

2015 JOINT CONFERENCE OF THE
IEEE INTERNATIONAL FREQUENCY CONTROL SYMPOSIUM
& EUROPEAN FREQUENCY AND TIME FORUM

April 12-16, 2015 | Colorado Convention Center | Denver, Colorado - USA

ABSTRACT BOOK

Organized and Sponsored by:

IEEE

UFFC

EFTF

Parametric Excitation in Geometrically Optimized Contour Mode AlN Resonators

Ruochen Lu, Anming Gao, and Songbin Gong
Dept. of Electr. & Comput. Eng., Univ. of Illinois at Urbana Champaign, Urbana, IL, USA
E-mail: rlu10@illinois.edu

Recently, a wide spectrum of applications, including computing, sensing, and noise squeezing in frequency sources, has been proposed leveraging parametrically excited resonances in nano and micro scale devices [1, 2]. These demonstrations, implemented with either electrostatic or piezoelectric actuations, all exploit the excitation of a fundamental resonance with a pump signal at twice the fundamental frequency. Despite the exciting potentials, these devices mostly employ flexural acoustic modes that require vacuum ambient for high Q and lack the scalability to higher frequencies. In this work, we report the first observation of parametric excitation in an Aluminum Nitride (AlN) contour mode resonator (CMR) that can be readily scaled in frequency, enhanced in efficiency, operated in dry air, and interfaced with auxiliary CMOS electronics.

The concept of parametric excited AlN CMRs harnesses the fact that the resonant frequencies of extensional mode vibrations along transverse and longitudinal direction can both be determined by resonator dimensions [3]. As seen in Fig. 1(a), the designed resonator consists of suspended AlN thin film with two sets of electrodes for inputting parametric excitation ($2f_0$) and outputting fundamental oscillations (f_0). By geometrically optimizing lateral dimensions to be around 200 μm and 50 μm, dual resonances can be respectively engineered at f_0 and $2f_0$ for lateral vibrations depicted in Fig. 1(c-e). This prototype device can be interpreted as a reproduction of Melde's experiment (Fig. 1(b)) on chip-level and micro scale. In operation, the parametric excitation amplifies an orthogonal oscillation at f_0 by periodically modulating the stiffness constants of AlN piezoelectric thin film via straining the structure at $2f_0$. Finite-element analyses were conducted to confirm that the device could be resonantly coupled at 36.2 MHz at 72.4 MHz for efficiently amplifying the pre-existing oscillation and absorbing the parametric excitation via input and parametric port respectively.

The fabricated resonator was tested by inputting an excitation of 72.4 MHz with an analog signal generator at the parametric port and measuring the admittance response at the input port with a VNA concurrently. An artificial enhancement in Q at f_0, from 40.9 to 143.9, was observed, confirming parametric amplification process in the prototype device. Upon further scaling and optimizations, we anticipate this type of devices will lead to the development of GHz low noise frequency sources and nanoelectromechanical logic.

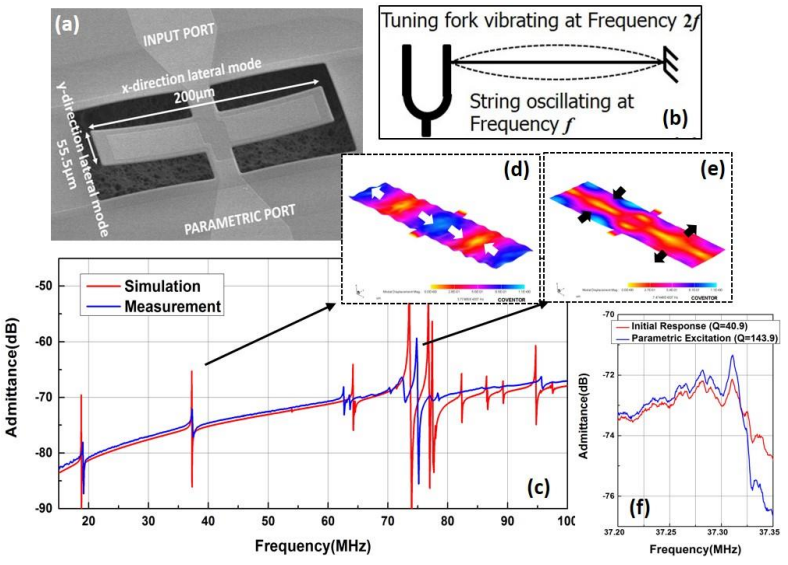


Fig. 1: (a) SEM image of the fabricated resonator; (b) Melde's experiment; (c) simulated and measured dual resonance response at input/output port; (d) Y-direction displacement mode shape; (e) X-direction displacement mode shape; (f) experimentally observed parametric excitation in the fabricated resonator.

[1] Karabalin R.B., Feng XL, Roukes ML., Parametric nanomechanical amplification at very high frequency. *Nano Letters* **9**(9), 116-23 (2009)

[2] Mahboob, I., & Yamaguchi, H. Bit storage and bit flip operations in an electromechanical oscillator. *Nature nanotechnology*, *3*(5), 275-279(2008).

[3] G, Piazza, P.J. Stephanou, A.P. Pisano, Piezoelectric aluminum nitride vibrating contour-mode MEMS resonators. *JMEMS*, *15*(6), 1406-1418. 2006

Third Order Intermodulation Distortion in Capacitive-Gap Micromechanical Filters

Jalal Naghsh Nilchi, Ruonan Liu, Scott Li, Clark T.-C. Nguyen,
EECS, University of California, Berkeley, Berkeley, CA, USA
E-mail: jalal.naghsh.nilchi@berkeley.edu

The third-order intermodulation distortion in properly terminated high-order bridged clamped-clamped beam (CC-beam) channel-select micromechanical filters [1] has been measured for the first time and found to be appreciably higher than seen on unterminated stand-alone CC-beams. In particular, a three-resonator bridged 8-MHz filter with 140nm gaps posts a measured IIP_3 of 25dBm and 36dBm for two-tone offsets of 200kHz and 400kHz, respectively, which are much larger than the -11.7dBm for a stand-alone 9.2MHz CC-beam with 200kHz two-tone offset [2]. The result matches well the prediction of a new model for nonlinearity that incorporates not only parallel-plate capacitor nonlinearity, but also the influence of the filter structure, where Q-loading by the termination reduces the degree of out-of-channel tone suppression, but also reduces the amplitude of resonator motion, which then improves the IIP_3. The full model to be described in the full paper incorporates these phenomena, plus dependencies on dc-bias, gap spacing, and electrode area.

Channel-select filters like those of this work, capable of rejecting all interferer signals and passing only the desired signal, greatly reduce dynamic range requirements on subsequent stages, e.g., the LNA and mixer, thereby greatly reducing power consumption. However, the degree of interferer suppression depends strongly on the linearity of the filter, which if not sufficiently linear, can also generate intermodulation spurs even after rejecting interferers. Here, third order nonlinearity with interferer signals at frequency offsets $\omega_0 \pm \Delta\omega$ and $\omega_0 \pm 2\Delta\omega$ are of most concern, for which the third-order intercept point IIP_3 is best maximized.

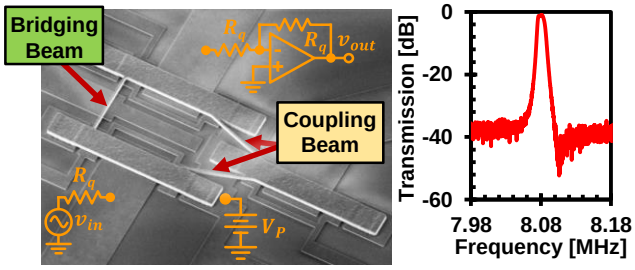


Fig. 1: SEM photo (left) and frequency response of a released and terminated 3CC-λ/4 bridged filter (right).

To validate our model's prediction that high-order filters improve IIP_3, bridged multi-CC-beam filters [1] were designed, fabricated and measured. Figure 1 shows the SEM and frequency response of a terminated 3rd order filter with λ/4 bridging (3CC-λ/4). This filter exhibits a measured bandwidth of 10.7kHz, an insertion loss of 1.2dB, and a 20dB shape factor of 2.08. Third order intermodulation distortion was measured by exciting the filter with two interferer signals at $\omega_0+\Delta\omega$ and $\omega_0+2\Delta\omega$ and measuring the output power at ω_0. As shown in Fig. 2, the 3CC-λ/4 bridged filter achieves a reasonable IIP_3 of 11dBm for $\Delta\omega=2\pi\times80$kHz and an even better value of 36dBm for $\Delta\omega=2\pi\times400$kHz. As predicted by the analytical model, filter IIP_3 increases with $\Delta\omega$ due to reduction in mechanical displacement as interferer signals move away from the filter center frequency, measured and shown in the left plot of Fig. 2.

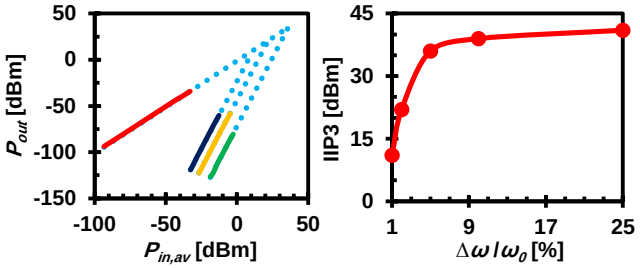


Fig. 2: IIP_3 measurement of 3CC-λ/4 bridged filter for interferer separation of 80, 160 and 400 kHz (Left). The figure on the right shows the IIP_3 dependency on interferer separation.

[1] S.-S. Li, M. U. Demirci, Y.-W. Lin, Z. Ren, C. T.-C Nguyen, "Bridged Micromechanical Filters," *Proceedings*, IEEE Int. Ultrasonics, Ferroelectrics, and Frequency Control 50th Anniv. Joint Conf., pp. 144-150, Aug. 2004.

[2] R. Navid, J. R. Clark, M. U. Demirci, and C. T.-C. Nguyen, "Third-order intermodulation distortion in capacitively-driven CC-beam micromechanical resonators," Technical Digest, Int. IEEE MEMS Conference, pp. 228-231, Jan. 2001.

Nonlinear Acceleration Sensitivity of Quartz Resonators

Jianfeng Chen, Yook-Kong Yong, Randall Kubena*, Deborah Kirby*, and David Chang*
Department of Civil and Environmental Engineering, Rutgers University, Piscataway, New Jersey, U.S.A.
*Sensors and Materials Laboratory, HRL Laboratories, Malibu, California, U.S.A.
E-mail: yyong@rci.rutgers.edu

We study the nonlinear effects of initial stress/strain of the quartz resonator on its acceleration sensitivity. The acceleration sensitivity of quartz resonators was considered an "old" problem and thought to be well understood. Since the acceleration sensitivity is a second order effect of frequency shift due to initial stress/strain induced by acceleration, the current assumption was that linear initial stress/strain would be sufficient for accurate predictions of acceleration sensitivity. We have recently found that comparisons of measured data by Fletcher and Douglas[1] with the results of models using the assumption of linear initial stress/strain were *inadequate*. The acceleration sensitivity is highly affected by the geometric nonlinearity of the initial stress/strain; particularly when the resonator is under high acceleration.

Figure 1 shows the effect of bending a circular 10 MHz AT-cut quartz plate on its resonant frequency[1]. A 2 gram-force (~ 0.02 N) is applied to the lever to provide the equivalent of about 200g acceleration to the plate clamped on one edge as shown. The angle ψ is the angle between the normal axis of the clamped edge to the crystal X-axis. The frequency change is recorded and is a measure of the acceleration sensitivity of the quartz plate for the ψ angle. The initial stress/strain caused by bending of the plate is calculated using linear elastic equations and nonlinear elastic equations with nonlinear strain. Figure 2 shows the model results of both the linear and nonlinear models compared with the Fletcher and Douglas measured results[1]. It shows that the nonlinear model is needed for good comparisons with the measured results. The 10 MHz quartz SC-cut plate was also studied, and good comparisons with the measured data could only be obtained when the nonlinear strain was included in the initial stress/strain of the acceleration sensitivity model. It was found that when the cantilever force was limited to less than 0.1 gram-force (~0.001 N) the linear acceleration sensitivity model yielded similar results as the nonlinear acceleration sensitivity model. Accurate models and designs of acceleration sensitivity of quartz resonators must include the nonlinear initial stress/strain.

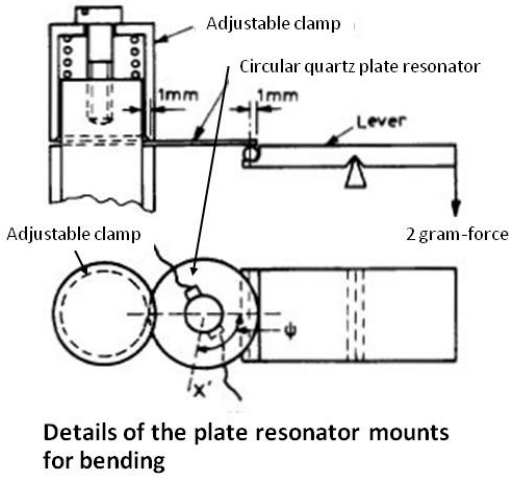


Fig. 1: Experimental setup for the study of effects of bending moment on a plate resonator frequency by Fletcher and Douglas[1]

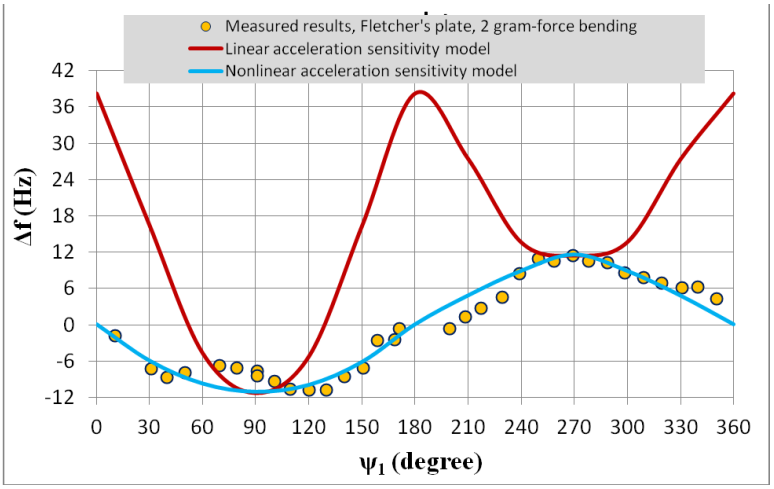


Fig. 2: Comparisons of linear and nonlinear acceleration sensitivity models with the measured results of Fletcher and Douglas [1]

[1] E.D. Fletcher and A.J. Douglas, "A Comparison of the Effects of Bending Moments on the Vibrations of AT and SC (or TTC) Cuts of Quartz", Proceedings of the 33rd Annual Symposium on Frequency Control, 1979, pp. 346-350.

MEMS-based UHF Monolithic Crystal Filters for Integrated RF Circuits

Kubena, Randall, Nguyen, Hung, Perahia, Raviv, Stratton, Fred, Joyce, Richard, Chang, David, and Kirby, Deb
HRL Laboratories, Malibu, Ca. USA
E-mail: rlkubena@HRL.com

UHF RF front ends are of wide use in present communication systems for commercial and military markets. For many applications, narrow-band, low insertion loss filters are needed for high sensitivity, high channel selectivity, and high noise rejection. Integrating the filters with the active electronics provides for miniaturization, low parasitics and loss, and simplification of the manufacturing assembly.[1] In this paper, we describe our work in developing UHF AT-cut quartz monolithic crystal filters for integration with Si electronics for highly compact RF front-end electronics. The AT-cut quartz crystal filters have demonstrated insertion losses of -2 dB and bandwidths of ~ 800 kHz (0.2%) with center frequencies below 400 MHz. In addition, the center frequency is highly stable over temperature as expected for AT-cut resonators.[2] Frequency uniformity over a 3" or larger quartz wafer can be maintained by using a combination of optical metrology and scanning ion beam truing techniques.

A micrograph of a completed device is shown in Fig. 1. Typical Qs for the resonators were approximately 17 – 20 K in vacuum with R_1s of 70 Ω, giving f x Q products of 6.5 – 7.5 x 10^{12}. A S_{12} filter response is shown in Fig. 2 for a symmetric single-pair 2-pole filter with 64 x 80 µm electrodes and a 4-µm gap between the electrodes. The electrodes were 80-nm-thick Al. The center frequency was 366 MHz, and the -3 dB bandwidth was 738 kHz. The insertion loss after impedance matching to the 2050 Ω impedance of the filter was -2 dB with a ripple of 0.19 dB. Out-of-band rejection was typically -35 dB. The temperature coefficient of the center frequency was -0.7 ppm/^{o} C measured from +10^o to +80^o C. The insertion loss change over this temperature range was ± 0.13 dB.

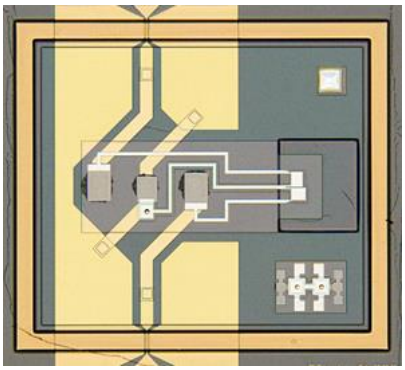


Fig. 1 Micrograph of single-pair, asymmetric electrode filter with an in-line mount to reduce bonding stress. Die size is 2.4 x 2.4 mm.

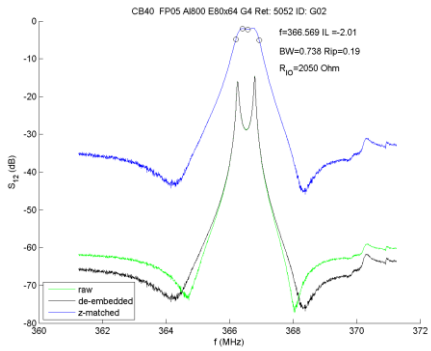


Fig. 2 S_{12} of a symmetric, single-pair, 2-pole filter showing the raw data and the de-embedded impedance matched results. The filter impedance was 2050 Ω.

In this paper, we will present data for both symmetric and asymmetric electrode designs, compare the experimental data to our filter models, and discuss work in using a commercial scanning ion beam truing system for maintaining frequency uniformity across the quartz wafer.

[1] R. L. Kubena, F. P. Stratton, D. T. Chang, R. J. Joyce, and T. Y. Hsu, "Next Generation Quartz Oscillators and Filters for VHF-UHF Systems," 2006 IEEE International Microwave Symposium, San Francisco, Ca., June 11-16, 2006.

[2] D. J. Kirby, Yook-Kong Yong, R. L. Kubena, R. Perahia, D. T. Chang, H. Nguyen, F. P. Stratton, R. J. Joyce, H. P. Moyer, R. G. Nagele, P. D. Brewer, "Optimizing UHF Quartz MEMS Resonators for High Thermal Stability," 2013 IEEE International Frequency Control Symposium, Prague, Czech Republic, July 22 – 26, 2013.

Multiple SAW Resonance Sensing Through One Communication Channel with Multiple Phase Detectors

TAKIZAWA, Yoshinori*; SHIBATA, Takayuki**; KASHIWADA, Shinji**; YAMAMOTO, Yasuo**; ESASHI, Masayoshi*; TANAKA, Shuji+

*WPI-AIMR, Tohoku University, Sendai-City, Miyagi Prefecture, Japan
**DENSO Research Laboratories, Nisshin-City, Aichi Prefecture, Japan
+Graduate School of Engineering, Tohoku University, Sendai-City, Miyagi Prefecture, Japan
E-mail: takizaway@wpi-aimr.tohoku.ac.jp

SAW device is a very strong tool in the various passive sensing such as temperature, pressure, torque measurements, etc [1]. However, in some applications, the measurement results are not stable in temperature. For example in the mechanical force sensing, the temperature response is larger than the mechanical force response, and the temperature compensation is required by using the multiple SAW devices.

Several measurement methods are proposed for the passive remote sensing. In most cases, Time Division (TD) measurement similar to a radar system is commonly used along with frequency domain analysis. This method has high accuracy capability, but the circuit size is large and the processing speed is slow because of the time-frequency domain conversion. In this paper, the Continuous Wave (CW) Phase-Lock-Loop (PLL) solution with SAW resonator is described. The biggest advantage of this method has the faster processing speed than the TD method, since the resonant frequency change can be seamlessly tracked by PLL.

Fig.1 shows the blockdiagram for the proposing system. If there are N resonators on the measuring object, the N PLL circuits are provided but combined signal are communicate through only the one sending/receiving channel. The Vco outputs are summed and feed to the parallel connected SAW circuit through the channel. The response to the resonators are the linear summation of resonators. When the combined signal is phased detected by the original Vco signal, the loop filter is tuned only in the targeted resonator phase shift (frequency change). If the loop gains are properly design to the corresponding SAW resonators, the PLL can detect and track the resonator phase shift.

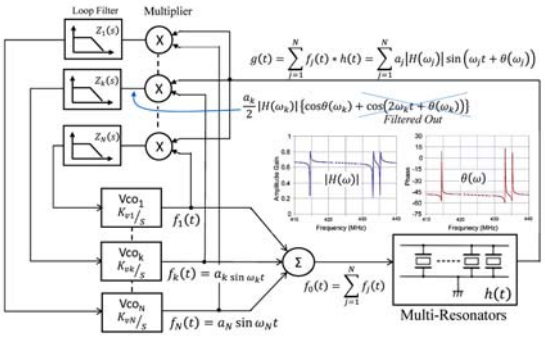


Fig. 1: Blockdiagram for the multiple SAW resonators measurement system with multiple PLLs

The hardware phase lock experiment results are summarized in table 1. The experiments were conducted with two and three SAW resonators, and the PLL locks were confirmed in the temperature change of 20-200°C. The temperature test with 203-204MHz LiNO3 showed the very linear characteristics over approximately 3MHz frequency range. This result indicates the system can be very useful in the temperature compensating measurement systems [2]. One important point when summing the Vco signals is that the zero signal point must not be happened in the Vco summed signal during the operation. This can be avoid by appropriately setting the Vco signal amplitudes. The proposed method can be applied to the wireless remote sensing in near electromagnetic filed, and successfully worked.

[1] Haekwan Oh, Weng Wang, Keeeun Lee, Ikmo Lee Park, and Sang Sik Yang, "Sensitive Improvement of Wireless Pressure Sensor by Incorporating A SAW Refrective Delay", Int. Journal on Smart Sensing and Intelligent System, VOl.1, No.4

[2] B.Dixon, V.Kalinin, J.Beckley, R.Lohr, "A Second Generation In-Car Tire Pressure Monitoring System Based on Wireless Passive SAW Sensors," International Frequency Control Symp., pp.374 – 380, 4-7 June 2006

# of SAW	Resonator Frequency	SAW Type TFC,
3	415MHz, 433.5MHz, 434MHz	Low TFC Type 2.5ppm/K
2	203MHz, 204MHz	LiNO3 70ppm/K
2	201MHz, 202MHz Passive wireless communication in near electromagnetic filed.	LiNO3 70ppm/K

Table 1: PLL Lock Experimental Results
Temperature Range: 20-200°C

Imaging the Static Magnetic Field Distribution in a Vapor Cell Atomic Clock

Christoph Affolderbach*, Guan-Xiang Du[+], Thejesh Bandi*, Andrew Horsley[+],
Philipp Treutlein[+], Gateano Mileti*
*Laboratoire Temps-Fréquence, Institute of Physics, University of Neuchâtel, Neuchâtel, Switzerland.
[+]Departement Physik, Universität Basel, Basel, Switzerland.
E-mail: Christoph.affolderbach@unine.ch

Precise knowledge of the microwave and static magnetic field ("C-field") distribution across an alkali vapor cell is crucial for the development and optimization of high-performance vapor-cell atomic clocks. We recently reported imaging of the microwave magnetic field distribution [1] in a compact microwave resonator cavity for vapor-cell atomic clocks [2]. In this approach, a CCD camera is used to record the laser intensity I_T transmitted through the alkali cell with high spatial resolution, and the microwave field amplitude is extracted from time-domain data obtained by pulsed laser and microwave interaction in the Rabi scheme [3].

Here we exploit a similar scheme for obtaining images of the C-field distribution across the Rb cell used in our vapor-cell atomic clock physics package [2]. In this case, we employ the Ramsey interaction scheme of two microwave pulses separated by a Ramsey time T_R, and a calibrated microwave frequency detuned by δ_R from a selected Zeeman component of the Rb ground-state transition. The signal $I_T(T_R)$ shows oscillation at a frequency corresponding to the microwave detuning δ_R that can be obtained from a fit to the $I_T(T_R)$ data in the time domain. The C-field amplitude is then calculated from this measure of the transition's Zeeman shift (using the Breit-Rabi formula), and common-mode shifts (e.g. buffer-gas shifts) are eliminated by measuring on two or more Zeeman transitions. Spatial resolution is again achieved using a CCD camera as optical detector.

Figure 1 shows an image of C-field amplitude distribution, obtained on the physics package of our vapor-cell atomic clock [2]. Very low variations (< 0.5 % only) in C-field amplitude across the imaging region are detected, with a central symmetry of the distribution originating from the C-field coil used. Images of the T2 relaxation time in the cell can be extracted from the same Ramsey data $I_T(T_R)$ and show a distribution very similar to the one found for the C-field, indicating inhomogeneous dephasing due to C-field gradients, but do not correlate with the microwave magnetic field distribution also measured for our clock. The presented method is useful for measuring the spatial distribution of C-field amplitude and relaxation times in vapor-cell atomic clocks that are otherwise difficult to assess experimentally in a fully assembled clock physics package. It is particularly interesting for detecting changes in magnetic field distribution after extended clock operation time, e.g. caused by magnetization of the magnetic shields.

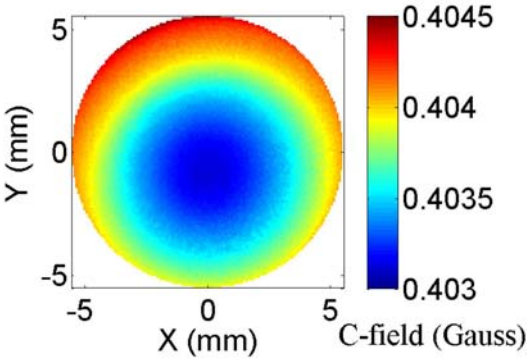


Fig. 1: Example of imaging the amplitude of the C-field applied to the vapor cell in our clock. The $m_1=1 \leftrightarrow m_2=1$ Zeeman transition was used here.

This work was supported by the Swiss National Science Foundation (SNSF) and the European Metrology Research Programme (EMRP project IND55-Mclocks). The EMRP is jointly funded by the EMRP participating countries within EURAMET and the European Union.

[1] A. Ivanov et al., "Experimental and numerical study of the microwave field distribution in a compact magnetron-type microwave cavity", *Proceedings* 28th EFTF, Neuchatel, Switzerland, June 22 - 26, 2014, pp. 208-211.

[2] T. Bandi et al., "Compact high-performance continuous-wave double-resonance rubidium standard with 1.4×10^{-13} $\tau^{-1/2}$ stability", *IEEE Trans. Ultrason. Ferroelectr. Freq. Control,* vol. 61, no. 11, pp. 1769 – 1778, Nov. 2014.

[3] A. Horsley et al., "Imaging of Relaxation Times and Microwave Field Strength in a Microfabricated Vapor Cell", *Phys. Rev. A*, vol. 88, no. 6, p. 063407, Dec. 2013.

^{87}Rb Isoclinic-Point Thermometry

N. Wells, T. Driskell, and J. Camparo

Photonics Technology Dept.
Physical Sciences Laboratories
The Aerospace Corporation, El Segundo, CA/USA

E-mail: nathan.p.wells@aero.org

The long-term temperature instability of vapor-phase atomic systems, at the tens of milliKelvin level, is known to have a significant effect on the frequency stability of Rb atomic clocks and atom-stabilized lasers. Building on previous work examining the isoclinic point in (nuclear spin) I = 3/2 alkalies [1], we demonstrate in this presentation an isoclinic-point thermometer.

We have previously shown that the minimum in the Doppler broadened D_1 ^{87}Rb absorption transition midway between the $F_g=2\rightarrow F_e=1$ and $F_g=2\rightarrow F_e=2$ lines, the "isoclinic point," is a suitable frequency reference for laser stabilization with a near zero temperature sensitivity [1]. Additionally the isoclinc point can be employed for the measurement of the energy dependence of optical transition collisional shifts [2]. Here we combine our previous work [1-3] to demonstrate isoclinic-point thermometry, where we sense the temperature of an atomic vapor in an all optical fashion [4].

We have designed two nearly identical laser stabilization systems consisting of 795 nm DBR lasers locked to different features of the ^{87}Rb D_1 absorption spectrum: one laser is locked to the isoclinic point, while the other is locked to a temperature sensitive resonance. Laser locking is achieved via frequency modulation (FM) spectroscopy using electro-optic modulators (EOMs), and we can lock to either Doppler or pressure broadened optical transitions. The unmodulated output of the two lasers are combined, and the resulting beat note is detected with a high speed photodiode. This beat note acts as an optical sensor of vapor temperature fluctuations in the absorption cell.

The sensitivity and long-term stability of this optical thermometer are inherently linked to the lasers' stabilization. We will discuss the influence of systematic FM spectroscopy effects on laser stabilization, and disentangle those effects from other instabilities of a purely atomic nature.

Our current system shows a laser frequency stabilization reaching ~ 2×10^{-11} at 1 s for a Doppler broadened feature (500 MHz), and flicker noise at this level out to 10^2 s. The laser beat note then shows a long term deviation of ± 1 MHz over tens of hours. The beat note's measured sensitivity to optical power and absorption cell temperature are too small to account for the long-term laser frequency instability. Instead, our measurements suggests that the long-term frequency variations are due to residual amplitude modulation (RAM) of the lasers, which we believe is due to thermal variations of the EOMs. Consequently, we are presently constructing thermal enclosures for the EOMs to improve their long-term stability.

Notwithstanding these limitations, we have been able to demonstrate an ability to sense vapor temperature changes down to ±0.3 K in an all optical fashion. Moreover, these are measurements of the vapor temperature itself; they are not point measurements of temperature made on the exterior of a glass resonance cell, which may or may not be reflective of the vapor's true temperature. We believe that with our planned improvements in the laser stabilization system, we should be able to increase this temperature sensing capability markedly.

Our results show a clear path forward for reaching long-term stabilization of Rb vapor cell temperatures based on isoclinic-point thermometry. This in turn should have a dramatic impact on the stability of vapor-cell atomic clocks (both lamp-pumped and laser-pumped), and atom-stabilized laser systems.

REFERENCES

[1] Wells, N. P.; Camparo, J. C. *Physical Review A* **2010**, *82*, 062505.

[2] Wells, N. P.; Driskell, T. U.; Camparo, J. C. *Physical Review A* **2014**, *89*, 052516.

[3] Wells, N. P.; Camparo, J. C. In *Frequency Control Symposium (FCS), 2010 IEEE International* 2010, p 329.

[4] Wells, N.; Driskell, T.; Camparo, J. In *Proceedings of the EFTF* Neuchâtel, Switzerland 2014.

Measuring Excited State Lifetime of Alkali Atoms with Novel Pump-Probe Technique

Xi Zeng, Dmitri L. Boiko
Centre Suisse d'Électronique et de Microtechnique, Neuchâtel, Switzerland
E-mail: dmitri.boiko@csem.ch

Exact knowledge of the excited state lifetime τ_{ex} in alkali vapor cells is vital for many applications in atomic physics, spectroscopy, and frequency standards. In alkali vapor cells with molecular buffer gases (e.g. Rb cell containing more than few tens of torr of N_2), the τ_{ex} lifetime may be quenched down to nanosecond scale. With a large pressure broadening of the absorption line and hence small absorption cross-section, measuring the τ_{ex} of such a cell with the standard technique of time-resolved fluorescence can be impractical because the photodetector must be extremely sensitive, have sub-nanosecond temporal resolution, and have wide collection angle.

We present an alternative pump-probe technique to measure τ_{ex} in an alkali vapor cell and apply it to the D_1 line in ^{85}Rb cells. The method is best explained in the framework of 3-level model of alkali atoms [1] and is depicted in Fig. 1(a). The model is suitable for cells with buffer gas pressure of more than a few tens of torrs and under excitation by linearly polarized (π) light. Initially, the alkali vapor cell is optically excited by two lasers. The pump laser (here, a DFB emitting 5 mW) excites the alkali atoms in dual frequency (DF) configuration, which is achieved by modulating the laser current at 1.5 GHz, half of hyperfine splitting frequency of the ground states in ^{85}Rb atoms. This laser produces non-zero atomic population in the excited state while keeping ground state populations close to thermal equilibrium. The second VCSEL laser of much smaller power (200 µW here) is used as single frequency (SF) probe laser and is tuned to one of the hyperfine resonances. After the atomic system reaches steady state, interaction with the pump laser is suddenly suppressed by removing the RF modulation. This results in a transient process in which the atomic populations move towards a new steady state where the atoms are under excitation by the SF probe laser only. The decay of the upper state population can be observed at the onset of the transient as indicated in Fig. 1(b). This feature is well reproduced by our model (Fig. 1(c)). The measured excited state lifetime quenching *vs* N_2 buffer gas pressure is in reasonable agreement with the literature value for quenching cross-section of N_2 on the Rb *D*-lines of 50 Å^2 [2] as indicated in Fig. 1(d). This technique can serve as a practical alternative to time-resolved fluorescence for cells heavily quenched by buffer gas.

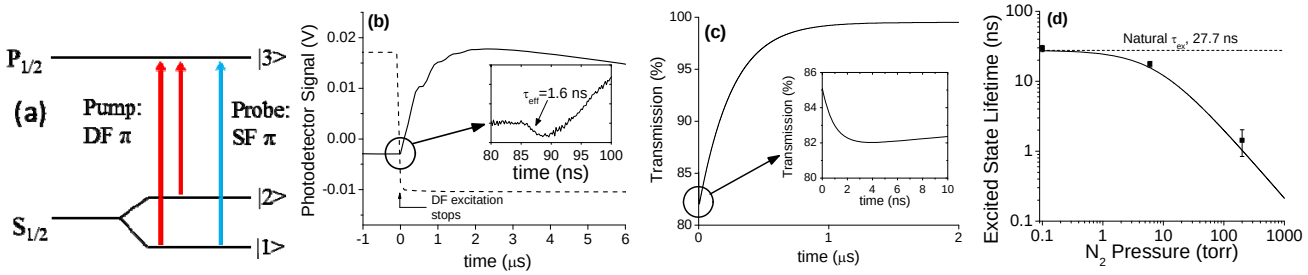


Fig. 1: (a) 3-level model of ^{85}Rb atom under optical excitation by pump and probe beams. Measured (b) and modeled (c) transmitted signal of the probe laser through a ^{85}Rb cell with 200 torr of N_2 buffer gas (solid curve) at 66° C. (d) Measured (points) and calculated (curve) excited state lifetimes τ_{ex} of ^{85}Rb under quenching by N_2.

[1] J. Vanier, "Atomic clocks based on coherent population trapping: a review," *Appl. Phys. B*, vol. 81, no. 4, pp. 421–442, Aug. 2005.

[2] E. S. Hrycyshyn and L. Krause, "Inelastic collisions between excited alkali atoms and molecules. VII. Sensitized fluorescence and quenching in mixtures of rubidium with H_2, HD, D_2, N_2, CH_4, CD_4, C_2H_4, and C_2H_6[1]," *Can. J. Phys.*, vol. 48, no. 22, pp. 2761–2768, Nov. 1970.

Spectroscopy and hyperfine clock frequency shift measurements in Cs vapor cells coated with octadecyltrichlorosilanes (OTS).

Abdel Hafiz Moustafa, Maurice Vincent, Chutani Ravinder, Gorecki Christophe, De Clercq Emeric, Guérandel Stéphane, Boudot Rodolphe.
FEMTO-ST, CNRS, UFC, 26 chemin de l'épitaphe, 25000 Besançon, France
LNE-SYRTE, Observatoire de Paris, 61 avenue de l'observatoire 75014 Paris, France
E-mail: rodolphe.boudot@femto-st.fr

The detection of long-lived spin polarized alkali atoms in vapor cells is of critical importance for the development of high-performance atomic clocks or magnetometers. Two main techniques are used to slow down the fast wall-induced depolarization of atoms. The first method is to dilute the alkali vapor with a pressure of buffer gas. In this so-called Dicke regime [1], slight collisions between buffer gas and alkali atoms increase the time for alkali atoms to collide against the cell walls and allow consequently to reduce the linewidth of the detected resonance. Drawbacks of the presence of buffer gas are to induce shift and broadening of the optical resonances and a collisional frequency shift of the clock transition. The second method consists in coating the glass walls with an anti-relaxation material. In this case, atoms experience multiple bounds against the cell walls before destruction of the population or coherence. Parafin and alkene-based coatings are known to exhibit excellent anti-relaxation properties with the demonstration of 10^4 to 10^6 bounces [2,3]. Most of the time, these coatings are used in magnetometry or quantum information experiments where Zeeman population or coherences are observed. Thus, understanding what the wall-coating mechanism actually relaxing the microwave clock coherence, how it operates and what the best material to use is, is far to be fully clear. Additionally, their drawback is their low temperature melting point preventing them to be used in chip scale atomic devices. At the opposite, octadecyltrichlorosliane (OTS) layers, thermally stable up to 170°C in presence of Rb vapor, are interesting candidates for miniature devices [4].

We report here the realization and characterization using coherent population trapping spectroscopy of a centimeter-scaled Cs vapor cell coated with octadecyltrichlorosilane (OTS). The dual structure of the resonance lineshape, with presence of a narrow structure at the top of a Doppler-broadened structure, is observed. We performed measurements of clock resonance linewidths and clock frequency shifts. The results show that cesium atoms collide about 12 times with the cell walls before relaxation of the CPT coherence. The adsorption energy, that relates to the kinetic energy an atom must have to escape the surface attraction, is measured to be 0.42 eV (+/- 0.03 eV), in good agreement with results reported in [2]. The zero-intensity CPT resonance linewidth in the Cs-OTS cell is measured to be a factor 2.4 higer than in a buffer-gas filled cell of similar dimensions. The Zeeman population lifetime T_1 is measured to be about 1.6 ms using the Franzen technique while the lifetime T_2 of the microwave coherence is about 500 us. Ramsey spectroscopy is also performed on this cell. Potential applications of OTS coatings to the development of a vapor cell atomic clock is discussed.

[1] DICKE, R. H. The effect of collisions upon the Doppler width of spectral lines. *Physical Review*, 1953, vol. 89, no 2, p. 472.
[2] BOUCHIAT, M. A, BROSSEL. J *Phys. Rev.*, 1966, vol. 147, no 1, 41.
[3] BALABAS M. et al... *Phys. Rev. Lett.*, 2010, vol. 105, 170801.
[4] STRAESSLE R. et al., *Appl. Phys. Lett.*, 2014, 105, 043205.

Buffer Gas Consumption in Rubidium Discharge Lamps

Jaduszliwer, Bernardo, Michael Huang, and James Camparo
Physical Sciences Laboratories, The Aerospace Corporation, El Segundo, CA, USA
E-mail: James.C.Camparo@aero.org

At the heart of a conventional rubidium atomic clock there is a simple rubidium vapor rf-discharge lamp, which enables the production of the atomic clock signal and the sensing of the rubidium atoms' response to resonant microwaves. Discharge electrons extract energy from the rf-field via elastic collisions with buffer noble gas (Kr or Xe) atoms. Unfortunately, the lamps slowly lose their buffer gas, giving rise to a life-limiting mechanism for the clock [1]. Data has recently become available in which lamp buffer gas pressure was measured as a function of operating time for lamps with different initial Xe fills. We have employed that data to develop a physics-based, empirical model of the noble gas loss process which, if validated, should allow high confidence predictions of lamp life against buffer gas exhaustion.

The first striking fact about the observed Xe loss to the lamp glass is that the loss of a noble gas atom to the glass wall is an extremely rare event. Simple kinetic theory considerations, when combined with typical measured loss rates, show that the probability of loss of a Xe atom in a collision with the wall is $\gamma \approx 4\times10^{-14}$. There are three plausible explanations: (1): *There are very few sites in the glass capable of capturing Xe.* (2)*: Xe capture is a very high activation energy process.* (3): *The lost Xe is not ground state neutral Xe, but either an excited Xe species or* Xe^+*, in either case present in very low numbers in the discharge*.

The second striking fact about the observed Xe loss to the lamp glass is its pressure dependence. The loss rate for any process mediated by collisions of ground state neutral Xe atoms with the walls should decrease as the collision rate decreases, *i.e.*, with decreasing Xe pressure p. But the loss rate is seen to increase with decreasing p in a manner inconsistent with (1) and (2) above, leaving (3) as the only possible alternative.

We are proposing noble gas ion capture (NIC) by the glass as the loss mechanism. We will show that it explains the low probability of Xe loss per wall collision and the dependence of loss rate on p. It also predicts a strong dependence of loss rate on discharge electron temperature, which has been confirmed by measurements.

In the NIC model, the Xe loss rate to the glass can be written in a most general way as

$$R = -\frac{dp}{dt} = -\frac{kT}{V}\frac{dN}{dt} = \frac{kT}{V}\oint_A dA \int_0^\infty dE\, \Phi(E,\vec{x})\,\gamma(E,\vec{x})$$

where Φ is the flux of Xe^+ ions of kinetic energy E impinging on the glass surface at point $\vec{x}$, and γ is the probability that one of them will be captured in the glass. Φ will be determined by discharge conditions, and γ by the properties of the glass surface (and possibly by the plasma conditions in its immediate vicinity).

A full calculation of $\Phi(E,\vec{x})$ would require complete modeling of a two-component (Rb and Xe) weakly ionized plasma in a non-homogeneous, non-isotropic electromagnetic field distribution, with ill-defined boundary conditions. It would also require full knowledge of all the relevant collision cross sections. Such a calculation is beyond the scope of a reasonable effort to understand and mitigate the buffer gas loss problem. Instead, we will use the results of empirical observations to guide us in the formulation of the simplest possible physics-based empirical model capable of reasonable lamp life predictions.

We assume the electrons in the discharge to follow a Boltzmann energy distribution at temperature T_e (typically ≈ 3200K). The Xe ionization threshold is 12.127 eV, and the first excitation threshold is 8.3204 eV. The fraction of electrons capable of exciting ground state Xe to its 1st excited state is $\mathcal{F}_{ex} \approx 2.7\times10^{-13}$, while the fraction capable of directly ionizing ground state Xe is $\mathcal{F}_{+} \approx 3.3\times10^{-19}$, 10^6 times smaller. Once a ground state Xe atom has been excited, sequential collisions can take it up a ladder of excited states leading to ionization. Since the subsequent energy steps in this ladder are much smaller than the first one, the numbers of available electrons are much higher, making multistep ionization a more likely path to Xe^+ production than direct ground state ionization. We will show that

(m+1)-step ionization leads directly to a p^{-m} dependence of the loss rate on Xe pressure, consistent with available data.

The probability of ionization after (m+1) collisions with electrons will be given by $P_+ = P_{0,1} \prod_{k=1}^{m} P_{k,k+1}$,where $P_{k,k+1}$ is the probability of promoting an atom by a collision with an electron from state k to a higher energy state k+1. $P_{0,1}$ will be independent of p, but for $k \neq 0$, $P_{k,k+1}$ will depend on p, since the atom in state k could be demoted to a lower energy state by a collision with another Xe atom before colliding with an electron and being promoted to state k+1. If n is the Xe number density, σ_k are de-excitation cross sections for collisions with other thermal Xe atoms and the ζ_k are the mean free paths for excitation to state k+1 by electron collision, it can be shown that

$$P_+ \approx \frac{P_{0,1} e^{-m}}{n^m} \prod_{k=1}^{m} \frac{1}{\sigma_k \zeta_k}.$$

The loss rate $R \propto P_+$; since $p \propto n$, $R \propto p^{-m}$. Of course, this behavior cannot continue indefinitely as $p \to 0$. We postulate the simplest possible expression for R(p) with $R \propto p^{-m}$ for $p << p_C$, and $R \propto p$ for $p << p_C$ (p_C is some critical pressure): $R = -dp/dt = \kappa p / \left(p^{m+1} + p_C^{m+1}\right)$. That expression can be integrated to yield p(t). Figure 1 displays measurements of p as a function of operating time for a lamp with an initial ≈ 1 torr Xe fill and the corresponding measured loss rates, as well as the corresponding NIC model fits.

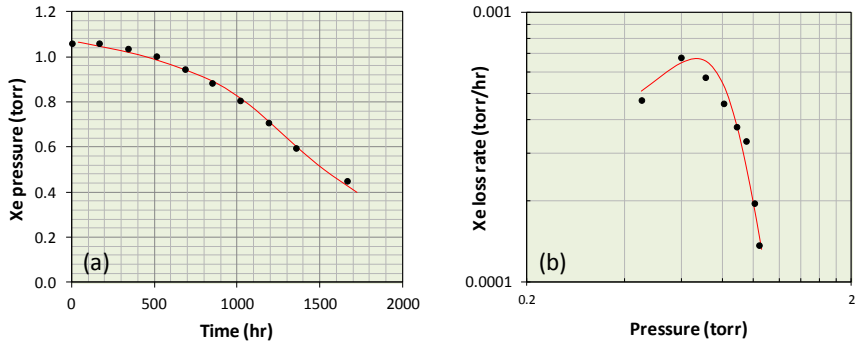


Figure 1: (a) p vs. t for a 1 torr fill lamp. Black dots: measurements; red curve: NIC model fit, with m = 8, $\kappa = 2.4 \times 10^{-4}$ torr^9/hr and p_C = 0.84 torr. (b) Xe loss rate vs. pressure; black dots derived from data in (a); red curve; NIC model

The multistep ionization rate is limited by $P_{0,1} \propto \mathcal{F}_{ex}$; R will be very small because of the very small $\mathcal{F}_{ex}$ value.

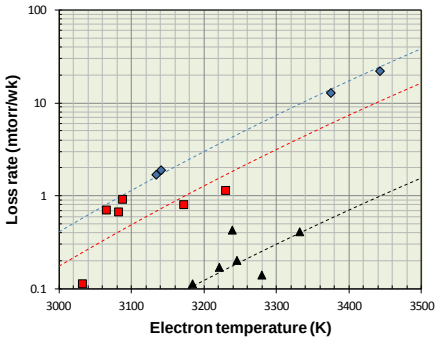


Figure 2 shows measured consumption rates for three sets of lamps (1 torr, 2.5 torr and 3.5 torr initial Xe fills) vs. measured discharge T_e, as well as $\mathcal{F}_{ex}$ vs. T_e, scaled to match each set of lamps. It can be seen that each set of lamps follows reasonably well the $\mathcal{F}_{ex}(T_e)$ trend, and that the consumption rate is extremely sensitive to T_e. It follows that the lowest possible value of T_e consistent with clock performance will maximize lamp life against buffer gas exhaustion.

Figure 2: R vs. T_e. Blue diamonds: 1 torr lamps. Red squares: 2.5 torr lamps. Black triangles: 3.5 torr lamps. Dash curves: $\mathcal{F}_{ex}$, scaled to match each set of lamps

This work was supported by the US Air Force Space and Missile Center under contract FA8802-09-C-001.

[1] S.A. Kazantsev, V. I. Khutorshchikov, G. H. Guthorlein and L. Windholz, "Practical Spectroscopy of High Frequency Discharges" (Plenum, New York, 1998), Ch. 8, and references therein

Track: Optical Frequency Standards And Applications

Title: Relativistic geodesy with clocks

Author: Jakob Flury, Institut fuer Erdmessung, Leibniz Universitaet Hannover

Abstract: The recent progress in optical atomic clocks and in long-distance frequency transfer by optical fiber together pave the way for using measurements of the gravitational frequency redshift for geodesy. The remote comparison of frequencies generated by calibrated clocks will allow for a purely relativistic determination of differences in gravitational potential and height between stations on Earth surface (chronometric leveling). Experiments for the proof of concept for this technique are currently in preparation at Leibniz Universität and Physikalisch-Technische Bundesanstalt (PTB). If successful, the technique could on the long run provide the basis for an atomic height reference and a relativistic geoid definition.

Highly-charged ions for atomic clocks and search for the variation of the fine-structure constant

Marianna Safronova[1,2], Vladimir Dzuba[3], Victor Flambaum[3], Ulyana Safronova[4,5], Sergey Porsev[1,6], Mikhail Kozlov[6,7]

[1]Department of Physics and Astronomy, University of Delaware, Newark, Delaware, USA
[2]Joint Quantum Institute, NIST and the University of Maryland, College Park, Maryland, USA
[3]School of Physics, University of New South Wales, Sydney, Australia
[4]Department of Physics, University of Nevada, Reno, Nevada, USA
[5]Department of Physics University of Notre Dame, Notre Dame, Indiana, USA
[6]Petersburg Nuclear Physics Institute, Gatchina, Russia
[7]St. Petersburg Electrotechnical University ``LETI", St. Petersburg, Russia
E-mail: msafrono@udel.edu

The modern theories directed toward unifying gravitation with the three other fundamental interactions suggest variation of the fundamental constants in an expanding universe. Development of ultra-precise atomic clocks allows laboratory tests of the α-variation at the present time. Despite very large ionization energies, some highly-charged ions (HCI) have transitions that lie in the optical range and have very large sensitivities to α-variation [1]. Highly-charged ions are less sensitive to external perturbations than either neutral atoms or singly-charged ions due to their more compact size. Some HCIs have several metastable states representing a level structure and other properties that are not present in any neutral and low-ionization state ions and are advantageous for the development of atomic clocks as well as provide new possibilities for quantum information storage and processing. The development of ultra-precise atomic clocks provides remarkable new opportunities for precision tests of fundamental science and development of new technologies.

One of the main obstacles for the HCI experimental work in this direction is the lack of data for these systems as well as difficulties in accurate theoretical predictions of the transition wavelengths. The goal of the present work was to resolve this problem. We carried out an exhaustive search of transitions in highly-charged ions that are particularly well suited for the experimental exploration [2-4]. We proposed 10 highly-charged ions as candidates for the development of next generation atomic clocks and search for α-variation [2-4]. These ions have long-lived metastable states with transition frequencies to the ground state between 170-3000 nm, relatively simple electronic structure, stable isotopes and high sensitivity to α-variation (e.g., Sm^{14+}, Pr^{10+}, Sm^{13+}, Nd^{10+}). We predict ion properties crucial for the experimental exploration using state-of-the-art theoretical approaches [5] and highlight particularly attractive systems for these applications.

[1] J. C. Berengut, V. A. Dzuba, and V. V. Flambaum, "Enhanced Laboratory Sensitivity to Variation of the Fine-Structure Constant using Highly Charged Ions", Phys. Rev. Lett., vol.105, 120801, 2010.

[2] M. S. Safronova, V. A. Dzuba, V. V. Flambaum, U. I. Safronova, S. G. Porsev, and M. G. Kozlov, "Highly-charged ions for atomic clocks, quantum information, and search for α-variation", Phys. Rev. Lett., vol. 113, 030801 (2014).

[3] M. S. Safronova, V. A. Dzuba, V. V. Flambaum, U. I. Safronova, S. G. Porsev, and M. G. Kozlov, "Study of highly-charged Ag-like and In-like ions for the development of atomic clocks and search for α-variation", Phys. Rev. A, vol. 90, 042513, 2014.

[4] M. S. Safronova, V. A. Dzuba, V. V. Flambaum, U. I. Safronova, S. G. Porsev, and M. G. Kozlov, "Atomic properties of Cd-like and Sn-like ions for the development of frequency standards and search for the variation of the fine-structure constant", Phys. Rev. A, vol. 90, 052509, 2014.

[5] M. S. Safronova, M. G. Kozlov, and Charles W. Clark, "Precision Calculation of Blackbody Radiation Shifts for Optical Frequency Metrology", Phys. Rev. Lett., vol. 107, 143006, 2011.

mSTAR: Testing Special Relativity in Space Using High Performance Optical Frequency References

Thilo Schuldt[1], Shailendhar Saraf[2], Alberto Stochino[2], Klaus Döringshoff[3], Sasha Buchman[2], Grant D. Cutler[2], John Lipa[2], Si Tan[2], John Hanson[4], Belgacem Jaroux[4], Claus Braxmaier[1,6], Norman Gürlebeck[6], Sven Herrmann[6], Claus Lämmerzahl[6], Achim Peters[3], Abdul Alfauwaz[5], Abdulaziz Alhussien[5], Badr Alsuwaidan[5], Turki Al Saud[5], Hansjörg Dittus[1], Ulrich Johann[7], Simon P. Worden[4], Robert Byer[2]

[1]Deutsches Zentrum für Luft- und Raumfahrt (DLR), Institut für Raumfahrtsysteme, Bremen, Germany
[2]Stanford University, Hansen Experimental Physics Laboratory, Stanford, California/USA
[3]Humboldt-Universität zu Berlin, Institut für Physik, Berlin, Germany
[4]NASA Ames Research Center (ARC), Mountain View, California/USA
[5]King Abdulaziz City for Science and Technology (KACST), Riyadh, Saudi-Arabia
[6]Zentrum für Angewandte Raumfahrttechnologie und Mikrogravitation (ZARM), Universität Bremen, Germany
[7]Airbus Defence and Space GmbH, Friedrichshafen, Germany
E-mail: thilo.schuldt@dlr.de

The proposed mini SpaceTime Asymmetry Research (mSTAR) mission will perform a test of special relativity. By comparing an absolute frequency reference to a length-based frequency reference, a Kennedy-Thorndike type experiment is carried out, testing the boost dependency of the speed of light using the large and rapid velocity modulation available in low Earth orbit (LEO). Using clocks with instabilities at or below the 10^{-15} level at orbit averaging time, the Kennedy-Thorndike coefficient will be measured with an up to two orders of magnitude higher accuracy than current ground-based experiments [1].

In the current baseline design, mSTAR utilizes an absolute frequency reference based on modulation transfer spectroscopy of molecular iodine near 532nm. A frequency-doubled Nd:YAG laser is foreseen as laser source. Part of the fundamental (1064nm) stabilized laser light is split off, frequency shifted using an acousto-optic modulator (AOM) and sideband locked to the resonance frequency of a high finesse optical cavity made of ultra-low expansion (ULE) glass using an electro-optic modulator and standard Pound-Drever-Hall technique. For the evaluation of the Kennedy-Thorndike experiment, the feedback signal to the AOM of the frequency lock is analyzed with respect to variations at the orbit frequency.

The mSTAR iodine clock is based on a DLR-funded setup on Engineering Model (EM) level, realized using specific assembly-integration technologies. A frequency stability below 5×10^{-15} at integration times between 10s and 100s was demonstrated [2]. The cavity is based on the space-qualified cavity setup under development at JPL within the GRACE follow-on mission. A design with adapted thermal shielding and fiber coupling to the cavity is currently realized at Stanford University.

The mSTAR mission is investigated in an international US-Saudi-German collaboration. In an ongoing Phase A study, the feasibility of the payload accommodation within the SaudiSat 4 satellite bus is evaluated. This especially includes the evaluation of a detailed payload design including corresponding budgets (volume, mass and power).

We will give an overview over the mission profile and the scientific measurement. Special emphasis will be placed on the optical frequency references that are foreseen for the mission.

[1] M. E. Tobar, P. Wolf, S. Bize, G. Santarelli, and V. Flambaum, "Testing local lorentz and position invariance and variation of fundamental constants by searching the derivative of the comparison frequency between a cryogenic sapphire oscillator and hydrogen maser," Phys. Rev. D, vol. 81, p. 022003, Jan 2010.

[2] T. Schuldt, J. Stühler, K. Döringshoff, J. Pahl, E.V. Kovalchuk, M. Franz, U. Johann, A. Peters, C. Braxmaier, "An Iodine-Based Ultra-Stable Optical Frequency Reference and its Application in Fundamental Physics Space Missions," Proceedings of the European Frequency and Time Forum 2014, Neuchatel, Switzerland

Geometrical scale-factor stabilization of square cavity ring laser gyroscopes

Belfi J[1], Beverini N[1,2], Cuccato D[3], Di Virgilio A[1], Maccioni E[2], Ortolan A[4], Santagata R[1,5]

[1]INFN, section of Pisa, Pisa, Italy
[2]Dept. of Physics, University of Pisa, Pisa, Italy
[3]Dept. of Information Engineering, University of Padova, Via Gradenigo 6/B, Padova, Italy
[4]Laboratori Nazionali di Legnaro, INFN, Legnaro (PD), Italy
[5]Dept. of Physics, University of Siena Via Roma 56, Siena, Italy

E-mail: belfi@pi.infn.it

Recent progresses in the field of large ring laser gyroscopes fostered the GINGER (Gyroscopes IN GEneral Relativity) proposal, aiming at the detection of the relativistic frame-dragging or Lense-Thirring effect, in a ground based observatory [1]. The idea is to built up a tri-axial gyroscope providing a local measurement of the Earth's rotation vector and to compare it with the measurement referred to an inertial reference system, given by the IERS (International Earth Rotation and Reference Systems Service). The target accuracy is of one part in 10^{10} of the Earth rotation rate. This requires a same level of accuracy on the geometrical the scale factor $k_s=(4A)/(\lambda P)$, that relates the gyroscope output to the angular velocity of its frame, being A the area enclosed by the laser beams, P the optical path length and λ the laser wavelength.

We present a method for controlling the scale factor of a single square cavity ring laser based on the accurate measurement and stabilization of the absolute length of the two diagonal resonators formed by the opposite mirrors of the cavity [2]. The idea is to determine both the optical resonance frequency and the Free Spectral Range (FSR) of the cavity. The experimental approach is based on the use of a single frequency-stabilized diode laser a 633 nm, phase modulated with a combination of three independent modulation frequencies [3]. The first phase modulation provides the Pound-Drever-Hall signals for locking the two cavities to the same laser optical frequency. The second modulation creates a set of sidebands spaced by a harmonic of the cavity FSR. The third modulation is a small dithering of the second frequency for shifting the FSR resonance detection down to few tens kHz. The optical reference frequency in the experiment is provided by a He-Ne laser, with a relative frequency stability of 10^{-11}. The accurate determination of the FSR is measured by locking a voltage controlled oscillator to the center of the cavity dynamic resonance.

Here we discuss the potential and the performances of the method as well as its implementation on the "GP2" ring laser gyroscope. This is a square cavity ring laser 1.6 m in side dedicated to the optimization of the cavity geometry by means of active controls and is equipped with a 6 d.o.f. cavity deformation control system.

[1] F. Bosi et al., "Measuring Gravito-magnetic Effects by Multi Ring-Laser Gyroscope", Phys. Rev. D 84, 1220022, (2011)

[2] R. Santagata et al., "Optimization of the geometrical stability in square ring laser gyroscopes", ArXiv:1411.2585.

[3] J.Belfi et al., "Interferometric length metrology for the dimensional control of ultra-stable Ring Laser gyroscopes", Class. Quant. Grav. 31, 22500, (2014).

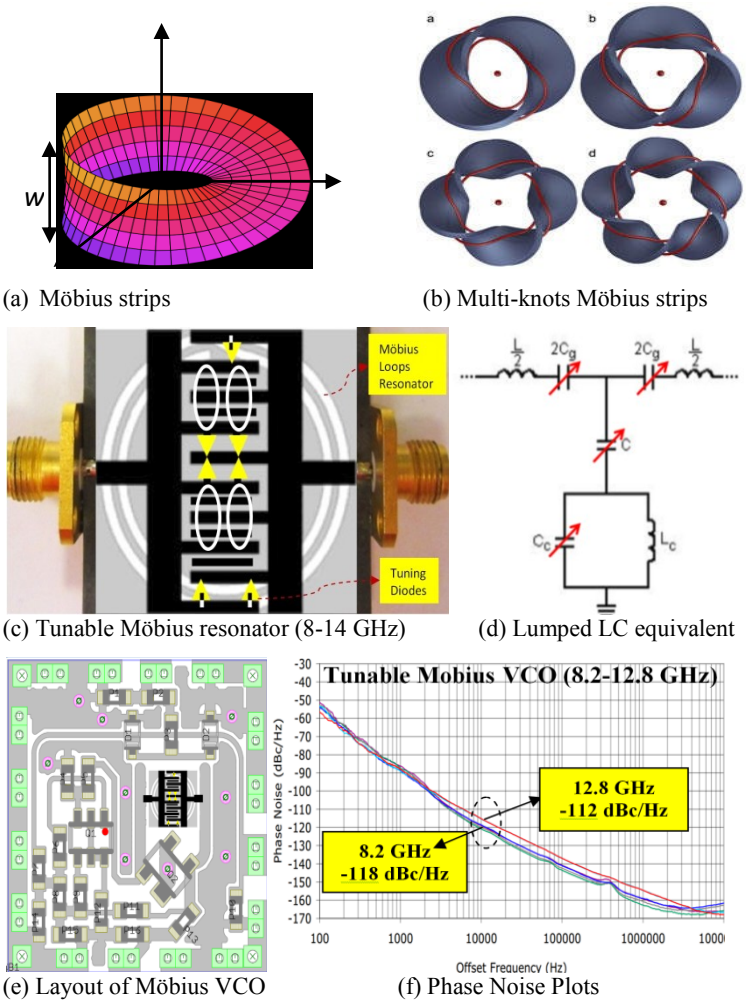
Möbius Metamaterial Symmetry: Resonators and Oscillators

Ajay K. Poddar, Ulrich L. Rohde*
Synergy Microwave Corp., NJ, USA
*Brandenburg Univ. of Tech., Cottbus, Germany
E-mail:akpoddar@synergymwave.com

Symmetry defined as a system feature or property, conserved when the system undergoes an alteration [1]. The electromagnetic symmetry discovered in metamaterial is equivalent to the structural symmetry of a Möbius strip, with the number of twists controlled by the sign change of the electromagnetic coupling between the meta-atoms. The negative index artificial material (metamaterial) with different coupling signs exhibit resonance frequencies that depend only on the number of turns but not the locations of the ''twists,'' thus confirming its Möbius Symmetry topological nature. Figure (1) shows Möbius strip, exhibits superior Q factor, enabling low phase noise signal sources. The Q-factor of Möbius resonator can be given by [2]

$$\overline{Q_a(\omega)}_{\omega\to\omega_0} = \left[\frac{\omega}{2(I_{max}-I_{min})}\int_{I_{min}}^{I_{max}} Q_a(\omega.i)\,di\right]_{\omega\to\omega_0} \quad (1)$$

where I_{min} and I_{max} are the minimum and maximum currents, and $Q_a(\omega,i)$ is the instantaneous quality factor at frequency ω and current i provides an effective mean to quantify the Q-factor of Möbius strips resonator when operated in a negative permeability (MNG: μ negative) or negative permittivity (ENG: ε negative) conditions. Möbius strips exhibit improved Q-factor (1280 @ 10.2 GHz) for a given size (0.3inch square), enables wideband tuning characteristics [2]. The Multi-Knots strips shown in Figure 1(b) conserve the quantity that gives invariance of solutions under a 2π rotation with a definite handedness, analyzed by solving the boundary condition using Green theorem. Figure (1e) shows the typical layout (0.5 inch square) fabricated using tunable Möbius strips resonator with a dielectric constant 2.2 and thickness of 8- mil. The circuits use SiGe HBT active device (BFP 740) and hyper-abrupt tuning diodes. The oscillator circuit offers promising phase noise performances (-118dBc/Hz @ 10 kHz offset for 8.2 GHz carrier frequency) with DC bias (3.5V, 18mA), measured O/P exceeds 1.5 dBm. To author knowledge, the reported phase noise performance is best to date for this class of VCO technology. In addition to this, Möbius metamaterial strips present several advantages: (i) high Q-factor, improved selectivity, (ii) easy integration in MMIC, (iii) small size (iv) concurrent multi-mode solution and (v) relatively insensitive to EMI and EMC.



(a) Möbius strips (b) Multi-knots Möbius strips
(c) Tunable Möbius resonator (8-14 GHz) (d) Lumped LC equivalent
(e) Layout of Möbius VCO (f) Phase Noise Plots

Fig. 1: Shows the typical Möbius strips resonator based VCO

[1] Chang et al, " Optical Mobius Symmetry in Metamaterials", Physical Review Letters, pp. 235501-1-235501-4, Dec 2010
[2] A. K. Poddar, "Slow Wave Resonator Based Tunable Multi-Band Multi-Mode Injection-Locked Oscillators" Dr.-Ing.-habil Thesis, BTU Cottbus, Germany, 2014

Frequency Source's PN Measurements:Challenges and Uncertainties

[1]*Ulrich L. Rohde,* [2]*Ajay K. Poddar*, [3]*Enrico Rubiola*

[1]*Brandenburg Univ. of Tech. (BTU), Cottbus, Germany*
[2]*Synergy Microwave Corporation, Paterson, New Jersey, USA*
[3]*CNRS/UFC FEMTO-ST Institute, Besancon, France*
E-mail:akpoddar@ieee.org

This paper describes the novel ultra low phase noise 2.4 GHz SAW Oscillator circuits and brief overview of phase-noise measurement techniques for the validation of noise floor below kT using cross-correlation methods. The prevailing cross-correlation method used in modern phase-noise measurement equipments can give erroneous results depending upon many factors (dynamic ranges of the measurement equipments, output cable length, and positive/negative phase inversion). This discussion is imperative for frequency sources, validated with 2.4 GHz SAW oscillator circuit as shown in Figure (1) on various test equipments to show both discrepancies and uncertainty associated with the equipments and measurement techniques.

Cross-spectral analysis is a mathematical tool for extracting the power spectral density of a correlated signal from two time series in the presence of uncorrelated interfering signals. A major crux of the system described is the inherent impossibility to divide the DUT (device under test) noise from any other correlated effect. It is self-evident that vibrations or EMI (electromagnetic interference) hitting simultaneously on the two channels as depicted in Figure (2) cannot be rejected. However disturbing, experience is often useful to identify these perturbations as artifacts. The cross-spectrum of two signals *x (t)* and *y (t)* is defined as the Fourier transform of the cross-covariance function of *x* and *y*. The O/P of each channel of Figure (2) is

$$x(t) = a(t) + c(t) \quad \leftrightarrow \quad X(f) = A(f) + C(f) \qquad (1)$$
$$y(t) = b(t) + c(t) \quad \leftrightarrow \quad Y(f) = B(f) + C(f) \qquad (2)$$

where α(t), b(t) and c(t) are random signals; α(t) and b(t) are the noise of the transducers, and c(t) is the DUT noise; all signals are sampled at a suitable rate, and each acquisition takes the measurement time T. Introducing a disturbing signal d(t) impacting on the two channels, from (1)-(2) rewrite as

$$x = a + c + \varsigma_x d \leftrightarrow X = A + C + \varsigma_x D \qquad (3)$$
$$y = b + c + \varsigma_y d \leftrightarrow Y = B + C + \varsigma_y D \qquad (4)$$

where ς_x and ς_y are the coefficients which describe the impact of d on the phase-to-voltage converters. Notice that ς_x and ς_y, and also the product $\varsigma = \varsigma_x \varsigma_y$, can be positive or negative.

The phase noise plots shown in Figure (3) is best performance (-150 dBc/Hz @ 10 kHz offset) reported to date for this class technology. As shown in Figure (3), the measurement shows an optimistic value of -202dBc/Hz at 1.2 MHz off the carrier and 15 dB inferior at 6 MHz offset depending upon +ve/-ve phase inversion respectively. As a part of the research work, the validation carried out on different oscillators (OCXO, VCSO, CRO, DRO), will be shown in full length paper; "simultaneous presence of correlated /anti-correlated signals leads to gross underestimation of the total signal in cross-spectral analysis, these effects are time varying, therefore measurements poses challenges and uncertiantity.

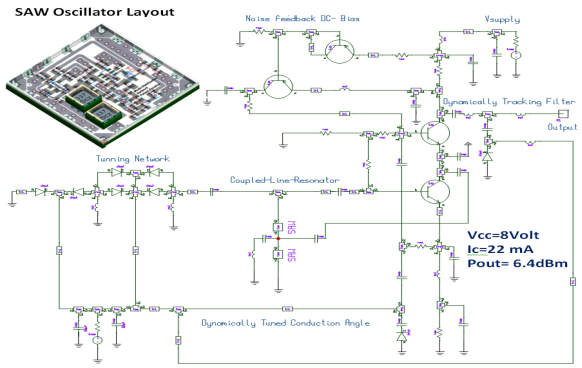


Fig. 1: Shows the typical schematic of 2.4 GHz SAW VCO

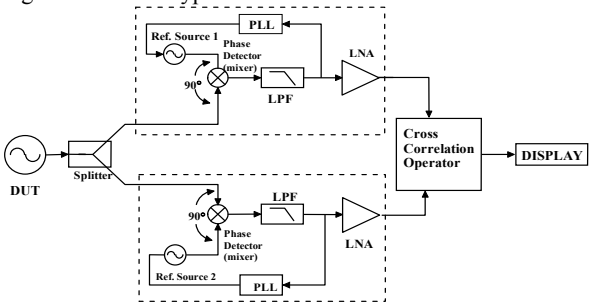


Fig. 2: Diagram of 2-channel cross-correlation technique

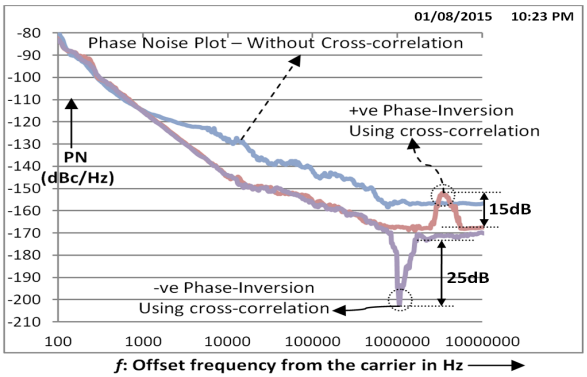


Fig. 3: Measured PN plots of 2.4GHz SAW oscillator circuit

Model for Acoustic Locking of Spin Torque Oscillators

Tanay A. Gosavi, Sunil A. Bhave
OxideMEMS Laboratory, Cornell University, Ithaca, NY, USA
Analog Devices Inc., Woburn, MA, USA
E-mail: tag75@cornell.edu

We present our model for locking Spin Torque Oscillator (STO) to AC strain generated using a mechanical transducer like High-Overtone Bulk Acoustic Resonator (HBAR). STOs are nanoscale octave tunable GHz frequency self-oscillating magnetic tunnel junctions (MTJ). In STOs, spin transfer torque generated from tunneling spin-polarized electrons overcomes damping. This causes oscillations of magnetization in the free layer. Using the Tunnel Magneto-Resistance effect these oscillations are read out as oscillations in output current. Low signal amplitude and poor phase noise are the challenges STOs face for practical applications. Locking multiple STOs to a common external reference oscillator improves noise performance and increases output signal. AC current based locking is limited in locking multiple devices due to problems in impedance matching and phase delays between STOs. To overcome challenges in scaling AC current-locked STO systems we propose acoustic locking which uses strain generated by HBAR and inverse magnetostriction effect for generating AC magnetic field in the free layer of MTJ [2]. This AC magnetic field which is in phase with transducer drive is the locking signal for STO.

AC dynamics of the STO are modeled using Landau-Lifshitz-Gilbert-Slonczewski (LLGS) equation (Eqn. 1), where precession, damping and the spin torque terms are shown on the right side. $\hat{m} = M/M_s$ is a unit vector representing magnetization of the free layer [1]. Eqn. 2 shows the components of H_{eff}, an effective field representing the total energy of the free layer. H_{app} is the applied field, while H_{an} and H_d are anisotropy and demagnetization fields due to material properties and shape of the free layer. $H_{st} = 2B_{eff}S/M_s$ is the locking AC magnetic field in direction $\hat{t}$ due to the AC strain S, also along $\hat{t}$, acting on the free layer [2]. B_{eff} is the magneto-elastic coupling coefficient. Thermal noise is accounted for using Gaussian-distributed Langevin term H_T whose amplitude is proportional to $\sqrt{\alpha}$ (Gilbert damping). We solve the LLGS for the parameters shown in Fig. 1(a).

$$\frac{d\hat{m}}{dt} = -\gamma\hat{m} \times [H_{eff}] + \alpha\,\hat{m} \times \frac{d\hat{m}}{dt} + \frac{\gamma\hbar J\eta}{2edM_s}\hat{m} \times [\hat{m} \times \hat{ep}] \quad (1)$$

$$\overrightarrow{H_{eff}} = \overrightarrow{H_{app}} + H_{an}\hat{n}[\hat{n}.\hat{m}] + H_d\hat{d}[\hat{d}.\hat{m}] + \overrightarrow{H_T} + H_{st}\hat{t}[\hat{t}.\hat{m}] \quad (2)$$

Fig. 1(b) shows the FFT of the output current of STO with (red) and without (blue) the locking AC strain signal, amplitude 33ppm, at STO oscillation frequency. From the figure it's clear that noise around the STO output signal is suppressed due to locking. Repeating experiments with frequency offsets in STO output and locking signal we trace a locking range linear over 130 MHz in Fig. 1(c). Acoustic locking demonstrated here is a platform for developing hybrid magnetic-acoustic oscillator systems. Using HBAR based acoustic locking in a feedback system with STO we can maintain lock over the entire tuning range of STO.

Free layer Size	170 nm x 100 nm x 1.5 nm
M_s	1100 erg/cm^3
H_{an}	219 Oe
$H_d = 4\pi M_{eff}$	13000 Oe
α	0.01
B_{eff}	$-7 * 10^7$ emu/cm^3
η	30%
H_{app}	300 Oe
Current	2.8 mA

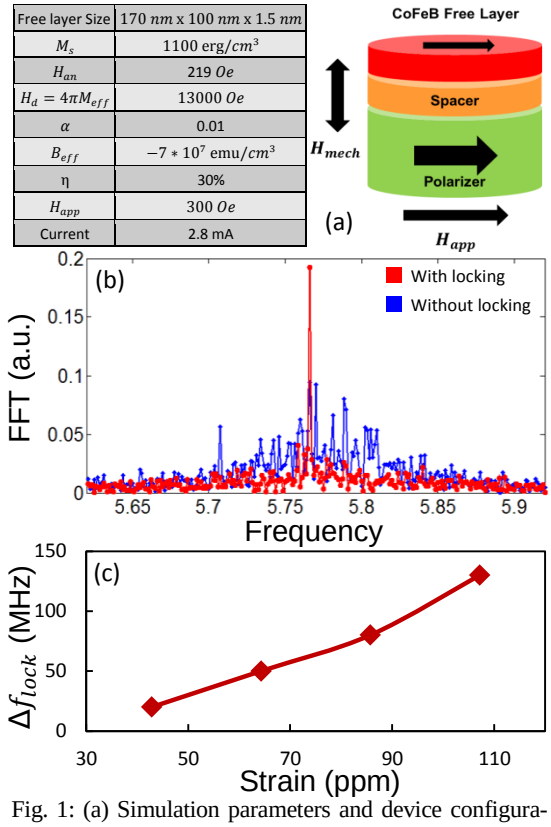


Fig. 1: (a) Simulation parameters and device configuration with field directions. (b) FFT of STO output with locking (red) strain signal at 5.77GHz and in absence of locking signal (blue). (c) Locking range of +/- 130MHz over 100ppm amplitude of strain for the given STO

[1] D. C. Ralph and M. D. Stiles, "Spin transfer torques," J. Magn. Magn. Mater., vol. 320, pp. 1190–1216, 2008.
[2] R. C. O'Handley, *Modern Magnetic Materials Principle and Applications*. Wiley Inter-Science Publication, 2000.

Piezoelectrically-Actuated Opto-Acoustic Oscillator

Ghosh, Siddhartha, Segovia-Fernandez, Jeronimo, Piazza, Gianluca
Department of Electrical and Computer Engineering, Carnegie Mellon University, Pittsburgh, PA, USA
E-mail: sidghosh@cmu.edu

This paper describes the first demonstration of a piezoelectrically-actuated Opto-Acoustic Oscillator (OAO). Previous demonstrations of photonic radio-frequency (RF) oscillators have included optoelectronic oscillators relying on long optical fiber delay lines [1] and MEMS-based OAOs using capacitively actuated air gaps in silicon [2]. The present device consists of a monolithic aluminum nitride acousto-optic modulator, in which the use of the piezoelectrically-driven resonator provides a better interface to RF signals.

The modulator (SEM in Fig. 1a) consists of two coupled rings, in which piezoelectric actuation in the first generates mechanical motion laterally transferred to the second. This second ring is simultaneously a whispering gallery mode photonic resonator, which is biased at a fixed wavelength to enable maximal modulation of the output signal (Fig. 1b). The optical output is converted back into the electrical domain through the use of an avalanche photodiode (APD). The oscillator loop may then be closed by feeding back the output from the APD to the electrical input. Other components used in the loop include a high pass filter, two cascaded amplifiers, a phase shifter, and a power splitter - which are employed to satisfy the Barkhausen condition for oscillation and lock to the desired mode at 652 MHz.

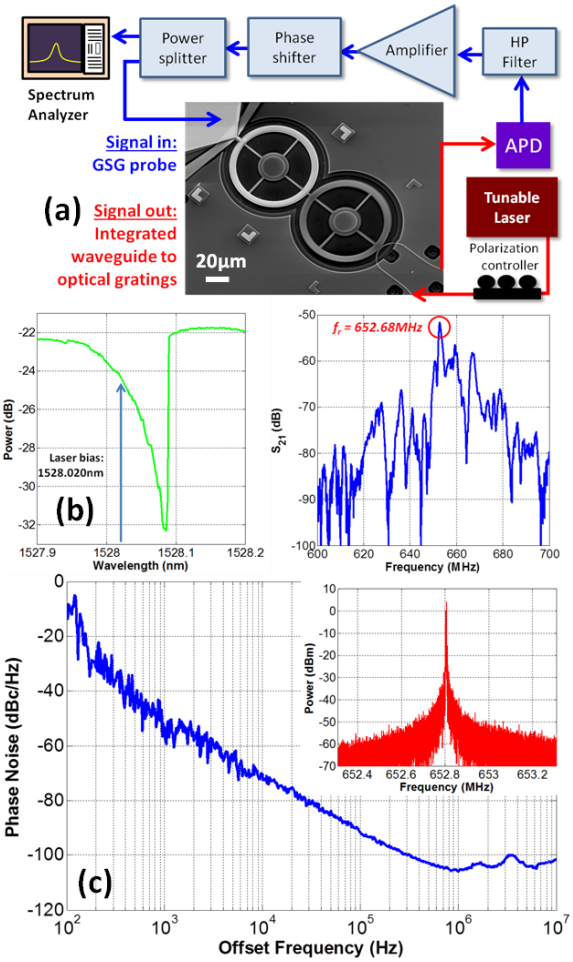


Fig. 1: (a) Setup schematic for the OAO with optical connections in red and RF in blue, (b) Optical resonance and Optomechanical transmission of modulator, (c) RF output of oscillator (inset) and corresponding phase noise.

An optical resonance with a high quality factor (~25,000) is selected, and the laser wavelength is biased at a point corresponding to the maximum optomechanical output. This response is measured by exciting the modulator piezoelectrically, and the transmission plot is shown in Fig. 1b. The mechanical resonance of the composite structure appears as a peak in the S_{21} plot corresponding to a frequency of 652.68MHz. A high-pass filter is used in the loop to filter out the mechanical resonances at lower frequencies, which are also possible to lock into. The two amplifiers are biased to produce approximately 62dB of gain to offset the losses in the modulator transmission and the rest of the closed loop. Once the loop is closed with the optimal phase condition, the oscillation is monitored on a spectrum analyzer. The carrier frequency for the oscillation is 652.80MHz. Phase noise (PN) for this oscillator was also measured with a signal source analyzer (Fig. 1c), and the phase noise is -72 dBc/Hz at 10 kHz offset from the carrier frequency. Based on the device's mechanical quality factor of ~450, the Leeson's frequency of 725 kHz is observed in the phase noise plot. The current phase noise performance is limited by the APD shot noise.

[1] X.S. Yao, and L. Maleki, "Optoelectronic Oscillator for Photonic Systems," IEEE J. of Quant. Elect., vol. 32, no. 7, pp. 1141-1149, Jul. 1996.

[2] S. Sridaran, and S.A. Bhave, "Opto-Acoustic Oscillator Using Silicon MEMS Optical Modulator," *Proceedings*, 16th Int. Conf. on Solid-State Sensors, Actuators and Microsyst., Beijing, June 5-9, 2011, pp. 2920-2923.

UHF SiGe Push-Pull VCO MEMS Oscillators

Y.Yoon, H.P. Moyer, D. J. Kirby, R.L. Kubena, R.J. Joyce, R.L. Bowen,
and D.T. Chang
HRL Laboratories, LLC, Malibu, CA, 90265 USA

Email: yyoon@hrl.com

Quartz reference oscillators commonly require temperature control enabled by a voltage controlled oscillator (VCO) which provides frequency tuning over temperature. Recent SiGe IC UHF quartz MEMS oscillators have utilized a push-pull topology to eliminate the need for large inductors that greatly increase chip size[1]. This work focuses on adapting the push-pull topology into a VCO for use in practical systems.

AT-cut quartz resonators operating in the fundamental thickness-shear mode formed the basis for the VCO's. Experiments utilized three resonators of two different designs, operating at 813, 920 and 1048MHz. The 920MHz resonator has 120x120μm aluminum electrodes and stress relieving spring tethers (S120 SPR) to de-couple bonding stresses from the active region. The remaining two resonators have 255 x 85μm aluminum electrodes (M V3 600). The 1048MHz resonator has an unloaded Q of 6,920 and a motional resistance of 31.7 ohms, as measured in a vacuum. This yields an fxQ product of 7.25×10^{12}, close to the expected limit for quartz devices of 1×10^{13}. Similarly, the fxQ products are 6.61×10^{12} and 6.64×10^{12} for the 814 and the 920MHz devices respectively.

As in previous work[1], the VCO is designed in the IBM 7WL BiCMOS process and uses devices biased with a cutoff frequency (f_T) of 30GHz. The push-pull topology consists of each device placed in a Pierce configuration with a common emitter buffer amplifier with a high input impedance. Tuning is achieved by replacing the phase shift capacitors on the active devices (n-p-n and p-n-p transistors) with 1.8V NMOS varactors that have a capacitive range of ~1 to 3pF and applying a bias from -1 to 1V. Fig. 1. shows measured results for the three resonators with phase noises ranging from -87dBc/Hz for the 1048MHz resonator to -100dBc/Hz for the 813MHz resonator at a 1KHz offset. Recent work using AlN contour-mode resonators at 1.16GHz demonstrates a phase noise of -82dBc/Hz at the same offset[2]. Overall tuning range varies with the number of tuning elements. The 1048MHz resonator was paired with an IC with four tuning elements and achieved an overall tuning range of ~62ppm which is equivalent to a total tuning range of ~65KHz. Setting the control voltages of three of the cells to 0V and tuning a single diode yields a tuning range of ~15-20ppm.

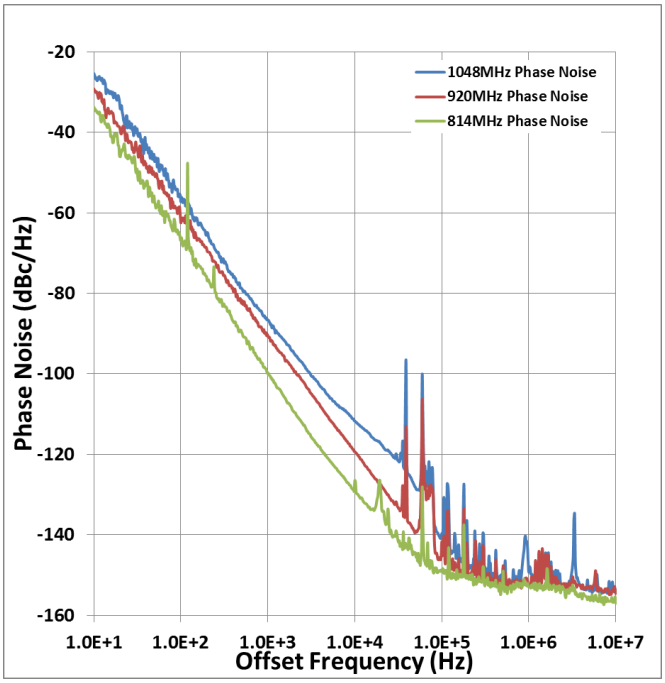


Fig.1. Plot of phase noise vs. frequency at a 1KHz offset for three different resonators.

[1] H.P. Moyer et al., "Nonlinear Behavior of an UHF Quartz Resonator in an Oscillating System," in Proc. 2012 IEEE International Frequency Control Symposium, Baltimore, MD, May 21-24, 2012, pp. 1-5.
[2] J. Koo et al., "A -173 dBc/Hz @ 1 MHz Offset Colpitts Oscillator Using AlN Contour-Mode MEMS Resonator," in Proc. 2013 IEEE Custom Integrated Circuits Conference, San Jose, CA, September 22-25, 2013, pp. 1-4.

This work was sponsored by DARPA'S MTO office under the DEFYS program, issued by DARPA /CMO under contract No. HR0011-10-C-0109. The views and conclusions contained in this document are those of the authors and should not be interpreted as representing the official policies, either expressly or implied, of DARPA or the U.S. Government.

An ultra low noise frequency synthesis chain for a high performance Cs compact vapor cell atomic clock

B. FRANÇOIS[a], C. E. CALOSSO[b], and R. BOUDOT[a]

[a]FEMTO-ST, Université de Franche-Comté, UMR CNRS 6174, 26 chemin de l'Épitaphe, 25030 Besançon, FRANCE
[b]INRIM, Strada delle Cacce 91 10135 Torino, ITALY

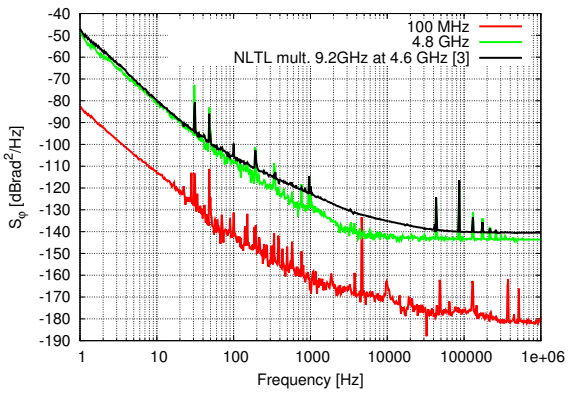
Email: bruno.francois@femto-st.fr

In order to prevent short term frequency stability degradation by the so-called Dick effect [1], compact vapor cell atomic clocks, based on coherent population trapping (CPT) or double resonance techniques, need microwave local oscillators exhibiting high spectral purity for Fourier frequencies typically in the 100−1 kHz range.

This paper aims to present a novel simple-architecture 4.596 GHz frequency synthesizer dedicated to the interrogation of a high performance Cs atomic clock based on CPT with an expected short term frequency stability of a few 10^{-13}. In order to reach such performances at 4.6 GHz, the LO phase noise has to be lower than -111 dBrad^2/Hz at f = $\frac{2}{T_c}$ = 330 Hz where T_c (6 ms) is the cycle time of the clock. In the present CPT clock, optical sideband generation is performed through modulation at 4.5963 GHz of a Mach-Zender electro-optic modulator [2].

We reported recently a microwave frequency synthesizer based on a non-linear transmission line (NLTL) [3]. In the latter, the absolute phase noise of the output signal was clearly limited by the residual noise of the NLTL component in the f = 100−1000 Hz range. Moreover, this key component is expensive and requires high input power. The new frequency synthesis chain is mainly based on a XM16 Pascall multiplication module (XM16-E-1600-E-12). This module integrates a state-of-the-art 100 MHz OCXO quartz oscillator (Pascall OCXOF-E) with an absolute phase noise of -140 dBrad^2/Hz at f = 100 Hz respectively, late frequency multiplied by 16 to 1.6 GHz without any phase noise degradation. The 1.6 GHz output signal is multiplied by 3 to 4.8 GHz and mixed with a with a 200 MHz from the synthesis chain and a 3.7 MHz from a direct digital synthesizer (DDS). The output is band-pass filtered to select the 4.5963 GHz signal.

The figure on the right shows preliminary absolute phase noise results of the synthesis. These measurements were performed with the signal source analyzer (Agilent E5052B) used in [3]. The 4.8 GHz output signal absolute phase noise is measured to be -108 dBrad^2/Hz at 100 Hz, -120 dBrad^2/Hz at f $\simeq$ 330 Hz and -143 dBrad^2/Hz at 1 MHz respectively. At f = 330 Hz, an improvement of about 3−4 dB is noticed in comparison with [3]. Nevertheless, a wide uncertainty mainly due the cross-spectral function in phasemeters [4] is present in our measurements. The work is still in progress also for reducing this source of uncertainty. Latest results will be shown at the conference.



[1]G.J. Dick. Local oscillator induced instabilities in trapped ion frequency standards. Proc. Precise Time and Time Interval, 1987, Redondo Beach, CA, pp. 133-147.

[2]X. Liu et al. Ramsey spectroscopy of high-contrast CPT resonances with push-pull optical pumping in Cs vapor, Optics Express, vol. 21, 2013, num. 10, pp. 12451-12459

[3]B. François et al. A low phase noise microwave frequency synthesis for a high-performance cesium vapor cell atomic clock. Review of Scientific Instruments, vol. 85, 2014, num. 9, pp. 094709

[4]C. W. Nelson, A collapse of the cross-spectral function in phase noise metrology, Review of Scientific Instruments, vo.l 85, pp. 024705-1 - 024705-7

Development of Transportable Atom Interferometer Gravity Gradiometer

Chiow, Sheng-wey; Williams, Jason; Botter, Thierry; Kellogg, James; Kohel, James;
Aveline, David; Thompson, Robert; Yu, Nan
Jet Propulsion Laboratory, California Institute of Technology, Pasadena, CA
E-mail: chiow@jpl.nasa.gov

Laser-cooled atomic gases in free fall provide ideal test masses for inertial and gravity measurements. Interferometric inertial sensors based on cold atoms in atom interferometers have demonstrated impressive performance in sensitivity and accuracy in laboratories. Adapting this promising technology for space-borne gravity measurements will provide the next generation instrument for global gravity mapping with higher resolution and better long-term stability. Furthermore, atom interferometers under microgravity provide advantages in fundamental science study over terrestrial experiments and will enhance our understanding of nature.

We will describe progress at JPL on the development of space-oriented atom interferometry for gravity mapping. Central to our work is the transportable atom interferometer instrument in operation at JPL, which is designed for operation in microgravity. Our recent advancements bringing the atom interferometer instrument to be competitive with the state of the art in gravity gradiometry will be reported, including discussions of technical challenges and mitigations.

Our instrument is composed of two Cs fountains in a single vacuum chamber, as depicted in Fig. 1. The two source regions are vertically separated by 1m, which defines the measurement baseline of the gradiometer. After launching the laser-cooled atoms with moving optical molasses, common high-power laser pulses from a tapered amplifier drive two-photon stimulated Raman transitions on both clouds for Zeeman state selection and velocity selection, and also serve as beam splitters in the Mach-Zehnder configuration. The phase difference of the interferometer outputs is extracted to infer the gravity gradient.

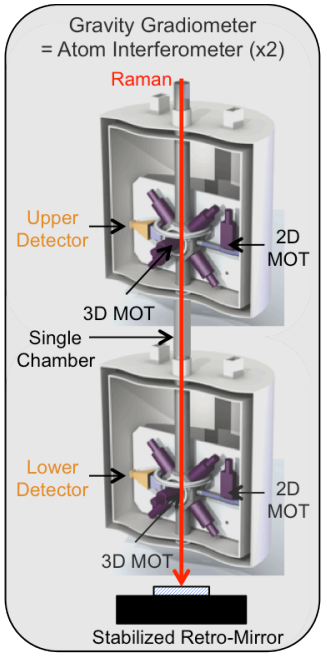


Figure 1. Gravity Gradiometer

The instrument was designed with a compact sensor head and compact laser/control modules. Processes of atom cooling, state preparation, and detection are all accomplished in the same sensor head regions such that the same atom interferometers can be operated in microgravity without launching atoms. Tests of operation under microgravity environment were conducted and found no degradation in atom sample preparation or in detection. With closed-loop operation, the instrument has a gravity gradient sensitivity of 40 E/Hz^{½}, where E is Eötvös=10^{-9}/s^2. This sensitivity was also verified with the proximity modulation of lead bricks of ~30 kg. Furthermore, similar atom interferometers are under development for deep space planetary applications and for fundamental physics measurements on the International Space Station.

This research was carried out at the Jet Propulsion Laboratory, California Institute of Technology, under a contract with the National Aeronautics and Space Administration.

A Novel Length Extensional Vibratory Gyroscope

Gobong Choi, and Yook-Kong Yong
Department of Civil and Environmental Engineering, Rutgers University, Piscataway, New Jersey, U.S.A.
E-mail: gobong.choi@rutgers.edu

We study and introduce a novel length extension vibratory gyroscope to detect the angular velocity rotation about z-axis. The proposed gyroscope is a new type of a gyroscope which utilizes a length extension mode as a driving mode and a flexure mode as a sensing mode to detect the Coriolis force generated by the rotation of the system. The gyroscope was designed and gyro-characteristics were simulated using COMSOL, finite element method (FEM) software. Quartz, langasite and langatate crystals are used for gyroscopes and compared. The driving frequencies and sensing frequencies of each gyroscope are obtained by optimizing the geometries of the each gyroscope using eigenfrequency analyses. Frequency response analyses were performed to simulate the gyro-characteristics of the gyroscopes which subjected to the angular velocity about z-axis. The results show that the length extension gyroscope can be used as a gyro-sensor. Moreover, we find that langasite and langatate crystals are suitable materials for higher precision piezoelectric gyro-sensors than quartz crystal.

Figure 1a shows the principle of operation of a length-extension gyroscope. The driving mode is a fundamental extension mode of driving arm in the x-y plane. Extensional vibrations of the driving arm along y-axis create vibration velocity, V_y as shown in figure 1b.The z-axis detection mode is an anti-symmetric flexure mode in x-y plane. When the gyroscope is subjected to a rotation about z-axis, a pair of Coriolis forces, F_c, acting on the driving arms is generated proportional to the angular rate of gyroscope, Ω_z, mass density, m, and vibration velocity, V_y. A pair of equal and opposite Coriolis force on each driving arms, which are generated by the rotation about z-axis, create the moment, M_c, that in turn induce the flexure mode of the sensing arms. The driving frequency and sensing frequency have to be tuned close to each other in order to achieve higher gyroscopic sensitivity.

We found gyro-sensitivity rotations about z-axis of quartz, langasite and langatate gyroscopes were respectively 2.78e-4 *V/(deg/s)*, -1.60e-2 *V/(deg/s)* and -1.6e-2 *V/(deg/s)*. The calculated optimum singly rotated cut angle for quartz, langasite and langatate were respectively θ =-9°, θ =24° and θ =24°.

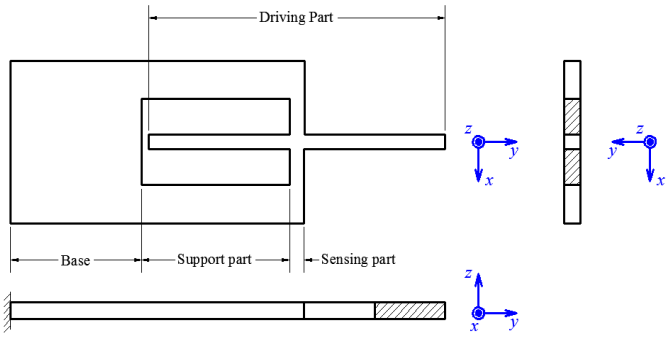


Fig. 1a: Structure of the main parts of a length extension gyroscope.

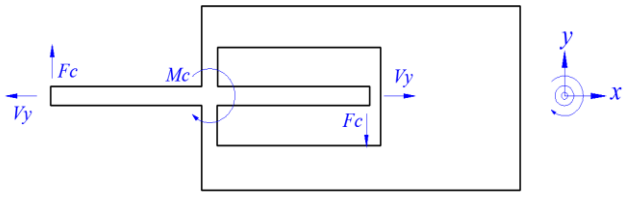


Fig. 1: Example figure. To ensure visibility try to use text font sizes in your figure on the same order as this figure caption font, "Times-New Roman 10pt".

Development of an Optically Pumped Atomic Magnetometer Array for Magnetoencephalography

Schwindt, Peter D. D., Anthony P. Colombo, Tony R. Carter, Yuan-Yu Jau, Christopher W. Berry, Jim McKay*, Michael P. Weisend†

Sandia National Laboratories, Albuquerque, NM/USA

*Candoo Systems, Coquitlam, British Colombia/Canada

†The Wright State Research Institute, Dayton, Ohio/USA

E-mail: pschwin@sandia.gov

Magnetoencephalography (MEG) is the measurement of the magnetic fields produced by the human brain. The primary magnetic sensor used for MEG is the super conducting quantum interference device (SQUID). Low-T_c SQUIDs must be operated within a liquid helium Dewar, and this cryogenic infrastructure adds significant size, expense, and complexity to SQUID-based MEG systems. In recent years, optically pumped atomic magnetometers (AMs) have demonstrated sub-femtotesla sensitivities [1] and have emerged as potential replacements for SQUIDs in MEG applications [2-3]. We will present measurements of MEG signals using our 4-channel AM [2] and discuss recent results in developing a complete MEG system, including a human-sized magnetic shield and a 36-channel array of magnetometers to provide partial head coverage for localizing sources within the brain.

In developing the 36-channel array, one of the primary tasks has been to improve the AM for the MEG application. The prototype used in Ref. [2] had a 5 fT/Hz$^{1/2}$ sensitivity but had several limitations. In the AM currently under development, we are maintaining the sensitivity while making multiple enhancements, including increasing the bandwidth from 20 Hz to >85 Hz, reducing the distance between the AM sensing volume and the sensor wall (and any external magnetic sources) from 25 mm to <10 mm, and reducing the active sensor volume (important for knowing precisely where the magnetic field is being measured) by a factor of >10 to ~15 mm^3. We are also increasing the channel separation from 5 mm to 18 mm to increase the baseline for gradiometer measurements.

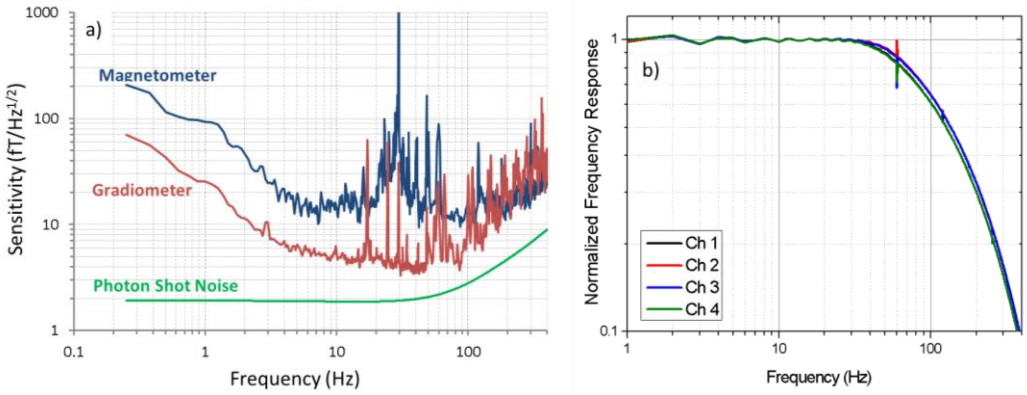


Figure 1. (a) Power spectral density of the magnetic noise of a single magnetometer channel and a gradiometer formed by subtracting two channels. (b) Frequency response of all four channels showing their near equivalence.

[1] I. K. Kominis, T. W. Kornack, J. C. Allred, and M. V. Romalis, "A subfemtotesla multichannel atomic magnetometer", Nature, vol. 422, pp. 596-599, 2003.

[2] C. Johnson, P.D.D. Schwindt, M.P. Weisend, "Magnetoencephalography with a two-color pump-probe, fiber-coupled atomic magnetometer", Applied Physics Letters, vol. 97, pp. 243703, 2010.

[3] T.H. Sander, *et al*, "Magnetoencephalography with a chip-scale atomic magnetometer", Biomedical Optics Express, vol. 3, pp. 981-990, 2012; and H. Xia, A. Ben-Amar Baranga, D. Hoffman, and M. V. Romalis, "Magnetoencephalography with an atomic magnetometer", Applied Physics Letters, vol. 89, pp. 211104, 2006.

Remote Atomic Vapor Magnetometer with Sub-pT Resolution Operating at Ambient Temperature

Lou, Janet W., Fatemi, Fredrik K.*, Cranch, Geoffrey A.*
C4ISR Division, Sotera Defense Solutions, Inc., Columbia, MD, USA
*Optical Sciences Division, U.S. Naval Research Laboratory, Washington, DC, USA
E-mail: janet.lou@soteradefense.com

Atomic vapor magnetometers are of interest for a range of applications from medicine to geological and military surveying. We have designed and characterized a magnetometry system specifically aimed at meeting the challenges of remote interrogation. Two key aspects of the remote system (>1.5 km) are the delivery and collection of the optical signals and the elimination of electrical power at the remote location. We demonstrate a practical system using standard, single-mode telecom optical fibers. In addition to the degradation due to optical losses (~2-3 dB/km), the greater challenge is in the fact that the optical polarization is not maintained in these fibers. We will show how polarization and modal walk-off can be used to mitigate the additional noise contribution. Additionally, the system must operate without temperature control.

Our system is based on a 15 mm^3 Cs vapor cell, which is optically pumped at the D1 transition ($S_{1/2}$ (F=3) $\rightarrow P_{1/2}$ (F=4)), and the laser amplitude is modulated at a fixed frequency. A probe laser is locked to the D2 transition ($S_{1/2}$ (F=4) $\rightarrow$ $P_{3/2}$ (F=4)). Both lasers are frequency locked using the DAVLL technique. The dependence of relaxation time on ambient temperature is characterized for a range of cells with varying Ne buffer gas pressures as well as paraffin coatings [1-2]. We characterize the vapor cells inside three layers of magnetic shielding, which reduces the ambient magnetic field to ~400 nT. A solenoid coil inside the chamber generates a controlled magnetic field parallel to the direction of beam propagation.

We demonstrate that it is possible to obtain as low as 0.1 $pT/Hz^{1/2}$ resolution at 1 Hz over the ambient temperature range of 0 to 35 C. For operation as a magnetometer, we choose a Cs cell filled with Ne at 200 Torr. Following the NMOR technique [3], as shown in Fig. 1, the output of the cell is sent through a Wollaston prism and the two orthogonal polarizations are detected. The difference between the detectors is demodulated with a lock-in amplifier and the dispersive component of the signal is used as the input to a feedback loop, which is used to drive the solenoid coil. Thus, variations in the residual magnetic field inside the shielding are partially compensated.

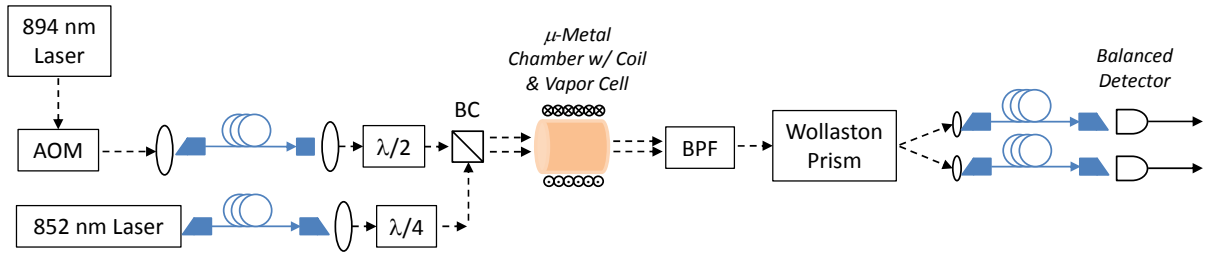


Fig. 1: Experimental setup. AOM=acousto-optic modulator. BC=beam combiner. BPF=bandpass filter.

[1] F. A. Franz and E. Luscher, "Spin Relaxation of Optically Pumped Cesium," Phys. Rev., vol. 135, no. 3A, pp. A582-A588, Aug. 1964.

[2] M. T. Graf, D. F. Kimball, S. M. Rochester, K. Kermer, C. Wong, D. Budker, E. B. Alexandrov, M. V. Balabas, and V. V. Yashchuk, "Relaxation of atomic polarization in paraffin-coated cesium vapor cells," Phys. Rev. A, vol. 72, no. 2, p.023401, Aug. 2005.

[3] W. Gawlik, L. Krzemien, S. Pustelny, D. Sangla, J. Zachorowski, M. Graf, A. O, Sushkov, and D. Budker, "Nonlinear magneto-optical rotation with amplitude modulated light," Appl. Phys. Lett., vol. 88, no. 13, p.131108, Mar. 2006.

Testing the isotropy of space by comparing two co-rotating precision quartz frequency standards

Anthony Lo, Philipp Haslinger, Eli Mizrachi, Lo¨ıc Anderegg, and Holger Mu¨ller
Department of Physics, University of California, Berkeley, CA 94720, USA

Michael Hohensee
Lawrence Livermore National Laboratory, Livermore, CA 94550, USA

Maxim Goryachev and Michael E Tobar
ARC Centre of Excellence for Engineered Quantum Systems, School of Physics, University of Western Australia, 35 Stirling Highway, Crawley WA 6009, Australia
E-mail: michael.tobar@uwa.edu.au

Experimental tests of Lorentz symmetry go back at least to A. A. Michelson's 1881 search for anisotropy in the propagation speed of light. The possibility that physics beyond the standard model might violate Lorentz invariance has motivated the development of experimental tests of Lorentz symmetry with higher and higher precision and tests with vastly broadened scope. In particular, experiments have now ruled out anisotropies in the laws of motion of the electron, proton and neutron based on, e.g., clock comparisons, electromagnetic cavities, magnetometry, ultracold neutrons and ion traps.

Some effects giving rise to anisotropic inertial masses are known to be below 10^{-28} GeV, but others are much more weakly constrained. The experiments often involve data taking over a year so that they can use Earth's orbit to modulate the velocity of the apparatus, and typically employ fragile and maintenance-intensive atomic, optical and/or cryogenic setups. The quest to close the remaining loopholes in the verification of Lorentz symmetry would benefit greatly from a simpler, yet accurate method. In this paper, we introduce crystal oscillators as a new, reliable and sensitive method and improve existing laboratory limits on the most weakly constrained mode of neutron-sector violations by almost six orders of magnitude to $(-3.8 \pm 2.4) \times 10^{-14}$ GeV from 10^{-8} GeV, a substantial improvement even compared to astrophysical bounds 2×10^{-13} [1]. This result closes all possibilities for Lorentz-violating anisotropies in the inertial mass of neutrons, protons and electron out at the $\sim 10^{-14}$ level or above. Future experiments with cryogenic oscillators could be used to perform more sensitive tests of Lorentz symmetry in the proton, neutron, electron, and photon sectors.

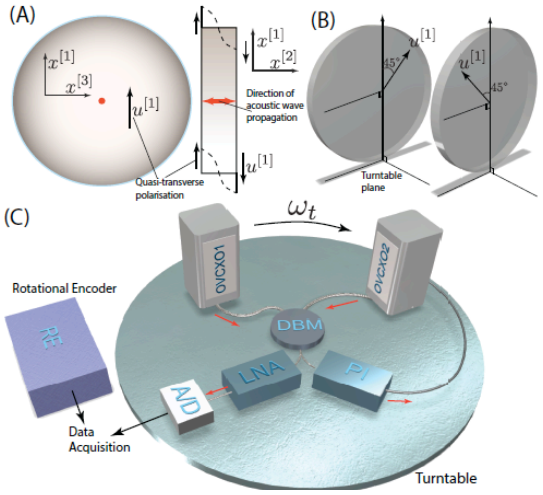


Fig. 1: Setup of the room temperature experiment. (A) Crystal blank showing coordinates x[1−3], the direction of propagation and the direction of the displacement of the shear mode. (B) Orientation of a shear relative to the turntable plane. (C) Frequency comparison on the turntable: The phase be- tween two 10-MHz ovenized, voltage-controlled crystal oscillators (OVCXO) is detected by homodyne detection using a double-balanced mixer (DBM). Phase-lock with a PI feedback controller keeps the DBM operating near zero output voltage. The feedback is very slow, leaving the oscillators essentially free-running on the timescale of the turntable rotation rate and its harmonics. The DBM output is amplified by a low noise amplifier (LNA) and acquired after Analog-to-Digital (A/D) conversion. All components are enclosed in a cylindrical dual-layer μ-metal magentic shield (not shown).

[1] A Lo, P Haslinger, E Mizrachi, L Anderegg, H Müller, M Hohensee, M Goryachev, ME Tobar, "Testing the isotropy of space using rotating quartz oscillators," arXiv:1412.2142 [gr-qc]

Optical Clock Based on the $^{171}Yb^{+}$ Octupole Transition with 3×10^{-18} Systematic Uncertainty

N. Huntemann, C. Sanner, B. Lipphardt, Chr. Tamm, Gerginov, S. Weyers, E. Peik
Physikalisch-Technische Bundesanstalt, Bundesallee 100, 38116 Braunschweig, Germany
E-mail: nils.huntemann@ptb.de

We aim at the realization of a very accurate optical clock that uses the electric octupole transition $^2S_{1/2}(F=0)\rightarrow{}^2F_{7/2}(F=3)$ of a single laser-cooled $^{171}Yb^{+}$ ion at 467 nm as a reference. This transition has a natural linewidth in the nHz range, and a low sensitivity to frequency shifts induced by electric and magnetic fields [1]. Both characteristics are advantageous for the realization of an optical clock, but because of the extremely small oscillator strength of the transition its excitation requires high spectral power density. The required intensity in turn introduces a significant light shift of the transition frequency.

To avoid the light shift, we have implemented the Hyper-Ramsey excitation scheme (HRS) [2] with a pulse sequence that is tailored to produce a resonance signal that is immune to frequency shifts during the interrogation pulses. In the HRS scheme, the effect of the light shift on the spectrum is compensated by introducing a frequency step of the probe light during the interrogation pulses and an additional pulse cancels the linear dependence of the resonance frequency on the necessary compensation frequency step. Our experiments demonstrate a suppression of the light shift by four orders of magnitude and immunity against its fluctuations. For the operation as a frequency standard, we have implemented a servo system that controls the step frequency of the HRS, so that slow variations of the light shift will not degrade its suppression and the uncertainty of the optical clock due to the light shift becomes negligible.

Recently, we have derived the static differential polarizability of the octupole transition from light shift measurements of near-infrared lasers at four different wavelengths between 0.85 and 1.54 μm to be $\Delta\alpha=-8.88(16)\times10^{-41}$ $JV^{-2}m^2$. Together with the improved knowledge of the thermal radiation emitted by the ion trap and its mounting structure, it allows us to correct the blackbody radiation shift with a fractional uncertainty of less than 2×10^{-18}, which no longer constitutes the leading contribution to the total systematic uncertainty of 3×10^{-18}.

Repeated frequency measurements over the last years of the octupole and the $^2S_{1/2}(F=0)\rightarrow{}^2D_{3/2}(F=2)$ quadrupole transition of the same ion against caesium fountain clocks with uncertainties as small as 4×10^{-16} provide stringent constraints on a temporal variation of the proton-to-electron mass ratio [4].

This work is partly funded by the EMRP project SIB04 Ion Clock. The EMRP is jointly funded by the EMRP participating countries within EURAMET and the European Union.

[1] N. Huntemann, M. Okhapkin, B. Lipphardt, S. Weyers, Chr. Tamm, and E. Peik, "High-Accuracy Optical Clock Based on the Octupole Transition in $^{171}Yb^{+}$," Phys. Rev. Lett. 108, 090801 (2012).

[2] V. I. Yudin, A. V. Taichenachev, C. W. Oates, Z. W. Barber, N. D. Lemke, A. D. Ludlow, U. Sterr, Ch. Lisdat, and F. Riehle, "Hyper-Ramsey spectroscopy of optical clock transitions," Phys. Rev. A 82, 011804(R) (2010).

[3] N. Huntemann, B. Lipphardt, M. Okhapkin, Chr. Tamm, E. Peik A.V. Taichenachev and V. I. Yudin, "Generalized Ramsey Excitation Scheme with Suppressed Light Shift," Phys. Rev. Lett. 109, 213002 (2012).

[4] N. Huntemann, B. Lipphardt, Chr. Tamm, V. Gerginov, S. Weyers, and E. Peik, "Improved limit on a temporal variation of m_p/m_e from comparisons of Yb^{+} and Cs atomic clocks," Phys. Rev. Lett. 113, 210802 (2014).

Frequency Comparison of Two $^{40}Ca^{+}$ Optical Frequency Standards

Yao Huang, Pei-Liang Liu, Wu Bian, Hua Guan, Ke-Lin Gao*
Wuhan Institute of Physics and Mathematics, Chinese Academy of Sciences, Wuhan 430071
*E-mail: klgao@wipm.ac.cn

Frequency comparison is one of the most efficient ways to evaluate the performance of a frequency standard. Based on the pre-existing $^{40}Ca^{+}$ optical frequency standard [1-2], we set up the second $^{40}Ca^{+}$ optical frequency standard, which has been improved in the materials and structure of ion trap for better control of the magnetic field. The scheme of the comparison of two $^{40}Ca^{+}$ optical frequency standards is shown in Fig. 1 [3]. In our experiment, two optical frequency standards have the similar structure and share the 397 nm, 866 nm, 854 nm and 729 nm lasers together. Two AOMs (AO3 and AO4) are used to cover the difference between the clock transition frequency and the super cavity's resonant frequency. During the locking, although the two frequency standards share the same probe laser, the probe laser is referenced to the clock transition by feeding back to AO3 and AO4 independently to compensate for changes of the magnetic field and addressing of individual Zeeman transitions. The frequency data applied to AO3 and AO4 indicate the offset values of clock transition frequencies for two $^{40}Ca^{+}$ optical frequency standards, whose frequency difference is reflected from the frequency difference of AO3 and AO4. To rule out the effects from the jitter of magnetic field and the drift of the probe laser frequency with time, the probe laser is locked to the clock transitions of the ions in two ion traps simultaneously and independently.

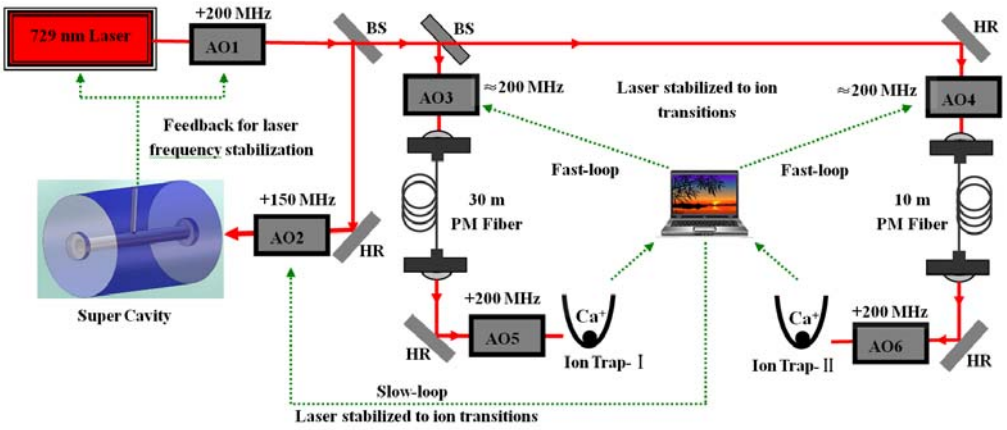


Fig. 1. The overview of setup on the frequency comparison of two $^{40}Ca^{+}$ optical frequency standards (AO: acousto-optic modulator; PM: polarization maintaining; BS: polarized beam splitter)

A preliminary optical frequency comparison experiment of two $^{40}Ca^{+}$ optical frequency standards is processed with the locking data of more than 3 days. A relative stability is $\sim 1\times10^{-14}\ \tau^{-1/2}$, which is shown in Fig. 2. In Fig.2, the result is much better than the relative stability of the first $^{40}Ca^{+}$ optical frequency standard vs. a hydrogen maser [2]. Through the comparison of two $^{40}Ca^{+}$ optical frequency standards, the relative stability is improved by more than an order of magnitude.

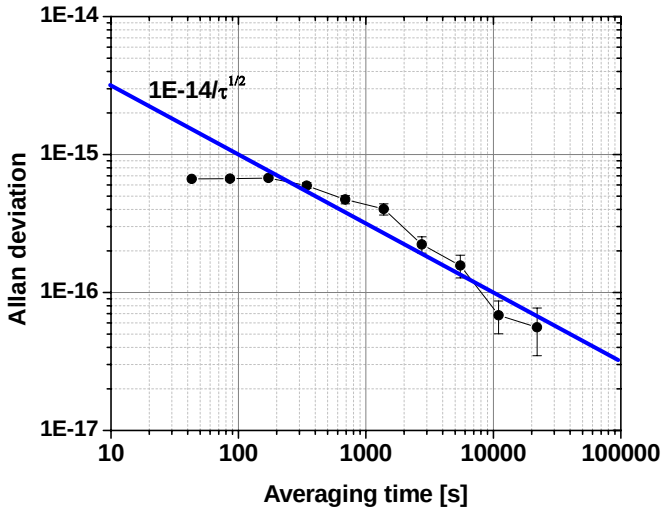


Fig.2. The relative stability of $^{40}Ca^{+}$ optical frequency standards.

[1] Y. Huang, Q. Liu, J. Cao, B. Ou, P. Liu, H. Guan, X. Huang, and K. Gao Phys. Rev. A **84**, 053841 (2011)
[2] Y. Huang, J. Cao, P. Liu, K. Liang, B. Ou, H. Guan, X. Huang, T. Li, and K. Gao Phys. Rev. A **85** 030503(R) (2012)
[3] P. Liu, Y. Huang, W. Bian, H. Shao, Y. Qian, H. Guan, K. Gao Chin. Phys. Lett. **31**, 113702(2014)

The Al^+ quantum-logic clock at NIST*

Brewer, S. M.[1,3], Bergquist, J. C.[1], Chen, J. S.[1,2], Hume, D. B.[1], Chou, C. W.[1], Hankin, A. M.[1], Wineland, D. J.[1,2], Rosenband, T.[1,4], and Leibrandt, D. R.[1]

[1]Time and Frequency Division, National Institute of Standards and Technology, Boulder, CO 80305, USA
[2]Department of Physics, University of Colorado, Boulder, CO 80309, USA
[3]Research Laboratory of Electronics, Massachusetts Institute of Technology, Cambridge, MA 02139, USA
[4]Department of Physics, Harvard University, Cambridge, MA 02138
E-mail: samuel.brewer@nist.gov

Optical atomic clocks based on quantum-logic spectroscopy of the $^1S_0 \leftrightarrow {}^3P_0$ transition in $^{27}Al^+$ have reached a fractional frequency uncertainty of 8.0×10^{-18} [1]. This accuracy is largely due to the insensitivity of the $^{27}Al^+$ ion to environmental perturbations such as electromagnetic fields. The largest contributions to the uncertainty of previous $^{27}Al^+$ quantum-logic clocks have been time dilation shifts due to driven motion (i.e., micromotion) and thermal motion of the trapped ions. In order to reduce these shifts, we have designed and built a new ion trap based on a gold-plated, laser-machined diamond wafer with differential RF drive.

Applications such as geodesy will require that such clocks be robust and packaged so that they can be deployed to and operated at sites of interest outside the laboratory. To this end, we have operated the clock using a robust, portable clock laser based on a spherical Fabry-Pérot cavity with a 1 second stability of 2×10^{-15} and an acceleration sensitivity below 10^{-12}/g [2]. We will present details of the trap design and operation as well as a preliminary characterization of the clock performance.

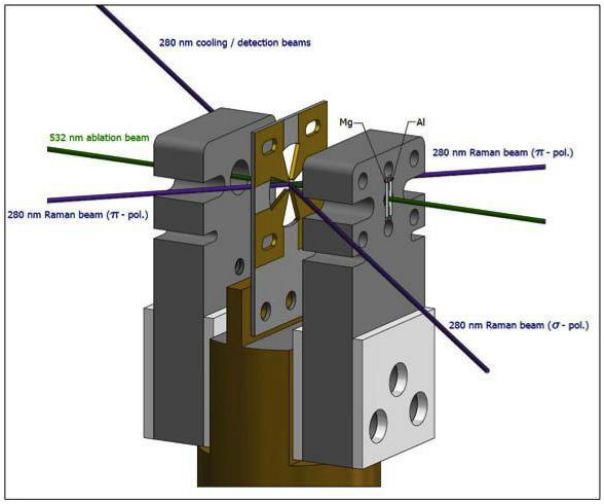


Figure 1: Schematic of $^{27}Al^+/^{25}Mg^+$ ion trap.

Reference:

[1] C. W. Chou, D. B. Hume, J. C. J. Koelemeij, D. J. Wineland, and T. Rosenband, Phys. Rev. Lett. **104**, 070802 (2010).
[2] D. R. Leibrandt, J. C. Bergquist, and T. Rosenband, Phys. Rev. A **87**, 023829 (2013).

* This work is supported by AFOSR, ARO, DARPA, and ONR.

Relative frequency shifts in scalable ion traps for optical clocks below 10^{-19}

Mehlstäubler, Tanja E., Keller, Jonas, Burgermeister, Tobias, Partner, Heather L., Doležal, Miroslav*, Balling, Petr*

Physikalisch-Technische Bundesanstalt, 38116 Braunschweig, Germany
*CMI, V Botanice 4, Prague, Czech Republic
E-mail: tanja.mehlstaeubler@ptb.de

Major limitations for the accuracy of optical ion clocks are today the blackbody shift due to the environmental temperature seen by the ion and 2nd Doppler shifts due to residual micromotion or excessive heating rates in the ion trap. The stability of the ion optical frequency standard suffers from the limited signal of a single atomic absorber and limited interrogation times due to excessive heating rates of the ion trap as well as the stability of the clock laser.

In our experiment, we develop scalable linear ion traps with reduced axial micromotion to store multiple ions for clock spectroscopy. Linear chains of $^{115}In^+$ ions are sympathetically cooled by $^{172}Yb^+$ ions. We currently operate a prototype trap made out of Rogers4350 with three trapping segments, including a separate loading and a protected spectroscopy segment, with on-board rf filter electronics. Using our ultra-stable spectroscopy laser at 411 nm [1] we implemented resolved sideband spectroscopy on the narrow $^2S_{1/2} \rightarrow {}^2D_{5/2}$ transition in $^{172}Yb^+$, which enables us to perform precise temperature measurements as well as to evaluate the sensitivity of different techniques for micromotion determination and compensation.

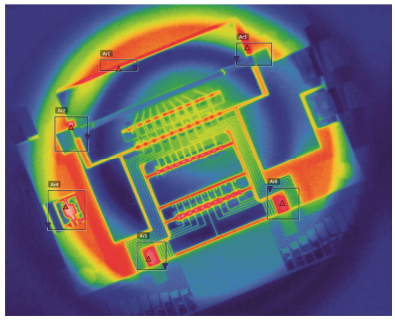


Fig. 1: Thermal image of the AlN ion trap in rf operation taken by a calibrated IR-camera. The AlN trap has integrated calibrated PT100 sensors on board of the ion trap.

By quenching the long-lived $^2D_{5/2}$ state with a laser at 1650 nm, we cooled a single Yb^+ ion to its quantum mechanical ground-state in the harmonic trapping potential. This allowed us to precisely determine the heating rate of the ion trap, to be as low as (1.2 ± 0.4) phonons/s, leading to a 2nd order Doppler shift of 2.3×10^{-20} per 1 second for an uncooled ion. A second source of systematic frequency shifts due to the motional effects in rf ion traps is residual micromotion. Several techniques have been proposed and implemented [2, 3] to measure the rf driven motion of ions in rf traps. However, for relative frequency shifts at the level of 10^{-18} and below, the various techniques show different limitations and systematic offsets. We present a quantitative comparison of three major techniques, utilizing spectroscopy on broad and narrow transitions, as well as parametric heating of the ions and demonstrate a sensitivity to motional effects corresponding to 2nd order Doppler shifts below 10^{-20}.

Based on the design of the prototype trap, we developed a new rf ion trap with improved heat conductivity and mechanical tolerances. The laser cut and gold coated trap was produced in the PTB clean room center. A first trap stack was completed and its thermal behavior in rf operation up to 3.3kV peak-peak voltage has been investigated at CMI. Simulations of the ion trap predict a maximum blackbody shift of 7×10^{-20} for the clock transition of $^{115}In^+$. First measurements indicate an elevated temperature rise corresponding to 7×10^{-19}. This work was supported by the EU through SIB04-Ion Clock. The EMRP is jointly funded by the EMRP participating countries within EURAMET and the European Union.

[1] Keller J. *et al.*, Appl. Phys. B (2013), DOI: 10.1007/s00340-013-5676-y.
[2] Berkeland, D.J. *et al.*, J. Appl. Phys. 83, 5025 (1998).
[3] Tanaka, U. *et al.*, Appl. Phys. B 107, 907 (2012).

Reducing field-related shift uncertainties to below 10^{-17} in a $^{88}Sr^{+}$ optical clock

Barwood G. P., Huang G., King S. A., Klein H. A. and Gill P.
National Physical Laboratory, Hampton Road, Teddington, Middx, TW11 0LW, UK
E-mail: geoffrey.barwood@npl.co.uk

Agreement between two trapped-ion $^{88}Sr^{+}$ optical clocks has recently been demonstrated at NPL with an uncertainty of 4 parts in 10^{17} [1]. One of the major uncertainty contributions stems from the blackbody shift which in turn depends on uncertainty in the knowledge of the differential polarisability between the ground and excited clock states. Measurements of AC scalar Stark shifts at several wavelengths will be reported; they complement a recent NRC measurement of the DC shift [2]. The estimated optical clock AC Stark shift as a function of laser wavelength is shown in figure 1. Preliminary results using a fiber laser at 1064 nm agree with calculated values to within ~3%. The effect of magnetic field noise on the frequency instability of our optical clock has also been modeled [3]. The 674 nm clock transition linear Zeeman shift is nominally cancelled by interrogating components symmetrically placed around line center, but magnetic field noise can degrade the frequency instability. Inclusion of the effect of this noise explains the observed two-trap frequency instabilities.

The Stark shift is observed by two-trap comparison, with a laser directed through one of the two traps and scalar, tensor and vector Stark shifts are all observed. The vector Stark shift depends on the magnetic quantum number m and so modifies the apparent Zeeman effect whereas the tensor Stark shift depends on m^2 and so changes the effective quadrupole shift. By averaging over different Zeeman components, the effect of both the tensor and vector Stark shifts is cancelled, leaving a measurement of the scalar Stark coefficient which is required for determination of the blackbody shift.

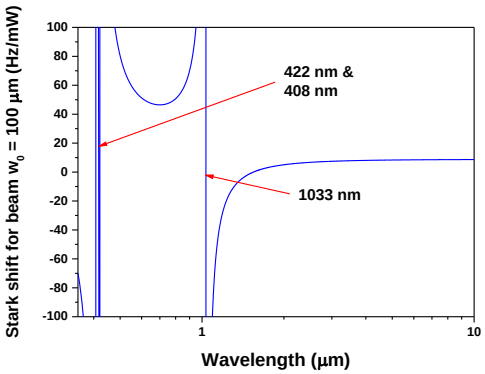


Fig. 1: Calculated Stark shifts for a beam focused to a 1/e amplitude radius of 100 µm and wavelengths between 350 nm and 10 µm.

Modelling the effect of magnetic field noise shows that, irrespective of whether the magnetic field noise has predominantly a white, flicker or random walk frequency character, this will always result in increased white frequency noise ($\sigma \propto \tau^{-1/2}$). The software controlling the frequency servo to the ion probes the higher and lower frequency Zeeman components alternately. These two components have the same field sensitivity, but opposite sign. Sensing the magnetic field differentially in this way alters the noise characteristic from random walk to white frequency noise.

Acknowledgement: This work was funded by the UK Department for Business, Innovation and Skills, as part of the National Measurement System Electromagnetics and Time program and also by the European Metrology Research Program (EMRP). The EMRP is jointly funded by the EMRP participating countries within EURAMET and the European Union.

[1] G.P. Barwood, G. Huang, H.A. Klein, L.A.M. Johnson, S.A. King, H.S. Margolis, K. Szymaniec, and P. Gill, "Agreement between two $^{88}Sr^{+}$ optical clocks to 4 parts in 10^{17}", Phys. Rev. A **89**, 050501(R) (2014)

[2] P. Dubé, A.A. Madej, M. Tibbo, and JE Bernard, "High-Accuracy Measurement of the Differential Scalar Polarizability of a $^{88}Sr^{+}$ Clock Using the Time-Dilation Effect", Phys. Rev. Lett. **112**, 173002 (2014)

[3] G.P. Barwood, G. Huang, S.A. King, H.A. Klein and P. Gill. "Frequency Noise Processes in a Strontium Ion Optical Clock", J. Phys. B: At. Mol. Opt. Phys. **48**, 035401 (2015)

Search for optical excitation of the low-energy nuclear isomer of Th-229

E. Peik[1], D. M. Meier[1], M. V. Okhapkin[1], A. Yamaguchi[1*],
M. Kolbe[2], H. Kaser[2], T. Reichel[2], A. Gottwald[2]
[1]Physikalisch-Technische Bundesanstalt, Bundesallee 100, 38116 Braunschweig, Germany
[2]Physikalisch-Technische Bundesanstalt, Abbestrasse 2-12, 10587 Berlin, Germany
E-mail: ekkehard.peik@ptb.de

The concept of an optical clock based on resonant excitation of the nuclear magnetic dipole transition between the ground state and the isomeric level of Th-229 at about 7.8 eV excitation energy with an expected linewidth in the mHz range is well established and advantages of this system in terms of achievable accuracy and stability have been pointed out [1-4]. An efficient isolation from external frequency shifting perturbations can be expected for the nuclear transition in $^{229}Th^{3+}$. Since the transition has been studied so far only indirectly in γ-spectroscopy, an optical excitation of the nuclear transition and a more precise determination of the transition energy are the missing links towards a study of this system as a precise nuclear clock. We present the status of two different experiments that are designed to achieve this goal.

We are using two-photon laser excitation via electronic bridge processes in Th^+ in a search for the nuclear excitation [5]. In resonant two-step laser excitation of trapped Th^+ ions, we have observed 43 previously unknown electronic energy levels within the search range from 7.3 to 8.3 eV [6]. The high density of states promises a strongly enhanced nuclear excitation rate. Using laser ablation loading of the ion trap and photodissociation of molecular ions that are formed in reactions of Th^+ with impurities in the buffer gas, we efficiently load and stably store ions of the radioactive Th-229 isotope. We have measured the hyperfine structure and isotope shifts of two resonance lines that are suitable as first stages of the electron bridge excitation and can be used to infer nuclear moments of the isomeric state. Presently, the search scan for the resonant electronic bridge excitation is ongoing.

For a different search approach of the isomeric transition in solid samples [7], we have developed a novel adsorption technique which prepares ^{229}Th on a surface of CaF_2. The adsorbed ^{229}Th is exposed to highly intensive undulator radiation in the wavelength range between 130 nm and 320 nm, which includes the indirectly measured nuclear resonance wavelength 160(10) nm. After the excitation, light emission from the sample is detected with a VUV sensitive photomultiplier tube. No clear signal relating to the nuclear transition is observed. A possible explanation by non-radiative relaxation of the nuclear excitation makes a more detailed analysis of the chemical environment of the adsorbed Th necessary.

*present address: Quantum Metrology Laboratory, RIKEN, Wako, Saitama 351-0198, Japan.

[1] E. Peik and Chr. Tamm, Europhys. Lett. 61, 181 (2003).

[2] C. J. Campbell, A. G. Radnaev, A. Kuzmich, V. A. Dzuba, V.V. Flambaum, and A. Derevianko, Phys. Rev. Lett. 108, 120802 (2012).

[3] W. G. Rellergert, D. DeMille, R. R. Greco, M. P. Hehlen, J. R. Torgerson, E. R. Hudson, Phys. Rev. Lett. 104, 200802 (2010).

[4] G. A. Kazakov, A. N. Litvinov, V. I. Romanenko, L. P. Yatsenko, A. V. Romanenko, M. Schreitl, G. Winkler and T. Schumm, New Journal Phys. 14, 083019 (2012).

[5] S. G. Porsev, V.V. Flambaum, E. Peik, Chr. Tamm, Phys. Rev. Lett. 105, 182501 (2010)

[6] O. A. Herrera-Sancho, N. Nemitz, M. V. Okhapkin, E. Peik, Phys. Rev. A 88, 012512 (2013)

[7] A. Yamaguchi, M. Kolbe, H. Kaser, T. Reichel, A. Gottwald, E. Peik, "Experimental search for the low-energy nuclear transition in ^{229}Th with undulator radiation", to be published

UHF acoustic attenuation and quality parameter limits in the diamond based HBAR

Telichko Arseniy*+, Sorokin Boris*+, Kvashnin Gennady+
*Moscow Institute of Physics and Technology, Russian Federation
+Technological Institute for Superhard and Novel Carbon Materials, Russian Federation
E-mail: arseny.telichko@phystech.edu, bpsorokin2@rambler.ru

High-overtone Bulk Acoustic Resonator (HBAR) is a perspective acoustoelectronic device, operating at high frequencies [1]. High operating frequencies f, quality factor Q, and low acoustic losses α depend mainly on the quality of a substrate material. Creation of devices on HBAR with high Q and f is important task of modern acoustoelectronic society. According to above, diamond is one of the best materials as a substrate for HBAR. But in order to predict the diamond HBAR behavior at high frequencies it is necessary to estimate physical limit of UHF acoustic attenuation.

It is known that the $Q\times f$ product (quality parameter) depends on phonon-phonon scattering [2] and in Akhiezer attenuation regime ($2\pi f\tau << 1$) it should remain a constant, while in Landau-Rumer regime it has linear frequency dependence [3, 4]:

$$Akh: Q\times f = \frac{\rho V_a^2\left[1+(2\pi f\tau)^2\right]}{C_v T\gamma^2\tau};\ L-R: Q\times f = \frac{30\rho V_a^5 h^3}{\pi^4\gamma^2(k_B T)^4} f. \qquad (1)$$

Here ρ is the density of substrate, V_a acoustic velocity, τ thermal relaxation time, γ Grüniesen parameter, C_v volumetric heat capacity, T temperature, and h Planck constant. The experimental results on resonance properties of Al/AlN/Mo/(100) diamond HBAR are represented on Fig. 1. It is known that the transition from Akhiezer to Landau-Rumer regime takes place at $2\pi f\tau \approx 1$. Beginning the 2 GHz one can observe a linear frequency dependence of the quality parameter associated with *L-R* regime (Fig. 1). The highest results on $Q\times f \approx 8\cdot 10^4$ GHz can be achieved at ~ 6.5 GHz.

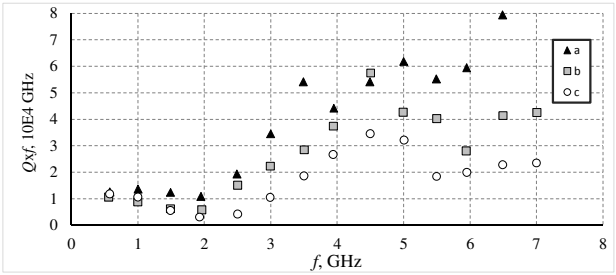


Fig. 1: Experimental results on $Q\times f$ of diamond based HBAR with different electrode form: a – triangle, b – square, c – circle.

In order to get theoretical predictions on the $Q\times f$ limit value for a diamond it is important to define the Grüneisen parameter for a given acoustical mode. Taking $\gamma_{L100} = 1.3$ we can estimate $Q\times f \approx 5.4\cdot 10^4$ GHz for Akhiezer regime, and $Q\times f \approx 1.1\cdot 10^6\times f$ GHz for *L-R* regime, as well as acoustic attenuation $\alpha_{Akh} = 0.2$ dB/cm at 1 GHz, and $\alpha_{L\text{-}R} = 0.07$ dB/cm at 9 GHz. For the fastest bulk acoustic wave travelling along [111], we have $\gamma_{L100} = 1.1$, so $Q\times f_{Akh} \approx 9.5\cdot 10^4$ GHz, and $Q\times f_{L\text{-}R} \approx 20\cdot 10^6\times f$ GHz, as well as $\alpha_{Akh} = 0.1$ dB/cm at 1 GHz, and $\alpha_{L\text{-}R} = 0.04$ dB/cm at 9 GHz.

[1] B. P. Sorokin, G. M. Kvashnin, A. P. Volkov, V. S. Bormashov, V. V. Aksenenkov, A. V. Telichko, and G.I. Gordeev, "AlN/single crystalline diamond piezoelectric structure as a high overtone bulk acoustic resonator," Appl. Phys. Lett., vol. 102, p. 113507, 2013.

[2] R. Tabrizian, M. Rais-Zadeh, and F. Ayazi, "Effect of phonon interactions on limiting the *f·Q* product of micromechanical resonators," *Proceedings*, 2009 Int. Conf on Solid-State Structures, Actuators and Microsyst., Denver, Colorado, June 21-25, pp. 2131–2134.

[3] A. Akhiezer, "About sound absorption in solids," JETF (in Russian), vol. 8, no. 12, pp. 1318-1329, 1938.

[4] L. Landau and G. Rumer, "On sound absorption in solids," Phys. Zs. Sowjet., vol. 11, no. 18, pp. 227-233, 1937.

How to qualify LGT crystal for acoustic devices?

M. Allani[1,2], X. Vacheret[1], A. Clairet[1], T. Baron[1], O. Bel[3], H. Cabane[4], JM Lesage[5], JJ Boy[1]
[1] FEMTO-ST Institute, UFC, CNRS, ENSMM, UTBM, 25000 Besançon, France
[2] INSAT, BP 676, 1080 Tunis cedex - Tunisie
[3] RAKON France, 10150 Pont Sainte Marie, France
[4] Cristal Innov – Université Lyon1, 73800 Sainte-Hélène du Lac, France
[5] DGA MI - 35998 Rennes Cedex 9
E-mail: maroua.allani@ens2m.fr

Before using any piezoelectric crystal to realize acoustic devices (sensors, transducers, actuators or ultra-stable resonators) and beyond its mechanical properties, the crystal material itself has to be characterized. Whether the very interesting properties of the LGT crystal (high acoustic quality, very good thermal stability and high electromechanical coupling factor) make it the best candidate to substitute quartz crystal for frequency output devices, we must take into account the crystal quality. Indeed, applications require homogeneous crystals with reproducible physical properties.

The presence of structural defects and inhomogeneity of the crystal composition significantly affect the physicochemical properties (optical, electrical, piezoelectric…), and can be revealed by chemical, optical, and electrical analytical methods. So, before manufacturing acoustic devices, we perform the following sequence:



Fig. 1: Photos if LGT and LGS crystals (CI06, LGS, FO02, CK03, FO01, CI03

Firstly, we chemically etch LGT samples in H_3PO_4 to reveal structural defects and compositional inhomogeneities. Then, we study the surfaces state by optical microscopy and roughness measurements. We observe that the roughness profiles reveal the presence of holes called “etch pits”, indicating the existence of bundles of dislocations.

Secondly, we analyze the stoichiometry of LGT crystals and their impurities levels by femtosecond laser ablation Inductively Coupled Plasma Mass Spectrometry (fs LA-ICP-MS). We also study the radial distributions of these impurities to explain the heterogeneous orange color of some LGT crystals. One of the most interesting results is that LGT crystal was contaminated by its raw materials impurities such as Iron ions and Lanthanides which can cause its color.

Third, considering that point defects significantly affect the optical properties, we record optical transmission spectra in UV-VIS and IR ranges. The band gap energy, which is a criterion to define the LGT crystal quality, is qualitatively determined from the edge of the intrinsic absorption of the UV-Vis spectrum. In IR spectrum, we observe that the intensity of absorption peak at 5350 cm^{-1} increases with the intensity of color. It seems to be related to a point defect responsible for the LGT (and LGS) color. We assign the absorption band at 3430 cm^{-1} to Ga-OH vibrations.

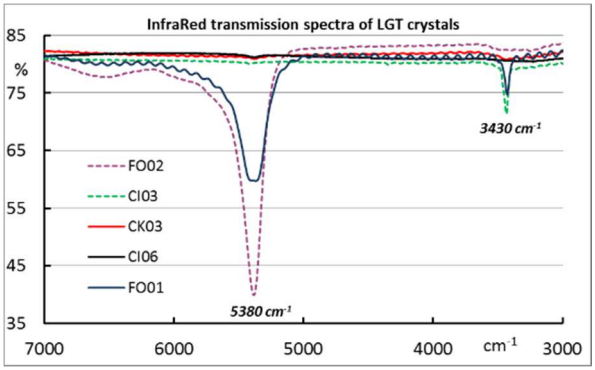


Fig. 2: Infra-Red transmission spectra of LGT crystals

After that, to test the acoustic properties, it seemed necessary to manufacture bulk acoustic waves resonators working at a given frequency, if possible not too sensitive to external parameters. Indeed, the Q-factor defining the quality of the resonant frequency depends on crystal quality but also on the resonator geometry. So, we have chosen to build very thin BAW resonators (about 100 µm thick) working at about 40MHz and also HBAR based on LGT substrate in which some overtones work at a few hundreds of MHz and present low frequency shift with temperature.

Langasite family crystals as promising materials for microacoustic devices at cryogenic temperatures

Smirnova, Elena [*], Sotnikov, Andrey[*,**], Schmidt, Hagen[**], Weihnacht, Manfred[**], Goetze, Jens[+], Sakharov, Sergey[++]

[*]A. F. Ioffe Physical-Technical Institute, Polytekhnicheskaya 26, St. Petersburg, Russia
[**]IFW Dresden, SAWLab Saxony, Helmholtzstr. 20, Dresden, Germany
[+]TU Bergakademie Freiberg, Department of Mineralogy, Brennhausgasse 14, Freiberg, Germany
[++]JSC Fomos-Materials, Buzhinova 16, 107023 Moscow, Russia
E-Mail: m.weihnacht@ifw-dresden.de

Future progress in microacoustic devices is highly determined by the revealing of new efficient piezoelectric single crystals. Langasite (LGS) itself and ordered single crystals from its family demonstrate moderately high electromechanical coupling, low acoustic attenuation as well absence of any phase transition between liquid helium temperature and their melting point. In addition to the normal and high temperature conditions, the ability for low (cryogenic) temperature operation is of special importance. Obviously, for successful application the crystals should preserve their physical properties at lowest temperatures without considerable worsening. To our best knowledge the only paper on LGS material parameters at low temperatures is [1]. Notice that low temperature elastic and dielectric behavior is also a direct approach for basic understanding of the crystal lattice dynamics.

In this contribution, we present a set of elastic and dielectric constants for $Sr_3NbGa_3Si_2O_{12}$ (SNGS) belonging to the ordered langasite family crystals at temperatures between 4.2 and 300 K. The common feature of the temperature dependences of the elastic constants C_{ij} is a gradual increase with decreasing temperature followed by a saturation at low temperatures (T < 20…50 K). In contrast to results obtained in [1] for LGS, we cannot find for SNGS any specific softening of C_{11}, C_{12} and C_{33} elastic constants at T ~ 150 K as well as a turnover point close to room temperature for C_{66}. Our results are corresponding to the Varshni expression based on the Einstein oscillator model [2]. Using this expression the Einstein temperature as well as the zero temperature decrement (difference between the harmonic elastic constant obtained by linear extrapolation from high temperatures and the observed value of the elastic constant at $T \rightarrow 0$) are derived. The latter effect is due to quantum zero point energy vibrations. As for the dielectric behavior, both $\varepsilon_{11}(T)$ and $\varepsilon_{33}(T)$ show a weak decrease with decreasing temperature. As also found, the piezoelectric activity of SNGS at 4.2 K is almost the same as at room temperature. High piezoelectric response together with flat $C_{ij}(T)$ dependencies in the temperature range from 4.2 to about 20…50 K indicates SNGS as a promising material for acoustic sensors and frequency stable devices at cryogenic temperatures. Similar measurements were also done for LGS crystals. In contrast to SNGS, $\varepsilon_{33}(T)$ increases with decreasing temperature and $C_{66}(T)$ shows a turnover point close to room temperature followed by a decreasing up to T ~ 4.2 K. Moreover, deviating from [1], we cannot confirm a specific softening of C_{11}, C_{12} and C_{33} elastic constants at temperatures around 150 K.

[1] R. Tarumi, H. Nitta, H. Ogi, M. Hirao, “Low-temperature elastic constants and piezoelectric coefficients of langasite ($La_3Ga_5SiO_{14}$)”, Philosophical Magazine, vol. 91, no. 16, 1 June 2011, pp. 2140-2153.

[2] Y.P. Varshni, “Temperature dependence of the elastic constants”, Physical Review B, vol. 2, no. 10, 15 Nov. 1970, pp. 3952-3958.

As-doped Si's Complex Permittivity Estimation and its Effect on Heating Curve at 2.45 GHz frequency

Varadan, Siddharth, Zhao, Zhao*,Pan George, Alford, Terry*
Department of Electrical Engineering, Arizona State University, Tempe, AZ/USA
*School of Matter, Transport and Energy, Arizona State University, Tempe, AZ/USA
E-mail: Siddharth.varadan@asu.edu

An analysis to determine the complex permittivity of arsenic-doped silicon wafer at 2.45 GHz and its impact on the susceptor-based heating curve of the material is presented. Complex permittivity estimation is based on closed-form analytical expressions for cylindrical symmetry. Experimental results in support with the numerical analysis and simulation results are presented. This analysis will further help analyze the capacitive heating of doped and undoped silicon wafer at microwave frequency; hence, this paper is a precursor to elucidation of capacitive heating of silicon substrates placed onto susceptors. This study indicates that when the dopant is added to the silicon the loss tangent decreases with increase in concentration of the dopant but upon annealing the loss tangent becomes constant with respect to concentration of the dopant.

The junction considered for this analysis, as show in Fig. 1, is a coaxial line with center conductor, entering the cylindrical waveguide through its flat face. The dimensions of the coaxial line are set such that it supports only quasi-TEM waves at the desired frequency. It is also assumed that all conductors have perfectly conducting surfaces.

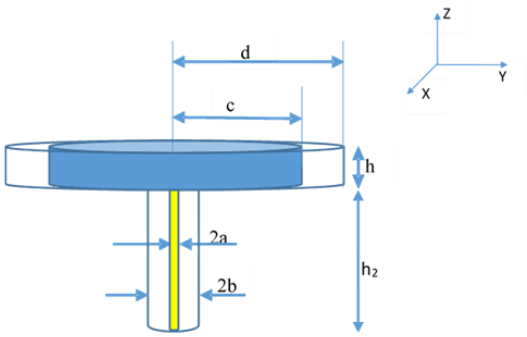


Fig. 1. Radial transmission line used in the experimental setup along with its dimensions, where *a*=15 mm, *b*=25 mm, *c*=101.6 mm, *d*=152.4 mm and *h*=0.6 mm. The center of junction between coaxial cable and the cylindrical waveguide is assumed to be the origin.

Analyses presented prior to this paper, such as [1], were for low-loss dielectric (i.e., loss tangent of 0.02) whereas the investigation done here estimates the complex permittivity of a highly lossy (.e.g., loss tangent close to 50) dielectric (arsenic-doped silicon wafer). The effect of annealing on the complex permittivity was compared by measuring the permittivity before and after annealing. Experiments were conducted to validate the numerical and simulation results. The reflection coefficients were obtained experimentally and were matched with the reflection coefficients obtained from the simulation results and analytical solutions. Three samples with varying doping concentration were analyzed and presented in this paper.

The results indicate that the assumption made in [2], that the heating curve is driven by the sheet properties of the sample and not the bulk properties, is correct. This also is a valid assumption considering the fact that in a good conducting material, the electromagnetic (microwaves) waves do not penetrate beyond the skin depth and this forms the sheet of this sample. To further validate this result, Hall Effect and four-point-probe measurements (before and after annealing) were conducted.

[1] Z. Guo, G.W. Pan, S. Hall and C. Pan, "Broadband characterization of complex permittivity for low-loss dielectrics: circular PC broad disk approach," *IEEE Trans. on Antenna and Propagation*, vol. 57, no. 10, pp. 3126-3155, (October) 2009.

[2] R. N. P Vemuri, M. J. Gadre, N. D. Theodore, W. Chen, S. S. Lau and T. L. Alford, "Susceptor assisted microwave annealing for recrystallization and dopant activation of arsenic-implanted silicon," *Journal of Applied Physics*, vol.110 issue 3, pp. 034907-034907-7, 2011.

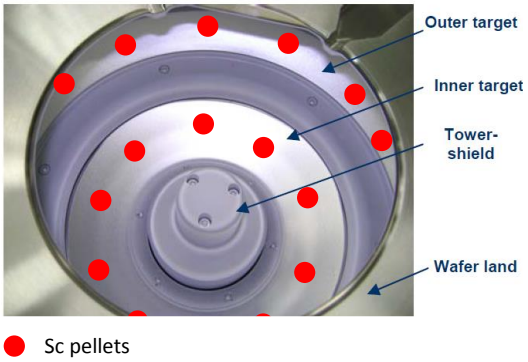
Sputtered $Al_{(1-x)}Sc_xN$ thin films with high areal uniformity for mass production

Felmetsger V*, Clement M+, Olivares J+, DeMiguel-Ramos M+, Mirea T+, Mikhov M* and Iborra E+
*OEM Group Inc. Gilbert, AZ, USA
+GMME-CEMDATIC ETSI de Telecomunicación. Universidad Politécnica de Madrid, Spain
E-mail: enrique.iborra@upm.es

AlScN thin films are an attractive material for high frequency (GHz range) resonators because AlScN piezoelectric activity is remarkably higher compared with pure AlN and increases with Sc content, reaching a maximum at about 40 at. %, although this material's elastic constants strongly decrease [1]. However, for some applications, even moderate enhancement of piezoelectric activity achievable with relatively low Sc concentrations can be very attractive, if elastic constants remain high.

For deposition of homogeneous thin films with a given Sc content on production size wafers (diameters 6" and 8"), alloyed Al-Sc targets would be desirable. However, the metallurgy of the Sc/Al system impedes to obtain Al-Sc alloys with Sc content greater than 10-12%. Usually co-sputtering is used to obtain AlScN films for research purposes. However, this method is not suitable for mass production, as the homogeneity is poor or the deposition rate is very low. In this communication, we present a method to obtain uniform, in composition and thickness, thin films of AlScN thin films on standard 6" Si wafers. The method was implemented in an Endeavor AT™ cluster tool from OEM Group, capable of deposit AlScN films on wafers up to 8" in diameter.

The method employs a dual-target S-gun magnetron for AC (40 kHz) reactive sputtering equipped with Al targets containing embedded Sc pellets (see figure 1) in a number adequate to provide the desired composition in the deposited film. For this work, 10 Sc pellets of 0.5" in diameter are embedded in the inner target, 7" in diameter, and 14 pellets of 0.5" in diameter are embedded in the outer target, 11" in diameter. Calculated Sc concentration in the sputter flux is about 6% based on area covered by the Sc surface and ion sputter yield of 0.6. Real concentration may be higher since erosion zone area may be lower than that used in calculation. Changing the number of pellets allows modifying the composition of the layers. AlScN films were deposited on nominally unheated wafers.



XRD measurements demonstrate films of pure *c*-axis oriented wurtzite. The plane spacing (from Bragg angle of the (00·2) reflection) is 5.00 ±0.005 Å and the rocking curve is 1.43˚-1.61˚ across the wafer.

Because of the particular geometry of the target assembly in this sputter tool, the uniformity is very good in both thickness (+/-0.9%, std. = 0.47% in 1 µm-thick films) and composition as estimated by using the position of the A1(LO) infrared absorption band and crystalline-plane spacing.

Solidly mounted bulk acoustic wave resonators were made on Al/Mo and SiO_2/Mo acoustic reflectors using Mo thin films as bottom electrode. The effective coupling is around 5.5 ± 0.2% with very good uniformity across the 6" wafer. This coupling factor is lower than expected, probably because Mo is not the best substrate for AlScN films. Other metals such as Ir, W, and Cr are now being tested for improving piezoelectric activity. Dielectric constant and sound velocity have also been evaluated giving values of 106 pF/m and 9500 m/s, respectively.

[1]. M. Akiyama, K. Kano, and A. Teshigahara, "Influence of growth temperature and scandium concentration on piezoelectric response of scandium aluminum nitride alloy thin films" Appl. Phys Lett. **95**, (2009) 162107.

Micro OXCO EWOS-0513: A 20 years space odyssey up to 67P/Churyumov-Gerasimenko

Philippe Guillemot, Gille Cibiel, Yves Richard*, Jean-Marie Tarot*, Guy Richard*
CNES – French Space Agency, Toulouse, France
*Syrlinks, Rennes, France
E-mail: philippe.guillemot@cnes.fr

The story probably started somewhere on the Mars planet in the middle of the 90s' when the Sojourner rover demonstrated that it was possible to make great space missions with 'low cost' systems. It was the beginning of the 'Better / Faster / Cheaper' period. It led space agencies and space industry to develop space equipment using 'professional' systems instead of full space qualified ones.

In 1995, the CNES, the French Space Agency, decided to develop a family of 'low cost' space miniaturized OCXOs. A so called EWOS-0500 micro OCXO, used up to then for distress beacons, was selected for this purpose. The EWOS-0500 was a very small size (DIL 14, 1.5 cm^3) and low power (150 mW) OCXO with a short-term stability in the 10^{-11} range (A-Dev) and a frequency stability of 0.2 ppm in the temperature range [-30 °C; +60°C]. A specific qualification program was set up, to demonstrate the performances and the capability of this OCXO to fulfil space missions. The EWOS-0513 micro OCXO was born.

The EWOS-513 was embarked on numerous space missions, mainly in low earth orbit. But some of them were also embarked on the Rosetta mission for a 10 years journey through the solar system up to the 67P/Churyumov-Gerasimenko comet. Once arrived, they contributed to the success of the mission, allowing telecommunication between the orbiter and the lander and being involved in the science program through the CONSERT instrument.

This paper redraws the main steps and the main performances of this program that led an oscillator initially intended for distress beacons to contribute to the success of the Rosetta mission.

Noise modeling methodology of an integrated circuit for quartz crystal oscillator

Vorobyev Nikolay, Imbaud Joël, Baron Thomas, Cibiel Gilles* and Galliou Serge
Time and Frequency Dept., FEMTO-ST Institute, UFC, CNRS, ENSMM, UTBM, Besançon, France
*Microwave and Time-Frequency Department, CNES, Toulouse, France
E-mail: nikolay.vorobyev@femto-st.fr

This paper reports the methodology and results about noise modeling and tests of a quartz crystal oscillator based on a dedicated integrated circuit (ASIC). Unfortunately, the phase noise of the inner sustaining amplifier is unknown. The challenge is then to evaluate the performance limits of this ASIC in an oscillator circuit.

Actually, the sustaining amplifier is an ASIC whose internal design is just partially known and whose electrical inputs-outputs are very restricted. This fact considerably complicates the parametric characterization process. The analysis of the core of the internal circuit shows that its noise modeling can be performed by defining four noise parameters. Thus, a set of four external configurations is designed to extract experimental data. These data allow to compare the measured noise to the simulated one and to identify the unknown parameters by an engineer tool like Advanced Design System (ADS).

Moreover the noise of usual grade BAW resonators, commercially available, is measured. Precision passive measurements of the quartz crystal resonator phase noise are conducted in our laboratory by using an interferometric bench [1]. The resonator noise model is matched according to the measurements and implemented in the simulation oscillator circuit [2].

Finally, the oscillator noise can be simulated from the knowledge of individual noise from the sustaining amplifier and the resonator respectively. The theoretical computation results are in very good agreement with the oscillator phase noise measurements: their difference is less than about 3 dB. As a consequence the developed model allows parametric and structural optimization of the electrical environment of the ASIC as well as resonator-type selection.

In addition, once the noise model of the ASIC is known, the oscillator phase noise can be predicted for any kind of resonator, according to it specified noise. Indeed, tests with a state-of-the-art 10 MHz resonator confirm the validity of the resulting noise model and give a phase noise level of -110dBc at 1Hz frequency-offset from the carrier.

[1] F. Sthal, S. Galliou, J. Imbaud, X. Vacheret, P. Salzenstein, E. Rubiola, and G. Cibiel, “About quartz crystal resonator noise: recent study,” in *Proc. Int. Conf. Noise and Fluctuations*, Pisa, Italy, 2007, pp. 607–610.

[2] M. Goryachev and S. Galliou, “Precision close-to-carrier phase noise simulation of BAW oscillators,” IEEE Transactions on Ultrasonics, Ferroelectrics and Frequency Control, vol. 58, no. 1, pp. 6–9, Jan. 2011.

The Prediction, Simulation and Verification of the Phase Noise in Low-Phase-Noise Crystal Oscillator

Huang Xianhe*, Jiao Junjie and Fu Wei
University of Electronic Science and Technology of China, Chengdu, China
xianhehuang@uestc.edu.cn

In order to achieve the prediction of the low phase noise crystal oscillator's phase noise, based on the classic Lesson phase noise model, the load Q value (Q_L) is calculated according to the selected oscillator circuit parameters after analysis and selection of appropriate oscillator noise factor F and transistor corner frequency f_c . Thus, on the basis of Lesson phase noise formula, the prediction results of low phase noise crystal oscillator's phase noise are obtained. Then, the transistor nonlinear model is constructed to simulate the low phase noise crystal oscillator's phase noise by using the ADS (Advanced Design System) simulation software of Agilent and obtain the simulation curve of the phase noise. At last, practical debugging and testing have been performed on this low phase noise crystal oscillator prototype. The testing result shows that: the prediction values of the oscillator's phase noise after reasonable selection of each parameter of Lesson model and the ADS simulation results obtained by using nonlinear transistor model are both close to the actual testing results, which are at 100Hz and far away offset the carrier frequency. After that, the existing of the deviation, which is near carrier frequency, is analyzed. The prediction and simulation methods given by this paper might be beneficial to simplify the design progress of the low phase noise crystal oscillator.

Tab. 1 the comparison among prediction values, simulation results and real test results of several low phase noise crystal oscillators' phase noise

Type	specification and parameters of the resonators	prediction values of the oscillator's phase noise	simulation results of the oscillator's phase noise	testing results of the oscillator's phase noise
LT10.7MHz low phase noise crystal oscillator	lithium tantalite C_1=0.579pF, Q_0=1.24K, C_0=4.0pF	-89dBc/Hz/10Hz -119dBc/Hz/100Hz -149dBc/Hz/1KHz -173dBc/Hz/10KHz	-88dBc/Hz/10Hz -118dBc/Hz/100Hz -147dBc/Hz/1KHz -173dBc/Hz/10KHz	-87dBc/Hz/10Hz -117dBc/Hz/100Hz -148dBc/Hz/1KHz -173dBc/Hz/10KHz
80MHz low phase noise crystal oscillator	Quartz, SC-cut 5th overtone C_1=0.142fF,Q_0=162K C_0=3.5pF	-115dBc/Hz/10Hz -145dBc/Hz/100Hz -165dBc/Hz/1KHz -172dBc/Hz/10KHz	-117dBc/Hz/10Hz -149dBc/Hz/100Hz -169dBc/Hz/1KHz -173dBc/Hz/10KHz	-108dBc/Hz/10Hz -145dBc/Hz/100Hz -164dBc/Hz/1KHz -176dBc/Hz/10KHz
100MHz low phase noise crystal oscillator	Quartz, AT, 3th overtone C_1=1.2fF, Q_0=132K C_0=2.5pF	-99dBc/Hz/10Hz -129dBc/Hz/100Hz -157dBc/Hz/1KHz -169dBc/Hz/10KHz	-100dBc/Hz/10Hz -130dBc/Hz/100Hz -159dBc/Hz/1KHz -174dBc/Hz/10KHz	-92dBc/Hz/10Hz -128dBc/Hz/100Hz -157dBc/Hz/1KHz -170dBc/Hz/10KHz
120MHz low phase noise crystal oscillator	Quartz, SC-cut 5th overtone C_1=0.2fF, Q_0=105K C_0=3.2pF	-108dBc/Hz/10Hz -138dBc/Hz/100Hz -162dBc/Hz/1KHz -169dBc/Hz/10KHz	-112dBc/Hz/10Hz -141dBc/Hz/100Hz -164dBc/Hz/1KHz -172dBc/Hz/10KHz	-104dBc/Hz/10Hz -138dBc/Hz/100Hz -161dBc/Hz/1KHz -170dBc/Hz/10KHz

References:

[1] John R. Vig, "Quartz Crystal Resonators and Oscillators for Frequency Control and Timing Applications-A Tutorial " http://www.ieee-uffc.org [Online]

[2] Xianhe Huang, Wei Fu, Pingping Chen and Hongyuan Huang, "Physical model of phase noise in feedback oscillator", *in Proc. IEEE Int. Freq. Control Symp. Joint with European Freq. and Time Forum*, 2013, pp. 952-955.

[3] M. M. Driscoll, "Modeling phase noise in multifunction subassemblies", *IEEE Trans. Ultrason., Ferroelectr., Freq. Control*, vol. 59, no. 3, pp. 373-381, Mar. 2012.

Thermal Fluctuations in Cryogenic Quartz Resonators

E. Ivanov , M. Goryachev, M. Tobar and S. Galliou*
School of Physics, The University of Western Australia, Perth, Australia
*Department of Time and Frequency, FEMTO-ST Institute, ENSMM, Besancon, France

Acoustic resonances at frequencies around 500 MHz and Q-factors exceeding one billion were reported in [1]. This was observed with the so-called BVA quartz resonators employing the non-contacting electrode technology [2]. Such resonators are the time-keeping elements of the most frequency-stable quartz oscillators [3].
By cooling the 400 MHz BVA resonator to 15 mK, which is well within the range of modern cryogen-free dilution systems (for example, http://www.bluefors.com), one can putatively observe the quantum behavior of macroscopic objects, as well as perform various high-precision tests of fundamental physics.

We report the first observations of thermal fluctuations in the BVA resonators at cryogenic (4 K) and ultra-cryogenic (20 mK) temperatures. The measurements were conducted with commercial DC SQUID readout system at frequencies up to 20 MHz.

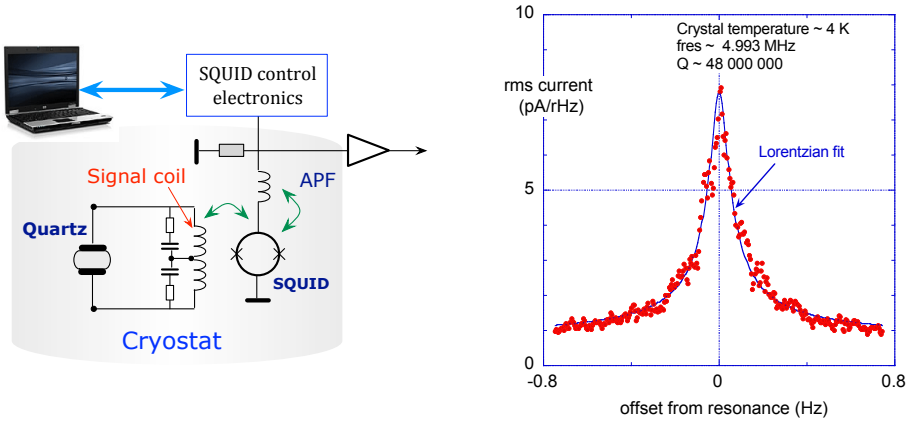


Fig. 1. Experimental setup and spectrum of current fluctuations through the SQUID signal coil at 4 K

Our investigation showed that:
- Spectra of thermal fluctuations are Lorentzian;
- Statistics of thermal fluctuations is Gaussian;
- At T~ 4K, mode temperatures of all acoustic resonances detected is close to physical temperature of the crystal;
- The Q-factors extracted from the thermal noise spectral fits are consistent with those measured with impedance analyser.

The following aspects of our study will be discussed in details at the conference:
- Calibration and noise floor measurement of the DC SQUID readout;
- Conversion of FFT voltage noise spectra into mode temperature;
- Comparison of thermal noise spectra at cryogenic and ultra-cryogenic temperatures.

[1] M. Goryachev, D. Creedon, S. Galliou, and M. Tobar, "Observation of Rayleigh Phonon Scattering through Excitation of Extremely High Overtones in Low-Loss Cryogenic Acoustic Cavities for Hybrid Quantum Systems Physical Review Letters, 111, 085502 (2013).
[2] R. J. Besson, Proc. of 31st Annual Symposium on Frequency Control (1977), pp. 147–152.
[3] P. Salzenstein, A. Kuna, L. Sojdr, F. Sthal, N. Cholley, and F. Lefebvre, "Significant step in ultra-high frequency stability quartz crystal oscillators", Electronic Letters, v. 46, issue 21, 686 (2010).

The Border Effect in Frequency Processing and the Phase Measurement with Different Nominal Frequency Signal

Wei Zhou, Lina Bai, Zhiqi Li, Faxi Chen, Xiaotian Cao, Yadong Duan
Dept. of Measurement and Instrument, Xidian University, Xi'an 710071,China
E-mail: wzhou@xidian.edu.cn

Abstract

Based on phase coincidence detection technique, the processing and elimination of quantization error is available in digital frequency measurement[1]. Because of the limited resolution of phase coincidence detection, a fuzzy area is found during the detection. The higher precision measuring technique is proposed in the paper by the processing of the border stability of the fuzzy areas. The decisive factor of the measuring precision is the resolution stability of fuzzy area's border, called the border effect[1]. Therefore, the circuit with ns resolution can obtain ps level or higher precision.

Using significant improvements of measuring resolution and the phase variation regularity of periodic signals[5] , through the frequency measurement with continuous phase, the measured frequency signal is compared with its theoretical nominal frequency[3] in multiple periods and with measuring gate time one by one. Eventually, the measurement of phase variation of any measured signal in a wide frequency range can be realized. Because the phase information is obtained between the different nominal frequency signals, higher frequency measurement precision[4] can be realized without any frequency transformation, for example, Table 1.shows the measurement precision with measurement time.

Table 1.the Variation of Measurement Precision with Measurement Time

Measurement Time/s	10	100	1000	10000
Measurement Precision	$6\sim9\times10^{-13}$	$5\sim10\times10^{-14}$	$6\sim11\times10^{-15}$	$7\sim13\times10^{-16}$

The realization of this new technique— phase change measurement or phase change recovery in a wide frequency range, has already provided a novelty approach in the development of time - frequency measurement and control [2]. We have seen its potential influence in other measurements, communication, electronic engineering, navigation positioning[4], etc.. Currently, this technique has already been used in precise phase comparison, frequency standard measurement, time synchronization system with wide frequency range and PLL (phase locked loop). It has also been partly used in frequency link, transmission of accuracy in atomic clock system. A lot of experiments have demonstrated its wide applications in the frequency control field.

References

[1] ZHOU Wei[1], LI Zhi-Qi[2], BAI Li-Na[3],etc. Verification and Application of the Border Effect in Precision Measurement[J]. CHIN. PHYS. LETT. Vol. 31, No. 10 (2014) 100602

[2]Diddams, S. A., Bergquist, J.C., Jefferts, S. R. & Oates, C. W. Standards of Time and Frequency at the Outs et of the 21st Century[J]. Science. 306, 1318-1324 (2004).11:42:4

[3]ZHOU Wei[1] , LI Zhi-Qi[2] , ,YU Jian-Guo[3], etc. A Frequency Measurement Method with Wide Frequency Range Recovery and Keeping Phase Information[P].2014.12.China,Invention Patent, 201410799225.8

[4] David J. Starling, P. Ben Dixon, Andrew N. Jordan, and John C. Howell. Precision frequency measurements with interferometric weak values[J]. Phys. Rev. A 82, 063822 – Published 20 December 2010.

[5]Zhou, W. The Greatest Common Factor Frequency and Its Application in the Accurate Measurement of Peri odic Signals[C]. Proceedings of the 1992 IEEE Frequency Control Symposium. 354-359 (1992).

A new 250nm CMOS low phase noise differential VCO circuit without varactors

Anatoly V. Kosykh, Konstantin V. Murasov Aleksandr N. Lepetaev, Sergey A. Zavyalov,
Omsk state technical university, Omsk, Russia.
E-mail: avkosykh@omgtu.ru

Quartz crystals are widely used as sources of reference frequency for various radio communication systems but they have some temperature dependence of frequency. Compensation of crystal oscillator frequency drift in most cases achieved by connecting in series to resonator voltage controlled capacity (varactor)

In most types of technological processes based on CMOS, implementation of high quality varactor (having high Q, low resistance and the necessary capacitance variability) is not possible. The using of MOS gate capacitance as an integrated varactor is related with a high level of initial gate capacitance and less than 50% ratio of relative tuning. To provide MOSFET gate operation mode as varactors capacitance it is necessary that the gate potential will be smaller than potentials of electrically connected regions of MOSFET drain and source. These requirements are realized by introduction of separation capacitance and supplying a bias voltage to transistor gate. These actions lead to reduction in Q-factor of MOS varactor and to on chip tuning system size enlarging. Moreover, in a number of oscillator circuits, MOS varactors do not apply at all because of it large initial capacitance.

If increasing of tuning range is necessary, switched MOSFET bank of capacitances [2], or combination of capacitances bank and MOS varactor can be used [3].

A fundamentally different way of oscillator frequency controlling may be implemented by changing of oscillator load. Schematic diagram of realized this method differential crystal oscillator is shown at Fig. 1. The differential pair with a negative resistance characteristic is assembled on transistors P3, P5. It should be noted that the use of p-channel transistors as a differential pair allows phase noise reducing at the offsets frequency of 1 kHz to 6 dB. C1, N1 and C3, N4 are used as a variable load circuit. Frequency vs. control voltage characteristic of this circuit has been modeling by special method described in [4]. Changing of control voltage from 0.9 V to 1.8 V leads to output oscillator frequency changing on 1.7 kHz that is more than enough to compensate the temperature dependence of the oscillator frequency

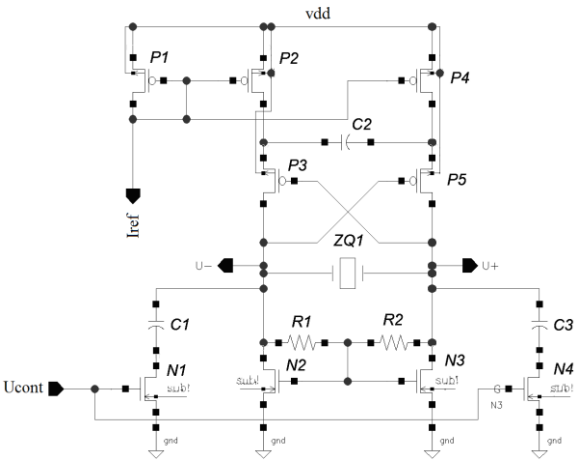


Fig. 1: Differential Xtal oscillator circuit

Nonlinearity of oscillator frequency vs. control voltage curve is about 7.9%. This characteristic with a high accuracy can be approximated as a polynomial of second degree. This non-linearity can be compensated by the introduction of relevant corrections to compensating function synthesizer.

Unlike common VCO based on Pierce oscillator circuit, the differential oscillator circuit has a good own temperature instability, not more than 300 Hz in a temperature range of -60 ... 125 C at commensurate level of phase noise, less than -155 dBc/Hz on offset frequency of 10 kHz.

The sufficient advantage of proposed circuit is considerably expanding of working frequency range in low end as low as a few MHz.

[1] R. L. Bunch, S. Roman, “Large-Signal Analysis of MOS Varactors in CMOS Gm *LC* VCOs”, *Proceedings*, IEEE JOURNAL OF SOLID-STATE CIRCUITS, VOL. 38, NO. 8, pp. 1325 – 1332, AUG. 2003.

[2] US Patent 5117206 A

[3] A. D. Berny, A.M. Niknejad, R. G. Meyer, “A Wideband Low-Phase-Noise CMOS VCO”, *Proceedings*, IEEE Custom Integrated Circuits Conference, pp. 555 – 558, Sept. 2003

[4] S. A. Zavyalov, A. N. Lepetaev, K. V. Murasov, A. V. Kosykh, “The method of modeling of VCO based on SPICE simulation”, *Proceedings* IEEE Frequency Control Symposium, 2009 Joint with the 22nd European Frequency and Time forum, Besanson, France, April 2009, pp. 978-981.

Novel gyroscopic mounting for crystal oscillator (payload) applied in high dynamic host vehicle (platform) to improve its short-term stability

Maryam Abedi, Tian Jin
Beihang University, School of Electronic and Information, Beijing 100191, China
E-mail: abedi_maryam@buaa.edu.cn

When crystal oscillator is used in high dynamic host vehicle, its output will be affected by a large number of environmental effects. One of them is mechanical environment in which crystal oscillator exposed to a variety of dynamic loads. The modulated frequency will disturb the oscillator output and phase noise and frequency jitter will impact oscillator short–term stability.

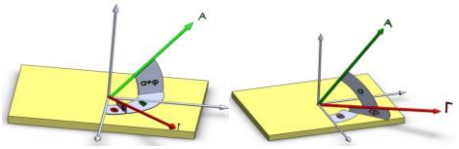


Fig. 1: orientation of applied dynamic load and g-sensitivity of quartz crystal (left) general state,(right) critical state (β=0)

In crystal oscillator; phase noise and frequency jitter calculated as:
Frequency jitter (τ=1s): $\Delta f = \Gamma.A\ f0 = f0\ \Gamma\ A \cos\alpha \cos\beta$ (Hz);
Phase jitter (Bn=1 Hz): $\Delta\varphi = 2\pi \int \Delta f\, dt = 2\pi\ f0\ \Gamma. \int A\, dt$ (rad);
Phase noise: $L(f) = 20 \log|\Delta\varphi/2|$ (dBc/Hz).

In order to reduce phase noise and frequency jitter, each mentioned parameter will be studied. Since frequency jitter is a function of α and β cosine, therefore when A moves away from Γ, improvements give arise in phase noise and frequency jitter. The first idea to suppress these disturbances is to fix the applied dynamic load perpendicular to Γ in any given moment. Since the angular orientation and magnitude of Γ is different from one given crystal to the other, the implementation of this idea is not feasible. As statistical study of angle φ in different crystal blanks shows that in most cases this angle tends to be close to the crystal surface not perpendicular to it (median value with 20% safety margin is $|\varphi|=30°$), The main idea is to hold the dynamic applied load perpendicular to the crystal surface in any given moment. By this method, angle α is increased as far as possible, therefore for a specified range $|\beta| < \cos^{-1}(\sin\varphi/\cos\alpha)$, phase noise and frequency jitter are reduced.

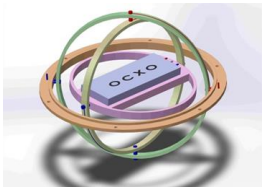
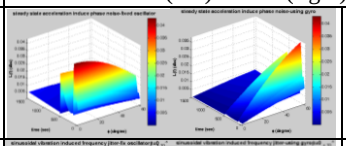
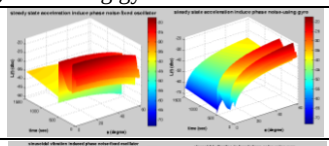
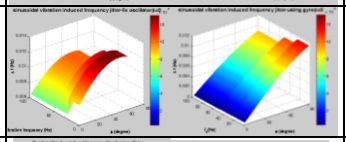
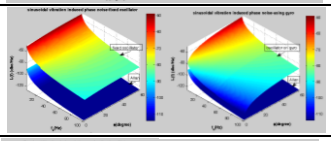
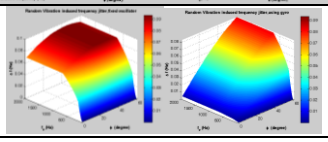
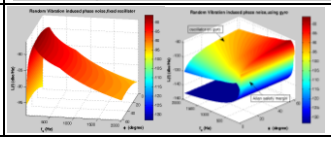


Fig. 2: gyro-mounting

In order to implement this idea a mounting is designed and manufactured for crystal oscillator for electronic board. Its structure is similar to gyroscope, so it is called as gyro-mounting. Numerical analysis is provided to illustrate the function of this mounting by assumption of GPS disciplined OCXO, f0=10.23 (MHz), Γ=10^ (-9) and Q factor=10^ (11), as a payload on launch vehicle ARIAN 5. The performances are compared under the dynamic environment before and after using gyro mounting.

A (Dynamic load)	Frequency jitter (Δf) (left) before (right) after using gyro	Phase noise L(f)	Max gyro effect on (Δf) (Hz)	Max gyro effect on L(f) (dBc/Hz)	Explanation
Steady state acceleration			-0.0414	-29.14	Gyro changes the disturbances, form most probable cases (φ<30°) to low probable ones.
Sinusoidal Vibration (2-100 Hz)			-0.0081	-25.43	In some cases Gyro reduces disturbances close to Allan deviation safety margin.
Random vibration (2-2000 Hz)			-0.0653	-26.43	In some cases Gyro reduces disturbances below Allan deviation safety margin.
attitude changes	Gyro-mounting Suppresses all attitude changes induced disturbances totally.				

[1] "Arian 5 User's Manual Issue 5", Revision 1, July 2011.
[2] Jaap Wijker, "Random Vibrations in Spacecraft Structures Design", © Springer Science +Business Media B.V.2009.
[3]Jacob Job Wijker,"Spacecraft Structures", © 2008 Springer Science-Verlag Berlin Heidelberg.
[4] John R.Vig, Arthur Ballato, "Frequency Control Devices", U.S Army Communications-Electronics Command,AMSEL-RD-C2-PT.

Frequency Performance of the New Horizons Ultra-stable Oscillators: Nine years of Continuous In-flight Monitoring

Jensen, J. Robert , Weaver, Gregory L.
Space Exploration Sector, Johns Hopkins University Applied Physics Laboratory, Laurel, MD/USA
E-mail: Bob.Jensen@jhuapl.edu

The New Horizons (NH) mission to the Pluto and subsequent exploration of the Kuiper Belt structure in our outer solar system is expected to achieve a major mission goal by its impending flyby of the Pluto-Charon double planet in July 2015. One of the primary science objectives for NH during the Pluto-Charon flyby is the chemical characterization of any possible atmosphere at Pluto, including assessment of atmospheric density and dynamic interaction with Pluto's surface. The measurement of Pluto's possible atmosphere will be accomplished by an NH on-board radio science experiment, known as REX. To achieve its science objectives, REX requires the frequency stability of an ultra-stable oscillator (USO) with Allan deviation of no more than $1x10^{-13}$ over time intervals from 1 to 1000 s.

REX is non-traditional in that signal interrogation will be performed on-board NH using the uplink provided by the NASA Deep Space Network ground stations. This is because, at over 30 AU from Earth, the NH downlink S/N would be too low to achieve the desired science return [1]. The two JHU/APL USOs A & B onboard NH are allowed to continuously operate during the spacecraft's flight to Pluto-Charon to assure the maximum state of readiness for REX, while improving their frequency stability and reducing drift (aging). Fig. 1 shows the placement of USOs A & B on the spacecraft. As well as supporting REX, the USOs provide the signal reference for the spacecraft's transceiver and non-coherent navigation system.

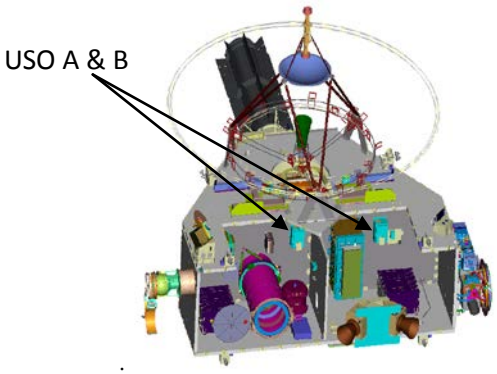


Fig. 1: The New Horizons spacecraft carries two JHU/APL ultra-stable oscillators (USO) to support the REX, radio science experiment of Pluto's possible atmosphere

The NH non-coherent navigation system provides the opportunity for precise determination of USO's A & B in-flight frequency performance during the entirety of every downlink pass [2]. This represents an unprecedented amount of data for USOs in deep space. In this paper, we will report on the frequency stability of each USO over the nine years since launch. We will discuss the treatment of general and special relativity, including the Shapiro delay. The frequency performance of each NH USO demonstrates distinct interactions with various space environments, such as with Jupiter's radiation belt in Feb. 2007 and the impact of the normal 5 RPM spin rate on the two USOs. The frequency drifts of USO A & B are currently $-0.83x10^{-12}$/day and $+0.90x10^{-12}$/day, respectively. It is possible both USOs may be on the cusp of a re-curve in their drift behavior. We will discuss our confidence in this possibility, and any concern to the performance of REX.

[1] G. L. Tyler, and et al., "The New Horizons radio science experiment (REX)," Space Science Reviews, Springer+Business Media, vol. 140, nos. 1-4, pp. 217-259, 2008.

[2] C. C. DeBoy, and et al., "The RF telecommunications system for the New Horizons mission to Pluto," *Proceedings*, 2004 IEEE Aerospace Conference, Big Spring, MT, paper #1369, version 4, pp.1463-1478.

A CMOS LC-Based Frequency Reference with ±40ppm Stability from -40°C to 105°C

D. Gaied, M. Khairy, M. Atef, A. Ahmed , M. Shadoufa, A. Hassanein, O. El-Aassar, M. Gamal, A. El-Sayed, A. Badawy, A. Adel, M. Erfan, N. Sinoussi and A. Helmy
Timing Products Division, Si-Ware Systems, Cairo, Egypt
E-mail: nabil.sinoussi@si-ware.com

For decades, quartz Crystal Oscillators (XOs) have been the de facto reference clock generators in electronic applications. They exhibit excellent frequency stability and phase noise performance. However, XOs impose stringent limitations on the cost and integration of electronic systems. This has driven a lot of research efforts to replace XOs by a cost efficient CMOS integrated solution.

In previous work [1–2], a CMOS Self-Compensated Oscillator (SCO) based on LC tank Temperature Null (TNULL) has been introduced. The SCO utilizes various oscillator architectures to force the LC tank to operate at its specific TNULL phase (Φ_{NULL}), where the oscillator frequency deviates only few tens of ppms across a given temperature range. The SCO can achieve ±100ppm frequency stability from -40°C to 85°C [2]. However, the frequency stability depends mainly on the tank circuit structure which limits the capability of the SCO to expand its temperature range.

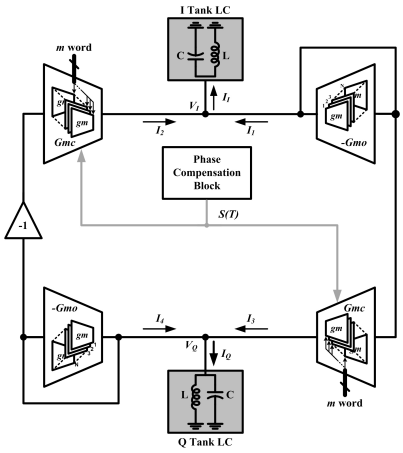


Fig. 1: Proposed phase compensation technique applied on a quadrature SCO.

This paper demonstrates a novel phase compensation technique which improves the SCO frequency stability significantly. Fig. 1 shows the quadrature SCO architecture [1] with the proposed technique applied. The phase compensation block generates a temperature dependent signal ($S(T)$) which modulates the coupling transconductance (G_{mc}). The variation of G_{mc} causes a temperature dependent modulation of the LC tank phase around the nominal TNULL phase. This, in turn, results in a temperature dependent frequency shift. The induced frequency shift is controlled to cancel the inherent frequency deviation of the SCO while operating at TNULL.

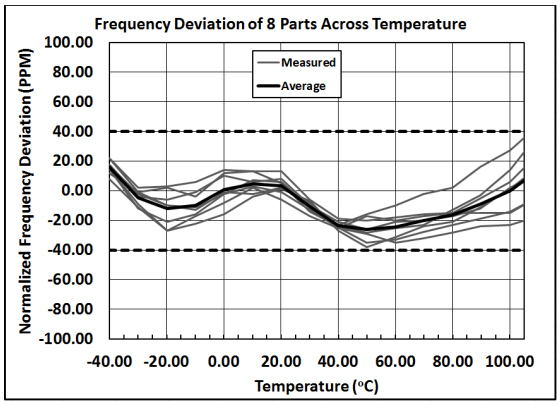


Fig. 2: Frequency deviation across temperature of 8 SCO parts utilizing the phase compensation technique. The output frequency is 25MHz.

The phase compensation block is integrated with the SCO in a standard 0.18µm CMOS technology. Fig. 2 shows the measured frequency deviation across temperature of 8 ceramic packaged SCO parts producing a 25MHz clock. Utilizing the new phase compensation technique, the SCO achieves a unique frequency stability of ±40ppm across the temperature range: -40 – 105°C. The novel technique paves the way to extend the SCO operation even further satisfying the requirements of automotive and industrial applications.

[1] A. Ahmed *et al.*, "A Highly Stable CMOS Self-Compensated Oscillator (SCO) Based on an LC Tank Temperature Null Concept," *Proceedings*, 2011 IEEE Int. Frequency Control Symp., San Francisco, California, May 1-5, 2011, pp. 443-447.

[2] N. Sinoussi *et al.*, "A Single LC Tank Self-Compensated CMOS Oscillator with Frequency Stability of ±100ppm from -40°C to 85°C," *Proceedings*, 2012 IEEE Int. Frequency Control Symp., Baltimore, Maryland, May 21-24, 2012, pp. 1-5.

2015 Joint IFCS-EFTF; Abstract for Submission

Practical Crystal Oscillator Parameter Measurement

Bischof, Glenn E.
Itron, Inc., West Union, South Carolina/U.S.A.
E-mail: glenn.bischof@itron.com

Verification of the selection of a quartz resonator, printed circuit layout of the oscillator circuit, and performance of the oscillator under environmental conditions is often neglected in rapid development of products utilizing highly integrated components with internal oscillator circuitry. This is often due to a lack of expertise and perceived equipment requirements in small to medium-sized development groups.

Simple, inexpensive procedures and techniques are presented which allow designers without quartz crystal oscillator design experience to analyze the component requirements for reference-design based oscillator circuits utilizing AT-cut quartz resonators. Published specifications for the oscillator sections of very highly integrated circuits are rarely sufficient for external component selection and PCB layout for reliable product design. This is particularly true of custom Application Specific Integrated Circuits (ASICs) designed by third parties. Experimental verification is usually required to avoid surprises in the form of field returns. The same techniques can often be applied to root cause analysis of oscillator field failures.

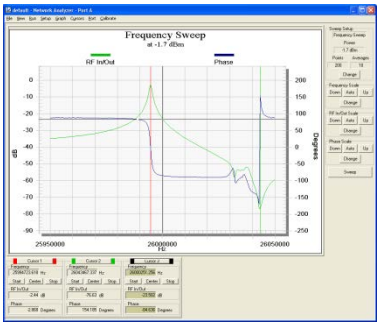


Figure 1 Crystal Parameter Measurement

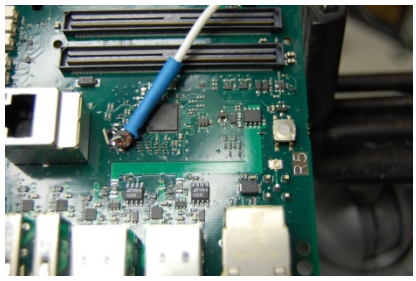


Figure 2 Crystal Current Measurement.

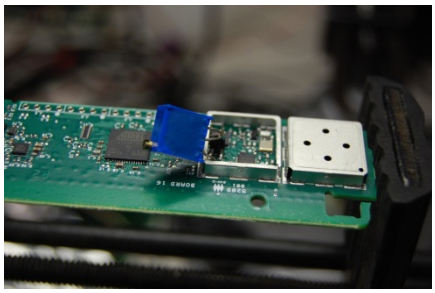


Figure 3 OSF Measurement.

Techniques are presented for using a spectrum analyzer with a tracking generator to measure the transfer characteristics of the crystal resonator, as illustrated in **Figure 1**. These parameters include static capacitance, resonant resistance, motional capacitance and inductance, and load-resonant frequency error.

Once the resonator parameters are measured, the remaining circuit parameters, such as stray capacitance, drive level (see Figure 2), Oscillation Safety Factor (see Figure 3), start-up time, jitter, and environmental dependencies of the oscillator circuit can be measured or calculated. Readily available equipment and home-made probes are the only required tools.

References

[1] Rose, D. “Load Resonant Measurements of Quartz Crystals” Saunders & Associates, Phoenix, Arizona, U.S.A.:.,. Pp 2-20, April 19, 2003.

[2] Engelson, Morris, “Crystal Device Measurements Using the Spectrum Analyzer”, Tektronix, Inc., Beaverton, OR, pp 2-8 February, 1977.

Effects of Pressure and Bias Voltage on the Phase Noise of CMOS-MEMS Oscillators

Wan-Cheng Chiu[1], Ming-Huang Li[1], Chao-Yu Chen[1], and Sheng-Shian Li[1,2]
[1]Inst. of NanoEngineering and MicroSystems, [2]Dept. of Power Mechanical Engineering
National Tsing Hua University, Hsinchu, Taiwan
E-mail: wancheng5990@gmail.com

In this work, we present a comprehensive study on the effects of environmental pressure (P) and resonator dc-bias voltage (V_P) for the phase noise (PN) of a monolithic CMOS-MEMS oscillator. The contributions of this work are: (1) demonstration of the ***lowest PN for a monolithic CMOS-MEMS oscillator at P = 760 Torr***, and (2) ***investigation of the phase noise at low V_P and low Q-factor*** under various operation conditions. In order to access the practical utility of CMOS-MEMS oscillators for versatile applications, a double-ended tuning fork (DETF) MEMS resonator oscillator [1] is used as a case study. The squeeze-film damping is expected to be the main loss mechanism that limits the Q-factor of the DETF resonator in ambient pressure (P = 760 Torr, Q = 150). In the ambient pressure, the oscillation ensues at a minimum V_P = 30V and shows a PN of -86 dBc/Hz at 1-kHz offset and -99 dBc/Hz at 1-MHz offset. The PN can be further improved using elevated dc biasing (e.g., V_P = 90V), which is a possible implementation in future if HV-CMOS or BCD technology platform is applicable. Moreover, if a vacuum-package is applied to the CMOS-MEMS oscillators, the required V_P for oscillation is dramatically reduced. In this work, a low-V_P CMOS-MEMS oscillator ***with IC compatible voltage (i.e., V_P = 3V, an equivalent motional impedance R_m of 100 MΩ)*** is also demonstrated in a vacuum chamber (P < 1 mTorr) with a PN of -94 dBc/Hz at 1-kHz offset and -98 dBc/Hz at 1-MHz offset, respectively.

Fig. 1 presents the measured frequency spectra of a CMOS-MEMS DETF resonator with on-chip amplifier, which shows the Q-factors of 1,700 in vacuum and 150 in air. Fig. 2(a) shows the oscillator phase noise under P = 760 Torr while the best-case PN is demonstrated at V_P = 90V. The oscillator performance is comparable to other state-of-the-arts that operated in air [2][3]. Fig. 2(b) shows the oscillator PN (operated in vacuum) with low-V_P (3V, R_m = 100MΩ) and high-V_P (33V, R_m = 1MΩ). The MEMS oscillator circuit typically consumes 1.3 mW.

[1] M.-H. Li, *et al.*, "Optimizing the close-to-carrier phase noise …," *Proc.*, *IEDM 2014*, pp. 22.3.1-22.3.4, Dec. 2014.
[2] J. Verd, *et al.*, "Monolithic CMOS MEMS …," *IEEE Electron Device Lett.*, vol. 29, no. 2, pp. 146-148, Feb. 2008.
[3] J. Pettine, *et al.*, "Power-efficient …" *IEEE Trans. Biomed. Circuits Syst*, vol. 6, no. 6, pp. 542-551, Dec. 2012.

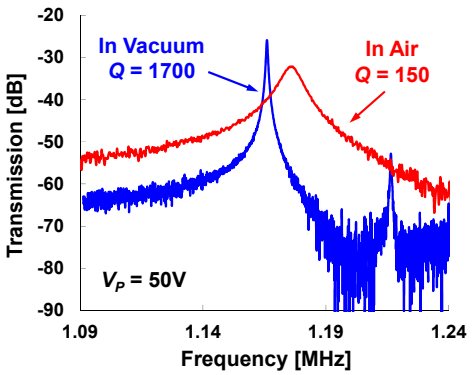


Fig. 1: Frequency responses of a CMOS-MEMS DETF resonator with amplifier. The measured Q-factor is 150 in air. The resonant spectra are taken from distinct chips.

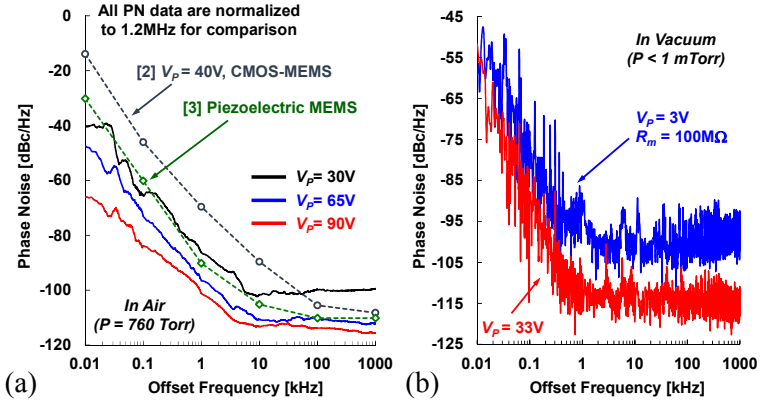


Fig. 2: (a) Comparison of PN for MEMS oscillators operated in air. All phase noise data are normalized to 1.2 MHz. (b) PN for CMOS-MEMS oscillators operated in vacuum. The resonator motional impedance (R_m) is around 100 MΩ for V_P = 3V and 1 MΩ for V_P = 33V.

Effect of the Nonlinearity in the Phase noise of a Monolithic MEMS on CMOS oscillator

G. Sobreviela, M. Riverola, A. Uranga, N. Barniol, E. Marigó* and M. Soundara Pandian*
Dept. of Electronic Engineering, Universitat Autònoma de Barcelona, Cerdanyola del Vallès, Spain
*SilTerra Malaysia Sdn Bhd, Kulim Hi Tech Park, Malaysia
E-mail: guillermo.sobreviela@uab.es

CMOS-MEMS oscillators are the technological alternative against oscillators based on quartz crystals since they can meet the current requirements of a market sector which demands higher integration capability reducing manufacturing cost for time reference systems. Despite this technological interest CMOS-MEMS oscillators suffers from a poor frequency stability (low phase noise) [1, 2, 3]. In this paper the effect of the nonlinearity of the MEMS resonator and the sustaining-amplifier over a 24MHz MEMS-on-CMOS oscillator is empirically studied.

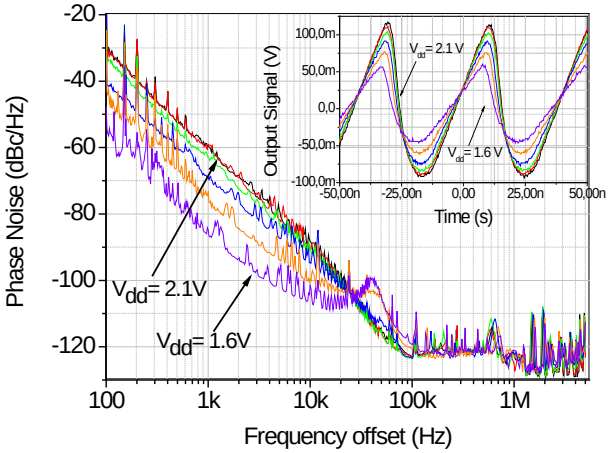


Fig.1 Phase noise behavior for the resonator biasing voltage V_{Bias} = 20V and a set of values for the power supply of the sustaining-amplifier (V_{dd}), from 2.1V to 1.6V with a step increase of 0.1V. Inset: Time response of the MEMS oscillator.

A paddle shaped out-of-plane MEMS resonator device has been implemented on top of a CMOS chip using the CMOS Silterra 0.18 µm commercial CMOS technology [4]. Electrostatic excitation and capacitive detection is used to interact with the MEMS. An electrical characterization of the MEMS resonator has been performed. The frequency response of the MEMS resonator has been measured in an open loop configuration for a set of excitation amplitude power values from -20dBm to 10dBm. As a result the linear/nonlinear region of operation of the resonator can be determined, being the critical power value -5dBm @ V_{Bias} = 20V. The phase noise of this MEMS-on-CMOS oscillator has been measured for different values of V_{dd} (CMOS amplifier power supply) and a fixed resonator biasing voltage of V_{Bias} = 20V, as is show in Fig 1. The variation of V_{dd} produces variations on the non-linear operation region of the MEMS resonator and the amplifier, obtaining as a result a decrease in the phase noise near the carrier frequency while the floor noise remains constant. Specifically an important improvement as large as a reduction of 25 dBc/Hz @ 1 kHz carrier offset on the phase noise is achieved, indicating the influence of a linear/non-linear operation for the MEMS resonator and the amplifier circuit.

[1] J. Verd et al. “A 3V CMOS-MEMS oscillator in 0.35um CMOS technology” Transducers and Eurosensors XXVI, pp. 806-809. 2013

[2] M-H Li et al. “Foundry-CMOS Integrated Oscillator Circuits Based on Ultra-Low Power Ovenized CMOS-MEMS Resonators”. IEDM13, pp 18.4.1-18.4.4. 2013

[3] Wen-Lung Huang et al. “Fully Monolithic CMOS Nickel Microelectromechanical Resonator Oscillator”. MEMS 2008, pp 10-13. 2013

[4] A. Uranga et al. “Dual-Clock with Single and Monolithical 0-Level Vacuum Packaged MEMS-on-CMOS Resonator”. MEMS 2015

1/*f* noise of quartz resonators: Measurements, modelization and comparison studies

Sthal Fabrice*, Devel Michel*, Imbaud Joel*, Bourquin Roger*, Bakir Ahmed*, Vuillemin Cedric*, Ghosh Santunu*, P. Abbe*, D. Vernier* and G. Cibiel+

*FEMTO-ST Institute, UFC, CNRS, ENSMM, UTBM, Besançon 25000, France

+Microwave and Time-Frequency, CNES, Toulouse 31000, France

E-mail: fsthal@ens2m.fr

The Centre National d'Etudes Spatiales (CNES), Toulouse, France and the FEMTO-ST Institute, Besancon, France, investigate the origins of noise in bulk acoustic wave resonators [1]. Several European manufacturers of high quality resonators and oscillators are involved in this partnership to achieve resonators. For this investigation, quartz crystal resonators have been cut from a quartz crystal block supplied specifically for this study on 1/*f* noise. This crystal block was grown from a seed which originated from a previous synthetic crystal which was grown from a natural seed. This kind of synthetic crystal is usually used to grow new generations of quartz crystal blocks.

In this paper, the reader is reminded the description of the resonator realization and the topology of the resonator prototype is exposed. The resulting resonators are SC-cut with a 5 MHz resonant frequency. A comparison of these resonators is given in terms of motional parameters. Then, we report the noise measurements made on these quartz crystal resonators using an advanced phase noise measurement system. Phase noise measurements on several batches of resonators are given. The resulting short term stability of some resonators has been measured lower than $8 \cdot 10^{-14}$. Fig. 1 shows the noise floor of the fractional frequency stability.

The noise results are discussed according to the position of the resonators inside the crystal block and several physical analyses of the crystal (inclusion, dislocation). The results are also compared according the Q-factors measured at room temperature and at low temperature. Measurements of resonator parameters have been done at low temperature in order to correlate them with noise results and expecting crystal defects. Theoretically, an approach, based on the fluctuation-dissipation theorem, is used in order to put numerical constraints on a model of 1/*f* noise caused by an internal (or structural) dissipation proportional to the amplitude and not to the speed. The order of magnitude of the noise is then discussed.

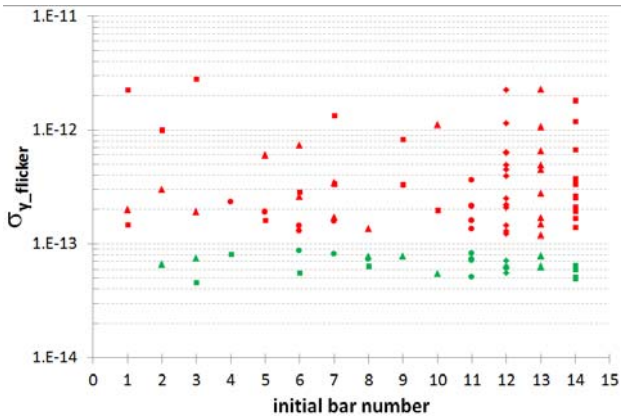


Fig. 1: Figure 1: Short-term stability of quartz crystal resonators according to the position in the mother block.

[1] S. Ghosh, F. Sthal, J. Imbaud, M. Devel, R. Bourquin, C. Vuillemin, A. Bakir, N. Cholley, P. Abbe, D. Vernier, G. Cibiel, "Theoretical and experimental investigations on 1/f noise of quartz crystal resonators," *Proceedings,* 2013 IEEE Joint UFFC, EFTF and PFM Symp., Prague, Czech Republic, 21-25 July, pp. 737-740.

Ultra Low Noise Frequency Divider

R. Boroditsky, J. Gomez,

NEL Frequency Controls, 357 Beloit Street, Burlington, WI 53105

Some applications, namely non-invasive medical monitoring, require Ultra Low Phase Noise Precision Frequency sources at lower than usually used in other industries frequencies in the range of 2 – 3 MHz. These requirements present challenges in several areas: availability of high quality low frequency crystal resonators, and real estate limitations. Low frequency resonators, even if available are much larger in size. Another option is to use crystal resonators in more conventional frequency range (8 – 12 MHz) and divide the frequency down. Available off the shelf frequency dividers, however, introduce significant phase noise degradation. The purpose of this work was to develop a divider with much improved phase noise performance with virtually no additional degradation. That goal was accomplished by combining "brute force" noise de-correlation with other innovative techniques. The result was the OCXO in small package (37x26x16 mm "Europack"), output frequency range 2 to 4 MHz and ultra low phase noise closely following 20 Log(N) law close to the carrier. Example of a phase noise plot at 3.000 MHz is presented on Fig.1.

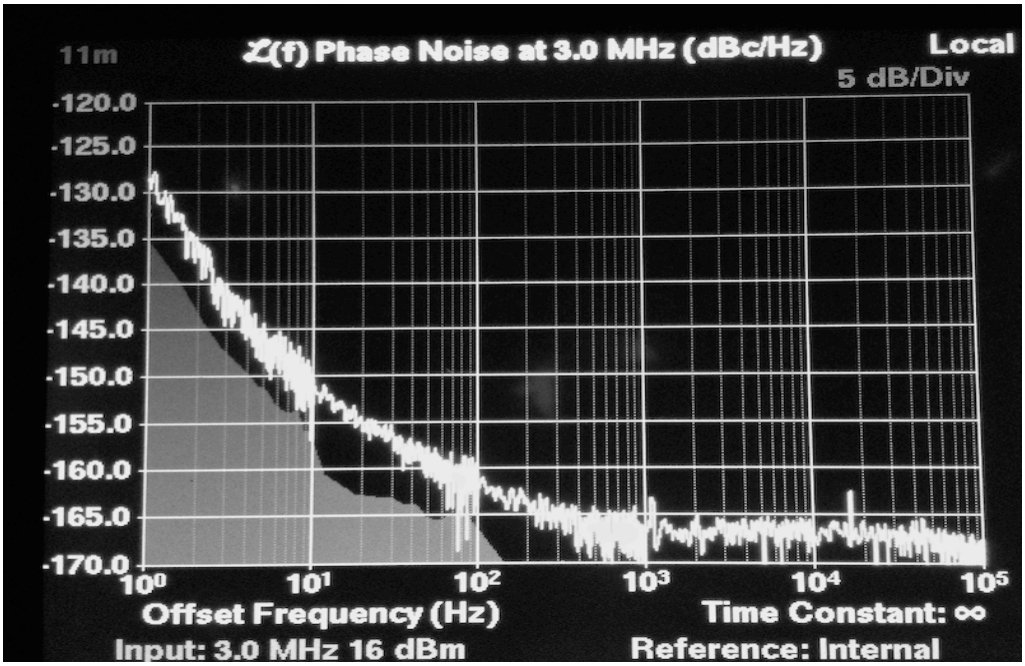


Fig.1. Phase Noise Plot of 3.000 MHz OCXO with ultra low noise divider

Low He Permeation Cells for CSACs

Dellis A., Knappe S., Donley E. A., Kitching J.
National Institute of Standards and Technology, Boulder, Colorado 80305, USA
E-mail: argyrios.dellis@nist.gov

Chip Scale Atomic Clocks (CSACs) [1] have been successfully used as low cost and low power frequency standards for about a decade. Their long-term stability is affected, among other parameters, by changes in the buffer gas pressure. Usually the windows of CSAC cells are made of Pyrex, a material known to be permeable to Helium. It can be estimated that atmospheric Helium can diffuse through the Pyrex, causing a drift in the clock frequency of about 10^{-12}/day. This result is consistent with the observed drift in CSACs after several years of operation. Replacing Pyrex with a low permeation rate material such as alumino-silicate glass (ASG) may solve the problem and improve the stability of the clock.

We have identified a suitable source of ASG that is fabricated in wafer form and can be anodically bonded to silicon. Moreover we have successfully fabricated micro-machined alkali vapor cells using this type of glass for the optical windows and we have developed a method for measuring the permeation rate. We have measured the permeation rate of ASG in our microfabricated cells and it was found to be about a factor of 100 lower than that of Pyrex at 90^{o}C. This result suggests that alumino-silicate glass can be used to suppress Helium permeation in microfabricated cells and thus can improve the long-term stability of chip scale atomic clocks.

In the future, alumino-silicate glass windows could be used in combination with passive pumping techniques, such as non-evaporable getters, in order to completely replace large vacuum pumps. In this way they could contribute to the miniaturization of instruments and sensors based on laser-cooled atoms [2].

[1] Knappe, S., Shah, V., Schwindt, P. D. D., Hollberg, L., Kitching, J., Liew, L.-A., & Moreland, J. (2004). A microfabricated atomic clock. *Applied Physics Letters*, *85*(9), 1460.

[2] Hoth, G. W., Donley, E. A., & Kitching, J. (2013). Atom number in magneto-optic traps with millimeter scale laser beams. *Optics Letters*, *38*(5), 661–3.

A CSAC based on CPT in Spaceon

Runchang Du, Yuanhong Cao, Leiji Liu, Lin Yang, Xingshi Zhen

Chengdu Spaceon Electronics, Chengdu, China

Email: sccyh@163.com

Traditional atomic clocks, including Rb clock, H-Maser and Cs beam, have excellent specialty in comparison with Cristal oscillator in frequency stability and accuracy. Unfortunately, the size, power dissipation and cost of the traditional clock cannot be shortened to the average level of Cristal oscillator, which always blocks application in telecom and other industry. Chip-Scale Atomic Clock (CSAC), a novel clock based on Coherent Population Trap (CPT), has no cavity and takes use of substitution in pump source by Laser to spectrum lamp. Therefore, the absorption cell can be made by Micro-Electromechanical System (MEMS) procession, and the cell will be downsized to millimeter scale. Among Laser development, a VCSEL diode arising recently has very low power dissipation and can be used as the optical pump source with bare chip. Therefore, the CPT atomic clock could be fabricated by semiconductor procession, such as MEMS and CMOS. In fact, the first CSAC has been made by Symmericom, and other companies have been studying and developing that clock after the prototype of CPT atomic clock was made by NIST. In recent years, a CSAC based on CPT has been developed in China.

There are several techniques adopted to mitigate its size and power in the CSAC. Firstly, atom cell is made by MEMS. In this way, there are many holes corroded in the silicon plate, and the atom produced by chemical activity will be filled into the holes before the silicon plate was bound with two glass plates. Subsequently, the tiny cell is assembled with VCSEL diode, quarter wavelength plate and photocell, and the physics system will be enclosed into a package in vacuum chamber in order to depress convection. Finally, a special 3.4GHz chip was designed and fabricated. This chip has 35mW power and -50dBc@1Hz phase noise, which ensures that the layout of the whole electronics can be allocated on a small board and the phase noise can not affect the clock's frequency stability.

In this clock, a Micro-Control Unit (MCU) with embodied program is to lock VCSEL wavelength, TCXO frequency with atomic fluorescence and CPT line simultaneously. The frequency standard is compensated according as VCSEL intensity fluctuation while environment temperature was changed. After developing the clock and optimizing the parameters, the CSAC demonstrated a performance with a frequency aging of -1.4×10^{-11} per day and a frequency stability is better than $3\times10^{-10}\tau^{-1/2}$ ($1 \sim 100$s). The volume of the CSAC is 24ml, and a consumed power is 0.6W at 25℃.

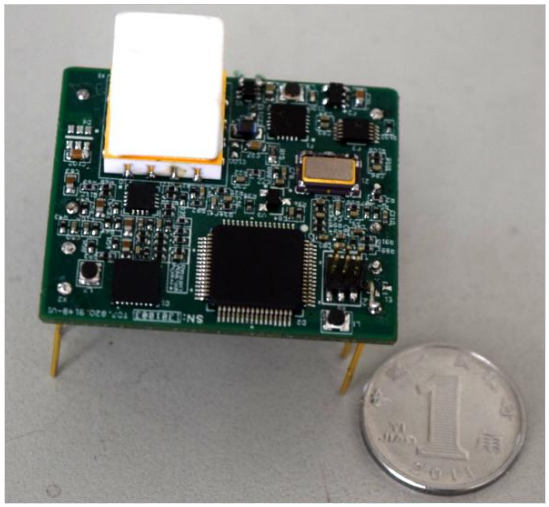


Fig. 1: The CSAC prototype without case. The white cubic structure is the physics package, and the besides are the whole electronics board.

The CSAC could be used in navigation satellite receivers, underwater navigation, and data chain of weapon system.

Quantime: low cost miniature atomic clock for telecom

Berthoud Patrick, Haldimann Manuel, Schneller Luc, Ducommun Christophe, Affolderbach Christoph*, Stojanovic Marko+, Farine Gaël+, Pétremand Yves°, Michaud Alain

Oscilloquartz SA, CH-2000 Neuchâtel, Switzerland
*University of Neuchâtel, CH-2000 Neuchâtel, Switzerland
+Ecole Polytechnique Fédérale de Lausanne, CH-1000 Lausanne, Switzerland
°Centre Suisse d'Electronique et de Microtechnique SA, CH-2000 Neuchâtel, Switzerland
E-mail: michaud@oscilloquartz.com

Frequency reference sources play a central role in telecommunication systems as being the heart of the synchronization network. With the migration from Frequency Division Multiplexing to Time Division Multiplexing, those reference sources require frequency accuracy in addition to frequency stability. Various reference sources cohabit in telecom networks going from cesium beam primary reference clock, GNSS receivers, rubidium vapor cell secondary standards and quartz oscillators. In case of failure of primary reference signals, quartz oscillators have to guarantee time holdover performances (sub-microsecond) for increasing holdover period (up to three days). Low cost quartz technology has reached its performance floor with some microseconds holdover over one day, which are mainly limited by residual thermal sensitivity, thermal hysteresis and long-term aging. The development of Chip Scale Atomic Clock, its proved performances and its capability to be mass produced yield this technology to replace quartz technology providing that the cost remain limited.

Oscilloquartz has started its Quantime development for a miniature atomic clock in partnership with three local technology labs. Its goal is to design an electronic component of volume $\leq 51\text{x}51\text{x}15$ mm^3, of power consumption ≤ 2 W, of frequency stability $\sigma_y(\tau) \leq 6\text{E-}10\ \tau^{-1/2}$ and of cost ≤ 200 USD. The physics package architecture is based on Coherent Population Trapping (CPT) of cesium atoms. The design has been oriented with off-the-shelf components, except for the cesium cell which is micro-fabricated with semiconductor wafer technologies (deep reactive ion etching, cesium dispensing, buffer gas filling and anodic bonding). The Fig. 1 shows the first Quantime prototype with the Physics Package integrated on the Electronics Package. All clock functionalities have been demonstrated (Cs cell and laser thermal regulation, laser frequency servo, CPT signal generation and frequency lock loop of the local oscillator on the atomic reference signal). The short-term frequency stability has been measured at $\sigma_y(\tau) = 1.5\text{E-}10\ \tau^{-1/2}$ up to $\tau \leq 500$ s, which complies with our goals. Long-term frequency stability improvement is under investigation.

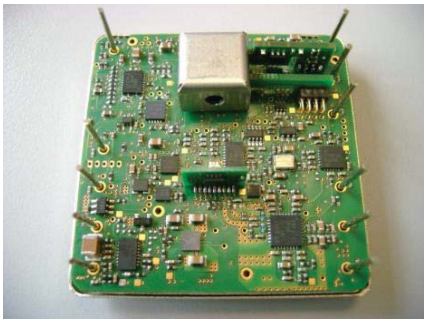


Fig. 1: Quantime miniature atomic clock prototype

This development has been partially financially supported by the Swiss Commission for Technology and Innovation (project number 13'818.2).

Double Resonance Spectroscopy Using a Magnetron-type Microwave Cavity for Compact Rubidium Frequency Standards

Hyun-Gue Hong, Sang Eon Park, Sangmin Lee, Myoung-Sun Heo, Sang-Bum Lee, Taeg Yong Kwon, Sin Hyuk Yim*, and Chang Bok Lee

Center for Time and Frequency, Korea Research Institute of Standards and Science, Daejeon, South Korea

* Agency for Defense Development, Daejeon, South Korea

E-mail: hghong@kriss.re.kr

The magnetron-type cavity is useful for building a compact cavity-based microwave interrogation component in an atomic clock [1]. Its dimension can be reduced well below the wavelength of the clock transition without degradation in the uniformity of the field. Thus it enables reduction in the volume, mass, and power consumption of the entire physics package, which is attractive for portable and space application.

We report on a recent progress at KRISS in the development of a compact laser-pumped Rb clock using the magnetron cavity of 66 cm^3 in volume. The cavity design is based on the finite-element-method simulation to include the frequency shift due to the vapor cell as well as the critically coupled microwave coupling antenna. The distributed Bragg reflector laser, stabilized in a compact setup with its stability better than $10^{-12}\ \tau^{-1/2}$, is used.

We obtained the continuous-wave double-resonance spectrum from a ^{87}Rb buffer-gas-filled vapor cell installed in our cavity. At optimal power of optical and microwave fields, we observed a Lorentzian signal having 233 Hz linewidth (full width at half maximum) with 28% contrast.

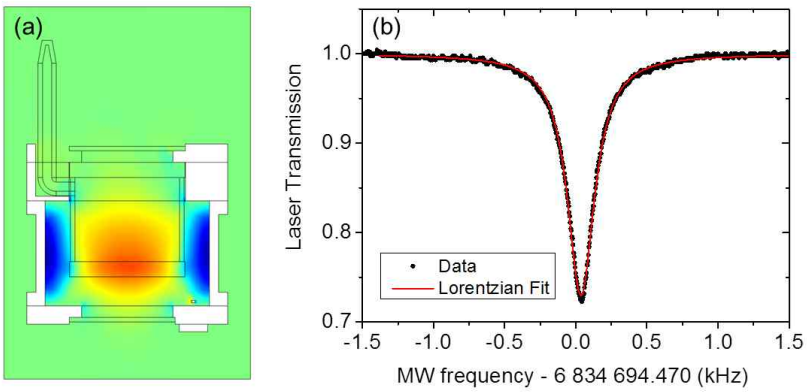


Fig. 1: (a) The magnetic field distribution along the quantization axis (vertical) obtained from the simulation using COMSOL Multiphysics®. (b) Double resonance spectrum of the magnetically insensitive transition (0-0) of rubidium ground state.

[1] C. Stefanucci, T. Bandi, F. Merli, M. Pellaton, C. Affolderbach, G. Mileti, and A. K. Skrivervik, "Compact microwave cavity for high performance rubidium frequency standards," Rev. Sci. Instrum., vol 83, pp.104706, Oct. 2012.

Estimation of the light shift in Ramsey- Coherent Population Trapping

Yuichiro Yano, Shigeyoshi Goka, Masatoshi Kajita*
Graduate School of Science and Engineering, Tokyo Metropolitan University, Hachioji, Tokyo Japan
*National Institute of Information and Communications Technology, Koganei, Tokyo Japan
E-mail: yano-yuichiro@ed.tmu.ac.jp

The light shift is one of the limitations for long-term frequency stability in CPT atomic clocks [1]. The Raman-Ramsey scheme significantly reduces the light shift to one or two orders of magnitude lower than that under continuous wave illumination. In our previous work, we investigated the light shift in the Raman-Ramsey scheme from both theoretical and experimental sides [2]. However, the relationship between the light shift and the pulse parameters, especially in terms of the free evolution time T and excitation duration time τ, is still unclear. In this work, we propose an estimation equation of light shift in Ramsey-Coherent Population Trapping (CPT) for enhancing long-term stability of Ramsey-CPT atomic clocks. The proposed equation expresses the relationship between light shift and all pulse parameters.

The estimation equation of light shift S is found to be

$$S = \frac{\tau_{\text{eff}}}{\tau_{\text{eff}} + Te^{-\tau_m/\tau_p}} S_{cw}$$

$$\because \tau_{\text{eff}} = \tau_p(1 - e^{-\tau/\tau_p})$$

S_{cw} is the light shift under cw illumination, which is proportional to the light intensity I ($S_{cw} = \alpha_{cw} I$). τ_p is the pumping time, which is inversely proportional to the light intensity[3].

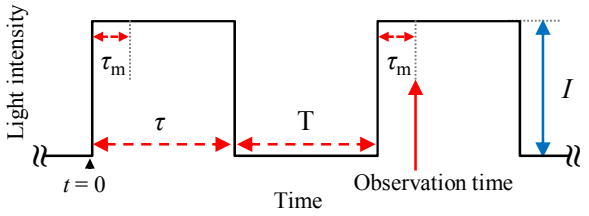


Fig. 1: Ramsey pulse sequence: τ is the excitation time, T is the free evolution time, and τ_m is the resonance signal observation time.

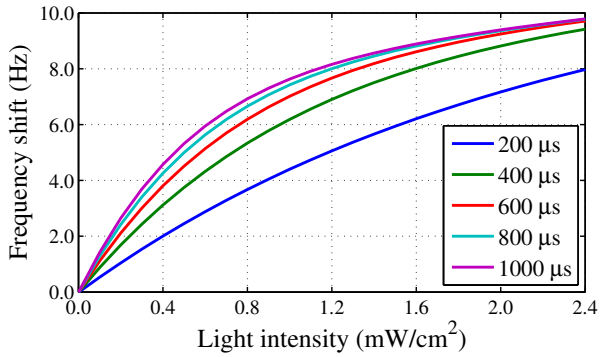


Fig. 2: Light shift as a function of light intensity under different excitation time τ. The free evolution time and the observation time are set to 800 µs and 10 µs, respectively.

Figure 2 shows the light shift as a function of light intensity under different excitation time τ. The light shift is calculated using density-matrix analysis of a Λ-type three-level system that was modeled on the ^{133}Cs D_1 line. The calculation method is shown in more detail in Ref. 2. A comparison of the results of the numerical calculations performed by density matrix analysis and the estimated values from the proposed equation shows that the relative error of the results is no more than 0.05%. The proposed equation is useful for practical purposes. And the light shift tendencies agree with experiment data.

At the conference, we will present the calculated results of the light shift in Ramsey-CPT and a derivation of the estimation equation.

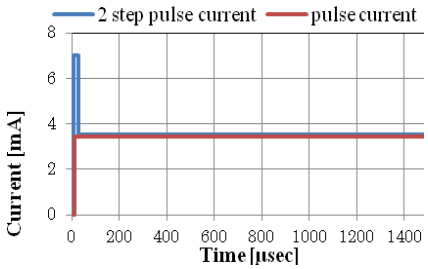
[1] O. Kozlova, J.-M. Danet, S. Guérandel, and E. de Clercq," IEEE Trans. on Instrum. Meas., vol. 63, no. 7, pp. 1863–1870, 2014.
[2] Y. Yano, W. Gao, S. Goka, and M. Kajita, Phys. Rev. A, **90**, 013826, 2014.
[3] T. Zanon-Willette, E. de Clercq, and E. Arimondo, Phys. Rev. A, **84**, 062502, 2011.

CPT pulse excitation method based on VCSEL current modulation for miniature atomic clocks

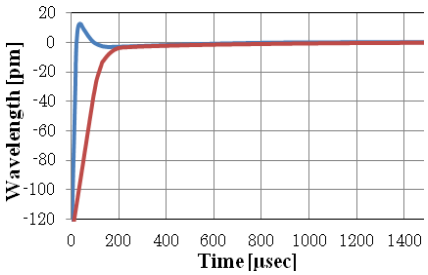
Ide Takumi, Goka Shigeyoshi*, Yano Yuichiro
Graduate School of Science and Engineering, Tokyo Metropolitan University, Hachioji, Tokyo 1920397, Japan
*E-mail: goka@tmu.ac.jp

We propose a novel coherent-population-trapping (CPT) pulse excitation method based on direct drive current modulation of a Vertical-Cavity Surface-Emitting LASER (VCSEL) for miniature atomic clocks (MACs). To excite Ramsey-CPT resonance, an external optical modulator is used to generate pulsed laser because very short rise time and laser wavelength stability are required for the Ramsey-CPT excitation [1]. Therefore, it is difficult to apply conventional pulse excitation methods to MACs. Since our method needs only simple device configuration without the external optical modulator, it is suitable for MACs including chip-scale atomic-clocks (CSACs) and is also possible to reduce the size, cost and power consumption. In this paper, we report the experimental results of Ramsey-CPT fringe excited by the proposed method.

In general, wavelength of a semiconductor laser is changed by temperature variation of the active layer caused by the drive current variation. Therefore, conventional drive current on/off modulation to generate the pulsed laser cannot be applied to the CPT pulse excitation in terms of the laser wavelength variation, which takes time until obtaining the required wavelength. To solve this problem, we split the drive current into 2 stages. Comparisons of the drive current and the output wavelengths for the conventional and proposed method are shown in Fig. 1 and Fig. 2. In Fig. 2, the vertical axis shows the wavelength difference from a wavelength used for the Ramsey-CPT excitation. In a first-stage, by setting drive current high, it is possible to greatly shorten the rise time to the required wavelength. In a second-stage, the drive current controls the wavelength required for the excitation process in the second half of the pulse. As a result, the rise time with the proposed method is 20 μs, although that with the conventional method is 1300 μs. It is shown that the proposed method can reduce the rise time, which is shorter than one-sixtieth that with the conventional method.



(a) Drive current of VCSEL



(b) Output wavelengths

Fig. 2: Comparison of the output wavelengths due to the drive current.

Figure 3 shows the Ramsey-CPT fringe observed by proposed method with a Cs gas cell contained 4 kPa Ne buffer gas. A single-mode 894nm VCSEL was used to excite Cs at the D1 line. The center frequency was 4.6 GHz, and the free evolution time was set at 300 μs. The full width at half maximum (FWHM) of the proposed method was 960 Hz, which was nearly one-seventh the continuous excitation value (6.55 kHz). These results indicate that our method can observe the Ramsey-CPT fringe without the external optical modulator and can be applied to the MACs.

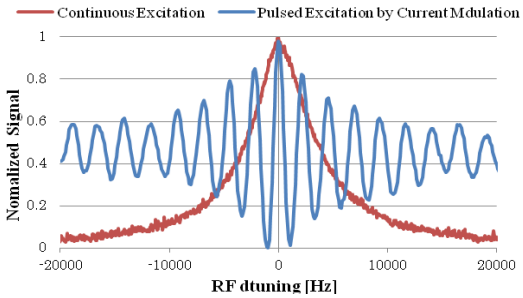


Fig. 3: CPT resonance of continuous excitation and Ramsey-CPT resonance with proposed method.

[1] S. Guêrandel, T. Zanon, N. Castagna, F. Dahes, E. Clercq, N. Dimarcq, A, Clairon, "Raman-Ramsey Interaction for Coherent Population Trapping Cs Clocks" IEEE Tranasactions on instrumentation and measurement, vol.56, NO.2, 2007.

Preliminar results of a Cs vapor cell CPT clock using push-pull optical pumping

M. Abdel Hafiz, R. Boudot

FEMTO-ST, CNRS, UFC, 26 chemin de l'épitaphe 25044 Besançon cedex, France.

Email: rodolphe.boudot@femto-st.fr

We developed an experimental set-up to detect high-contrast CPT resonances in buffer-gas-filled Cs vapor cells using push-pull optical pumping (PPOP) [1]. The laser source of the system is a distributed-feedback (DFB) diode laser tuned on the Cs D_1 line at 894.6 nm. A Mach-Zehnder electro-optic modulator (MZ EOM) is driven by a 4.596 GHz local oscillator to generate two first-order optical sidebands frequency-separated by 9.192 GHz. The dc electrode bias voltage of the MZ EOM is actively controlled using an original microwave synchronous detector technique to stabilize optical carrier rejection (~28dB) at the output of the EOM. A Michelson-like interferometer allows to generate the so-called push-pull interaction scheme [2]. The laser light is transmitted through a Cs vapor cell filled with a buffer gas mixture of N_2 and Ar. The laser power at the output of the cell is detected by a photodiode. The laser can be frequency stabilized onto the Cs-buffer gas cell into the bottom of the absorption line. The local oscillator frequency can be locked to the atomic 0-0 clock transition frequency.

In a first point, the impact of several experimental parameters (laser intensity, cell temperature, RF power, ..) on the clock resonance lineshape parameters was evaluated to find conditions that will optimize the clock short term frequency stability. The clock resonance is about 560 Hz with a contrast of about 22% for an input laser power in the cell of about 700 uW. The clock relative frequency stability is measured to be $4.2\ 10^{-13}$ at 1s, in good agreement with the signal to noise ratio limit, that is encouraging compared to state-of-the-art vapor cell atomic clocks based on double-resonance or CPT techniques. Nevertheless, the clock frequency stability performances are currently strongly limited after one or a few seconds, preventing Allan deviation to decrease as expected with a $\tau^{-1/2}$ slope, signature of a white frequency noise.

Investigations are currently in progress in order to understand the origin of this strong limitation. Laser power effects are strongly suspected, including total laser power variations and slight independent fluctuations of sidebands power at the output of the EOM. The sensitivity of the clock resonance frequency to various experimental parameters such as the EOM temperature, the EOM bias point, the EOM RF driving power, the static magnetic field, the optical path difference in the Michelson interferometer and laser variations will be studied with attention.

Progress, first conclusions of these investigations and last frequency stability results will be reported at the conference.

[1] Y. Y. Jau et al., Phys. Rev. Lett. 93, 160802 (2004).

[2] X. Liu et al., Phys. Rev. A 87, 013416 (2013)

Alkali Metal Source Tablet for Vapor Cells of Atomic Magnetometers

K. Ban, K. Tsujimoto*, Y. Hirai*, A. Terao, N. Mizutani, T. Kobayashi[+], O. Tabata*
Frontier Research Center, Canon Inc., Tokyo, Japan
*Department of Micro Engineering, Kyoto University, Kyoto, Japan
[+]Department of Electrical Engineering, Kyoto University, Kyoto, Japan
E-mail: ban.kazuhiro@canon.co.jp

Optically pumped atomic magnetometers (OPAMs) using alkali metal vapor can measure extremely small magnetic fields without cryogenic cooling. They are applicable to biomagnetic measurements such as magnetoencephalography as their sensitivity is comparable to that of superconducting quantum interference devices [1]. Toward practical implementation of OPAMs, we have fabricated an OPAM module that uses potassium [2] and operates under spin-exchange relaxation-free (SERF) conditions. Potassium was chosen for its long T_2 time, which enables high intrinsic sensitivity. In an OPAM array system, the quantity of potassium enclosed in each vapor cell should be uniform to suppress differences in atomic density and OPAM sensitivity. Uniform cells can be made using potassium sources that feed fixed amounts of the potassium to the cells.

For the potassium reagent, we selected potassium azide (KN_3), which is an explosive powder whose melting point and relatively low decomposition temperature are close to each other under high vacuum. The drawback here is that when a layer of KN_3 placed in a tiny vessel or on a flat substrate is heated, thermal decomposition of the azide takes place explosively and patches of KN_3 splash the surrounding area, which might contaminate the cell walls. We found that a porous alumina plate covered with a layer of alkali azide such as KN_3 or CsN_3, which we call the alkali metal source tablet (AMST), keeps alkali azide from splashing.

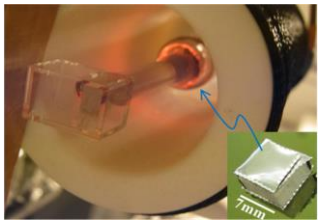


Fig.1: RF heating of AMST for vapor cell fabrication.

AMST was prepared by a simple two-step process: Droplets of KN_3 aqueous solution were put onto a porous alumina substrate and the water was removed under vacuum. The yield of potassium was dependent on the pore size. The highest yield was 65% for a KN_3 tablet with an average pore size of 60 μm. Additionally, the AMST was covered with niobium foil to enable RF wave heating, leaving only one or two faces open as a potassium outlet. Fabrication takes about 20 min per cell when using an AMST for the following two reasons. Potassium generation with RF heating takes only 10 min, and the time to deliver potassium to the cell is also shortened because AMSTs can be placed adjacent to the cell. The brevity of this process contrasts with the length of the conventional process of cell fabrication, which entails heating a glass tube with a gas burner and requires a great deal of skill and an hour of careful operations per cell. Twelve potassium cells were fabricated using AMSTs. The atomic vapor densities were measured to be within 50-70% of the theoretical value. The cells operated as OPAMs with sensitivity of 3.3-3.8 $fT_{rms}/Hz^{1/2}$ at a frequency of 10 kHz, indicating small variation in sensitivity. The next step is to realize an OPAM array system for biomagnetic measurements and imaging using these uniform alkali metal vapor cells as sensor heads.

[1] J.C. Allred, R.N. Lyman, T.W. Kornack, and M.V. Romalis, Phys. Rev. Lett. **89**(13), 130801 (2002).
[2] K. Okano, A. Terao, K. Ban, S. Ichihara, N. Mizutani, and T. Kobayashi, IEEE Sensors, 2012.

Rubidium Metal Consumption by Rb Discharge Lamps Fabricated from GE-180 Aluminosilicate Glass

Klimcak, Charles, Huang, Michael, Camparo, James
Photonics Technology Department, The Aerospace Corporation, El Segundo, CA
E-mail: charles.m.klimcak@aero.org

For the Rb atomic clocks flying on GNSS satellites, the rf-discharge lamp is a critical component, providing the light necessary for optical pumping, and thereby atomic signal generation, and the light for sensing the atoms' interaction with the resonant microwave field. Traditionally, discharge lamp envelopes have been fabricated from Corning type 1720 aluminosilicate glass due to its superior chemical resistance to alkali vapor, and such lamps have demonstrated decade-long continuous operation on orbit. Specifically, the diffusion of alkali atoms into this lamp glass has been shown to be sufficiently slow that lifetimes in excess of ten years can be obtained using only moderate initial alkali fill levels (<400 μg) [1]. However, Corning 1720 glass is no longer being manufactured. It is therefore important to identify an alternative glass type that offers comparable alkali chemical resistance, and that is readily available. Although Schott type 8436 aluminosilicate glass has been shown to be a suitable substitute for fabricating rf-discharge lamp envelopes, it would be advantageous to identify an alternate glass type produced in higher volume. An alternative to Corning 1720 glass, which is manufactured in very high volume for use in automotive lamps, is GE-180 glass. Although this glass is also known to offer high alkali chemical resistivity due to its aluminosilicate composition, the rate of diffusion of alkali atoms into this material when employed as the glass envelope of a Rb clock's rf-discharge lamp has not been evaluated. We present here our initial results obtained by differential scanning calorimetry of the rate of diffusive consumption of rubidium by operating pre-conditioned discharge lamps that have been manufactured with GE-180 glass envelopes. Our results suggest that GE-180 is an excellent substitute for Corning 1720 glass in Rb clock rf-discharge lamps. We will also discuss some unusual experimental issues that have been observed during calorimetric measurements on a set of twelve of these discharge lamps, and we will outline optimum methods for attaining an accurate measurement of the rubidium fill.

(1) C.H. Volk, R. P. Frueholz, T.C. English, T.J. Lynch, and J. Riley, "Lifetime and Reliability of Rubidium Discharge Lamps for Use in Atomic Frequency Standards," Proc. 38th Annual Symp. Freq. (IEEE Press, New York, 1984), pp. 387-400.

R. P. Frueholz, M. Wun-Fogle, H.U. Eckert, C.H. Volk, and P. F. Jones, "Lamp Reliability Studies for Improved Satellite Rubidium Frequency Standards," Proc. 13th Annual Precise Time and Time Interval (PTTI) Applications and Planning Meeting, (NASA Conference Publication 2220, 1982). pp 767-790.

Light Shift Compensation in Optically Oriented Alkaline Vapors with Laser Pumping

Baranov Alexey, Ermak Sergey, Sagitov Eduard, Smolin Roman, Semenov Vladimir
Department of Quantum Electronics
St. Petersburg State Polytechnic University
St. Petersburg, Russia
Vladimir_semenov@mail.ru

As it is known, long term stability of vapor-cell atomic discriminators with optical pumping used in quantum magnetometers and atomic clocks is mostly determined by technical (flicker) noise due to slow apparatus's properties variation such as working substance temperature, vapor pressure, pumping source spectrum and intensity instabilities. Due to synchronous effect of the technical noises of a different kind a certain noise component cannot be distinguished and therefore its contribution to the frequency drift of a quantum device cannot be analyzed separately. This situation complicates quantum device construction optimization, which leads to metrological characteristics improvement. Nevertheless, numerous studies in this field allow concluding that the light shift of a resonance frequency due to pumping light spectrum non-resonance components is a major destabilizing factor in such devices. For alkaline vapors in presence of a circular polarized light the light shift contains three components [1]:

- The scalar shift, which is identical for all magnetic sublevels of a hyperfine structure F or F*.
- The vector light shift, caused by an effective magnetic field due to circular polarized light (an inverse Faraday Effect).
- Tensor light shift caused by ground state atoms alignment. It depends on a magnetic quantum number m_F.

Circular polarization sign (right or left) of the pumping light cause either summation or subtraction of the scalar and vector components that allows their mutual compensation on atomic level. Hence, pumping source influence on a frequency stability of a quantum device can be significantly reduced. This paper presents experimental studies of such an effect with respect to Rb^{87} atoms pumped by a laser source tuned to D_2 line of the doublet, which was chosen because of the tensor component small contribution compared to D_1 line.

Error signals of the microwave transition (end resonance) and Zeeman transition (spin generator) were simultaneously detected to capture magnetic field residuals in the area of the absorption cell. The signals were subtracted and processed in terms of Allan variation.

Analytical studies showed that LF noise components of the two signals can be suppressed in a case of a correct choice of the circular light polarization sign. A significant role plays spin generator frequency choice that is defined by the magnitude of the magnetic field. For instance, an order of a magnitude improvement in Allan variance (1000 s) was obtained after magnetic field tripling. This result matches theoretical studies of the work [2].

[1] W. Happer, B.S. Mathur, Phys. Rev., v163, no. 1, pp. 12-25, 1967.

[2] V.V. Semenov, P.V. Zimnitsii, R.V. Smolin, S.V. Ermak "The Effect of Flicker Processes on the Resolution of Self-Oscillating Magnetometers Optically Pumped in the Saturation Regime", Technical Physics Letters, vol. 3, no 40, pp. 271-273, 2014.

Mercury Lamp Studies in Support of Trapped Ion Frequency Standards

Lin Yi, Eric A. Burt and Robert L. Tjoelker

Jet Propulsion Laboratory, California Institute of Technology, Pasadena, USA
Email: Lin.Yi@jpl.nasa.gov

The mercury linear ion trap frequency standard (LITS) [1] at JPL continues to advance with multiple potential applications. In particular, the outstanding long-term stability [2] and practicality of the ground-based clock have attracted significant academic and commercial interests for time-keeping and metrology. However, the mercury RF discharge lamp used in these clocks for optical pumping and state detection may limit the ultimate stability performance of the clock [3-4], constraining even broader application.

For mercury ion frequency standards, the operational lamp behavior is described by the ratio of useful light at 194nm and unwanted background light at 254nm (194/254). This ratio depends on several lamp fabrication factors: buffer gas pressure, lamp inner diameter (ID) and the quantity of mercury. However, the quantitative relationship is not known well, which constrains fabrication optimization and repeatability. Increasing the 194nm output decreases optical pumping times and an increase of the 194/254 ratio improves the clock signal-to-noise ratio (SNR). These improvements lead to an improvement in clock short-term stability and enable the use of an even broader range of local oscillators.

We have carried out several experiments to unfold the relationship between the 194/254 and the fabrication factors: buffer gas pressure, lamp ID, and the quantity of mercury. The quantitative results may be used to improve the process of lamp fabrication for mercury ion frequency standards. The research presented here may also shed light on other lamp-based applications and atomic clocks.

References

[1] R.L. Tjoelker, C. Bricker, W. Diener, R.L. Hamell, A. Kirk, P. Kuhnle, L. Maleki, J.D. Prestage, D. Santiago, D. Seidel, D.A. Stowers, R.L. Sydnor, T. Tucker "A mercury ion frequency standard engineering prototype for the NASA deep space network." In *Frequency Control Symposium, 1996. 50th., Proceedings of the 1996 IEEE International.*, pp. 1073-1081. IEEE, 1996.

[2] Eric A. Burt, William A. Diener, and Robert L. Tjoelker. "A compensated multi-pole linear ion trap mercury frequency standard for ultra-stable timekeeping." *Ultrasonics, Ferroelectrics and Frequency Control, IEEE Transactions on* 55, no. 12 (2008): 2586-2595.

[3] L. Yi, S. Taghavi-Larigani, E. A. Burt, and R. L. Tjoelker. "Progress towards a dual-isotope trapped mercury ion atomic clock: Further studies of background gas collision shifts." In *Frequency Control Symposium (FCS), 2012 IEEE International*, pp. 1-5. IEEE, 2012.

[4] L. Yi et al., "Sub-mm Scale Fiber Guided Deep/Vacuum Ultra-Violet Optical Source for Trapped Mercury Ion Clocks," Proc. Of the Precise Time and Time Interval Systems and Applications(2013), Dec 2-5, Bellevue, WA

Preliminary results for a hydrogen maser cavity in the TE_{111} mode

E. Van der Beken, D. Léonard*, A. Counet*, and T. Bastin
Institut de Physique Nucléaire, Atomique et de Spectroscopie, University of Liège,
Sart-Tilman B15, Liège, Belgium
*Gillam-Fei, Mont Saint-Martin 58, Liège, Belgium
E-mail : evanderbeken@ulg.ac.be

We present results of our preliminary investigations on a hydrogen maser cavity in the TE_{111} mode. Hydrogen masers use the transition at 1420.405 MHz between the two hyperfine levels $F = 0$ and $F = 1$ of the $1s_{1/2}$ ground state of the hydrogen atom [1]. Standard hydrogen masers are heavy devices. They are based on the use of a TE_{011} cylindrical cavity with dimensions of the order of 27 cm [1]. In contrast, the TE_{111} mode is the lowest frequency mode of a cylindrical cavity in the usual regime $D/L < 0.985$ where D and L are the diameter and the length of the cavity, respectively [2]. In comparison with the standard masers, the TE_{111} mode makes thus possible to reduce dimensions significantly to obtain resonance at 1420.405 MHz, which is very interesting for space applications and in particular in the context of the global positioning system.

In the TE_{111} mode the cavity exhibits two regions with opposite directions of the magnetic field (see figure 1). Therefore the cavity has to be divided in two storage regions for hydrogen atoms. So far, few studies have been realized about this type of cavity (see for example [3]). The electromagnetic cavity is the fundamental component of the maser device. In view of a future development of a hydrogen maser in the TE_{111} mode we performed a thorough analysis of the maser physics for this mode. Studies of the maser oscillation condition have been performed to determine the ideal length over radius ratio for the cavity. Different simulations have been carried out for the modeling of the TE_{111} electromagnetic field. They allowed us to estimate the frequency and quality factor for different configurations of the cavity. In these simulations we have also investigated a means of cavity frequency tuning by inserting a screw inside the cavity.

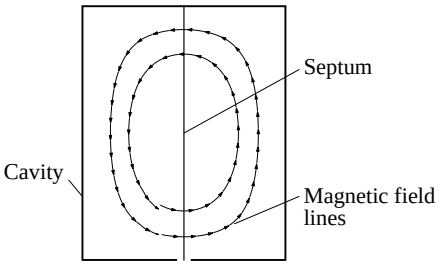


FIG. 1 – Magnetic field lines of a TE_{111} cavity [3].

Our studies and simulations led to the realization of a test cavity in aluminum. This cylindrical cavity has been cut in two according to its longitudinal axis of symmetry and a 1 mm thickness has been withdrawn (0.5 mm for each half). The two halves clamp a thin Teflon FEP sheet which is used as a septum for the separation between the two storage regions. This test cavity allowed us to perform several measurements of its frequency and quality factor in order to validate our cavity model. All of these results will be presented.

[1] D. Kleppner, H. C. Berg, S. B. Crampton, N. F. Ramsey, R. F. C. Vessot, H. E. Peters, et J. Vanier, Phys. Rev. A **138**, 972 (1965).

[2] J. D. Jackson, *Classical electrodynamics*, Wiley, New York, 1962.

[3] Q. Wang, Z. Zhai, W. Zhang, et C. Lin, IEEE Transactions on ultrasonics, ferroelectrics, and frequency control **47**, 197 (2000).

Preliminary Results for an Atomic Gravimeter Developing at KRISS

Lee, Sang-Bum, Kwon, Taeg Yong, Park, Sang Eon, Heo, Myoung-Sun, Hong, Hyun-Gue, Park, Chang Yong, Lee, Won-Kyu, and Yu, Dai-Hyuk
Center for Time and Frequency, Korea Research Institute of Standard and Science, Daejeon 305-340, Korea
E-mail: lsbum@kriss.re.kr

An gravimeter using stimulated Raman transition is employed for a variety applications ranging from measurement of Newtonain constant of gravity G, a fine-structure constant, and test of general relativity to inertial navigation, underground structure detection, locating natural resources such as oil, geophysics, and geodesy. Furthermore, the atom interferometry is currently being proposed for measurement of gravitational wave as well as for a gravity field characterization for a Watt balance project aiming at redefining the unit of mass, the kilogram, in the future. Here we introduce Preliminary results about the gravimeter developing at KRISS.

Fig.1 a) shows Rabi oscillations of atom numbers between two ground states ($|F=1, m_f=0\rangle$, $|F=2, m_f=0\rangle$) for the free falling Rb^{87}atoms with the temperature of 5μK by two counter-propagating Raman pulses. The decay of the Rabi oscillation amplitude for increasingly longer pulse lengths is attributed to Gaussian envelope of Raman beam intensity with finite size. The phase difference accumulated by three Raman pulses of Mach-Zehnder-type configuration corresponding to $\pi/2$-π-$\pi/2$ pulses (τ=40μs) is given by $k_{eff}\cdot g\cdot T^2$, which is proportional to gravity acceleration g, where $k_{eff}=k_1+k_2$ (k_1 and k_2 are wave numbers for two counter- propagating beams) and T is the spacing time between two pulses. By compensating for the acceleration-induced Doppler shift by the variation of frequency sweeping rate **a**, we can find the minimum fringe of population N_2/N_T (N_2 is the atom number of $|F=2, m_f=0\rangle$ state and N_T is total atom number) whose the phase is independent of T and the sweeping rate **a** corresponds to $g\cdot k_{eff}/2\pi$ (**a**≈25.1MHz/s), as shown Fig.1 b).

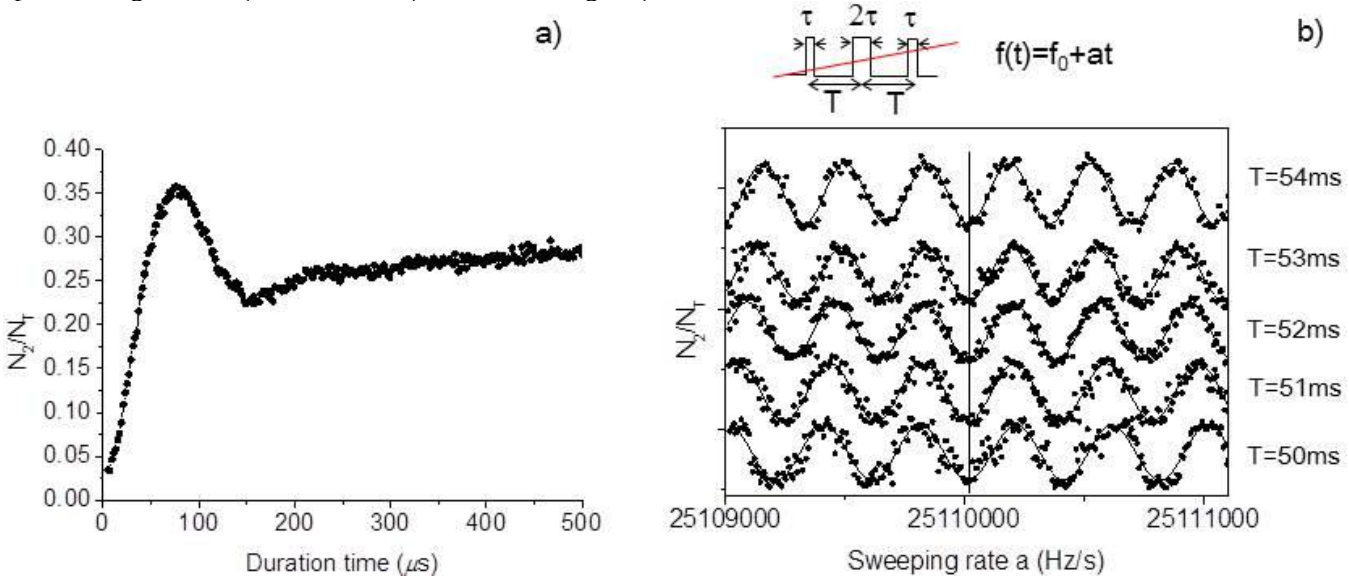


Figure. 1: a) Rabi oscillations and b) interference signals in Mach-Zehnder-type configuration corresponding to $\pi/2$-π-$\pi/2$ pulses (τ=40μs), for two counter-propagating Raman pulses.

Precision interferometry with ultra-cold atoms

Christian Schubert, Naceur Gaaloul, Wolfgang Ertmer, Ernst M. Rasel
Institut für Quantenoptik, Leibniz Universität Hannover, Hanover, Germany
E-mail: schubert@iqo.uni-hannover.de

Atom interferometry is widely used for measuring rotations and accelerations with applications in navigation, geophysics/geodesy, and fundamental physics. In our group, an atomic gyroscope [1] measured earth rotation at the percent level, a dual species gravimeter resolved the tides [2] and performed a test of the universality of free fall at parts in 10^7 [3]. As the scaling factor in these kind of experiments depends on the square of the free evolution time, the extension of this time in microgravity is investigated with compact experiments operated in a drop tower [4,5] and sounding rocket experiments for future space borne applications [6], in parallel to large ground based setups.

Currently, most precision atom interferometers are based on molasses cooled atoms with temperatures in the micro Kelvin regime, offering fast cycle times and high atom numbers [1-3]. The drawback is the residual expansion limiting beam splitting and lattice launch efficiencies, detection after extended free evolution times, and imposing systematic uncertainties. Overcoming these is crucial for the improvement of current experiments and future setups. Therefore, fast generation of ultra-cold ensembles with suitable atom numbers is an actively pursued research topic.

Within the microgravity experiments, atom chips are employed for the generation of magnetic traps and implementation of delta kick cooling techniques. When operating QUANTUS I in the drop tower, an effective temperature of 1 nK was reached which enabled a Bragg interferometer with a total free evolution time of 675 ms [4]. The successor, QUANTUS II, demonstrated the production of ^{87}Rb Bose-Einstein-condensates in a compact device with a flux of 10^5 atoms/s [7], opening the era of maturity for use in quantum precision interferometers.

[1] G. Tackmann, P. Berg, C. Schubert, S. Abend, M. Gilowski, W. Ertmer, and E. M. Rasel, New J. Phys 14, 015002 (2012)
[2] N. Gaaloul, J. Hartwig, C. Schubert, W. Ertmer, and E. M. Rasel, Precision interferometry with Bose-Einstein condensates, in: Atom Interferometry, edited by G. M. Tino and M. A. Kasevich, Amsterdam: IOS (2014)
[3] D. Schlippert, J. Hartwig, H. Albers, L. L. Richardson, C. Schubert, A. Roura, W. P. Schleich, W. Ertmer, and E. M. Rasel, Phys. Rev. Lett. 112, 203002 (2014)
[4] H. Müntinga et al., Phys. Rev. Lett. 110, 093602 (2013)
[5] J. Rudolph, Microgravity Sci. Technol. 23, 287 (2011)
[6] D. N. Aguilera et al., Class. Quantum Grav. 31, 115010 (2014).
[7] J. Rudolph et al., arXiv:1501.00403 (2015)

A new method to select Cs fountain clock state by optical pumping with a de-pumping procedure

Fang Fang, Kun Liu, Weiliang Chen, Nianfeng Liu, Rui Suo and Tianchu Li

National Institute of Metrology (NIM), Beijing, P. R. China

Email: fangf@nim.ac.cn

A new cesium fountain clock NIM6 is under developing in NIM. Besides some improvements, NIM6 is also aiming to collect more atoms from a MOT loading optical molasses and optical pumping, leading to a better signal to noise ratio at the detection.

The optical pumping has been used to accumulate the $m_F = 0$ sublevel population in NPL's fountains[1]. Here, we propose a new method to do optical pumping. The atoms, distributed evenly in the F=4 sublevels after launch, are first de-pumped to the F=3 state with a linearly polarized light to make a F=4 → F'=3 π transition. Theoretical calculation indicates that the atom population on the |3,0> sublevel reaches 92% with only scattering 2 photons per atom in an ideal case, as shown in figure 1(a). The atom distribution on each Zeeman sublevel of F=4 state is assumed to be 1. Then, atoms are optical pumped to the |F=3, m_F=0> state with a pumping light on resonance with F=3 → F'=3 transition. The theoretical results of atom distribution on the F=3 sublevel after optical pumping is shown in figure 1(b). The atom number on the clock state |F=3, m_F=0> is increased 2.3 times compared to the number with a routine method only selecting |F=4, m_F=0> state. The total population on the other $m_F \neq 0$ states is less than 3% of the atom number on the clock state, while the averaged scattering photon number per atom is less than 4. More number of atoms on the clock state can be obtained if the de-pumping light is presented during the optical pumping.

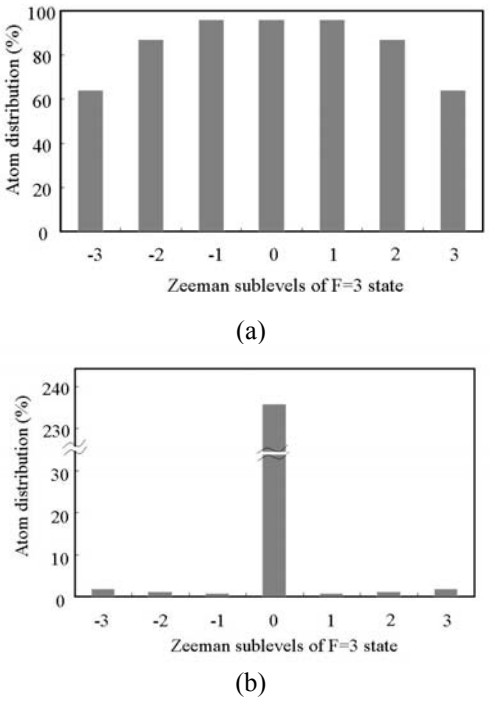


Fig. 1: Atom distribution on Zeeman sublevels of F=3 state. The original atom distribution on each Zeeman sublevel of F=4 is assumed to be 100%. (a) Distribution after de-pumping; (b) Distribution after optical pumping.

The advantage of the proposed method is not only increasing the atom number on the clock state, but also selecting the clock state by optical pumping, so the state selection microwave cavity is not necessary anymore.

[1] [1] K. Szymaniec and S. E. Park, "Primary Frequency Standard NPL-CsF2: Optimized Operation near the Collisional Shift Cancellation Point," IEEE Trans. Instrum. Meas., vol. 60, pp. 2475–2481, 2011.

Towards thermodynamics of cold Cesium atoms in Cs fountain clocks

Espinosa María[1], de Carlos Eduardo[1], López Sergio[1] and López Mauricio[1]
Time and Frequency Metrology, CENAM, Querétaro, México
E-mail: mauricio.lopez@cenam.mx

A novel analytical method for temperature measurement in Cs fountain clocks has been recently introduced [1], it is called the point by point (PBP) method. In this article we further analyze the velocity distributions of the ultra cold atoms obtained with the PBP method. This analysis is performed on experimental data obtained from the CENAM cesium fountain clock (CENAM CsF-1). We performed a double Gaussian fit to the PBP velocity distribution data. Then, we analyze the contribution of each Gaussian to the temperature of the whole system. Our results show that a double Gaussian fit provides a new scheme to assign a value to the cloud´s temperature. We fit the PBP velocity distribution of the CENAM CsF-1 cold atoms to a double Gaussian. Temperature computation of the CENAM CsF-1 ultra cold atoms is presented when applying different criteria. Commonly, the temperature in ultra cold gasses is defined as a kinetic temperature, which in turn is related with the width of the velocity distribution, i.e., $e^{-1/2}$ when a Maxwell–Boltzmann distribution for velocity distribution is assumed. However, the assumption on the Maxwell–Boltzmann shaped velocity distribution could be not true. Then, in order to have a better analysis of the experimental velocity distributions, we fit the velocity distribution to a double Gaussian. We will show that this constitute a best fit to the experimental velocity distributions when certain MOT´s operational parameters are used. In Figure below we show two CENAM CsF-1 velocity distributions (red color) with non-Gaussian profiles. We analyze the red colored graph by fitting it to a double Gaussian. The two Gaussians that, added each other, result in the blue colored velocity distribution. The double Gaussian fitting performs better than a single Gaussian approximation. The cold atoms cloud, can be modeled by composed of two groups of atoms each of them in thermodynamic equilibrium, and so with a very well defined temperature. On the other hand, because the Cs cloud atoms constitute a very dilute gas, the two groups of atoms are not in thermal contact, and then the thermal equilibrium is reached after a very long time. In other words, the atoms cloud is formed by two groups of atoms, sharing the same space, not in thermal contact, each of them in very well defined temperature state.

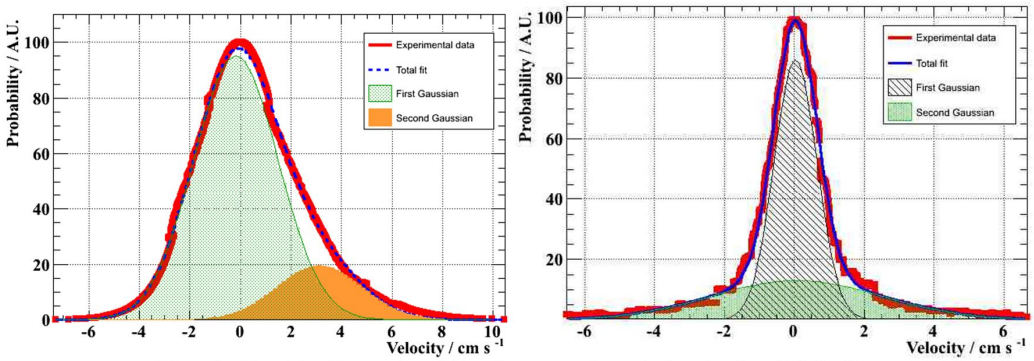


Fig. 1. *Double Gaussian fit in the experimental velocity distribution.*

References:

[1] M. G. Espinosa, E. de Carlos, J. M. López and S. López, "*Alternative Algorithm for Temperature Measurements of Cold Atoms in Cs Fountain Clocks*", in press, IEEE Trans. on Ins. and Meas.

Studies of electromagnetic frequency shifts on FoCS-2

Antoine Jallageas[1], Michael Petersen[1], Laurent Devenoges[2], Laurent-Guy Bernier[2], Thomas Südmeyer[1], Jacques Morel[2]

[1] Laboratoire Temps-Fréquence, Université de Neuchâtel, Neuchâtel, Switzerland

[2] Federal Institute of Metrology METAS, Bern, Switzerland

Email: antoine.jallageas@unine.ch

We are reporting on the latest improvements of the continuous Cs fountain clock FoCS-2 at METAS. An in depth analysis of possible microwave leaks [1] and of their effects on the clock frequency was carried out. This demonstrated that a microwave leak occurring at the rotating microwave feedthrough located on the top of the vacuum chamber was responsible for a so far unexplained frequency offset which limited the performance of FoCS-2. Due to a first reduction of the leak the resulting clock frequency offset is now within the estimated total clock uncertainty.

Furthermore, a dependency of the clock frequency on the vertical atomic velocity has been reduced by a factor of 5. This was achieved by improving the microwave distribution in Focs-2, indicating a possible perturbation due to the proximity of the microwave cables and the free falling atoms inside the free evolution zone in between the two microwave interaction regions and the possibility of microwave common mode surface currents circulating on the coaxial cables. Different original methods for completely eliminating this effect are currently being evaluated and will be discussed.

[1] S. Weyers and al., ”Effects of microwave leakage in caesium clocks: theoretical and experimental results,” in *Proc. Eur Time Freq. Forum*, 2006.

Brazilian National Frequency Standards Framework

De Martin Jr J, Müller S T, Valappil S K N, Salas A R*, Pechoneri R D, Rubio E L[+], Junqueira S[#], Bagnato V S*, Cruz F C[+], Tarelho L V G[&], Garcia G A[&], Courteille P W*, Magalhães D V

EESC - USP, São Carlos, SP/Brazil
*IFSC - USP, São Carlos, SP/Brazil
[+]IFGW - UNICAMP, Campinas, SP/Brazil
[&]DMTIC - INMETRO, Xerém, RJ/Brazil
[#]DSHO - ON, Rio de Janeiro, RJ/Brazil
E-mail: jairdemartinjr@usp.br

Atomic frequency standards play a fundamental role in communications, navigation systems and timekeeping. To support these areas, different kinds of atomic frequency standards, in both microwave and optical domain, are the responsible for the achievement of high-performance measurements. Our research group has been working intensively to establish various experiments of frequency standards and to consolidate partnerships for the development of national references in Brazil. This is crucial for a country aiming stronger influence worldwide and that needs to reinforce strategic areas, such as defense and national industry.

In the microwave domain, we have developed an atomic fountain, based on 133Cs atoms, that is currently being upgraded aiming a better performance. Other experiment in this domain concerns a compact system to probe cold atoms magneto-optically trapped in a microwave cavity [1] and we have also been working on the commissioning of a thermal beam standard, optically operated, in the Brazilian NMI, in order to provide an operational structure to this area [2]. Envisaging time dissemination, we have worked on remote comparisons and data treatment for GNSS receivers [3]. In the optical domain, we have an experiment under construction, to use 88Sr as the atomic reference [4] and an ultra-stable laser in 1.55 m is being developed to be used with a high finesse F-P cavity. The optical and microwave domains are going to be linked by the use of a commercial frequency comb system and we have also worked on the establishment of optical links, using existing optical fibers from the campuses infra-structure and possible expansion should be discussed to fiber connect all the participating institutes.

[1] Müller, S. T. ; Pechoneri, R. D. ; Martin Jr, J. ; Otoboni, F. A. ; Bagnato, V. S. ; Magalhães, D. V. . *Development of a Mobile Atomic Frequency Standard based on Cold Atoms*. OSA Trends in Optics and Photonics, v. 1, p. LM2A.12, 2012.

[2] Tarelho, L. V. G. ; Garcia, G. A. ; Baratto, A. C. ; Souza, R.S.L ; Martin Junior, J. ; Muller, S. T. ; Magalhães, D. V. ; Bebeachibuli, A. ; Bagnato, V. S. ; Rovera, G. D. . *Joint Effort to Commissioning a Thermal Cesium Beam with Optical Pumping as Primary Frequency Standard to Brazilian NMI*. In: 29th Conference on Precise Electromagnetic Measurements, 2014, Rio de Janeiro. Digest of 29th Conference on Precise Electromagnetic Measurements. Rio de Janeiro: IEEE, 2014.

[3] Tarelho, L. V. G. ; Garcia, G. A. ; Baratto, A. C. ; Raymundo, E.V. ; Junqueira, S. ; Souza, R.S.L . *Determination of Environmental Effects on GPS Signals by Using a Geodetic Receiver and several online PPP softwares.* In: 29 th Conference on Precise Electromagnetic Measurements, 2014, Rio de Janeiro. Digest of 29th Conference on Precise Electromagnetic Measurements. Rio de Janeiro: IEEE, 2014.

[4] P.H. Moriya ; Holynski, M. S. ; Courteille, P. W. . *Collective effects in a strontium cloud*. In: Young Atom Opticians Conference 2014, 2014, Barcelona. Young Atom Opticians Conference, 2014. p. 48.

Multimode SiC Trampoline Resonators Manipulate Microbeads to Create Chladni Figures

Hao Jia[†], Hao Tang[†], Philip X.-L. Feng[*]
Electrical Engineering, Case Western Reserve University, Cleveland, OH 44106, USA
[†]Equally Contributed Authors. [*]Email: philip.feng@case.edu

We report, for the first time, the experimental demonstration of two-dimensional (2D) microscale Chladni figures created by using SiC square trampoline resonators with multimode responses. At least 5 flexural modes of a trampoline resonator (50×50×0.2μm) are resolved by interacting with a group of microbeads (3.62μm-in-diameter) atop *in an aquatic environment* with piezoelectric excitation from 200kHz to 5MHz. Microbeads are observed to quickly stabilized along the nodal lines or circles (within ~30–40s), and 2D Chladni patterns, such as circle ('○'), cross ('×'), line ('\') and even complex higher mode patterns are formed. Such results show opposite phenomena to the previous work [1], in which 1D microscale Chladni patterns are first reported using cantilevers, but microbeads (4μm-in-diameter) are observed moving toward antinodes. Chladni patterns using 2D micromechanics offer new exciting opportunities for patterning and manipulating micro/nanoscale particles and biological cells in a fast manner with simple device fabrication and engineerable mode shapes, and such SiC MEMS platform, with its outstanding mechanical, optical properties, and more interestingly, biocompatibility, may also be attractive to size-based cell sorting, cellular behavior, cell-cell interactions and other biophysics and biosensing applications.

Background & State-of-the-Art

In recent years, there is an increasing interest and need in patterning and manipulating particles and more interestingly, biological cells on surfaces of devices. Chemical surface patterning [2], which requires pre-patterned chemicals, is a passive patterning approach with low controllability. Optical tweezers [3] can manipulate single cell in non-contact mode with high force resolution, but time consumption and laser induced heating effect limit itself in patterning cells in large quantities. Microfluidic-based method [4], by confining cells in microscale structures induce unwanted mechanical stimuli which may potentially interfere cellular interactions. Surface acoustic wave (SAW) method [5] can pattern and manipulate cells in a very fast manner with high controllability, but only simple patterns are currently achieved and the device structure is relatively bulky. Chladni figures, first demonstrated using cantilevers [1], open our minds of patterning particles using mechanical resonances. However, to date no 2D Chladni patterns has been demonstrated using micro/nanodevices, which makes it even more appealing for automated cell patterning because of its fast response and diverse engineerable modes.

Device Fabrication & Experimental System

The SiC trampoline resonators (50×50×0.2μm) are patterned based on a SiC-on-Si device platform using a simple 2-step fabrication process: (i) focused ion beam (FIB) milling; (ii) HNA etching ($HF:HNO_3:H_20$=1:2:1). The resulted devices are shown in Fig. 1b and 1c. The device surfaces are flat enough to avoid undriven spontaneous movement. Multimode resonances of the SiC trampoline resonator are characterized in DI water using an optical actuation/detection module (Fig.2) [6] to predetermine the piezo-driving frequencies in the next step. Silica microbeads (Cospheric, 3.62μm-in-diameter) are then delivered onto the device surface using a custom-built pressure-controlled microinjection module (Narishige IM-6-2). The detailed microbead transfer process is shown in Fig.4. A piezoelectric actuator is used to excite the resonances in water (Fig. 2). We sweep the driving frequency from 5MHz to 200kHz (from high to low, for convenience of introducing the mode shapes), with an step of 100kHz within 5–1MHz and 50kHz within 1MHz–200kHz. Time-lapse images are taken with an interval of 10s and duration of ~300s for each frequency step. After microbeads are successfully delivered to device surface, the whole chip, already immersed in DI water in a package, is sealed by simply covering an optical window (Fig. 1d).

Experimental Results & Discussions

Figure 3 shows the multimode resonance characteristics of the SiC trampoline resonators in water. At least 5 resonance modes within 500kHz–5MHz are evident when varying the detecting laser positions on the device surface. Figure 5 shows that 2D Chlani patterns of 5 flexural modes are continuously resolved as the driving frequency sweeping from 5MHz to 200kHz. Microbeads are observed quickly stabilized along the nodal lines or circles (within ~30–40s), forming a variety of geometric patterns, such as '○', '×', '\' and even more complex higher modes. Such Chladni patterns show excellent agreement with the theoretically predicted mode shapes. By varying the frequency range, we are able to automatically accumulate microbeads (even from off-device), to create clear patterns on the device surface, and visualize mode shape transitions in both frequency and time domains. Comprehensive data and detailed analysis will be presented in the full paper.

References

[1] M. Dorrestijn, *et. al.*, *Phys. Rev. Lett.* **98**, 026102(4), 2007. [2] H. Zhang, *et. al.*, *J. R. Soc. Interface* **5**, 671–690, 2008. [3] C. Zheng, *et. al.*, *Anal. Chem.* **84**, 2088–2093, 2012. [4]. F. Guo, *et. al.*, *PNAS*, **112**, 43–48, 2015. [5] D. T. Chiu, *et. al.*, *PNAS* **97**, 2408–2413, 2000. [6] H. Jia, *et. al.*, *IFCS'2014*, Taipei, May 19-22, 2014.

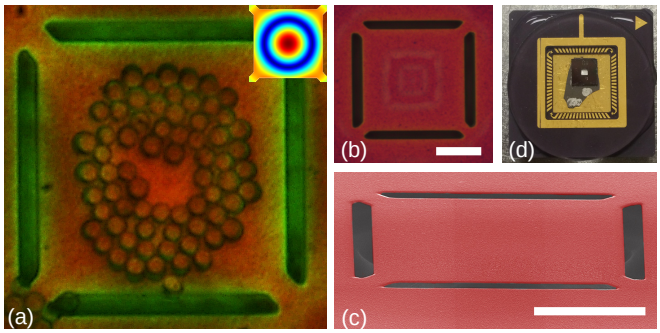


Fig. 1: 2D Chladni figure generated by SiC trampoline resonator (50×50×0.2μm). (a) An example of high-order resonance mode (inset shows the simulated mode shape) is resolved as silica microbeads (3.62μm-in-diameter) are stabilized along the nodal circle. (b) Optical and (c) SEM images show the suspended and flat trampoline structure after a 2-step fabrication process based on a SiC-on-Si platform: FIB patterning and HNA etching. (d) The whole chip is fixed onto a PZT piece in a package, immersed in DI water and sealed by covering an optical window.

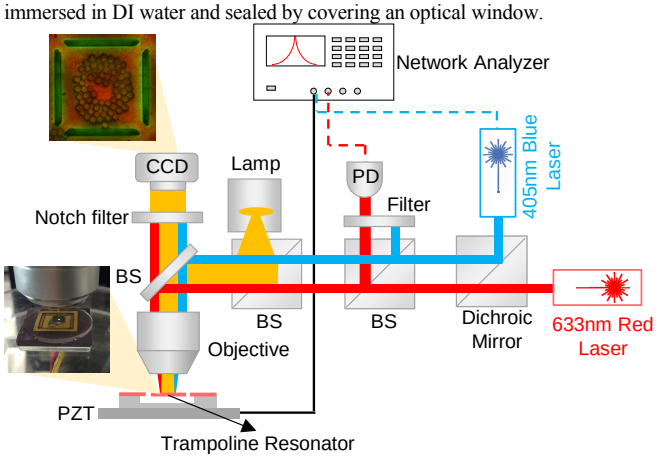


Fig. 2: Schematic illustration of the experimental system. Optical actuation/detection module is integrated to characterize the multimode resonances of the SiC trampoline resonator in water, where an amplitude-modulated 405nm blue laser is used to excite the resonances and a 633nm red laser is used to detect the flexural displacements interferometrically. Piezoelectric actuation module is then used to strongly excite the resonances while the microbead distributions on the device surface are recorded by a time-lapse imaging module.

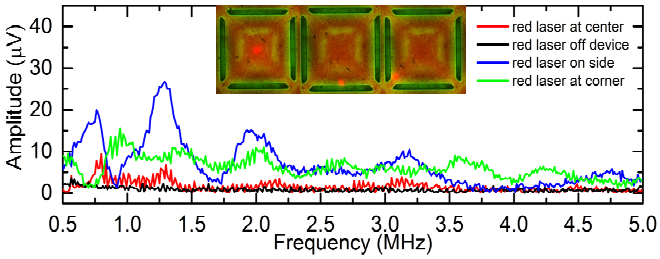


Fig. 3: Multimode resonance characteristics of the SiC trampoline resonator in water measured by the optical actuation/detection module. At least 5 flexural modes within 500kHz–5MHz are observed when the detecting (red) laser is focused at center (red curve), side (blue curve) and corner (green curve), as shown in the insets. Black curve shows a flat background spectrum when moving off the device.

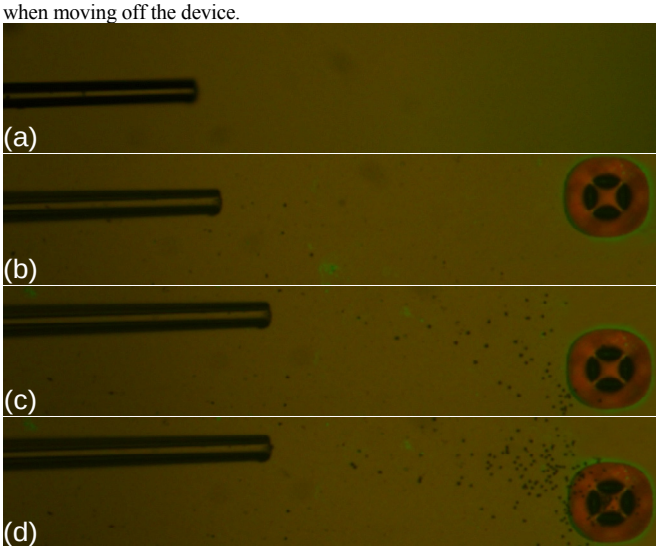


Fig. 4: Microbead delivery using a custom-built microinjection module. Microbeads are initially sonicated in DI water and sampled by a pressure-controlled micropipette (~40μm-in-diameter). (a) Micropipette is first focused under the microscope objective by adjusting a XYZ-stage. (b) The whole chip is then raised up (by another XYZ-stage) to the same focal plane with target device next to the pipette tip. (c) Adjust the injection speed and distance by controlling the pressure and relative position between the pipette and target device. (d) A number of microbeads are delivered onto (or near) the device surface while still moveable *in the aquatic environment*.

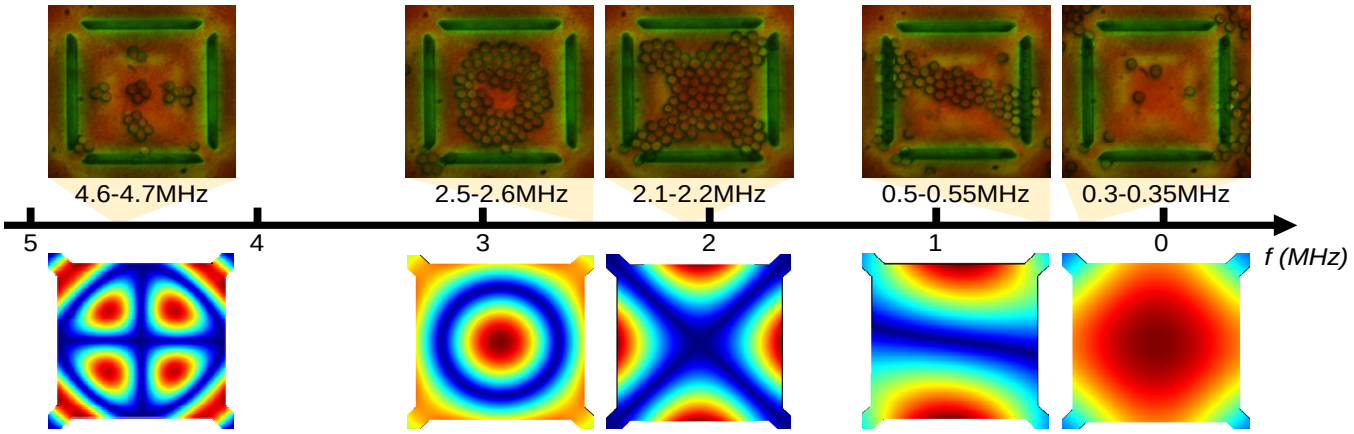


Fig. 5: 2D Chladni figures generated by the SiC trampoline resonator. Piezoelectric driving frequency is swept from 5MHz to 200kHz with an step of 100kHz within 5–1MHz and 50kHz within 1MHz–200kHz. Time-lapse images are taken with an interval of 10s and duration of ~300s for each frequency step. 5 flexural modes are clearly resolved as microbeads are stabilized along the nodal lines or circles. Experimental results show a good agreement with the simulated mode shapes. Note that a few microbeads are occasionally stuck to the device surface and no longer moveable at the end.

Calibrating Temperature Coefficient of Frequency (TCf) and Thermal Expansion Coefficient (α) of MoS_2 Nanomechanical Resonators

Rui Yang*, Zenghui Wang, Philip X.-L. Feng*
Electrical Engineering, Case Western Reserve University, Cleveland, OH 44106, USA
*E-mail: rui.yang@case.edu; philip.feng@case.edu

We report on experimental calibration of temperature coefficient of frequency (TCf) and laser heating effect in vibrating two-dimensional (2D) resonators, and through which, a new method for determining the thermal expansion coefficient (α) in 2D crystals. Nanomechanical resonators based on MoS_2 2D crystal have exhibited high frequencies and potential for frequency scaling thanks to attractive mechanical properties and unconventionally high strain limit [1]. To date MoS_2 resonators vibrations are mostly transduced via optical detection schemes, while laser heating is known to affect characteristics of micro/nanoelectromechanical systems (MEMS/NEMS) [2], it is thus desirable to systematically calibrate laser heating effects on MoS_2 resonators. Here we show the TCf measurement through which we extract α of the MoS_2 device, and the calibration of the resonance frequency (f_{res}) shift under different laser power levels. This type of device is promising for frequency-shift-based temperature sensors and other thermal sensing functions previously demonstrated in MEMS [3], as well as laser power meters and photodetectors shown with MoS_2 transistors [4]. As we can measure frequency and time with very high accuracy, and the device has very high TCf (-0.396%/K) and excellent power responsivity (-4.116%/mW), this technique will be very sensitive for such thermal sensing or monitoring applications.

Device resonance is optothermally driven using an RF modulated 405nm laser, and detected by interferometry with a 633nm laser. Figure 1a shows the TCf of a 56nm-thick MoS_2 resonator (Fig. 1e) measured by regulating the device temperature using an integrated temperature controller. Combining the experimental data with FEM simulations, we determine the thermal expansion coefficient to be α=3.7×10^{-6}/K. We also measure the f_{res} shift under various 633nm laser power levels, which exhibits highly linear relationship (Fig. 1b).

Figure 1c and 1d show the mode shape and temperature profile of the MoS_2 resonator under laser heating, respectively. To calibrate the heating effects for both 633nm and 405nm laser, and to evaluate the effects due to laser spot (or fiber) positioning, we measure both undriven thermomechanical spectra and driven resonances. We find that the 405nm laser has very little heating effect as we defocus it and move it away from the device to prevent overheating, and the 633nm laser position will affect the f_{res} shift (Fig. 1f). Complete experimental details and analysis, including results for devices with different sizes and thicknesses, will be presented in the full paper.

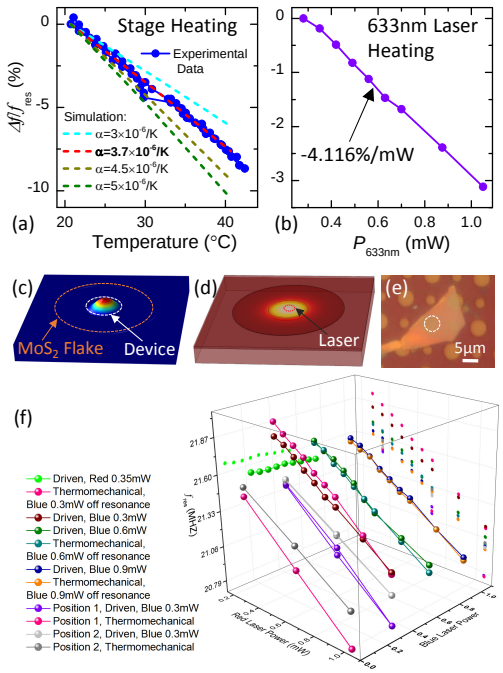


Fig. 1: Calibration of TCf and laser heating effects of a 56nm-thick MoS_2 diaphragm resonator suspended on a 5μm-diameter cavity. (a) Experimental data and simulations of f_{res} shift with different device heating temperature, for obtaining α. (b) Experimental data of f_{res} shift at different 633nm laser power levels. (c) & (d) Simulation results of (c) mode shape and (d) temperature profile of the device under laser heating. (e) Optical microscope image. (f) Calibration of red and blue laser effect on f_{res} under different conditions.

[1] J. Lee, *et al.*, "High frequency MoS_2 nanomechanical resonators," *ACS Nano*, vol. 7, pp. 6086-6091, Jun. 2013.

[2] K.L. Aubin, *et al.*, "Laser annealing for high-Q MEMS resonators," *Proc. SPIE*, vol. 5116, pp. 531-535, Apr. 2003.

[3] C.M. Jha, *et al.*, "CMOS-compatible dual-resonator MEMS temperature sensor with milli-degree accuracy," *Proceedings of the 14th Int. Conf. on Solid-State Sensors, Actuators & Microsystems* (*Transducers'07*), pp. 229-232, Lyon, France, Jun. 10-14, 2007.

[4] O. Lopez-Sanchez, *et al.*, "Ultrasensitive photodetectors based on monolayer MoS_2," *Nature Nanotech.*, vol. 8, pp. 497-501, Jun. 2013.

Performance Evaluation of CMOS-MEMS Thermal-Piezoresistive Resonators in Ambient Pressure for Sensor Applications

Jung-Hao Chang[1], Cheng-Syun Li[2], Cheng-Chi Chen[2], and Sheng-Shian Li[1,2]
[1] Dept. of Power Mechanical Engineering, [2] Inst. of NanoEngineering and MicroSystems
National Tsing Hua University, Hsinchu, Taiwan
E-mail: g123869443@hotmail.com

In this work, we report a thermally driven and piezoresistively sensed (i.e., thermal-piezoresistive) CMOS-MEMS resonator with high quality factor (Q ~ 2,000) in air and decent power handling capability. The combination of (i) no tiny transducer gap spacing resulting from thermal-piezoresistive transduction, (ii) the use of high-Q SiO_2/polysilicon structural materials from CMOS back-end-of-line (BEOL), and (iii) a bulk-mode resonator design leads to ***resonator Q more than 2,000 in ambient pressure and 10,000 in vacuum***. Key to attaining sheer Q in ambient pressure relies on significant attenuation of air damping effect under thermal-piezoresistive transduction as compared to capacitive resonators which necessitate tiny transducer's gap for reasonable electromechanical coupling. With such high Q and inherent circuit integration capability, the proposed CMOS-MEMS thermal-piezoresistive resonators can potentially be implemented as highly sensitivity mass/gas sensors based on resonant transducers. The resonators with center frequency around 5.1 MHz were fabricated using a standard 0.35 μm 2-poly-4-metal (2P4M) CMOS process, thus featuring low cost, batch production, fast turnaround time, easy prototyping, and MEMS/IC integration.

Fig. 1 shows the measured frequency spectra of CMOS-MEMS thermal-piezoresistive resonators developed in this work. The Q-factor in vacuum is six times higher than that in air while Q of 2,000 in ambient pressure is still very attractive among all CMOS-MEMS counterparts. The transmission loss between vacuum and air (around 10 dB) can be compensated using higher dc-power operation. Fig. 2 presents the power handling capability of the resonator in air. Due to the high-stiffness vibration mode and thermal driving, the decent power handling is achieved as compared to capacitive resonators which suffer strong capacitive nonlinearity.

[1] S. J. Hyeong *et al.*, "High-Q-factor in-plane-mod…," *IEEE J. Microelectromech. Syst.*, vol. 17, pp. 483-493, Apr. 2008.
[2] A. Rahafrooz and S. Pourkamali, "High-Frequency…," *IEEE Trans. Electron Devices*, vol. 58, pp. 1205-1214, Apr. 2011.

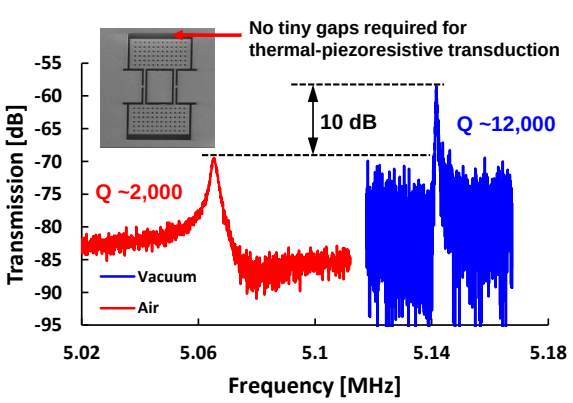


Fig. 1: Frequency responses of the proposed CMOS-MEMS thermal-piezoresistive resonator. The red and blue curves indicate the transmission in air and vacuum. The Q-factors are 2,000 and 12,000, respectively.

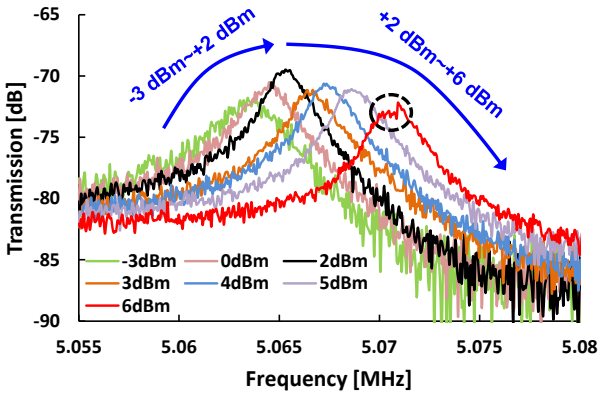


Fig. 2: Power handling of the CMOS-MEMS thermal-piezoresistive resonator tested in air. It shows the transmission under different driving power levels, from -3dBm to +6dBm. And the resonator becomes malfunction under +6dBm driving power.

Comparison of Acoustic Wave Pressure Sensors for TPMS applications

Nagaraju Manohar*, Sridaran Suresh†, Lingley Andy*, Larson John†, Otis Brian*, Ruby Richard†
*Department of Electrical Engineering, University of Washington, Seattle, WA, US
†Wireless Semiconductor Divison, Avago Technologies, San Jose, CA
E-mail: manohar@uw.edu

In this work, we demonstrate a Rayleigh Lamb wave (RL) mode resonator based pressure sensor suitable for TPMS applications. A FBAR-based pressure sensor for TPMS applications with sensitivity of 2.2 ppm/psi was proposed in [1]. We extend on the work and propose to improve the pressure sensitivity. The processing of the sensor is similar making it attractive to design highly sensitive, fully integrated pressure sensors for a TPMS.

The resonant frequency of an acoustic resonator is sensitive to the in-plane stress in the membrane and is expressed as in equation (1). 'V_a' is the phase velocity of the acoustic wave propagating in a piezoelectric membrane with a wavelength of 'λ', 'C', the stiffness matrix & 'ρ' the mass density of the membrane. A differential pressure induces a bending stress in the horizontal plane of the membrane. This changes the resonant frequency of the resonator creating a relative pressure-to-frequency transducer.

$$f_{resonant} = V_a / \lambda$$

$$V_a = (C/\rho)^{1/2} \qquad \text{(Eq. 1)}$$

In this paper, we compare measured data of an FBAR pressure sensor resonator vs several RL mode resonators (or larger area). For the RL membrane, we use an inter-digitated resonator structure as shown in the Fig. 1a to excite the Lamb waves in the membrane. A wafer-scale process as described in [1] is used to build a RL-mode resonator in a hermetically sealed package. The thickness of the piezoelectric membrane is 1µm. After processing the FBAR and RL resonators and hermetically sealing them, a standard Dry Reactive Ion Etching (DRIE) process was used in a post fabrication process to provide a channel for pressure input to the sensor.

The frequency shift of the RL-mode resonator was monitored on a network analyzer. The pressure sensitivity across different areas of the resonator was measured. As the data suggests, sensitivity trades with the area of the RL resonator (Figure 1(b)) and measured 7.08ppm/psi for the largest area device fabricated.

In summary, we demonstrate a RL-mode resonator based pressure sensor to improve the sensitivity for TPMS applications. We achieve this in a wafer scale fabrication process using standard micromachining process throughout, making it commercially viable in mass production

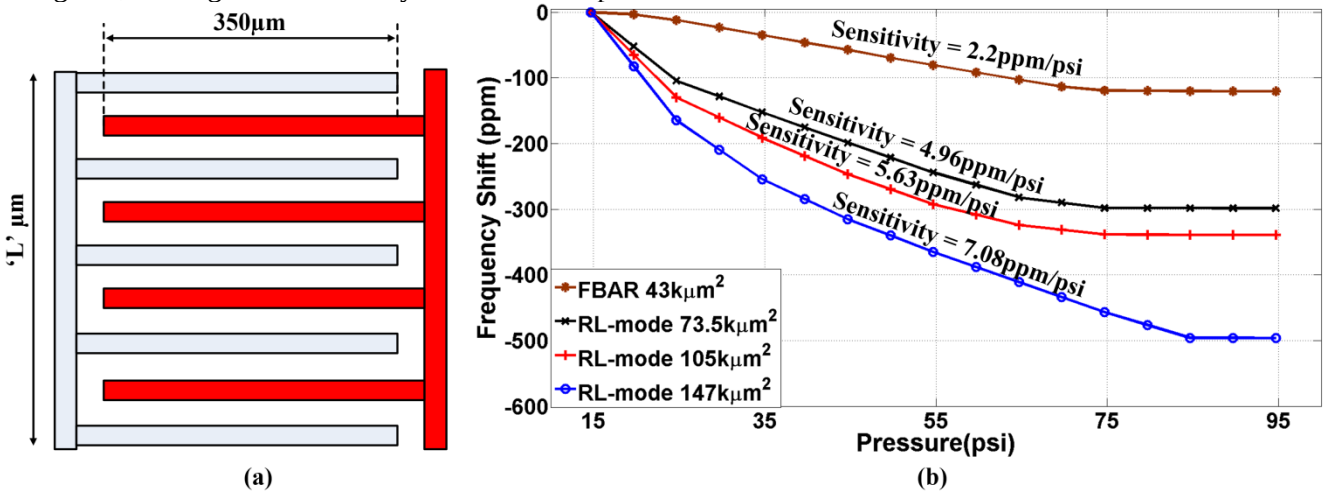


Figure 1 : a) Structure of the Interdigitated RL-mode resonator. b) Response of the RL-mode (for different areas) and FBAR resonators to pressure.

References :

[1] Nagaraju, Manohar et. al,. "A 0.8mm3, ±0.68psi Single-Chip Wireless Pressure Sensor for TPMS Applications." Solid State Circuits Conference, International (ISSCC), February 2015

Micromechanical Piezoelectric-on-Silicon BAW Resonators for Sensing in Liquid Environments

Prasad, Abhinav, Charmet, Jérôme, Seshia, Ashwin A.
Department of Engineering, University of Cambridge, Cambridge, United Kingdom
E-mail: ap676@cam.ac.uk

MEMS technology enables batch-fabrication of miniaturized mechanical sensors that may be co-integrated with chip-scale electronics and microfluidic handling systems to realize portable platforms of small form-factor for bio-chemical sensing and environmental monitoring. Particular implementations of such mechanical transducers are micro/nanomechanical resonators where the interaction between the analyte/surrounding media and the resonator surface results in a shift in the resonant frequency response. However, when these resonators are operated in viscous environments (air and liquids), they suffer from degradation in performance due to high levels of fluidic damping. The quality factors of bulk-acoustic resonators are typically higher than corresponding flexural mode resonators thereby offering the potential for higher resolution sensing in liquid environments [1], [2].

This abstract reports on micromachined AlN thin-film piezoelectric-on-silicon BAW resonators (Fig. 1a) operating in the square-extension mode at ~3.16 MHz in liquid environments. The devices were fabricated using the foundry PiezoMUMPs process incorporating a 0.5 μm thick AlN piezoelectric film deposited on a 10 μm thick silicon structural layer. The devices were piezoelectrically transduced in a two-port open loop configuration. Relatively high quality factors in the range of 110 to 190 were observed with one surface in contact with water. Various Glycerol-Water mixtures (varying the viscosity-density product of the fluid medium in contact with the resonator) were introduced resulting in corresponding negative resonant frequency shifts recorded as shown in Fig. 1 (b). Using analytical expressions for liquid loading for such devices [3], resonant frequency shift predictions were compared to experiment with agreement seen to within 10%.

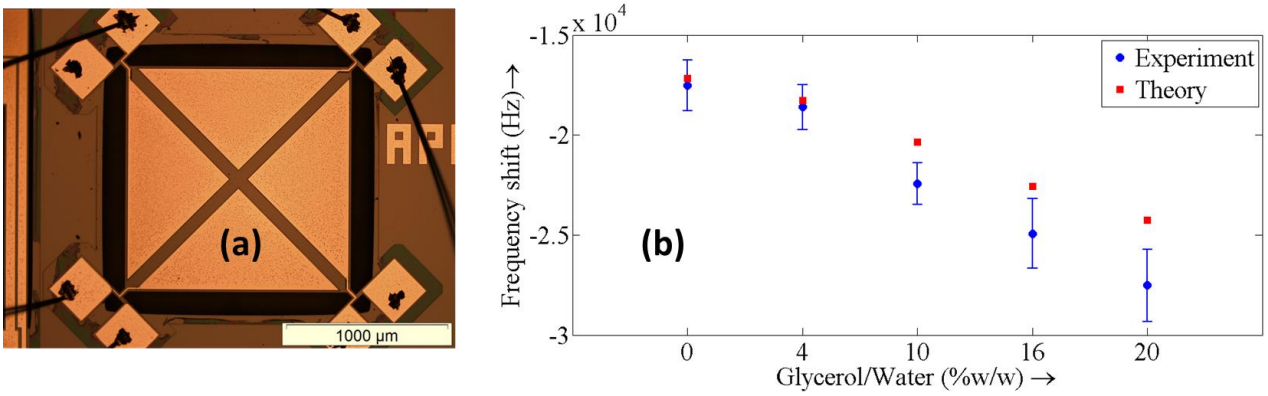


Fig. 1: (a) Optical micrograph of the piezoelectric square resonator, and (b) Frequency shifts observed for the square-extension mode (experiment, theory) for different Glycerol-Water (% w/w) mixtures in contact with one surface of the resonator.

[1] A. T.-H. Lin, J. Yan, and A. A. Seshia, "Electrically addressed dual resonator sensing platform for biochemical detection," *J. Micromechanical Syst.*, vol. 21, no. 1, pp. 34-43, Feb. 2012.

[2] T. Manzaneque, V. Ruiz-Diez, J. Hernando-Garcia, *et al.*, "Piezoelectric in-plane microplate resonators based on contour and flexure-actuated modes," *Microsyst. Technol.*, vol. 20, no. 4-5, pp. 691-699, Dec. 2013.

[3] A. Prasad, A. T.-H. Lin, V. R. Rao, and A. A. Seshia, "Monitoring sessile droplet evaporation on a micromechanical device," *Analyst*, vol. 139, pp. 5538-5546, Aug. 2014.

Stress sensitivity coefficients of HBAR

BARON Thomas, PETRINI Valérie, MARTIN Gilles, COMBE Guillaume, CLAIRET Alexandre, LAROCHE Thierry*, LESAGE Jean-Marc+, DULMET Bernard, BALLANDRAS Sylvain*
Time & Frequency department, FEMTO-ST, UMR CNRS-UFC-ENSMM-UTBM 6174, Besançon, France
*frec|n|sys SAS, Besançon, France
+ DGA – Information Superiority, Bruz, France
E-mail: thomas.baron@femto-st.fr

Previous work has demonstrated experimentally a low vibration sensitivity of High-overtone Bulk Acoustic Resonators (HBAR) [1]. The corresponding experimental results show a global vibration sensitivity of 3.9×10^{-11}/g for HBAR based on ALN on Sapphire, and 2.6 or 2.9×10^{-9}/g for HBAR based on $LiNbO_3$ piezoelectric layer on Quartz or $LiTaO_3$. To reproduce and improve such results, the resonator design must be supported by accurate computation. However, the calculation of the stress sensitivity of HBAR resonators imposes some theoretical developments and the implementation of an *ad hoc* simulation tool.

A first attempt to calculate the stress sensitivity coefficients of thin film resonators (FBARs) has been proposed by Masson *et al.* [2] but this approach did not reveal easily adaptable to the treatment of HBARs resonators which are composed of several crystalline materials. We here consider the Sinha-Tiersten perturbation method [3] [4] [5] which involves the computation of static and dynamic terms. We adapt the method to carry all necessary integrations across the different layers of the stacked HBARs structures. Assumption of constant stress in the various layers is done allowing the derivation of HBAR stress sensitivity coefficients of frequency ($^s\alpha_{mn}$). Only mechanical terms are taken into account and the contribution of the piezoelectric constants were deliberately omitted in the perturbation equations since electromechanical coupling rarely approach the percent in HBAR.

Fig. 1 shows the evolution of stress sensitivity coefficients for the case of HBAR based on (YX*l*)/163° $LiNbO_3$ piezoelectric layer and (YX*lt*)/35°/90° quartz substrate. The stress sensitivity coefficients are slowly changing along the overtone number but we note a maximum variation near the piezoelectric layer fundamental resonance. For other overtones, stress sensitivity coefficients are almost constant and remain close to the coefficient of the single substrate plate. As the stress coefficients obtained using the proposed calculation are very close to those obtained with the calculation of BAW $^s\alpha_{mn}$ on single-crystal substrates, usual low sensitivity cuts for BAW can be used also for HBAR. All non-linear constants of material were found in [6]. As a conclusion, Comparisons with experimental results of acceleration sensitivity of HBAR oscillators based on sapphire and quartz are achieved to validate the proposed model.

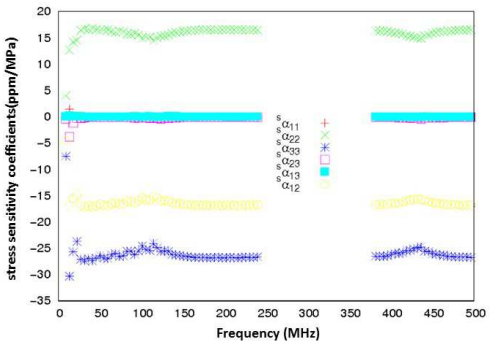


Fig. 1: HBAR Sensitivity coefficient for HBAR based on (YX*lt*)/35°/90° quartz substrate (thickness equal to 350µm) with (YX*l*)/163° LiNbO3 layer of 15 µm thickness.

[1] Baron T., *et al.*, "Low-g sensitivity of HBAR Oscillator", in *European Frequency and Time Forum*, 2014
[2] Masson, J.; Reinhardt, A.; Ballandras, S.; "Simulation of stressed FBAR thanks to a perturbation method," *Microwave Symposium Digest*, 2005 IEEE MTT-S International , vol., no., pp. 4 pp., 12-17 June 2005
[3] Sinha, B.K., Tiersten, H.F., "On the temperature dependence of the velocity of surface wave in quartz", *J. Appl. Phys.*, Vol.51, n°9, pp. 4659-4665, 1980
[4] J.C. Baumhauer, H.F. Tiersten, J. *Acoust. Soc. Am.*, 54, 1017, 1973
[5] H.F. Tiersten, *J. Acoust. Soc. Am.*, 64, 832, 1978
[6] Landolt-Bornstein

A 400µW serial interface circuit for FBAR pressure sensor

Nagaraju Manohar*, Sridaran Suresh†, Lingley Andy*, Parker Reed†, Ruby Richard†, Otis Brian*
*Department of Electrical Engineering, University of Washington, Seattle, WA, US
†Wireless Semiconductor Divison, Avago Technologies, San Jose, CA
E-mail: manohar@uw.edu

We have demonstrated fully-integrated FBAR-based pressure sensors previously [1]. However, the instantaneous power consumption of the interface circuitry, 12.69mW, is prohibitively high to be used with standard coin-cell batteries, considering that a Tire Pressure Monitoring System (TPMS) would include an additional accelerometer, memory and an on-chip controller. In this work, we propose to reduce the instantaneous power consumption by processing the sensor information in the digital domain. The output variable from the FBAR sensor/oscillator can readily be processed by standard digital cells. A digital interface will also benefit from scaling to advanced nodes and is easily reconfigurable.

Figure 1 shows the architecture of the digital FBAR pressure sensor system. Two FBAR's are integrated in close proximity to cancel the resonant frequency drift due to temperature, stress etc. The sensor resonator is exposed by a backside etch at the wafer level while the reference FBAR is hermetically sealed. Both core oscillators use the Pierce topology. The sensor oscillator frequency is measured on-chip with a 26-bit counter. The clock for the measurement is derived from the reference oscillator by a programmable divider. The measurement period is a function of the resolution requirement of the sensor. A higher divide ratio reduces the quantization error in the measurement, however also increasing the average power consumption for one measurement cycle. The output of the counter provides a digital value representative of the pressure input. In this case, we read the output value through a serial communication interface.

The proposed digital sensor interface was fabricated in a 130nm IBM CMOS process. We integrate the dual FBAR die with the circuit die by flip chipping at the die level, due to unavailability of the processing. However, the processing proposed in [1] could be followed in a similar fashion.

The digital interface consumes 530µW from a 0.75V supply, sufficiently low to enable integration with standard coin-cell batteries available in the market. Detailed results of the pressure sensor will be discussed in the final paper.

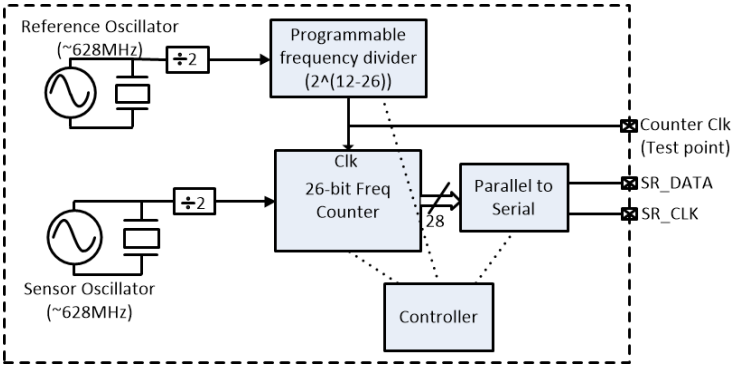


Figure 1: Architecture of the digital interface for a FBAR pressure sensor

[1] Nagaraju, Manohar et. al,. "A 0.8mm^3, ±0.68psi Single-Chip Wireless Pressure Sensor for TPMS Applications." *Solid State Circuits Conference, International (ISSCC), February* 2015

Dual-Mode NEMS Self-Oscillator for Mass Sensing

Gourlat, Guillaume, Sansa M., Jourdan G., Villard P., Sicard G., Hentz S.
LETI, CEA (Commissariat à l'énergie atomique et aux énergies alternatives), Grenoble, France
E-mail: guillaume.gourlat@cea.fr

We report the first experimental demonstration of a heterodyne self-oscillator operating alternatively on the first and second resonance mode of a silicon NEMS resonator. This oscillator is a step towards all applications requiring dense integration of multimode-resonator arrays, like single-particle mass sensing applications.

Nano Electro Mechanical Systems (NEMS) constitute a promising solution for mass sensing applications [1], which require very high capture efficiency of the analytes, only achievable by co-integration of arrays of sensors with CMOS circuitry [2]. Two architectures have been reported in the literature. The homodyne self-oscillating scheme is the most compact, but it is very sensitive to parasitic coupling and it is not able to handle multimode operation (necessary to deduce the mass of a particle landing on an unknown position on the NEMS). On the other hand, the Phase Lock Loop handles multimode resonator with robustness to parasitic capacitances but it implies power-consuming and bulky circuitry, which does not scale favorably for large arrays of sensors. In this context, we present an improved heterodyne self-oscillator [3] capable of handling multimode operation with the reduced footprint and consumption of the self oscillator scheme.

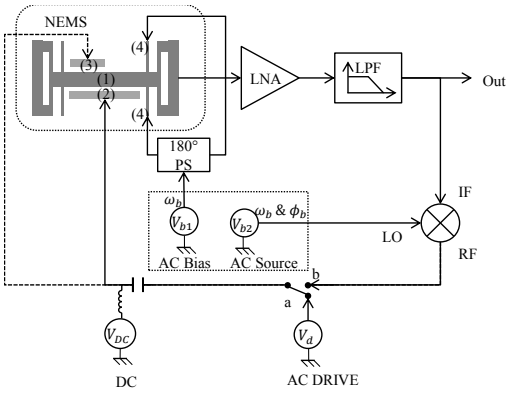


Fig. 1: Diagram of the oscillator setup used for both modes. Switch position (a) and (b) corresponds to the open loop and closed loop scheme respectively. The dashed connection is used for the second mode of operation.

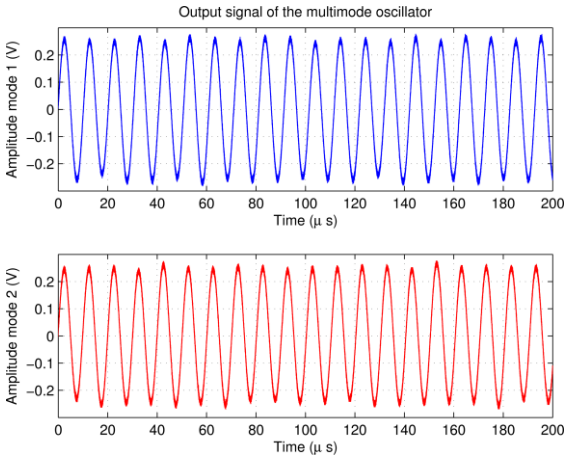


Fig. 2: Output of the closed loop for mode 1 (Top) and for mode 2 (Bottom) of the heterodyne oscillator.

The nanomechanical resonator used here [4] is a monocrystalline silicon doubly-clamped beam with compliant anchors for enhanced dynamic range. It is electrostatically-actuated and its motion is transduced in the electrical domain thanks to two piezoresistive nanoscale gauges in bridge configuration. It operates under vacuum (typically 10^{-5} mbar) at room temperature. The frequency response spectrum and the intrinsic frequency stability of the resonator are first obtained by an open loop characterization. Our implementation Fig. 1 allows the closing of the loop with only an amplifier, a low pass filter and a phase shifter. Sustained oscillations on the first two mode of resonance are easily obtained without tedious parameter tuning Fig. 2. From a sensing point of view, the frequency stability was measured and is not degraded with this new implementation and very fast response to external perturbations is demonstrated.

In conclusion, this work demonstrates for the first time the multimode operations of our heterodyne NEMS self-oscillator scheme which promises a reduced silicon footprint and power consumption compatible with the readout of dense sensor arrays required by mass sensing applications.

[1]M. S. Hanay, S. Kelber, A. K. Naik et al., *Nat. Nanotechnol.*, vol. 7, no. 9, pp. 602–608, Sep. 2012.
[2]G. Arndt, C. Dupre, J. Arcamone et al., Proc. *ISSCC, 2012 IEEE International*, pp. 320–322, 2012.
[3]G. Jourdan, E. Colinet, J. Arcamone et al., *Sens. Actuators Phys.*, vol. 189, pp. 512–518, Jan. 2013.
[4]E. Mile, G. Jourdan, I. Bargatin, S. Labarthe et al., *Nanotechnology*, vol. 21, no. 16, p. 165504, Apr. 2010.

GPS-based frequency comparison of $^{171}Yb^{+}$ ion optical clocks at PTB and NPL

N. Huntemann[1], B. Lipphardt[1], Chr. Tamm[1], R. M. Godun[2], J. M. Jones[2], S. A. King[2], H. S. Margolis[2], P. B. R. Nisbet-Jones[2], V. Gerginov[1], S. Weyers[1], P. Głowacki[2,4], S. N. Lea[2], K. Szymaniec[2], J. Leute[1], P. Whibberley[2], A. Wallin[3], M. Merimaa[3], P. Gill[2], E. Peik[1]

[1]Physikalisch-Technische Bundesanstalt (PTB), Bundesallee 100, 38116 Braunschweig, Germany
[2]National Physical Laboratory (NPL), Hampton Road, Teddington, TW11 0LW, UK
[3] MIKES Metrology, VTT Technical Research Centre of Finland ltd, Espoo, Finland
[4]Poznań University of Technology, Poznań, Poland

E-mail: ekkehard.peik@ptb.de

Optical frequency standards based on single laser-cooled $^{171}Yb^{+}$ ions are investigated at NPL, UK and at PTB, Germany, and in other laboratories. The ytterbium ion is of particular interest since it provides two narrow transitions suitable for the realization of an optical frequency standard with low systematic uncertainty: the $^{2}S_{1/2}(F=0)$-$^{2}D_{3/2}(F=2)$ electric quadrupole transition (E2) and the $^{2}S_{1/2}(F=0)$-$^{2}F_{7/2}(F=3)$ electric octupole transition (E3). Both transitions have been recommended by the CIPM as secondary representations of the SI second and very good agreement between independent transition frequency measurements against cesium fountain clocks has been obtained over recent years [1-3]. However, a significant contribution to the total uncertainty of these comparisons resulted from the local microwave reference. Therefore, a direct, remote frequency comparison during simultaneous operation is favorable, as has recently been demonstrated between two Sr lattice clocks [4].

Since no optical fiber link is yet available between the institutes, our comparison is based on the well-established GPS Carrier-Phase based time and frequency transfer using the Precise Point Positioning technique. In this way, the frequency difference of hydrogen masers located at PTB and NPL has been determined. Simultaneously, the unperturbed frequency of the $^{171}Yb^{+}$ E2 transition has been realized at both sites and compared to the hydrogen masers via frequency combs. From data recorded during more than 38 hours of simultaneous measurement, we are able to investigate relative frequency differences with an uncertainty on the order of 10^{-15}. To further increase the confidence in the data and to check for consistency with previous results, the optical frequency was compared to cesium fountain clocks during the measurement at PTB and NPL.

From the data obtained using the E2 transition, in principle, even tighter limits can be inferred indirectly for the agreement of the E3 transition frequency realized with the same ion trap at each institute due to its significantly smaller sensitivity against external electric and magnetic fields. This fact can also be used in another way of comparing the two optical frequency standards of the distant laboratories by comparing the ratio of the two transition frequencies measured at each site.

This work is funded by the EMRP project SIB04 Ion Clock. The EMRP is jointly funded by the EMRP participating countries within EURAMET and the European Union.

[1] R. M. Godun, P. B. R. Nisbet-Jones, J. M. Jones, S. A. King, L. A. M. Johnson, H. S. Margolis, K. Szymaniec, S. N. Lea, K. Bongs, and P. Gill, "Frequency ratio of two optical clock transitions in $^{171}Yb^{+}$ and constraints on the time variation of fundamental constants," Phys. Rev. Lett. 113, 210801 (2014).

[2] Chr. Tamm, N. Huntemann, B. Lipphardt, V. Gerginov, N. Nemitz, M. Kazda, S. Weyers, and E. Peik, "Cs-based optical frequency measurement using cross-linked optical and microwave oscillators," Phys. Rev. A 89, 023820 (2014).

[3] N. Huntemann, B. Lipphardt, Chr. Tamm, V. Gerginov, S. Weyers, and E. Peik, "Improved limit on a temporal variation of m_p/m_e from comparisons of Yb^{+} and Cs atomic clocks," Phys. Rev. Lett. 113, 210802 (2014).

[4] H. Hachisu, et al., "Direct comparison of optical lattice clocks with an intercontinental baseline of 9000 km," Opt. Lett. 39, 4072 (2014).

Uncertainty Evaluation of 2013 TL METODE Link Calibration Tour

Shinn-Yan Lin, Yi-Jiun Huang, and Wen-Hung Tseng
Telecommunication Laboratories Chunghwa Telecom Co., Ltd., Taoyuan Taiwan
E-mail: sylin@cht.com.tw

From MJD 56595 to 56650 (30 Oct. – 24 Dec. 2013), the BIPM METODE [1] calibrators (StdB, composed of BIPM GNSS traveling receivers BP0U and BP1C) visited TL to calibrate the TL's GNSS reference station, TWTF, and the UTC link from PTB to TL. The BP0U and BP1C's total electronic delays, denoted by DlyR(BP0U) and DlyR(BP1C) respectively, from the phase center of their antennae (PCA) to the calibration reference 1 PPS point had been calibrated based on PTBB (the GNSS pivot reference station of UTC) DlyR(PTBB) before this calibration tour, thus we could use DlyR(BP0U) and DlyR(BP1C) to calibrate/align the total electronic delay from the PCA of TWTF to the UTC(TL) 1 PPS reference point, DlyR(TWTF), and link delay between PTBB and TWTF (denoted as DlyL(PTBB, TWTF)).

The link delay, DlyL(PTBB, TWTF), was used for zeroing the stations bias to measure the time differences remotely. Based on METODE, the link delay DlyL(PTBB, TWTF) was the difference between the total delays DlyR(PTBB) and DlyR(TWTF) by definition [1]. In this paper, we analyzed DlyL(PTBB, TWTF) and expressed it as 3 individual groups, the first group contained the uncompensated GPS CCD (common clock difference) measurements in PTB and TL, the second was the cable delay measurements. The third was the total delay migration of station PTBB, TWTF, and the travelling calibrator StdB (BP1C or BP0U) in this tour. The uncertainty of the first group was statistical uncertainty, the uncertainty of second group was typically limited by the systematic uncertainty of time interval counter, before we had more precise method to measure the GPS timing and cable delay, it's not easy to reduce the uncertainty introduced by items of group 1 and 2.

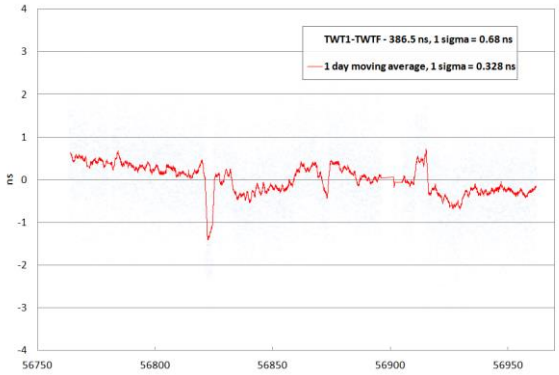


Fig. 1: The P3 CCD of 2 Ashtech Z12T GPS receivers of TL over 300 days.

The third group contained non-white-noise terms of the TOTDLY of GPS stations, including their delay instability of antennae, cables, receivers, and any other unknown terms. For PTBB and TWTF, they were both fixed (antennae, cables, receiver) Ashtech Z12T Metornome stations. In this paper, we monitored the long-term behavior of Ashtech Z12T Metornome over 300 days to evaluate the non-stationary effects of PTBB and TWTF; for the BIPM travel stations BP0U and BP1C, we used a moving cesium clock method to evaluate their instability of total delay in different antenna position over 25 km baseline. Although the long-baseline behavior was not evaluated here, our study was helpful for clarifying the uncertainty composition of the current PTB-TL link and could reduce it in a reasonable limitation.

[1] Z. Jiang et al, "BIPM Calibration Scheme for UTC Time Links," Proc. EFTF 2011, pp 1064–1069

[2] S. Y. Lin, Y. J. Huang, and W. H. Tseng, "Upper Limit Uncertainty Estimation of TL METODE Calibration Tour Using Moving Cs Clock Method" *Proceedings*, 2014 Precise Time and Time Interval, Boston, Ma, Dec 1-4, 2014.

Link calibration or receiver calibration for accurate time transfer ?

Z Jiang
Time Department, Bureau International des Poids et Mesures (BIPM)
zjiang@bipm.org

Calibration is essential for accurate time transfer. The time transfer techniques so far used for clock comparisons in UTC are (1) for Two-Way Satellite Time and Frequency Transfer, the *link* calibration using a TWSTFT mobile ground station [1-3] has in *Circular T* conventional value 1 ns for the Type B uncertainty (u_B); and (2) for GNSS time transfer, the classical differential receiver calibrations [4]. The conventional value of u_B in *Circular T* is larger than that of TWSTFT.

Many authors started implementing GPS link calibrations. The latest developments [5-10] suggest that the u_B at the moment of the calibration can be 1 to 1.5 ns. This is a great achievement which suggests that link calibrations can bring an improvement in the uncertainty of time links in Circular T in a factor of about 2 or 3, with a positive equivalent impact on the uncertainty of [*UTC-UTC*(*k*)]. An advantage of the link calibration is to be able to calibrate all types of time transfer techniques over the same baseline, e.g., a physical TWSTFT *link* calibration can be used to calibrate the respective GPS link, and vice versa.

In earlier studies [1-10], the *receiver* calibration and the *link* calibration had been discussed and implemented separately as if the two calibrations were independent. In fact, the difference between the *receiver* and *link* calibrations is not how to perform the calibration measurement but how to use the measurement data. The two calibration results are convertible to each other. We discuss the advantages and disadvantages of the *link* and *receiver* calibrations, the method for the conversion, their uncertainties, and in particular, of which their application to the computation of [*UTC-UTC*(*k*)].

Key word: time transfer, uncertainty, calibration, link calibration, differential receiver calibration

[1] Piester D., A. Bauch, L. Breakiron, D. Matsakis, B. Blanzano, O. Koudelka (2008): Time transfer with nanosecond accuracy for the realization of International Atomic Time, *Metrologia*, vol. 45, 185 – 198, 2008

[2] Niessner A, W. Mache, B. Blanzano, O. Koudelka, J. Becker, D. Piester, Z. Jiang, and F. Arias (2008), *Calibration of the BEV GPS receiver using TWSTFT*, Proc. PTTI 2008

[3] Jiang Z et N. A. Niessner, *Calibrating GPS with TWSTFT for Accurate Time Transfer*, Proc. PTTI 2008

[4] Petit G., Jiang Z., Moussay P., White J., Powers E., Dudle G, Uhrich P., Progresses in the calibration of geodetic like GPS receivers for accurate time comparisons, Proc. 15th EFTF, p.164, 2001a

[5] Esteban H, J. Palacio, A. Bauch, D. Piester, G. Cerretto, T. Feldmann (2012) EURAMET Project 1156, GPSCALEU, Results of two years GPS receiver calibration campaign. Proc. 2012 European Frequency and Time Forum, 24-26 Apr 2012, Gothenburg, Sweden, pp. 354-360, 2012

[6] Feldmann T., A. Bauch, D. Piester, P. Alvarez, D. Autiero, J. Serrano, G. Brunetti (2013) Relative Calibration of the Time Transfer Link between CERN and LNGS for Precise Neutrino Time of Flight Measurements. Proc. 44th Annual Precise Time and Time Interval (PTTI) Systems and Applications Meeting, Reston, Virginia, USA, pp. 141-150, 2013

[7] Cerretto G., H. Esteban, M. Pallavicini, Va. Pettiti, C. Plantard, A. Razeto (2012) Measurement of CNGS Muon Neutrinos Speed with Borexino: INRIM and ROA Contribution. Proc. 44th Annual Precise Time and Time Interval (PTTI) Systems and Applications Meeting, Reston, Virginia, USA, pp. 133 - 140, 2012

[8] Liang K. Feldmann T., Bauch A. , Piester D. ; Zhang A., Gao X. (2011) Summary of the Link Calibration between NIM and PTB Using a Traveling GPS Receiver， Proc. IFCS&EFTF2011

[9] Lin Calvin S.Y., Huang Y. J., Tseng W. H. (2014) Upper Limit Uncertainty Estimation of TL METODE Calibration Tour Using Moving Cs Clock Method, Proc. ION PTTI 2014

[10] Jiang Z (2014) Accurate time link calibration for UTC time transfer -- Status of the BIPM pilot study on the UTC time link calibration, Proc. EFTF 2014

The performance evaluation of the BD one-way time service

Wei Li[1,2],Wei Guang[1,2], Jihai Zhang[1,2], Zhe Gao[1,2], Yongliang Xu[1]
[1]Natioanl Time Service center,CAS, Xi'an China
[2]Key Laboratory of Time & Frequency Primary Standard, CAS, Xi'an China

The capability of one-way time service as an important index of satellite navigation system reflects the ability that a satellite navigation system broadcast the system time to the clients.In this paper, the performance evaluation method of BD one-way time service is designed standing in the clients' position. The evaluation system is shown as Figure.1.

The UTC(NTSC)-BDT result via Space signal reception method is obtained in NTSC. The remote time comparison methods between UTC(NTSC) and BDT include GPS CV、BD CV and TWSTFT. It is shown in Table.1 that the results of the three links have strong consistency. In this paper, the results of BD CV is chose as the reference to evaluate the performance of BD one-way time service.

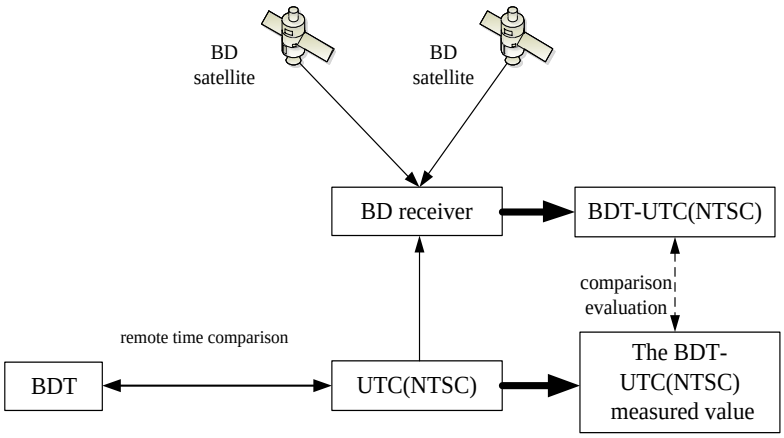


Figure.1 The performance evaluation system of the BD one-way time service

Table.1 residual statistics of three links

	BDSCV-TW	GPSCV-TW	GPSCV-BDSCV
RMS	0.79ns	1.83 ns	1.46 ns

The residual between one-way time service and BD CV is shown in Figure.2, from June 27,2013 to November 10,2013.

Calculating the root mean square error of residual, The uncertainty of one-way time service is 3.01 ns, the result shows that the pricision of BD one-way time service have higher level.

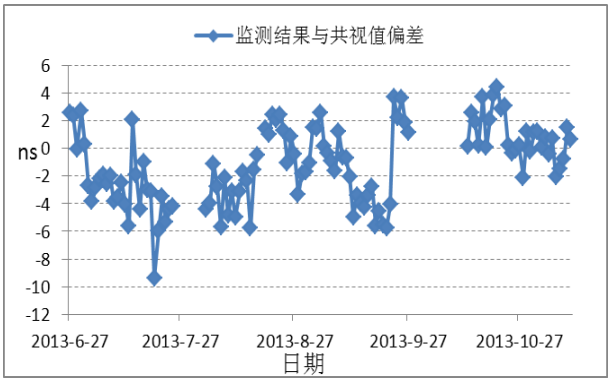


Figure.2 The residual between one-way time service and BD CV

[1] Haitao Wu, Xiaohui Li, Xiaochun Lu. The base of Satellite navigation system time[M]. Beijing: The Chinese Science Press. 2011，54~62.

[2] Yuan Haibo, Guang wei. Common View Time Transfer by a GEO Navigation Satellite[C], IEEE IFCS. 2012.

Techniques of antenna cable delay measurement for GPS time transfer

Rovera Giovanni Daniele, Abgrall Michel, Uhrich Pierre, Siccardi Marco†
LNE-SYRTE, Observatoire de Paris - LNE - CNRS - UPMC, Paris, France
†SKK Electronics, Cuneo, Italia
e-mail: daniele.rovera@obspm.fr

In principle, the global delay of an ensemble GPS receiver plus antenna and antenna cable in a station used for time transfer can be evaluated by absolute or relative calibration techniques, disregarding for individual delay contributions as the one due to the antenna cable in the latter case. Relative calibration might be performed with a traveling receiver, which needs to be installed in a common-clock set-up at the station site. However, subsequent modifications to the station's hardware might invalidate the calibration, which proves to be very expensive in either time, money, or logistic. In order to mitigate the issue, the measurement of the antenna cable delay plays an important role. In any cases, absolute calibration requires the proper measurement of the antenna cable delay.

In this paper we will compare the measurement results of antenna cable delay obtained by different techniques, including methods that allow the measurement of the cable installed in-situ. Among these techniques, the reflection of a pulse from the open end of the cable will be analyzed in detail and compared with the results obtained with other methods.

The pulse method is based on transmission line theory. When a pulse enters in a cable, if the cable has the same characteristic impedance of the signal generator, no reflection is produced and the voltage at the input connector rises from 0 to half of the available voltage at the output of the generator. When the pulse reaches the open end of the cable it will be reflected back from the impedance mismatch and the voltage at the input of the cable will raise to the maximum available voltage of the generator. By recording the rising edge of the pulses is then possible to estimate the delay introduced by the cable.

We will provide actual measurement results and a proposal on how to estimate the related uncertainty.

Analysis of System Time Performance in BeiDou Satellite Navigation System

Lu Jun, Ren Ye* †,Xiaohui Li* † , Ya Liu*†
Beijing Institute of Tracking and Telecommunication Technology, Beijing, China
*National Time Service Center, Xi'an, China
†Key Laboratory of Precision Navigation and Timing, National Time Service Center, Xi'an, China
E-mail: renye@ntsc.ac.cn

As same as other satellite navigation systems, the time difference is considered as one of the basic observations in Beidou satellite navigation system. Therefore, an accurate and stable system time is crucial to realize the system function. Based on the inverse decomposition method, this paper analyzes the requirements of Beidou system time (BDT) on behalf of the Beidou System service.

Three time transfer links, The Two-Way Satellite Time transfer, GPS Common-View Time Comparison and Beidou Common-View Time Comparison, are established between National Time Service Center and the Beidou system time center in order to obtain the time difference between BDT and UTC(NTSC). At last, the accuracy and stability of BDT, as Fig1-4 shows, are discussed based on the performance of these three links.

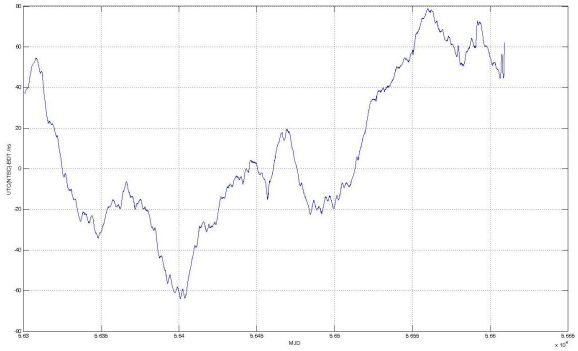


Fig 1 : BDT and UTC(NTSC) time difference

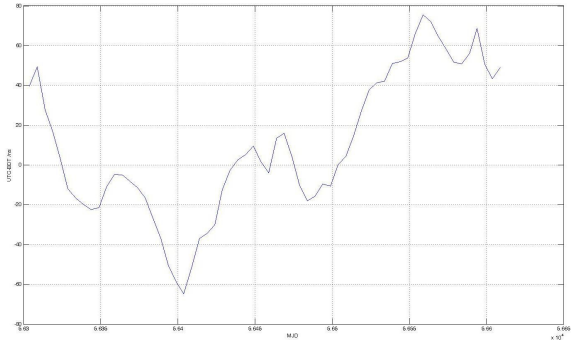


Fig 2 : BDT and UTC time difference

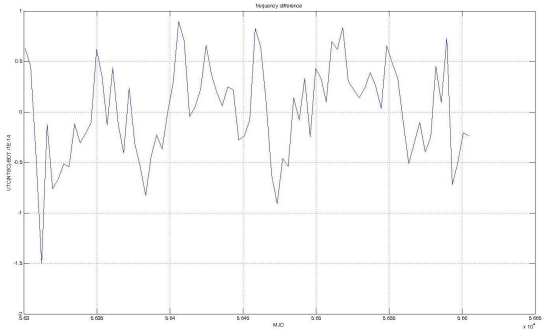


Fig 3 : Frequency difference of BDT-UTC

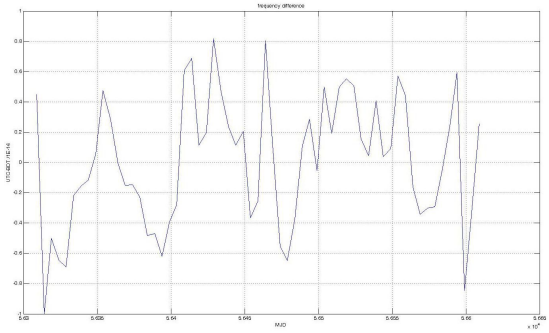


Fig 4 : Frequency difference of BDT-UTC(NTSC)

Relative Calibration of Galileo Receivers within the Time Validation Facility (TVF)

Píriz, Ricardo, D. Rodríguez, P. Roldán, A. Mudrak*, A. Bauch+, J. Leute+, A. Kuna++
GMV, Madrid, Spain
*ESA/ESTEC, Noordwijk, The Netherlands
+Physikalisch-Technische Bundesanstalt, Braunschweig, Germany
++UFE, Prague, Czech Republic
E-mail: rpiriz@gmv.com

GMV is the prime contractor for the Time and Geodetic Validation Facility (TGVF) in the Galileo FOC phase (Full Operational Capability), a contract of the European Space Agency (ESA). Within the TGVF, the Time Validation Facility (TVF) is the subsystem in charge of steering Galileo System Time (GST) to UTC, among other duties. The TVF is operated at GMV headquarters in Madrid, Spain.

Calibrated Galileo receivers are needed in the frame of TVF activities to, among other tasks, assess the GST-UTC offset broadcast in the Galileo navigation message. In a calibrated Galileo receiver connected to a UTC(k) time scale, generated CGGTTS files provide the offset between UTC(k) and GST estimated from the signals of each Galileo satellite in view. Averaging satellites per epoch and applying the UTC-GST offset from the Galileo Signal-In-Space (SIS) we obtain the UTC(Galileo SIS)-UTC(k) difference, which is monitored on a daily basis.

Absolute receiver calibration is a complex activity involving the availability of a signal simulator and a calibrated reference antenna. An alternative data-based method to evaluate the Galileo receiver delay in E5 signals has been proposed by ORB [1]. The key feature of the proposed method is the cancellation of the GPS and Galileo ionospheric delays when combining pseudoranges from two satellites with a close position in the sky. It is assumed that the receiver GPS L1 and L2 delays and the Galileo E1 delay are known. *Differential Code Biases* (DCBs) for GPS and Galileo satellites are also needed as input. The method has been validated at ESTEC by comparing results from a PolaRx4 with the ones obtained from a timing Test User Receiver which had absolute calibration. The results were consistent at nanosecond level.

Normally the GPS L1 and L2 delays of a new receiver can be easily calibrated relative to an existing calibrated receiver connected to the same antenna (or an antenna nearby) and to the same clock or time reference. The Galileo E1 delay should be similar but not identical to the GPS L1 delay, given the shared frequency but different modulations involved. For Septentrio receivers, the manufacturer states that the difference should be at the sub-nanosecond level. DLR [2] measured a difference of 0.9 ns between the two biases on a Septentrio PolaRx4, using absolute calibration techniques. For other receiver types larger differences have been found.

A software tool called *gecal* has been developed by GMV within the Galileo TVF, implementing the ORB method and processing RINEX 3.x observation files. Satellite positions are read from a SP3 orbit file. The tool allows the rapid E5 calibration of a new or existing Galileo receiver. So far three receivers have been calibrated in the frame of TVF activities: a PolaRx4 at UTC(ESTEC); a GTR51 and a PolaRx4 at UTC(PTB). The PolaRx4 at PTB is at the core of a new *Galileo Experimental Sensor Station* (GESS) installed at PTB (named GPTB), thus becoming the first fully calibrated station of the Galileo infrastructure.

This paper describes in detail the *gecal* tool and the calibration results obtained for the three Galileo receivers used in the TVF. Galileo SIS validation results obtained using such receivers are also presented.

[1] P. Defraigne et al., Calibration of Galileo signals for time metrology, IEEE transactions on Ultrasonics, Ferroelectrics, and Frequency control 12/2014 61(12):1967-75.

[2] B. P. B. Elwischger, S. Thoelert, M. Suess, J. Furthner (DLR), "Absolute Calibration of Dual Frequency Timing Receivers for Galileo", European Navigation Conference ENC 2013, 23.-25. Apr. 2013, Vienna, Austria.

A New Modem for Two Way Satellite Time and Frequency Transfer

Zhang, Shengkang*+, Wang, Xueyun*, Wang, Haifeng*, Wang, Hongbo*, Zhang, Victor+, Feng, Keming*
*Science and Technology on Metrology and Calibration Laboratory, Beijing Institute of Radio Metrology& Measurement, Beijing, China
+Time and Frequency Division, National Institute of Standards and Technology, Boulder, Colorado/U.S.A.
E-mail: Zhangsk@126.com

Two Way Satellite Time Frequency Transfer (TWSTFT) is a highly precise time & frequency remote comparison technique, which is widely used in time metrology, satellite navigation, etc. Nowadays, most of the time metrology laboratories in Europe, America and Asia established TWSTFT links. Time transfer Modem is the most crucial instrument in the TWSTFT system. By means of the Modem, the one pulse per second (1PPS) is modulated into intermediate frequency (IF) at the local site. The signal is then up-converted to the radio frequency (RF), amplified, and transmitted to the satellite. At the remote site the RF signal is again amplified, down-converted to the IF, and demodulated by the modem. The time interval between the local 1PPS and reconstructed 1PPS from the received TWSTFT signal is measured on each site. Based on the reciprocity of the TWSTFT signals' bidirectional paths, the time offset of the two clocks are gained by exchanging and differencing the time interval measurements at the two sites.

A new time transfer Modem for TWSTFT is developed recently at Beijing Institute of Radio Metrology and Measurement (BIRMM). In this instrument, we use direct sequence spread spectrum and BPSK modulation to generate the IF signal. And the FFT fast parallel algorithm is applied to quickly acquire the pseudo noise modulated signal. A 2nd order FLL assisted a 3rd order PLL are designed in order to solve the paradox of the performance of loop dynamic stress and carrier phase tracking accuracy. A 2nd order DLL is used to track and measure the code phase. The receiver unit of Modem is accomplished by an all-digital structure. The FFT algorithm and correlation process are realized on a FPGA chip. The carrier & code phase discriminator, loop filter, etc. are realized on a DSP processor. Using this structure, we can maximize the processing ability of the chips. So the receiving channel can be extended easily to about 8 channels or even more without any changes on the hardware, which will brings great benefits in the future.

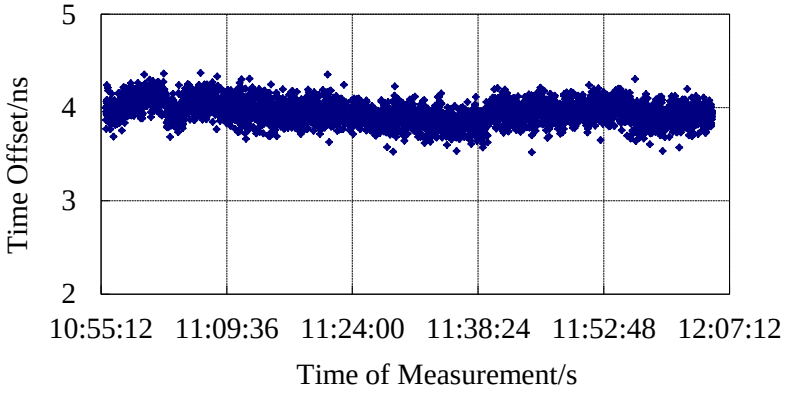


Fig. 1 Zero baseline Measurement of BIRMM Modem with ChinaSat 10 Geostationary satellite (2.5Mchip/s, 1σ=0.13ns).

In the first phase to evaluate the performance of the Modem, a zero baseline experiment was done. Two Rubidium clocks are used as the time & frequency references for two BIRMM Modems. Then TWSTFT link is established by two 1.2m dish earth stations using the ChinaSat 10 satellite. The Modems measured the time difference of the two clocks. The Modem outputs the 1PPS measurements at 1sample/s without any smooth processing. Meanwhile a commercial TIC is used to measure the two clocks' time differences. Then a double difference is made between them as Fig. 1 illustrates, which shows quite small instability with 1σ equals 0.13ns totally.

Development of pulsar-based time scale with NANOGRAV data

Dongshan Yin*+, Paul Demorest&,Yuping Gao*,Shuhong Zhao*
* National Time Service Center,Chinese Academy of Sciences, Xi'an,China
+University of Chinese Academy of Sciences, Beijing,China
&National Radio Astronomy Observatory,Socorro,USA
E-mail: yds@ntsc.ac.cn

We developed ensemble pulsar time scale using NANOGRAV pulsar timing data, which has comparable precision to international atomic time-scale(TAI), and it can lead to a new realization of terrestrial time(TT). Any shift in reference time scale TT(TAI) will lead to completely correlated signal in pulsar timing residuals, we identified significant discrepancy in TT(TAI) with respect to TT(BIPM11). We also discussed various phenomena that lead to a correlated signal in the timing residuals and therefore limit the stability and precision of ensemble pulsar time scale.

Reference

[1] G.Hobbs, W.Coles, R.N.Manchester, et al., Mon. Not. R. Astron. Soc. 427, 2012, 2780-2787.
[2] Petit G., 2003, in 35th Annual Precise Time and Time Interval (PTTI) Meeting, San Diego,
[3] Hobbs G. B., Edwards R. T., Manchester R. N., 2006, MNRAS,369, 655
[4] Champion D. J. et al., 2010, ApJ, 720, L201
[5] Coles W., Hobbs G., Champion D. J., Manchester R. N., Ver-biest J. P. W., 2011, MNRAS, 418, 561
[6] Cordes J. M., Kramer M., Lazio T. J. W., Stappers B. W., Backer D. C., Johnston S., 2004, New Astronomy Reviews, 48, 1413
[7] D.R.Lorimer, M.Kramer, Handbook of Pulsar Astronomy
[8] Andrew Lyne, Francis Graham-Smith, Pulsar Astronomy, 3rd edition

SASO Time Scale and Measurement Capability

Khalid S. AlDawood, Ahmed H. AlJawan, Fahed A. AlMutari
Saudi Standards, Metrology and Quality Organization (SASO)
National Measurement and Calibration Center (NMCC)
Riyadh, 11471, P.O.Box 3437, Kingdom of Saudi Arabia
E-mail: k.dawood@saso.gov.sa

SASO Time and Frequency Laboratory is a responsible for national time scale generation and dissemination on Saudi Arabia. Recently at SASO NMCC the Time and Frequency Laboratory was developed using primary 5 Cs atomic clocks, 2 GNSS receivers and high technology modern equipments, The national time scale was generated with an uncertainty better than 2x10-14 and disseminated through the internet for industrial applications using an NTP time dissemination system with an uncertainty less than 50 ms. The fully automatic time and frequency calibration system that was developed is traceable to the national time scale and has the capability for frequency generation and measurement in the DC – 50 GHz range including signal analysis and phase noise measurements. Currently SASO is a member of BIPM Atomic Time Club in order to contribute to the Universal Coordinated Time (UTC) time scale and the realization of the international traceability of the SASO time scale.

SASO time scale generated by using 5 Cs atomic clocks with high performance tubes (5071) and calibrated 2 multichannel GNSS receivers (TTS-4). Time signals from the GPS, GLONASS and GALILEO systems are received using 2 GNSS antennas which are installed on the metrology (NMCC) building. The time signals from the antenna are received by a TTS-4 model multi-channel GNSS receiver using a 35 m low noise cables. The reference one pulse per second (PPS) time signal from the reference atomic clock is also sent to GNSS receivers and these receivers measures the time difference between satellite clocks and reference SASO Cs atomic clocks in accordance with the BIPM satellite tracing schedule. Time difference between atomic clocks is measured by computer controlled counter trough switch box. All cables delay is measured by counter and 50 GHz oscilloscope with an uncertainty less than 100 ps. SASO time scale was compared by GPS common view with UME and MTC scale with an uncertainty less than 5 ns. In additionally for uncertainty evaluation 2 Cs clock in SASO same time interval compared trough counter and 2 GNSS receiver using GPS common view method. Currently SASO time scale generated with type A uncertainty 0.7 ns and with type B uncertainty 7.3 ns.

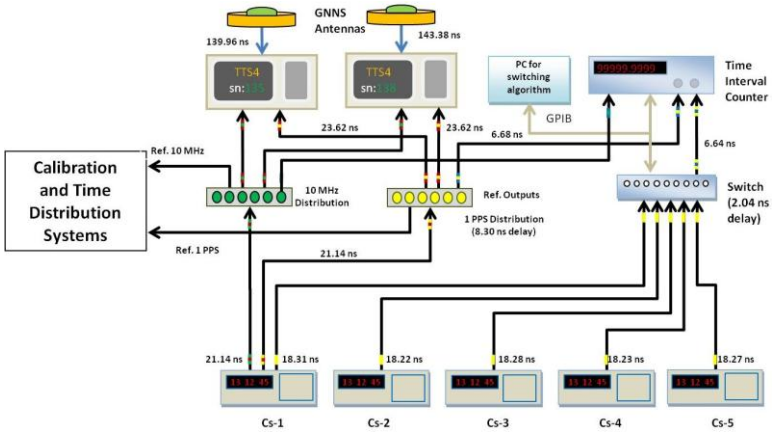


Fig.1: Block diagram of SASO time and frequency system

The developed fully computer controlled automatic time and frequency calibration system in the DC – 50 GHz range including signal analysis and phase noise measurements was verified by manual measurement and used for atomic clock, signal generator, spectrum analyzer, counter and timer calibrations. Time interval measurement with <10 ps uncertainty and high frequency oscilloscope calibration system was developed by using fs laser and 50 GHz oscilloscope system. In additionally, comparison SASO and UME phase noise measurement system using low noise oscillators in progress.

Stability analysis of the French timescale UTC(OP)

Abgrall M., Bize S., Chupin B. , Guéna J., Laurent Ph., Rosenbusch P., Uhrich P., Rovera G. D.

LNE-SYRTE, Observatoire de Paris – LNE- CNRS –UPMC, Paris, France
E-mail: michel.abgrall@obspm.fr

This poster presents the performances of UTC(OP) generated at LNE-SYRTE, Observatoire de Paris (OP). In operation since October 2012, the current version of the timescale is based on a hydrogen maser steered by one of the SYRTE atomic fountains FO1, FO2 or FOM [1]. The algorithm has already been presented in details in [2]. The steering of the maser is performed using a microphase stepper and is updated daily. It is the sum of two main components. First, the current frequency of the maser is estimated daily by extrapolating data of the frequency comparison between the maser and the fountain. Second, a small steering to maintain UTC(OP) close to UTC is added. This term is updated monthly using data published in the last available Circular T published by the BIPM, to compensate for the slope and for the phase offset of UTC – UTC(OP). We are currently working on the improvement of the system hardware by setting up the new generation of microphase stepper [3] at the input of a switch allowing a hot swapping between nominal and backup timescales with a negligible impact.

This new version of UTC(OP) is now one of the best real time realization of UTC. Since the end of 2012, the departure of UTC(OP) from UTC remained continuously well below 10 ns. In this poster, we will present the latest results together with an analysis of the stability of UTC(OP) against other national and international timescales.

[1] J. Guéna, et al, "Progress in atomic fountains at LNE-SYRTE," Ultrasonics, Ferroelectrics and Frequency Control, IEEE Transactions on, vol. 59, pp. 391 –409, march 2012.

[2] M. Abgrall, et al "Performances of UTC(OP) based on LNE-SYRTE atomic foutains", in Proc. of the 28th European Frequency and Time Forum, Neuchâtel, Switzerland, 2014.

[3] D. Rovera, et al, "Characterization of an auxiliary offset generator for steering of H masers," in Proc. of the 26th European Frequency and Time Forum, Gothenburg, Sweden, 2012.

Preliminary step for a UTC(IT) steering algorithm based on the ITCsF2 primary frequency standard measurements

G. Signorile*, P. Tavella*, D. Calonico*, F.Levi*, G. Costanzo*+, G.Cerretto*, R. Costa*, E. Cantoni*, I. Sesia*
*Optics Division, INRIM, Turin, Italy
+ Electronics Department, Politecnico di Torino, Turin, Italy
E-mail: g.signorile@inrim.it

The generation of the Italian reference time scale UTC(IT) is currently based on commercial Caesium frequency standards and Hydrogen masers. Our plan is to introduce also the frequency measures referenced to the primary frequency standard, to improve the stability and accuracy of the UTC(IT) time scale.

We have developed, implemented and tested a new steering algorithm based on the measurements of the ITCsF2 Caesium Fountain developed and operated in the INRIM Optics Division.

The algorithm implementation is described and the results that could be obtained with almost one year of real fountain data are reported, and compared with similar results that could be obtained by steering the same H maser by using only BIPM products, UTC and rapid UTC.

The performances on the test period are finally analyzed and discussed and the benefits of using fountain measures in the steering algorithm are pointed out.

Acquisition Method of Loran-C Signal Based on Matched Filter

GAO Yuanyuan*, HUA Yu, LI Shifeng

National Time Service Center /Key Lab of Precision Navigation and Timing Technology, Chinese Academy of Sciences, Xi'an, Shannxi China

*University of the Chinese Academy of Sciences, Beijing, China

E-mail: gaoyy @ntsc.ac.cn

Loran-C system is considered as an enhancement or backup for global navigation satellite system (GNSS) to reduce the Position Navigation Timing (PNT) service risk of navigation system. Because the traditional Loran-C system can't satisfy all requirements of the satellite navigation system backup, many countries have to Loran-C system with modern transformation and upgrade, which is of great significance to improve the reliability and the integrity of national navigation timing system.

Loran-C system achieves the capture of Loran-C signal mainly through the detection and recognition of phase encoding, while phase code detection needs a high SNR conditions. In the case of using the traditional capture methods, amplitude modulated signal of Loran-C system is more sensitive to noise, which makes the Loran-C receiver can't work under heavy noise environment. Therefore, capturing weak Loran-C signal with low SNR effectively, is first solved a problem for Loran-C navigation digital receiver.

In this paper, a novel acquisition method of Loran-C signal based on matched filter is proposed to improve the acquisition performance of Loran-C signal under heavy noise environment. The difference between Loran-C signal and noise in the spectral distribution and statistical properties is employed in this method, which is based on the study of the characteristics of Loran-C signal and digital matched filter. Higher SNR could be obtained through matched filtering the received signals. Then outputs are correlated with standard pulse signal and the correlation peaks are judged. Theoretical analysis and simulation experiments show that the proposed method can eliminate the noise effectively, the anti-noise performance is superior to -20dB, improving about 10dB compared with the traditional methods, and higher acquisition processing gain is obtained, while its implementation is simple.

[1] LEI Wenying and CHEN Baixiao, "Low complexity sparse noise reduction method for Loran-C sky-wave delay estimation," IEEE Electronics Letters, vol.49, no. 24, pp. 1572-1574, Nov. 2013.

[2] LI Shifeng, WANG Yulin, and HUA Yu, "Loran-C signal fast acquisition method and its performance analysis," IEEE Jounal of Electronics & Information Technology, vol..35, no. 9, pp. 2175-2179, Sept. 2013.

[3] S. H.Yang, C.B.Lee, and Y. K.Lee, "Accuracy Improvement Technique for Timing Application of LORAN-C Signal," IEEE Transactions on Instrumentation and Measurement, vol.60, no.7, pp. 2648-2654,July 2011.

[4] D. Last, and YI Bian, "Carrier Wave Interference and Loran-C Receiver Performance," IEE Proceeding-F, Radar and Signal Processing,vol.140, no.5, pp. 273-283,1993

Verification of Time Telegrams in Long Wave Radio Systems

Schneider, Matthias, Ruland, Christoph
Institute for Data Communication Systems, University of Siegen, 57068 Siegen, Germany
E-mail: matthias.schneider@uni-siegen.de

Long wave radio systems are widely used to distribute the actual date and time information, because wireless transmission guarantees timeliness. The provision of timeliness and reliability of time information is very important for many devices, which are controlled by time stamped telematic telegrams or time triggered events, and play an essential role for public and private safety. The correct behavior of the devices of any system is only possible, if a synchronized and correct system time is available in all devices.

The distribution of time telegrams is used to synchronize the system clocks of the receivers and their real time clocks. These received time messages, which contain the actual system time, can-not be securely verified by the Long Wave Radio Receiver, because there is no backchannel. No receipt or confirmation can be requested by the transmitting station without the existence of a back channel.

Time telegrams can be manipulated or generated by "man-in-the-middle" attacks. Therefore it is possible to manipulate the system clocks of groups of devices or individual devices depending on the location of the attacker. By manipulating the receiver´s system clock the control behavior of the device can be completely changed. Even the application of digital signatures and encryption to time telegrams doesn´t protect against man-in-the-middle attacks, for example by delaying the time telegrams.

Possible attack scenarios on broadcast data services have been published [1].

This paper describes a method to verify received time telegrams distributed by Long Wave Radio systems on the example of the radio ripple control technology.

By this approach, the time between two time telegrams is continuously measured and compared with the time difference calculated by the time information contained in the time telegrams. In other words, physical and logical information is compared. The physical time difference is directly calculated using the carrier frequency of the transmission system (for example: DCF49 transmission system uses a carrier frequency of 129.1 kHz with FSK modulation ± 170 Hz). A counter is clocked by the received carrier frequency of the system. The physical time difference between the transmission of two time telegrams can be derived by the number of oscillations. The logical time difference is given by the content of the time telegrams.

The comparison of physical and logical time differences is continuously verified to detect time jumps, which may appear during the transmission of time telegrams. Manipulated or delayed time telegrams can be accurately identified. This method can be applied without changing the time distribution protocol and can applied to other time distribution services.

[1] M. Schneider; Ch. Ruland: Sicherheit von Broadcast-Datendiensten im Smart Grid am Beispiel der Rundsteuertechnik. Tagungsband des 13. BSI-Kongresses. S. 483–496.

Two-Way Coherent Frequency Transfer in a Commercial WDM Communication Network in Sweden

Sven-Christian Ebenhag, Martin Zelan, Per Olof Hedekvist, Magnus Karlsson* and Börje Josefsson+
Department of Measurement Technologies, SP Technical Research Institute of Sweden, Borås, Sweden
* Microtechnology and Nanoscience, Photonics Laboratory, Chalmers University of Technology, Göteborg, Sweden
+Swedish University Computer Network, Stockholm, Sweden
E-mail: sven-christian.ebenhag@sp.se

An experimental fiber link is being established between SP Borås and Chalmers University of Gothenburg in Sweden. The fiber length one way is about 60 km and implemented in SUNET (Swedish University Network). The network connection is DWDM-based (Dense Wavelength Division Multiplexing) and connects the network routers in a central node with the client network, where each channel can be configured with terminal equipment based on user needs, such as Ethernet or POS (Packet-Over-SONET / SDH) technology at different bit rates.

SP Technical Research Institute of Sweden is the National Metrology Institute (NMI) responsible for the national frequency and time as well as the development and distribution of these to users within Sweden. Through participation in EMRP-project NEAT-FT, there is also development of techniques useful on a European scale. As part of these efforts, SP has achieved funding for an optical frequency comb and an ultra-stable laser from Menlo Systems. The ultra-stable laser is unique equipment in Sweden but there are several users, such as Chalmers University of Technology that would benefit of access to this type of equipment in in their areas of research, such as development of optical combs.

The aim of the project is to evaluate the signal quality when sending a stable optical coherent frequency utilizing a wavelength in a DWDM system fiber pair. The experiment uses a channel in the DWDM with the wavelength of 1542.14 nm which also is the wavelength of our ultra-stable laser. This wavelength is within the C band and is therefore compatible with common Erbium doped amplifiers in this network. The experiment uses a fiber pair, i.e. one fiber for transmission from east to west and another, parallel fiber from west to east. This will introduce an asymmetry that will be monitored and evaluated. Another aim of the system is to be ultra-stable which corresponds to a stability of 10^{-13} for $\tau = 1$ sec (Overlapping Allan Variance), as well as providing the ability to distribute monitored ultra-stable frequency with a future traceability to UTC (SP) (National realization of Universal Time Coordinated within Sweden) to multiple users within the network.

Frequency distribution in delay-stabilized optical DWDM network over the distance of 3000 km

Śliwczyński Ł, Krehlik P, Lipiński M, Turza K*, Binczewski A*
Department of Electronics, AGH University of Science and Technology, Krakow, Poland
Poznań Supercomputing and Networking Center, Poznań, Poland
E-mail: sliwczyn@agh.edu.pl

The best strategy for implementing fiber-based systems for time/frequency distribution is a dark-fiber approach, where an effective cancellation of the phase fluctuations of the signals propagating in two opposite directions is possible thanks to the highest possible symmetry of the optical path. This approach proved to be very effective for transferring an optical carrier [1], radio frequencies [2] or time (pulse per second) signals. The dark fiber, however, may not always be available, especially in long-distance links, spanning hundreds or even thousands of kilometers. Implementing bidirectional transfer scheme within a standard fiber telecommunication network carrying a live traffic, although in principle possible [3], faces substantial technical problems and requires bypassing each active node with special bidirectional optical amplifiers. In this situation an attractive option would be to exploit the capabilities of modern optical transport networks (OTN), equipped with reconfigurable optical add-drop multiplexers (ROADM), erbium-doped and Raman amplifiers, chromatic dispersion compensators, etc. In such a network it is possible to configure fully-transparent optical DWDM channels that, on the basis of so-called alien-lambda, may carry optical signals in both directions using two separate fibers running in the same cable. Good stability of the frequency distribution in the closed-loop delay-stabilized link exploiting such fiber pair may be expected because fibers sharing the same cable also share very similar thermal and mechanical conditions.

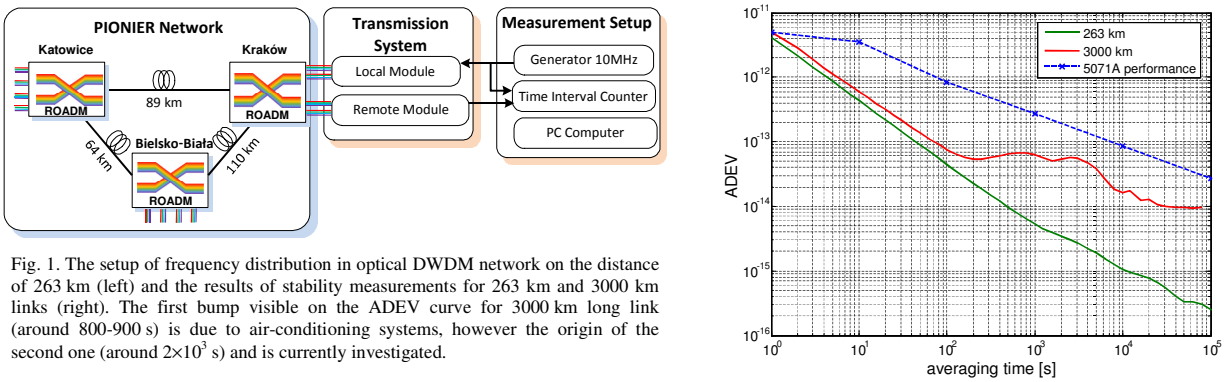


Fig. 1. The setup of frequency distribution in optical DWDM network on the distance of 263 km (left) and the results of stability measurements for 263 km and 3000 km links (right). The first bump visible on the ADEV curve for 3000 km long link (around 800-900 s) is due to air-conditioning systems, however the origin of the second one (around 2×10^3 s) and is currently investigated.

In proposed paper we will present the results of our experiments with the distribution of 10 MHz frequency signal in optical DWDM network in Poland. A systematic investigation of the effects limiting the stability will be presented. Our measurement results show (see Fig. 1) that even at the distances exceeding 3000 km the stability of the delay-stabilized link outperforms the stability of commercial 5071A cesium standards.

[1] K. Predehl, G. Grosche, S. Raupach, S. Droste, O. Terra, J. Alnis, T. Legero, T. Hänsch, T. Udem, R. Holzwarth, H. Schnatz, "A 920-Kilometer Optical Fiber Link for Frequency Metrology at the 19th Decimal Place", Science, vol. 336, pp. 441-444, 2012

[2] Ł. Śliwczyński, P. Krehlik, A. Czubla, Ł. Buczek and M. Lipiński , "Dissemination of time and RF frequency via a stabilized fibre optic link over a distance of 420km," Metrologia vol. 50, pp. 133–45, 2013.

[3] O. Lopez, A. Kanj, P-E. Pottie, D. Rovera, J. Achkar, Ch. Chardonnet, A. Amy-Klein, G. Santarelli, "Simultaneous remote transfer of accurate timing and optical frequency over a public fiber network", Applied Physics B, vol. 110, pp 3-6, 2013.

Distributed Raman amplification in multiplexed and long-haul coherent optical links

Clivati Cecilia[1], Bolognini Gabriele[2], Calonico Davide[1], Faralli Stefano[3], Mura Alberto[1], Levi Filippo[1]

[1]Optics Division, Istituto Nazionale di Ricerca Metrologica, Turin, Italy

[2]Consiglio Nazionale delle Ricerche, IMM Institute, Bologna, Italy

[3]Scuola Superiore Sant'Anna, TeCIP Institute, Pisa, Italy

E-mail: c.clivati@inrim.it

The advent of Doppler-stabilized optical fiber links for frequency metrology opened a number of new possibilities in experimental physics, as they offer a resolution which is several orders of magnitude better than that of satellite techniques [1]. In the more recent years, attention has been posed to the realization of a continental network of atomic clocks in Europe and this requires the bridging of ultra-long distances through Doppler-stabilized optical fibers. A critical issue is related to optical amplification, as chained bidirectional Erbium-Doped Fiber Amplifiers (b-EDFA) present several drawbacks, related to Amplified Spontaneous Emission and Rayleigh scattering. As an alternative, distributed Brillouin and Raman amplification (DRA) [2,3] have been proposed. In this work, we studied for the first time the behavior of DRA in deployed metrological links and successfully employed it on two Doppler-stabilized links based on different fiber architectures. Both links have the remote end in the launching laboratory, to allow the metrological characterization.

In a first experiment, we realized a 94-km long Doppler-stabilized link on a wavelength-division multiplexed architecture, where the metrological signal shares the fiber with Internet users. A Raman laser is launched from the fiber remote end with about 1 W of optical pump power. This provides a 23 dB optical gain of the metrological signal and a 14 dB optical gain of the data channels as well. In spite of this, we did not observe any deterioration of the data transmission or of the optical signal and we obtained a robust, cycles-slips-free link operation, with an ultimate 10^{-19} uncertainty on the delivered signal.

In a second experiment we investigated the maximum achievable distance on a single span optical link 180-km long, based on an inter-city dedicated fiber. In this case, we identified significant loss events on the first 20 km of optical fiber, that severely deteriorated the DRA performance; for this reason, a b-EDFA was used to boost the signal at the remote end. The hybrid scheme allowed us to investigate the synergy between the two techniques and to achieve robust link operation across the 180 km link without intermediate amplification.

We propose a detailed analysis of our experiments and highlight some possible impairments arising from the interaction between DRA and b-EDFA and from the Spontaneous Brillouin Scattering. Nevertheless, our results demonstrate that DRA can be a viable choice as an alternative to b-EDFA in ultra-long Doppler-stabilized links.

This work was supported by the Italian Ministry of Research under Progetti Premiali Programme and by the European Metrology Research Programme (EMRP) under SIB-02 NEAT-FT, SIB-02 REG3 and SIB-55 ITOC. The EMRP is jointly funded by the EMRP participating countries within EURAMET and the European Union.

[1] S. Droste, F. Ozimek, Th. Udem, K. Predehl, T.W. Hansch, H. Schnatz, G. Grosche, and R. Holzwarth, "Optical-Frequency Transfer over a Single-Span 1840 km Fiber Link," Phys. Rev. Lett., Vol. 111, no. 11, pp. 110801, Sept. 2013.

[2] S. M. F. Raupach, A. Koczwara, and G. Grosche, "Optical frequency transfer via a 660 km underground fiber link using a remote Brillouin amplifier," Opt. Expr., Vol. 22, no. 22, pp. 26537-26547, Nov. 2014.

[3] C. Clivati, G. Bolognini, D. Calonico, S. Faralli, F. Levi, A. Mura, and N. Poli "Distributed Raman Optical Amplification in Phase Coherent Transfer of Optical Frequencies," Photon. Techn. Lett. Vol. 25, no. 17, pp. 1711-1714, Sept. 2013.

The Research Progress of Two Way Time Synchronization with Optical Fiber Based on Spread Spectrum Signal

Zhu Xiangwei, Gong Hang, Liu Zengjun, Sun Guangfu
Department of Electronic Science and Engineering, National University of Defense Technology, Changsha, Hunan, China
E-mail: zhuxiangwei@nudt.edu.cn, zxwnudt@gmail.com

High-precision time synchronization is a basic element in some areas of aeronautical engineering, such as satellite navigation and deep space exploration. It is more accurate and stable to use the optical fibers while performing time-frequency transfer than using other media such as GNSS common view (GNSS CV) and two way satellites time and frequency transfer (TWSTFT). Most of the current researches in optical fiber time-frequency transfer focus on stable frequency transfer. However, there is little study on time transfer, and the accuracy of time transfer is commonly in nanosecond level. In this paper, a two way time transfer method based on spread spectrum ranging is studied. Most of the optical fiber link error is canceled out because the two way spread spectrum signals are transferred with the same fiber. The picosecond level time delay measurement based on spread spectrum ranging under high SNR is used to realize the absolute high precision time synchronization.

In the beginning of this paper, the characteristics of optical fiber time-frequency transfer techniques are summarized. Then, the performances of widely used high precision optical fiber time-frequency transfer techniques are compared, and this article mainly focused on the analysis of the principle and errors of the two way optical fiber time-frequency transfer methods. The error cause by 1PPS phase coding and recovery in traditional two way optical fiber may affect the time transfer accuracy, and extra two way data transfer link makes the system more complex. On the contrast, the presented new time-frequency transfer method based on pseudo code ranging with single optical fiber is more simple and accurate.

For the proposed method, the accuracy is improved and extra data links are not needed any more. Theoretical analysis shows that the time alignment accuracy is less than 10ps, which is helpful to remote time synchronization. The designing schemes and the implementation progress of the engineering prototype are introduced. The experimental results indicate that the time accuracy is better than 50ps by use of the proposed method with 2km optical fiber transmission distance. In the future, it could be expected that time delay measurement accuracy is better than one picosecond by optimizing signal architecture, transfer link and ranging algorithms. So, it's an appropriate solution for precise remote time-frequency transfer, which may be widely used in satellite navigation, deep space exploration and international atomic time scale, etc.

High Precise Time Synchronization Based on Ultra-short Pulse

Fan Shi, Shengkang Zhang, Huaiying Shang, Hongbo Wang, Haifeng Wang, Hang Yi,
Zhenggang Ding, Feng Nian, Keming Feng

Science and Technology on Metrology and Calibration Laboratory, Beijing Institute of Radio Metrology & Measurement, Beijing 100854, China

Email: shifan_chinese@sina.com

High precise timekeeping, measurement and synchronization are the most important technological tasks in many fields of science and engineering, such as distributed radars system, global navigation satellite system (GNSS), particle accelerators, free-electron lasers and phased-array antennas for radio-astronomy. With advances in modern technologies, the time synchronization system has become even precise. Traditionally, precise time synchronization is achieved by satellite-based techniques [1] such as two-way satellite time and frequency transfer (TWSTFT) or GPS-based measurements, but these techniques are hard to enable the synchronization accuracy to be better than picoseconds.

Ultra-short pulse, whose pulse duration is usually several femtoseconds to several hundred femtoseconds, is generated by a femtosecond laser system. Theoretically, shorter pulse is helpful to achieve higher precise synchronization. Moreover, because femtosecond laser has ultralow noise, it has been anticipated that ultra-short pulse would be applied in scientific and engineering facilities requiring extremely high timing accuracy.

In this paper, we describe the idea of a high precise time synchronization system(Fig.1) based on ultra-short pulse using auto-correlation method. The local pulse train is generated by a femtosecond laser system tightly locked to a local atomic clock. Then the optical pulse train is distributed to remote location. The backward propagating pulses and local pulses are combined and applied to the second-harmonic generation (SHG) crystal auto-correlator which is used for precise time delay measurements. The time compensation block is constructed by an optical delay line. We have measured calibration curve of the system. The time synchronization measurement precision is 10fs. Our work is promising to be applied in the designing and operating of high-precision facilities and future communication networks.

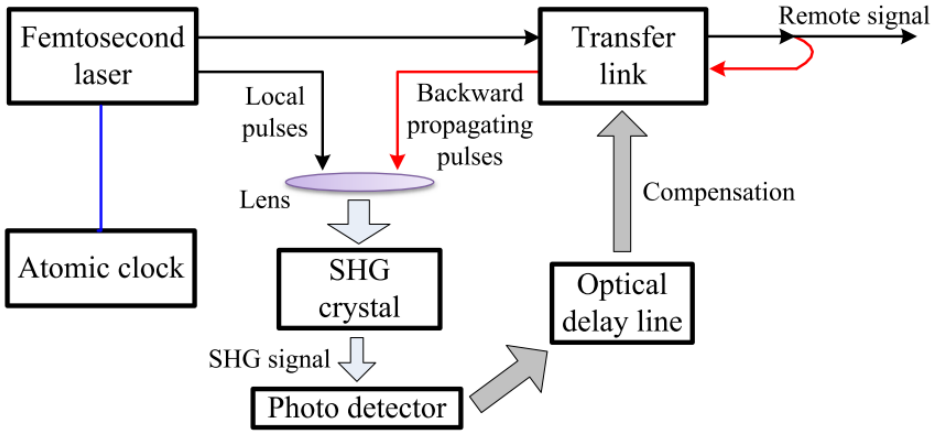


Fig. 1: High precise time synchronization system based on ultra-short pulse.

[1] Shengkang Zhang, et al., "Ultra-Short Term Clock Offset Prediction for Two-Way Satellite Time Synchronization", European Time and Frequency Forum (EFTF), Prague, July 2013.

Comparison of UTC time links

Z. Jiang[1], W Wu[1,2] and J Yao[3]

1 Bureau International des Poids et Mesures (BIPM), Pavillon de Breteuil F-92312,
SÈVRES CEDEX, France, zjiang@bipm.org
2 National Time Service Center (NTSC), Xian, China
3 National Institute of Standards and Technology (NIST), Boulder, USA

The BIPM has the most complete data base of time transfer results using all techniques and methods, from the first GPS/GLONASS multichannel satellite tracking to most refined methods such as GPS P3, GPS PPP, Two-Way Satellite Time and Frequency Transfer (TWSTFT), and more recently one optical fibre link. These data are provided by more than 70 institutes that contribute to the computation of UTC at the BIPM. Since 2005 the BIPM has been publishing, after issuing the monthly Circular T, the results of time links and time link comparisons with different methods/techniques at its web site ftp://tai.bipm.org/TimeLink/LkC/. In 2010, long-term comparisons have been added and available at ftp://tai.bipm.org/TimeLink/LkC/LongTerm/. These comparisons allow the study of the short-, middle- and long-terms behavior of different time transfer techniques and methods, and in particular, to compare the two major space techniques used for clock comparison in UTC, TWSTFT and GNSS. Because they are completely independent, a non-constant difference between them would suggest the instability of the reference of the receiver system or the variation of the 'calibration' of one or both techniques. Furtherly, this investigation is important for the study of the uncertainty of UTC time link calibrations. The-state-of-the-art of the time link calibration uncertainty is about 1.5 ns. This value is close to the amount of the annual variations between the TWSTFT and GPS, present in the long-term link comparisons. This paper completes the 2012 study [1] with new data, and includes the latest developments: accurate optical fiber [2], the improved GPS PPP solutions [3,4] and the impact of the diurnals in the TWSTFT time links [5]. We present our observations and analysis based on the five years' data sets.

Key Words: UTC Time transfer, Time link, Uncertainty, Calibration, GPS, GLONASS, TWSTFT

Reference

[1] Jiang Z and Lewandowski W (2012) Inter-comparison of the UTC time transfer links, IN. *Proc. EFTF2012*
[2] Jiang Z, Czubla A, Nawrocki J, Lewandowski W and Arias F (2014), "Towards accurate optical fibre time transfer in UTC", IN. *Proc. EFTF2014*
[3] Yao J and Levine J (2014) GPS Measurements Anomaly and Continuous GPS Carrier-Phase Time Transfer, *ION-PTTI 2014, 1-4 Dec. 2014, Boston, USA*
[4] Jian Yao, and Judah Levine (2014) An improvement of RINEX-Shift algorithm for continuous GPS carrier-phase time transfer, IN. *Proc. 27th ION GNSS+ 2014 Conference*, pp. 1253–1260, 2014
[5] Wu W (2014) Some consideration on the diurnal in TWSTFT, IN *IFCS-EFTF2015 Proc.*

Study on Autonomous and Distributed Time Synchronization Method for formation UAVs

Liu Tao*, Hu Yonghui, Hua Yu, Wu Meifang

National Time Service Center /Key Lab of Precision Navigation and Timing Technology, Chinese Academy of Sciences, Xi'an, Shannxi China

*University of the Chinese Academy of Sciences, Beijing, China

E-mail: liutao@ntsc.ac.cn

Unmanned Aerial Vehicles (UAV) has an irreplaceable role in modern warfare, and high-precision time synchronization is a key technology to implement multi-UAVs formation flight, cooperation and co-strike reconnaissance. However, the existing mode of that depending the GNSS satellite navigation system, or ground control station to achieve time synchronization, its autonomy is subjected to certain restricted, exist serious strategic security risks, especially in wartime. Consequently, it is necessary to study autonomous high precision time synchronization method in the absence of any external time source.

For distributed architecture such as formation of large-scale UAVs, because of the large numbers of UAVs and complex topology, the traditional master-slave time synchronization method is no longer applicable. The firefly synchronization model which's been studied in other areas such as biology, chemistry and mathematics, has provided a new way to solve the problem of time synchronization in distributed system. In this paper, we introduce the synchronize model of fireflies into UAV formation network, and proposed a kind of distributed time synchronization methods based on broadcasting, make use of existing communication links between UAVs, each UAV broadcasts his current time information, its neighbor UAVs receive the information, and make simple arithmetic average, use the average value as the current time, and then broadcasts it again. This process is carried out repeatedly until all the UAVs meet the same clock tick, which means the whole network achieves distributed synchronization.

In order to prove the feasibility of the method and its performance, in this paper, we conducted some simulation experiments, and the results showed that, in a network consisting of 50 nodes, with the topology of all-to-all, synchronization accuracy can be achieved 100us. Meanwhile, we also built one test platform uses 10 GAINGS-3 nodes to implement and test the algorithm, the experimental results show that the maximum synchronization error between two nodes is 258us, and the minimum is 78us. There is no doubt that this method can effectively achieve time synchronization autonomously in the absence of any external time source.

[1] Daniel Gonzales, John Hollywood, Gina Kingston. Network-Centric Operations Case Study: Air-to-Air Combat With and Without Link 16. ADA437368: National Defense Research Institute，2005.

[2] King-Yip Cheng, A Distributed Multi-hop Time Synchronization Protocol for Wireless Sensor Networks using Pair-wise Broadcast Synchronization. IEEE Transactions on Wireless Communications, Vol. 8, No. 4, April 2009.

[3] WeiWu and Tianping Chen1, Desynchronization of pulse-coupled oscillators with delayed excitatory coupling, Nonlinearity 20 (2007) 789–808.

[4] Alexander Tyrrell, Gunther Auer, Fireflies as Role Models for Synchronization in Ad Hoc Networks, I1-4244-0463-0/06/$20.OO ©2006 IEEE.

Optical Lattice Clocks: paving the road towards ultimate stabilities

Le Targat Rodolphe, Robyr Jean-Luc, Shi Chunyan, Eismann Ulrich, Lodewyck Jérôme
LNE-SYRTE, Observatoire de Paris, CNRS, UPMC, Paris, France

The large number of atoms (>10^4) probed simultaneously in Optical Lattice Clocks raises the prospect of unprecedented frequency stabilities: the atomic Quantum Projection Noise (QPN) allows in principle a statistical resolution at the 10^{-17} level after 1s of integration. Several directions of research are at the moment pursued in order to reach this limit, either with state-of-the-art laser systems (see for instance [1,2,3]) or with refined interrogation strategies [4]. In this presentation we will describe two complementary works that we are leading to progress towards the QPN limit.

At LNE-SYRTE, the laser probing the narrow strontium clock transition at 698 nm is stabilized on an ultrastable cavity characterized by a frequency flicker floor at 5×10^{-16}. In order to preserve this level of stability and to transfer it from the cavity to the atoms, all the optical paths, both fibered and in free space, must be actively compensated in order to make the phase immune to temperature or acoustic noise. We present a scheme in which the input of the ultrastable cavity itself is used to close the interferometer compensating phase fluctuations between the laser and the cavity, therefore leaving no uncontrolled propagation. On the atom side, we present a scheme based on a two-frequency optical carrier: the first frequency component is off-resonance, switched on permanently, and is used to stabilize an interferometer between the laser and the lattice-trapped atoms. The second frequency component is phase-locked to the first one, offseted to be at resonance with the atoms and is pulsed when the spectroscopy phase starts. The characterization of this overall scheme shows that it is compatible with the dissemination of an ultrastable carrier at the 10^{-17} level.

Beyond these developments, in order to minimize the impact of the residual noise of the laser on the clock stability (Dick effect), we are elaborating a new detection method. At the end of each clock cycle, we aim at detecting the populations in a non-destructive way, in order to keep the atoms trapped in the lattice and thus ready to be probed again at the next cycle. This would open the way to duty cycles as high as 80 % (instead of 15 % in the present configuration) and push the Dick effect contribution down to the 10^{-17} range. The strategy is based on the measurement of the phase imprinted by the atoms on a weak, far-detuned beam probing the lattice–trapped atoms. Our cavity based approach leads to an increase of the sensitivity scaling as the finesse of the cavity. We will describe the theory, as well as the possible issues of this method, and we will present the preliminary results.

The research leading to these results has received funding from the EMRP Joint Research Program EXL-01 QESOCAS (Quantum Engineered States for Optical Clocks and Atomic Sensors). The EMRP is jointly funded by the EMRP participating countries within EURAMET and the European Union.

[1] B. J. Bloom *et al.*, "An optical lattice clock with accuracy and stability at the 10^{-18} level", Nature 506, 71-75 (2014)

[2] N. Hinckley *et al.*, "An Atomic Clock with 10^{-18} Instability", Science 341, p.1215 (2013)

[3] C. Hagemann *et al.*, "Providing 10^{-16} short-term stability of a 1.5 µm laser to optical clocks", IEEE Trans. Instrum. Meas. 99, p.1 (2013)

[4] J. Lodewyck *et al.*, "Nondestructive measurement of the transition probability in a Sr optical lattice clock", Phys Rev. A 79 061401 (2009)

Advances of the mercury optical lattice clock at LNE-SYRTE

[Favier, Maxime], [Tyumenev, Rinat], [De Sarlo, Luigi], [Bize, Sebastien]
SYRTE - Observatoire de Paris, LNE, CNRS, UPMC, Paris, France
E-mail: maxime.favier@obspm.fr

Optical lattice clocks are among the most interesting prospects to realize a definition of the SI second based on an optical frequency standard. To reach this goal, an ensemble of two Sr lattice clocks and one Hg lattice clock is being developed at LNE-SYRTE, and routinely compared to state of the art microwave fountains via optical frequency combs. Sensitivity to thermal electromagnetic fields and static electric fields are limiting the performances of lattice clocks, and in this regard, the low sensitivity of the $^1S_0 - {}^3P_0$ clock transition to blackbody radiation, 30 times smaller than in the case of Sr and 15 times smaller than in the case of Yb, as well as the high vapor pressure of Hg at room temperature, eliminating the need for strong temperature gradients in the setup, make it a truly promising element to build an optical lattice clock with record stability and accuracy. Furthermore, Hg can be laser cooled to temperatures as low as 30µK using only a single stage magneto-optical trap on the $^1S_0 - {}^3P_1$ intercombination line, and loaded directly in the trapping optical lattice.

In this poster, we will present our on-going efforts to overcome the main challenges of this experiment which lie in the need for three reliable laser sources operating in the UV region of the spectrum respectively at 253.7nm, 265.6nm and 362.5nm for the cooling, probing and trapping of neutral Hg atoms.

Several major modifications of the setup were made, notably regarding the reliability and performances of the cooling and trapping laser systems. These improvements have allowed for a significant increase of the depth of the trap from less than 20 recoil energies E_R to more than 50 E_R, and as a result the number of atoms trapped in the vertical optical lattice was raised by one order of magnitude. We will show a study of the trapped atomic sample properties, and improved spectroscopic measurement of the clock transition in mercury. From 11Hz published by our group in 2012 [1], we are now able to perform Rabi spectroscopy down to a 6Hz linewidth. We will also present a characterization of the performances of the setup when locked to the clock transition, namely a measurement of the improved short term stability of the clock over the previous value of $5.4.10^{-15}/\tau^{1/2}$ [2], and a study of a few systematic effects down to 10^{-16}.

[1] J. J. McFerran, L. Yi, S. Mejri, S. Di Manno, W. Zhang, J. Guéna, Y. Le Coq, and S. Bize, Phys. Rev. Lett., vol. 108, 183004, 2012.

[2] J. J. McFerran, D. V. Magalhães, C. Mandache, J. Millo, W. Zhang, Y. Le Coq, G. Santarelli, and S. Bize, Optics Letters, vol. 37, pp. 3477, 2012

Development of a strontium optical lattice clock for space applications

Lyndsie Smith, Wei He, Dariusz Świerad, Joshua Hughes, Ole Kock, Stefano Origlia*, Stephan Schiller*, Yeshpal Singh, Kai Bongs and the SOC2 team+

School of Physics and Astronomy, University of Birmingham, Birmingham, UK
* Institut für Experimentalphysik, Heinrich-Heine-Universität Düsseldorf, Düsseldorf, Germany
And the remaining of the SOC2 team and affiliations.
E-mail: l.l.smith@pgr.bham.ac.uk

With timekeeping being of paramount importance for modern life, much research and major scientific advances have been undertaken in the field of frequency metrology, particularly over the last decade. New Nobel-prize winning technologies have enabled a new era of atomic clocks; namely the optical clock. These have been shown to perform significantly better than the best microwave clocks reaching an inaccuracy of $2.1 \cdot 10^{-18}$[1].

With such results being found in large lab based apparatus, the focus now has shifted to portability - to enable the accuracy of various ground based clocks to be measured by use of this improved, portable setup, and to compact autonomous performance - to enable such technologies to be tested in space. This could lead to a master clock in space, improving not only the accuracy of technologies on which modern life has come to require such as GPS and communication networks. But also more fundamentally, this could lead to the redefinition of the second and tests of fundamental physics.

Within the European collaboration, Space Optical Clocks 2 (SOC2) [2] consisting of various institutes and industry partners across Europe we have tried to tackle this problem of miniaturization whilst maintaining stability, accuracy ($5 \cdot 10^{-17}$) and robustness whilst keeping power consumption to a minimum – characteristics ideal for space applications.

I will present the most recent results of the Sr optical clock in SOC2 and also the novel compact design features, techniques for reducing BBR, new methods employed in the scheme of realizing the sample of ultra-cold strontium and outlook for the future advances of the project.

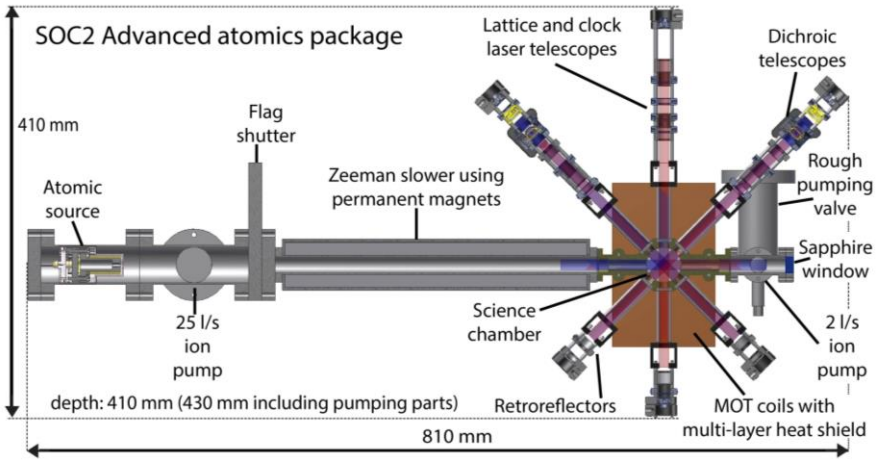


Fig 1: Schematic diagram showing the novel, compact vacuum apparatus employed for the SOC2 atomics package.

[1] B. J. Bloom, T. L. Nicholson, J. R. Williams, S. L. Campbell, M. Bishof, X. Zhang, W, Zhang, S. L. Bromley, and J. Ye, "An optical lattice clock with accuracy and stability at the 10^{-18} level," Nature **506**, issue 7486, 71-75, Feb. 2014.

[2] S. Schiller, et. Al., "The Space Optical Clocks Project: Development of high-performance transportable and breadboard optical clocks and advanced subsystems," EFTF 2012 contribution, arXiv:1206.3765 [quant-ph], Jun. 2012.

Ytterbium optical lattice clock at INRIM

Pizzocaro Marco[1,*], Milani Gianmaria[1,2], Rauf Benjamin[1,2], Thoumany Pierre[1,2], Costanzo Giovanni Antonio[1,2], Levi Filippo[1] and Calonico Davide[1]

[1]*INRIM, Istituto Nazionale di Ricerca Metrologica, Strada delle caccie 91 10135 Torino, Italy*
[2]*Politecnico di Torino, Corso duca degli Abruzzi 24 10129 Torino, Italy*
[*]E-mail: m.pizzocaro@inrim.it

The development of optical frequency standards benefit many applications, such as realization of SI units, quantum simulations, test of fundamental physics and relativistic geodesy. Among other the clock transition of ytterbium 171Yb neutral atom is recommended as secondary representations of the SI second reflecting the measurements made at NIST [1] and NMIJ [2]. Additional measurements are needed to consolidate the knowledge of the system in view of a possible future redefinition of the SI second.

We present an optical lattice clock based on ytterbium atoms developed in the laboratories of INRIM. In the experiment, we cool and trap ytterbium atoms in a two stage magneto-optical trap (MOT) (at 399 nm and 556 nm for the first and second stage, respectively). Atoms are then transferred in a horizontal, one-dimensional optical lattice at the magic wavelength (759 nm). Here the clock transition at 578 nm is probed by a laser stabilized on an ultra-stable cavity. We describe the generation of all the laser sources, the physic package and the operation of the clock. Lasers at 399 nm, 556 nm and 578 nm are obtained, with different techniques, using non-linear crystals starting from infrared sources [3,4]. The clock laser is stabilized using a high finesse notched ULE cavity. The lattice is made with a titanium-sapphire laser. The aluminum vacuum chamber is designed for wide optical access and its temperature is measured by 8 thermistors for blackbody shift evaluation. Our system allows for fast loading of the lattice with $1x10^4$ atoms trapped in the lattice in 200 ms.

Our ytterbium lattice clock is part of the EMRP project "International Timescales with Optical Clocks", where a comparison campaign with other clocks is planned, both local and remote, that will allow a proof-of-principle relativistic geodesy experiment. As well, the Yb clock is part of the project AQUASIM, aiming to compare INRIM's clock to a ytterbium degenerate Fermi gas experiment at LENS using an optical fiber link. So far, INRIM's ultrastable cavity has been used in the LENS apparatus to stabilize a 578 nm laser radiation and study a quantum property of the Yb degenerate Fermi gas [5].

At the conference we will discuss a preliminary uncertainty budget for the clock and we will present the first comparison with the cryogenic cesium fountain IT-CsF2 which has an uncertainty of $2x10^{-16}$ [6]. As well, we will briefly describe the INRIM contribution to the two main experiments in which the Yb clock is involved.

This work was supported by the European Metrology Research Programme EMRP. The EMRP is jointly funded by the EMRP participating countries within EURAMET and the European Union.

[1] N. D. Lemke, A. D. Ludlow, Z. W. Barber, T. M. Fortier, S. A. Diddams, Y. Jiang, S. R. Jefferts, T. P. Heavner, T. E. Parker, and C. W. Oates, "Spin-1/2 optical lattice clock," Phys. Rev. Lett., vol. 103, no. 6, p. 063001, Aug 2009.

[2] M. Yasuda, H. Inaba, T. Kohno, T. Tanabe, Y. Nakajima, K. Hosaka, D. Akamatsu, A. Onae, T. Suzuyama, M. Amemiya, and F.-L. Hong, "Improved absolute frequency measurement of the 171 Yb optical lattice clock towards a candidate for the redefinition of the second," Applied Physics Express, vol. 5, no. 10, p. 102401, 2012.

[3] M. Pizzocaro, G. A. Costanzo, A. Godone, F. Levi, A. Mura, M. Zoppi, and D. Calonico, "Realization of an ultrastable 578-nm laser for an Yb lattice clock," IEEE Trans. Ultrason., Ferroelect., Freq. Cont., vol. 59, no. 3, pp. 426–431, march 2012.

[4] M. Pizzocaro, D. Calonico, P. C. Pastor, J. Catani, G. A. Costanzo, F. Levi, and L. Lorini, "Efficient frequency doubling at 399nm," Appl. Opt., vol. 53, no. 16, pp. 3388–3392, Jun 2014.

[5] G. Cappellini, M. Mancini, G. Pagano, P. Lombardi, L. Livi, M. Siciliani de Cumis, P. Cancio, M. Pizzocaro, D. Calonico, F. Levi, C. Sias, J. Catani, M. Inguscio, and L. Fallani, "Direct observation of coherent interorbital spin-exchange dynamics," Phys. Rev. Lett., vol. 113, p. 120402, Sep 2014.

[6] F. Levi, D. Calonico, C. E. Calosso, A. Godone, S. Micalizio, and G. A. Costanzo, "Accuracy evaluation of ITCsF2: a nitrogen cooled caesium fountain," Metrologia, vol. 51, no. 3, p. 270, 2014.

Making optical clocks more stable

Schioppo, M., Beloy, K., Hinkley, N., McGrew, W.,
Sherman, J. A., Phillips, N. B.*, Oates, C. W., and Ludlow, A. D.
Time and Frequency Division, National Institute of Standards and Technology, Boulder, CO, USA
*present address: Stable Laser Systems, Boulder, CO, USA
E-mail: marco.schioppo@nist.gov

Improving the frequency stability of atomic clocks is crucial for the pursuit of higher accuracy and to exploit new timing applications. Here we present our strategies applied to an optical lattice clock based on Yb atoms towards the target instability of $1x10^{-18}$ in 1000s.

The sequential nature of clock operation sets an important stability limit known as the Dick effect [1]. We are currently exploring two approaches to overcome this limit targeted in reducing the dead time in the interrogation scheme and in improving the frequency stability of the interrogation laser.

An interleaved, anti-synchronized interrogation scheme of two atomic systems is under study to realize a zero dead time operation, which has the potential to virtually eliminate the aliasing phenomenon at the base of the Dick effect [1,2]. We have operated two Yb systems with the requisite for 50% duty cycle and we are currently implementing control logic to enable unified operation of two interleaved lattice systems alternated [2].

In parallel a new interrogation laser is under construction (see Fig.1). This system is based on a 29cm long ULE cavity with near-infrared super-high reflectivity mirrors. In order to reduce the fundamental stability limit due to the thermal noise the cavity is operated near the unstable-resonator regime with 10 meters long radius of curvature mirrors. This allows the effect of the Brownian motion of the dielectric coating to be averaged over a large beam size [3]. The operation in the near-infrared has the advantage of very high reflectivity dielectric mirrors with losses of few ppm and provides a more reliable wavelength for the interface with the frequency comb systems. To enhance the long-term thermal stability the cavity is placed in an ultra-high-vacuum enclosure having three layers of low emissivity aluminum radiation shield enabling a thermal passive low-pass filter with a 1/e time constant of few days.

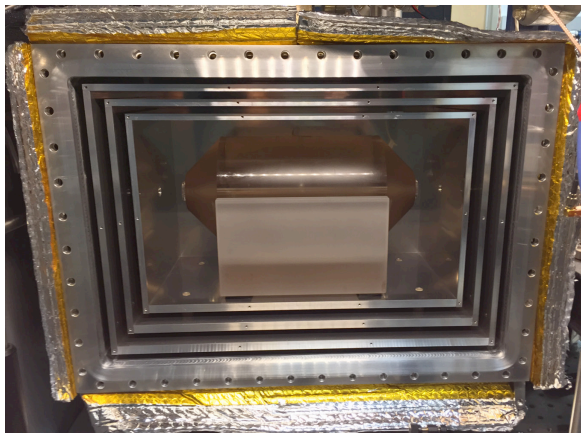


Fig.1: High finesse ULE cavity shown in the low emissivity ultra-high-vacuum enclosure.

Additionally, active study has been carried on in the characterization and optimization of the optical properties of high reflectivity mirrors based on crystalline AlGaAs Bragg reflectors, which have the potential for a lower thermal noise because of their high mechanical quality factor [4]. The results of these measurements will be presented highlighting feasibility for their use in low-thermal-noise cavities.

[1] Dick, G. J., et al., in Proceedings of the 22nd Precise Time and Time Interval Meeting (NASA Conference Publication 3116, Washington, DC, 1990), pp. 487–508.

[2] Hinkley, N., Sherman, J. A., Phillips, N. B., Schioppo, M., Lemke, N. D., Beloy, K, Pizzocaro, M, Oates, C. W., Ludlow, A. D., *Science* **341**, 1215–1218 (2013).

[3] Jiang, Y. Y., Ludlow, A. D., Lemke, N. D., Fox, R. W., Sherman, J. A., Ma, L. S., Oates, C. W., *Nat. Photon*. **5**, 158-161 (2011)

[4] Cole, G. D., Zhang, W., Martin, M. J., Ye, J., Aspelmeyer, M., *Nat. Photon.* **7**, 644-650 (2013)

Higher-order constraints on precision of clocks of neutral Sr, Yb and Hg atoms in optical lattices

V. G. Palchikov, H. Katori[*], S. I. Marmo[+] and V. D. Ovsiannikov[+]
FGUP VNIIFTRI, Mendeleevo, Moscow Region, 141570, Russia, and
National Research Nuclear University "MEPhI", Moscow, 115409, Russia
[*]Department of Applied Physics, Graduate School of Engineering,
The University of Tokyo, Bunkyo-ku, Tokyo 113-8656, Japan,
Innovative Space-Time Project, ERATO, Japan Science and Technology Agency, Bunkyo-ku, Tokyo 113-8656, Japan,
and Quantum Metrology Laboratory, RIKEN, Wako-shi, Saitama 351-0198, Japan.
[+]Voronezh State University, Voronezh, 394006, Russia.
E-mail: vitpal@mail.ru

Recent progress in optical lattice clocks based on the use of ionized [1] and neutral [2,3] atoms requires unprecedented precision in controlling systematic uncertainties at the level of 10^{-18}. Evidently, the target uncertainties at such level of accuracy require more and more precise estimates of the lattice-atom interaction effects with account of inhomogeneity of the lattice field spatial distribution, multipole, nonlinear, and anharmonic contributions to uncertainties [4].

In this paper, we propose new strategies to eliminate light shift perturbations without relying on a zero-extrapolation procedure. We show that the dependence of the clock-level shifts on the lattice-wave frequency and the hyperpolarizability dependence on the lattice-wave polarization can be used to tailor the intensity dependence of the light shift. As was demonstrated in [4], the dependence of the lattice-induced shift $\Delta\nu_{cl}^{latt}(\omega_l,\xi,n,I)$ of the clock frequency on the lattice-laser intensity *I*, with account of hyperpolarizability and the lowest-order anharmonic effects, may be written as a four-term polynomial

$$\Delta\nu_{cl}^{latt}(\omega_l,\xi,n,I)=c_{1/2}(\omega_l)(n+1/2)I^{1/2}+c_1(\omega_l,\xi,n)I+c_{3/2}(\omega_l,\xi)(n+1/2)I^{3/2}+c_2(\omega_{latt},\xi)I^2 \quad (1)$$

All coefficients here depend on the lattice-wave frequency ω_l. The dependence on the circular polarization degree ξ of the lattice wave comes from the hyperpolarizability effects. The quantum number *n* of vibrations of atoms in lattice potential wells appears in all terms of equation (1), except for last one. The half-integer powers of *I* account for the difference of vibration frequencies of an atom in its upper and lower clock states, in particular, the factor (*n*+1/2) is set off explicitly from coefficients $c_{1/2}$ and $c_{3/2}$. Tuning the lattice laser to the magic frequency ω_{mag} aims at reducing the shift (1) to its minimal value. Therefore, the basic target of ω_{mag} was equalization of the polarizability-dependent terms, providing principal contributions to the clock-state shifts. However, the multipole (electric-quadrupole E2 and magnetic-dipole M1) interactions give opposite contributions into the Stark shifts for free and lattice-well-trapped atom. Therefore, to minimize the shift (1), three different strategies may be used for determining ω_{mag}:

1. Equalization of the clock-level shifts in a traveling wave;
2. Equalization of the clock-level shifts in a standing wave;
3. Equalization of E1 polarizabilities of the clock states.

In this paper, the numerical calculations for E1, M1 andE2 polarizabilities and dipole hyperpolarizabilities are presented for the frequencies of $^1S_0$ -$^3P_0$ clock transitions in Sr, Yb, and Hg atoms, which are used to demonstrate the feasibility of the proposed strategies to achieve the lattice-induced systematic uncertainty of 10^{-18}.

[1] C. W. Chou, D. B. Hume, J. C. J. Koelemeij, D. J.Wineland, and T. Rosenband, Phys. Rev. Lett. **104**, 070802 (2010).
[2] B. J. Bloom, T. L. Nicholson, J. R. Williams, S. L. Campbell, M. Bishof, X. Zhang, W. Zhang, S. L. Bromley, and J. Ye, Nature **506**, 71 (2014).
[3] I. Ushijima, M. Takamoto, M. Das, T. Ohkubo, and H. Katori, arXiv:1405.4071 (2014).
[4] V. D. Ovsiannikov, V. G. Pal'chikov, A. V. Taichenachev, V. I. Yudin, and H. Katori, Phys. Rev. A **88**, 013405 (2013).

Determination of the magic wavelength for the clock transition in Magnesium-24

Fim Dominika, Kulosa André, Rühmann Steffen, Zipfel Klaus, Jha Nandan, Sauer Steffen, Ertmer Wolfgang and Rasel Ernst M.
Gottfried Wilhelm Leibniz Universität Hannover Germany, Institut für Quantenoptik, Hannover, Germany
E-mail: fim@iqo.uni-hannover.de

Cooling and trapping of magnesium-24 is done by two magneto-optical traps (MOT), respectively in the singlet and the triplet manifold. A direct loading of the optical lattice is not sufficient enough due to the high temperature and low densities in the MOT. Therefore we introduce a dark state in our second MOT which allows for continuous loading of an optical trap [1]. Since the lattice light ionize the atoms from the higher MOT states, we first accumulate up to 10^5 atoms in a dipole trap at 1064 nm and subsequently transfer to the lattice.

Up to 10^4 magnesium-24 atoms can be trapped near the magic Wavelength in a power enhanced optical lattice. A magnetic field induced spectroscopy of the $^1S_0 - {}^3P_0$ clock transition allows direct excitation of the spin forbidden transition [2]. The interrogation laser is stabilized to a ULE cavity with fused silica mirrors demonstrating an instability of 5×10^{-16} at 1s averaging time.

Two important parameters can be evaluated by a frequency scan over the blue and red sideband and the carrier. At first, the difference in high of the sidebands gives access to the temperature of the trapped atoms, which we could estimate to 7 μK. Secondly, a frequency shift of the carrier versus the trap depth provides information of the differential AC stark shift. From this measurement the magic wavelength for magnesium was determined to be at 468.4(0.1) nm which is in a good agreement with theoretical calculations.

[1] M. Riedmann et al., *Phys. Rev. A*, **86**, 043416 (2012)
[2] A. V. Taichenachev et al., *Phys. Rev. Lett.* **96**, 083001 (2006)

A Sr Optical Lattice Clock at NPL

Hill, Ian R, Hobson, Richard*, Bowden, William*, Menchetti, Marco+, Curtis, E Anne, Donnellan, Sean**, Williams, Ross, Gill, Patrick.
Time and Frequency, National Physical Laboratory, Teddington, UK
*Clarendon Laboratory, Oxford University, Oxford, UK
+School of Physics and Astronomy, University of Birmingham, Birmingham, UK
**Blackett Laboratory, Imperial College London, South Kensington Campus, London, UK
E-mail: ian.hill@npl.co.uk

We report on our first frequency measurement of the $^1S_0$-$^3P_0$ clock transition in ^{88}Sr in a 1D magic-wavelength optical lattice using magnetically induced spectroscopy (MIS) [1]. The clock laser is locked to the atoms using a software locking algorithm fed by a normalised fluorescence signal. We achieve shot-to-shot atom number fluctuations of <5% owing to intensity and frequency stabilization of all cooling lasers which are referenced through a transfer cavity to the clock laser frequency. In addition we have performed initial clock spectroscopy of ^{87}Sr.

Bosonic optical lattice clocks present several advantages compared to their fermionic counterpart. Owing to the absence of nuclear spin, the clock states experience almost no vector or tensor lattice Stark shifts and no first order Zeeman shift. The former relaxes the constraints on lattice polarization, allowing the simple implementation of a 3-D optical lattice, while the latter potentially reduces the noise requirements of the magnetic field environment. In Sr preparation of the atomic sample also favours the boson, with a cooling scheme simplified by the absence of hyperfine structure, and ^{88}Sr outnumbering ^{87}Sr approximately 10 to 1 in natural abundance. However, these advantages come at a cost: The ultra-forbidden clock transition in bosons is not easily accessible, and s-wave atomic interactions cause large collisional decoherence and shifts [2].

Interactions may be addressed in a system containing one or fewer atoms per lattice site and with sufficient confinement to suppress tunneling effects [3]. Alternatively, it may be possible to use a higher-dimensional optical lattice to spectrally resolve the collisional energy shift [4], reducing interactions to a line-pulling effect. We discuss the implementation of a 2-D optical lattice for investigation of these regimes in ^{88}Sr. To address the large ac-Stark and quadratic Zeeman shifts associated with MIS, in the first instance we plan to implement Hyper-Ramsey spectroscopy [5]. A promising alternative approach is to use an all-optical multiphoton excitation which mitigates limitations associated with the applied mixing field present in MIS.

We present current status of the NPL optical lattice clock, including the implementation of an in-house FPGA-based experimental control system using open-source software suite “Labscript” [6], and plans for an accurate bosonic optical clock.

[1] A.V. Taichenachev, V.I. Yudin, C.W. Oates, C.W. Hoyt, Z.W. Barber, and L. Hollberg, “Magnetic Field-Induced Spectroscopy of Forbidden Optical Transitions with Application to Lattice-Based Optical Atomic Clocks,” Physical Review Letters, vol. 96, no. 083001, Mar. 2006.

[2] Ch. Lisdat, J.S.R. Vellore Winfred, T. Middelmann, F. Riehle, and U. Sterr, “Collisional losses, decoherence, and frequency shifts in optical lattice clocks with bosons,” Physical Review Letters, vol. 103, no. 090801, Aug. 2009.

[3] T. Akatsuka, M. Takamoto, and H. Katori, “Optical lattice clocks with non-interacting bosons and fermions,” Nature Physics, vol. 4, no. 954-959, Oct. 2008.

[4] M. Bishof, Y. Lin, M.D. Swallows, A.V. Gorshkov, J. Ye, A.M. Rey, “Resolved Atomic Interaction Sidebands in an Optical Clock Transition,” Physical Review Letters, vol. 106, no. 250801, Jun. 2011.

[5] V.I. Yudin, A.V. Taichenachev, C.W. Oates, Z.W. Barber, N.D. Lemke, A.D. Ludlow, U. Sterr, Ch. Lisdat, and F. Riehle, “Hyper-Ramsey spectroscopy of optical clock transitions,” Physical Review A, vol. 82, no. 011804, Jul. 2010.

[6] P.T. Starkey, C.J. Billington, S.P. Johnstone, M. Jasperse, K. Helmerson, L.D. Turner, and R.P. Anderson, “A scripted control system for autonomous hardware-timed experiments,” Review of Scientific Instruments, vol. 84, no. 085111, Aug. 2013.

Prospects for a Bosonic Sr Optical Lattice Clock

Hobson, Richard*, Hill, Ian R, Bowden, William*, Menchetti, Marco+, Curtis, E Anne, Williams, Ross, Baird, Patrick E G*, Gill, Patrick
Time and Frequency, National Physical Laboratory, Teddington, UK
*Clarendon Laboratory, Oxford University, Oxford, UK
+School of Physics and Astronomy, University of Birmingham, Birmingham, UK
E-mail: richard.hobson@npl.co.uk

Optical lattice clocks with fermionic ^{87}Sr have recently demonstrated exceptional accuracy and stability [1], with further reductions in clock uncertainty possible in the near future. However, bosonic optical lattice clocks with ^{88}Sr present several advantages over fermions: No vector or tensor lattice Stark shifts, no first order Zeeman shift, ten times higher natural abundance, and a simpler cooling sequence. These advantages come at a cost: The ultra-forbidden clock transition in ^{88}Sr is not easily accessible, and s-wave interactions cause large collisional decoherence and shifts.

The $5s^2\ ^1S_0 \rightarrow 5s5p\ ^3P_0$ clock transition can be made accessible using magnetically-induced spectroscopy [2], where an external magnetic `mixing' field induces a small electric dipole moment between the two states. However, this typically introduces quadratic Zeeman and Stark shifts at the level of several parts in 10^{14}. These could be mitigated using Hyper-Ramsey spectroscopy [3], but such techniques are potentially undermined by experimental limitations on the control of the magnetic field. A promising alternative approach is to use all-optical multiphoton excitation, driving either an E1-M1 [4] or an E1-E1-E1 [5] transition. We propose one such scheme which all but eliminates the quadratic Zeeman shift while reducing probe Stark shifts to a few parts in 10^{15}; these shifts could be further cancelled to below a part in 10^{18} using Hyper-Ramsey spectroscopy.

Supplementing their high accuracy, optical lattice clocks can achieve very low quantum projection noise instability using many atoms in parallel [1]. However, due to the long dead time required to prepare new atomic samples, the Dick effect typically prevents lattice clocks from reaching their full stability potential. In order to reduce our Dick limit we propose a non-destructive clock readout scheme using fluorescence detection from a quench molasses. To this end we have successfully driven the $5s^2\ ^1S_0 \rightarrow 5s5p\ ^3P_1 \rightarrow 5p^2\ ^1D_2$ transition, scattering photons at a $\approx 10^6$ s^{-1} rate through the $5p^2\ ^1D_2 \rightarrow 5s5p\ ^1P_1 \rightarrow 5s^2\ ^1S_0$ cascade. As well as retaining the atoms in our 1.5 MHz-deep lattice, this scheme should allow us to filter out spurious laser scatter by exploiting the different wavelengths of incident and fluorescing light.

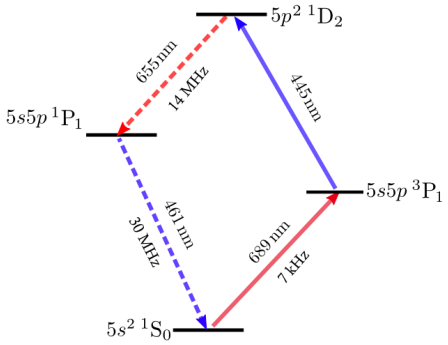


Fig. 1: Quench molasses detection scheme

[1] T.L. Nicholson, S.L. Campbell, R.B. Hutson, G.E. Marti, B.J. Bloom, R.L. McNally, W. Zhang, M.D. Barrett, M.S. Safronova, G.F. Strouse, W.L. Tew, and J. Ye, "2 x 10^{-18} total uncertainty in an atomic clock", Arxiv:1412.8261, Dec. 2014.

[2] A.V. Taichenachev, V.I. Yudin, C.W. Oates, C.W. Hoyt, Z.W. Barber, and L. Hollberg, "Magnetic Field-Induced Spectroscopy of Forbidden Optical Transitions with Application to Lattice-Based Optical Atomic Clocks," Physical Review Letters, vol. 96, no. 083001, Mar. 2006.

[3] V.I. Yudin, A.V. Taichenachev, C.W. Oates, Z.W. Barber, N.D. Lemke, A.D. Ludlow, U. Sterr, Ch. Lisdat, and F. Riehle, "Hyper-Ramsey spectroscopy of optical clock transitions," Physical Review A, vol. 82, no. 011804, Jul. 2010.

[4] T. Zanon-Willette, S. Almonacil, E de Clercq, A.D. Ludlow, and E. Arimondo, "Quantum engineering of atomic phase shifts in optical clocks," Physical Review A, vol. 90, no. 053427, Nov. 2014.

[5] T. Hong, C. Cramer, W. Nagourney, and E.N. Fortson, "Optical Clocks Based on Ultranarrow Three-Photon Resonances in Alkaline Earth Atoms," Physical Review Letters, vol. 94, no. 050801, Feb. 2005.

A dual optical lattice clock driven by clock lasers stabilized to a narrow linewidth comb

Daisuke Akamatsu[1], Takumi Kobayashi[1, 2], Masami Yasuda[1], Hajime Inaba[1], Takehiko Tanabe[1], Sho Okubo[1], Atsushi Onae[1], Feng-Lei Hong[1, 2], and Kazumoto Hosaka[1]

[1]National Metrology Institute of Japan (NMIJ), National Institute of Advanced Industrial Science and Technology (AIST), 1-1-1 Umezono, Tsukuba, Ibaraki 305-8563, Japan

[2]Department of Physics, Yokohama National University, 79-5 Tokiwadai, Hodogaya-ku, Yokohama 240-8501, Japan

E-mail: kazu.hosaka@aist.go.jp

In the past several decades, uncertainties of the optical frequency standards have been dramatically reduced, so that some of the optical frequency standards based on narrow linewidth forbidden transitions in either laser-cooled single ions or neutral atoms have already surpassed the caesium-fountain microwave primary standards used to realise the SI unit of time. For the process of the re-definition of the SI unit of time using optical frequency standards, it would be significant important to measure the optical frequency ratios between optical clocks. At NMIJ we have developed Yb and Sr optical lattice clocks [1, 2]. In the case of the second system that has been used for the Sr optical lattice clock, since the oven is filled with Sr and also Yb, it can be operated as a dual optical lattice clock. In this system, some of the systematic uncertainties of the optical frequency ratio can be reduced, because both atomic species are trapped in the same vacuum chamber. In this paper, we will describe recent progress of the Yb/Sr dual optical lattice clock developed at NMIJ.

To generate the narrow linewidth lasers for both clock transitions in Yb and Sr, we have used linewidth transfer scheme using a fibre based optical frequency comb, which is stabilised to a narrow linewidth laser. As the master laser, we employ a Nd:YAG laser operated at 1064 nm that is locked by the Pound-Drever-Hall technique to a high finesse Fabry–Pérot etalon made by ultra-low expansion glass. We have developed a high-speed controllable optical frequency comb with an erbium-doped fibre and an intra-cavity electro-optic modulator, which is inserted into a free space section of the cavity to change the effective cavity length with fast response [3-5]. Output power from the mode-locked fibre oscillator is split into five branches. The two branches are used to stabilise the comb itself, so that all of the comb modes have same linewidth of the master laser. Using the other two branches, the light sources at 578 nm and 698 nm required for the Yb and Sr optical lattice clocks, respectively, are stabilised to the comb. The last branch is used to observe the beat between the comb and another ultra-stable laser at 1.5 μm for evaluation of the system. As the light source at 578 nm, we have employed the external cavity laser diode operated at 1156 nm with the second harmonic generation scheme by using a periodically poled lithium niobate. Owing to the relatively large servo bandwidth (> 4 MHz), pre-stabilisation is not needed for phase locking to the comb. The cold ^{87}Sr atoms are bound within a vertically oriented one-dimensional optical lattice at 813 nm. On the other hand, a horizontally oriented optical lattice at 759 nm can trap cold ^{171}Yb atoms. Using the clock lasers stabilised to the same narrow linewidth optical frequency comb, narrow Zeeman components of both clock transitions in ^{171}Yb and ^{87}Sr are observed, having linewidths of less than 50 Hz.

[1] M. Yasuda *et al.*, "Improved absolute frequency measurement of the ^{171}Yb optical lattice clock towards a candidate for the redefinition of the second", Appl. Phys. Express, vol. 5, pp. 102401(3 pages), September 2012.

[2] D. Akamatsu *et al.*, "Spectroscopy and frequency measurement of the ^{87}Sr clock transition by laser linewidth transfer using an optical frequency comb", Appl. Phys. Express, vol. 7, pp. 012401(4 pages), January 2014.

[3] Y. Nakajima *et al.*, "A multi-branch, fiber-based frequency comb with millihertz-level relative linewidths using an intra-cavity electro-optic modulator", Opt. Express, vol. 18, pp. 1667 − 1676, January 2010.

[4] K. Iwakun *et al.*, "Narrow linewidth comb realized with a mode-locked fiber laser using an intra-cavity waveguide electro-optic modulator for high-speed control", Opt. Express, vol. 20, pp. 13769 − 13776, June 2012.

[5] H. Inaba *et al.*, "Spectroscopy of ^{171}Yb in an optical lattice based on laser linewidth transfer using a narrow linewidth frequency comb", Opt. Express, vol. 21, pp. 7891 − 7896, April 2013.

Development of Ytterbium Optical Lattice Clocks

Zhou Min, Zhang Xiaohang, Chen Ning, Gao Qi, Han Chengyin, Yao Yuan, Xu Peng, Xu Yilin, Li Shangyan, Jiang Yanyi, Bi Zhiyi, Ma Longsheng, Xu Xinye
State Key Laboratory of Precision Spectroscopy, East China Normal University, Shanghai 200062, China
E-mail: xyxu@phy.ecnu.edu.cn

The optical lattice clocks employing the alkaline-earth(-like) elements such as strontium (Sr) and ytterbium (Yb), have been developed worldwide [1-2]. Both accuracy and stability of the optical lattice clocks have been better than that of the best cesium atomic fountain clocks, enabling the high-precision measurements in the fields of fundamental physics and quantum physics. The optical lattice with the magic wavelength can provide a tight and state-insensitive confinement for in-trap cold atoms, and the cold atoms in the lattice can reach the Lamb-Dicke regimes where the Doppler and recoil effects can be eliminated. Therefore, the narrow-linewidth clock-transition spectrum in such kind of the optical lattice can be obtained so that the optical lattice clocks can have the superior precision and accuracy.

We have done the experiment on developing ytterbium optical lattice clocks. After two-stage cooling, the cold ^{171}Yb atoms with the number of 10^4 and temperature of 10 μK are loaded into a one-dimensional optical lattice with the magic-wavelength of 759 nm. By using the 578-nm narrow-linewidth laser we have observed the spectroscopy of the $^1S_0$-$^3P_0$ clock transition of ^{171}Yb atoms. We have improved the signal-to-noise ratio of the clock signal by the normalization method, which two repumping lasers with the wavelengths of 649 nm and 707 nm are utilized.

We have further studied the clock-transition spectrum of cold ^{171}Yb ytterbium atoms in a one-dimensional optical lattice. A typical clock-transition spectrum with a carrier-sideband structure is observed. After minimizing the power broadening effect and compensating the stray magnetic field, the carrier linewidth is narrowed to about 16 Hz for a 60-ms interrogation time. By increasing the interrogation time, the linewidth is further reduced to 6 Hz as shown in Fig. 1. In addition, by applying the bias magnetic field parallel to the clock-laser polarization, the two-peak spectrum corresponding to two π transitions is obtained. Finally, spin polarization of atoms to a single desired Zeeman sublevel of the ground state is demonstrated.

We have locked the 578-nm clock-laser frequency at the clock transition of ^{171}Yb atoms. We have also measured the stability of the ytterbium optical lattice clock by the self-comparison method. The results show that the instability of the ^{171}Yb lattice optical clock at a level of 1E-16 with the averaging time of 1000 s. Recently, we are doing the experiment on the frequency comparison between two ytterbium optical lattice clocks.

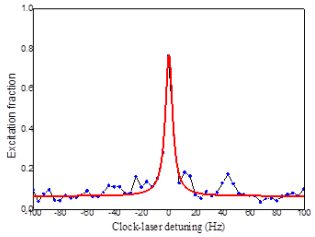


Fig. 1: The clock-transition spectrum of cold ^{171}Yb atoms, where the linewidth is about 6 Hz.

.This work is partially supported by the National Key Basic Research and Development Program of China (Grant No. 2012CB821302), the National Natural Science Foundation of China (Grant Nos. 11134003 and 10774044), and Shanghai Excellent Academic Leaders Program of China (Grant No. 12XD1402400).

[1] B. J. Bloom, T. L. Nicholson, J. R. Williams, S. L. Campbell, M. Bishof, X. Zhang, W. Zhang, S. L. Bromley, and J. Ye, "An optical lattice clock with accuracy and stability at the 10^{-18} level," Nature, Vol. 506, pp.71-75 (2014)..

[2] N. Hinkley, J. A. Sherman, N. B. Phillips, M. Schioppo, N. D. Lemke, K. Beloy, M. Pizzocaro, C. W. Oates, A. D. Ludlow, "An atomic clock with 10^{-18} instability," Science, Vol. 341, 1215-1218 (2013).

Development of Ytterbium Optical Lattice Clocks

Zhou Min, Zhang Xiaohang, Chen Ning, Gao Qi, Han Chengyin, Yao Yuan, Xu Peng, Xu Yilin, Li Shangyan, Jiang Yanyi, Bi Zhiyi, Ma Longsheng, Xu Xinye
State Key Laboratory of Precision Spectroscopy, East China Normal University, Shanghai 200062, China
E-mail: xyxu@phy.ecnu.edu.cn

The optical lattice clocks employing the alkaline-earth(-like) elements such as strontium (Sr) and ytterbium (Yb), have been developed worldwide [1-2]. Both accuracy and stability of the optical lattice clocks have been better than that of the best cesium atomic fountain clocks, enabling the high-precision measurements in the fields of fundamental physics and quantum physics. The optical lattice with the magic wavelength can provide a tight and state-insensitive confinement for in-trap cold atoms, and the cold atoms in the lattice can reach the Lamb-Dicke regimes where the Doppler and recoil effects can be eliminated. Therefore, the narrow-linewidth clock-transition spectrum in such kind of the optical lattice can be obtained so that the optical lattice clocks can have the superior precision and accuracy.

We have done the experiment on developing ytterbium optical lattice clocks. After two-stage cooling, the cold ^{171}Yb atoms with the number of 10^4 and temperature of 10 μK are loaded into a one-dimensional optical lattice with the magic-wavelength of 759 nm. By using the 578-nm narrow-linewidth laser we have observed the spectroscopy of the $^1S_0$-$^3P_0$ clock transition of ^{171}Yb atoms. We have improved the signal-to-noise ratio of the clock signal by the normalization method, which two repumping lasers with the wavelengths of 649 nm and 707 nm are utilized.

We have further studied the clock-transition spectrum of cold ^{171}Yb ytterbium atoms in a one-dimensional optical lattice. A typical clock-transition spectrum with a carrier-sideband structure is observed. After minimizing the power broadening effect and compensating the stray magnetic field, the carrier linewidth is narrowed to about 16 Hz for a 60-ms interrogation time. By increasing the interrogation time, the linewidth is further reduced to 6 Hz as shown in Fig. 1. In addition, by applying the bias magnetic field parallel to the clock-laser polarization, the two-peak spectrum corresponding to two π transitions is obtained. Finally, spin polarization of atoms to a single desired Zeeman sublevel of the ground state is demonstrated.

We have locked the 578-nm clock-laser frequency at the clock transition of ^{171}Yb atoms. We have also measured the stability of the ytterbium optical lattice clock by the self-comparison method. The results show that the instability of the ^{171}Yb lattice optical clock at a level of 1E-16 with the averaging time of 1000 s. Recently, we are doing the experiment on the frequency comparison between two ytterbium optical lattice clocks.

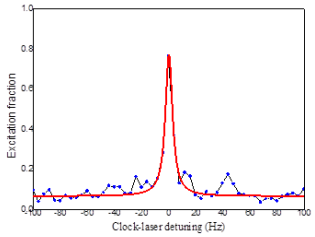


Fig. 1: The clock-transition spectrum of cold ^{171}Yb atoms, where the linewidth is about 6 Hz.

.This work is partially supported by the National Key Basic Research and Development Program of China (Grant No. 2012CB821302), the National Natural Science Foundation of China (Grant Nos. 11134003 and 10774044), and Shanghai Excellent Academic Leaders Program of China (Grant No. 12XD1402400).

[1] B. J. Bloom, T. L. Nicholson, J. R. Williams, S. L. Campbell, M. Bishof, X. Zhang, W. Zhang, S. L. Bromley, and J. Ye, "An optical lattice clock with accuracy and stability at the 10^{-18} level," Nature, Vol. 506, pp.71-75 (2014)..

[2] N. Hinkley, J. A. Sherman, N. B. Phillips, M. Schioppo, N. D. Lemke, K. Beloy, M. Pizzocaro, C. W. Oates, A. D. Ludlow, "An atomic clock with 10^{-18} instability," Science, Vol. 341, 1215-1218 (2013).

Progress of the Strontium Optical Clock at NIM

Lin, Yige, Wang, Qiang*, Li, Ye*, Lin, Baike*, Meng, Fei, Zang, Erjun, Li, Tianchu, Fang, Zhanjun
Time and Frequency Division, National Institute of Metrology, Beijing, China
*Department of Precision Instruments and Mechanology, Tsinghua University, Beijing, China
E-mail: linyige@nim.ac.cn

A strontium optical lattice clock based on ^{87}Sr is being developed at National Institute of Metrology (NIM). The atoms are cooled firstly by a 461nm laser. The absolute frequency of the 461 nm laser is locked to a strontium hot beam spectrometer. The atoms are then further cooled by a dual frequency 689 nm laser system. The master 689 nm laser is an external cavity diode laser (ECDL) which is locked to a reference cavity with Pound-Drever-Hall(PDH) method to reduced its linewidth. Two slave lasers are lock to the master laser by phase lock and injection lock respectively. After the cooling stage, the atoms are loaded into a 1-dimensional optical lattice at the wavelength of 813 nm. The lattice laser frequency is also locked to a high finesse cavity held in a vacuum chamber and measured by an Erbium fiber optical frequency comb.

The reference cavity for the master 698 nm clock laser has a finesse of 200,000. The support structure of the cavity is optimized by finite element analysis. The vacuum chamber of the cavity is mounted inside a copper box whose temperature is controlled by heating wires. A passive vibration isolation platform is used to reduce the vibration noise. The whole cavity system is held inside a homemade acoustic isolation box to isolate the acoustic noise and acts as a passive heat shield at the same time. The power of the master 698 nm laser is amplified to ~20 mW by injection lock a F-P diode laser. The output of the slave laser is then delivered to the atoms with a single mode polarization maintaining fiber. Active fiber noise cancellation technique is introduced to keep the narrow linewidth of the 698 nm laser.

By measuring the transition probabilities while scanning the clock laser frequency, lattice trapping sidebands resolved spectrum can be obtained. From the trapping sidebands, the temperature of the atoms trapped inside the lattice can be calculated to be ~3 μK in the longitudinal direction and ~7 μK in the transverse direction respectively. When the 698 nm probe laser pulse width is set to 300 ms, an atomic transition as narrow as 3.5 Hz can be obtained as showed in Fig 1. Preliminary lock is made based on a transition linewidth ~20 Hz. Interleaved lock of two atomic servos is applied to estimate the stability of the clock. The Allan deviation is 1.6E-16 @ 2000 s as showed in Fig 2.

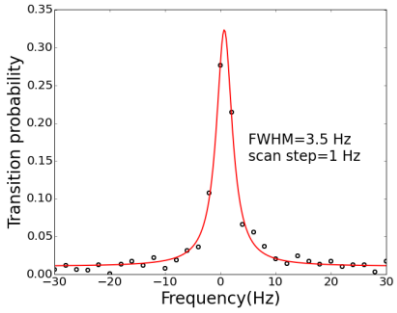


Fig. 1: Clock transition with a linewidth of ~3.5 Hz. The probe laser pulse width is 300 ms.

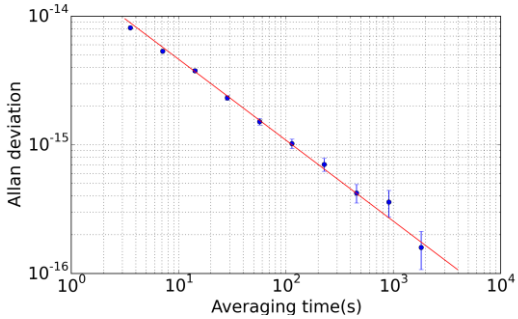


Fig. 2: The Allan deviation of the comparison between two interleaved atomic servos.

[1] Q. Wang, Y. Lin, Y. Li, B. Lin, F. Meng, E. Zang, T. Li, and Z. Fang, "Observation of Spin Polarized Clock Transition in 87 Sr Optical Lattice Clock," Chinese Physics Letters, vol. 31, no. 12, p. 123201, Dec. 2014.

[2] Y. Li, Y. Lin, Q. Wang, S. Wang, Y. Zhao, F. Meng, B. Lin, J. Cao, T. Li, Z. Fang, and E. Zang, "A Hertz-Linewidth Ultrastable Diode Laser System for Clock Transition Detection of Strontium Atoms," Chinese Physics Letters, vol. 31, no. 2, p. 024207, Feb. 2014.

Two independent strontium optical lattice clocks for practical realization of the meter and secondary representation of the second

Zawada M, Bober M, Morzyński P, Cygan A, Lisak D, Zachorowski J*, Masłowski P, Ozimek F+, Prymaczek M, Piotrowski M*, Wcisło P, Ablewski P, Piwiński M, Wójtewicz S, Bielska K, Bartoszek-Bober D, Ciuryło R, Gawlik W*, Radzewicz C+

Institute of Physics, Faculty of Physics, Astronomy and Informatics, Nicolaus Copernicus University, Grudziądzka 5, PL-87-100, Toruń, Poland

*M. Smoluchowski Institute of Physics, Faculty of Physics, Astronomy and Informatics, Jagiellonian University, St. Łojasiewicza 11, PL-30-348, Kraków, Poland

+Institute of Experimental Physics, Faculty of Physics, University of Warsaw, Hoża 69, PL-00-681 Warsaw, Poland

E-mail: zawada@fizyka.umk.pl

Ultracold neutral atoms in an optical lattice [1] are seen as an alternative to single-ions [2] for development of optical frequency standards. We report a system of two independent strontium optical lattice standards probed with a single shared ultra-narrow laser. This allows verification of relative stability of both optical standards. The absolute frequency of the clocks can be roughly verified by the use of a frequency-doubled Er:fiber polarization-mode-locked optical frequency comb with GPS-disciplined Rb frequency standard [3] or, more accurately, by a long distance stabilized fiber optic link with the UTC(AOS) and UTC(PL) via the OPTIME network [4].

The $^1S_0$ - $^3P_0$ transition in neutral strontium was recommended by the International Committee for Weights and Measures for practical realization of the meter and secondary representation of the second. Although best realizations of the strontium atomic clocks reached accuracy and stability at the 10^{-17} level or better [5-9], the International Bureau of Weights and Measures (BIPM) limited practical relative uncertainties to above 1×10^{-15} in case of fermionic isotope ^{87}Sr and 1×10^{-14} in case of bosonic isotope ^{88}Sr. The conservatism of this recommendation stems from the BIPM policy of taking into account only the independently obtained clock/transition frequencies and a limited pool of optical strontium atomic clocks working worldwide. Enlarging this pool is an essential prerequisite for a possible redefinition of the second.

[1] T. Ido, H. Katori, “Recoil-Free Spectroscopy of Neutral Sr Atoms in the Lamb-Dicke Regime”, Phys. Rev. Lett., vol. 91, p. 053001-4, 2003

[2] T. Rosenband, D. B. Hume, P. O. Schmidt, C. W. Chou, A. Brusch, L. Lorini, W. H. Oskay, R. E. Drullinger, T. M. Fortier, J. E. Stalnaker, S. A. Diddams, W. C. Swann, N. R. Newbury, W. M. Itano, D. J. Wineland, and J. C. Bergquist, “Frequency Ratio of Al+ and Hg+ Single-Ion Optical Clocks, Metrology at the 17th Decimal Place”, Science, vol. 319, p. 1808, 2008

[3] P. Morzyński, P. Wcisło, P. Ablewwski, R. Gartman, W. Gawlik, P. Masłowski, B. Nagórny, F. Ozimek, C. Radzewicz, M. Witkowski, R. Ciuryło, and M. Zawada, “Absolute frequency measurement of rubidium 5S-7S two-photon transitions”, Opt. Lett., vol. 38, p. 4581, 2013

[4] Ł. Śliwczyński, P. Krehlik, A. Czubla, Ł. Buczek, and M. Lipiński, “Dissemination of time and RF frequency via a stabilized fibre optic link over a distance of 420 km,” Metrologia, vol. 50, p 133, 2013

[5] B.J. Bloom, T.L. Nicholson, J.R. Williams, S.L. Campbell, M. Bishof, X. Zhang, W. Zhang, S.L. Bromley, and J. Ye, “An optical lattice clock with accuracy and stability at the 10^{18} level,” Nature, vol. 506 p. 7175, 2014

[6] R. Le Targat, L. Lorini, Y. Le Coq, M. Zawada., J. Guéna, M. Abgrall, M. Gurov, P. Rosenbusch, D.G. Rovera, B. Nagórny, R. Gartman, P.G. Westergaard, M.E. Tobar, M. Lours, G. Santarelli, A. Clairon, S. Bize, P. Laurent, P. Lemonde, and J. Lodewyck, “Experimental realization of an optical second with strontium lattice clocks.” Nature Commun., Vol. 4 p. 2109, 2013

[7] N. Hinkley, J.A. Sherman, N.B. Phillips, M. Schioppo, N.D. Lemke, K. Beloy, M. Pizzocaro, C.W. Oates, and A.D. Ludlow, “An atomic clock with 10^{-18} instability,” Science, vol. 341, p. 1215-8, 2013

[8] S. Falke, N. Lemke, C. Grebing, B. Lipphardt, S. Weyers, V. Gerginov, N. Huntemann, C. Hagemann, A. Al-Masoudi, and S. Häfner, “A strontium lattice clock with 3×10^{-17} inaccuracy and its frequency,” New J. Phys., vol. 16, p. 073023, 2014

[9] I. Ushijima, M. Takamoto, M. Das, T. Ohkubo, and H. Katori, “Cryogenic optical lattice clocks with a relative frequency difference of 1×10^{-18}”, arXiv 1405.4071v1, 2014

Dual stage magneto-optical trap for Yb I with sub-100μK temperatures for bosons and fermions

John J. McFerran, Nikita Kostylev and Michael E. Tobar
School of Physics, University of Western Australia, 35 Stirling Highway, Crawley, 6009, Australia*
Email: john.mcferran@uwa.edu.au

The use of neutral ytterbium for optical lattice clocks has shown striking results [1] and it is the atom of choice for a number of atomic clock projects around the globe [2]. With the goal of participating in future ground-clock to space-clock frequency comparisons we are developing a 1D, vertical aligned, optical lattice clock based on Yb. Having additional ground-clocks located in non-common-view with other prominent Time and Frequency laboratories should extend the capabilities of these space-clock missions through the increased clock comparison time. Hence the motivation for a stable and accurate frequency reference in a remote southern hemisphere location.

We have put in place a two-stage magneto-optical trap (MOT) that uses the $^1S_0$ - $^1P_1$ and $^1S_0$ - $^3P_1$ lines in neutral ytterbium. Preliminary measurements show temperatures of ~60μK for ^{171}Yb (fermionic) and ~100μK for ^{172}Yb (bosonic). The temperature of the ^{172}Yb atoms is a factor of 10 below that achieved using the $^1S_0$ - $^1P_1$ line alone. Optimization of the event sequence has just begun and lower temperatures are expected in the near future. The 399nm and 556nm beams are overlapping in the MOT and achromatic quarter wave plates are used to set the circular polarization of both wavelengths. Approximately 8mW of 556nm light is produced by frequency doubling 1111.6nm light in a resonant cavity containing a periodically poled potassium titanyl phosphate crystal. The IR light is generated by injection locking a 50mW semiconductor laser with a narrow linewidth fibre laser (specified linewidth of 60 kHz). By performing spectroscopy of ^{172}Yb atoms held in the $^1S_0$ - $^1P_1$ MOT we have confirmed that the linewidth of the 556 nm light is less than 410kHz [3]. Stabilization of the 556nm light is made by directing 300μW of the green light to the Yb thermal beam that loads the MOT (before a Zeeman slower). The light is aligned at right angles with respect to the atom stream and retro-reflected. Frequency modulation is applied to the light by use of a voltage controlled oscillator (plus RF amplifier) driving an acousto-optic modulator (AOM), through which the 556nm light passes. The fluorescence is spatially filtered and captured by a photo-multiplier cell, whose signal, containing modulation, is sent to a lock-in amplifier that generates the required error signal. Negative feedback (with a few Hertz bandwidth) is applied to a high-voltage driver that tunes the frequency of the 1111.6nm master fibre laser. Despite the FWHM of the spectroscopic line from the thermal beam being ~37 MHz, the S/N of ~160 is sufficient to produce ~230kHz stability at 1s (compare with $\Gamma_{556nm} \approx 190$kHz).

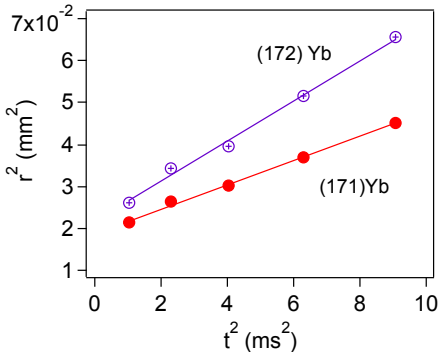


Fig. 1: Mean squared radius vs t^2 (t=free expansion time) for ^{171}Yb and ^{172}Yb. The corresponding temperatures are 60μK and 100μK, respectively ($I \approx 250 I_{sat}$).

In conjunction with the preparation of the Yb atoms for a lattice trap, a frequency comb has been generated to cover the relevant wavelengths of the lattice clock; for example; 1156nm, 1112nm and 759nm. The mode-locked light from one of the available ports of a Menlo Systems master oscillator (centred at 1.55μm) has been amplified and coupled into a section of highly nonlinear fibre (high step index) to extend the wavelength range below 1.1μm. An optical beat has been produced between the 1111.6nm master laser and an adjacent element of the frequency comb. This provides greater resolution for monitoring the frequency (detuning) of the 556nm light. The frequency comb mode spacing is referenced to a hydrogen maser that has been calibrated against UTC at the National Measurement Institute, Sydney.

[1] N. Hinkley, *et al*. Science, 341, 1215, 2013; J.A. Sherman, *et al.*, Phys. Rev. Lett.., 108, 153002, 2012
[2] M. Yasuda *et al.*, Appl. Phys. Exp., 5 102401, 2012; C. Ning *et al.,* Chin. Phys. B., 22, 090601, 2013; C.Y. Park *et al.*, Metrologia 50, 119, 2013
[3] N. Kostylev *et al.*, arXiv physics.optics 1410.4680v2

*This work was supported by the Australian Research Council: LE110100054, FT110100392

BBR-induced shifts and broadening of states in atoms and ions of alkaline-earth elements

Palchikov V.,*, Ovsiannikov V.[+], Kamenski A.[+], Glukhov I.[+], Mokhnenko S.[+], Nikitina E.[+], Chernushkin V[+], Bratchenko P*.

*FGUP VNIIFTRI, Mendeleevo, Moscow Region, 141570, Russia, and
National Research Nuclear University "MEPhI", Moscow, 115409, Russia
[+] Department of Physics, Voronezh State University, Voronezh, 394006, Russia
E-mail: vitpal@mail.ru

Deeply cooled neutral and singly ionized atoms of alkaline-earth-metal elements are considered as the most perspective candidates for the newest standards of time and frequency. The basic feature of a neutral atom is an extremely narrow clock transition between the ground $ns^2(^1S_0)$ and metastable $nsnp(^3P_0)$ states. Ions also may have metastable states of about 1 Hz width, such as the $nd_{J=3/2,5/2}$ states in Ca^+, Sr^+ and Yb^+ which may be used for ion clocks. In addition, the rare-earth ions may be used as logic elements for sympathetic cooling and interrogation of the clock transition in ions of the group III elements (Al^+, Tl^+).

The development of the highest-precision ion and neutral-atom clocks requires accurate account for the influence of surrounding environmental fields on the clock uncertainties. Significant perturbations of clock frequency come from the field of the ubiquitous blackbody radiation (BBR). The BBR cannot disappear unless the absolute temperature T of environment is zero. Consequently, the energy of a state $|nl\rangle$ in an atom (neutral or ionized) in really existing laboratory conditions is shifted and broadened by the BBR due to the dynamic Stark effect. The corresponding energy of the BBR-atom interaction includes both real (shift) and imaginary (broadening) parts: $\delta\varepsilon_{nl}(T) = \delta E_{nl}^{BBR}(T) - i\Gamma_{nl}^{BBR}(T)/2$.

General properties of $\delta E_{nl}^{BBR}(T)$ and $\Gamma_{nl}^{BBR}(T)$ were studied and asymptotic equations for high ($R_{nl}(T) >> 1$) and low ($R_{nl}(T) << 1$) values of the ratio $R_{nl}(T) = |E_{nl}|/kT$ of the state $|nl\rangle$ binding energy and the BBR thermal energy were derived already long ago (see for example [1], [2]). Inequality $R_{nl}(T) >> 1$ holds for the lowest-energy states (in particular, for the clock states) in the temperature ranges $T<3000$ K, here the BBR-induced width is exponentially small, $\Gamma_{nl}^{BBR}(T) \propto \exp\{-R_{nl}(T)\}$ and may be neglected in comparison with the natural (spontaneous-decay) width Γ_{nl}^{sp}. An opposite inequality, $R_{nl}(T) << 1$, for the room temperature $T=300$ K holds for states with their principal quantum numbers $n>100$ – in neutral atoms and for $n>160$ – in ions.

In this communication we present detailed calculations of the shift $\delta E_{nl}^{BBR}(T)$ and broadening $\Gamma_{nl}^{BBR}(T)$ of the clock levels in ions of the group IIa (Be^+, Mg^+, Ca^+, Sr^+, Ba^+) and IIb (Zn^+, Cd^+, Hg^+) elements, calculated on the basis of the Fues' Model Potential (FMP) [3] approach and in the Quantum Defect Method (QDM) [4] for determining the single-electron radiation transition amplitudes. Asymptotic equations are derived for estimating $\delta E_{nl}^{BBR}(T)$ and $\Gamma_{nl}^{BBR}(T)$ of Rydberg states, which may be useful for determining the BBR temperature and corresponding uncertainties in high-accuracy measurements of the clock frequency.

[1] T.F. Gallagher, "Rydberg Atoms", Cambridge University Press, New York, 1994.

[2] J.W.Farley and W. H. Wing, "Accurate calculation of dynamic Stark shifts and depopulation rates of Rydberg energy levels induced by blackbody radiation. Hydrogen, helium, and alkali atoms", Phys Rev A, Vol. 23, no. 5, pp. 2397-2424, 1981.

[3] N.L. Manakov and V.D. Ovsiannikov, "The use of a model potential for the calculation of dynamic polarizabilities, dispersion forces and the light shifts of atomic levels" J.Phys.B: Atom.Molec.Phys., Vol. 10, no. 4, pp. 569-581.

[4] D.R. Bates and A. Damgaard. "On the absolute strengths of spectral lines", Phil. Trans. Roy. Soc., Vol. A242, p. 101, 1949.

ITOC: International Timescales with Optical Clocks

H. S. Margolis[1], E. Benkler[2], D. Calonico[3], H. Denker[4], P. Delva[5], R. M. Godun[1], C. Lisdat[2], J. Achkar[5], S. Bize[5], J. Gersl[6], P. Gill[1], T. Lindvall[7], M. Merimaa[7], M. Pizzocaro[3], D. Piester[2], F. Riedel[2], I. Sesia[3], S. L. Shemar[1], U. Sterr[2], L. Timmen[4], C. Voigt[4], S. Vogt[2], S. Weyers[2], P. B. Whibberley[1]

[1]National Physical Laboratory (NPL), Teddington, UK
[2]Physikalisch-Technische Bundesanstalt (PTB), Braunschweig, Germany
[3]Istituto Nazionale di Ricerca Metrologica (INRIM), Torino, Italy
[4]Institut für Erdmessung (IfE), Gottfried Wilhelm Leibniz Universität, Hannover, Germany
[5]LNE-SYRTE / Observatoire de Paris, LNE, CNRS, UPMC, Paris, France
[6]Cesky Metrologicky Institut (CMI), Brno, Czech Republic
[7]MIKES Metrology,VTT Technical Research Centre of Finland Ltd, Espoo, Finland
E-mail: helen.margolis@npl.co.uk

A key prerequisite for a redefinition of the SI second based on optical atomic clocks is their integration into the international timescales TAI and UTC. This requires a coordinated programme of clock comparisons to be carried out, to validate the uncertainty budgets of the optical clocks, to anchor their frequencies to the present definition of the second, and to establish the leading contenders for a new definition. Such a comparison programme is underway within the EMRP-funded project "International Timescales with Optical Clocks" (ITOC). Illustrated in Fig. 1, this involves four different types of measurement and optical clocks in five different laboratories.

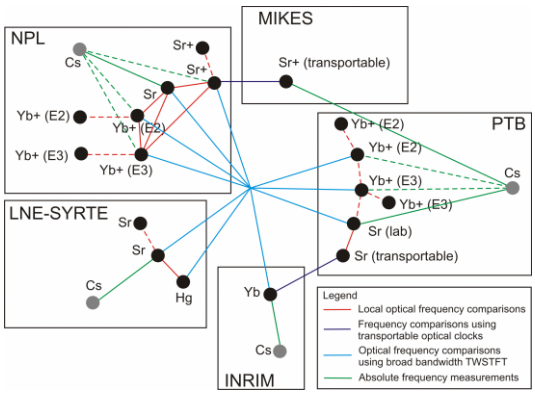


Fig. 1: ITOC clock comparison programme. Dotted lines indicate measurements to be carried out within other projects, but included within the self-consistency analysis.

Locally, comparisons are being carried out between optical clocks developed in individual laboratories, either by direct beat frequency comparison or by using femtosecond combs to measure optical frequency ratios. To compare optical clocks developed in different laboratories, two different techniques are being explored, both of which have the potential to be applied on an intercontinental scale. Two comparisons will be performed using transportable optical clocks, and an improved two-way satellite time and frequency transfer (TWSTFT) technique based on an increased chip rate is being investigated. In addition to the direct optical clock comparisons, absolute frequency measurements of the optical clocks are also being performed. Several new measurements have already been completed and the current status of the clock comparison programme will be reported at the conference. New methods developed to analyze the self-consistency of the clock comparison data and to derive optimized values for the frequency of each optical clock transition will also be described.

To support the clock comparison programme, a complete evaluation is being made of all relativistic effects influencing time and frequency comparisons at the 10^{-18} level of accuracy, including the gravitational redshifts of the clock transition frequencies. Significant progress has been made towards improved determination of the gravity potential at the sites participating in the optical clock comparisons; gravity surveys have been carried out at all locations and will feed into the computation of a revised European geoid model.

Finally, an experiment is in preparation to demonstrate the future impact that optical atomic clocks could have on the field of geodesy. This aims to measure with high temporal resolution the gravity potential difference between two well-defined locations separated by a long baseline (≈ 90 km) and a height difference of 1000 m.

The EMRP is jointly funded by the EMRP participating countries within EURAMET and the European Union.

Reducing the statistical uncertainty of clock comparisons by stable flywheel oscillators

Grebing, C.; Riehle, F.; Lisdat, C.; Sterr, U.
Physikalisch-Technische Bundesanstalt, Bundesallee 100, D-38116 Braunschweig, Germany
E-mail: christian.grebing@ptb.de

The best clocks, both microwave and optical are sophisticated laboratory devices and special care has to be taken to correctly account for all the known systematic effects. This often prevents their continuous operation, which is needed to e.g. realize a timescale [1] or desirable in frequency comparisons that require long averaging times. To bridge gaps in the clock operation, stable and reliable flywheel oscillators are employed. We propose a simple approach to evaluate the uncertainty of the average frequency of the flywheel oscillator, which is running for a long period but is measured only from time to time with a high performance clock. Applying this method allowed us to extend the measurement time of a comparison between a Sr lattice clock and a Cs fountain clock from 74 h to ~300 h.

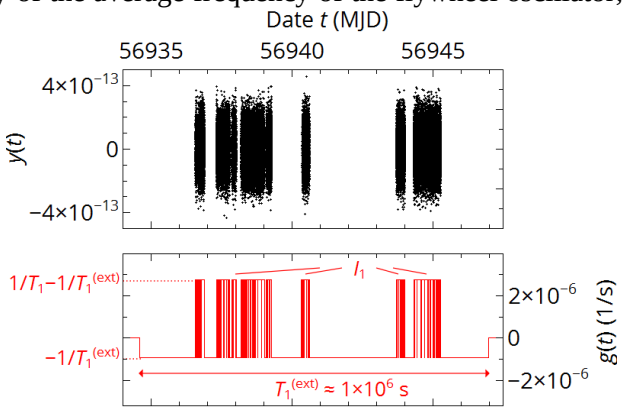


Fig. 1: Fractional frequency fluctuations between a Sr optical lattice clock and a maser as flywheel oscillator (upper curve). Corresponding sensitivity function $g(t)$ of an optimized extended measurement interval for the comparison to a Cs fountain clock with uncertainty $u^{(ext)}$ of 1.6×10^{-16}.

When comparing the frequency of two clocks $(k = 1, 2)$ the sets of uptime intervals I_k with total duration T_k typically do not fully overlap. If only the overlapping intervals $I^{(ov)} = I_1 \cap I_2$ with total duration $T^{(ov)}$ are used, the statistical uncertainty u is limited, e.g. in case of white frequency noise in atomic standards to $u^{(ov)} \propto {T^{(ov)}}^{-1/2}$. Especially when a Cs clock strongly dominates the instability in a comparison with an optical clock or when comparing remote clocks via TWSTFT or GPS, the statistical uncertainty can increase significantly. If we introduce a stable and continuously running flywheel oscillator that is compared to both clocks, the comparison intervals can be extended to $I_k^{(ext)}$ of total durations $T_k^{(ext)}$, thus gaps in the measurements can be interpolated and the statistical uncertainty of the clocks can be improved at the cost of an additional uncertainty $u^{(ext)}$ due to the unobserved fluctuations of the flywheel oscillator.

We present a simple mathematical treatment of this uncertainty for arbitrary measurement scenarios based on the methods of [2] and [3]. It uses a sensitivity function $g(t)$ [3] to describe the effect of the missing knowledge about the behavior of the flywheel during intervals, where only one clock is operating. The corresponding uncertainty $u^{(ext)}$ can then be calculated from the Fourier transform of the sensitivity function and the power spectral density of the flywheel's frequency fluctuations. This method was applied to optimize the interpolation strategy with a hydrogen maser in a comparison of a Sr optical lattice clock and a Cs fountain clock, minimizing the total statistical uncertainty $(\sigma_1^2 + \sigma_2^2 + {u^{(ext)}}^2)^{1/2}$. Over an extended interval of 12 days the uncertainty $u^{(ext)}$ of the mean maser frequency amounts to 1.6×10^{-16}, corresponding to a time error of 160 ps.

This work was supported by the Centre of Quantum Engineering and Space-Time Research (QUEST) and the EMRP projects IND14 and SIB55. The EMRP is jointly funded by the EMRP participating countries within EURAMET and the European Union.

[1] T. E. Parker, *Rev. Sci. Instrum.*, vol. 83, p. 021102, 2012
[2] D.-H. Yu, M. Weiss, and T. E. Parker, *Metrologia*, vol. 44, pp. 91−96, 2007
[3] G. J. Dick, *Proceedings of the 19th PTTI Applications and Planning Meeting*, pp. 133−147, 1988

Towards 10^{-18}-level frequency comparisons with a $^{171}Yb^{+}$ optical clock

King, S. A.[1], Jones, J. M.[1,2], Godun, R. M.[1], Nisbet-Jones, P. B. R.[1], Baynham, C.[1,3] and Gill, P.[1]
[1]National Physical Laboratory (NPL), Teddington, UK
[2] School of Physics and Astronomy, University of Birmingham, UK
[3]Clarendon Laboratory, University of Oxford, Oxford, UK
E-mail: steven.king@npl.co.uk

Optical clocks based on laser-cooled atomic ions have now demonstrated systematic uncertainties superior to the best primary frequency standards. Progress continues to be made, with the best systems having uncertainties at or below the 10^{-17} level. At this level, optical clocks are powerful tools for tests of fundamental physics [1,2,3] and could be used to redefine the SI second leading to a new generation of primary frequency standards.

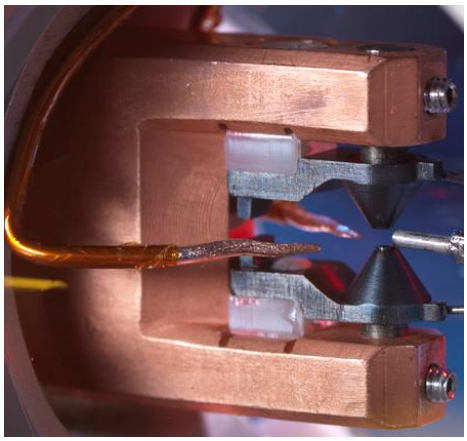


Fig 1: Next-generation single-ion end-cap trap in use at NPL. Improved dielectric materials and good thermal contact significantly limit the electrode temperature rise.

The systematic shift currently limiting the NPL Yb^{+} octupole optical frequency standard is the blackbody radiation shift, arising from the interaction of the atomic polarizability with the thermal radiation that the ion is exposed to. Improved knowledge of both the polarizability and the blackbody environment are key to achieving an uncertainty in the low 10^{-18} range. We present the first data from a new ion trap (see fig. 1) designed specifically to address the issue of blackbody radiation. Careful choice of construction materials and thermal design should limit the frequency shift uncertainty from the temperature of the trap structure to below 10^{-18}. The vacuum chamber is fitted with a MgF_2 window that permits direct thermal imaging of the trap, allowing verification of the thermal modelling undertaken at the Czech Metrology Institute (CMI), Prague [4]. Since the window transmits IR radiation up to around 7 μm, a mid-IR laser beam of known intensity can be applied to the ion to measure directly the differential polarizability close to the static limit.

As optical frequency standards perform at ever lower levels of instability and systematic uncertainty, comparisons with other optical frequency standards, both local and international, must also be improved. Direct optical-optical comparisons are free from the limitations imposed by referencing to local microwave standards. At NPL we have directly measured the ratio of two optical clock transitions in Yb^{+}, with an uncertainty half that achieved when taking the ratio of the absolute frequencies and superior stability at a given averaging time. Recent improvements made to the apparatus will also allow international intercomparison of the NPL Yb^{+} standard with other optical clocks, both via microwave satellite links and direct optical-optical comparison via phase-stabilized fiber links. Presentations regarding these campaigns will be given elsewhere at this conference.

This work is funded by the EMRP project SIB04 Ion Clock. The EMRP is jointly funded by the EMRP participating countries within EURAMET and the European Union.

[1] T. Rosenband *et al.*, *Science* **319** pp. 1808-1812 (2008)
[2] R. M. Godun *et. al.*, *Phys. Rev. Lett.* **113**, 210801 (2014)
[3] N. Huntemann *et al.*, *Phys. Rev. Lett.* **113**, 210802 (2014)
[4] CMI, private comms as part of EMRP project SIB04 Ion Clock

A transportable optical clock based on single $^{40}Ca^{+}$

Jian Cao[1,2,], Kaifeng Cui[1,2,3], Junjuan Shang[1,2,3],Shaomao Wang[1,2,3], Hualin Shu[1,2], Xueren Huang[1,2]

[1]State Key Laboratory of Magnetic Resonance and Atomic and Molecular Physics, Wuhan Institute of Physics and Mathematics, Chinese Academy of Sciences, Wuhan 430071, China

[2]Key Laboratory of Atomic Frequency Standards, Wuhan Institute of Physics and Mathematics, Chinese Academy of Sciences, Wuhan 430071, China

[3]Graduate School, Chinese Academy of Sciences, Beijing 100080, China

E-mail: caojian@wipm.ac.cn

With the advent of the era of optical frequency standard, developing a transportable optical clock attracts much attention in areas of global positioning, advanced communications, and tests of fundamental constant variation. We present a transportable optical clock based on laser-cooled single $^{40}Ca^{+}$ confined in a miniature Paul trap. This prototype is composed of a compact ion trapping apparatus and a transportable frequency stabilized laser system, with the whole volume about $0.5m^3$ excluding electronics. A Preliminary measurement demonstrates the clock transition to be performed with 20Hz resolution, and the Allan deviation fits to be $6 \times 10^{-14}/\sqrt{\tau}$ in 3 hours clock self-comparison.

Double-EIT Cooling: Shortcut to the Ground State

Jannes Wübbena, Nils Scharnhorst, Stephan Hannig, Ian D. Leroux and Piet O. Schmidt*
QUEST Institute for Experimental Quantum Metrology, Physikalisch-Technische Bundesanstalt, Braunschweig, Germany
*Institute for Quantum Optics, Leibniz Universität Hannover, Hannover, Germany
E-mail: idleroux@quantummetrology.de

Laser cooling using the Lorentzian scattering resonances of (effective) two-level atoms suffers from a fundamental conflict between low equilibrium temperatures, which require narrow cooling resonances, and fast cooling, which requires frequent scattering to remove entropy from the atom's motion and broad resonances to address multiple motional modes at once.

In multi-level atoms, coherences between levels can be used to design non-Lorentzian scattering spectra that selectively suppress heating processes [1,2]. Given enough levels, it is possible to suppress all the laser-heating processes that compete with laser cooling at leading order [3]. This allows laser cooling with a speed and bandwidth typical of Doppler cooling to equilibrium temperatures normally only reached through slow sideband cooling on narrow transitions. We demonstrate that so-called double-EIT cooling, based on a tripod level scheme, can be used to cool a $^{40}Ca^{+}$ ion to the motional ground state several times faster than optimized sideband cooling. Such fast cooling has important applications in state-of-the-art optical frequency standards, which we briefly discuss.

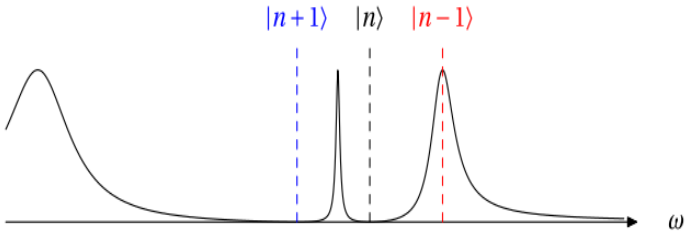


Figure 1: Non-Lorentzian scattering spectrum in double-EIT cooling. Dark resonances suppress the scattering processes that increment motional phonon number or leave it unchanged ($|n+1\rangle$ and $|n\rangle$) but leave a broad scattering resonance for the phonon-removing process ($|n-1\rangle$).

[1] G. Morigi, J. Eschner and C. H. Keitel, "Ground State Laser Cooling Using Electromagnetically Induced Transparency" Phys. Rev. Lett., vol. 85, pp. 4458, Nov. 2011.

[2] G. Morigi, "Cooling atomic motion with quantum interference," Phys. Rev. A., vol. 67, pp. 033402, Mar. 2003.

[3] J. Evers and C. H. Keitel, "Double-EIT ground-state laser cooling without blue-sideband heating", EPL, vol. 68, pp. 370, Oct. 2004.

Simulation of Raman sideband cooling of $^{25}Mg^{+}$ ions

Huang Che, Zetian Xu, Wenhao Yuan, Yapeng Ge, Ke Deng, Jie Zhang, and Zehuang Lu*
MOE Key Laboratory of Fundamental Quantities Measurement, School of Physics,
Huazhong University of Science and Technology, Wuhan, P.R. China
*Email: zehuanglu@mail.hust.edu.cn

Al^{+} ion clock based on quantum logic technique [1] has been one of the most accurate optical clocks ever made. To perform quantum logic process, a logic ion should be chosen. In our laboratory， $^{25}Mg^{+}$ ion is chosen to be the logic ion. Raman sideband cooling of $^{25}Mg^{+}$ ion to its vibration ground state needed before applying quantum logic technique. The sideband cooling rate significantly influences the information transfer velocity of quantum logic. Generally a faster cooling rate is preferred. In this paper we investigate theoretically approaches to cool $^{25}Mg^{+}$ ion to its vibration ground more efficiently. Through density matrix calculation, we simulate the evolution of $^{25}Mg^{+}$ ion motional states varying with time and laser frequency.

Before Raman sideband cooling, the ion is prepared at the state of F=3, m_F=3 by Doppler cooling. After that, π and σ^{+} lasers are simultaneously applied as Raman beams to cool $^{25}Mg^{+}$ ion. Figure 1 shows the Raman carrier spectroscopy for different Raman pulse times through wavefunction evolution of internal and external motional eigenstates.

In order to perform efficient Raman sideband cooling, it is necessary to obtain the initial average motional quantum number of $^{25}Mg^{+}$ ion by comparing the carrier and first order red Raman spectroscopy. Then sideband cooling is simulated. Both second order cooling and first order cooling can be used in the cooling sequence. Figure 2 shows three Raman cooling processes. At the beginning, the average motional quantum number is $\bar{n} = 15$. It can be seen that second order sideband pulses are more efficient at the beginning of cooling. At the later stage started from $\bar{n} = 5$ it can be seen that first order sideband pulses are more efficient. Therefore there is a more efficient combination of first and second order cooling. For different initial motional states, the best combination sequence will be calculated out in this paper.

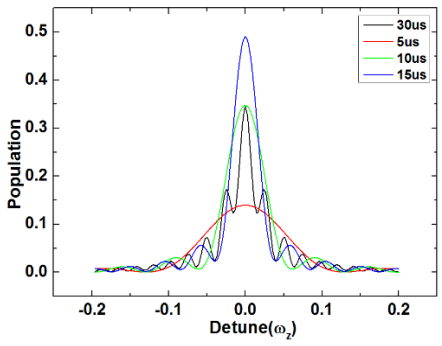


Fig. 1 Raman carrier spectroscopy

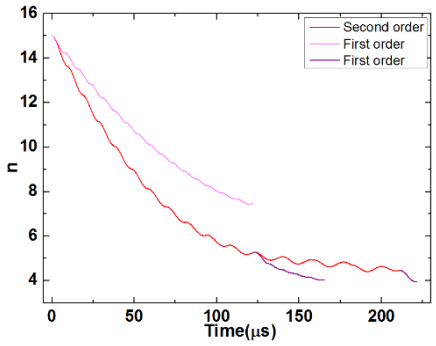


Fig. 2 Motional quantum number ***n*** in Raman cooling process

[1] P. O. Schmidt, T. Rosenband, C. Langer, W. M. Itano, J. C. Bergquist, and D. J. Wineland, "Spectroscopy using quantum logic," Science, vol. 309, p. 749, 2005.

Ion Trap Design for High-Accuracy $^{27}Al^{+}$ Clocks*

Chen, J. S.[1,2], Brewer, S. M.[1,3], Hume, D. B.[1], Chou, C. W.[1],Hankin, A. M.[1], Wineland, D. J.[1,2], Rosenband, T. R.[1,4], and Leibrandt, D. R.[1]

[1]Time and Frequency Division, National Institute of Standards and Technology, Boulder, CO 80305, USA
[2]Department of Physics, University of Colorado, Boulder, CO 80309, USA
[3]Research Laboratory of Electronics, Massachusetts Institute of Technology, Cambridge, MA 02139, USA
[4]Department of Physics, Harvard University, Cambridge, MA 02138, USA
E-mail: jwo-sy.chen@nist.gov

Low sensitivity to environmental electromagnetic fields and a narrow natural line width have enabled optical clocks based on the $^{1}S_0 \leftrightarrow {}^{3}P_0$ transition in $^{27}Al^{+}$ to achieve a fractional frequency uncertainty of 8.0×10^{-18} [1]. This can provide precise gravitational red-shift measurements with possible applications in geodesy and hydrology, as well as fundamental tests of physics [2, 3]. The accuracy of $^{27}Al^{+}$ optical clocks to date has been limited by second order time dilation shifts due to micromotion and residual motion of the ions in the RF pseudopotential well. To suppress these shifts, we have designed and built a new $^{27}Al^{+}$ ion clock based on a laser-machined, gold-plated diamond wafer with differential RF drive, as shown in Figure 1. Improved trap symmetry reduces micromotion, and low heating rates reduce the thermal motion of the trapped ions. Furthermore, the high thermal conductivity of diamond combined with good heat sinking reduces resistive RF heating of the ion trap, enabling sufficiently accurate measurement of the blackbody radiation environment. Here we will present details of the new trap design and also a preliminary evaluation of the trapped $^{27}Al^{+}$ micromotion and blackbody radiation environment.



Figure 1: Picture of a diamond wafer ion trap.

Reference:

[1] C. W. Chou, D. B. Hume, J. C. J. Koelemeij, D. J. Wineland, and T. Rosenband, "Frequency Comparison of Two High-Accuracy Al^{+} Optical Clocks," Phys. Rev. Lett. **104**, 070802 (2010).

[2] T. Rosenband, D. B. Hume, P. O. Schmidt, C. W. Chou, A. Brusch, L. Lorini, W. H. Oskay, R. E. Drullinger, T. M. Fortier, J. E. Stalnaker, S. A. Diddams, W. C. Swann, N. R. Newbury, W. M. Itano, D. J. Wineland, and J. C. Bergquist, "Metrology at the 17th Decimal Place," Science **319**, 1808 (2008).

[3] C. W. Chou, D. B. Hume, T. Rosenband, and D. J. Wineland, "Optical Clocks and Relativity," Science **329**, 1630 (2010).

A Zynq based Digital Phase and Amplitude Measurement System

G. W. Bres-Saix [1,2], C. W. Nelson[2], Hati A.[2], G. Goavec-Merou[1], P.-Y. Bourgeois[1], E. Rubiola[1] and D.A. Howe[2]
[1]FEMTO-ST, Besancon, France
[2]National Institute of Standards and Technology, Boulder, CO/USA
E-mail: guillaume.bressaix@gmail.com

We will present the progress in the development in a digital phase/amplitude noise measurement system (DPAMS) utilizing the Xilinx Zynq system on a chip (SoC) platform. Most current DPAMS only perform the data acquisition and the initial decimation in the FPGA fabric. All further analytical processing occurs in software after transfer from the FPGA to the external CPU. This results in a system that is computationally limited, discarding vast amounts of useful data and greatly limiting the averaging rate for the high offset frequency fast Fourier transforms (FFT). The data required for a single 25 MHz 1024 point FFT can be acquired in 41 µs. This corresponds to 24k FFT/s and would allow 10^6 spectra to be averaged in 41 seconds supporting a cross-spectral improvement of 30 dB at a 10 MHz offset frequency. The goal of this project is to make a DPAMS that is entirely acquisition time limited and allows for each acquired data point to be fully utilized in analysis. At the effective analysis sample rate of 25 MHz, we would like to calculate and average one frequency-domain point for each time-domain point processed. The system will be implemented on the ZYNC ZC706 platform. The ZYNC architecture incorporates dual CPU processors with Kintex-7 FPGA fabric all co-located on the same die. This architecture enables fast communication and tight integration between the hardware data acquisition, hardware and software computational engines. The source and reference signals will be sampled redundantly [1,2] with four 310 MHz - 16 bit analog to digital converters. The acquired data will be processed with four parallel channels of I/Q digital demodulation and hopefully achieve a cross-spectral noise floor of S_ϕ(10 MHz) = –180 dBc/Hz in a few minutes for a 100 MHz carrier signal. Solving the data flow bottleneck between the FPGA, in charge of simple yet high bandwidth processing steps, and the general purpose CPU is potentially solved by the high bandwidth bus shared between both peripherals in the Zynq architecture. However, current investigations in which polled data exchange is performed are limited to an 80 kS/s bandwidth. Reaching the bandwidths targeted for our DPANMS will require dedicated transfer mechanisms including Direct Memory Access, freeing the general purpose CPU for data processing and preventing the CPU, running a user-friendly operating system for high level processing description over the GNURadio framework, from limiting transfer bandwidth. Previous applications using similar architectures demonstrated we could process in the FPGA fabric and avoid a FPGA-CPU bottleneck [3].

[1] J. Grove, J. Hein, J. Retta, P. Schweiger, W. Solbrig, and S. R. Stein, “Direct-digital phase-noise measurement,” in *Frequency Control Symposium and Exposition, 2004. Proceedings of the 2004 IEEE International*, 2004, pp. 287–291.
[2] C. W. Nelson and D. A. Howe, “A sub-sampling digital PM/AM noise measurement system,” in *Frequency Control Symposium (FCS), 2012 IEEE International*, 2012, pp. 1 –4.
[3] G. Goavec-Merou, N. Chretien, J.-M. Friedt, P. Sandoz, G. Martin, M. Lenczner, and S. Ballandras, “Fast contactless vibrating structure characterization using real time field programmable gate array-based digital signal processing: demonstrations with a passive wireless acoustic delay line probe and vision,” *Rev. Sci. Instrum.*, vol. 85, no. 1, p. 015109, Jan. 2014.

Sub-100 µm resolution imaging of dc and microwave magnetic fields using atomic vapor cells

Andrew Horsley. Guan-Xiang Du, and Philipp Treutlein
Department of Physics, University of Basel, Switzerland
E-mail: andrew.horsley@unibas.ch

We have developed techniques for imaging dc [1] and microwave [2,3] magnetic fields using alkali vapor cells, detecting the respective fields through Ramsey and Rabi oscillations on hyperfine transitions. The parallel nature of our dc imaging technique could be advantageous in measurements requiring high spatial and time resolution, such as in microfluidics in chemistry and biology. For microwave fields, there are currently no established imaging techniques. Microwave devices form an essential part of modern technology, finding applications in telecommunications, defence, and scientific instrumentation. Our technique could prove transformative in the design, characterisation, and debugging of such devices, and is already being employed in the characterisation and debugging of vapor cell atomic clocks [4].

We present results, including the first for our dc imaging technique, from a new imaging system providing spatial resolutions of 40-100 µm, an order of magnitude improvement from previous experiments [2]. More importantly, our vapor cell allows imaging of fields as close as 150 µm above structures of interest, through the use of extremely thin external cell walls. This is crucial in allowing us to take practical advantage of the high spatial resolution, as feature sizes in near-fields are on the order of the distance from their source. We demonstrate our system through the imaging of dc and microwave fields above a selection of devices.

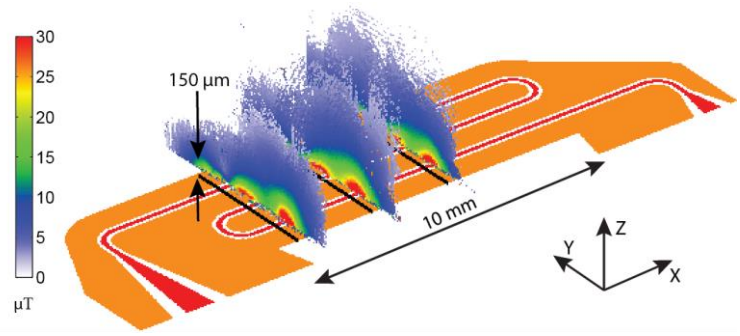


Figure 1: Experimentally obtained images of the microwave magnetic field at several positions above a microwave circuit. The central signal line of the circuit is shown in red, and the ground planes are in orange.

In a 140x140 pixel image, we achieve dc and microwave sensitivities up to 1 µT $Hz^{-1/2}$ per 40x40x100 μm^3 pixel. To achieve the same sensitivity with a single scanning probe, a sensitivity of 7 nT $Hz^{-1/2}$ is required. Our current sensitivity is limited by the low experiment duty cycle, and an improvement in sensitivity by up to 6 orders of magnitude is in principle possible, to the atomic projection noise limit.

Our spatial resolution, sensitivity, and approach distance are now sufficient for characterising a range of real world devices at fixed frequencies. However, the development of a broadband microwave imaging technique is essential for wider applications. We also present progress on a frequency-tunable setup, allowing us to image microwaves at any frequency, from sub-GHz to 10s of GHz.

[1] A. Horsley et al., "Imaging of Electromagnetic Fields in Alkali Vapor Cells With 40-100 µm Resolution", in preparation
[2] P. Böhi and P. Treutlein, "Simple microwave field imaging technique using hot atomic vapor cells" Appl. Phys. Lett. 101, 181107 (2012)
[3] A. Horsley et al., "Imaging of Relaxation Times and Microwave Field Strength in a Microfabricated Vapor Cell" Phys. Rev. A 88 063407 (2013)
[4] A. Ivanov et al., "Experimental and numerical study of the microwave field distribution in a compact magnetron-type microwave cavity", *Proceedings* 28th EFTF, Neuchatel, Switzerland, June 22 - 26, 2014, pp. 208-211.

A Magnetometer Based on Coherent Population Beating

LIU Li, WANG Yigen, ZHAO Xiaona, ZHUANG Yuxin and WANG Zhong,
School of Electronics Engineering & Computer Science, Peking University, Beijing, 100871, P. R. China
E-mail: zw@pku.edu.cn

We proposed a novel magnetic field measurement method extended from the CPT method. It is based on the coherent population beating (CPB) phenomenon [1]. CPB occurs in a typical three-level system, when the frequency difference of the two pump laser fields have a detuning from the ground states splitting, and the CPB oscillation frequency is equal to the detuning. The CPB phenomenon enables us to directly obtain the beat frequency between the RF signal and the atomic transition frequency. For m_F=0 ground state hyperfine energy levels (Fig.1), they are insensitive to external magnetic field, which can be used to achieve a CPB atomic clock [2]. Here we move the CPB effect to the ground levels of m_F=1 or m_F=-1, which are sensitive to external magnetic field. When the atoms are placed in a magnetic field, the Zeeman sublevels of the atoms will shift with the magnetic field intensity changing. Then we are able to detect the beat frequency shift with the external magnetic field changing via digital processing, thus we can acquire the Zeeman frequency shift and then calculate external magnetic field intensity accurately.

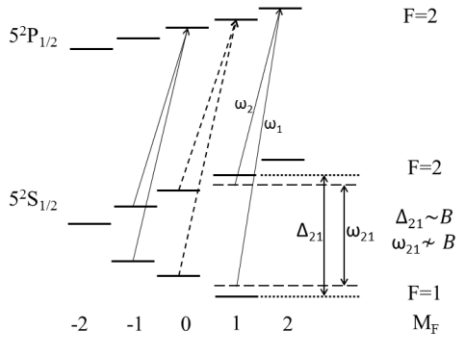


Fig.1: ^{87}Rb atom's energy levels of D1 line in magnetic field and the Λ-type configuration. The two laser fields different frequency $\omega_{21} = \omega_1-\omega_2$.

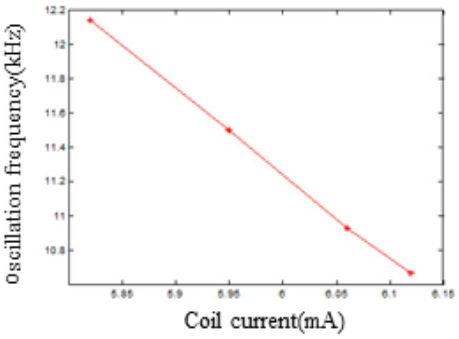


Fig.2: The relationship between coil current (which is proportional to magnetic field intensity) and CPB oscillation frequency.

In the procedure of frequency measurement, the CPB oscillation frequency $\Delta=|\Delta_{21}-\omega_{21}|$, where Δ_{21} is the ground levels hyperfine splitting and ω_{21} is the difference of the coherent laser fields. The beat frequency Δ can be accurately measured through digital signal processing, which is capable of up to mHz or higher frequency resolutions (for GHz signal). Taking ^{87}Rb for example, the gyromagnetic constant is 7Hz/nT, so according to $\Delta\nu=\gamma B$, the magnetic field intensity resolution can reach up to 1pT. In experiment we have proved a good linear relationship between coil current (which is proportional to magnetic field intensity) and oscillation frequency (Fig.2), showing that it's a feasible way to measure magnetic intensity.

[1]. T. Guo, K. Deng, X. Chen, and Z. Wang, "Atomic clock based on transient coherent population trapping", Appl. Phys. Lett. 94, 151108 (2009).

[2]. Dawei Li, Daiting Shi Ermeng Hu, Yigen Wang, Lu Tian, Jianye Zhao, and Zhong Wang*. "A frequency standard via spectrum analysis and direct digital synthesis" Applied Physics Express 7, 112203 (2014)

A Compact Atom Interferometer Based on an Expanding Ball of Atoms

Gregory W. Hoth, Stefan Riedl, Bruno Pelle, John Kitching, Elizabeth A. Donley
NIST, Boulder, CO
E-mail: gregory.hoth@nist.gov

Atom interferometers have proven to be powerful tools for measuring gravity, acceleration, and rotation [1]. So far, these tools have largely been confined to laboratory environments by their large size, but there are applications, such as inertial navigation and geodesy, that could benefit from the precision and stability offered by atom interferometers if they could be made small enough to be taken outside the lab. Toward this end, we have developed an atom interferometer that is capable of measuring both rotations and accelerations with an active evacuated volume of 5 cubic centimeters. Our interferometer set up is sketched in Figure 1a.

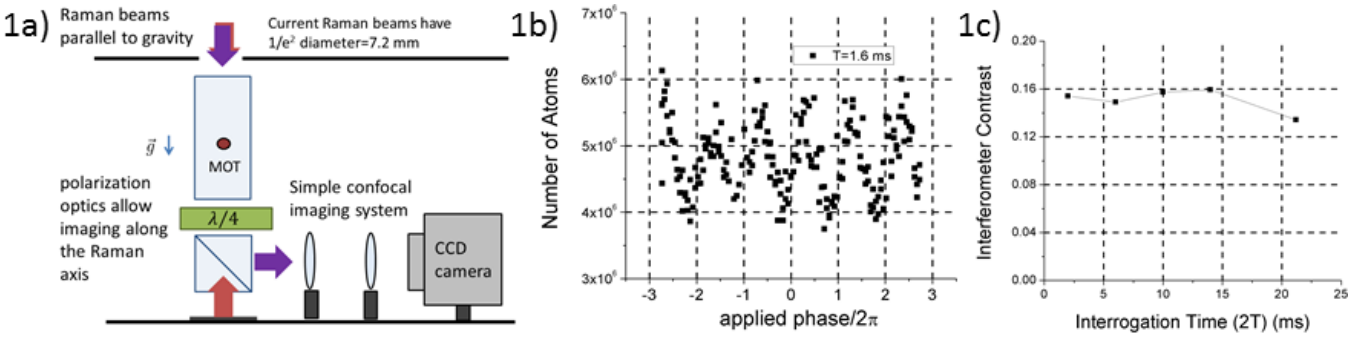


Figure 1a) A sketch of our set up illustrating our detection geometry. The volume used to trap and interrogate the atoms is about 5 cc. The volume of our vacuum system is about 300 cc. 1b) Interferometric fringes in the number of atoms detected in the F=2 ground state. 1c) Interferometer contrast versus interrogation time.

In order to measure both accelerations and rotations, we apply a π/2-π-π/2 pulse sequence to an expanding cloud of ^{87}Rb atoms using stimulated Raman transitions and image the final cloud onto a CCD. In this spatially resolved, point source imaging scheme, rotations cause spatial fringes to appear across the cloud while accelerations shift the overall phase of the fringe pattern [2]. In particular, it is possible to simultaneously measure two components of the rotation vector and one component of the acceleration vector. By extracting three measurements from a single shot of our interferometer, we make efficient use of our compact evacuated volume.

We are able to observe interferometric fringes in the atom number with a contrast of about 15% and interrogations times up to 2T=20 ms (Figs 1b and 1c). In the near future, upgrades to our system will allow us to detect both hyperfine states in a single shot of our interferometer, extend the interrogation time to 2T=100 ms, and characterize the performance of our interferometer as a sensor of accelerations and rotations.

[1] A. D. Cronin, J. Schmiedmayer, and D.E. Pritchard, "Optics and interferometry with atoms and molecules," Rev. Mod. Phys., vol. 81, no. 1051. July 2009.

[2] S. M. Dickerson, J. M. Hogan, A. Sugarbaker, D. M. S. Johnson, and M. A. Kasevich, "Multiaxis Inertial sensing with Long-Time Point Source Atom Interferometry," Phys. Rev. Lett., vol. 111, no. 083001 Aug. 2013.

Repetition rate stabilization of an optical frequency comb to a high quality factor optical fiber delay line

Jung, Kwangyun and Kim, Jungwon*
Korea Advanced Institute of Science and Technology (KAIST), Daejeon 305-701, South Korea
*E-mail: jungwon.kim@kaist.ac.kr

Optical frequency combs have enabled revolutionary applications for astronomy, metrology, and spectroscopy. Repetition rate stabilization of optical frequency combs is a core technology for various comb applications such as ultralow phase noise microwave generations, photonic analog-to-digital converters, particle accelerators, and high performance radars. For high performance short-term (below ~ 10 s time scale) stabilization, repetition rate should be locked to high quality factor (Q) RF/microwave references or optical references. Mode-locked laser repetition rate can be stabilized to high-Q RF or microwave oscillators such as ultralow phase noise sapphire oscillators, optoelectronic oscillators (OEO), and oven controlled crystal oscillators (OCXO). However, for the ultimate performance, optical references such as high-Q ($\sim 10^{11}$) ultra-stable cavities (Fabry-Perot cavity) [1] or optical fiber delay lines [2] are required. Generally, continuous wave (CW) lasers are used as connecting links between optical references and mode-locked lasers. First, CW laser frequency is stabilized to an ultra-stable cavity using PDH technique, and then, carrier-envelope offset frequency of a mode-locked laser is stabilized to a separate RF oscillator. Finally, mode-locked laser repetition rate is locked to the cavity-stabilized CW laser. The use of CW lasers results in multi-stage phase-locked loops, complexity, and high cost. In addition, ultra-stable cavities and their shielding systems are fragile, alignment sensitive, and expensive. Although mode-locked laser repetition rate stabilization based on cavity-stabilized CW lasers results in ultimate phase noise performance (-105 dBc/Hz at 1 Hz offset frequency with 10 GHz carrier [1]), its maintenance, cost, and complexity may limit their applications in well-controlled metrology laboratory environment.

In this paper, we demonstrate direct repetition rate stabilization of a mode-locked Er-fiber laser to a 2.5 km fiber delay line (Q $\sim 10^{10}$) without any CW laser. The demonstrated repetition rate stabilization method is all-fiber configuration, nearly repetition rate independent, simple, and robust. The basic structure is an all-fiber Michelson interferometer including a km scale optical fiber delay line [2]. We use a 77-MHz repetition rate mode-locked laser, instead of a CW laser that was used in ref. 2. By optical carrier interference between a reference arm and a delayed arm of the interferometer, absolute frequency noise of comb modes is detected. As we use the comb directly, combined frequency noise (*nfrep+fceo*) is detected. In order to eliminate the *fceo* frequency noise, we apply two separate spectral components of the frequency comb into the interferometer. The common mode *fceo* noise is rejected by mixing two frequency noise signals detected from different spectral regions [3]. The detected *nfrep* noise is stabilized to the 2.5 km delay line using a pzt and an electro-optic phase modulator (EOM) inside the laser cavity. A preliminary out-of-loop result shows 3×10^{-13} Allan deviation at 1 s averaging time without any environment isolation such as shielding box, vacuum chamber, vibrational isolation, and temperature control. Further improvement is in progress, and the results will be reported at the time of meeting.

[1] T. M. Fortier, M. S. Kirchner, F. Quinlan, J. Taylor, J. C. Bergquist, T. Rosenband, N. Lemke, A. Ludlow, Y. Jiang, C. W. Oates, and S. A. Diddams, "Generation of ultrastable microwaves via optical frequency division," Nature Photon., vol. 5, no. 7, pp. 425-429, Jul. 2011.

[2] F. Kéfélian, H. Jiang, P. Lemonde, and G. Santarelli, "Ultralow-frequency-noise stabilization of a laser by locking to an optical fiber-delay line," Opt. Lett., vol. 34, no. 7, pp. 914-916, Apr. 2009.

[3] R. J. Jones, I. Thomann, and J. Ye, "Precision stabilization of femtosecond lasers to high-finesse optical cavities," Phys. Rev. A, vol. 69, no. 5, pp. 051803, May 2004.

Yellow solid state laser for Yb atomic clock application

Bolognesi Giacomo[1,2,3*], Parisi Daniela[4], Pizzocaro Marco[1], Calonico Davide[1], Costanzo Giovanni Antonio[2], Levi Filippo[1], Metz Philip Werner[5], Kränkel Christian[5,6], Huber Günter[5,6] and Tonelli Mauro[3,4]

[1]*INRIM, Istituto Nazionale di Ricerca Metrologica, Strada delle caccie 91 10135 Torino, Italy*
[2]*Politecnico di Torino, Corso duca degli Abruzzi 24 10129 Torino, Italy*
[3]*Dipartimento di Fisica, Università di Pisa, Largo B. Pontecorvo 3 56127 Pisa, Italy*
[4]*Nest-istituto Nanoscienze-CNR, Pz. San Silvestro 12 56127 Pisa, Italy*
[5]*Institut für Laser-Physik, Universität Hamburg, Luruper Chaussee 149, 22761 Hamburg, Germany*
[6]*The Hamburg Centre for Ultrafast Imaging, Universität Hamburg, Luruper Chaussee 149,*
[*]E-mail: g.bolognesi@inrim.it

INRIM, the Italian institute for metrology, is developing an optical lattice clock based on ^{171}Yb. The Yb clock transition $^1S_0 \rightarrow {}^3P_0$ is in the yellow range of the spectrum at 578.14 nm [1]. So far the clock laser radiation at 578 nm has been produced by sum frequency generation (SFG) [2] of 1030 nm and 1319 nm laser radiation in a non-linear crystal, or by second harmonic generation (SHG) of 1156-nm laser radiation [3]. We have investigated the possibility of direct solid-state laser emission at 578 nm.

A solid-state laser source is beneficial due to its simpler and more robust set-up, enhanced reliability, larger output power and possible miniaturization of the device. The latter is an extremely important feature in the development of transportable optical clocks and space applications. A new attractive candidate for visible laser emission is the trivalent dysprosium ion Dy^{3+} as a dopant in fluoride crystals.

We present laser results obtained from a Dy^{3+},Tb^{3+} codoped $LiLuF_4$ crystal [4], pumped by a blue InGaN laser diode, aiming for the generation of a compact 578 nm source. We exploit the yellow Dy^{3+} transition $^4F_{9/2} \rightarrow {}^6H_{13/2}$ to generate yellow laser emission. The lifetime of the lower laser level is quenched via energy transfer to co-doped Tb^{3+} ions in the fluoride crystal. We report the room temperature continuous wave (cw) laser results in a hemispherical cavity at 574 nm and with a highly reflective output coupler at 578 nm. A yellow laser at 578 nm is very relevant for metrological applications, in particular to excite the forbidden $^1S_0 \rightarrow {}^3P_0$ Ytterbium clock transition, which is recommended as a secondary representation of the second. At the conference we will report the characterization of the laser and the results achieved in the Yb optical clock application.

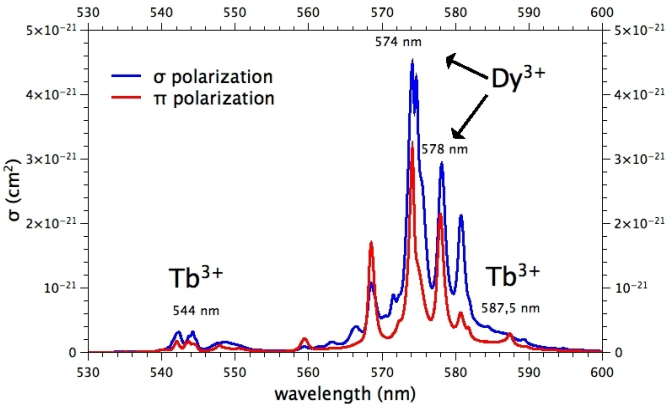


Fig. 1 Room temperature emission cross sections σ in the yellow spectral region for the two possible polarizations of Dy^{3+}(4%), Tb^{3+}(1%): $LiLuF_4$ relative to the optical axis.

[1] N. D. Lemke, A. D. Ludlow, Z.W. Barber, T. M. Fortier, S.A. Diddams, Y. Jiang, S. R. Jefferts, T. P. Heavner, T. E. Parker, and C.W. Oates, Phys. Rev. Lett. 103, 063001 (2009).

[2] M. Pizzocaro, G. A. Costanzo, A. Godone, F. Levi, A. Mura, M. Zoppi, D. Calonico, {IEEE} Trans. Ultrason., Ferroelect., Freq. Contr. **59**, 426-431 (2012).

[3] A. Yu. Nevsky, U. Bressel, I. Ernsting, Ch. Eisele, M. Okhapkin, S. Schiller, A. Gubenko, D. Livshits, S. Mikhrin, I. Krestnikov, and A. Kovsh, Appl. Phys. B 92(4), 501–507 (2008).

[4] Giacomo Bolognesi, Daniela Parisi, Davide Calonico, Giovanni Antonio Costanzo, Filippo Levi, Philip Werner Metz, Christian Kränkel, Günter Huber, and Mauro Tonelli, Optics Letters, Vol. 39 Issue 23, pp.6628-6631 (2014).

Delivery of Optical Frequency via 34 km Urban Fiber Link with a Linewidth Broadning of 1 mHz

Ma C Q, Wu L F, Jiang Y Y, Bi Z Y, Yu H F, Ma L S
State Key Laboratory of Precision Spectroscopy, East China Normal University, Shanghai, China
E-mail: yyjiang@phy.ecun.edu.cn

We demonstrate a coherence transfer of an optical frequency operating at 1556nm (192.8 THz) through a pair of cascaded 17 km urban fiber link between East China Normal University and Shanghai South Railway Station. The light source used for transfer is provided by a diode laser which is frequency stabilized to a Fabry-Pérot cavity with finesse of 270000 using the Pound-Drever-Hall technique [1]. By measuring the beat note of two independent cavity-locked diode lasers, the most probable linewidth of the beat note is 0.75 Hz, corresponding to 0.5 Hz for each cavity-locked laser.

When the light travels through the 34 km fiber link, the optical carrier is suffering from a random phase modulation induced by fiber length fluctuation, resulting in linewidth broadening and degraded frequency stability. To obtain the servo signal for compensate the phase noise, we transfer the light through the fiber for a round-trip and mix it with the original light. The error signal is sent to a servo control system to compensate the fiber noise by modifying the driving frequency of an acousto-optic modulator [2]. Due to the delay effect, the performance of the compensation system is limited by a servo bandwidth of $1/4\tau$ [3]. Here, τ stands for the delay time of light single-pass in fiber.

After compensation, we measure the frequency of the beat note between remote light and the original light for about 45 hours using a Λ-type counter with a gate time of 1 s. The frequency instability after transfer is about 4×10^{-17} at an averaging time of one second, as shown in Fig. 1. The linewidth broadening caused by the fiber noise is suppressed as narrow as 1 mHz, as shown in Fig. 2. This work shows that both the frequency instability and monochromaticity of the optical frequency can be delivered to the remote site through fiber.

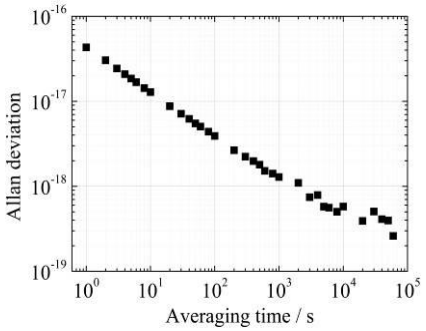


Fig. 1: Frequency instability after transfer of 34 km fiber with fiber noise compensation

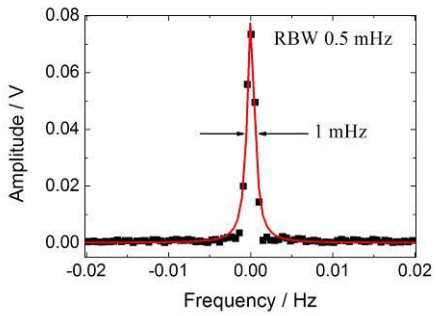


Fig. 2: Beat note between remote and original light with fiber noise compensation.

[1] R. W. P. Drever, J. L. Hall. F. V. Kowalski, J. Hough, G. M. Ford, A. J. Munley, and H. Ward, "Laser phase and frequency stabilization using an optical resonator," Applied Physics B, 1983, pp.97-105.

[2] L. S. Ma, P. Jungner, J. Ye, and J. L. Hall, "Delivering the same optical frequency at two places: accurate cancellation of phase noise introduced by an optical fiber or other time-varying path," Optics Letters, 1994, pp.1777-1779.

[3] N. R. Newbury, P. A. Williams, and W. C. Swann, "Coherent transfer of an optical carrier over 251 km," Optical Letters, 2007, pp.3056-3058.

Research on the New Steering Strategy for the NTSC Master Clock

Shuhong Zhao*+,Shaowu Dong*+,Haibo yuan*+,Dongshan Yin*+&
* National Time Service Center,Chinese Academy of Sciences, Xi'an 710600,China
+Key Laboratory of time and frequency standards, Chinese Academy of Sciences, Xi'an 710600, China
& University of Chinese Academy of Sciences, Beijing,China
E-mail: yds@ntsc.ac.cn

NTSC(National Time Service Center, Chinese Academy of Sciences) has taken the charge of the national standard time UTC(NTSC). |UTC-UTC(NTSC)| has been kept within 20ns since 2012,which is the notable achievements on high precision time-keeping .But the shortage of UTC(NTSC) is poor short-term stability, and we also want to reduce the absolute time difference between UTC(NTSC) and UTC, therefore the new realization of UTC(NTSC) is described, the time scale algorithm and steering algorithm are presented in detailed.

From Cir T,UTC(NTSC) works much better than before because of the new steering strategy, and the results of new steering UTC(NTSC) in 2013.09~2014.11 are discussed. Fig.1shows that the new steering strategy can control the absolute time offset within 10ns, and Fig.2 shows that the new steering strategy can improve the short-term stability and long-term stability.

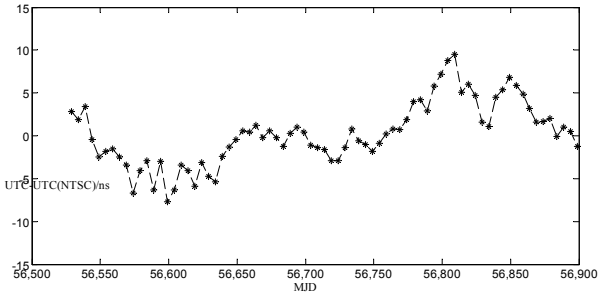


Fig. 1 :UTC-UTC(NTSC) (2013.09-2014.11)

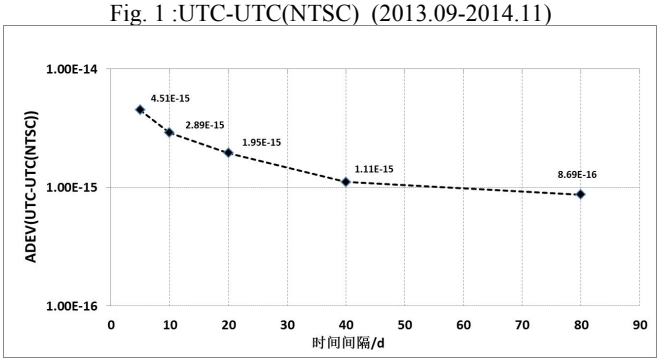


Fig. 2 :the stability of UTC(NTSC) (2013.09-2014.11)

Reference

[1] Demetrios Matsakis etc. "Steering Strategies for the Master Clock of the U.S. Naval Observatory (USNO)", in proc 34th precise time and time interval(PTTI) appl.2003.

[2] P. Koppang,D.Johns，J.Skinner.Application of Control Theory in the Formation of a Timescale, in proc 35th precise time and time interval(PTTI) appl.2004.

[3] Yuan Haibo,Wang Zhengming.Automatic steering strategy for UTC(NTSC) ,Asia-Pacific workshop on Time and Frequency 2004,225-229.

[4] Panfilo G, Harmegnies A, Tisserand L. A new prediction algorithm for the generation of International Atomic Time[J]. Metrologia, 2012, 49 (1), 49~56.

[5] Shuhong Zhao, Dongshan Yin, Shaowu Dong, Haibo Yuan, Lili Qu,Ruan Jun. A New Steering Strategy for UTC(NTSC).

IFCS2014,210-213.
[6] Information on BIPM FTP site: ftp://ftp2.bipm.org/pub/tai/publication/.

Balanced Low-Loss 2-IDT Double Mode SAW Filter with Narrowed Passband and Improved Selectivity

Doberstein Sergei
PJSC «Omskiy Nauchno Issledovatelskiy Institut Priborostroenia» (ONIIP), Omsk, Russia
E-mail: info@oniip.ru

There are many applications for the narrowband SAW filters with a fractional bandwidth of less than 1% having low loss and high selectivity. Recently the low-loss 3-IDT double mode SAW (DMS) filter with the fractional bandwidth of 0.96 % and high selectivity was developed [1]. But the further narrow passband on the retention of the low loss and high selectivity is required for front-end of the VHF receivers for example.

This paper presents the new balanced low-loss DMS filter with the narrowed passband and improved selectivity on 42º YX $LiTaO_3$. The filter is realized as a two-transducer scheme on the longitudinal first and second resonance modes. A passband of DMS filter depends on a frequency difference between these modes and is determined by the gap length between the input and output IDTs. The frequency difference between the first and second resonance modes in the two-transducer filter is always less than frequency difference between the first and third resonance modes in the three-transducer filter, all things being equal [2]. Also the frequency responses of the input weighted IDT, output IDT and reflectors affect on the passband width. Then the both long weighted input IDT and reflectors are used for narrowing passband.

A shape of the frequency response of the filter depends on the weighting the input IDT, frequency responses of the output IDT and reflectors. This shape is determined by the weighting function of the input IDT, number of the electrodes in the output IDT and reflectors, relationship between the electrode pitch in the input IDT, output IDT and reflectors. An optimization of the mentioned parameters allows to get the specified high selectivity of the filter with a fractional bandwidth of 0.5-0.6 % under condition that the insertion loss are low and input and output impedances are close to the specified real values. In this case the passband is considerably narrowed as opposed to known methods [1-3]. The balanced operation of the filter is made by symmetrical connection of the input IDT and output IDT to the loads because these IDTs have not a common grounded busbar. To decrease the input and output impedances the parallel connection of the two filters in the different acoustic tracks is used. To improve the selectivity of the filter the cascaded connection and phase weighting the input IDT are employed. The constructional and topological optimization of the SAW filter is provided with a computer simulation using an equivalent circuit model.

The 300 MHz sample of the balanced SAW filter have shown an insertion loss of 3 dB, 2-dB bandwidth of 1.2-1.5 MHz, stopband attenuation of 60-70 dB at ±13 MHz offsets from a center frequency in a 75-Ω balanced system. The filter did not require the matching elements and housed in the 9.1x7.1x2mm SMD package. Our new 2-IDT DMS filter has narrowed passband and improved selectivity than its known prototypes [1-3] and it will be widely used as IF and front-end filter in the telecommunication equipment.

[1] S. A. Doberstein, “Balanced Low-Loss Narrowband 3-IDT Double Mode SAW Filters with Improved Selectivity,” *Proceedings*, 2013 IEEE Joint UFFC, EFTF and PFM Symposium, Prague, Czech Republic, July 21-25, 2013, pp. 1069-1072.

[2] T. Morita, Y. Watanabe, M. Tanaka and Y. Nakazava, “Wideband Low Loss Double Mode SAW Filters,” *Proceedings*, 1992 IEEE Ultrason. Symp., Tucson, Arisona, October 20-23, 1992, pp. 95-104.

[3] S. A. Doberstein, “2-IDT Double-Mode SAW Filters with Decreased Insertion Loss and Advanced Functionalities,” *Proceedings*, 2011 Joint Conf. of the IEEE Int. Frequency Control Symp. and EFTF, San Francisco, California, May 1-5, 2011, pp. 1-4.

Switchable and Tunable Resonators with Barium Strontium Titanate on GaN/Saphire Substrates

T.S. Kalkur[1], Milad Hmeda [1], Almonir Mansour[1], Pamir Alpay [2], Nick Srockey [3]and G.S. Tompa[3]

[1] Department of Electrical and Computer Engineering
University of Colorado, Colorado Springs, CO 80918, USA
[2] Department of Materials Science and Engineering and Institute of Materials Science
University of Connecticut, Storrs, Connecticut 062269
[3] Structured Materials Industries, Inc., Piscataway, New Jersey, 08854, USA
Contact author: tkalkur@uccs.edu

Gallium nitride (GaN) has emerged as an in-demand semiconductor technology for future radar, electronic warfare and communications technologies. GaN is becoming very important in the implementation high frequency, high power integrated circuits for future communication circuits. Most of the effort in GaN technology is directed towards the fabrication of high power transistors for power amplifiers. For the implementation of RF circuits, we need a variety of RF blocks such as amplifiers, oscillators and filters. Resonators play an important role in the fabrication of RF circuits such as filters and low phase noise oscillators. A solidly mounted tunable barium strontium titanate (BST) based resonator was fabricated on a GaN/Sapphire substrate using a metalorganic solution deposition (MOSD) technique. An acoustic Bragg reflector was first formed on the GaN/sapphire substrate consisting of alternating layers of silicon dioxide and tantalum oxide deposited using a-spin on technique. Lower and upper electrodes were fabricated using sputter deposited platinum. The resonant frequency of the resonator could be tuned from 5.17 GHz to 5.20 GHz by applying a voltage of 8 V, resulting in tunability of about 0.6%. The quality factor of the resonator was found to depend on the applied voltage, with a maximum quality factor of 218 observed for an applied bias voltage of 8 V. The effective electromechanical coupling coefficient (k^2) of the resonator was found to be 10% at 8 V.

Resonant transformation of acoustic waves observed for the diamond based HBAR

Kvashnin Gennady+, Telichko Arseniy*+, Sorokin Boris*+
+Technological Institute for Superhard and Novel Carbon Materials, Russian Federation
*Moscow Institute of Physics and Technology, Russian Federation
E-mail: arseny.telichko@phystech.edu, bpsorokin2@rambler.ru

High-overtone Bulk Acoustic Resonator (HBAR) based on synthetic diamond substrate has showed the excellent UHF resonant properties [1]. But one can observed the appearance of the additional resonant peaks which depends on the structure, dimensions and topology of thin film piezoelectric transducer (TFPT). As a result a deterioration of HBAR's fundamental resonant properties takes place. The nature of such undesirable effect should be investigated for a more detail in order to design an improved HBAR at a given frequency band. Recall that such effect was observed for HBARs incorporating other crystalline substrates [2]. The main objective of this paper is the modeling and experimental investigation of the resonant peculiarities for HBAR based on the layered piezoelectric structure as Al/AlN/Mo/(100) diamond (164 nm/624 nm/169 nm/392 μm).

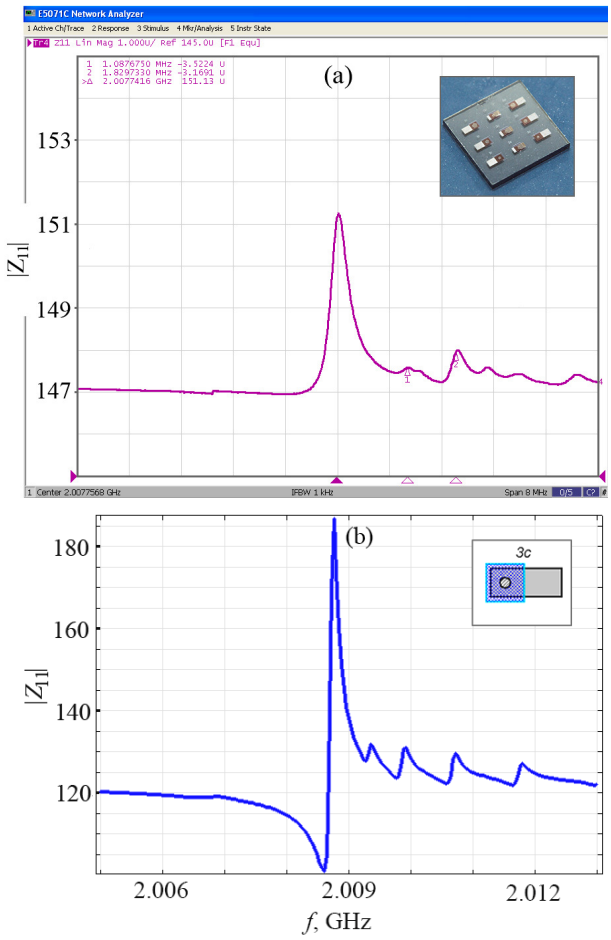


Fig. 1: Frequency dependence of Z_{11} for the "Al/AlN/Mo/(100) diamond" HBAR: experimental (a) and modeling (b) results.

HBAR's microwave acoustic properties were tested by M-150 Multipurpose Probing System and E5071C Network Analyzer at room temperature. Modeling calculation of frequency dependence of HBAR parameters was based on 2D FEM simulation.

Main origin of a HBAR's complex resonant behavior is associated with the finite dimensions of TFPT elements in lateral directions. It was shown that if AlN and Al thin films have the finite lateral dimensions, the additional resonant peaks can arise in the frequency band above the given overtone (Fig. 1). For example, the peak nearest to fundamental overtone is associated with the dissection of the TFPT area on 4 parts (in the case of square TFPT), and as a result an ultrasonic beams will be placed below each small area. Note that the more complicated behavior as the peaks arising between the resonance and anti-resonance can exist at lower frequencies. Ways to suppress such undesirable resonant effects have been proposed.

[1] B. P. Sorokin, G. M. Kvashnin, A. P. Volkov, et al, "AlN/single crystalline diamond piezoelectric structure as a high overtone bulk acoustic resonator," Appl. Phys. Lett., vol. 102, p. 113507, March 2013.

[2] E. Lebrasseur, G. Martin, T. Baron, et al, "A feedback-loop oscillator stabilized using laterally-coupled-mode narrow-band HBAR filters," *Proceedings*, 2011 IEEE Int. Ultrasonics Symp., Orlando, Florida, October 18-21, 2011, pp. 1222-1225.

An Analysis of Thickness-shear Vibrations of an Annular Plate with the Mindlin Plate Equations

Wang J, Chen H, Ma TF, Du JK, Yi LJ, Huang DJ, Yong Y-K*
School of Mechanical Engineering & Mechanics, Ningbo University, 818 Fenghua Road, Ningbo, Zhejiang 315211, CHINA
*Department of Civil and Environmental Engineering, Rutgers University, 623 Bowser Road, Piscataway, NJ 08854, USA
E-mail: wangji@nbu.edu.cn

The Mindlin plate equations with the consideration of thickness-shear deformation as an independent variable have been used for the analysis of vibrations of quartz crystal resonators of both rectangular and circular types. The objective of such analysis is always on identifying optimal parameters of plates and resonator structures to enhance the strong and pure vibrations of thickness-shear mode, which is the functioning mode of thickness-shear type resonators of both AT- and SC-cut quartz crystal. This goal can only be sufficiently achieved through accurate analysis of vibrations of coupled modes in a finite crystal plates with the consideration of closely clustered modes and complication factors such as electrodes and mounting supports which can affect the frequency and stability under loadings like impact and temperature. The Mindlin or Lee plate theories that treat thickness-shear deformation as an independent higher-order mode in a coupled system of two-dimensional variables are the choice of theory for analysis [1, 2].

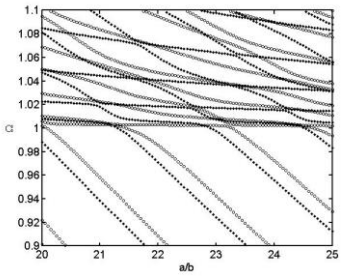


Fig. 1 Frequency spectra of a free circular plate (·) vs. annular plate (°) with the Mindlin plate equations.

For circular plates, we derived the Mindlin plate equations in a systematic manner as demonstrated by Mindlin and others and obtained the truncated two-dimensional equations of closely coupled modes in a finite circular plate [3]. We simplified the equations for modes in the vicinity of fundamental thickness-shear frequency and validated the equations and method. To explore newer structures of quartz crystal resonators, we utilized the Mindlin plate equations for the analysis of annular plates with fixed inner and free outer edges for frequency spectra with the finding that we can obtain similar spectra and vibration modes of a free circular plate for isotropic materials as shown in Fig. 1. The radial thickness-shear, flexural, and the transverse thickness-shear modes are considered in the analysis. The detailed analysis of vibrations of plates for the normalized frequency versus dimensional parameters will provide guidelines for optimal selection of plate parameters based on the principle of strong thickness-shear mode and minimal presence of other modes to enhance energy trapping through maintaining the strong and pure thickness-shear vibrations insensitive to many complication factors such as thermal and initial stresses.

[1] R. D. Mindlin, H. Deresiewicz, "Thickness-Shear and Flexural Vibrations of a Circular Disk," J. Appl. Phys., vol. 25, pp. 1329-1332, 1954.

[2] P. C. Y. Lee, R. Huang, X. Li, W.-H. Shih, "Vibrations and Static Responses of Asymmetric Bimorph Disks of Piezoelectric Ceramics," IEEE Trans. Ultrason., Ferroelect., Freq. Contr., vol. 47, no. 3, pp. 706-715, 2000.

[3] H. Chen, J. Wang, T.F. Ma, J.K. Du, "An Analysis of Free Vibrations of Isotropic, Circular Plates with the Mindlin Plate Theory," *Proceedings*, 2014 Symp. on Piezoelectricity, Acoustic Waves, and Device Applications, Beijing, China, Oct. 30 – Nov. 2, 2014, pp. 397-400.

Thickness-shear Vibration Frequencies of an Infinite Plate with a Generalized Material Property Grading along the Thickness

Wang J, Zhang WL, Huang DJ, Ma TF, Du JK, Yi LJ
Piezoelectric Device Lab, School of Mechanical Engineering & Mechanics, Ningbo University,
818 Fenghua Road, Ningbo, Zhejiang 315211, CHINA
E-mail: wangji@nbu.edu.cn

For quartz crystal resonators of thickness-shear type, the vibration frequency and mode shapes, which are key features of resonators in circuit applications, reflect the basic material and structural properties of the crystal plate and its variation with time under various factors such as erosive gases and liquids that can cause surface and internal damage and deterioration of crystal blanks. The accumulated damages and erosions eventually will change the surface conditions in terms of elastic constants and stiffness and more importantly, the gradient of such properties along the thickness direction. This is a typical functionally graded materials (FGM) structure and has been studied extensively in structural applications under multiple loadings such as thermal and electromagnetic fields. As for acoustic wave resonators, such studies are equally important and the wave propagation in FGM materials can be used in the evaluation and assessment of performance, reliability, and life of sensors based on acoustic waves such as the quartz crystal microbalance (QCM). We have studied the thickness-shear vibrations of FGM plates with properties of AT-cut quartz crystal varying along the thickness in a symmetric pattern represented by a cosine function of the thickness coordinate [1]. We have obtained the frequency changes of the fundamental and overtone modes which are coupled and frequencies are no longer integers as we can expect.

Effects of FGM Index on Thickness-shear Frequency

FGM index	1	3	5	7	9
N=5	0.995991	2.998690	4.999215	6.999439	8.999564
N=10	0.998990	2.999665	4.999799	6.999856	8.999888
N=15	0.999550	2.999850	4.999910	6.999936	8.999950
N=20	0.999747	2.999916	4.999949	6.999964	8.999972
N=25	0.999838	2.999946	4.999968	6.999977	8.999982
$N\rightarrow\infty$	1.000000	3.000000	5.000000	7.000000	9.000000

As the continuation of earlier studies, we now extend the FGM pattern of the plate in thickness-shear vibrations to a generalized variation scheme in the form of $f(x_2) = \alpha + \beta_1 \cos\frac{x_2}{Nb} + \beta_2 \sin\frac{x_2}{Nb}$ $(\alpha, \beta_1, \beta_2 - \text{constants}, N - \text{integer})$ that can cover both symmetric and asymmetric functions along the thickness. The solution procedure is based on the Fourier expansion of deformation with both sine and cosine harmonics. It shows both symmetric and anti-symmetric modes can be excited in vibrations with material grading, thus shown that changes of plate properties can cause more complicated resonances and the accuracy and performances of resonator structures will deteriorate with more coupled modes. This is to be avoided in actual sensors and devices for sensing and measurement applications. The results can be used as a reference for the monitoring and evaluation of conditions of sensors and other devices based on thickness vibrations of plates.

[1] J. Wang, W.L. Zhang, D.J. Huang, T.F. Ma, J.K. Du, "Thickness-Shear Frequencies of an Infinite Quartz Plate of Material Property Variation along the Thickness," *Proceedings*, 2014 IEEE International Frequency Control Symposium, Taipei, May 19-21, 2014. [DOI: 10.1109/FCS.2014.6859865]

Monitoring the Adhesion Process of Tendon Stem Cells with Shear-Horizontal Surface Acoustic Wave Sensors

Huiyan Wu , Hongfei Zu , Guangyi Zhao*, James H-C. Wang*, Qing-Ming Wang
Department of Mechanical Engineering & Materials Science, University of Pittsburgh, Pittsburgh, PA/USA
* MechanoBiology Laboratory, Department of Orthopaedic Surgery, University of Pittsburgh, Pittsburgh, PA/USA
E-mail: qiw4@pitt.edu

Cell adhesion to a substrate or extracellular matrix plays an important role in a variety of cellular functions, such as cell-to-cell communication, cell proliferation and differentiation, and tissue formation [1]. Some measurement techniques have been developed for real-time detection of cell adhesion, including electric cell-substrate impedance sensing and quartz thickness shear mode (TSM) resonance sensing. Shear-horizontal surface acoustic wave (SH-SAW) sensors are promising in biological and biomedical engineering, detecting cell behaviors in liquid in a non-invasive, simple and quantitative manner [2]. Nevertheless, because of a lack of proper bio-interface, most studies neglected their innovative applications as cell-based sensors. Parylene-C (poly(2-chloro-p-xylylene)) has been proven as ideal acoustic-wave guiding layer due to its good uniformity, compactness and adhesion to the substrate [3]. Furthermore, of comparable cell and protein compatibility to the tissue culture substrates, parytlene-C films also have preferable effects as the bio-sensitive interference on SH-SAW sensor surface [4].

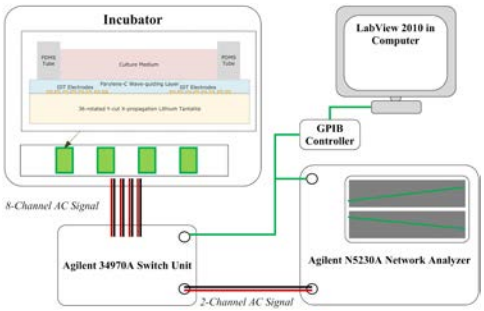


Fig. 1: The schematic diagram of SH-SAW sensor measurement system

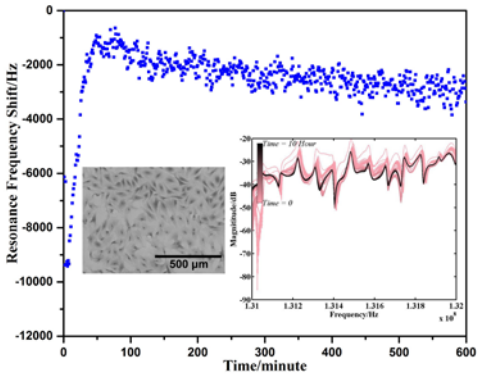


Fig. 2: Resonance frequency shift of SH-SAW sensor with TSC adhesion (insets are a SEM photo of TSCs and a corresponding admittance spectrum set where the resonance frequencies were collected)

In this study, SH-SAW sensors with parylene-C guiding layer were adopted to monitor the adhesion process of tendon stem cells (TSCs), a newly discovered stem cell type in tendons. Fig.1 schematically shows the measurement system of SH-SAW sensors for TSCs. TSC suspensions with a series of concentrations (4.0×10^5, 2.0×10^5, 1.0×10^5, 0.5×10^5 */ml*) were added to PDMS wells successively and maintained in wells for 10 *hr*, during which corresponding S_{21} loss curves were acquired every 1 *min*. Fig. 2 is the effective resonance frequency shift of SH-SAW sensor during TSC adhesion (1.0×10^5 */ml*). For TSC suspensions of various concentrations, extracted resonance frequency exhibits similar variation of three regions: (I) rapid decrease, (II) reverse increase, and (III) slow decrease to keep stable. These changes are considered to be related to corresponding different stages in adhesion process (attachment, spreading, and formation of focal adhesions and stress fibers), especially surface interactions within relatively short distance. In addition, the results demonstrate an approximately linear relationship between effective resonance frequency shift and TSC concentrations. SH-SAW sensors show high sensitivity and stability in TSC adhesion monitoring, indicating their potential for investigating cell adhesion in particular as well as cell biology in general.

[1] Hardin, J., G. Bertoni, and L.J. Kleinsmith, "Becker's World of the Cell". 2012: Pearson Education.
[2] Ballantine, D.S., et al., "Acoustic Wave Sensor: Theory, Design, and Physico-Chemical Applications". 1997: Academic Press.
[3] Lange, K., S. Grimm, and M. Rapp, "Chemical Modification of Parylene C Coatings for SAW Biosensors". Sensors & Actuators B, 2007. vol.125: pp. 441-446.
[4] Chang, T.Y., et al., "Cell and Protein Compatibility of Parylene-C". Langmuir, 2007. vol. 23: pp. 11718-11725.

A novel microwave reflector-antenna as a resonant wireless passive mechanical sensor

Taimur Aftab, Adnan Yousaf, Thomas Ostertag, Leonhard M Reindl
Department of Microsystems Engineering (IMTEK), University of Freiburg, Freiburg, Germany
E-mail: taimur.aftab@imtek.de

Wireless passive sensors (WPS) provide a promising solution to the problem of sensing in harsh environments where batteries and wiring are undesirable. The sensing system comprises of a reader unit and a sensor connected together only by a wireless link. One of the ways to momentarily store the RF energy in the sensor before retransmission is to use high-Q resonators. Historically, a significant research effort has been made on using acoustic resonators and delay lines as WPS [1]. More recently alternate approaches to chipless wireless sensing are being explored using electromagnetic structures [2].

The original WPS revealed in this abstract is a dielectric resonator (DR) confined in an open ended waveguide (OEWG) as shown in Fig 1. The DR-OWEG device is designed for the $TE_{01\delta}$ mode of the DR which resonates well below the cutoff frequency of the waveguide. The motivation for doing so is that the $TE_{01\delta}$ mode loses a large majority of its energy to radiation losses. The rectangular "under-moded" waveguide limits the radiation coupling and increases the effective (loaded) quality factor. The OEWG also acts as a directional antenna, improving the operational range of the wireless resonator.

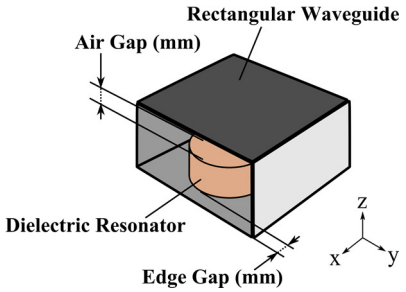


Fig. 1: A new chipless resonant wireless passive sensor concept. The resonant frequency and Q-factor are dependent on edge-gap and air-gap respectively.

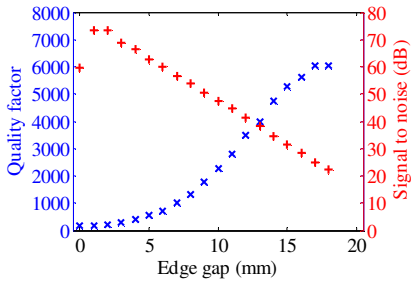


Fig. 2: The signal to noise ratio (SNR) and loaded quality factors as a function of edge gap.

Fig 2 shows the experimentally observed effect of changing the distance of the DR from the edge of the OEWG. At low edge-gaps the device behaves like a radiating DR antenna. As the edge-gap is increased the quality factor improves, finally reaching saturation caused by conduction losses. In Fig 2, the SNR is the maximum magnitude of the time domain ringing of the resonator minus the noise floor. It is calculated by isolating the resonance signal from environmental reflections using time-domain-gating. The SNR quantifies the coupling with 'free space' and is observed to be directly related to the radiation Q-factor.

The device is used as a mechanical force sensor by applying a force and bending the top of the OEWG. The air-gap change caused by the deformation shifts the resonant frequency. The mathematical models for the bending beam and the parallel plate dielectric resonator predict a displacement force sensitivity in the order of 10 ppm/µm and 100 ppm/N respectively. A sensor with 2.46 GHz center frequency is interrogated using a commercial tracking mode SAW resonator interrogation unit from RSSI GmbH. A wireless measurement range of at least 3 m is obtained with the loaded-Q tuned to 3000. The mathematical models for force to frequency conversion agree strongly with the experimental results.

[1] A. Pohl, "A review of wireless SAW sensors.," IEEE Trans. Ultrason. Ferroelectr. Freq. Control, vol. 47, no. 2, pp. 317–32, Jan. 2000.

[2] M. Schüßler, C. Mandel, B. Kubina, and R. Jakoby, "Realization Concepts for Chipless Wireless Temperature Sensing," in Sensors and Measuring Systems 2014; 17. ITG/GMA Symposium; Proceedings of, 2014, pp. 1–6.

Wireless Monitoring of Eye Intraocular Pressure Using Transparent Graphene LC Sensors

[Zeng, Peng], [Wu, Chung-Tse Michael], [Cheng, Mark Ming-Cheng]
Electrical and Computer Engineering Wayne State University, Detroit MI, E-mail: mcheng@wayne.edu

This paper presents a new wearable and wireless pressure sensor for continuous intraocular pressure (IOP) monitoring using a LC tank resonant circuit made of a transparent and flexible graphene capacitor in series with a coil. Measuring IOP is essential in the diagnosis and monitoring of glaucoma, one of the leading causes of blindness. In recent years, implantable polymer based pressure sensors made of LC tank have been developed [1] [2] [3]. However, all the capacitor designs have been based on opaque and rigid metal such as gold and nickel, which essentially limits the vision. Because of the limited space, curvature of the cornea and dilation of the pupil, a capacitor using flexible and transparent electrodes is highly desirable. To the best of authors' knowledge, this paper presents **for the first time** an integrated graphene capacitor in series with a coil for IOP measurements.

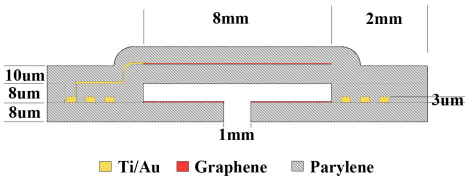


Fig 1 *The cross-section of graphene LC sensors for IOP monitoring*

Figure 1 shows the cross-section of the sensor, which consists of a transparent variable capacitor made of graphene, parylene C and an air gap, a wounded coil made of copper and a parylene substrate. The capacitor was designed 42 pF, where the diameter of the membrane was 8mm and the thickness of air gap was 8 μm. The inductor was designed 0.325 μH, making the resonant frequency approximately 43 MHz. The IOP (up to 100 mmHg) was monitored by the shift of resonant frequency, which results from the fact that IOP causes the membrane deformation and capacitance change. The RF signal could be detected by an external coil, making the device adequate for passive wireless sensing without power consumption on the implanted sensor. Figure 2 shows the simulation results for the frequency shift as a result of the pressure change in wireless inductive coupling. The device was fabricated using surface micromachining. 8μm parylene was deposited and patterned on a silicon substrate, followed by graphene transfer and patterning. A 3μm Au layer was deposited and patterned as a planar coil. An 8μm photoresist layer was spin-coated and patterned as a sacrificial layer. The second 8μm parylene was coated, followed by the second graphene transfer. A 0.5μm Au was deposited and patterned for the interconnection. A 10μm parylene layer was deposited to increase the thickness of the membrane. The sacrificial layer was removed by acetone after the underneath silicon was etched by deep reactive ion etch (DRIE). Figure 3 shows the prototype of fabricated IOP sensors, where the transparent graphene-based capacitor can be clearly observed.

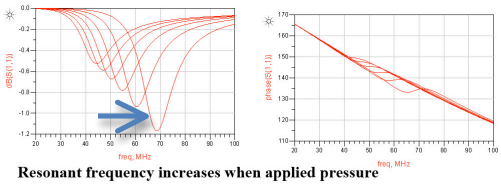


Fig 2. *Simulation results of LC tank when the pressure (and corresponding capacitor) increases*

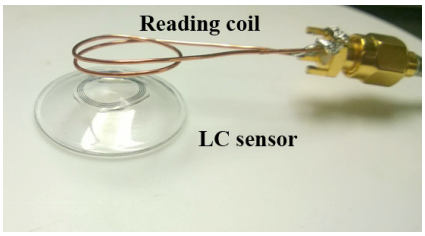


Fig 3. *The prototype of a LC sensor and a reader coil*

References:

1 Chen, P.J., Rodger, D.C., Agrawal, R., Saati, S., Meng, E., Varma, R., Humayun, M.S., and Tai, Y.C.: 'Implantable micromechanical parylene-based pressure sensors for unpowered intraocular pressure sensing', J. Micromech. Microeng., 2007, 17, (10), pp. 1931-1938

2 Xue, N., Chang, S.P., and Lee, J.B.: 'A SU-8-Based Microfabricated Implantable Inductively Coupled Passive RF Wireless Intraocular Pressure Sensor', J. Microelectromech. Syst., 2012, 21, (6), pp. 1338-1346

3 Varel, C., Shih, Y.C., Otis, B.P., Shen, T.S., and Bohringer, K.F.: 'A wireless intraocular pressure monitoring device with a solder-filled microchannel antenna', J. Micromech. Microeng., 2014, 24, (4), pp. 8

A Wireless Temperature Sensor Powered by a Piezoelectric Resonant Energy Harvesting System

Peng Wang[1*], Robert Gray[1,2], Philip X.-L. Feng[1*]
[1]Electrical Engineering, Case Western Reserve University, Cleveland, OH 44106, USA
[2]Hawken High School, Gates Mills, OH 44040, USA
[*]E-mail: peng.wang9@case.edu, philip.feng@case.edu

Wireless temperature sensor networks are a key to energy-efficient smart buildings in urban areas for more sustainable and resource-conversing development. However, large-scale temperature sensor networks have high maintenance costs due to required periodical replacements of batteries, which constrain real-world applications and deployments. Vibration energy harvesting offers an alternative to battery-free wireless temperature sensor networks. Here we report on an experimental demonstration of using a piezoelectric resonant energy harvesting system to power a wireless temperature sensor (WTS). The energy harvesting system stores the energy from a PZT resonant transducer to a capacitor, and uses the stored energy to power a commercial wireless temperature sensor (EZ430-RF2500, Texas Instruments Inc.). The main functions of the harvesting system are implemented by a power management application specific circuit (ASIC) [1]. The ASIC shows a peak charging power of 416μW and an efficiency of ~55%. The PZT transducer resonates at the same frequency (120Hz) with the vibration source (a small service pump) and generates 96μW of power, which is well sufficient for charging the capacitor. The WTS transmits measured temperature signal at a distance of 9m, and consumes ~13.4μW (10s reading interval) or 4μW (10mins interval) of power, all provided by the energy harvester, with surplus.

The PZT transducer is a cantilever resonator (15mm×12mm×200μm), laser machined to have an optimized 2/3 length coverage of metal electrode. After tuned to 120Hz, the PZT transducer can output 96μW when installed on the small pump that generates 1.5g peak acceleration (Fig. 1, a-c). We characterize the frequencies and accelerations of vibrating energy sources (pump, coffee machine, *etc.*) with a 3-axis accelerometer (ADXL325, Analog Devices, Inc.). We tune the frequency of PZT transducer by changing proof mass.

The frequency tuning of the PZT transducer is verified in both time and frequency domain. In time domain, the PZT cantilever's output voltage is measured during oscillating after released from an initial deflection. For frequency domain, the S_{21} parameter is measured with a network analyzer (Agilent 4395A) (Fig. 1, d-f). The impedance of the PZT transducer is 40.79-j53kΩ (complex variable, 25nF||69MΩ@120Hz), characterized by a LCR meter (HP 4263B).

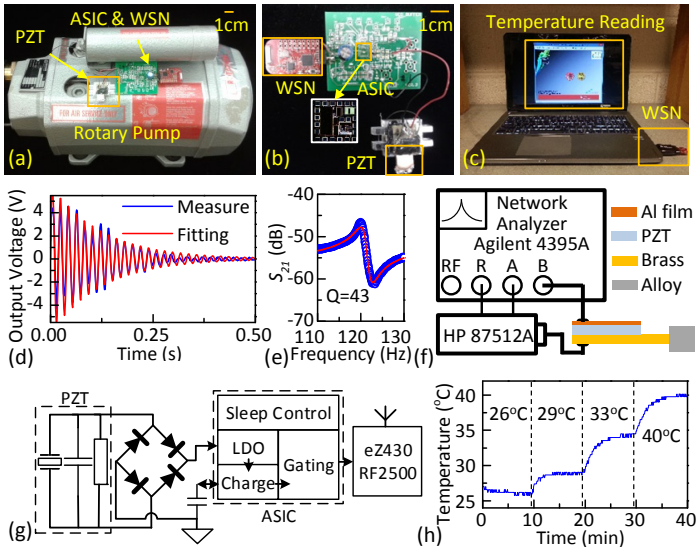


Fig. 1: Experimental results. (a) Photographs of the piezoelectric harvester mounted on a small service pump. (b) The energy harvesting system. (c) The sensor reading software interface. (d) Data from ring down test. (e)-(f) Transmission loss data and testing scheme. (g) Schematic of the energy harvesting system and the WTS. (h) Monitoring of controlled temperature changes, recorded by the PZT energy harvester powered WTS.

The output AC energy of PZT is rectified and regulated to charge a capacitor to 3.0V (Fig. 1-g). The ASIC saves energy by turning off WTS's power, and only drains 5pA when waiting for external wake up signal. We have also developed a new design of the ASIC featuring a CMOS resonant circuit module, which could further boost the PZT energy harvester's output by a factor of 7.

[1] P. Wang, B. Liang, X. S. Ye, W. H. Ko, and P. Cong, "A simple novel wireless integrated power management unit (PMU) for rechargeable battery-operated implantable biomedical telemetry systems," in *Proc. 4th Int. Conf. on Bioinformatics & Biomed. Eng. (iCBBE)*, Chengdu, China, Jun. 18-20, 2010, DOI:10.1109/ICBBE.2010.5517158.

ALD-Enabled NanoElectroMechanical Systems

Prof. Victor M. Bright
Department of Mechanical Engineering
University of Colorado Boulder, USA

Abstract

Atomic Layer Deposition (ALD) and Molecular Layer Deposition (MLD) can be effectively used to deposit custom-designed, multi-material layers with atomic resolution on any micro- or nano-scale device surface. The nano-scale ALD/MLD coating can protect the devices from electrical short, charge accumulation, moisture-induced adhesion, wear, corrosion, creep, fatigue or anodic oxidation during short-term prototyping or long-term product life. The nano- and micro-electro-mechanical systems (N/MEMS) community has been looking for effective antistiction and environmental protection coatings for many years. ALD/MLD films achieve these goals similar to what CVD Si_3N_4 has been for CMOS. As devices further shrink toward nano-scale, ALD-based processes offer a new strategy for depositing conformal and precise films that may have important applications as a novel dielectric, a sacrificial layer for gap control in nanofabrication, or as a structural layer for NEMS. ALD relies on sequential, self-limiting surface reactions to deposit ultra thin films with the following characteristics: ALD film thicknesses can be precisely deposited from a few angstroms to hundreds of nanometers; ALD films can be deposited at low temperatures compatible with CMOS; ALD films are pinhole-free, dense, smooth and highly conformal; ALD films can be deposited on silicon, silicon nitride, metals, polymers, and ceramics; ALD can coat high surface area to volume ratio structures with complex geometries; ALD can deposit dielectric or conductive layers; ALD can deposit hydrophobic or hydrophilic layers covalently bonded to the surface. ALD materials can be selectively etched to create nano-scale gaps and free standing structures. The ALD technologies for N/MEMS, pioneered at the University of Colorado Boulder, represent breakthrough in nano-scale processes that can be used to fabricate custom-designed, multi-material layers with atomic resolution. These methods are proven, mature, and are available to serve the nano-scale systems community.

GPS TIMING SERVICE

Edward Powers, USNO

ABSTRACT

The Global Positioning System (GPS) will celebrate the 20th anniversary of achieving full operational capability (FOC) on April 27, 2015. GPS has revolutionized the world's ability to precisely position and synchronize activities. The GPS timing service is often overlooked, but it is critical for many industries such as telecommunication, financial, scientific and the power industry. This paper provides an overview of how the GPS timing service operates its performance, USNO's role and a historical look at impact of the GPS timing service.

New Level of Timekeeping Advancement in Russian Federation and Time Reference Frame for GLONASS

Sergey Donchenko, Igor Blinov, Vitaly Palchikov, Alexander Goncharov,
Yury Smirnov, Yury Domnin

FGUP VNIIFTRI, Mendeleevo, Moscow Region, 141570, Russia
E-mail: vitpal@mail.ru

The new national time and frequency standard (NTFS) of Russian Federation in pursuance of Decree No 1226 28 December 2012 of Federal Agency on Technical Regulation and Metrology have been commissioned. Along with it new realization of atomic time scale TA(SU) based on new time algorithm have been introduced on MJD 56289 – 28th December 2012.

Composition of the new NTFS consists of:

1. Primary Cs standards for national realization of the SI unit;
2. Clocks comparison and time keeping instrumentation;
3. Time and frequency transfer and dissemination instrumentation;
4. Infrastructure.

This paper provides information on the composition and main characteristics of the formation complex of the national time scale UTC (SU) and represents the prospects of its development.

The national time scale of the Russian Federation is reproduced and maintained based on the State standard of time and frequency operated at a facility located in Mendeleevo, Moscow Region. The UTC(SU) time scale is a representation of UTC; it is maintained in accordance with the BIPM requirements, based on the results of comparisons by GPS with the time scales of PTB, USNO, NIST with other time laboratories, and with time scales of Eu-Asian TWSTFT workgroup, including laboratories of Germany, China, Korea, India, Japan and Taiwan.

The UTC(SU) time scale is currently transmitted to the GLONASS Ground Control Segment using signal receivers.

The national atomic time scale TA(SU) is computed in accordance with the definition of the SI second and the values of the units of time and frequency realized by primary cesium standards of the CSFO fountain, with an error of 5×10^{-16} or below. Since 2014 CSFO2 is officially included in calculations TAI.

The units of time and frequency are maintained independently during periods between the last official publication of UTC data and the next, by an upgraded ensemble of hydrogen frequency and time standards of type CH1-75A with a daily frequency instability of 5×10^{-16}.

UTC(SU) is computed based on TA(SU), monitored and corrected against UTC as soon as the next BIPM publication becomes available.

Galileo System Status

Edrich Yau, BEng MSc (ESA)
Edrich.Yau@esa.int

Abstract:

The Galileo system is continuing with the roll-out and deployment. More satellites are scheduled to be launched and the supporting ground infrastructure continues to be updated and improved. As time goes on, the progress of Galileo and the overall capabilities increase and improve inline.

This presentation will provide an update on the current status of the Galileo System, touch also on the recent GSAT 0201 and 0202 recovery, and summarise the current system performance.

The Time Validation Facility (TVF): An All-New Key Element of the Galileo Operational Phase

Píriz, Ricardo, D. Rodríguez, P. Roldán, A. Mudrak*, A. Bauch+, F. Riedel+, E. Staliuniene+, J. Galindo§, H. Esteban§, I.Sesia¶, G. Cerretto¶, C. Rieck⌘, K. Jaldehag⌘, P. Uhrich✪, D. Rovera✪
GMV, Madrid, Spain
*ESA/ESTEC, Noordwijk, The Netherlands
+Physikalisch-Technische Bundesanstalt, Braunschweig, Germany
§ROA, San Fernando de Cádiz, Spain
¶INRiM, Turin, Italy
⌘SP, Borås, Sweden
✪LNE-SYRTE, Observatoire de Paris, LNE, CNRS, UPMC, Paris, France
E-mail: rpiriz@gmv.com

GMV is the prime contractor for the Time and Geodetic Validation Facility (TGVF) in the Galileo FOC phase (Full Operational Capability), a contract of the European Space Agency (ESA). Within the TGVF, the Time Validation Facility (TVF) is the subsystem in charge of steering Galileo System Time (GST) to UTC, among other duties. The TVF is operated at GMV headquarters in Madrid, Spain. TVF operations rely on the contribution of five European timing laboratories, located at INRiM, OP, PTB, ROA, and SP.

Two independent Precise Timing Facilities (PTFs) generate GST, one located at Fucino in Italy (master) and the other located at Oberpfaffenhofen in Germany (backup). At each PTF, the frequency output of the primary hydrogen maser is tuned using a frequency offset generator according to the steering corrections computed by the TVF (nominally one per day), to generate the final GST scale. The robustness of GST steering by TVF is enhanced by the operation of an Alternative Time Service Provider (ATSP) operated by SP in Sweden. Fig. 1 shows the GST-UTC evolution (Fucino) over three months in 2014.

For the time-transfer links between the PTFs and the timing laboratories, two different methods are used: TWSTFT and GPS. Two calibration campaigns have taken place during 2014: one for TWSTFT conducted by ROA, and one for GPS conducted by OP.

Other TVF activities include the monitoring and validation of UTC and GGTO parameters broadcast in the Galileo navigation message. Another key task of the TVF is the characterization of the Galileo satellites' PHM and RAFS clocks.

In the frame of the TGVF contract the *Galileo Experimental Sensor Stations* (GESS) have been upgraded with Septentrio PolaRx4 receivers. Three of them are installed at timing laboratories (INRiM, ESTEC, and USNO), and a new GESS has been installed at PTB.

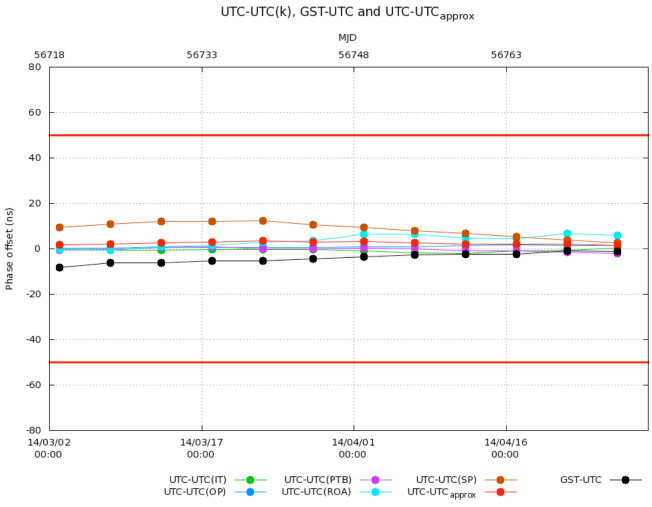


Fig. 1: Evolution of GST-UTC and UTC-UTC(k) from BIPM Circular T.

This paper provides a general description of the TVF element and its related activities for the FOC phase, and presents the main results and findings of the TVF operation until now.

Measuring the Yb/Sr clock frequency ratio with cryogenic optical lattice clocks

Nemitz, N.[a], Ohkubo, T.[a,b,c], Takamoto, M.[a,b,d], Ushijima, I.[a,b,d], Das, M.[a,b,d], Ohmae, N.[a,b,c], Katori, H.[a,b,c,d]

a) Quantum Metrology Laboratory, RIKEN, Wako, Saitama, Japan
b) Innovative Space-Time Project, ERATO, Japan Science and Technology Agency, Bunkyo-ku, Tokyo, Japan
c) Dep. of Applied Physics, Graduate School of Engineering, The University of Tokyo, Bunkyo-ku, Tokyo, Japan
d) RIKEN Center for Advanced Photonics, Wako, Saitama, Japan

E-mail: Nils.Nemitz@riken.jp

Optical lattice clocks now approach an overall fractional uncertainty of 10^{-18} [1,2,3]. In this regime, remote clock comparisons require dedicated fiber links and do not yet seem feasible over intercontinental distances. For this reason, frequency ratio measurements of optical clocks using different atomic species will play an important role in demonstrating performance and reproducibility in the light of an eventual redefinition of the SI second: The result of such a comparison is a dimensionless number that is easily transferred and can be tested by any laboratory with access to the same combination of clocks.

Working towards this goal, RIKEN's cryogenic optical lattice clocks have been designed to allow operation with Yb in addition to Sr. For the experiments described here, Yb atoms are trapped and interrogated in the clock Sr2, while Sr1 provides a reference measurement of the Sr clock frequency with an overall uncertainty of 7×10^{-18} [3]. In both clocks the effect of blackbody radiation – at room temperature the largest contribution to the systematic frequency shifts – is suppressed to below 10^{-16} by interrogating atoms in a cryogenic chamber kept at a temperature of 95 K. A frequency comb with high control bandwidth [4] transfers the stability of the Sr clock laser to the Yb clock laser. In this way, a significant fraction of the residual phase noise is common between both clock lasers [Fig. 1] and can be suppressed by the technique of synchronous interrogation [5]. Comparisons have shown an instability below 10^{-17} for one hour of averaging time, corresponding to $\sigma_y(\tau) = 6\times10^{-16}\ (\tau/\mathrm{s})^{-1/2}$ [Fig. 2].

In this talk, I will present the uncertainty budget of the cryogenic Yb optical lattice clock and our progress towards a measurement of the Yb/Sr frequency ratio beyond the limit of the current definition of the SI second.

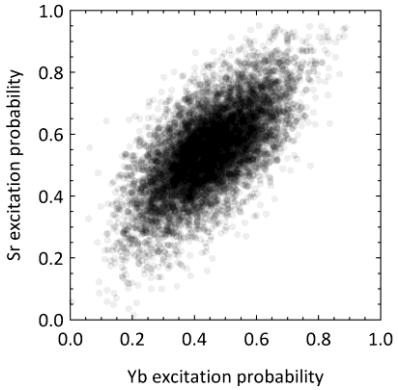
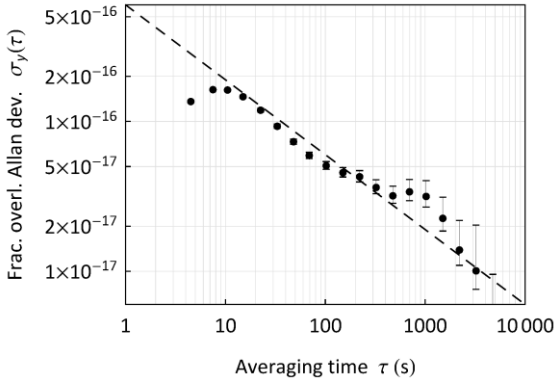


Figure 1 (left):
Shared laser noise causes a strong correlation of the excitation probabilities in the Yb and Sr clocks for synchronous interrogation.

Figure 2 (right):
Ratio measurement fractional instability, dashed line shows $\sigma_y(\tau)=6\times10^{-16}\ (\tau/\mathrm{s})^{-1/2}$.



[1] T. L. Nicholson *et al.*, "2×10^{-18} total uncertainty in an atomic clock", arXiv:1412.8261, Dec. 2014

[2] K. Beloy *et al.*, "An atomic clock with 1×10^{-18} room-temperature blackbody Stark uncertainty", arXiv:1412.1029, Dec. 2014

[3] I. Ushijima *et al.*, "Cryogenic optical lattice clocks with a relative frequency difference of 1×10^{-18}", arXiv:1405.4071, May 2014

[4] K. Iwakuni *et al.*, "Narrow linewidth comb realized with a mode-locked fiber laser using an intra-cavity waveguide electro-optic modulator for high-speed control", Optics Express, vol. 20, no. 13, pp. 13769-13776, June 2012

[5] M. Takamoto *et al.*, "Frequency comparison of optical lattice clocks beyond the Dick limit", Nature Photonics, vol. 5, pp. 288-292, April 2011

2×10^{-18} Total Uncertainty in an Atomic Clock

T.L. Nicholson[1], S.L. Campbell[1], R.B. Hutson[1], G.E. Marti[1], B.J. Bloom[1], R.L. McNally[1], W. Zhang[1], M.D. Barrett[1,2], M.S. Safronova[3,4], G.F. Strouse[5], W.L. Tew[5], and J. Ye[1]

[1]JILA, National Institute of Standards and Technology, and University of Colorado, Boulder, Colorado, USA
[2]Centre for Quantum Technologies, Singapore
[3]University of Delaware, Newark, Delaware, USA
[4]Joint Quantum Institute and the University of Maryland, College Park, Maryland, USA
[5]National Institute of Standards and Technology, Gaithersburg, Maryland, USA
E-mail: nicholtl@jilau1.colorado.edu

We present fractional stability of 2.2×10^{-16} at 1 s by using seconds-long coherent interrogations of our clock transition in a low-density system not limited by atomic interactions [1]. With this stability, we perform a new systematic evaluation of our clock, improving many uncertainties that limited our previous measurements [2], such as the lattice ac Stark and blackbody radiation (BBR) shifts.

Effect	Shift ($\times 10^{-18}$)	Uncertainty ($\times 10^{-18}$)
Lattice Stark	-1.3	1.1
BBR static	-4562.1	0.3
BBR dynamic	-305.3	1.4
dc Stark	0.0	0.1
Probe Stark	0.0	0.0
1st-order Zeeman	-0.2	0.2
2nd-order Zeeman	-51.7	0.3
Density	-3.5	0.4
Line pulling + tunneling	0.0	<0.1
2nd-order Doppler	0.0	<0.1
Background gas	0.0	<0.6
Servo offset	-0.5	0.4
AOM phase chirp	0.6	0.4
Total	-4924.0	2.1

Table 1: Uncertainty budget for the JILA ^{87}Sr optical lattice clock. The shifts and their corresponding 1σ uncertainties are quoted in fractional frequency units. The statistical uncertainties for each effect are inflated by the square root of the reduced chi-square statistic, χ^2_{red}, when $\chi^2_{red} > 1$. Typical values of χ^2_{red} are between 1 and 1.5. Statistical uncertainties are summed in quadrature with the systematic uncertainties for each effect.

For the lattice ac Stark systematic, we identify the lattice laser frequency where the scalar and tensor components of the shift cancel, allowing for state-independent trapping with clock shifts at the 1×10^{-18} level (Table 1) [1].

For the BBR systematic, we collaborated with NIST Sensor Science Division to improve our measurement of the atoms' thermal environment using accurate radiation thermometry, which is traceable to the NIST ITS-90 absolute temperature scale [1]. We also directly measure the component of the strontium atomic structure that is chiefly responsible for the spectral response to room-temperature BBR [1,3].

Our combined measurements have reduced the total uncertainty of the JILA Sr clock to a new record of 2.1×10^{-18} in fractional frequency units (Table 1), which is a factor of 3 improvement over the previous best.

[1] T.L. Nicholson, *et al*, "2×10^{-18} total uncertainty in an atomic clock," *arXiv preprint* 1412:8261, Dec. 2014.
[2] B.J. Bloom, *et al*, "An optical lattice clock with accuracy and stability at the 10^{-18} level," *Nature* 506, pp 71-75, Jan. 2014.
[3] K. Beloy, *et al*, "Determination of the 5d6s $^3D_1$ state lifetime and blackbody radiation clock shift in Yb," PRA 86, 051404, Nov. 2012.

Measurements of high-order Stark effects at the 10^{-18} level in an Yb optical lattice clock

Phillips, N. B.*, Beloy, K., Hinkley, N., Schioppo, M.,
McGrew, W., Sherman, J. A., Oates, C. W., and Ludlow, A. D.
Time and Frequency Division, National Institute of Standards and Technology, Boulder, CO USA
*present address: Stable Laser Systems, Boulder, CO USA
E-mail: nathaniel.phillips@nist.gov

Recently, optical lattice clocks have demonstrated the ability to reach fractional stability at the 10^{-18} level [1,2,3]. This level of measurement capability facilitates the detailed characterization of systematic effects influencing lattice clocks. Recent systematic evaluations of optical lattice clocks based on Sr are reporting total systematic uncertainties in the 10^{-18} decade [2,3] and agreement between two such clocks has been observed at the 10^{-18} level [3]. We have begun such an evaluation at NIST for the Yb optical lattice clock. Now that a formidable blackbody-Stark-effect is controlled $\leq 1\text{x}10^{-18}$ [4], the most significant uncontrolled perturbations originate from light shifts due to the optical lattice. Scalar Stark shifts are typically nulled by operating at the magic wavelength, and vector Stark shifts are minimized by interrogation of opposing atomic spin states. However, for lattice clocks with 10^{-18} uncertainty, hyperpolarizability effects, scaling as E^4, can be significant [5], as can higher-multipolar effects through M1/E2 terms [6]. Here we report direct measurements of such effects in an Yb optical lattice clock using a lattice power-enhancement-cavity. Operating intentionally with a small detuning from the magic wavelength, we demonstrate measurement and control of all lattice Stark effects near the 10^{-18} level. We also provide updates on other systematic effects that have recently been investigated.

[1] N. Hinkley, J. A. Sherman, N. B. Phillips, M. Schioppo, N. D. Lemke, K. Beloy, M. Pizzocaro, C. W. Oates, and A. D. Ludlow, "An atomic clock with 10^{-18} instability" Science, vol. 341, pp. 1215-1218, 2013.

[2] B. J. Bloom, T. L. Nicholson, J. R. Williams, S. Campbell, M. Bishof, X. Zhang, W. Zhang, S. L. Bromley, and J. Ye, "An optical lattice clock with accuracy and stability at the 10^{-18} level" Nature, vol. 506, pp. 71-75, 2014.

[3] I. Ushijima, M. Takamoto, M. Das, T. Ohkubo, and H. Katori, "Cryogenic optical lattice clocks with a relative frequency difference of $1\text{x}10^{-18}$" arXiv:1405.4071, 2014.

[4] K. Beloy, N. Hinkley, N. B. Phillips, J. A. Sherman, M. Schioppo, J. Lehman, A. Feldman, L. M. Hanssen, C. W. Oates, and A. D. Ludlow, "An atomic clock with $1\text{x}10^{-18}$ room-temperature blackbody Stark uncertainty," Phys. Rev. Lett., vol. 113, 260801, 2014.

[5] P. G. Westergaard, J. Lodewyck, L. Lorini,A. Lecallier,E. A. Burt,M. Zawada,J. Millo,and P. Lemonde, "Lattice-Induced Frequency Shifts in Sr Optical Lattice Clocks at the 10^{-17} Level," Phys. Rev. Lett., vol. 106, 210801, 2011.

[6] A. V. Taichenachev, V. I. Yudin, V. D. Ovsiannikov, V. G. Pal'chikov, and C. W. Oates, "Frequency Shifts in an Optical Lattice Clock Due to Magnetic-Dipole and Electric-Quadrupole Transitions," Phys. Rev. Lett., vol. 101, 193601, 2008.

Operational Sr clock at LNE-SYRTE

[Shi, Chunyan], [Robyr, Jean-Luc], [Bilicki, Sławomir], [Guéna, Jocelyne], [Abgrall, Michel], [Le Coq, Yann], [Nicolodi, Daniele], [Rosenbusch, Peter], [Laurent, Philippe],[Bize, Sébastien], [Le Targat, Rodolphe],[Lodewyck, Jérôme]

LNE-SYRTE, Observatoire de Paris, UPMC, CNRS, 61, avenue de l'Observatoire, Paris, France

E-mail: jerome.lodewyck@obspm.fr

Thanks to their large quality factor and the large number of simultaneously interrogated atoms, Optical Lattice Clocks beat stability and frequency records [1][2].

Here, we propose the demonstration of an operational lattice clock using strontium atoms. It features an uncertainty budget of 7.6×10^{-17} entirely limited by the black-body radiation shift, and a frequency stability of 1.0×10^{-15}, after a 1s integration time. The clock has been operated during a full week, as part of the EMRP-funded project "International Timescales with Optical Clocks" (ITOC), with minimal human intervention. During this period, the clock, linked to a fiber-based frequency comb, provided integration points every second with an uptime larger than 93%. These developments are essential steps towards international comparisons of optical clocks, either by fiber links or via the PHARAO/ACES space clock project.

During this measurement campaign, the Sr clock has been compared to Cs and Rb microwave fountains, providing frequency ratio measurements with a statistical resolution below 10^{-16}, and an improved overall uncertainty over our previous measurement [3]. Moreover, these ratio measurements agree within the error bars with the results publish in [3], reinforcing our confidence in the reproducibility of the clocks, and further constraining a possible drift of fundamental constants.

Finally, we take profit from the reliability of the clock to investigate a pending issue that could have compromised the ultimate performances of OLCs. We propose a study of lattice induced effects by comparing various laser sources for the optical lattice: Semi-conductor tapered amplifiers, slaves lasers and a titanium-sapphire laser. We show that careful characterization of the light is necessary to ensure ultimate accuracy.

The EMRP is jointly funded by the EMRP participating countries within EURAMET and the European Union.

[1] B.J. Bloom *et al*, An optical lattice clock with accuracy and stability at the 10^{-18} level. Nature **506**, 71 (2014)

[2] N. Hinkley *et al*, An Atomic Clock with 10^{-18} Instability, Science **341**, 1215 (2013)

[3] R. Le Targat *et al*, Experimental realization of an optical second with strontium lattice clocks. Nature Communications **4**, 2109 (2013)

Frequency measurement of an optical clock with 4×10^{-16} uncertainty assisted by an H-maser as flywheel oscillator

Al-Masoudi, A.; Dörscher, S.; Häfner, S.; Grebing, C.; Gerginov, V.;
Weyers, S.; Lipphardt, B.; Riehle, F.; Sterr U.; Lisdat, C.
Physikalisch-Technische Bundesanstalt, Bundesallee 100, D-38116 Braunschweig, Germany
E-mail: christian.lisdat@ptb.de

Though optical clocks have excellent stability, often long measurements durations are required to achieve small statistical uncertainty, because either extremely high accuracy is aimed at or because the clocks are used in combination with systems that limit the measurement stability. In the latter case, it is very desirable to reduce the necessary up-time of the optical clock by the application of a highly reliable flywheel oscillator like a hydrogen maser. During an absolute frequency measurement of the PTB Sr lattice clock with our primary fountain clock CSF2, we have applied a method to estimate the average frequency ratio of an H-maser and the lattice clock from interrupted measurements over a long period of time. During this period, the maser frequency is measured quasi continuously by CSF2. The approach used ideas given in [1] and [2] and allows for a useful extension of measurement time from 74 h to about 300 h, which reduces the statistical uncertainty significantly. Details are given in [3].

During the measurement campaign, the lattice clock was operated under conditions similar to the ones of our last frequency measurement [4]. The clock instability was further reduced to about $2.6 \times 10^{-16}\,(\tau/\mathrm{s})^{-0.5}$ by a new 698 nm clock laser system with a 48 cm reference cavity (see Fig. 1). A detailed investigation of the noise sources in the lattice clock shows that the clock stability is still degraded by the Dick effect.

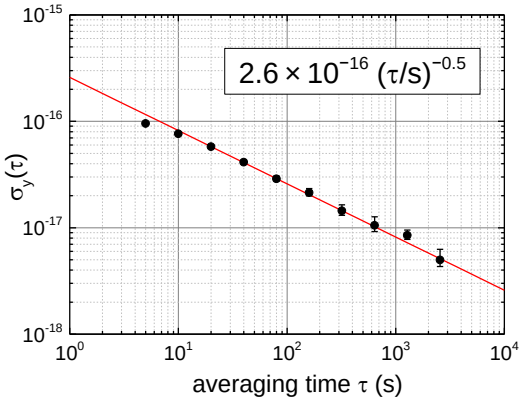


Fig. 1: Fractional frequency instability σ_y of the PTB strontium lattice clock estimated from a self-comparison. A new clock laser system with instability of below 10^{-16} from 1 s to more than 1000 s considerably improved the clock.

The measurement did not aim at interruption-free operation of the lattice clock (though uninterrupted over-night operation was achieved) but showed breaks of more than two days. With the total up-time of the Sr lattice clock of about 74 h, statistics would have a large contribution to the measurement uncertainty. Using a highly stable hydrogen maser as flywheel oscillator allows extending the measurement time on cost of additional uncertainty due to the interpolation [1],[3]. This uncertainty and reduction of statistics have to be trade-off; the combined uncertainty is minimized at an interval of 300 h. Finally, we have achieved a frequency measurement with a total fractional uncertainty of 4×10^{-16} of the measured frequency, which is in very good agreement with previous measurements [4],[5].

This work was supported by the Centre of Quantum Engineering and Space-Time Research (QUEST) and the EMRP projects ITOC and QESOCAS. The EMRP is jointly funded by the EMRP participating countries within EURAMET and the European Union.

[1] D.-H. Yu, M. Weiss, and T. E. Parker, *Metrologia*, vol. 44, pp. 91–96, 2007
[2] G. J. Dick, *Proceedings of the 19th PTTI Applications and Planning Meeting*, pp. 133–147, 1988
[3] C. Grebing, F. Riehle, C. Lisdat, U. Sterr, *Joint IFCS – EFTF meeting*, 2015
[4] S. Falke et al., *New J. Phys.*, vol. 16, p. 073023, 2014
[5] R. Le Targat et al., *Nature Com.*, vol. 4, p. 2109, 2013

Mercury Optical lattice clock at LNE-SYRTE

[De Sarlo, Luigi], [Tyumenev, Rinat], [Favier, Maxime], [Bize, Sébastien]
SYRTE – Observatoire de Paris, CNRS, LNE, UPMC, Paris France
E-mail: Luigi.de-sarlo@obpspm.fr

Among the different atomic species considered for optical clocks, neutral mercury has several favorable atomic properties that reduce the impact of most of the systematic effects currently limiting the accuracy of optical lattice clocks. The $^1S_0 - {}^3P_0$ clock transition in Hg is weakly coupled to thermal radiation and to static electric fields. For instance blackbody radiation sensitivity in Hg is a factor of ~30 less than in Sr. Mercury has a high vapor pressure at room temperature, which allows eliminating large temperature gradients in the experimental setup due to heating systems. Furthermore the isotope 199 has a spin ½ which suppresses systematic effects related to the lattice trap. Finally Hg atoms can be laser-cooled to rather low temperature of 30 μK with a single stage magneto optical trap (MOT), performed directly on $^1S_0 - {}^3P_1$ intercombination transition, and then straightforwardly loaded in the optical lattice.

The biggest challenges in the Hg-based optical lattice clock operation lie in the difficulty of operating the three required UV lasers (253.7nm, 265.6 nm and 362.5nm for cooling, probing, and trapping at the magic wavelength, respectively) and in the reduced polarizability that makes obtaining deep trap experimentally demanding. In spite of these challenges our group demonstrated high resolution spectroscopy of the 1.1PHz clock transition [1], experimental determination of the magic wavelength [1,2], absolute frequency measurement of the transition with a relative accuracy of 5.7×10^{-15} [3] and lattice clock operation with fractional frequency instability of $5.4 \times 10^{-15}/\tau^{1/2}$ for $\tau < 400$s [4]. All of these results, limited by the modest depth of the lattice, lead to the inclusion of the mercury clock transition in the list of the BIPM recommended atomic transition by CCTF in 2012.

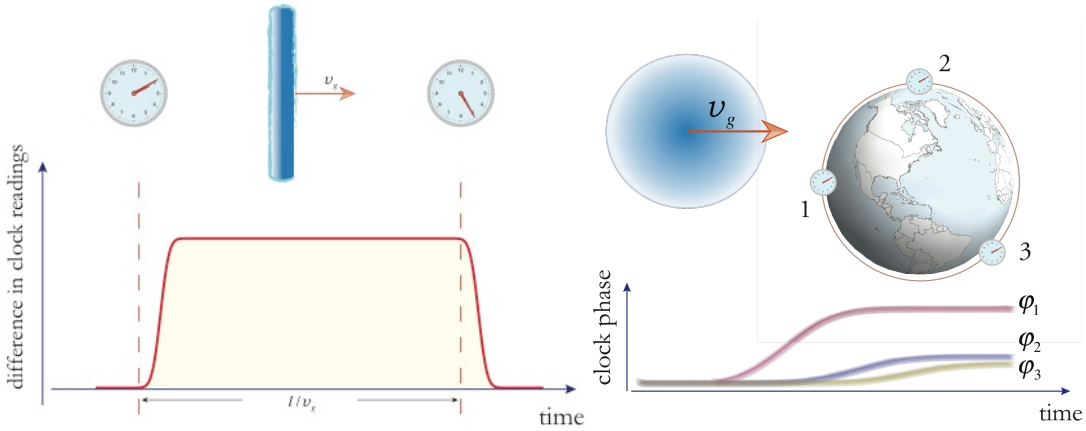
A novel implementation of the lattice trap allowed us to more than double the available trap depth with the capability of further increase it to more than 100 recoil energies. This and other important improvements of the experimental setup that we will detail in this presentation allowed us to improve by one order of magnitude the number of trapped atoms and by a factor of two our spectroscopic resolution. We will also report a new value of the short term stability of the clock and we will also present the measurement of a few systematic effects with uncertainty of a few 10^{-16}. At the end of the presentation we will briefly discuss the future plans for our experiment. In particular we plan to introduce a finer control over the magic trapping wavelength, another important step in the quest for the limits of the Hg system which are expected in the low 10^{-18} range, at room temperature.

[1] L. Yi *et al.*, Phys. Rev. Lett., vol. 106, 073005, 2011.
[2] S. Mejri *et al.*, Phys. Rev. A, vol. 84, 032507, 2011.
[3] J. J. McFerran *et al.*, Phys. Rev. Lett., vol. 108, 183004, 2012.
[4] J. J. McFerran *et al.*, Optics Letters, vol. 37, pp. 3477, 2012.

Dark matter search with atomic clocks and GPS

Andrei Derevianko
Physics Department, University of Nevada, Reno, USA
E-mail: andrei@unr.edu

Atomic clocks are arguably the most accurate scientific instruments ever built. Modern clocks are astonishing timepieces guaranteed to keep time within a second over the age of the Universe. Attaining this accuracy requires that the quantum oscillator be well protected from environmental noise and perturbations well controlled and characterized. This opens intriguing prospects of using clocks to study subtle effects, and it is natural to ask if such accuracy can be harnessed for dark matter searches.



By monitoring correlated time discrepancy between two spatially separated clocks one could search for passage of topological defects (TD), such as the domain wall pictured here (left panel). Domain wall moves at galactic speeds ~ 300 km/s. Before the TD arrival, the two clocks are synchronized. As the TD sweeps through the first clock, it runs faster (or slower), with the clock time difference reaching the maximum value. Time difference stays at that level while the defect travels between the two clocks. Finally, as the defect sweeps through the second clock, clocks resynchronize. For intercontinental scale network, l~ 10,000 km, the characteristic time is 30 seconds. The right panel shows correlated response to a monopole TD.

The cosmological applications of atomic clocks so far have been limited to searches of the uniform-in-time drift of fundamental constants. We argue that a transient in time change of fundamental constants can be induced by dark matter objects that have large spatial extent, and are built from light non-Standard Model fields. The stability of this type of dark matter can be dictated by the topological reasons. A correlated network of atomic clocks (see figures), such as atomic clocks onboard satellites of the GPS constellation, can be used as a powerful tool to search for the topological defect dark matter. In other words, one could envision using GPS as a 50,000 km-aperture dark-matter detector.

[1] A. Derevianko and M. Pospelov, *Nature Phys. 10, 933 (2014)*, *arXiv:1311.1244*

Stable Time and Frequency Transfer in the Atacama Large Millimeter Array

William Shillue,
Central Development Laboratory, National Radio Astronomy Observatory, Charlottesville, VA, USA
E-mail: bshillue@nrao.edu

The ALMA (Atacama Large Millimeter Array) is a single radio telescope of advanced design, composed of sixty-six high-precision 12-meter antennas located on the Chajnantor plateau in the Atacama Desert of Northern Chile. The plateau is at an elevation of 5,000 meters which gives a high degree of radio transparency due to low atmospheric water vapor. The telescope combines radio waves from all antennas to image the sky at frequencies between 30-950 GHz. To construct a high-fidelity image, exceptional stability is needed not just in the atmosphere but also the radio antenna structure, the millimeter wave radio receivers, and especially the first local oscillator in the receiver. Additionally, all receivers must be mutually coherent which requires a high-precision central timing and distribution system. A fiber optic transmission system sends timing and local oscillator (LO) signals to each telescope, with the central building and radio telescopes arranged as a hub with spokes. The maximum distance to an antenna is 15 km, and the antennas are movable to allow scientists to scale the array size to fit the science objective.

This paper will describe the ALMA LO and timing system. The receiver outputs are digitized and sent from the telescopes to the central building by optical fiber, where they are combined in a massive digital correlator, thus forming a multiple element interferometer. In order to construct high fidelity images, the entire signal path and the local oscillators must be highly stable. The specification for the phase stability level was determined so that contributions from the engineered elements: telescope, receivers, and local oscillators, would be less than the atmosphere under the best observing conditions. The specifications were very challenging, especially for the 1st LO which needed to provide stable phase (22 fsec RMS) for frequencies up to 938 GHz over a 15 km distance. The engineering of the system to meet this requirement will be described which consisted of a centrally based dual-laser heterodyne with low phase-noise (Laser synthesizer) transmitted by optical fiber which is used to phase-lock an antenna-based oscillator-multiplier frequency chain. Additionally, the fiber and many components in the path are stabilized by a round-trip phase-correction system that uses a stable laser reference (master laser).



Fig. 1: Four of the ALMA radio telescopes on the Chajnantor plateau in Chile (credit: ALMA (ESO/NAOJ/NRAO))

The ALMA radio telescope has been in scientific use since 2011. Recent results including instrumental perfomance over long baselines will be included. Also detailed will be the addition, in 2014, of further synchronization hardware which now allows ALMA to operate as a single telescope in a global millimeter-wave radio array for testing theories of general relativity and providing unprecedented imaging of black holes.

[1] J.F. Cliche, B. Shillue, "Precision timing control for radioastronomy: maintaining femtosecond synchronization in the Atacama Large Millimeter Array," IEEE Control System, Vol. 26, No. 1, pp. 19-26, 2006

[2] W. Shillue, et al, "A High-Precision Tunable Millimeter-Wave Photonic LO Reference for the ALMA Telescope," 2013 International Microwave Symposium Digest, Jun 2-7, 2013

Quantum Tests of the Einstein Equivalence Principle on Ground and in Space

Invited Speaker: Ernst Rasel rasel@iqo.uni-hannover.de

The Einstein equivalence principle is a corner stone of general relativity and therefore challenged with growing precision by experimental tests on ground [1,2] and in space [3]. In the recent past several atom-interferometric experiments were started with the aim to perform precise tests of the universality of free fall with quantum matter displaying unique features such as a long coherence length or pure sin polarisation [9-10]. They aim to reduce the present sensitivity gap between current ground based tests and a future space mission STE-QUEST [11,12], which will allow to improve on the ultimate systematic uncertainties of ground based experiments. A more elaborate version of STE-QUEST is proposed for The ESA M4-mission. It will host a dual species interferometer for testing the universality of free fall as well as enable intercontinental comparisons of state-of-the-art ground clocks for a test of the sun and moon gravitational redshift.

Acknowledgement: The M4 proposal of STE-QUEST was established by a consortium of European scientists under the lead of Peter Wolf.

Core scientists:
Kai Bongs, Philippe Bouyer, Claus Braxmaier, Davide Calonico, A. Michael Cruise, Naceur Gaaloul, Luciano Iess, Philippe Jetzer, Wolf D.C. von Klitzing, Steve Lecomte, Ernst Rasel, Markus Rothacher, Stephan Schiller, Carlos F. Sopuerta, Guglielmo M. Tino, Philip Tuckey, Martin Zelan

Additional contributions:
Holger Ahlers, Peter Berg, Michael Chwalla, Robert Ecoffet, Thorsten Feldmann, Domenico Gerardi, Christine Guerlin, Jonas Hartwig, Thierry Martin, Didier Massonnet, Katerine Posso-Trujillo, Christian Schubert, Thilo Schuldt, Drazen Svehla

[1] J. G. Williams, S. G. Turyshev, D. H. Boggs, Phys. Rev. Lett. 93, 261101 (2004).
[2] S. Schlamminger, K.-Y. Choi, T. A. Wagner, J. H. Gundlach, and E. G. Adelberger, Phys. Rev. Lett. 100, 041101 (2008).
[3] P. Touboul, G. Métris, V. Lebat, and A. Robert, Class. Quantum Grav. 29, 184010 (2012).
[4] S. Fray and M. Weitz, Space Sci. Rev. 148, 225 (2009).
[5] A. Bonnin, N. Zahzam, Y. Bidel, and A. Bresson, Phys. Rev. A 88, 043615 (2013)
[6] M. G. Tarallo, T. Mazzoni, N. Poli, D.V. Sutyrin, X. Zhang, and G. M. Tino, Phys. Rev. Lett 113, 023005 (2014)
[7] G. Varoquaux, A. Landragin, R. A. Nyman, R. Geiger, P. Cheinet,and P. Bouyer, New J. Phys. 11, 113010 (2009).
[8] S. M. Dickerson, J. M. Hogan, A. Sugarbaker, D. M. S.Johnson, and M. A. Kasevich, Phys. Rev. Lett. 111, 083001 (2013).
[9] A. Sugarbaker, S. M. Dickerson, J. M. Hogan, D. M. S.Johnson, and M. A. Kasevich, Phys. Rev. Lett. 111,113002 (2013).
[10] H. Müntinga et al., Phys. Rev. Lett. 110, 093602 (2013).
[11] D. N. Aguilera et al., Class. Quantum Grav. 31, 115010 (2014)
[12] G. M. Tino and M. Kasevich (eds) 2013 Precision interferometry with Bose-Einstein condensates (Atom Interferometry vol 188) (Proceedings of the International School of Physics "Enrico Fermi") N. Gaaloul, J. Hartwig, C. Schubert, W. Ertmer, and E. M. Rasel

Front-End Communication System-: Recent & Emerging Trends

Ulrich L. Rohde
Brandenburg University of Tech., Cottbus, Germany
Bayerische Ackademie, Munich, Germany

The recent security requirement has revealed an intensive data gathering for fiber or radio communication. Besides the fiber technology, there are varieties of wireless activities, which are typically analyzed by off the air monitoring. The spectral density of signals these days is very high and therefore such monitoring receivers require high performance. The technique in designing such receivers is a composition of microwave engineering of the building blocks preamplifier, mixer, synthesizer and necessary filters and this presentation will cover important highlights about pros and cons of these designs. What is needed: high dynamic range, typically the highest in the frequency range between 80 and 160 MHz, as the broadcast band is full of strong signals (80- 109 MHz) and the frequency range above covers the aircraft radio band, the amateur radio band (144-148 MHz) and the mobile communication above the 160 MHz [1]-[3].

A typical receiver consists of an input stage, first mixer stage including the necessary synthesizer, a possible second mixer stage, and then the output is fed to signal processing down at the IF level of choice. There is a variety of important receiver parameters. The noise figure determines the minimum discernible signal, sometimes also called minimum detectable signal, typically expressed in dBm and overall dynamic range, the key intermodulation distortion products [1]-[2]. System noise and noise floor defines the spurious free dynamic range. Second order intermodulation distortion products can be reduced by the appropriate input filters. This signal is then up converted to an IF of about 20 GHz using a highly cleaned-up LO chain (detailed schematics will be shown in full length paper). This is achieved by frequency-doubler and very large amount of filtering of the signals. Spectral purity of the oscillator chain is of the essence. Finally, a second converter is used to down convert the signal to the IF level. This arrangement allows a very high performance signal analysis. Fig. 1 shows a frequency panorama display and a waterfall time event. On the left hand of the frequency display, there are a large number of FM broadcast stations, and on the right side shows air traffic control frequency range, police and other mobile radioactivity. The waterfall display shows the various transmissions, which are useful for frequency occupancy analysis over time, and the spectral display shows a range where demodulation of transmission is possible while observing all the activity. Fig. 2 shows a five-channel arrangement for signal analysis. The wideband monitoring receiver can handle five individual channels simultaneously, including transmission monitoring. In this case, two ATC frequencies and two FM broadcast stations. The systems performance s determined by hardware, firmware and software. Even if everyone has access to the same chip-set the implementation may differ depending upon the market price of the equipment. The detailed implementation of modern receivers will be shown in full-length paper.

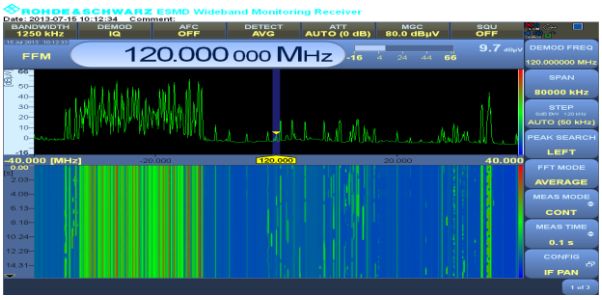


Fig. 1: Wide bandwidth waterfall

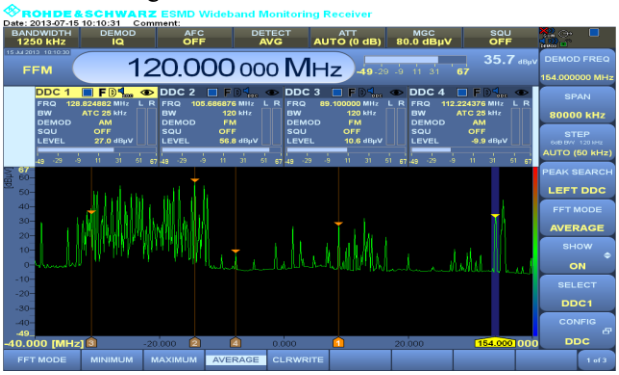


Fig. 2: Five channel arrangement for signal analysis

[1] U. L. Rohde and A. K. Poddar, "A Digital Frequency Synthesizer Using Adaptive Mode-Coupled Resonator Mechanism for Low Noise and Low Jitter Applications", IEEE International Symposium on Circuits and Systems (ISCAS), pp. 414-417, May 15-18, 2011, Brazil

[2] Ulrich L. Rohde and David Newkirk, "RF/Microwave Circuit Design for Wireless Applications", John Wiley & Sons, April 2000, ISBN 0-471-29818-2

[3] James Tsui, Special Design Topics in Digital Wideband Receivers, 2010

Oscillator Phase Noise: A 50-year Retrospective

Leeson, David B.
Department of Electrical Engineering, Stanford University, Stanford, CA
E-mail: leeson@stanford.edu

Oscillator instabilities are a fundamental concern for systems tasked with keeping and distributing precision time or frequency. Also, oscillator phase noise limits the demodulated signal-to-noise ratio in communication systems that rely on phase modulation, such as microwave relay systems, including satellite and deep-space links. Comparably important are the dynamic range limits in multi-signal systems resulting from masking of small signals of interest by oscillator phase noise on adjacent large signals. For example, Doppler radar targets are masked by phase noise on the much larger ground clutter return.

Fifty years ago I had the good fortune to write a brief summary, now widely cited, of emerging thoughts regarding modeling the power spectral density of phase noise in oscillators [1]. My early interest in oscillator noise came as solid-state signal sources began to be applied to the radars that had been under development since the days of the MIT Radiation Laboratory. I was initiated into the phase-noise requirements of airborne Doppler radar through my work on those signal sources.

In 1964 an IEEE committee was formed to prepare a standard on frequency stability. Thanks to a supportive mentor, the late W. K. Saunders, I became a member of that group, which included J. A. Barnes and L. S. Cutler. It was noted that the separate use of frequency-domain and time-domain definitions stood in the way of development of a common standard. The first step of the program to craft a standard that would define frequency stability was to understand and meld the frequency- and time-domain descriptions of phase instability to a degree that was predictive and permitted analysis and optimization. To promote focused interchange, we sponsored the November 1964 IEEE/NASA Conference on Short Term Frequency Stability and subsequently edited the February 1966 Special Issue on Frequency Stability of the *Proceedings of the IEEE*.

By the time the subcommittee edited the *Proc. IEEE* special issue, the wide exchange of viewpoints and concepts provided the environment in which to synthesize concise summaries of the work in both domains, of which my own model was one that owed a special indebtedness to the late L. C. Cutler. The committee published its summary work in 1971 [2]. This ultimately led to the establishment of IEEE Std 1139 [Vig, *et al*].

The frequency-domain work that preceded the 1964 symposium had focused primarily on linewidth rather than spectrum of phase, both in electronic circuits [*e.g.*, Edson, Golay] and quantum devices [*e.g.*, Schawlow and Townes]. The 1966 model recognized nonlinear effects by an approximation, and provided results that sufficed then for high-Q oscillators. Given the limitations of any model, evolutionary improvements and verification of the 1966 work have occupied many during the intervening five decades [*e.g.*, Rhode, Everard, among many]. Measurements have come to play a key role in confirming the usefulness of the basic model [*e.g.*, van der Merwe].

The search for new understanding and techniques has been spurred by this requirement for low phase noise in oscillators and synthesizers whose primary character is integration and its accompanying cost benefits. Today, numerical nonlinear circuit analysis supports additional design variables, such as the timing of the current pulse in nonlinear oscillators, that have become feasible because of the improved capabilities of both semiconductor devices and computation [*e.g.*, Lee and Hajimiri, Kärtner, and Demir *et al*]. The field is still alive and vigorous, with emerging players eager to find a role on the stage for their own scenarios.

[1] D. B. Leeson, "A Simple Model of Feedback Oscillator Noise Spectrum," *Proc. IEEE*, Vol. 54, Feb. 1966, pp. 329-330.

[2] J. Barnes, A. Chi, L. Cutler, D. Healey, D. Leeson, *et al*, "Characterization of Frequency Stability," *IEEE Trans. Inst. and Meas*., Vol. IM-20, No. 2, May 1971, pp. 105-120.

The measurement of frequency fluctuations with Ω counters and AVAR-like least-square-fit wavelets

F. Vernotte$^{\diamondsuit}$, M. Lenczner, P.-Y. Bourgeois, and E. Rubiola

FEMTO-ST Institute, Besançon, France
$\diamondsuit$ UTINAM, Besançon, France

home page http://rubiola.org

The Allan variance (AVAR) is good at rendering the largest τ for a given time series of measured data. This feature, highly desired for timekeeping, comes at expenses of poor resolution of white and flicker phase noise. By contrast, high resolution in the presence of white and flicker phase noise is mandatory for the measurement of short-term fluctuations (μs to s), and useful for medium-term fluctuations (up to days). This is the case of optics and of the generation of pure microwaves from optics. The same features are of paramount importance for radars, VLBI, geodesy, space communications, etc. Needless to say, extending the time-domain measurements to lower τ overcomes some issue in the numerical conversion from spectra to variances.

The modified Allan variance (MVAR) helps in the analysis of fast fluctuations, at a moderate cost in terms of computing power. Frequency counters specialized for MVAR are available as a niche product, chiefly intended for research labs[1]. The least-square method is a milestone in applied statistics. It provides the lowest-energy (or lowest-power) fit of a data set, which is in most cases considered the optimum approximation. For our purposes, the least-square fit finds an obvious application in the estimation of the frequency from a time series of phase data, and opens the way to improvements in fluctuation analysis. Besides, new digital hardware — like FPGAs and SoCs — provides bandwidth and computing power at an acceptable complexity, and makes possible least-square fitting in real-time.

We apply least-square estimation of frequency to fast time stamping. The simplest estimator if this family is the linear regression (LR) on phase data. The LR can be interpreted as a filter that processes frequency fluctuations. The shape of such filter is parabolic. We call the corresponding instrument 'Ω counter,' for the graphical analogy with the Greek letter, and in the continuity of the Π and Λ counters[2,3]. The Ω estimator is similar to the Λ estimator, but exhibits higher rejection of the instrument noise, chiefly of white phase noise. This is important in the measurement of fast phenomena, where the cutoff frequency f_H is necessarily high, and the white phase noise is integrated over the wide analog bandwidth that follows.

In the same way as the Π and Λ estimators yield the AVAR and the MVAR, respectively, we define a variance based on the Ω estimator, and we extend the analysis to higher-order least-square fits. Like in the AVAR and MVAR, the weight functions are similar to wavelets, but for the trivial difference that they are normalized for power-type signals. We provide the response to polynomial-law noise types as analytical formulae and as the result of extensive simulations, and some experimental results using cryogenic oscillators. Finally, we discuss the computation complexity and its impact on digital hardware requirements.

[1] For example, G. Kramer and K. Klitsche, "Multi-channel synchronous digital phase recorder," Proc. *2001 IFCS*.

[2] E. Rubiola, "On the measurement of frequency and of its sample variance with high-resolution counters," Rev. Sci. Instrum. 76(5) article no. 054703, May 2005.

[3] Dawkins ST, Mc Ferran JJ, A.N. Luiten, "Considerations on the Measurement of the Stability of Oscillators with Frequency Counters," IEEE Transact. on UFFC 54(5), 2007.

SDR and Self-Focusing Radar Techniques for milliHerz Measurement of Multi-Component Phase Noise Spectra?

Underhill, Michael J
Underhill Research Limited
Lingfield, UK
E-mail: mike@underhill.co.uk

This paper shows that Synthetic Aperture Radar (SAR) Self-Focusing Post-Processing Techniques can be used for faster higher precision Phase Noise and Allan Variance Measurement on more than one signal component at a time. One key essential is to use Software Radio (SDR) techniques [1, 2] to sample, acquire and process the signals, on a continuous basis, for record lengths of up to a few days. The RFSpace SDR-IP has an 16bit ADC sampling at 80MHz and this creates data at a rate of 160 megabytes/second, or a gigabyte in 6.25 seconds, or 14 terabytes a day. A second key essential is to process (or decimate) this data in real time while it is being collected, so that only the required information is recorded and stored with the maximum accuracy, resolution and precision depending and the available equipment and measurement time. Easily available PCs of modest specifications can host several simultaneous Allan variance or Phase noise measurement processes all in real time.

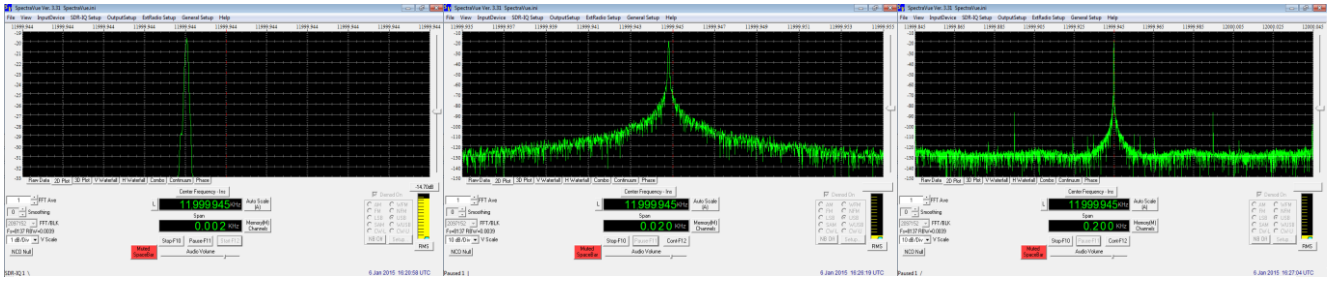


Fig. 1: Example of three simultaneous phase noise spectra plots of 10MHz signal from an HP8457D source with spans of 2Hz, 20Hz and 200Hz, with 3.9mHz resolution (RBW), and using Blackman-Harris windowing function. 1db vertical scale steps on left plot and 10dB steps on centre and right plots. No spectrum or time averaging was used. The data record length was about 260 seconds. Decimated sample rate was 8137Hz and a two million point FFT was used.

Figure 1 shows three simultaneous close in phase noise plots of a 10MHz source, all with 3.9 milliHerz resolution and obtained in about 260 seconds. The RFSpace 14 bit SDR-IQ with SpectraVue 'freeware' was used with a Samsung NC10 Notebook PC.

Key questions are what processes to use, and whether better results may be achieved by coupling two processes together? For example one proposal for phase noise measurement of an uncompensated oscillator is to compensate for any oscillator frequency drift (or wander) in the software only. This allows long integration times to improve the dynamic range of the phase noise measurement. Then increasing the record length from 1 to 1000 seconds can extend the measurement dynamic range by 30dB. This process is essentially the same as the 'self-focusing' that is used in space and airborne Synthetic Aperture Radar (SAR), to compensate for aircraft or satellite trajectory variations down to a few millimeters.

Assessment of Ionospheric Carrier Frequency Shifts require such SDR techniques to separate and plot the spectra of two or more components a few tenths to a few Hz apart [3].

[1] M. J. Underhill., "Time jitter and phase noise — Now and in the future?", *Proceedings*, 2012 IEEE Int. Frequency Control Symp., Baltimore, Maryland, 21-24 May 2012, 2012, pp. 1-8.

[2] M. J. Underhill., "Coupling Theory for Fluctuating Spurs in Oscillators", *Proceedings*, 2014 IEEE Int. Frequency Control Symp., Taipei, Taiwan, 19-22 May 2014, pp. 1-5.

[3] M. J. Underhill., "Discovery of Persistent Ionospheric Frequency Shifts of a few Herz and Impact on Time and Frequency Transfer.", submitted to Group 5 of this conference.

Characterization of a set of Cryocooled Sapphire Oscillators at the 10^{-16} level with the three-cornered-hat method

Christophe Fluhr[1], Serge Grop[1], Timothée Accadia[1], Benoît Dubois[2], Ahmed Bakir[1]
Yann Kersalé[1], Enrico Rubiola[1] and Vincent Giordano[1]

[1]FEMTO-ST Institute, Time and Frequency Dpt, 26 Chemin de l'Epitaphe, 25000 Besançon, France
[2] FEMTO Engineering, 15B Avenue des Montboucons, 25030 Besançon Cedex, France

The latest improvements of the Cryogenic Sapphire Oscillators (CSO) was realized in the frame of the ULISS project [1] and presented during the last EFTF in Neuchâtel [2]. Since, a third instrument, named Absolut, was built. The design of the new cryostat has been developed by Absolut System [3] in collaboration with FEMTO-ST. It has been optimized in term of thermal and mechanical configurations. A bellows has been added between the pulse tube cryocooler and the cryostat reducing the residual vibration level by a factor of two. A new design of thermal ballast has been tested improving the thermal control stability.

Absolut incorporates a Kyroupolos sapphire crystal [4] instead of the common HEMEX sapphire resonator [5] used for their high purity. We observed that the two growth methods achieved equivalent performances. The loaded Q-factor is up to 500.10^6 for X-band frequencies and the whispering gallery modes presents a frequency/temperature turnover at around 5.5K. These characteristics permit to Absolut to reach identical level of relative frequency instabilities and phase noise than the two previous CSOs.

A set of three nearly identical CSOs constitutes an unique tool permitting to reach an unprecedented noise floor in the frequency stability measurement. These three CSOs has been compared with the three-cornered-hat method, which permits to extract the individual frequency stabilities. The measurement set-up has been fully characterized. Two frequency counters were tested requiring two different data processing, both methods achieved the same results.

The CSOs reach a frequency stability better than $7x10^{-16}$ between 1 s and 3,000 s integration times. One CSO presents a noise floor of $1.5x10^{-16}$ @200s and the two others a noise floor of $3.5x10^{-16}$ @20s.

[1] www.uliss-st.com

[2] Serge Grop, Christophe Fluhr, Benoit Dubois, Jean-Louis Masson,Yann Kersale, Enrico Rubiola, Gregory Haye and Vincent Giordano: *Latest Improvements in the Performances of a Cryogenic Sapphire Oscillator,* Proceedings of the 2014 EFTF, 23-26 June 2014, Neuchâtel (CH)

[3] Absolut System SAS: www.absolut-system.com

[4] Precision Sapphire Technologies, Ltd.: http://www.sapphire.lt

[5] GT Advanced Technologies: http://www.gtat.com

Enhancing Clocks with Collective Effects: Spin Squeezing and Superradiance

Justin G. Bohnet, Kevin C. Cox, Matthew A. Norcia, Joshua M Weiner, Zilong Chen, James K. Thompson
JILA and Dept. of Physics, University of Colorado, Boulder, CO, USA
E-mail: jkt@jila.colorado.edu

The field of atomic and optical physics has developed a myriad of tools to gain nearly complete control over the quantum state of individual atoms and ions: both their internal and external states. These tools have been leveraged to build extremely precise and accurate sensors of time, fields, and motion. A new frontier of atomic and optical physics is to learn how to extend these single-atom tools to now realize, control, and exploit interactions *between* atoms in order to create interesting quantum and classical correlations between the atoms. This effort is at the heart of both quantum computers and the simulation of condensed matter systems.

We are interested in understanding how to create correlations and collective states of atomic ensembles that are useful for enhancing precision measurements. The goal is to move away from a purely single-atom paradigm of precision measurement, and move toward a many-body paradigm in which collective effects will provide new tools to advance the precision and accuracy of quantum sensors. In this talk, we will discuss two proof-of-principle experiments, entangled state generation and superradiant lasing, that may one day lead to improved optical lattice clocks and perhaps matter-wave interferometers.

We will present collective measurements that project an ensemble of $N = 4.8 \times 10^5$ ^{87}Rb atoms into an entangled state [1]. We directly observe an entangled, spin-squeezed state with quantum phase resolution improved in variance by a factor of 10.5(1.5), or 10.2(6) dB, compared to the initially unentangled ensemble of atoms. Crucially, the reported number reflects no background subtractions or corrections for experimental imperfections.

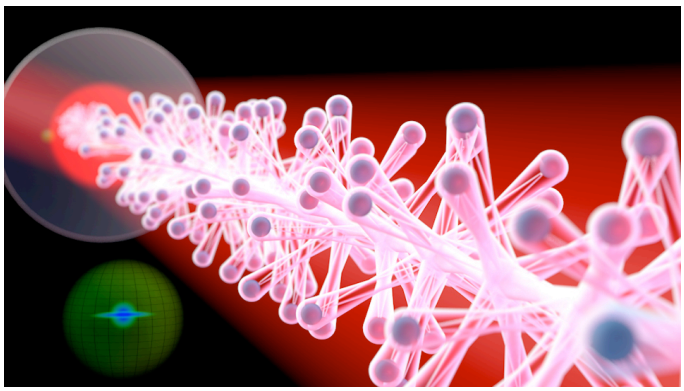


Fig. 1 Rubidium atoms (balls) become quantum entangled (visualized as links) when probed by laser light (red glow) inside an optical cavity. By forging quantum connections between the atoms, the intrinsic quantum noise of the atoms can be squeezed ten times below the standard quantum limit, visualized by the squeezing and antisqueezing of the blue quantum noise distribution on the green Bloch sphere.

We will next discuss the realization of a proof-of-principle Raman laser that operates with <1 photon on average inside the laser cavity [2]. In this deep superradiant regime, almost all of the laser's phase information is collectively stored inside the ensemble of atoms where it is strongly protected from corruption by motion of the laser cavity's mirrors—whether it arises from technical sources of vibration or the thermal vibration noise that limits today's most narrow linewidth lasers. We will briefly discuss our new effort to realize a superradiant laser using the mHz optical clock transition in strontium. Such a laser might one day achieve a mHz linewidth, advance both time keeping and long baseline optical interferometry, and provide a way to move narrow linewidth lasers out of low-vibration laboratory environments for both scientific and practical applications.

[1] Justin G. Bohnet, Kevin C. Cox, Matthew A. Norcia, Joshua M. Weiner, Zilong Chen, J. K. Thompson, "Reduced spin measurement back-action for a phase sensitivity 10 times beyond the standard quantum limit," *Nature Photonics* **8**, 731-736 (Sept. 2014)

[2] J. G. Bohnet, Z. Chen, J. M. Weiner, D. Meiser, M. J. Holland, J.K. Thompson, "A Steady State Superradiant Laser with <1 Intracavity Photon," *Nature* **484** 78-81, (April 5, 2012).

Laser Stabilization on Velocity Dependent Non-linear Dispersion of Sr Atoms in an Optical Cavity

Christensen, Bjarke T. R.[1], Henriksen, Martin R.[1], Schäffer, Stefan A.[1], Tieri, David[+] , Holland, Murray[+], Cooper, John[+], Westergaard, Philip G.[*], Ye, Jun[+], and Thomsen, Jan W. [1]

[1]Niels Bohr Institute, University of Copenhagen; Blegdamsvej 17, 2100 Copenhagen, Denmark
*Danish Fundamental Metrology; Matematiktorvet 307, 1. sal, DK-2800 Kgs. Lyngby, Denmark
+JILA, National Institute of Standards and Technology and University of Colorado, Boulder, CO
E-mail: bjarkesan@nbi.ku.dk

Nonlinear effects from coupling of atoms with a narrow transition to an optical cavity has been proposed as an alternative strategy to improve the stability and reduce the complexity of state-of-the-art laser frequency stabilization [1-4]. The development of simple and reliable high stability optical clock lasers are important for future state-of-the-arts optical clocks [5-7] and transportable optical clocks [8-9].

Laser cooled atomic samples with narrow optical transitions provides a domain where the Doppler energy scale is several orders of magnitude larger compared to the linewidth of the optical transition. A system in this domain is sensitive to velocity dependent multi-photon scattering events (Dopplerons) [10] which affects the system's performance as a frequency discriminator [11]. However, the dynamics of those velocity dependent processes have not yet been fully understood. Here we present experimental studies of the velocity dependent dynamics relevant for laser stabilization to atoms with narrow transitions probed inside an optical cavity.

The investigated frequency discriminator consisted of a sample of laser cooled strontium-88 atoms with sample temperatures of few mK strongly coupled to a low-finesse optical cavity, see figure 1. The collective cooperativity of this system has been measured to C = 630. The system is thus placed in a regime with strong atom-light coupling but not in the collective CQED regime [12], as the collective atom-light coupling parameter of this system, g = 2.8 MHz, is less than the cavity decay rate, κ = 5.8 MHz. In this regime, the system has no bi-stability limiting its performance. The cavity transmitted intensity and non-linear phase shifts of the system was measured by cavity-enhanced FM spectroscopy and shown to be significantly modified by velocity dependent processes, see figure 2.

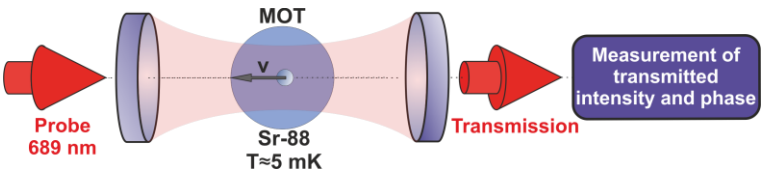


Fig. 1: Experimental setup. A sample of cold Sr-88 atoms prepared in a Magneto Optical Trap (MOT) inside a low finesse cavity (F = 85). We probe the atoms at 689 nm while the cavity is held at resonance with the probe laser. Both the cavity transmitted intensity and phase shift are measured by cavity- enhanced FM spectroscopy.

The slope and the signal-to-noise ratio of the measured phase dispersion determines the ultimate frequency stability of the system. The phase dispersion slope depends nonlinearly on the optical intra-cavity power, which makes the optimal choice of parameters non-trivial. This non-trivial dynamics is investigated experimentally in order to optimize the laser stabilization performance of the system.

Whereas the velocity dependent multi-photon scatterings are found to be degrading the ultimate frequency stabilized linewidth of the system, the shot-noise-limited linewidth of the current unoptimized system is estimated to be 480 mHz. The same system with optimized input power is estimated to have a shot-noise-limited linewidth comparable with the state-of-the-art laser stabilization [13]. Furthermore, our theoretical model shows that the merit in terms of frequency stability from further cooling of the atomic sample is minimal. This opens the prospects for implementations of a simple and compact transportable optical atomic clock with high stability.

The understanding of relevant motional effects presented here has direct implications for other atomic clocks and superradiant laser sources involving ultranarrow transitions.

Furthermore, two following Sr-based experimental systems are under preparation to reach the full potential for applying velocity dependent non-linear phase dispersions as quantum discriminators: 1) A sample of laser cooled strontium-88 coupled to a monolithic high finesse cavity inside a vacuum chamber to reach previously unachieved laser stabilization performance. 2) A beam of strontium-88 probed inside an optical cavity in order to perform continuous clock operation. The latest progresses in these works will be presented at IFCS 2015.

[1] D. Meiser, J. Ye, D. R. Carlson, and M. Holland, "Prospects for a Millihertz-Linewidth Laser" Phys Rev. Lett., vol. 102, issue 16, 163601, Apr. 2009.

[2] D. Meiser, and M. Holland, "Steady-state superradiance with alkaline-earth-metal atoms" Phys. Rev. A, vol. 81, issue 3, 033847, Mar. 2010.

[3] M. J. Martin, D. Meiser, J. W. Thomsen, J. Ye, and M. Holland, "Extreme nonlinear response of ultranarrow optical transitions in cavity QED for laser stabilization" Phys. Rev. A, vol. 84, issue 6, 063813, Dec. 2011.

[4] J. G. Bohnet, et al., "A steady-state superradiant laser with less than one intracavity photon", Nature, vol. 484, pp. 78-81, Apr. 2012.

[5] B. J. Bloom et al, "An optical lattice clock with accuracy and stability at the 10^{-18} level", Nature, vol. 506, pp. 71-75, Feb. 2014.

[6] N. Hinkley et al, "An Atomic Clock with 10^{-18} Instability", Science, vol. 341, pp. 1215-1218, Sep. 2013.

[7] I. Ushijima, M. Takamoto, M. Das, T. Ohkubo and H. Katori, "Cryogenic optical lattice clocks with a relative frequency difference of 1×10^{-18}", arXiv:1405.4071.

[8] N. Poli et al., "A transportable strontium optical lattice clock", J. Applied Physics B, vol. 117, issue 4, pp. 1107-1116, Dec. 2014.

[9] D. R. Scherer et. al., "Progress on a Miniature Cold-Atom Frequency Standard", arXiv:1411.5006.

[10] A. Tallet, "Raman Emission Versus Dopplerons in a Two-level Atomic Cell", J. Opt. Soc. Am. B, vol. 11, issue 8, pp. 1336-1349, 1994.

[11] P. G. Westergaard et al. "Observation of Motion Dependent Nonlinear Dispersion with Narrow Linewidth Atoms in an Optical Cavity", arXiv:1408.3983.

[12] H. Tanji-Suzuki et al., "Interactions between atomic ensembles and optical resonators: Classical Description", Adv. At. Mol. Opt. Phys, vol. 60, pp. 201, Jul. 2011.

[13] T. Kessler et al., "A sub-40-mHz-linewidth laser based on a silicon single-crystal optical cavity", Nature Phot., vol. 6, pp. 687-692, Jul. 2012.

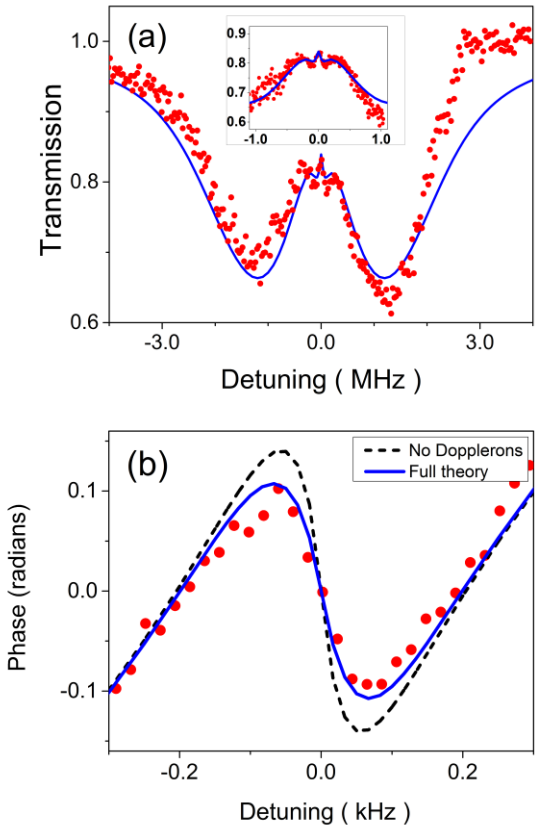


Fig. 2: The solid and dashed lines are theoretical predictions based on our theoretical model [11]. The dots are data measured by cavity-enhanced FM spectroscopy. (a) Frequency scan of the cavity transmitted intensity normalized to the transmitted intensity without atoms inside the cavity for input power of 575 nW, total number of atoms of $N = 5.0\cdot10^8$ and atom temperature T = 5.0 mK. The asymmetry of the experimental data is expected to be due to mechanical effects of the probe light on the atoms. Inset: Zoom on the central region with enhanced transmission due to saturation. A detailed structure around resonance predicted by our theoretical model is clearly visible. The units on the inset axes are the same as in (a). (b) Frequency scan of the cavity transmitted phase shift close to resonance for input power of 650 nW, total number of atoms of $N = 4.0\cdot10^8$ and atom temperature T = 4.1 mK . Here, two theoretical plots are shown. The solid blue line take the velocity dependent Dopplerons and higher order saturation processes into account, while the dashed black line does not. The slope of the phase dispersion around resonance is affected by the Dopplerons and the effect of the Dopplerons is readily apparent.

Ten Years of Active Optical Frequency Standards

Jingbiao Chen, Wei Zhuang*, Duo Pan, Xiaobo Xue, Xiaogang Zhang, Mo Chen, and Zhichao Xu
State Key Laboratory of Advanced Optical Communication System and Network, School of Electronics Engineering and Computer Science, Peking University, Beijing 100871,China.
*National Institute of Metrology, Beijing10013, China.
E-mail: jbchen@pku.edu.cn

The concept of active optical clock was proposed ten years ago [1, 2]. In this paper, after a simple review, we will mainly present the most recent experimental progresses of active optical frequency standards in Peking University, including 4-level Cesium active optical frequency standards and active Faraday optical frequency standards.

The first part focuses on the 4-level Cesium active optical frequency standards. When Cesium atoms within a FP cavity with a finesse of 4.3, which is at deep bad-cavity regime, are pumped by 455.5 nm and 459.3 nm laser, the stimulated emission radiations at 1469.9 nm from $7S_{1/2}$-$6P_{3/2}$ is realized. The measured threshold, linewidth, cavity-pulling reduction, saturation effect of pumping laser, hyperfine structure effect, etc. will be discussed in detail.

The second part emphases on active Faraday optical frequency standards, including the active Faraday optical frequency standard at good-cavity regime named as ultralong Faraday laser with Rubidium atoms at 780 nm, and active Faraday optical frequency standard at deep bad-cavity regime with Cesium atoms at 852 nm. The Faraday effect of magneto-optical rotation discovered by Michael Faraday in 1845, is applied to realize new-mechanism optical clocks in two different finesse regimes of laser FP cavities.

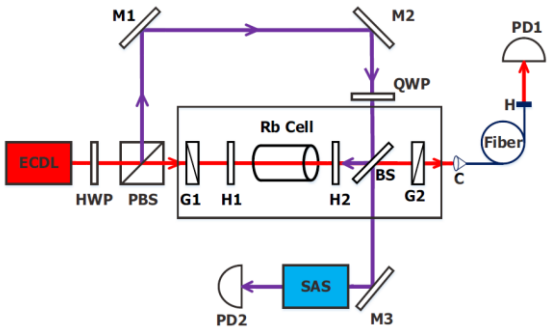


Fig. 1: Experimental setup of ultralong Faraday laser with 800 m fiber external cavity. ECDL: external cavity diode laser, SAS: saturated absorption spectrum, HWP/QWP: half-wave plate, quarter wave plate, BS/PBS: beam splitter, polarizing beam splitter, M1/M2/M3: 780 nm total re flection mirrors, G1/G2: A pair of orthogonally polarized Glan-Taylor prisms, H1/H2: permanent magnets, C: fiber coupler, H: high-reflection mirror coated to fiber, PD1/PD2: photodetec-

At good-cavity regime, the active Faraday optical frequency standard is named as ultralong Faraday laser, based on the Faraday anomalous dispersion atomic filter with ultra-narrow bandwidth of 26 MHz at Rubidium 780 nm transition line and the ultralong fiber extended cavity of 800 m with extremely small free-spectra-range of 0.125 MHz. The stability around (6-9)E-12 has been measured at sampling time from 0.01 s to 1 s. An ultralong Faraday laser with 100 km fiber cavity is undergoing.

The active Faraday optical frequency standard at bad-cavity regime [3], has advantages of much narrowed linewidth and reduced cavity pulling effect. Measured by the optical heterodyne beat between two similar independent active Faraday optical frequency standards, results show the frequency linewidth reaches 281(23) Hz, which is 19000 times smaller than the natural linewidth of the Cesium 852 nm transition line.

[1] J. Chen, X. Chen, "Optical lattice laser," Proceedings, 2005 IEEE Int. Frequency Control Symp., Vancouver, Canada, August 29-31, 2005, pp. 608-610.
[2] J. Chen, "Active optical clock", Chin. Sci. Bull., vol.54(3), pp. 348-352, 2009. http://arxiv.org/abs/physics/051209.
[3] W. Zhuang, J. Chen, "Active Faraday optical frequency standard," Opt Lett, vol. 39, no. 21, pp. 6339-6342, 2014.

Laser frequency stabilization based on steady-state spectral-hole burning in $Eu^{3+}:Y_2SiO_5$*

Cook, Shon, Rosenband, Till, and Leibrandt, David
National Institute of Standards and Technology, Boulder, CO, USA
E-mail: shon.cook@nist.gov

Frequency stable laser local oscillators (LLOs) are key tools in the field of metrology. Applications of such LLOs include tests of general relativity, searches for variation of fundamental constants, relativistic geodesy, and optical atomic clocks. The best lasers to date are stabilized to Fabry- Pérot reference cavities, and their stability is intrinsically limited by thermomechanical length fluctuations of the cavity.

Spectral holes in cryogenically cooled $Eu^{3+}:Y_2SiO_5$ are a promising alternative to the use of a mechanical frequency reference for laser frequency stabilization. At 4 K, this material supports spectral holes at 580 nm with linewidths as narrow as 122 Hz and lifetimes of 10^6 s. The frequency shifts due to fluctuations in the magnetic and electric fields, temperature, pressure, optical probe power, and acceleration are all small enough to allow laser frequency stability at the 10^{-17} fractional frequency level [1, 2]. However, prior laser frequency stabilization experiments with $Eu^{3+}:Y_2SiO_5$ have been limited to run times of a few thousand seconds due to degradation of the spectral holes caused by the probe laser [3].

In this work, we demonstrate laser frequency stabilization to a steady-state pattern of spectral holes in $Eu^{3+}:Y_2SiO_5$. This pattern consists of three sets of spectral holes spaced in frequency by 42.6 MHz and 36.4 MHz, corresponding to the ground-state hyperfine splittings of $^{151}Eu^{3+}$. The Eu^{3+} population reaches steady-state as the spectral holes are burned, and additional interleaved probing does not modify the absorption spectrum. Using this spectral-hole pattern, laser frequency stabilization experiments can run indefinitely. We measure the frequency stability of a laser locked to such a steady-state spectral hole pattern relative to an independent cavity-stabilized laser and a Yb optical lattice clock, demonstrating a spectral-hole stability of $1.0\times10^{-15}\ \tau^{-1/2}$ for $0.01\text{ s} < \tau < 20$ s, which averages to 8.5×10^{-17} at $\tau = 73$ s.

[1] M. J. Thorpe, L. Rippe, T. M. Fortier, M. S. Kirchner, and T. Rosenband, "Frequency stabilization to 6×10-^{16} via spectral-hole burning," Nature Photonics 5, 688 (2011).

[2] M. J. Thorpe, D. R. Leibrandt, and T. Rosenband, "Shifts of optical frequency references based on spectral-hole burning in $Eu^{3+}:Y_2SiO_5$," New Journal of Physics 15, 033006 (2013).

[3] D. R. Leibrandt, M. J. Thorpe, C.-W. Chou, T. M. Fortier, S. A. Diddams, and T. Rosenband, "Absolute and relative stability of an optical frequency reference based on spectral hole burning in $Eu^{3+}:Y_2SiO_5$,"Physical Review Letters 111, 237402 (2013).

* This work is supported by ONR, AFOSR, and DARPA.

Precision isotope shift measurements of Ca^+ ions using photon recoil spectroscopy

Gebert, F., Wan, Y., Wolf, F., Berengut, J.*, Schmidt, P.O.
QUEST Institut, Physikalisch-Technische Bundesanstalt, Braunschweig, Germany and
Institut für Quantenoptik, Leibniz Universität Hannover, Hannover, Germany
*School of Physics, University of New South Wales, Sidney, Australia
E-mail: Piet.Schmidt@quantummetrology.de

Precision laser spectroscopy of trapped atoms typically comes in two flavors: Laser induced fluorescence of short-lived excited states and laser excitation of long-lived states followed by internal state detection via electron shelving. We present a novel spectroscopy technique combining the high detection efficiency of the electron shelving technique with background-free spectroscopy of short-lived excited states. This is accomplished by detecting photon recoil during laser induced fluorescence of a single ion through a co-trapped ion, which also provides sympathetic laser cooling. Starting from the ground state of motion of a common motional mode [1], photon recoil from probing the spectroscopy transition results in motional excitation of the two-ion crystal, which is detected through a motional sideband transition on the cooling ion. Spectroscopy pulses are synchronized with the motion of the ions in the trap to enhance the sensitivity through resonant driving while reducing systematic frequency shifts of the technique. This way, we are able to detect the scattering of around 10 photons with a SNR of 1 on the $^2S_{1/2}$-$^2P_{1/2}$ Ca^+ spectroscopy transition using Mg^+ as the cooling ion [2]. In an extension of the technique, we were able to obtain single-photon detection efficiency as required for spectroscopy of the non-closed $^2D_{3/2}$-$^2P_{1/2}$ transition in Ca^+. Excitation of this transition results in dominant decay to the $^2S_{1/2}$ state. We then use resonant driving of the $^2S_{1/2}$-$^2P_{1/2}$ transition for motional excitation, thus amplifying the signal from a single absorbed photon. Using these two photon recoil spectroscopy (PRS) schemes, we performed absolute frequency measurements of the $^2S_{1/2}$-$^2P_{1/2}$ and $^2D_{3/2}$-$^2P_{1/2}$ transitions for the isotopes 40, 42, 44, 48 of Ca^+ with accuracy below 100 kHz. A multi-dimensional King's plot analysis provides significantly improved relative field and mass shift constants together with nuclear charge radii. This system can serve as a benchmark for atomic structure and nuclear calculations of complex atomic systems. PRS can be seen as an extension of the quantum logic spectroscopy technique used for optical clocks [3] to short-lived excited states. Future applications include spectroscopy of rare isotopes and atoms or molecules with a complex level structure that do not possess closed cycling transitions. In particular, isotope shifts of metal ions relevant for astronomical searches of a possible variation of the fine-structure constant [4] could be measured with unprecedented precision.

References:

[1] B. Hemmerling, F. Gebert, Y. Wan, D. Nigg, I. V. Sherstov, and P. O. Schmidt, *A Single Laser System for Ground State Cooling of $^{25}Mg^+$*, Appl. Phys. B **104**, 583–590 (2011).

[2] Y. Wan, F. Gebert, J. B. Wübbena, N. Scharnhorst, S. Amairi, I. D. Leroux, B. Hemmerling, N. Lörch, K. Hammerer, and P. O. Schmidt, *Precision spectroscopy by photon-recoil signal amplification*, Nat Commun **5**, 4096 (2014).

[3] P. O. Schmidt, T. Rosenband, C. Langer, W. M. Itano, J. C. Bergquist, and D. J. Wineland, *Spectroscopy Using Quantum Logic*, Science **309**, 749–752 (2005).

[4] M. T. Murphy and J. C. Berengut, *Laboratory atomic transition data for precise optical quasar absorption spectroscopy*, MNRAS **438**, 388–411 (2014).

Precise Cascade Synchronization of Two Digitally Tuned Space Clocks to UTC (GPS)

Wang, H. and Iyanu, G. H.
The Aerospace Corporation, El Segundo, California/USA
E-mail: he.wang@aero.org

A satellite constellation usually has multiple time and frequency reference clocks on orbits. Some satellites may carry atomic clocks while others have crystal oscillator clocks on board. For applications such as satellite communication networks, all on-orbit clocks in the constellation are required to be precisely synchronized to UTC through the reference clocks in the ground control system. In order to efficiently synchronize all on-orbit clocks, the satellite timekeeping system could be designed such that the ground control only manages one on-orbit clock, the constellation Master clock, to which all other on-orbit clocks are synchronized through the constellation crosslink. Such a cascade timekeeping architecture is particularly useful if the satellite system has crystal oscillator clocks on board. In general a crystal oscillator clock has poorer long term frequency stability than an atomic clock and is more sensitive to space environmental effects. Therefore it is important to know how well a crystal oscillator clock can be slaved to a Master atomic clock through satellite crosslink, and how well the Master clock can be synchronized to the ground reference clock through ground to satellite link.

In order to answer those questions, we have constructed a unique hardware-software spacecraft atomic clock flight simulation and test station at The Aerospace Corporation, which is capable of simulating and studying the algorithms and synchronization performance of a multiple-clock timekeeping system. Briefly, our test station has two subsystems: one simulates the space segment and the other simulates the function of the ground control segment of a satellite system. The simulated space segment has two flight model rubidium master oscillators (RMO) housed in a vacuum chamber. A computer (PC1) operates as the on-board computer of the satellite system. A second computer (PC2) and a Cs reference clock (Symmetricom 4065C/075) form the simulated ground control system. Our Cs clock is calibrated against a GPS receiver. In our experiment, we assign one RMO as the Master atomic clock and set the second RMO to operate in its crystal master oscillator (XMO) mode as a Slave clock. The phase differences between the slave and master clocks and the master and Cs reference clock are measured simultaneously by a multiple clock phase counter, and the data are processed in real-time by the simulated 'space" and "ground" computers PC1 and PC2, respectively. Once the accumulated time offset of the slave clock relative to the master clock passes a pre-set time-offset threshold, PC1 will estimate the frequency offset of the slave clock using a real-time linear regression algorithm and send a frequency correction command to the slave clock to syntonize its frequency with the master clock. At the same time, the slave clock's time is reset. Similarly, PC2 independently synchronizes the master clock to the Cs reference clock. Thus, in a cascaded way both space clocks are precisely synchronized to UTC (GPS).

In this paper we first describe our hardware-software timekeeping simulation testbed and present a real-time linear regression clock synchronization algorithm. Then we report the results of a three-clock, cascade synchronization experiment, in which a crystal oscillator clock (XMO) is synchronized to an Rb atomic clock (RMO) while the RMO is independently synchronized to a Cs reference clock. With this cascade timekeeping scheme, we are able to precisely synchronize the two digitally-tuned space clocks with the Cs clock to an averaged residual frequency offset of 5×10^{-13} (or 2.5 μHz for a nominal clock frequency of 5 MHz). As a result of the precise cascade synchronization, the two space clocks' long-term frequency drift rates have significantly reduced to 1.7×10^{-14} per day and 2.5×10^{-13} per day for the RMO clock and the XMO clock, respectively. Furthermore, we demonstrate that the real-time linear regression algorithm is able to efficiently detect and mitigate large frequency jumps of the crystal oscillator clock caused by temperature variations.

Robust Clock Ensemble for Time and Frequency Reference System

Qinghua Wang, Fabien Droz, Pascal Rochat
Orolia Switzerland Inc. (Spectratime), Neuchâtel, Switzerland
E-mail: qinghua@spectratime.com

A novel concept of a robust clock ensemble for the Time and Frequency Reference System was proposed by Spectratime (SpT) in 2009. Over the last years SpT has conducted studies on the feasibility of hardware and algorithm approaches. With minimum three clocks powered, all clocks are kept in phase and frequency via the steering loop. The system performs corrections on the master clock in function of weighted averaging of clocks named as ONe CLock Ensemble (ONCLE). A simple approach of the real-time Clock Fault Detection and Compensation (CFDC) based on low-pass recursive filters is implemented. This allows reliable detection of the clock feared events (including clock hard failure, phase jump, frequency jump and white frequency noise level increase), as well as jump correction, failed clock removal, healthy clock inclusion, and clock switchover. This clock ensemble generates a frequency output signal with improved robustness and performances.

The feasibility concept has been demonstrated under the European GNSS Evolutions Program. SpT with the support of GMV has developed an Elegant Breadboard of the Robust On-board Frequency Reference Subsystem (FRS) as an improved version of the on-board Clock Monitoring and Control Unit in present Galileo system. The self-standing unit is able to receive and process a number of on-board clock signals (from Rubidium Atomic Frequency Standards or Passive Hydrogen Maser) and generate an output signal with improved availability and robustness. Tested under various clock degradation scenarios, this unit has demonstrated its capability to autonomously detect, correct, isolate and remove (or include) the identified clock with very minor impact on the output signal.

The solution of the robust clock ensemble is proposed for the next generation of Precise Timing Facility (PTF), a key element of the Ground Mission Segment to generate the Galileo System Time (GST). An ensemble of at least three Active Hydrogen Masers (AHM) provides the physical realization of GST with advantages of simple, robust, fully redundant and improved performance. It ensures a fully continuous GST, real-time clock anomaly detection, and automatic correction or switch-over. A mathematic model has been developed to simulate the expected ensemble output versus four AHM inputs. The principal function of Phase-Locked Loop based on Femtostepper, phase comparator and Proportional-Integral filtering controller, functions of ONCLE and CFDC have been established in the model. All functions could be implemented into a small industrial micro-controller or signal processor. The simulation under various test cases has demonstrated its capability to provide a smooth timing output even in presence of clock feared events.

This paper will describe the concept of the robust clock ensemble, and provide verification test results achieved on the FRS. Simulation results with the proposed robust solution for next PTF will also be presented.

Time and Frequency Transfer from an Almost Freely-Falling Satellite

Ashby, Neil, Jefferts, Steven, Patla, Bijunath, Weiss, Marc
National Institute of Standards and Technology, Boulder, CO/USA
E-mail: ashby@boulder.nist.gov

We discuss the metric of general relativity in a falling reference frame that has small non-gravitational accelerations. The Principle of Equivalence implies that in a local, freely falling reference frame of a satellite carrying an atomic clock, the only significant effects arise from tidal terms. However a satellite such as the ISS is not in free fall since it experiences non-gravitational forces. We discuss transformations of the metric tensor between Earth-Centered Inertial Frame, an "almost freely falling" frame, and the rotating Earth-Centered Earth Fixed frame. We approach estimation of errors on an orbiting clock using variations of terms in a classical Lagrangian, showing the conditions under which the clock is insensitive to errors in position and velocity. Applying this approach to constants of the motion of the ISS, with data from the SIGI2 GPS receiver on the ISS, we characterize noise in the GPS measurements of position and velocity and the resulting errors in proper time on the orbiting clock. Contributions to noise on an orbiting clock placed on the ISS appears to be similar to flicker PM. Requirements for precision measurement leading to an improved test of the gravitational part of the total frequency shift of the orbiting clock are discussed.

Impact of correlations on the uncertainties of [UTC-UTC(k)]

Panfilo Gianna, Petit Gérard, Harmegnies Aurélie
BIPM, Sèvres, France
E-mail: gpanfilo@bipm.org

The Time Department of the BIPM is responsible for the calculation and for the publication of the Universal Time Coordinated (UTC). UTC is calculated monthly by averaging about 450 atomic clocks spread all round the word. The results, expressed as the difference between UTC and UTC(k) are published monthly in the official document called Circular T. In particular in the Section 1 the values of UTC-UTC(k) with the respective uncertainties are reported.

The network of UTC time links until now is supported by two independent techniques, the two-way satellite time and frequency transfer (TWSTFT, or shorter, TW) and those based on GNSS observations. Several types of measurements exist for GNSS time transfer, e.g. single frequency code, dual frequency code, dual frequency code and phase for GPS. For the TW in Europe, in North America and in Asia a complete set of redundant measurements is available, but only a non-redundant set of TW links is used for UTC.

The calculation of the uncertainties [1, 2] used in UTC is based on the time link uncertainties and on the atomic clock weights. Until now GNSS data are expressed as time links to a pivot laboratory and are considered uncorrelated. The consequence is that the pivot laboratory has its uncertainty underestimated and the value doesn't correspond to a physical real value.

In this paper we investigate different ways to use time transfer data in order to better use all available data, better account for correlations and in the end better evaluate the uncertainty of [UTC-UTC(k)], expanding on earlier suggestions [3]. A first approach is to consider, instead of GNSS links, the original GNSS data expressed with respect to a reference timescale acting as a virtual pivot to which an uncertainty can be attributed from the metrological point of view. In such a way the current algorithm used for evaluating the uncertainty of [UTC-UTC(k)] remains still valid but the uncertainties of the virtual pivot will effectively introduce correlations. A second approach is to use the complete set of redundant TW links, in which case the system of time links is solved by the least square method where each link is weighted with the corresponding uncertainty.

Tests and simulations for both approaches will be presented and discussed.

[1] W. Lewandowski , D. Matsakis, G. Panfilo, P. Tavella, "The evaluation of uncertainties in [UTC-UTC(k)]", Metrologia, vol. 43, No. 3, pp. 278-286, 2006.

[2] G. Panfilo, "A mathematical model of the atomic clock error",PhD Thesys in Metrology, Politecnico of Torino, Turin, 2005.

[3] G. Petit, Z. Jiang, "Redundancy and correlations in TAI time links", *Proceedings* FCS/PTTI Meeting (Vancouver), pp. 346–349, 2005.

A status report on time scale generation in PTB

Bauch, Andreas, Gomah, Gihan*, Staliuniene, Egle
Physikalisch-Technische Bundesanstalt, 38116 Braunschweig, Germany
*National Institute for Standards, Tersa St. Elharam , Giza, Egypt
E-mail: andreas.bauch@ptb.de

Since February 2010 UTC(PTB) has been realized using an active hydrogen maser as signal source whose frequency is steered via a commercial high resolution offset generator. Steering is based primarily on the comparison between the maser involved and PTB's primary fountain clocks CSF1 and CSF2 [1]. In the long term, UTC(PTB) is steered towards UTC based on the data published in the BIPM Circular T. Between July 2010 and July 2014 the time difference UTC – UTC(PTB) was always less than 9 ns and typically below 5 ns. During that period the maximum absolute rate of UTC-UTC(PTB) during any standard 5-day interval was 0.44 ns/d. In our paper we discuss further properties of UTC(PTB) and of TA(PTB) that is generated in a similar way (but no time steering to an external reference). UTC(PTB) serves as the basis for all of PTB's time services and international time comparisons. It will also serve directly as the time and frequency reference for the future ACES campaign [2], and we are going to describe the signal interface to the future location of the ACES microwave-link ground terminal.

From early on it was foreseen that the steering of UTC(PTB) could also be derived from the ensemble of caesium beam clocks operated in PTB, described as Option 2 in [1]. It turned out that CSF1 and CSF2 provided data with greatest reliability so that this option needed hardly ever be applied, UTC(PTB) practically is a fountain-based time scale. Since several months a timescale generation "test bed" is used to realize another time scale, named UTT(PTB), based on the inputs of five thermal beam clocks. Contrary to the expectations, a considerable difference between UTC(PTB) and UTT(PTB) was noted and motivated a study into the causes thereof. The steering commanded to the UTT(PTB) phase stepper consists of two clock specific summands and a common term, $\delta f_{\mathrm{Steer}} = w_{\mathrm{i}}\{\delta f_{\mathrm{Clock}}(\mathrm{i}) + \delta f_{\mathrm{Rate}}(\mathrm{i})\} + \delta f_{\mathrm{Offset}}$. The term $\delta f_{\mathrm{Clock}}(\mathrm{i})$ is the predicted frequency offset of clock(i) from the maser used to generate UTT(PTB) for the current day, based on 16 or 25 days averaging, depending on the clock type. $\delta f_{\mathrm{Rate}}(\mathrm{i})$ is the rate of clock(i) with respect to TAI, and the weight w_{i} (weights normalized to 1) has been calculated based on the weights of the clocks in the ALGOS process, both quantities published monthly by BIPM. $\delta f_{\mathrm{Offset}}$ has been determined so that a time offset UTT(PTB)-UTCr that appears at the end of a week is steered to zero within 20 days.

Our analysis based on a few months of data showed that the averaging times mentioned should be changed, and in particular that the statistical weights published by BIPM deviate substantially from values that one would generate autonomously based on the instability of the clock frequency prediction. The findings will be explained in details. Starting January 2015, UTT(PTB) will be generated using the new strategy, and first results will be available at the time of the conference.

Acknowledgment

G.G. gratefully acknowledges the support of the Egyptian Government funding her stage at PTB. The quality of the PTB time scales is highly dependent on the team operating the fountain clocks and the team managing the daily operations of the hardware and software involved, and the authors are grateful for their support.

[1] A. Bauch, S. Weyers, D. Piester, E Staliuniene and W. Yang, "Generation of UTC(PTB) as a fountain-clock based time scale," Metrologia 49 (2012) 180–188 doi:10.1088/0026-1394/49/3/180.

[2] L. Cacciapuoti and Ch. Salomon, "Atomic Clock Ensemble in Space", Journal of Physics: Conference Series 327 (2011) 012049.

Makkah Time Scale Generation and Measurement Capability

Yaseen M. Almleaky, Alaa Almleaky, Hamza Almleaky, Samy Khadem-Al-Charieh
King Abdullah Centre for Crescent Observation and Astronomy (KACCOA)
Makkah Time Center, Makkah, Saudi Arabia
E-mail: yaseen.almleaky@kaccolr.org

In this work we will present Makkah time scale generation and traceability with a type A uncertainty 1 ns and Type B uncertainty 7.3 ns using 11 Cs atomic clocks and calibrated TTS-4 GNSS receiver. GNSS signal detected by antenna and passed through 5 m cable with lighting arrestor, 85 m low noise cable, amplifier, last 5 m low noise cable and received by TTS-4 receiver (Fig.1). Reference Cs clock (Cs-1) was steered with an uncertainty better than $1x10^{-14}$. Reference Cs-1 clock and other 4 clocks (Cs-2 – Cs-5) are located in same laboratory and other 6 clocks (Cs-6 – Cs-11) was located in the another laboratory with temperature controlling better than 0.2^{o}C. Time difference between reference Cs-1 clocks and other 6 clocks is measured through fiber cable with a length of 200 m and Timetech counter. Time difference between reference Cs-1 clock other 4 Cs clocks (Cs-2 – Cs-5) which is measured in a same time by 2 computer controlled SRS-620 and Timetech counters. All cables used in time interval measurements were specially prepared and cable delay is measured with uncertainty less than 100 ps. For evaluation of uncertainty in time interval measurements we have compare results with 2 different counters and investigate influence of counter parameters to time difference measurements. Comparison of 2 Cs clocks in a same time interval using 2 different counters and also using GPS common view method including similar GNSS receiver is in a progress. Additionally, comparison of time interval and cable delay measurement using different counters and 50 GHz oscilloscope which is calibrated by femtosecond laser pulses also in scope of our activity.

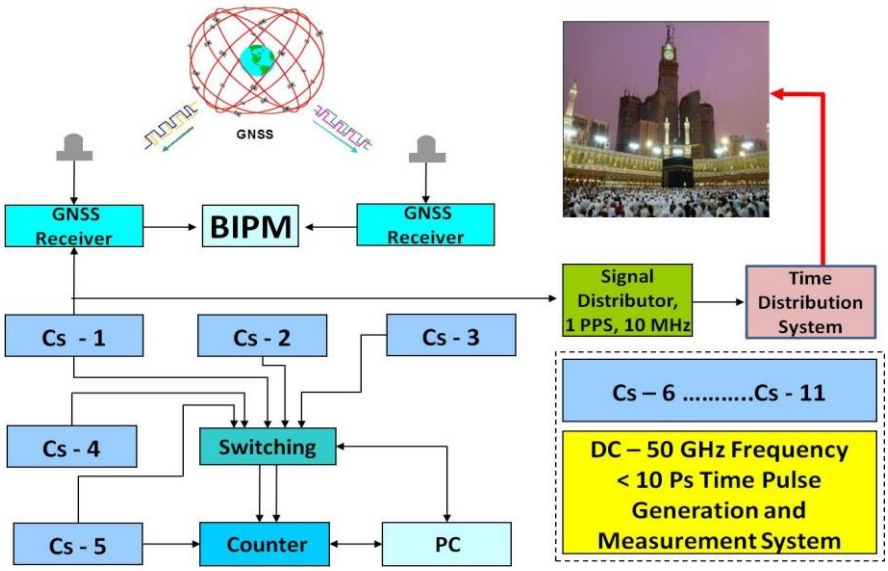


Fig. 1: Block diagram of time and frequency system of Makkah Time Center

Traceable time information disseminated trough NTP server with an uncertainty < 5 ms in a LAN. This dissimilated reference time used for synchronization of main Makkah tower clock with a size of 50 m trough step motors.

Finally we will present our planned research and development activity including generation and measurement capability at frequency range DC- 50 GHz, phase noise measurements, 200 fs – 2 ps pulse generation and measurement system, development of optical clocks based on fiber lasers.

Wideband Ladder Filters Fully Covering Digital TV Band based on Shear Horizontal Plate Wave

Michio Kadota and Shuji Tanaka
Graduate School of Engineering, Tohoku University, Sendai, Miyagi, Japan
E-mail: mkadota@mems.mech.tohoku.ac.jp

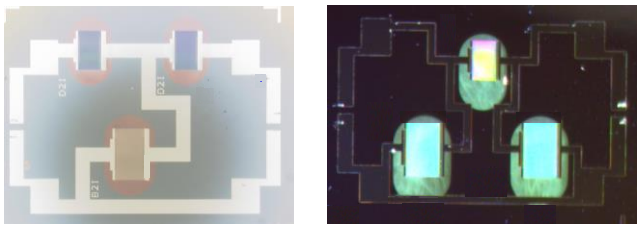
Currently, the wide spread of smartphones and other mobile terminals has led to the depletion of available frequencies. To address this problem, cognitive radio technology using a vacant frequency band of digital TV channels (TV white space), which is standardized as IEEE 802.11af, is receiving a lot of attention [1]. A key device in a cognitive radio terminal is the tunable acoustic wave filter which can largely change the center frequency and bandwidth to select an available TV white space. The authors developed a monolithic bandwidth-tunable SAW filter with BST varactors [2, 3], but the fractional tuning range is limited to ten-odd % by this type of configuration [4].

A wider tuning range can be realized by restricting a wide passband using band rejection filters [5]. For TV white space cognitive radio application, therefore, a bandpass filter fully covering the digital TV band (470-710 MHz in Japan) is primarily needed. The authors presented 0-th mode shear horizontal (SH_0) plate wave resonators with large electromechanical coupling factor in an ultrathin 30ºYX-$LiNbO_3$ plate, and numerically synthesized a wideband filter covering the digital TV band based on the measured frequency characteristics of the resonators [5]. In this study, T-type and π-type ladder filters using SH_0 plate wave were fabricated, and the full coverage of the digital TV band was first demonstrated.

The T-type and π-type ladder filters are composed of three SH_0 resonators, and fabricated in a 30ºYX-$LiNbO_3$ plate of 0.61 μm thickness supported with a Si substrate, as shown in Fig. 1. The wavelength ratio (WR) of the series/parallel resonators is 1.32 to 1.47 for T-type and 1.32 for π-type. Fig. 2 shows the frequency characteristics of the T-type ladder filter with a WR of 1.47 and the π-type one with a WR of 1.39. The bandwidth at 6 dB attenuation is 51% and 45% for the T-type and π-type ladder filter, respectively. The bandwidth can be adjusted by WR, and 45% is enough to fully cover the digital TV band, even if some margin is considered for temperature compensation. The insertion loss is as low as 0.8 to 1.8 dB. Passband ripples due to transverse mode are observed, but they can be suppressed using an apodized IDT, as demonstrated in [4].

References

[1]H. Harada, IEICE Tech. Rep., vol. J91-B, no. 11, 2008, pp. 1320-1331.
[2]H. Hirano *et al.*, Proc. IEEE Ultrason. Symp., 2014, pp. 803-806.
[3]T. Kimura *et al.*, Proc. IEEE Ultrason. Symp., 2014, pp. 795-798.
[4]M. Kadota *et al.*, IEEE Trans. Ultrason. Ferroelec. Freq. Contr., vol. 60, no. 10, pp. 2129-2136, 2013.
[5]M. Kadota *et al.*, Proc. IEEE Ultrason Symp., 2014, pp. 2031-2034.



(a) (b)

Fig. 1 (a) T-type and (b) π-type ladder filters.

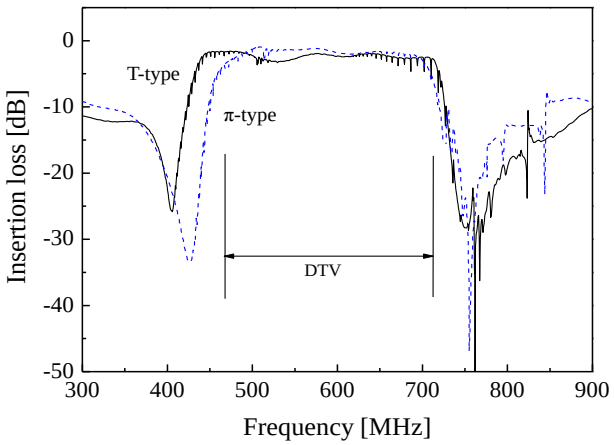


Fig. 2 Frequency characteristics of (a) T-type and (b) π-type ladder filters.

Enhancement of Effective Electromechanical Coupling Factor by Mass Loading in Layered SAW Device Structures

Gongbin Tang[1,2], Tao Han[1], Akihiko Teshigahara[3], Takao Iwaki[3], and Ken-ya Hashimoto[2]
[1]Department of Electronic Information and Electrical Engineering, Shanghai Jiao Tong University, Shanghai 200240, China
[2]Graduate School of Engineering, Chiba University, 1-33 Yayoi-cho, Inage-ku, Chiba, Chiba 263-8522, Japan,
[3]Research Laboratories, DENSO CORPORATION, 500-1 Minamiyama, Komenoki, Nisshin, Aichi 470-0111, Japan
E-mail: gongbin.tang@chiba-u.jp

Nowadays, ScAlN thin films are paid much attention for their extraordinary strong piezoelectricity among paraelectric materials. The authors reported that large SAW velocity, small attenuation with propagation, and large effective electromechanical coupling factor (K_e^2) are simultaneously achievable when the film is combined with a high velocity base substrate such as single crystal diamond (SCD) and SiC.

This paper describes drastic enhancement of K_e^2 by mass loading in layered SAW device structures such as the ScAlN film/single crystal diamond (SCD) substrate. It is shown that this phenomenon is obvious even when an amorphous SiO_2 film is deposited uniformly on the top surface for temperature compensation. This enhancement is caused by SAW energy confinement to the top surface of the ScAlN layer where the IDT is placed. This means this phenomenon does not occur when the IDT is placed in another interface.

Here we choose SAW properties on a structure composed of SiO_2 overlay/Cu IDT/piezoelectric $Sc_{0.43}Al_{0.57}N$ film/SCD base substrate for the discussion. Resonance and anti-resonance frequencies, f_r and f_a, respectively, of the second mode (Sezawa mode) were calculated for the structure and then K_e^2 was estimated by the relation of $K_e^2 = (\pi f_r / 2f_a)\cot(\pi f_r / 2f_a)$.

Fig. 1 shows variation of K_e^2 with the ScAlN and Cu thicknesses, h_{ScAlN} and h_{Cu}, respectively, when the SiO_2 thickness h_{SiO2} is zero. In the figure, λ is the SAW wavelength. When h_{ScAlN}~0.8λ and h_{Cu}~0.11λ, K_e^2 takes a maximum of 9.9%. This value is significantly larger than the value of 5.9% achievable when h_{Cu}=0. Although required electrode thickness changes with the employed electrode material, the maximum K_e^2 is mostly unchanged.

Fig. 2 shows variation of K_e^2 with h_{SiO2} when h_{ScAlN} is fixed at 0.8λ. In this analysis, we assume that the SiO_2 film covers not only one the electrodes but also the gap between electrodes uniformly (See the inset in Fig. 2). It is seen that the maximum K_e^2 of 8.1% is achievable when both h_{SiO2} and h_{Cu} are set properly. The maximum K_e^2 is scarcely dependent on h_{Cu}, and h_{SiO2} giving the maximum value becomes small with an increase in h_{Cu}. This is because the K_e^2 enhancement is mainly caused by the mass loading. The maximum K_e^2 for this case is a little lower than that the value of 9.9% achievable when h_{SiO2}=0 owing to increased static capacitance of the IDT.

This K_e^2 enhancement is also found when other electrode and/or substrate materials are employed. For example, the SiO_2/Cu/ScAlN/Si structure offers almost the same maximum K_e^2 with the SiO_2/Cu/ScAlN/SCD structure although the SAW velocity for the former case (~5,000 m/s) is somewhat smaller than the latter case (~5,600 m/s).

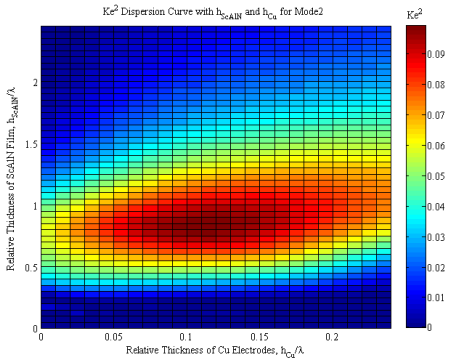


Fig. 1 Variation of K_e^2 with h_{Cu}/λ and h_{ScAlN}/λ at h_{SiO2}=0

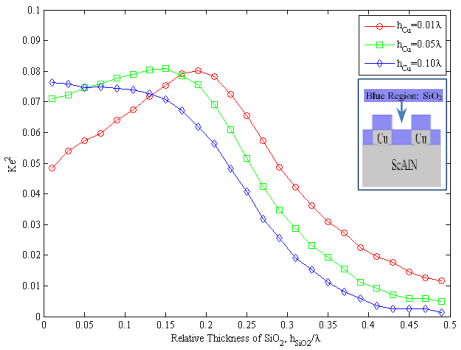


Fig. 2 Change of K_e^2 with h_{SiO2}/λ when h_{ScAlN}=0.6λ

Second Order Temperature Compensated Piezoelectrically Driven 23 MHz Heavily Doped Silicon Resonators with ±15 ppm Temperature Stability

Antti Jaakkola, Panu Pekko, James Dekker, Mika Prunnila, Tuomas Pensala
VTT Technical Research Centre of Finland, Espoo, Finland
E-mail: antti.jaakkola@vtt.fi

We report quartz level temperature stability of a silicon MEMS resonator. A frequency variation of less than ±15 ppm is measured for a 23 MHz extensional mode resonator over a temperature range of T= -40 … +85°C. The temperature compensation mechanism is entirely passive, relying on the tailored elastic properties of heavily doped silicon with a doping level of $n > 10^{20}\text{cm}^{-3}$, and on an optimized resonator geometry.

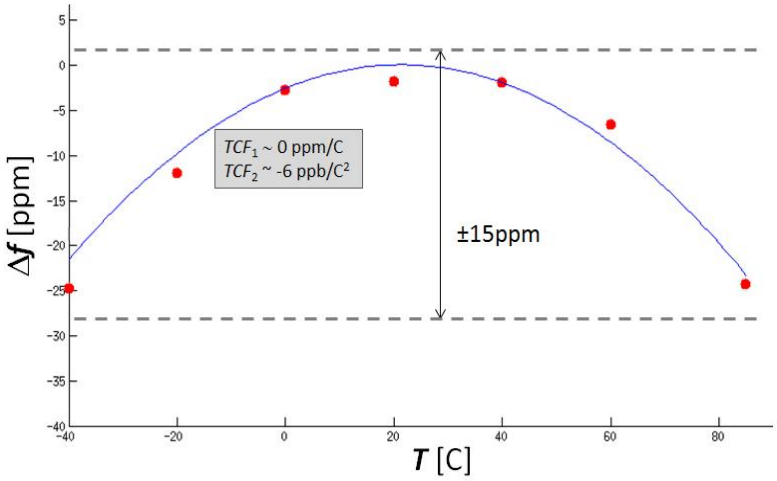


Fig. 1: Frequency-vs-temperature curve of a temperature compensated 23 MHz extensional mode resonator.

The resonators are piezoelectrically driven with a sputtered 0.5 µm thick AlN film between the aluminum top electrode and the silicon resonator body. The bulk of the resonator is formed of silicon, the temperature dependency and thickness of which are made such that the linear and quadratic temperature dependency contribution from the AlN and aluminum thin films are canceled out. Recent studies have shown that silicon elastic properties can be controlled by using very high doping levels [1]. The resonator f-vs-T curves (Fig. 1) were measured on wafer level in atmospheric pressure by measuring their frequency response with an impedance analyzer. Resonator performance parameters were: R_m~100 Ω, C_0~11 pF, Q~4000, f_p-f_s~750 ppm, and k^2~0.15%. Further optimization of the design will enable increasing the quality factor and reduction of C_0 to such a level that the resonator can be driven with a standard oscillator IC intended for quartz crystals.

The result greatly improves the competitiveness of silicon based resonator technology in timing and frequency reference applications, and presents an attractive alternative to current silicon MEMS approaches using active (PLL-based) temperature compensation.

[1] A. Jaakkola, M. Prunnila, T. Pensala, J. Dekker, P. Pekko, "*Determination of Doping and Temperature Dependent Elastic Constants of Degenerately Doped Silicon from MEMS Resonators*", IEEE Transactions on Ultrasonics Ferroelectrics and Frequency Vol. 61, No. 7, pp. 1063-1074, 2014.

Highly Tuneable X-Band Bragg Resonator- Initial Results

Pratik D Deshpande, Simon Bale, Mark Hough and Jeremy Everard
Department of Electronics, University of York, Heslington, York, YO10 5DD, United Kingdom
E-mail: pd617@york.ac.uk

Summary: This paper describes the design and measurement of a broad tuning aperiodic Bragg resonator at X-band. The resonator utilizes an aperiodic arrangement of non $(\lambda_g/4)$ low loss alumina plates (ε_r=9.75, loss tangent of ~2×10^{-5}) mounted in a cylindrical metal waveguide.

The initial results demonstrate a spurious free tuning range of 100MHz. The insertion loss, S_{21}, varies from -5.6dB to -4dB while the unloaded Q varies from 40,000 to 60,000 over the tuning range. (The loaded Q varied from 20,000 to 23,000).

However it is possible to tune over a range of 400MHz with similar unloaded Qs up to 64,000, but on occasion the required TE_{011} mode passes through several low Q modes which degrades the unloaded Q.

Introduction: Broad tuning ultra-high Q cavities enable versatile ultra-low phase noise tunable oscillators offering broadband electromechanical course tuning and electronic fine tuning. These could achieve noise floors below −200dBc at X band. Fixed frequency alumina based aperiodic cylindrical Bragg resonators, developed by this group, show unloaded Qs exceeding 200,000 with some sapphire structures demonstrating unloaded Qs exceeding 500,000. The reflectivity of Bragg type reflectors can offer very low loss high reflectivity over a broad frequency range exceeding 10% of the centre frequency. Significant tuning can therefore be achieved simply by changing the length of the center section. Changing this length using concentric cylinders has not been possible without energy loss from the wanted high Q mode. Further, to achieve low insertion loss the probes (or probe for a one port) have to be in the correct position in the cavity.

Design: The initial prototype of the resonator is shown in the Fig. 1. A cylindrical enclosure was chosen because it offers a simple mechanical construction. The dielectric plates and air waveguide dimensions were optimized to achieve maximum quality factor by redistributing the energy loss within the cavity. Simulations were performed using ABCD waveguide matrices and in house field solvers. The central section comprises two bellows and a solid middle section for the probes. The bellows are copper sheets with etched solder release rings in order to control the position of the solder. Different temperature solders (highest first) are used during assembly to ensure the structure does not disintegrate during assembly. The length and the orientation of the probes were optimized in order to maximise the quality factor. Finally, Micrometers were used to tune the length of the central section. The insertion loss and the loaded Q were measured on a network analyser and change in the frequency was noted. The highest unloaded Q obtained was 64,000.

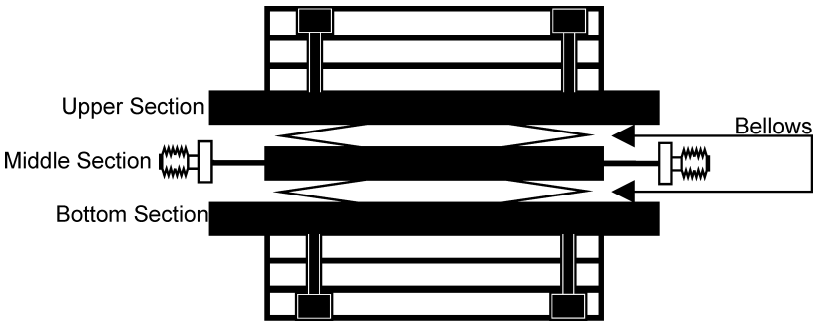


Fig. 1: Side view of a 6 plate tuneable aperiodic Bragg resonator

Discussion: The unloaded Q is significantly lower than the numerical simulation results (215,000). This may be due to conductor losses in and around the bellows including losses in the solder as well as leakage and mode conversion due to the discontinuities in the structure. Further improvements in Q and unwanted mode suppression are under investigation.

Acknowledgement: We wish to thank Mr. John Clapham for his help in the construction of the main cavity.

2015 Joint IFCS-EFTF; Abstract for Submission

The effect of contour concentricity on the acceleration sensitivity of quartz crystal resonators

Morley, Peter E.
Vectron International, 4914 Gray Road, Cincinnati, OH 45232, USA
E-mail: pmorley@vectron.com

Optimization of the acceleration sensitivity of quartz crystal resonators has been a challenging problem for resonator designers for decades. The structural symmetry of the resonator and mount combination has been shown in past work, both theoretical and practical, to have a strong influence on acceleration sensitivity, and specialized structures have been developed [1,2] that have greatly improved performance. However, especially with applications such as airborne radar systems, there is a persistent demand for further improvement.

The design of many of the practical high-stability resonator products that have a need for good acceleration sensitivity is also constrained by other attributes, such as high quality factor, and these constraints typically result in a fully contoured resonator element design. In this paper, the effect in contoured resonators of the concentricity of the contour shape on the quartz disk is considered, and results are presented that demonstrate a strong correlation between the contour offset from the blank center and the acceleration sensitivity of the resonator. Methods are also described for measurement of the contour position relative to the disk edge.

[1] R.B. Haskell, P.E. Morley, and D.S. Stevens, “High Q, Precision SC Resonators with Low Acceleration Sensitivity”, *Proceedings*, 2002 IEEE Int. Frequency Control Symp., New Orleans, Louisiana, USA, May 29-31, 2002, pp. 111-118.

[2] R.B. Haskell, J.E. Buchanan, P.E. Morley, M.A Esmiol, M.E. Martin and D.S. Stevens, “State-of-the-Art in Design and Manufacture of Low Acceleration Sensitivity Resonators”, *Proceedings*, 2004 IEEE Int. Frequency Control Symp., Montréal, Canada, Aug 23-27, 2004, pp. 672-677.

Resonant Cold-Switching Test for 3-Terminal CMOS-NEM Relays using Nonlinear Capacitive Transduction

Riverola, Martín, Vidal-Álvarez, Gabriel, Sobreviela, Guillermo, Uranga, Arantxa, Torres, Francesc, and Barniol, Núria
Department of Electronic Engineering, Universitat Autònoma de Barcelona, Cerdanyola del Vallès, Spain
E-mail: martin.riverola@uab.es

In this paper, a 3-terminal NEMS relay integrated monolithically in the back end of line of a standard CMOS technology [1] is driven into contact due to a sinusoidal signal of frequency similar to the resonance of the movable structure, commonly known as tapping mode. A SEM image of the switching device is shown in Fig. 1. This approach has been recently applied to the M/NEM relay field [2]. There, the dynamical tapping mode phenomenology of silicon carbide relays under cold-switching conditions is measured by using a complex optical interferometry system. However, they do not report any result related to the evolution of the on-state contact resistance. Furthermore, an impacting micromechanical switch known as "resoswitch" exploits such contact dynamic phenomenon for implementing switched power amplifiers and converters [3]. In this case, the actuation and detection is performed electrically under linear operation conditions. In our case, we present a fully electrical resonant cold-switching test for assessing the lifetime of a switching device under nonlinear conditions based on the capacitive detection of its tapping mode.

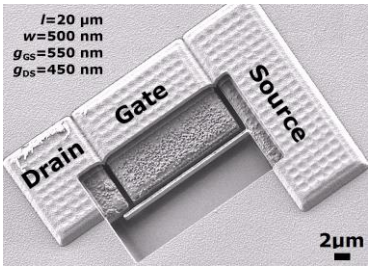


Fig. 1: Top view SEM image of a released relay of length 20 µm.

Increasing significantly the driving power, the amplitude vibration of the cantilever is large enough to impact against the drain electrode. In this way, the measured frequency response shows a flattened plateau for a defined frequency region as depicted in Fig. 2. Note that the phenomenon takes place separately for both frequency sweep up and down responses (Fig. 2(a) and 2(b) respectively). In order to study the intrinsic lifetime of the presented switch, we drive the cantilever for 16,000 seconds (which is more than 4 hours) setting the applied power to 5 dBm and the driving frequency to 738 kHz, biasing the device to 25 V. In this way, the switch operates more than 10 billion (10^{10}) of cycles in tapping mode (1.35 µs per cycle for more than 4 hours of test) without failure as reveal the I-V curves showed in Fig. 3 taken at the beginning of the cold-switching test, after 8,000 seconds and in the end of the test. This test reveals that the tungsten relay has a consistent and repetitive pull-in voltage and shows a decrease in the contact resistance up to 735 MΩ from an initial value of 2 GΩ, possibly due to the surface oxide removal by the tapping of the cantilever tip on the drain or contact electrode.

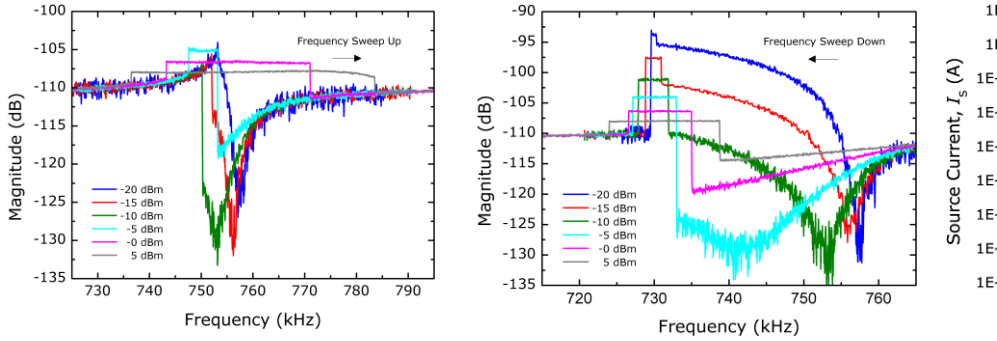


Fig. 2: Magnitude of experimental electrical frequency responses of the tungsten cantilever sensed capacitively reaching the flattened plateau which is sign that the cantilever is operating in tapping mode. The phenomenon takes place separately for the frequency sweeps up (left) and down (right). The bias voltage V_G is fixed at 25 V during the entire experiment.

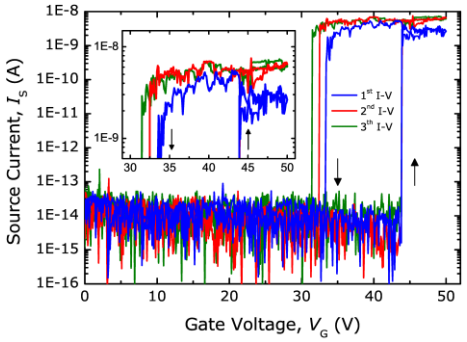


Fig. 3: I-V curves (setting the drain voltage at 5 V) taken at the beginning (1st), in the middle (2nd) and in the end (3th) of the resonant cold-switching test.

[1] M. Riverola, G. Vidal-Alvarez, F. Torres and N. Barniol, "CMOS-NEM Relay based on Tungsten VIA Layer", in *Proc. IEEE Sensors*, Valencia, Spain, Nov. 2014, pp. 162-165.

[2] T. He, J. Lee, Z. Wang and Philip X.-L. Feng, "Interrogating Contact-Mode Silicon Carbide (SiC) Nanoelectromechanical Switching Dynamics by Ultrasensitive Laser Interferometry", in *Proc. IEEE 27th Int. Conf. MEMS*, San Francisco, CA, Jan. 2014, pp. 1079-1082.

[3] Y. Lin, W.-C. Li, Z. Ren and Clark T.-C. Nguyen, "A Resonance Dynamical Approach to Faster, More Reliable Micromechanical Switches", in *Proc. IEEE Int. Frequency Control Symp.*, Honolulu, Hawaii, May 2008, pp. 640-645.

Anchor Loss Suppression using Butterfly-Shaped Plates for AlN Lamb Wave Resonators

Jie Zou[1], Chih-Ming Lin[2], and Albert P. Pisano[1,3]

[1]Department of Mechanical Engineering, University of California, Berkeley, CA 94720, USA
[2]Silicon Laboratories, Inc., Sunnyvale, CA 94085, USA
[3]Department of Mechanical and Aerospace Engineering and Department of Electrical and Computer Engineering, University of California, San Diego, CA 92093, USA

Email: jiezou@berkeley.edu

Aluminum nitride (AlN) Lamb wave resonators (LWRs) have attracted much interests since they have high frequencies, low motional impedances (R_m), and capability of multiple frequencies on a single chip. However, the AlN LWR usually shows a quality factor (Q) below 2000 so an improvement in the Q of the AlN LWRs is highly desirable. There is growing evidence that a large portion of mechanical energy dissipation via the support tether of the LWR, and one effective way of reducing the anchor loss is to design the resonator geometry itself to concentrate the acoustic energy far from the supporting area. To effectively reduce anchor loss and without scarifying the other performance, for the first time, a novel AlN Lamb wave resonator utilizing a butterfly-shaped thin plate is investigated to enhance the Q in this work.

Three different designs of AlN LWRs are designed and compared in this work, including butterfly-shaped LWRs with straight and curved edges and conventional rectangular LWRs, as is shown in Fig. 1. The PML-based finite element analysis verifies that the use of the butterfly-shaped plates, instead of the conventional rectangular plates, can bring evident reduction in tether vibration that is directly related to the energy dissipated through the supporting tethers, and the curved edges yields a highest Q_{anchor}. The measured frequency response for the butterfly-shaped resonator with curved edges yields a Q of 2,433 which represents a 2.24× increase in Q over the conventional rectangular resonator, and butterfly-shaped resonator with straight edges represents a Q of 1,779 which represents a 1.64× increase in Q (Figure 2). Moreover, the butterfly-shaped AlN plate does not introduce any other spurious mode within a 1.5 GHz frequency band and exhibits smaller R_m thanks to the high Q.

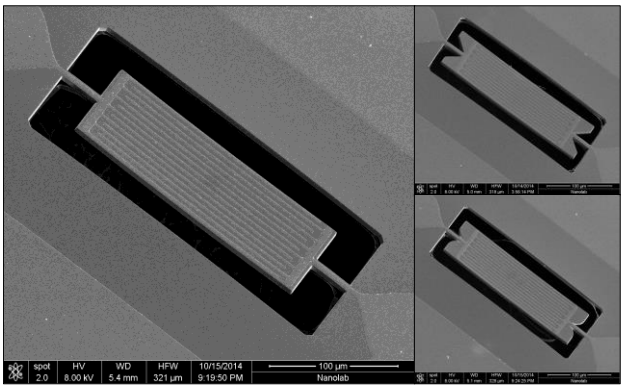


Fig. 1: SEM images of the fabricated conventional and butterfly-shaped Lamb wave resonators with straight and curved edges on a 4.1-μm-thick AlN plate.

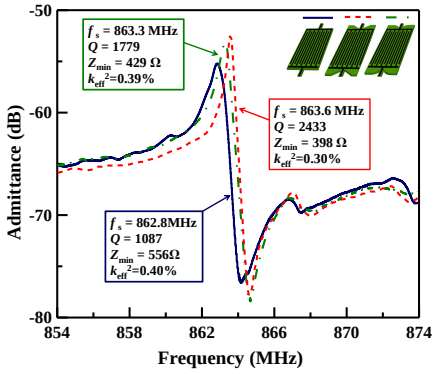


Fig. 2: Comparison of measured frequency responses for Lamb wave resonators with rectangular plate and butterfly-shaped plates with straight and curved edges.

Ultra-low noise all fiber mode-locked laser

Yaolin Zhang, Quansheng Ren, Dong Hou, and Jianye Zhao*
School of Electronics Engineering and Computer Science, Peking University, Beijing, China
zhaojianye@pku.edu.cn

High repetition rate optical pulse generators with low phase noise are becoming more and more popular in many applications such as high-speed communication, arbitrary waveform generation, high-speed and high-resolution optical analog-to-digital conversion [1-4]. Mode-locked lasers are ideal optical pulse generators and are recognized as the purest microwave generators [5] in the world. In this letter, we report a cascaded mode-locked fiber laser, which generates ultralow phase noise microwave and high repetition rate optical pulses simultaneously. Such mode-locked fiber lasers have numerous advantages such as low noise, low cost, high stability, and compact construction.

The cascaded mode-locked fiber laser we proposed includes an Er-doped passively mode-locked laser (PMLL) based on nonlinear polarization rotation (NPR) and an actively mode-locked laser (AMLL) based on intracavity intensity modulator. Our scheme utilizes the PMLL to generate ultra-low noise radio frequency (RF) and then extracts one high harmonic component of the RF to drive the AMLL. In the PMLL, the medium gain was provided by a 0.4 m highly Er-doped fiber. To ensure the facility of adjusting the repetition rate, we used spatial optical components including two collimators, one half-wave plate, two quarter-wave plates, one isolator and one polarizing beam splitter (PBS). The PMLL operates at a repetition rate of ~74.5 MHz, corresponding to a cavity length of ~2.68 m. ~3dBm power of the optical pulses was divided by the PBS and was injected into a fast photodiode (PD) with 3.2 GHz bandwidth and reponsivity of 0.8 A/W. The AMLL was mode-locked at ~1.117 GHz via gain modulation of an intensity modulated electro-optical modulator (EOM, KG-DDMZ1510PS). The EOM has a bandwidth of 10 GHz and a half-wave voltage of 2.6 V. The cavity length of the AMLL was set at about ~14.8 m, corresponding to a fundamental repetition rate of ~13.46 MHz. A 1.2 m highly Er-doped fiber was used for laser pump and an isolator was used to guarantee unidirectional light propagation in the cavity. The EOM was biased at 0 V, and approximately 5 dBm of RF power from the low noise amplifier was applied to the EOM. Before the EOM, a fiber stretching based three-paddle polarization controller (PC, Thorlabs FPC561) was used to restrict the polarization state of the light entering the EOM. The laser diode generates ~600mw maximum optical power at 980 nm and all of the power was injected into the cavity via a 980nm/1550nm wavelength division multiplexer. ~10% power of the optical pulses was coupled to another high speed PD through a fiber coupler for signal detection and phase noise measurement. By this scheme, a ~1.117 GHz optical pulse train and microwave with -158 dBc/Hz of low phase noise at 1 MHz offset frequency were obtained. To our knowledge, this is the first time that a very cost effective way of generating ultra-low noise, high repetition rate optical pulse train and microwave based on a cascaded fiber ring laser was explored.

[1] G. Eisenstein, R. S. Tucker, U. Koren, and S. K. Korotky, "Active mode-locking characteristics of InGaAsP-single mode fiber composite cavity lasers," IEEE J. Quantum Electron. 22 (1986), 142-148.

[2] P. W. Juodawlkis, J. C. Twichell, G. E. Betts, J. J. Hargreaves, R. D. Younger, J. L. Wasserman, F. J. O'Donnell, K. G. Ray, and R. C. Williamson, "Optically sampled analog-to-digital converters," IEEE Trans. Microwave Theory Tech. 49 (2001), 1840-1853.

[3] S. T. Cundiff, and A. M. Weiner, "Optical arbitrary waveform generation," Nat. Photon. 4 (2010), 760-766.

[4] G. E. Villanueva, M. Ferri, and P. Perez-Millan, "Active and passive mode-locked fiber lasers for high-speed high-resolution photonic analog-to-digital conversion," IEEE J. Quantum Electron. 48 (2012), 1443-1452.

[5] E. Rubiola and G. Santarelli, "FREQUENCY COMBS: The purest microwave oscillations," Nat. Photon. 7 (2013), 269-271.

Time and frequency metrology in flicker noise context

Vernotte F, Lantz E*
UTINAM/Observatory THETA, University of Franche-Comte/CNRS, Besançon, France
*Femto-ST/Optics department, University of Franche-Comte/CNRS, Besançon, France
E-mail: francois.vernotte@obs-besancon.fr

The flicker noise, or *1/f* noise, may be encountered everywhere from atomic physics to astrophysics through nano-technologies, electronics, … [1]. Although its origin is better understood [2], it remains a difficult issue and the nightmare of metrologists because of the strong correlations of its samples inducing a fundamentally duration dependent behavior. For example, unlike the white noise, the *1/f* noise does not decrease by averaging but remains almost the same. Moreover, this is one of the way to be faced with the flicker noise: very often, we observe that the dispersion of measurements decreases as $1/\sqrt{N}$, where N is the number of averaged measurements, until a certain value of N for which the decrement stops. The flicker floor is reached.

It is then of importance to identify when we pass from a white noise to a *1/f* context and what is the optimal average number.

However, once the flicker floor is reached, it is still possible to perform metrology but some precautions must be taken. Firstly, we must keep in mind that the *1/f* noise takes its name from the dependency of its spectral density versus frequency: it means that the spectral density tends toward infinity for $f=0$. We have thus to ensure the convergence of the statistical parameters, such as the mean, by introducing a low cut-off frequency, below which the spectral density tends toward 0. But the existence of such a low cut-off frequency may be puzzling. This paper will give some clues to understand its physical meaning and the way to model it. Then, it is necessary to be able to define confidence intervals in such a context. Of course, the classical relationships which are designed for white noise are not valid for flicker.

This paper intends to determine rigorously new relationships giving confidence intervals over statistical parameters (arithmetic mean, drift coefficients) versus the number of measurements, the variance of the residuals and the hypothetic low cut-off frequency. In order to obtain such relationships, approximations will be performed on the autocorrelation function of the *1/f* noise and on the variance calculation. These results will be validated by both numerical computations and Monte-Carlo simulations. Then, a methodology will be proposed for handling properly measurements in a *1/f* context. Finally, this method will be applied to experimental cases.

But more than practical recipes, this paper aims to give a general method for finding such relationships for other types of noise in other contexts and for carefully validating the results.

[1] W.H. Press, “Flicker noises in astronomy and elsewhere”, in Comments on Modern Physics, Part C - Comments on Astrophysics, vol 7(4), Gordon and Breach Science Publishers Ltd, 1978, pp 103-119.

[2] G. Liu, S. Rumyantsev, M.S. Shur and A.A. Balandin, “Origin of 1/f noise in graphene multilayers: Surface vs. volume”, Applied Physics Letters, vol. 102, no. 9, pp. 093111.1-093111.5, 2013.

Phase Group Characteristics and Phase Coincidence Detection Based Phase Noise Measurement Method

Dong Shaofeng, Zhou Wei, Hu Wei, Zhan Jinsong, Qin Hongbo
School of Electro-Mechanical Engineering, Xidian University, Xi'an, Shaanxi/China
E-mail: shaofengdong@126.com

Phase noise is an important parameter in time-frequency measurement and control. The available phase noise measurement methods, such as phase discrimination method and high-speed A/D sampling method, are founded on the phase processing between two signals at the same frequency. Frequency normalization is needed for the phase noise measurement between two different frequency value signals, which increases the system complexity and introduces additional phase noise. By analysising the phase difference variation regularity between two different frequency signals, the paper reveals the phase group synchronization and quantized phase step phenomena between every two cyclical signals, shown as Fig.1. With these phase group characteristics, a wide-band and fast-response phase noise measurement method can be achieved.

A high-stability and low-noise OCXO is used as the reference frequency, two adjacent phase coincidence points which are detected between the measured frequency and the reference frequency are used as the start and stop signals of the gate,. Theoretical analysis shows that the fluctuate of gate time between multiple consecutive measurement reflects the close-in phase noise. To measure the far-out phase noise, a short gate time, such as several milliseconds, is required. However so short a measurement gate is difficult to generate. The experiment observed that the output of the phase coincidence detection between two different frequency signals is not a singular pulse, but a pulse group containing millions of pulse, shown as Fig.2. There is a discontinuity in phase coincidence detection pulse group, and the discontinuity is the reflection the far-out phase noise. The method achieves the far-out phase noise by counting phase coincidence detection pulse and data processing.

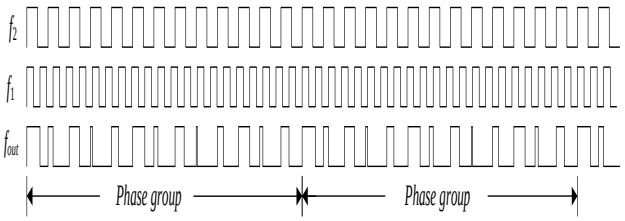


Fig. 1: Phase group variation between different frequency.

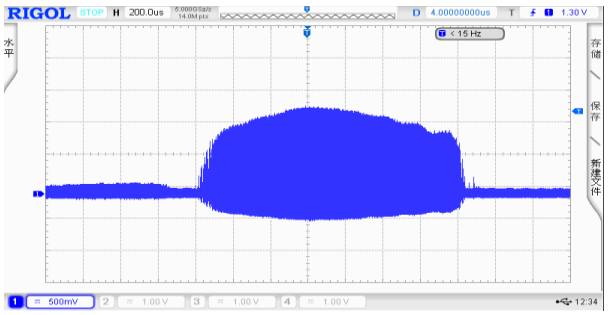


Fig. 2: Phase coincidence detection pulse group observing from the oscilloscope.

Combing the fluctuate of gate time and the discontinuity of the phase coincidence detection pulse, the SSB phase noise of the measured frequency can be obtained by FFT. Fig.3 shows the SSB phase noise of 10MHz generated by HP8662.

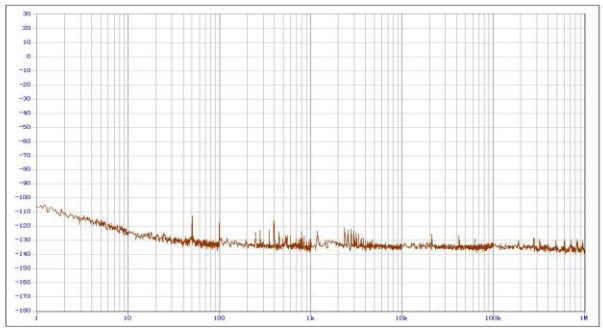


Fig. 3: SSB phase noise of 10MHz generated by HP8662.

Compared with the available phase noise measurement methods, the method has the advantages in simpler structure, wider measurement band, smaller additional noise.

Supported by the National Natural Science Foundation of China under Grant No 11403017, and the Fundamental Research Funds for the Central Universities under Grant No 7214508606.

High-stability Frequency Synthesis Based on a Cryocooled Cryogenic Sapphire Oscillator

Myoung-Sun Heo, Sang Eon Park, Sang-Bum Lee, Hyun-Gue Hong, Taeg Yong Kwon, Chang Yong Park, Won Kyu Lee, Dai Hyuk Yu, Andre N. Luiten*, Ashby Hilton*, and John G. Hartnett*
Center For Time and Frequency, Korea Research Institute of Standards and Science, Daejeon, South Korea
*IPAS and the School of Physical Sciences, the University of Adelaide, Adelaide, SA, Austraila
E-mail: hms1005@kriss.re.kr

The short-term frequency stability of the Cs fountain clock being developed at KRISS in South Korea is governed by that of the local oscillator (LO), BVA crystal oscillator (~1×10^{-13} at 1 s) even though it is among best crystal oscillators. This not only limits the performance of atomic clock, but it also takes significant amount of time for accuracy uncertainty to reach below the 10^{-15} level. To overcome these limitations we have introduced an ultra-stable cryocooled cryogenic sapphire oscillator (cryoCSO), designed and assembled in the University of Adelaide [1]. Its stability (~2×10^{-15} at 1 s) is much better than the BVA quartz oscillator, so it is expected that the fountain clock is not limited by LO stability any more but by quantum projection noise (QPN) [2].

Since the output frequency of the cryoCSO is around 11.2 GHz, we need to build a frequency synthesizer to produce 9 GHz for the Cs clock operation and 7 GHz for the Rb clock operation. Fig. 1 shows the schematic of the frequency synthesis chain. After subtracting a 44 kHz frequency offset using an IQ mixer we obtain the required output frequencies using low-phase-noise digital dividers and mixers. It is not possible to measure the absolute stability or phase noise of output signals without an additional cryoCSO, but it is confirmed that the residual stability of the frequency synthesizer is well below 10^{-14} by comparison with another low-phase-noise synthesizer. The Cs fountain clock is now operating with this highly stable LO and shows a frequency stability of about 5×10^{-14} at 1 s.

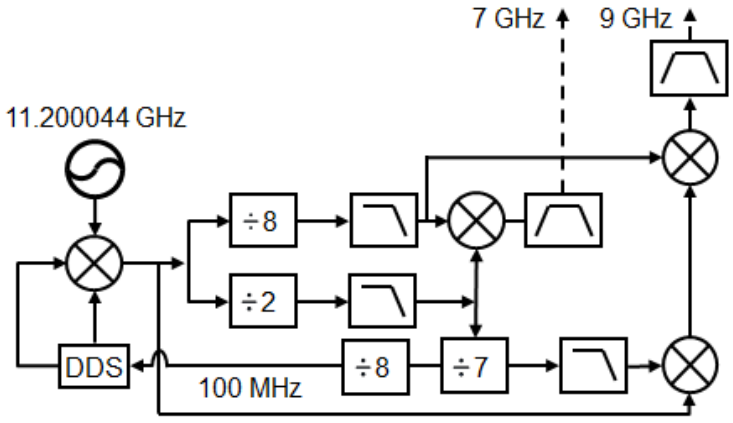


Fig.1 Schematic diagram of the frequency synthesizer

[1] J. G. Hartnett et al., "Ultra-low-phase-noise cryocooled microwave dielectric-sapphire-resonator oscillators," Appl. Phys. Lett., vol. 100, pp. 183501, Apr. 2012

[2] J. Guena et al., "Progress in atomic fountains at LNE-SYRTE." IEEE Trans. Ultrason., Ferroelect., Freq. Contr., vol. 59, no. 3, pp. 391-409, Mar 2012.

All optical 10 GHz ultra-low phase noise signal generation with commercial devices

Didier Alexandre, Millo Jacques, Grop Serge, Dubois Benoît*, Bigler Emmanuel, Rubiola Enrico, Lacroûte Clément and Kersalé Yann

FEMTO-ST Institute, UMR 6174 : CNRS/ENSMM/UFC/UTBM ,

Time and Frequency Dpt., 26 ch. de l'Epitaphe, 25030 Besançon Cedex, France

* FEMTO Engineering, 15 B avenue des Montboucons, 25030 Besançon Cedex, France

E-mail: alexandre.didier@femto-st.fr

We present a setup based on commercial devices for the all-optical generation of a microwave signal at 10 GHz with ultra-low phase noise. A commercial, fibered femtosecond laser is locked to a laser that is stabilized to a commercial ULE Fabry-Perot cavity. A 10 GHz microwave signal is extracted from the femtosecond laser output using a fast photodiode. The resulting signal exhibits a phase noise $\mathcal{L}(f) = -104$ dBc/Hz at 1 Hz Fourier frequency, at the level of the best value obtained with such "microwave photonics" laboratory experiments [1]. We measure the phase noise spectrum of the RF beat-note between our "all-optical" microwave signal and one of our cryogenic sapphire oscillators (CSO).

The contributions of the ultra-stable cavity, the CSO and environmental noises are discussed. Such a setup will make it possible for laboratories outside the frequency metrology field to generate ultralow phase noise microwave signals, opening up new possibilities in various domains.

[1] T. M. Fortier, M. S. Kirchner, F. Quinlan, J. Taylor, J. C. Bergquist, T. Rosenband, N. Lemke, A. Ludlow, Y. Jiang, C. W. Oates, and S. A. Diddams, "Generation of ultrastable microwaves via optical frequency division," Nature Phot. 5, 425–429

Precise measurement of complicated frequency signals

Bai Lina, Zhou Wei, Ye Bo

Department of Measurement and Instrumentation, Xidian University, xi'an, P.R.C.

E-mail: lnbai@mail.xidian.edu.cn

Based on the border effect found by us, the decisive factor that determines the measurement precision is the resolution stability, not the resolution itself.[1] Resolution stability is obviously finer than resolution itself by two-three orders of magnitude; therefore, it is possible to significantly improve the measurement precision with this new finding. In the fields of quantum frequency standard and telecommunications, there are many complicated frequency-signals of which measurements are of great significance. Discrete fuzzy areas result when any complicated frequency-signal in a wide range of frequency is measured with only one frequency-signal as the standard.[2] By exactly capturing the border information of a discrete fuzzy area, we can obtain higher measurement precision when measuring complicated frequency-signals, as shown in Fig.1.

f_0 is the reference signal, f_x the measured signal, f_D is the phase-difference, f_{out} is phase-coincidence detection. After slight phase-shifting, two types of f_{out} are gained. It can be seen from Fig.1 that state a_2 in f_{out1} disappears in f_{out2}, so does state b_2. Some phase-coincidence states, which do not exist in f_{out1}, appear in f_{out2}, and some that are in f_{out1} disappear in f_{out2}; meanwhile the states between those states that change remain and do not alter. The changed states are exactly the borders of discrete fuzzy areas, which generate the actual gate.

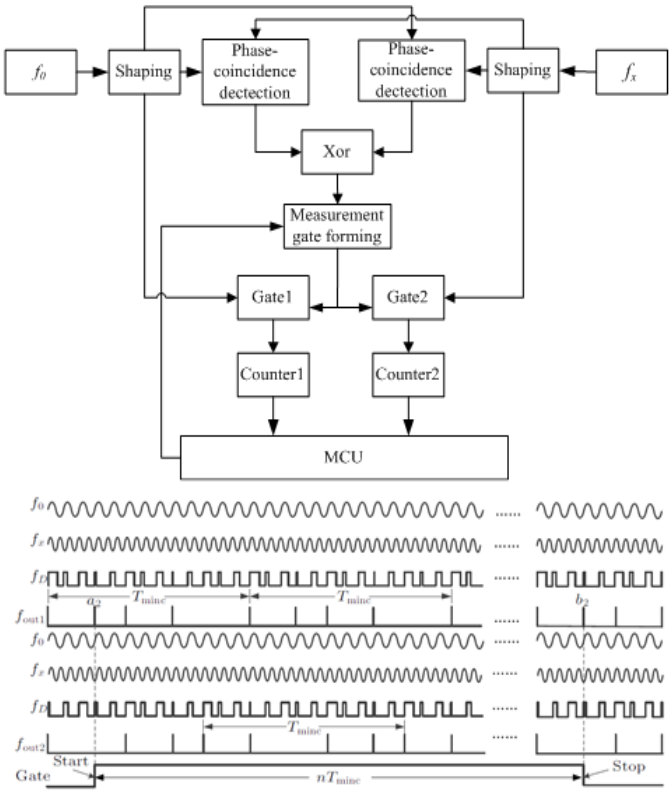


Fig. 1 Precise measurement of complicated signals and waveforms

A reference signal 10MHz is produced by OSA 8607 to measure complicated signals such as 8.2201MHz, 16.384MHz, and 19.44MHz etc., and the frequency stability can reach 10^{-12} level.

[1] ZHOU Wei, LI Zhi-Qi, BAI Li-Na, et al., Verification and Application of the Border Effect in Precision Measurement, CHIN. PHYS. LETT. vol. 31,no. 10, Sept.2014

[2] Zhou W, 2005Chinese Journal of Scientific Instrument, vol. 26, pp:764

Single-Bit-Output All-Digital Frequency Synthesis Using Multi-Step Look-Ahead Band-Pass Σ-Δ Modulator-Like Quantization Processing

Basetas Charis, Sotiriadis Paul
Department of Electrical & Computer Engineering, National Technical University of Athens, Greece
E-mail: pps@ieee.org

A new approach to all-digital frequency synthesis [1] is proposed, where a sinusoidal signal $\{x_n\}$ of desirable frequency ω_0 is generated by a LUT with high-resolution output of N Bits, exactly as in standard DDS. Then $\{x_n\}$ is fed into a Band-Pass (BP) Σ-Δ modulator-like nonlinear digital filter performing the 1-BIT quantization and shaping the quantization noise away from the carrier frequency ω_0. In principle the quantization step can be performed using a conventional BP 1-BIT ΣΔ modulator. However, the stability of conventional BP 1-BIT ΣΔ modulators of order 2M, M=2,3,… requires sacrifices in noise suppression, i.e. the choice of the Noise Transfer Function (NTF) is very limited. Instead, the Σ-Δ modulator-like filter used here offers superior stability and therefore a significantly larger design space for the NTF. It is an optimization algorithm predicting the optimal current 1-BIT output sample taking into account the next k input samples. This is described by the following equations: $y_n = \arg\min_{v_0\in\{\pm1\}}\left(\min_{v_1,v_2,\ldots,v_k\in\{\pm1\}}\sum_{i=0}^{k}\left|x_{n+i}+e_{n+i}-v_i\right|\right)$, where y_n is the n-th output sample, x_n is the n-th input sample, and, $e_m=\sum_{i=0}^{n-1}(x_i-y_i)g_{n-1-i}+\sum_{i=n}^{m-1}(x_i-v_{n-i})g_{m-1-i}$, $m=n,n+1,\ldots,n+k$, is the filtered error sequence $\{x_i-y_i\}$ which is also a function of the optimization variables $v_1,v_2,\ldots,v_k$. $\{g_i\}$ is the impulse response of the noise-shaping filter G and k is the number of future input samples that we take into account. G must be a BP filter. Here we choose $G(z)=(1-H(z))/H(z)$, $H(z)=\left(1-e^{-j\omega_0}z^{-1}\right)^2\left(1-e^{j\omega_0}z^{-1}\right)^2$ and $\omega_0=2\pi\cdot0.365$. So the quantization noise is shaped by a double pair of conjugate zeros placed on the unit circle at frequency ω_0. In Fig. 2 the spectrum of output $\{y_n\}$ is shown when the amplitude of the sinewave $\{x_n\}$ is 0.7. Dynamic range of 120 dB near-in is achieved for $2\cdot10^6$ samples and $k=2$. NTF zeros may be split to broaden the useful bandwidth near in.



Fig. 1: All-Digital Frequency Synthesis Using the Multi-Step Look-Ahead (MSLA) Band-Pass Σ-Δ Modulator

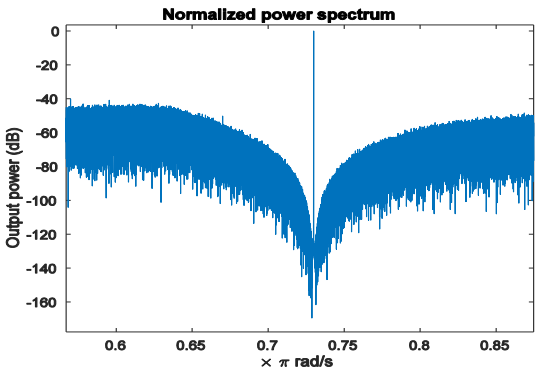


Fig. 2: Spectrum of the architecture in Fig.1

[1] P. P. Sotiriadis, K. Galanopoulos, "Direct All-Digital Frequency Synthesis Techniques, Spurs Suppression, and Deterministic Jitter Correction", IEEE Trans. on Circuits and Systems-I, Vol. 59, No. 5, May 2012, pp. 958-968

Hardware Implementation Aspects of Multi-Step Look-Ahead Σ-Δ Modulation-Like Architectures for All-Digital Frequency Synthesis Applications

Basetas Charis, Sotiriadis Paul
Department of Electrical & Computer Engineering, National Technical University of Athens, Greece
E-mail: pps@ieee.org

All-digital frequency synthesis is an ongoing research subject and many of its challenges have not yet been completely resolved [1]. E.g., dithering techniques have been used as a remedy for spurious tones, while 1-bit output has been proposed for DAC-less architectures. Dithering however leads to an elevated noise floor, which makes all-digital frequency synthesis unsuitable for many noise-sensitive applications. Noise shaping using Σ-Δ modulation type techniques may be used to lower the noise floor within a specific frequency band. Yet, noise shaping filters of order higher than two and high input amplitude may result in stability problems of the loop. Increased dynamic range and stability may be achieved, simultaneously, if future inputs and states of the modulator are taken into account when calculating the next output sample. The proposed technique is summarized by equation

$$u_n = \arg\min_{y_0\in\{\pm1\}}\left(\min_{y_1,y_2,\ldots,y_k\in\{\pm1\}}\sum_{j=0}^{k}\left|A_j-\sum_{i=0}^{j}c_{j-i}y_i\right|\right)$$

where u_n is the *n*-th output sample, A_j is a function of the past outputs and current and *k* future inputs, and c_j are coefficients depending on the noise shaping filter.

The proposed implementation shown in Fig. 1 is comprised of an IIR filter, which filters in parallel the current and future inputs of the modulator, and a combinational logic circuit or LUT, which chooses the value of the output depending on the values of its $k+1$ inputs $A_0 \ldots A_k$. Here x_n is the current input sample, x_{n+k} is the *k*-th future input sample, *a* and *b* are the IIR filter coefficients, $e_n^{'}$ is the current output of the IIR filter, $e_{n+k}^{'}$ is the *k*-th future output of the IIR filter and $C_1 \ldots C_k$ are coefficients depending on the values of c_j. As a demonstration of the mapping between $A_0 \ldots A_k$ and u_n implemented by combinational logic, Fig. 2 depicts this mapping for $k=1$ and $(1-z^{-1})^2$ as the noise shaping filter. Similar mappings in higher dimension are obtained for higher values of *k*, while different filters change the mapping region boundaries. The paper presents implementation strategies minimizing the hardware complexity. The technique can be used for both base-band and pass-band 1-bit quantization.

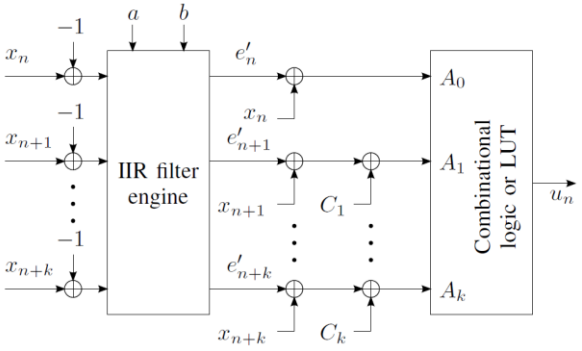


Fig. 1: Proposed hardware implementation of the Multi-Step Look-Ahead Σ-Δ Modulator-Like architecture.

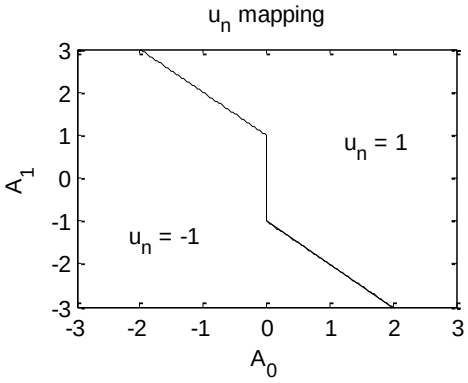


Fig. 2: u_n mapping regions.

[1] U.L. Rohde, Microwave and Wireless Synthesizers: Theory and Design, 1st ed. Singapore: Wiley-Interscience, 1997.

Oscillator improvements utilizing AM-PM correlations

A. Hati., C.W. Nelson and D.A. Howe.
Time and Frequency Division/ NIST, Boulder, CO/USA
E-mail: archita.hati@nist.gov

One can sense and correct an oscillator's phase modulation (PM) noise by measuring its PM noise in real time. However, such measurement requires a higher quality reference oscillator or a stable high-quality factor (Q) element to measure against. Recently we have shown a new technique that reduces oscillator's PM noise from AM (amplitude modulation)-PM noise correlation [1]. This technique is much simpler; it requires a measurement of AM noise only which is easier than a PM noise measurement, requiring only a diode and a few capacitors, rather than a reference oscillator. In this paper we will elaborate on three factors, listed below, that strengthen the merits of the technique.

Steady state: Whenever the gain of the sustaining amplifier only marginally exceeds the loss in oscillator loop, the loop amplifier may not be operating in deep saturation. Under this operating condition(s) we observed strong correlation between PM and AM noise. We implemented our circuitry and successfully improved the PM noise of oscillators. The phase noise of an oscillator improves if this correlation originates from the amplifier, resonator, phase shifter, or all components simultaneously.

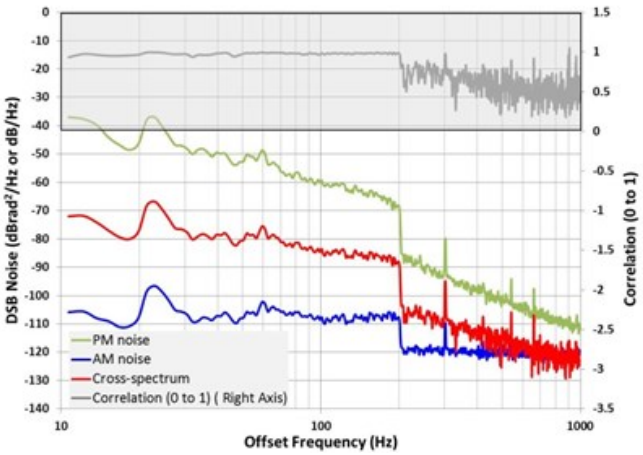


Fig. 1: Left axis: Plot of double-sideband (DSB) PM noise, AM noise, and the cross-spectrum between them for a quartz-MEMS oscillator at 635 MHz under vibration. The oscillator was subjected to a constant acceleration white noise of amount equal to 500 mg^2/Hz between 20 – 200 Hz (integrated acceleration = 0.95 g_{rms}). Right axis: The plot at the top shows the strong degree of correlation ($\rho = 0.97$) within the range of vibration frequencies.

Under vibration: We observed strong correlation (> 90%) between vibration induced PM and AM noise when different classes of oscillators were subjected to vibration as shown in Fig. 1. This high level of vibration induced correlation exists even if oscillators showing low levels of steady-state correlation. This electronic circuit is equally applicable in reducing the phase noise of an oscillator under vibration and hence improves the vibration insensitivity. This scheme will also reduce undesired spurious resonances occurring under vibration.

AM noise: Another advantage of the proposed circuit is that in addition to PM noise it can also reduce the AM noise of the oscillator simultaneously. AM noise is usually higher if the loop amplifier is not saturated moderately.

[1] A. Hati, C.W. Nelson, and D.A. Howe, "Reducing oscillator PM noise from AM-PM noise correlation," Electron. Lett., vol. 50, pp. 1195-1197, Aug. 2014.

Automatic control of amplitude-to-phase conversion in photo-detection of femto-second pulses for low phase-noise microwave generation

Nicolodi Daniele, Bouchand Romain, Xie Xiaopeng, Abgrall Michel, Le Coq Yann
LNE-SYRTE, Observatoire de Paris, CNRS, UPMC, 61 Avenue de l'Observatoire, 75014 Paris, France
E-mail: daniele.nicolodi@obspm.fr

Ultra-stable microwave signals are of great interest in a broad range of applications, such as radar, telecommunication, deep-space navigation systems, timing distribution and synchronisation at large scale facilities, and precision microwave spectroscopy. Femto-second lasers provide a phase coherent link between optical and microwave frequencies and thus allow to transfer the unrivaled spectral purity of modern ultra-stable continuous wave lasers to the microwave domain. The conversion from the optical to the microwave domain is based on the synchronization of the pulse repetition rate of the femto-second laser with the optical frequency of the cw laser. The subsequent detection of the optical pulse train with a fast photodiode provides access to the microwave signal. The photo-detection process is, however, accompanied by excess phase noise which limits the stability of the microwave frequency generation. One of the main causes for this excess phase noise is the amplitude-to-phase conversion in the fast photodiode, combined with the unavoidable intensity noise of the femto-second laser [1, 2, 3].

The amplitude-to-phase conversion coefficient arises in part due to saturation and nonlinearities in the photodiodes. Therefore, it depends on the operational conditions of the photo-detector. At a given bias voltage, scanning the optical energy per pulse of the incident light, the amplitude-to-phase conversion coefficient is found to alternate between positive and negative values, going through vanishing points. State-of-the art low phase noise generation via optical frequency comb frequency division of optical references relies on operating the photodiodes at one of the null point of the amplitude-to-phase conversion coefficient, in order to reject the intensity noise of the femto-second laser. However, drift in any of the operational parameters may cause deviation from the amplitude-to-phase conversion null point.

We will present an automatic system for the measurement of the amplitude-to-phase conversion and continuous control of the system parameters for operation at a null point of the amplitude-to-phase conversion. The system operates modulating the intensity of the frequency comb output and coherently demodulating the relative phase between the microwave signal obtained from the photodiode and a reference oscillator. The beatnote between the photo-detected microwave signal and the reference oscillator is digitized and phase measurement, demodulation, and control loop are implemented digitally, allowing for great flexibility in the choice of modulation parameters and control loop optimization. The sensitivity of the system to the amplitude-to-phase conversion coefficient is limited by the phase noise of the reference oscillator and by the sensitivity of the digital phasemeter. However, adjusting the modulation frequency and amplitude, the sensitivity to the amplitude-to-phase conversion coefficient can be tuned, obtaining an arbitrary large rejection of the intensity noise.

1. W. Zhang, T. Li, M. Lours, S. Seidelin, G. Santarelli, and Y. Le Coq, "Amplitude to phase conversion of InGaAs pin photo- diodes for femtosecond lasers microwave signal generation," Applied Physics B, 106, pp. 301-308, 2012.
2. J. Taylor, S. Datta, A. Hati, C. Nelson, F. Quinlan, A. Joshi, and S. Diddams, "Characterization of Power-to-Phase Conversion in High-Speed P-I-N Photodiodes," IEEE Photonics Journal, 3, pp. 140-151, 2011.
3. T. M. Fortier, F. Quinlan, A. Hati, C. Nelson, J. A. Taylor, Y. Fu, J. Campbell, and S. A. Diddams, "Photonic microwave generation with high-power photodiodes," Optics Letters, 38, pp. 1712-1714, 2013.

Compact Clocks for Industrial Applications: the EMRP Project IND 55 MClocks

S. Micalizio[1], F. Levi[1], A. Godone[1], C. E. Calosso[1], S. Guérandel[2], D. Holleville[2], E. De Clercq[2], L. De Sarlo[2], P. Yun[2], J. M. Danet[2], M. Langlois[2], R. Boudot[3], B. François[3], G. Mileti[4], C. Affolderbach[4], F. Gruet[4], S. Kang[4], M. Gharavipour[4], R. Hamid[5], E. Sahin[5], B. Desruelle[6]

[1]Optics Division, INRIM, Torino, Italy
[2]LNE-SYRTE, Observatoire de Paris, Paris, France
[3]Femto-St, CNRS, UFC, Université de Franche Comté, Besançon, France
[4]Laboratoire Temps Fréquence, Université de Neuchâtel, Neuchâtel, Switzerland
[5]National Metrological institute of Turkey, Tubitak, Kocaeli, Turkey
[6]Muquans, Talence, France

E-mail: s.micalizio@inrim.it

Atomic frequency standards provide the ultimate source of accuracy and stability for all modern communication, navigation and timekeeping systems, and nowadays commercially available devices are deployed in many strategic industrial fields. As these industrial activities are essentially exploiting microwave frequencies, it turns out that vapor-cell clocks are particularly suited to fulfil industrial requirements. In fact, besides working in the microwave regime, vapor-cell clocks are compact, portable, reliable, with low power consumption and exhibit a good short-term frequency stability.

However, the development of compact and high performing frequency standards is of interest in several scientific and technological applications, such as, improved local oscillators for future primary frequency standards or improved clocks for the Galileo space segment in view of forthcoming Galileo services, such as autonomous landing of airplanes, mooring of ships or vehicle autopilots [1]. Compact atomic clocks with 10-times improved performance will help bringing metrological precision into industry, with better stability than current commercial Cs beam clocks and reduced size and cost compared to hydrogen masers.

Recently, due to better performing laser sources and to innovative techniques to prepare and detect the atoms, several cell-based prototypes exhibiting unprecedented frequency stability have been developed.

Examples of these techniques are pulsed laser pumping, coherent population trapping (CPT), isotropic laser cooling and light shift suppression methods. For certain laboratory prototypes of such clocks frequency stabilities in the order of 10^{-13} at 1 s and in the range of 10^{-14} or better for the medium-long term were measured, a result even better than passive H-masers. In addition, the clocks based on cold atoms are on the way to providing an accuracy rivaling Cs atomic clocks, which can drastically reduce the need for periodic frequency calibration.

In this context, the project IND55-MClocks funded by EMRP* addresses the following objectives: 1) to develop a vapor-cell clock based on the pulsed optical pumping (POP) principle with a fractional frequency stability of 10^{-13} at 1 s and in the 10^{-15} range at 10^5 s; the clock will be targeted on industrial applications in terms of size, power consumption and reliability; 2) to develop a vapor-cell clock based on cold Rb atoms with performance comparable to that of POP in the short term but with better long term performance including an accuracy within an order of magnitude of that of primary standards; the project will identify the compromises required in order to obtain the expected performance while still targeting industrial applications; 3) to investigate alternatives principles such as CPT, to study the possibility of realizing a clock optimized in terms of compactness.

At the conference, the status of the project will be presented and the impact of the project's outcomes on metrology and industrial capabilities will be discussed.

[1] esamultimedia.esa.int/docs/galileo/GalileoE3web_copy.pdf

*This work is supported by the European Metrology Research Programme (EMRP project IND55-MClocks). The EMRP is jointly funded by the EMRP participating countries within EURAMET and the European Union.

Advances of Chip-Scale Atomic Clock in Peking University

Zhao Jianye[1]*, Zhang Yaolin[1], Lu Haoyuan[1,2], Hou Dong[1], Zhang Shuangyou[1]
[1]Department of Electronics, Peking University, Beijing, China
[2]Department of Electronic Engineering, Fudan University, Shanghai, China
zhaojianye@pku.edu.cn

Since the idea to combine the CPT spectroscopy with the micro-electromechanical systems (MEMS) for the fabrication of Chip-scale atomic clocks (CSACs) is proposed in [1], CSACs based on the Coherent Population Trapping (CPT) [2] have been an active research area for a few years. Many great research institutions are devoting to the realization of small-size, highly stable and low-power atomic clock. The MEMS vapor cells and Vertical Cavity Surface Emitting Lasers (VCSELs) are the key parts of the miniature atomic clocks, which can make the atomic clock (CSAC) physics packages with size less than 1 cm^3 and frequency stabilities below $2\times10^{-10}/\tau^{1/2}$ [3] .

The authors are developing a chip-scale atomic clock based on the ^{85}Rb CPT transition. As an intermediate milestone, we have developed a miniature atomic clock prototype. Combing the miniature physics part, low-power digital control circuits and low-power microwave system, the prototype has an overall size of 30 cm^3 volume with power consumption less than 400 mW. The current power consumption is limited by the physics package. The physics package, thermal management and control need to be addressed. The MEMS ^{85}Rb vapor cells with inner dimensions of 3 mm length and 3 mm radius [4] are fabricated by using anodic bonding and chemical reaction between BaN_6 and RbCl, and the 10% CPT resonance contrast (CPT Signal/Optical Absorption) is observed with the temperature at 50. The miniaturized control electronics provide the current supplies, and phase-lock the laser frequency and local oscillator to the ^{85}Rb 795nm D1 absorption transition and CPT resonance, respectively. A new microwave frequency modulation scheme is achieved by directly injecting triangular current signal into the charge-pump of voltage-control oscillator (VCO) [5]. Phase-sensitive detection is implemented for the phase locking of center of the optical and local oscillator. In our prototype, a new servo algorithm based on DFT algorithm is developed to optimize the long-term stability, and reduce the complexity. Our miniature atomic clock is demonstrated with frequency stability of 2.9×10^{-10}@1s and 2.9×10^{-11}@100s.

[1] S. Knappe, V. Shah, P. D. D. Schwindt, L. Hollberg, J. Kitching, L. A. Liew, and J. Moreland, “A microfabricated atomic clock,” Appl. Phys. Lett. 85, 1460-1462, 2004.

[2] G. Alzetta, A. Gozzini, M. Moi, and G. Orriols, “An experimental method for the observation of rf transitions and laser beat resonances in oriented Na vapour”, Nuovo Cim. B 36, 5-20, 1976.

[3] The MAC – A Miniature Atomic Clock A. U. Name, A. U. Name2, and A. U. Name3, “Interesting micro-scale stuff based on nanotechnology,” IEEE Trans. Ultrason., Ferroelect., Freq. Contr., vol. 51, no. 12, pp. 1607-1628, Dec. 2004.

[4] Zhang Chang, Zhang Shuangyou, Guo Dengzhu, Wang Zhong and Zhao Jianye Micro Rb Atomic Vapor Cells for the Chip-Scale Atomic Clock

[5] Xing Cheng, Zhang Yaolin, Wu Jiutao and Zhao Jianye Low Power Chip-scale CPT Atomic Clock with New Microwave Frequency Modulation Technique

An Atomic Frequency Micrometer Based on the Coherent Population Beating Phenomenon

WANG Zhong , ZHAO Jianye, ZHAO Xiaona， LIU Li, ZHUANG Yuxin and LI Dawei
School of Electronics Engineering & Computer Science, Peking University, Beijing, 100871, P. R. China
E-mail: zw@pku.edu.cn

We have demonstrated a frequency measuring method, and it can be seen as an atomic frequency measuring micrometer. It is based on the coherent population beating (CPB) phenomenon [1], which occurs in a typical three level system, when the frequency difference of the two pump laser fields have a detuning from the ground states splitting. The CPB phenomenon enables us to directly obtain the beat frequency between the measured RF signal and the atomic transition frequency. The main portion of the measured high frequency signal is equal to the atomic transition frequency, and the small portion of the frequency difference between the measured signal and the atomic transition frequency will be obtained. It allows us to measure this "magnified" beat frequency with a relative lower stability reference, which is a manner similar to the fine measurements of a micrometer. Hence, we have named this frequency measurement system the "atomic frequency micrometer" (Fig.1).

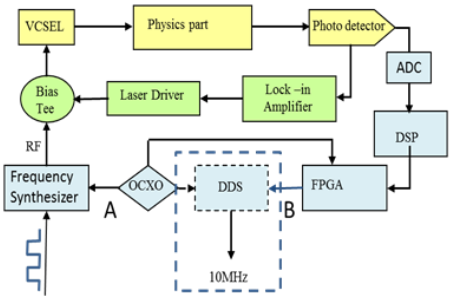


Fig.1: The block diagram of the atomic frequency micrometer （without the dotted DDS in the dashed region), and CPB atomic clock (with the dotted DDS).

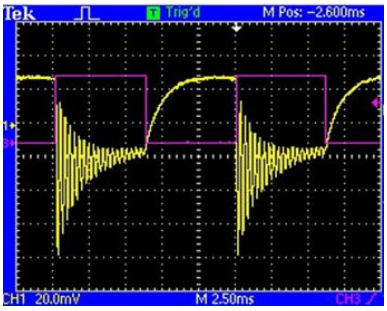


Fig.2: The CPB oscillation signal detected by the photo detector (Fig.1).

The CPB oscillation signal will be periodically excited (Fig.2). Then the beat frequency and its fluctuations can be detected and accurately measured through digital signal processing, which is capable of up to mHz or higher frequency resolutions (for GHz signal). The frequency discrimination via this CPB method is comparable to the Ramsey fringes method, and the working range is no longer limited by the width of the atomic transition line shape.

This CPB method enables us to achieve an atomic clock with better frequency stability [2] by actively compensating the measured RF signal frequency shift. The CPB atomic clock eliminates the need for the phase locking loop to lock the standard frequency, and broadens the working range with increasing reliability. This novel scheme could be extended to the optical frequency region, implying possible future applications in optical atomic clocks, optical frequency comb, atomic spectroscopy, magnetometer and other related researches.

[1]. T. Guo, K. Deng, X. Chen, and Z. Wang, "Atomic clock based on transient coherent population trapping", Appl. Phys. Lett. 94, 151108 (2009).

[2]. Dawei Li, Daiting Shi, Ermeng Hu, Yigen Wang, Lu Tian, Jianye Zhao and Zhong Wang*. "A frequency standard via spectrum analysis and direct digital synthesis" Applied Physics Express 7, 112203 (2014)

Digital servo system based on FPGA for optically pumped magnetometer

Zhou Sheng, Liu Chang, Wang Yanhui

Institute of Quantum Electronics, School of Electronics Engineering and Computer Science, Peking University, Beijing, China

Email: wangyanhui@pku.edu.cn

As the development of analog to digital converter (ADC) and digital to analog converter (DAC) technology, the convert between analog signal and digital signal becomes more precise. Digital signal process makes a difference in computing, filtering and displaying. Additionally, digital electronics could be easily realized by field programmable gate array (FPGA). Thus, this paper shares a digital servo system based on FPGA, ADC, and DAC for one optically pumped magnetometer. The Zeeman transition frequency is detected and locked by this digital servo system. This method is not only simple in hardware but also flexible to apply in other servo system.

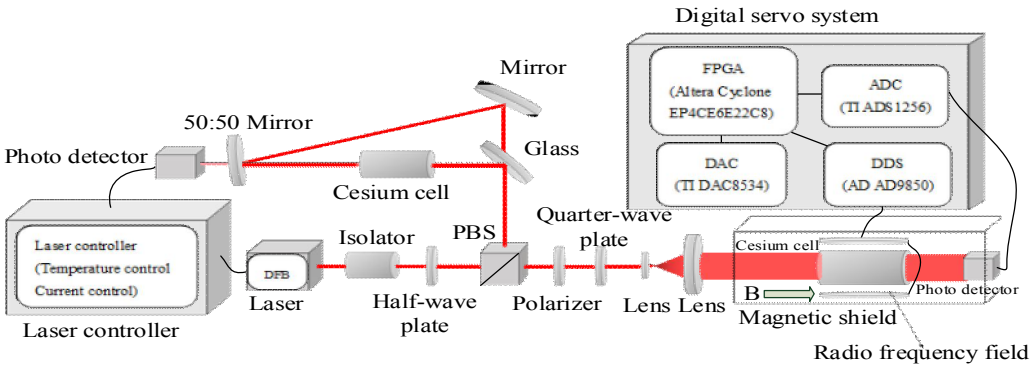


Fig. 1 M_z configuration cesium optically pumped magnetometer

The schematic diagram of M_z configuration cesium optically pumped magnetometer is shown in Fig.1, which consists of two parts, one is the laser system; the other is detecting the Zeeman transition signal and Zeeman transition frequency locking system.

The frequency of pumping light which is from a DFB laser is locked in D1 line ($6^2P_{1/2}$, F=4-$6^2S_{1/2}$, F'=3) of cesium by saturated absorption spectroscopy. The digital servo system which contains ADC, FPGA, DAC and DDS is applied to detect Zeeman transition signal and lock the Zeeman transition frequency. Particularly, the intensity of light is detected by a photo detector and converted to digital signals by ADC. The Zeeman transition frequency is detected by sweeping the frequency of the radio frequency field which is generated by DDS controlled by FPGA and also locked by frequency switching method[1] based on FPGA.

The digital servo system is flexible to apply in other servo system. With a minor change, this digital servo system is already applied in our atomic clock.

[1] R. Y. Shi, C. Liu, S. Zhou, Y. H. Wang, "Digital-locking optically pumped cesium magnetometer", *Proceedings*, 28th European Frequency and Time Forum, Neuchatel, Switzerland, June 23-26, 2014, pp. 144-146.

Measuring Buffer-Gas Pressure in Sealed Glass Cells

Travis Driskell, Michael Huang, and James Camparo

Physical Sciences Laboratories
The Aerospace Corporation
2310 E. El Segundo Blvd., El Segundo, CA 90245
Email: james.c.camparo@aero.org

In atomic clock resonance cells and the rf-discharge lamps employed in atomic clocks, a buffer-gas is present. In the former case, the buffer-gas plays a critical role in defining the clock's frequency and stability. In the case of the rf-discharge lamp, the buffer-gas (either Kr or Xe) is present in order to allow electrons to extract energy from the rf-field via elastic collisions with the buffer gas atoms. Contrary to naïve intuition, rf-discharge lamps can lose their noble-gas buffer over time, and should the buffer-gas drop to too low a level the lamp can fail [1]. Recently, we began a long-term experimental program to better understand the mechanism of noble-gas loss in rf-discharge lamps, and as a consequence needed a non-destructive means of measuring buffer-gas pressure in sealed glass cells. We are presently employing the technique of Kazantsev, Smirnova, and Khutorshchikov (KSK) [2] for that purpose, which is based on inferring buffer-gas pressure from the collision shift of an alkali ground-state hyperfine transition. We note that the KSK technique can also be used to measure buffer gas pressures in any sealed glass cell: a vapor-cell clock's resonance cell or the cell in a precision optical spectroscopy experiment [3], and so has very broad applicability.

In this presentation, we outline the basic concept behind the KSK technique, and two modifications of the technique that we have implemented for its improvement: use of a diode laser for better signal-to-noise ratios, and a change in method to better control for one of the larger systematic effects in the technique (*i.e.*, the quadratic Zeeman shift). We then discuss the sensitivity of the pressure measurements to various parameters: laser polarization, glass cell temperature, laser intensity, and microwave power. Finally, we discuss the technique's precision and stability. In our system, we have a precision that is better than 13% for total pressures between one and 100 torr, and a measurement reproducibility of about 0.18%. Additionally, we have examined the long-term stability of our measurement system for over a year, and find a long-term drift in our pressure measurement system for Xe of only 1.3 ± 0.4 mtorr/month.

---

[1] *Noble-gas loss in alkali rf-discharge lamps and its possible dependence on electron temperature*, N. L. Encalada, B. Jaduszliwer, W. E. Lybarger, and J. C. Camparo, IEEE Trans. Instrum. & Meas. 63(11), 2642-2650 (2014).

[2] *Radiospectroscopic method for precision measurement of gas pressure*, S. A. Kazantsev, G. M. Smirnova, and V. I. Khutorshchikov, Opt. & Spectrosc. 80(1), 10-21 (1996).

[3] *Kr-collision shift of the Rb D_1 transition: The isoclinic point and precision optical spectroscopy*, N. P. Wells, T. U. Driskell, and J. C. Camparo, Phys. Rev. A 89, 052516 (2014).

Measurement of Buffer Gas Collisional Clock Frequency Shift in Cs Vapor Cells in Presence of He and Xe

Eric Kroemer, Moustafa Abdel Hafiz, Vincent Maurice, Vincent Giordano, Rodolphe Boudot.
Time & Frequency Dpt., Femto-ST Institute, CNRS, 26 chemin de l'épitaphe, 25000 Besançon, France
E-mail: rodolphe.boudot@femto-st.fr

Introduction of buffer gas in vapor atomic cells is necessary to reduce the Doppler effect and to narrow the linewidth of the CPT resonance using the Dicke effect [1]. Femto-ST Institute developed an original technology for fabrication and filling of Cs vapor microcells with buffer gases [2]. The Cs vapor is generated after the complete sealing of the microcell by laser activation of a Cs dispenser developed by SAES Getters. Additionally, the cell is filled with a single Ne buffer gas permitting to cancel the temperature-dependence of the Cs clock frequency at a temperature inversion of about 80℃ [3]. This temperature is not enough for harsh environmental constraints applications and our Cs dispenser for- bids to use a N2-Ar buffer gas mixture, absorbing N2 buffer gas. We decided to investigate Cs clock frequency shift measurements in presence of other buffer gases, mainly Xe and He.

We implemented a laboratory-prototype Cs cell clock based on coherent population trapping. The laser source is a 1 MHz-linewidth distributed-feedback (DFB) diode laser turned on the Cs D1 line at 894.6 nm. The laser can be frequency stabilized onto Cs resonance by saturated absorption spectroscopy technique. A pigtailed phase electro-optic modulator (EOM), driven at 9.192 GHz, was used to generate 9.192 GHz frequency-splitted optical lines and to realize a CPT spectroscopy. We bought cm-scale commercially-available Cs cells filled with buffer gas (Xe and/or He). The cell was inserted in a physics package to be temperature-controlled and surrounded by a static magnetic field. The ensemble was inserted into a double-layer mu-metal magnetic shield.

First, we measured the actual buffer gas pressure in sealed cells through optical red shift measurements [4,5]. Then, once the buffer gas pressure was well known, we were able to determine the buffer gas collisional clock frequency shift coefficients by measuring the clock frequency shift as a function of cell temperature. The first estimations of these coefficients will be reported during the conference. Additionally, measurements of collisional frequency shift realized on microfabricated cells with new buffer gas mixtures will be reported.

[1] A DICKE, R. H. The effect of collisions upon the Doppler width of spectral lines. *Physical Review*, 1953, vol. 89, no 2, p. 472.

[2] HASEGAWA, M., CHUTANI, R. K., GORECKI, C., *et al.* Microfabrication of cesium vapor cells with buffer gas for MEMS atomic clocks. *Sensors and Actuators A: Physical*, 2011, vol. 167, no 2, p. 594-601.

[3] MILETIC, Danijela, DZIUBAN, P., BOUDOT, R., *et al.* Quadratic dependence on temperature of Cs 0–0 hyperfine resonance frequency in single Ne buffer gas microfabricated vapour cell. *Electronics letters*, 2010, vol. 46, no 15, p. 1069-1071.

[4] KOZLOVA, Olga, GUÉRANDEL, Stéphane, and DE CLERCQ, Emeric. Temperature and pressure shift of the Cs clock transition in the presence of buffer gases: Ne, N 2, Ar. *Physical Review A*, 2011, vol. 83, no 6, p. 062714.

[5] PITZ, Greg A., WERTEPNY, Douglas E., et PERRAM, Glen P. Pressure broadening and shift of the cesium D1 transition by the noble gases and N2, H2, HD, D2, CH4, C2H6, CF4, and 3He. *Physical Review A*, 2009, vol. 80, no 6, p. 062718.

About Signals' Correlation in a Spin Generator-Microwave Discriminator Dual Scheme

Baranov Alexey, Ermak Sergey, Sagitov Eduard, Smolin Roman, Semenov Vladimir
Department of Quantum Electronics
St. Petersburg State Polytechnic University
St. Petersburg, Russia
Vladimir_semenov@mail.ru

This paper presents the results of two double resonance signals correlation investigation. These signals were observed synchronously in optically oriented Rb^{87} vapors with laser pumping in a dual scheme: low frequency spin generator and HFS frequency discriminator.

Experiment was provided on a 1 cm^3 Rb vapor cell with antirelaxation wall coating in presence of a constant magnetic field of 100 nT magnitude. Laser source was tuned to the long-wave component of the D_2-line. Two types of atomic transitions were observed: magnetic-dependent (end resonance) and magnetic-independent 0-0 resonances.

The signals were subtracted after reducing to magnetic field units and processed to determine Allan deviation as a function of time average. During data handling correlation coefficient was found. Its value defines the detected signals coupling, which is a function of pumping rate and RF field intensity in the vapor cell area. During experiment optimal configuration of applied fields, when long-term stability of the quantum device reached its maximum, were obtained. Particularly, wall coated cell demonstrated the best efficiency at following configuration (in terms of dark line width 200 Hz): 20% - pumping light, 20% - microwave field, 10% - spin generator field corresponding to 50% signal level (100% - saturation regime).

Microwave and low frequency signals interference appeared in spin generator frequency shift while microwave resonance frequency being changed. This shift isn't referred to magnetic field variation, it corresponds to coherence circulation between hyperfine sublevels "covered" with radio frequency and depends on circular polarization sign of the pumping light, RF field intensity and type of magneto-dipole transition in microwave absorption spectrum. An absolute value of this shift for magnetic dependent transitions was an order of magnitude less than for conventional 0-0 transitions. Spin generator frequency shift had different signs for σ^+ и σ^- pumping light while microwave transition frequency shift preserved its sign.

This dual scheme works for a long-wave electro-dipole transitions only, when maximum amount of atoms on the hyperfine sublevels interacts with pumping light. The demand of self-excitation was not fulfilled on a short-wave transition due to low atom concentration. The results may be implemented in experiments with D_1-line optical pumping, when magnetic field orientation dependent tensor component of the light shift is sufficient [1]. High correlation of the tensor component in microwave and Zeeman transitions allows reducing orientation dependence of the atomic sensor.

[1] Семенов В.В. "О вкладе тензорной компоненты в световой сдвиг частоты радиооптического СВЧ резонанса в парах рубидия", Изв. Вузов, Физика, №2, с.86-90, 1999.

F-State Quenching Gas for $^{171}Yb^{+}$ Clock

Jau, Yuan-Yu, Hunker, Jeffery David, and Schwindt, Peter D.D.
Sandia National Laboratories, Albuquerque, NM/USA
E-mail: yjau@sandia.gov

The miniature, microwave ^{171}Yb ion clock [1] developed at Sandia National Labs has demonstrated good clock performance, comparable to a commercial Cs beam frequency standard. *F*-state trapping, however, has been a critical issue that prevents us from using all the trapped ions for the clock signal interrogation. As shown in Fig. 1, throughout the normal optical pumping, each Yb ion can eventually fall into the $F_{7/2}$ state before decaying back to the ground state. This *F*-state has a very long lifetime (6 years natural lifetime), and usually a laser is introduced to intentionally clear out the *F*-state, such as the 760-nm laser shown in Fig. 1.

In our buffer-gas cooled Yb ion clock, a few microtorr of helium buffer gas is present inside the ion-trap vacuum package. The *F*-state lifetime is shorter compared to the ultra-high vacuum environment. Without the *F*-state clearing laser, we still observe greater than 70% of the ions being in the *F*-state that cannot contribute to the clock signal. For the purpose of making a miniaturized Yb ion clock, the *F*-state laser is not preferred due to the additional power consumption of the laser and the complication of locking its frequency. Utilizing a buffer gas that can quench the *F*-state without relaxing the ground state and shifting the clock frequency is therefore very important for a miniature trapped ion clock. The nitrogen molecule (N_2) is known to be good for *F*-state quenching [2]. Unfortunately N_2 is pumped by the passive getter used inside the vacuum package. We have conducted a series of experiments and identified that methane (CH_4) can serve as a good quenching gas. We find its relative frequency shift coefficient to be -2.9×10^{-6} /torr and its ground-state decoherence rate coefficient to be 9.7×10^{4} s^{-1}/torr. For our clock operating conditions, the required CH_4 pressure to achieve sufficient *F*-state quenching is around 10^{-8} torr. Hence the frequency shift and the linewidth broadening of the clock resonance are negligible. In principle CH_4 cannot be pumped by the gas getter we use below 300C. Therefore CH_4 can be used to boost up the signal and improve the ^{171}Yb ion clock performance. We will present more details regarding this work.

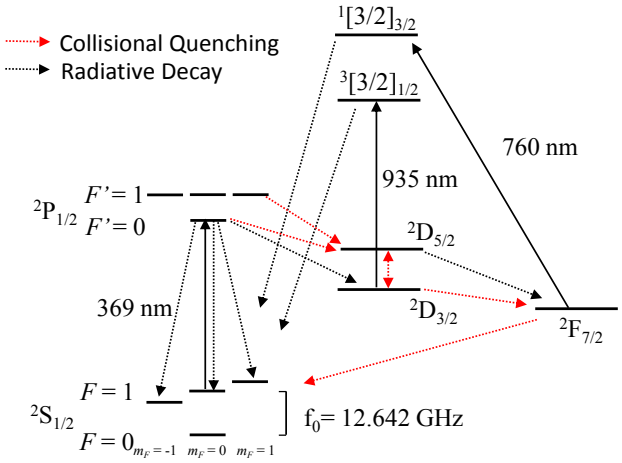


Fig. 1: Energy-level diagram of ^{171}Yb ion with optical pumping scheme and the decaying paths.

[1] Y.-Y. Jau, H. Partner, P.D.D. Schwindt, et al. "Low-Power, Miniature ^{171}Yb Ion Clock Using an Ultra-Small Vacuum Package," Appl. Phys. Lett. 101, 253518 (2012)

[2] D. J. Seidel and L. Maleki, "Efficient quenching of population trapping in excited Yb+," Phys. Rev. A 51, R2699 (1995).

Demonstration of long vacuum integrity lifetime of trapped ion standard package

Thejesh Bandi, John Prestage, Sang Chung, Thanh Le, Nan Yu
Jet Propulsion Laboratory, California Institute of Technology,
Pasadena, California, USA.
E-mail: thejesh.n.bandi@jpl.nasa.gov

Space navigation and deep-space tracking can be enhanced by precise onboard clocks. A promising avenue for future precision space clocks is the trapped Hg^+ standard [1, 2]. An Hg^+ standard has advantages over other compact standards. For instance, it does not require lasers; therefore there is no complexity associated with operating and stabilizing lasers. The Hg ions in the trap are optically pumped by spectral lamp as used in compact rubidium clocks. Further benefits of Hg^+ clock are that it requires no shutters, has low magnetic field sensitivity and no wall collisions (as in a Rubidium vapor cell clock). It is made of a completely sealed vacuum tube with no active pump, no consumables (as in cesium tube standards and hydrogen masers), no cryogenics, and no microwave cavities. The absence of wall-collisions offers a high atomic line-Q.

We describe a compact Hg ion quadrupole linear trap package (volume of 1 liter) that was vacuum-sealed since 2005 (about 9.5 years) in our laboratory. Presently, it is still able to store ions for 400 days without any replenishment. We demonstrate this package is still operational with excellent vacuum integrity, showing the long shelf life of these vacuum tubes. Since the sealing of this package it has been passively pumped using a getter pump. The investigations made with this package when in active pump stage has already been reported [3]. The long trap-lifetime and longer shelf life indicates the ultra-high vacuum environment inside the package and its reliability for portable applications. In addition to the vacuum trap package, we also used original optical and detection packages along with new lamps for the current studies.

The long ion trap lifetime presents an opportunity to study interesting phenomena that cause the relaxation of ions in the trap. We investigate the effect of charge transfer relaxations induced by the neutral Hg atoms on the trapped Hg ions. Significant effects on Rabi signals are observed with the neutral Hg density, which provide a measure of the charge transfer collisions between the trapped ions and neutral Hg atoms. Understanding the charge transfer relaxation phenomenon is of great value for improving the Hg+ clock performance as well as for fundamental physics process investigations.

Acknowledgements: This work was carried out at the Jet Propulsion Laboratory (JPL), under contract with the National Aeronautics and Space Administration (NASA). Thejesh Bandi thank Swiss National Science Foundation (SNSF) for the fellowship through Early Postdoc Mobility (EPM) grant.

[1] J.D. Prestage, M. Tu, S.K. Chung, and P. MacNeal, "Compact microwave mercury ion clock for space applications", Proceedings of the 39th Annual Precise Time and Time Interval (PTTI) Meeting, Long Beach, CA, pp. 249-256, 2007.

[2] J.D. Prestage, S. Chung, L. Lim, and T. Le, "Miniaturized mercury ion clock for ultra-stable deep space applications", Proceedings of the 38th Precise Time and Time Interval (PTTI) systems and applications meeting, Washington DC, pp. 95-104, 2006.

[3] J.D. Prestage, S. Chung, T. Le, M. Beach, L. Maleki, and R.L. Tjoelker, "One-liter ion clock: new capability for space-flight applications", Proceedings of the 35th Annual Precise Time and Time Interval (PTTI) Systems and Applications Meeting, San Diego, California, USA, pp. 427-433, 2004.

Measuring Speed of Light Isotropy to 10^{-18} with Cryogenic Microwave Oscillators

Parker, Stephen, Nagel, Moritz*, Kovalchuk, Evgeny*, Stanwix, Paul, Hartnett, John+, Ivanov, Eugene, Peters, Achim*, Tobar, Michael

School of Physics, The University of Western Australia, Crawley, Australia
*Institut für Physik, Humboldt Universität zu Berlin, Berlin, Germany
+School of Chemistry and Physics, University of Adelaide, Adelaide, Australia
E-mail: stephen.parker@uwa.edu.au

Lorentz symmetry is a foundational property of modern physics, but it is suspected that at high enough energies it could be broken, with observable effects appearing at Planck-suppressed levels. The most significant consequence of Lorentz symmetry is the isotropic nature of the speed of light, which remains invariant under rotation and boost transformations. Thus precision measurements of the isotropy of the speed of light provide a powerful portal for exploring the frontiers of physics.

We present the results of our modern Michelson-Morley experiment [1] that uses two ultra-stable cryogenic sapphire oscillator microwave frequency sources [2] to make the most precise measurement to date of the spatial isotropy of the speed of light, constraining $\Delta c/c$ to $9.2\pm10.7\times10^{-19}$ (95% C.I.). This is an order of magnitude improvement over the current state-of-the-art and is the first terrestrial test of Lorentz symmetry in electrodynamics at the Planck-suppressed electroweak unification scale. Our data is used to set new limits on Lorentz violating coefficients of the Standard Model Extension [3].

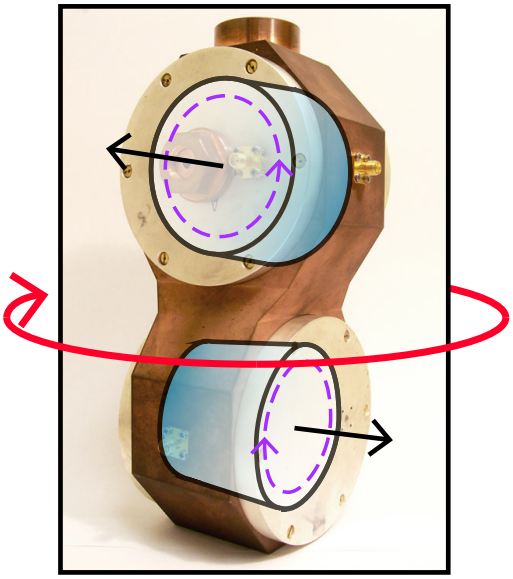


Fig. 1: Sketch of the experimental setup, showing the two sapphires with their crystal axes (black arrows) aligned orthogonally. The Poynting vectors for the resonant modes are sketched in purple, and the red arrow shows the active turntable rotation.

Two sapphire loaded cavity resonators are mounted in the same copper block and aligned such that their crystal axes are orthogonal (Fig. 1). Two independent oscillators are built by locking each to one of the sapphire loaded cavities. An orientation or velocity dependent fractional change in the speed of light would induce a fractional change in the beat frequency comparison of the two oscillator circuits. The cavities were cooled with liquid helium and rotated continuously on a high-precision air-bearing turntable with a period of 100 seconds, which corresponds to the optimal performance of the experiment. Data was collected over the course of a year, with the sensitivity ultimately dictated by the frequency stability of the oscillators. Sources of systematic noise and plans for current and future updates will be discussed.

[1] M. Nagel, S.R. Parker, E.V. Kovalchuk, P.L. Stanwix, J.G. Hartnett, E.N. Ivanov, A. Peters, and M.E. Tobar, "Direct Terrestrial Measurement of the Spatial Isotropy of the Speed of Light to 10^{-18}," arXiv:1412.6954v1, 2014.

[2] C.R. Locke, E.N. Ivanov, J.G. Hartnett, P.L. Stanwix and M.E. Tobar, "Design techniques and noise properties of ultrastable cryogenically cooled sapphire-dielectric resonator oscillators," Rev. Sci. Instrum., 79(5), 051301, 2008.

[3] V.A. Kostelecky and M. Mewes, "Signals for Lorentz Violation in Electrodynamics", Phys. Rev. D 66, 056005, 2002.

Simple Method for Minimizing Background Fields Using Coherent Effects in Cold Atoms

Paul D. Kunz, David H. Meyer, Qudsia Quraishi
Quantum Sciences Group, Army Research Laboratory, Adelphi, MD, USA
E-mail: paul.d.kunz.ctr@mail.mil, qudsia.quraishi.civ@mail.mil

Within the class of coherent nonlinear optical effects that exhibit sub-natural linewidth features, coherent population trapping (CPT) and nonlinear magneto-optical rotation (NMOR) have had a dramatic impact on compact atomic clocks [1] and sensing with atomic magnetometers [2]. A related effect, known as electromagnetically induced absorption (EIA) [3], has received less attention in the literature, though it has comparable sub-natural linewidths. Previous work on EIA has been largely carried out in warm atomic vapors, which can provide strong signals due to the large atom number, but this brings velocity changing collisions and Doppler broadened transitions. To avoid this we use a magneto-optical trap (MOT) as a source for cold ^{87}Rb atoms, and characterize EIA with respect to parameters such as transverse fields, polarization, and optical power. We find that this effect provides a simple, real-time, method for minimizing background DC magnetic fields for cold atom experiments, as it does not rely on additional equipment or post-processing of data. A schematic of our experiment is shown in Figure 1. Our magnetic field is controlled by three orthogonal sets of Helmholtz coils, and the simultaneous detection of transmission and polarization rotation signals is achieved with two photodetectors in a polarimeter configuration.

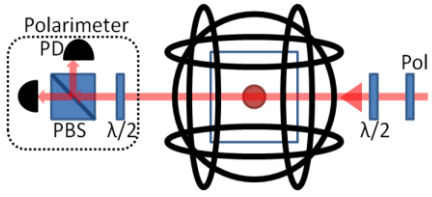


Fig. 1: Schematic showing single linearly polarized beam interrogating cold ^{87}Rb atoms centered in 3-axis Helmholtz coils.

We report on the first observation of EIA in cold atoms using the Hanle configuration, where a single laser beam is used to both pump and probe the atoms while sweeping an axial magnetic field through zero. We find that, associated with the EIA peak, a "twist" appears in the corresponding NMOR signal (see inset of Figure 2) when transverse magnetic fields are present. This twist, which is nested within the NMOR signal, has been previously noted by Budker et al., in the context of warm vapor optical magnetometry [4], and was described as being due to optical pumping through nearby hyperfine levels. By studying these features with cold atoms, thus rendering the hyperfine levels well resolved, we aim to enhance the understanding of the optical pumping mechanism behind it, and elucidate its relation to EIA. We demonstrate the ease and efficacy of using these coherent effects for nulling our background fields, thereby increasing spin coherence lifetime and improving sub-Doppler optical cooling, important aspects in nearly all cold atom experiments.

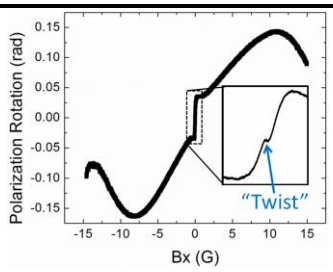


Fig. 2: Data showing nested optical rotation features. The broad dispersion curve is linear Faraday rotation, and the narrow feature is NMOR. Inset shows NMOR with visible "twist" in the center.

[1] J. Vanier, "Atomic clocks based on coherent population trapping: a review," *Appl. Phys. B*, vol. 81, no. 4, pp. 421–442, Aug. 2005.
[2] D. Budker and M. Romalis, "Optical magnetometry," *Nat. Phys.*, vol. 3, no. 4, pp. 227–234, Apr. 2007.
[3] A. Lezama, S. Barreiro, and A. M. Akulshin, "Electromagnetically induced absorption," *Phys. Rev. A*, vol. 59, no. 6, pp. 4732–4735, Jun. 1999.
[4] D. Budker, V. Yashchuk, and M. Zolotorev, "Nonlinear Magneto-optic Effects with Ultranarrow Widths," *Phys. Rev. Lett.*, vol. 81, no. 26, pp. 5788–5791, Dec. 1998.

Majorana atomic transition research in H-maser's magnetic state selection region

Aleynikov Mikhail
Time and Frequency Department, National Research Institute for Physical-Technical and RadioTechnical Measurements
FSUE VNIIFTRI, Moscow Region, Russia
E-mail: alejnikov@vniiftri.ru

For efficient performance of a single state selection system when using Majorana method, it's extremely important to know how eventual angle of rotation for atom's spin depends on a total magnetic field in a region between selection magnets[1]. As it was shown in previous work, the angle of rotation for spinor F = 1 greatly depends on a transverse (in regard to the hydrogen beam axis *z*) displacement of the zero-value total field[2]. In this work, for the first time, the dependence of single-state selection system performance (or H-maser's output power *P*) on the currents I_x and I_y of the transverse coils, that are placed at the region between magnets, is experimentally obtained. In figure 1 the angles of rotation for spinor, that are equal to $0,\pi/2,\pi$ under corresponding quantity of the currents, i. e. transverse coordinates of the zero field, are evidently shown. The optimal values of the currents, when the maximum of the single-state selection efficiency (the angle of rotation is equal π) is achieved, are defined. Moreover, the operation of the single-state selection system is confirmed by exploration of the H-maser's power curve and also by double resonance method. The relative amount of the operating atoms in the beam, that defines single-state selection system efficiency, is approximately 70%.

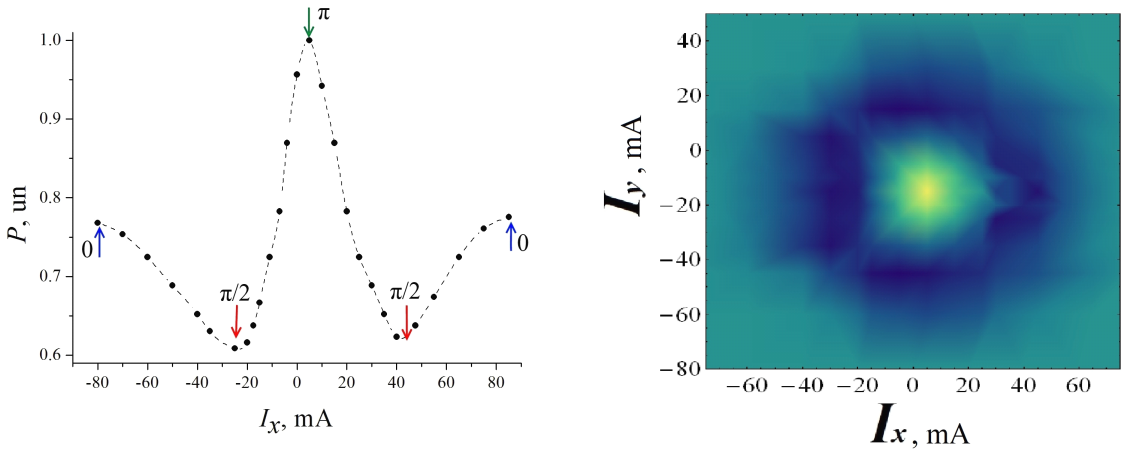


Figure 1. Normalized dependence of the H-maser's output power on the current of the transverse coil I_x under fixed value of the another coil current $I_y = -15\ mA$ (left) and general shape of such dependence on the both currents (right). Under turning of the spin to the angle π, in the atomic beam are predominantly presented operating atoms $F = 1,\ m_F = 0$, that corresponds to the maximum H-maser power. Under turning of the spin to the angle $\pi/2$ the number of the operating atoms decreases in comparison with previous case, but the number of the undesired atoms increases and leads to additional spin-exchange interaction in the storage bulb, that corresponds to the minimum H-maser power. When the turning is absent, the amount of the operating atoms is equal to the angle π case, but the amount of the undesired atoms exceeds angle π case.

[1] S. Urabe, K. Nakagiri, Y. Ohta, M. Kobayashi, and Y. Saburi, "Majorana Effect on Atomic Frequency Standards", IEEE Trans. On Instrum. and Measur., vol. IM-29, N. 4, pp. 304-310, 1980.

[2] Aleynikov M. S., Boyko A. I., "On the single-state selection for H-maser and its signal application for fountain atomic standard", *Proceedings*, 2014 IEEE European Frequency and Time Forum, Neuchatel, June 23-26, 2014, pp. 169-172.

Noise Investigation on Optical Detection in a Cesium Beam Clock with magnetic state selection

Liu Chang, Zhou Sheng, Wang Yanhui
Institute of Quantum electronics, School of Electronic Engineering and Computer Science,
Peking University, Beijing, China
E-mail: wangyanhui@pku.edu.cn

Cesium beam clocks have good performance on long-term stability and accuracy. We try to apply optical detection in a conventional compact cesium beam clock with magnetic state selection. Laser-based optical detection is successfully realized, as we reported in [1]. The difference in this paper is that the collecting bulb is removed and the atomic beam is detected directly. The general view of the clock is shown in Fig.1, where a fluorescence collector is mounted at the detection region instead of the traditional magnet B and electron multiplier. An external cavity diode laser, which is locked on 4-5 transition of cesium D2 line by means of saturated absorption spectroscopy, acts as the light source. Short-term stability of $1.0\times10^{-11}\cdot\tau^{-1/2}$ is achieved at oven temperature of 102 °C.

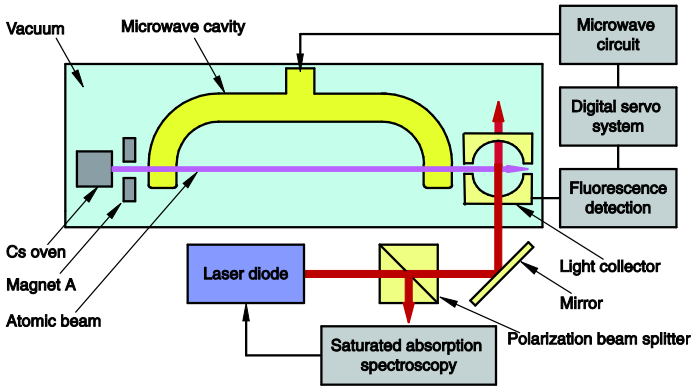


Fig. 1: Schematic diagram of our cesium beam clock.

The noise sources in an optically pumped cesium beam resonator, including atomic shot noise, photon noise, laser frequency noise and photon detection noise, are discussed in [2]. The condition is similar in our case. In this paper, we mainly focus on the noise induced by the optical detection, which largely depends on the laser's status, including its linewidth, frequency detuning and modulation parameters. The laser frequency noise is of most concern, since its power spectral density is proportional to the square of atomic flux intensity. In our beam tube, the number of invalid atoms which increase this noise, such as F=4 atoms surviving the selection, is larger than that in an optically pumped one. Besides, the scattered light brings the laser intensity fluctuation into the fluorescence signal.

A simple experimental method of estimating the noise in detection is presented and the noise analysis result is given. We discuss suitable parameters for the laser in our experiment and methods to reduce noise in the detection.

[1] C. Liu, R. Shi, Y. Wang, S. Liu and T. Dong, "An optically detected cesium beam frequency standard with magnetic state selection" *Proceedings*, 28th European Frequency and Time Forum, Neuchatel, Switzerland, June 23-26, 2014, pp. 175-177.
[2] N. Dimarcq, V. Giordano, P. Cerez and G. Theobald, "Analysis of the noise sources in an optically pumped cesium beam resonator," IEEE Trans. Instrum. Meas., vol. 42, no. 2, pp. 115-120, Apr. 1993.

The effect of bend on the Ramsey cavity

Sun Fuyu*, Huang Xianhe
University of Electronic Science and Technology of China, Chengdu, China
fuyusun@std.uestc.edu.cn

The Ramsey cavity is one of core components that compose the Cs beam tube in the Cs atomic beam clocks. In this work, the contribution from the waveguide bend on the field distribution of the cavity is carefully investigated by using combination method of Maxwell equations and Finite element simulation. We find that there exists TM_{11} mode inside cavity in addition to standing wave TE_{10p} mode. Meanwhile, we also find that the cavity resonance frequency is closely related to the bend radius.

Fig.1 is a demonstration structure of the Ramsey cavity. It is bent in the E-plane of the standard X-band waveguide and closed at the extremities. The total cavity longitudinal length is $L = 2l + l_{drift} + \pi r_{bend} = 186mm$, thus TE_{108} mode is fundamental operating mode, where l_{drift} is drift region length, r_{bend} is mean bend radius. The dimension of the cross-section of the beam hole is $3mm \times 6mm$. The net transverse magnetic field in right straight arm that excites the clock transition is H_x.

In order to investigate unknown mode inside cavity when the cavity resonant at clock transition frequency f, the longitudinal electric field E_z is investigated, since TE_{108} mode has not contribution to E_z. As a proof of presence of TM_{11} mode, the dependence of E_z on the x and y are plotted for $y = 3mm$ and $x = 7mm$ in Fig.2 respectively, where $z = 26mm$, l_{drift} =110mm and $r_{bend} = 6mm$. Simulation results reveal that E_z is the field component of TM_{11} mode, this can be easily explained via Maxwell theory. We let $H_x = H_{x-TE} + H_{x-TM}$, where H_{x-TE} and H_{x-TM} denote the transverse magnetic field of TE_{108} mode and TM_{11} mode respectively, and we have $H_{x-TM} \propto \sin(\pi x/a)\cos(\pi y/b)\left(e^{-\alpha z} + e^{\alpha z}\right)$, Furthermore, we can evaluate the contribution of TM_{11} mode on H_x. In the center of the beam hole $(x = a/2, z = 3mm)$, the variation of the microwave magnetic field as a function of y is calculated, we have $|H_{x-TM}/H_x| \approx 2.25\times10^{-4}\left|\cos(\pi y/b)\right|$. Lastly, a simulation result of the cavity resonance frequency change related to the drift region length under different bend radius is also investigated (Fig. 3), intuitively, the operating frequency may can be regards as the superposition of a constant frequency and an oscillation frequency for a given bend radius and a total longitudinal cavity length.

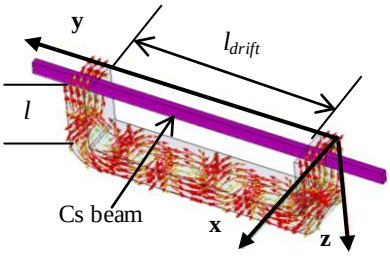


Fig. 1: Cavity Structure.

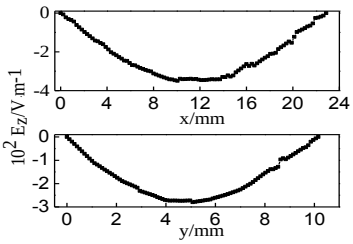


Fig. 2: E_z vs x, y.

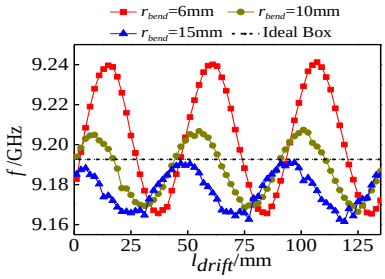


Fig. 3: f vs l_{drift}.

The similar conclusions hold for the cavity with a phase difference of π between the two interaction regions. Our work may help in designing cavity and providing a more accurate description of the cavity operating mode.

[1] Lacey R F, "Phase shift in microwave Ramsey structures," in *Proc.22nd Freq. Contr. Symp.*, Atlantic City, New Jersey, April 22-24, 1968, pp. 545-558.

[2] Drullinger R E, Shirley J H, Lowe J P and Glaze D J, "Error analysis of the NIST optically pumped primary frequency standard," IEEE Trans. Instrum. Meas. , vol. 42, no. 2, pp. 453-456, Jun. 1993.

Development of a transportable optically-pumped cesium beam clock

Berthoud Patrick, Haldimann Manuel, Kundermann Stefan*, Hermann Virgile+, Michaud Alain
Oscilloquartz SA, CH-2000 Neuchâtel, Switzerland
*Centre Suisse d'Electronique et de Microtechnique SA, CH-2000 Neuchâtel, Switzerland
+Thales Electron Devices, F-78140 Vélizy, France
E-mail: michaud@oscilloquartz.com

Commercial primary reference clocks are using the principle of magnetic deflection of a cesium atomic beam propagating in a vacuum sealed tube. While this technology is well mastered by a few worldwide manufacturers, its frequency stability and its operational lifetime must be traded off: for long life operation (10 years) the frequency stability is $\sigma_y(\tau) \leq 2.7\text{E-}11\ \tau^{-1/2}$, while increased performances to $\sigma_y(\tau) \leq 8.5\text{E-}12\ \tau^{-1/2}$ reduces its lifetime (3 years). This limitation is inherently due to the operation principle (magnetic deflection), in which only a small fraction of the cesium beam flux contributes to the useful error signal. In order to overcome this limitation, optical pumping of the cesium atomic beam dramatically increases the useful cesium beam flux with limited impact on the atomic quality factor, which yields finally a ten-fold improvement of the clock frequency stability at $\sigma_y(\tau) \leq 3\text{E-}12\ \tau^{-1/2}$ without compromising its lifetime (10 years). Several past developments have paved the way with technological proves of feasibility [1-4].

Oscilloquartz has developed a breadboard of transportable optically-pumped cesium clock in partnership with TED for the Cs tube, and CSEM for the Laser and Optics module. The collimated Cs beam is produced by an oven operated at 110°C. The atomic beam preparation and detection processes are achieved by a single optical pumping transition (D2:44' transition). The laser is a monolithic DFB module emitting at 852 nm. The microwave Ramsey cavity is designed with π phase shift between both arms ("dark fringe" design). The Fig. 1 shows the breadboard of transportable clock fitting in a standard 19 inches and 3U high frame. The short-term frequency stability has been measured at $\sigma_y(\tau) \leq 2.75\text{E-}12\ \tau^{-1/2}$ for $\tau \leq 100$ s. For longer integration time, the clock frequency stability is limited by the high sensitivity of the laser diode to optical feedback and acoustic noise.



Fig. 1: Transportable optically-pumped cesium beam clock breadboard

This development has been partially financially supported by the European Space Agency (project number 21603/08/D/JR).

[1] S. Guérandel et al, "Compact cesium beam frequency standard: improvements of the frequency stability towards the $10^{-12}\ \tau^{-1/2}$ level", Proc. of the EFTF conference, St-Petersburg, Russia, 2002, pp. E-028-E029
[2] S. Lecomte et al, "Performance demonstration of a compact, single optical frequency cesium beam clock for space applications", Proc. of the EFTF conference, Geneva, Switzerland, 2007, pp. 1127-1131
[3] P. Berthoud et al, "Optically-pumped space cesium clock for Galileo: first results of the breadboard", Proc. of the EFTF conference, 2008, Toulouse, France
[4] R. Lutwak, "Optically pumped cesium-beam frequency standard for GPS-III", Proc. of the PTTI meeting, 2001, Long Beach, CA, USA, pp. 19-32

Phase transients in the PHARAO microwave source

François-Xavier Esnault, Michel Abgrall*, Philippe Laurent*

Centre National d'Etudes Spatiales, Toulouse, France
*LNE-SYRTE / Observatoire de Paris, Paris, France
E-mail: francois-xavier.esnault@obspm.fr

This works presents the different issues related to the phase transients on the PHARAO microwave source and its impact on the ACES/PHARAO signals. Due to the sequential operation of cold atom clock, events synchronous with clock cycle (microwave and AOM switches, shutters,…) can lead to phase perturbations of the interrogation signal and thus to a frequency shift [1].

The PHARAO microwave source, designed and manufactured by Thales Airborne Systems, provides 3 metrological signals. Based on a 5 MHz USO, a 100 MHz signal is synthesized and phase-locked to the output of the Space Hydrogen Maser (SHM). This intermediate signal is then multiplied up to 9.192GHz for preparation and interrogation of the Cs atoms. Different events of the PHARAO operation induce perturbations on these metrological signals, like the preparation signal switch, the mechanical shutters of the laser beams or even serial link commands.

Phase transients can affect PHARAO frequency in two different ways. Direct perturbations on the interrogation signal at 9.192 GHz only matter if they occur during the Ramsey sequence. However, transients on the 100MHz signal are seen by the PLL and give rise to a phase drift downstream. Even though great efforts have been made by the manufacturer between engineering and flight models to minimize sensitivity, the phase transients-related shift is still not negligible at the 10^{-16} accuracy level.

We will present the measurements done to characterize these phase transients on both the 100 MHz and 9.192 GHz signals. We will also assess the impact of these perturbations on the PHARAO accuracy and describe the strategies to tackle this effect once in orbit.

[1] Santarelli, G., G. Governatori, D. Chambon, M. Lours, P. Rosenbusch, J. Guena, F. Chapelet, et al. "Switching Atomic Fountain Clock Microwave Interrogation Signal and High-Resolution Phase Measurements." *IEEE Transactions on Ultrasonics, Ferroelectrics and Frequency Control* 56, no. 7 (July 2009): 1319–26. doi:10.1109/TUFFC.2009.1188.

Design of the new NIM6 fountain with collecting atoms from a 3D MOT loading optical molasses

Fang Fang, Weiliang Chen, Nianfeng Liu, Kun Liu, Rui Suo and Tianchu Li

National Institute of Metrology (NIM), Beijing, P. R. China

Email: fangf@nim.ac.cn

A new cesium fountain clock NIM6 is under construction in the National Institute of Metrology China. Besides some improvements on the design of the Ramsey cavity to reduce the Distributed cavity phase shift and microwave leakage, NIM6 is also aiming to collect more atoms from a MOT loading optical molasses (OM) and optical pumping, leading to a better signal to noise ratio at the detection.

The design of the physical package of NIM6 is shown in figure 1. Cesium atoms are first collected in the lower MOT and launched to the upper OM with a small angle (10°) to prevent Cs atoms flying into the detection chamber directly. With atom temperature of 70 μK adjusted by the intensity and detuning of the cooling beams, the diameter of the cloud is about 6.5 mm when reaching the OM center. The launching velocity and atom temperature will be re-manipulated by the OM and launched vertically. The advantage of this design is not only able to collect more atoms, compared to the directly OM loading like NIM5 does, the background Cs gas in the detection chamber is also reduced due to a differential pumping between MOT and OM chambers. Furthermore, the atom density distribution is more uniform than that of 2D-MOT loading OM. The cooling lights for the MOT and OM work alternatively in one fountain cycle so could be supplied by one TA with time division multiplexing.

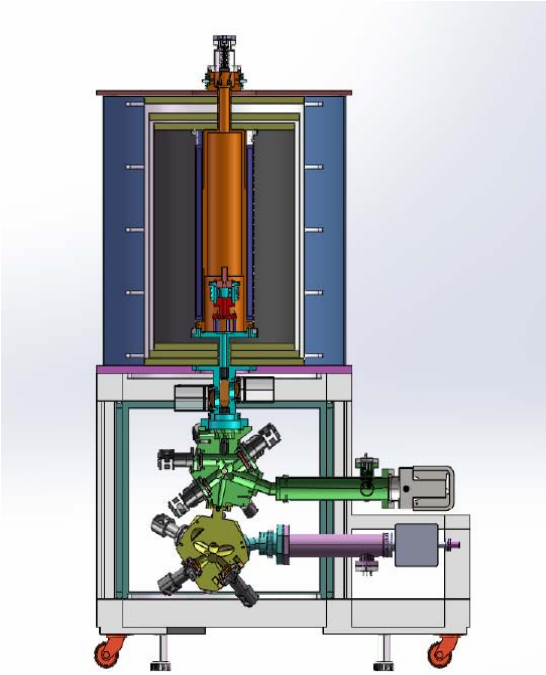


Fig. 1: The vacuum system design of NIM6 with a MOT loading optical molasses.

The atom numbers can be further increased by a de-pumping - optical pumping procedure. The atoms, distributed evenly in the F=4 sublevels after launch, are first de-pumped to F=3 state, then, atoms in are optical pumped to the $|F=3, m_F=0\rangle$ clock state with a linear pumping light on resonance with F=3 → F'=3 transition. The atom number on the clock state $|F=3, m_F=0\rangle$ is increased compared to the atom number using a routine selecting method, and the atoms in the other $|F=3, m_F\neq 0\rangle$ are less than 3% of the clock state in an ideal case.

A new microwave frequency synthesizer using Cryogenic Sapphire Oscillator (CSO) as a local oscillator is also under developing to reduce the phase noise, thus improve the short term instability of NIM6 to reach the quantum projection noise. NIM6 with better short term instability is going to be used to compare the absolute frequency of the Sr lattice optical clock with uncertainty of E-16 in the future.

Progress in Cs Fountain Clock Research in NTSC

Dandan Liu[1,2,3], Xinliang Wang[1,2,3], Jiang Chen[1,3], Rui Lin[2,3], Yong Guan[1,3], Hui Zhang[1,3], Jun Ruan[1,3], Fengxiang Yu[1,2,3], Junru Shi[1,2,3], Shougang Zhang*[1,3]

1.National Time Service Center, Chinese Academy of Science, Xi'an, Shaanxi, 710600, China

2. University of Chinese Academy of Science, Beijing 100039, China

3. Key Laboratory of Time and Frequency Primary Standards, Chinese Academy of Science, Xi'an, Shaanxi, 710600, China

E-mail: liudandan@ntsc.ac.cn, *szhang@ntsc.ac.cn

A cesium fountain clock operated in National Time Service Center (NTSC) will extend the time-keeping capabilities and improve UTC(NTSC). We present a current status of the Cs fountain clock (NTSC-F1) developing at NTSC. Since last year we have made many improvements to the NTSC-F1 physics package, laser system and frequency servo system where the NTSC-F1 physics package has undergone several major maintenance and upgrade procedures, resulting in a reduction by over a factor of 1 in the stability. The short-term fractional frequency instability of cesium atomic fountain clock measured against an H-maser is 3.1×10^{-13} at 1 s. The resulting Ramsey resonance signal with a full-width half-maximum linewidth (FWHM) as narrow as 0.8 Hz and signal noise ratio (SNR) with 110 are obtained by launching the atoms to a height of 45 cm above the interrogation cavity (see Fig. 1). The improvements are discussed in detail in this paper. A first measurement of the magnetic field homogeneity yields 0.8 nT (rms) (see Fig. 2). The C field map is generated by measuring the transition frequency $|3,0\rangle\rightarrow|3,m\neq0\rangle$ of the magnetically sensitive transition using a low-frequency excitation coil transverse to the flight path. The other evaluation procedure of the systematic frequency shifts are under performed.

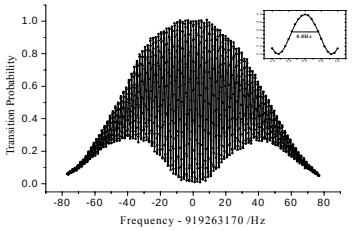


Fig. 1: Ramsey fringes obtained in the cesium fountain clock. The inset shows an enlargement of the central fringe which has a line-width of 0.8 Hz at half maximum of the transition probability.

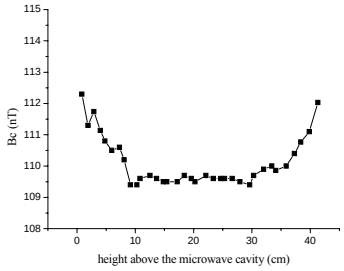


Fig. 2: Map of the magnetic field above the Ramsey cavity

[1] S. Weyers, U. Hiibner, R Schr8der, Ch. Tam and A.Bauch, "Uncertainty evaluation of the atomic caesium fountain CSF1 of the PTB," *Metrologia*, vol. 38, no. 4, pp. 343-352, 2001.

[2] S. Weyers, A. Bauch, D. Griebsch, U. Hiibner, R Schr8der and Ch. Tam, "First results of PTB's atomic caesium fountain," *Proceedings*, 1999 and the IEEE International Frequency Control Symposium, 1999., Proceedings of the 1999 Joint Meeting of the European, pp. 16-19, 1999.

[3] S. R. Jefferts, J. Shirley, T. E. Parker, T. P. Heavner, D. M. Meekhof, C. Nelson, F. Levi, G. Costanzo, A. De Marchi, R. Drullinger, L. Hollberg, W. D. Lee and F. L. Walls, "Accuracy evaluation of NIST-F1," *Metrologia*, vol. 39, no. 5, pp. 321-336, 2002.

Towards the entirely operation of cesium fountain clock with an ultra stable laser

de Carlos-López Eduardo, Ortiz-Cardona Carlos Andres*, López-Romero J. Mauricio, López-López Sergio
Dirección de Metrología de Tiempo y Frecuencia, Centro Nacional de Metrología (CENAM), Querétaro, México
* Centro de Investigación y de Estudios Avanzados del Instituto Politécnico Nacional (IPN), CINVESTAV, Unidad Querétaro, Querétaro, México
E-mail: edlopez@cenam.mx

Laser frequency stabilization by Ultra Low Expansion (ULE) optical cavities is a recent strategy to create ultra-stable optical oscillators which are fundamental, among other applications, for the new atomic clocks generation based on optical transitions. In this work we describe the implementation process of an ultra-stable optical oscillator using an optical Ultra Low Expansion (ULE) cavity and an Extended Cavity Diode Laser (ECDL) in order to use it as a master laser in a Cs fountain clock. With the aim of operate the CENAM cesium fountain clock (labeled as CENAM CsF-1) based on an ultra-stable optical master oscillator, some improvements on the CENAM CsF-1 set up (particularly in the optical part) have been done. The CENAM CsF-1 master laser is a continuous wave commercial ECDL equipped with a low loss interference filter, with 852 nm wavelength (near to the cesium D2 line), and 20 kHz linewidth. In order to reduce the linewidth of master laser, an ULE optical cavity is used (Advanced Thin Films, model ATF-6020-4 A - 50mm Notched Cavity Assy). The cavity linewidth is less than 2.3 kHz with a quality factor (Q) of 1.52×10^{11} and a free spectral range Δf_{fsr} of 1.49 GHz.

In order to measure and evaluate the frequency differences between the optical cavity and the ^{133}Cs D2 line, an experimental arrangement using polarization spectroscopy to stabilize the frequency of an Acousto-Optic Modulator (AOM) is implemented, with the ECDL frequency stabilized prior to the optical cavity. Therefore, the RF generator's output frequency of the AOM contains information about the frequency differences between the cavity and cesium spectroscopy. Due to its special characteristics, the short time stability of the ULE cavity is much better than the stability offered by the cesium saturation spectroscopy. In order to resolve the changes in frequency difference that could be attributable to the cavity, it is necessary to take measurements for long periods of time and ensure that variations are not associated with the saturation spectroscopy technique. Figure 1 shows preliminary results from the Allan deviation corresponding to the frequency differences between the optical cavity and cesium's spectroscopy. Once characterized, the ultra-stable laser can serve as a frequency reference to stabilize a frequency comb [1] in order to generate microwave frequencies to interrogate the clock transition in the atomic fountain. Thus it will be possible to operate the cesium fountain clock entirely using an ultra stable laser as a master oscillator.

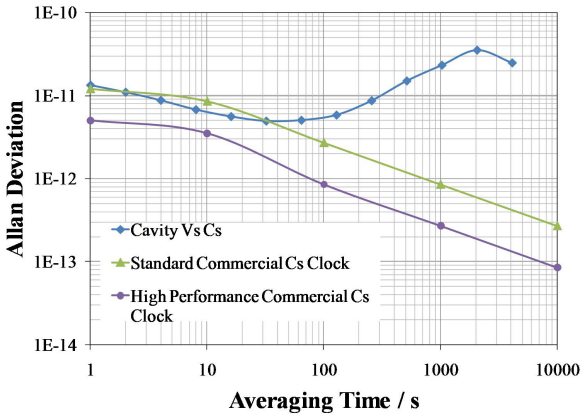


Fig. 1: Allan deviation corresponding to the frequency differences between the optical cavity and cesium's spectroscopy.

[1] T. M. Fortier, M. S. Kirchner, F. Quinlan, J. Taylor, J. C. Bergquist, T. Rosenband, N. Lemke, A. Ludlow, Y. Jiang, C. W. Oates and S. A. Diddams, "Generation of ultrastable microwaves via optical frequency division," *Nature Photonics*, 2011, pp. 425-429.

Phase Transient Analyzer for Precision Spectroscopy

M. Kazda, V. Gerginov, N. Huntemann, B. Lipphardt, S. Weyers

Physikalisch-Technische Bundesanstalt (PTB),
Bundesallee 100, 38116 Braunschweig, Germany
E-mail: Michael.Kazda@ptb.de

Progress in the development of atomic fountain clocks necessitates increasing care of frequency shifting effects which appeared comparatively small before or even have not at all been taken into account before. The pulsed operation modus of fountain clocks involves a number of cyclic switching processes, which may cause cycle synchronous phase variations of the microwave interrogation signal, which in turn may cause frequency shifts. In a fountain very small phase variations at the µrad level already result in frequency shifts at the 10^{-16} level, which is comparable to the dominant uncertainty contributions in today's most advanced fountain clocks. To detect such small phase variations sophisticated phase transient analyzing techniques have been developed [1], capable of coherent averaging synchronous to the fountain cycle.

We have developed a phase transient analyzer consisting of a commercially available FGPA-system with a 120 Ms/s 16 bit analog-digital converter front-end. The data acquisition and filtering is entirely carried out within the FPGA, making it possible to use advanced digital signal processing technologies and high-order filters. We have implemented an entirely digital I/Q demodulation and phase detection. Due to the large on-board memory, high-resolution measurements can be implemented on a long time scale. For our caesium fountain clocks [2,3], the analyzer allows us to determine cycle-synchronous phase excursions that would cause frequency shifts of less than 10^{-16}.

Due to its superior spectral resolution, Ramsey spectroscopy can have advantages in optical frequency standards. However, it requires higher phase stability during the interrogation pulses compared to Rabi spectroscopy [4]. We successfully employ a Ramsey-type excitation scheme in a single-ion Yb^{+}-clock to suppress otherwise dominating frequency shifts [5]. To investigate the effect of cycle synchronous phase excursions for example from optical pass length instabilities of the clock laser, we complemented our phase analyzer for the analysis of optical beat signals. From the recorded data we are able to determine phase excursions that correspond to frequency shifts of less than 10^{-18}.

[1] G. Santarelli, G. Governatori, D. Chambon, M. Lours, P. Rosenbusch, J. Guéna, F. Chapelet, S. Bize, M.E. Tobar, P. Laurent, T. Potier and A. Clairon, "Switching atomic fountain clock microwave interrogation signal and high-resolution phase measurements", IEEE Trans. Ultrason., Ferroelect., Freq. Contr. 56, 1319 (2009).

[2] S. Weyers, U. Hübner, R. Schröder, Chr. Tamm and A. Bauch, "Uncertainty evaluation of the atomic caesium fountain CSF1 of the PTB ", Metrologia 38, 343 (2001).

[3] V. Gerginov, N. Nemitz, S. Weyers, R. Schröder, D. Griebsch and R. Wynands, "Uncertainty evaluation of the caesium fountain clock PTB-CSF2", Metrologia 47, 65 (2010).

[4] S. Falke, M. Misera, U. Sterr and C. Lisdat, "Delivering pulsed and phase stable light to atoms of an optical clock", Applied Physics B 107, 301 (2012).

[5] N. Huntemann, B. Lipphardt, M. Okhapkin, Chr. Tamm, E. Peik, A.V. Taichenachev and V. I. Yudin, "Generalized Ramsey Excitation Scheme with Suppressed Light Shift", Phys. Rev. Lett. 109, 213002 (2012).

Improvements on the atomic fountain in SIOM

Yuanbo Du*+, Rong Wei*, Richang Dong*+, Fan Zou*+, Yuzhu Wang*
*Key Laboratory of Quantum Optics, Center for Cold Atom Physics, Shanghai Institute of Optics and Fine Mechanics, Chinese Academy of Science, Shanghai, 201800, China
+University of Chinese Academy of Sciences, Beijing, 100049, China
E-mail: weirong@siom.ac.cn

Abstract— We present several improvements on a rubidium 87 atomic fountain clock at Shanghai Institute of Optics and Fine Mechanics (SIOM), Chinese Academy of Sciences. The improvements include decreasing the quality factor of the interrogation cavity from 18000 to 10000, optimizing the coupling of microwave, adjusting the working temperature of interrogation region from 53.2°C to 29.0°C, and locking the local oscillator directly by a lower-noise control circuit. A comparison between the fountain clock and a local H-maser was carried out, demonstrating a short-term relative frequency stability of $2.7\times10^{-13}\tau^{-1/2}$, which reached 1.6×10^{-15} at the average time of 32 800 seconds. An uncertainty of 6×10^{-16} at the average time of 300 000 seconds was obtained in a self-comparing experiment. And a remote chain of GPS common view has been also set up to comparing our fountain clock with the time and frequency standards in other time-keeping laboratories.

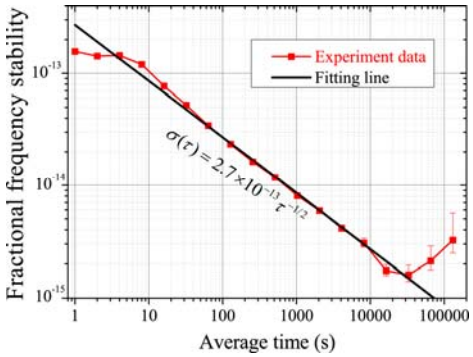


Figure 1. The short-term frequency stability of the atomic fountain compared with the H-maser, with the fitting curve $2.7\times10\text{-}13\tau^{-1/2}$, and it reaches 1.6×10^{-15} at the average time of 32800 seconds

Reference

[1] Weyers, S., et al. (2001). "Uncertainty evaluation of the atomic caesium fountain CSF1 of the PTB." Metrologia 38(4): 343.

[2] Chun-Yan, S., et al. (2011). Progress in rubidium fountain clock research at SIOM. Frequency Control and the European Frequency and Time Forum (FCS), 2011 Joint Conference of the IEEE International.

[3] Petit, G. and Z. Jiang (2008). "Precise point positioning for TAI computation." International Journal of Navigation and Observation 2008.

[4] Guéna, J., et al. (2014). "Contributing to TAI with a Secondary Representation of the SI Second." Metrologia 51(1): 108.

Comparison of Frequency Estimators for Interrogation of Wireless Resonant SAW Sensors

Kalinin, Victor
Transense Technologies plc, Bicester, Oxfordshire, UK
E-mail: victor.kalinin@transense.co.uk

Wireless resonant SAW sensors are often interrogated by means of a pulsed RF excitation of the SAW resonators and a measurement of the frequency of their free oscillations. Estimation of the frequency of the SAW response is usually performed by means of DFT and quadratic interpolation to find the maximum of the energy spectrum [1]. This method is known to be very close to a maximum likelihood estimator (MLE) for a complex sine wave in the presence of AWGN and it attains Cramer-Rao lower bound (CRLB) within a wide range of SNR values. However, there are a number of other frequency estimators [2,3] that have been recently developed by a signal processing community for the complex sine wave in the presence of AWGN. Some of them might be less computationally complex than MLE. The problem is that SAW interrogators do not just add a Gaussian noise to the signal. They also introduce a phase noise, limit the SAW response amplitude and distort its phase. Besides, the SAW response may or may not contain a parasitic mode response in addition to the main one so the analysis of [2,3] relying on CRLB as a benchmark is not sufficient. The aim of the paper is to investigate performance of three parametric estimators in a realistic SAW reader and compare them with the DFT-based estimator.

The first one [2] is a phase-based frequency estimator (PBFE) employing weighted least-squares estimate of the phase difference between neighbouring filtered signal samples. The second one [3] uses singular value decomposition (SVD) to separate signal and noise subspaces and then applies a generalized weighted linear predictor (GWLP) to the left and right principal singular vectors to find the phase difference between their components. Both methods were developed for a constant amplitude sine wave. The last one [3] was developed for a damped sine wave. It also employs SVD and then finds the phase difference between the components of the left and right principal singular vectors by means of an iterative weighted least squares (WLS) method.

First, a statistical simulation was performed using a numerical model of the reader [1]. It was found that, for a low SAW response magnitude corresponding to the AWGN domination region, PBFE performs much worse than the other three methods due to its high SNR threshold (Fig. 1). However, for a high SAW response magnitude corresponding to the phase noise domination region, PBFE performs better than the other methods. Influence of the signal nonlinear distortions and parasitic modes on all four estimators was also investigated. After that, experiments were performed for closely coupled sensor and reader antennas. They showed that PBFE performed just slightly better than DFT and SVD+WLS but SVD+GWLP was the worst one.

[1] V. Kalinin, "Influence of receiver noise on resolution of passive wireless resonant SAW sensors," *Proceedings*, 2005 IEEE Int. Ultrasonic Symp., Rotterdam, Holland, 19-21 Sep. 2005, pp. 1452 – 1455.

[2] M. L. Fowler, and J. A. Johnson, "Extending the threshold and frequency range for phase-based frequency estimation," IEEE Trans. Signal Process., vol. 47, no. 10, pp. 2857-2863, Oct. 1999.

[3] W. Sun and H. C. So, "Efficient parameter estimation of multiple damped sinusoids by combining subspace and weighted least squares techniques", *Proceedings*, 2012 IEEE ICASSP, Kyoto, Japan, 25-30 Mar. 2012, pp. 3509-3512.

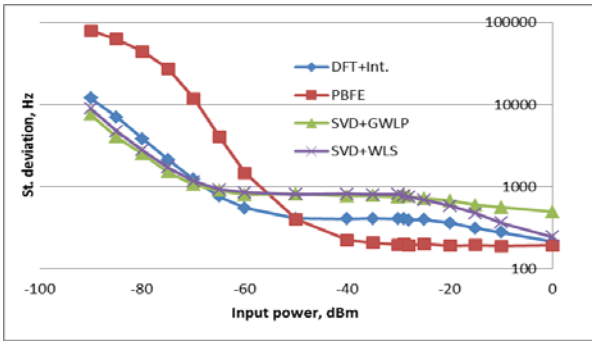


Fig. 1: Simulated standard deviation of the measured frequency against the SAW response input power.

Acoustic power gain induced by 2D electron drifting

Shao, Lei*, and Pipe, Kevin P.*+
*Department of Mechanical Engineering, University of Michigan, Ann Arbor, MI 48109-2125, USA
+Department of Electrical Engineering and Computer Science, University of Michigan, Ann Arbor, MI 48109-2122, USA
E-mail: shaolei@umich.edu

Interactions between acoustic waves and electrons have been extensively studied for more than half a century. Hutson, McFee, and White demonstrated that bulk ultrasonic waves could be substantially amplified by electron drift in a bulk piezoelectric semiconductor if the electron velocity exceeds the ultrasonic wave speed [1]. Later studies examined coupling between surface acoustic waves (SAWs) and electrons in a bulk or thin-film semiconductor. Following numerous demonstrations of acoustoelectric devices such as resonators, convolvers, and correlators, attention shifted to coupling between SAWs and two-dimensional electron gases (2DEGs), in particular the attenuation of SAWs by a 2DEG [2], the generation of SAWs in a dynamically screened 2DEG [3], and the transport of electrons by SAWs [4]. In this work, we analytically study the amplification of SAWs by electron drift in a 2DEG as shown in Fig. 1.

To model the acoustoelectric amplification of SAWs by electron drift in a 2DEG, we first revisit the amplification of SAWs in a bulk piezoelectric semiconductor [5]. We then adapt the well-known equation to a nanometer-scale conductive 2DEG layer of thickness d << 1/k on an insulating piezoelectric substrate, where k is the SAW wavevector and 1/k is the typical SAW penetration depth into the substrate.

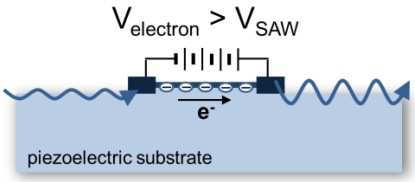


Fig. 1: Illustration of a layer structure and applied bias supporting SAW interaction by electron drift in a 2DEG which is located on top of a piezoelectric dielectric substrate.

The distinctive difference for amplification of SAWs in a 2DEG versus bulk is that the physical overlap between the SAW penetration depth (which extends a distance of approximately 1/k into the piezoelectric substrate) and the 2DEG conducting layer is very small as shown in Fig. 2. In a 2DEG-on-pieozelectric-insulator structure, the field modulation associated with the incident SAW relaxes by producing displacement currents within the conductive 2DEG channel. We show that this effect leads to frequency-independent gain per radian, which only occurs in the SAW-2DEG interaction among all types of structures used for acoustoelectric amplification. Furthermore, these calculations show that the peak power gain per radian for a SAW propagating through a 2DEG occurs at a sheet carrier density that is readily achievable, whereas for a SAW propagating through a piezoelectric bulk semiconductor, it occurs at a carrier density below practical limits.

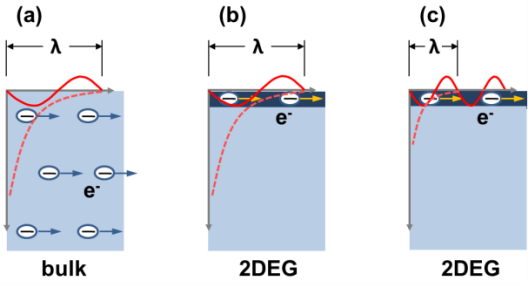


Fig. 2: Illustration of SAW penetration depth and its overlap with the conducting layer. (a) SAW interacts with a bulk piezoelectric semiconductor. (b) Low-frequency and (c) high-frequency SAWs interact with a 2DEG located on top of a piezoelectric insulator.

[1] A. R. Hutson, D. L. White, and J. H. Mcfee, Phys Rev Lett **7**, 237 (1961).
[2] A. Wixforth, J. P. Kotthaus, and G. Weimann, Phys Rev Lett **56**, 2104 (1986).
[3] L. Shao, M. Zhang, A. Banerjee, P. Bhattacharya, and K. P. Pipe, Appl Phys Lett **99**, 243507 (2011).
[4] S. Hermelin, S. Takada, M. Yamamoto, S. Tarucha, A. D. Wieck, L. Saminadayar, C. Bauerle, and T. Meunier, Nature **477**, 435 (2011).
[5] J. H. Collins, K. M. Lakin, C. F. Quate, and H. J. Shaw, Appl Phys Lett **13**, 314 (1968).

Modeling and control of a traveling wave in a finite beam, using multimodal approach and vector control method

GHENNA, Sofiane[1], F. GIRAUD[1], C. GIRAUD-AUDINE[1,2], M. AMBERG[1], and B. LEMAIRE-SEMAIL[1]
[1]Laboratoire d'Electrotechnique et d'Électronique de Puissance, Université Lille1
IRCICA, 50 avenue Halley, 59650 Villeneuve d'Ascq, France
[2]Ecole Nationale des Arts et métier Paris-tech, Lille, France
8 Boulevard Louis XIV, 59800 Lille
E-mail: sofiane.ghenna@ed.univ-lille1.fr

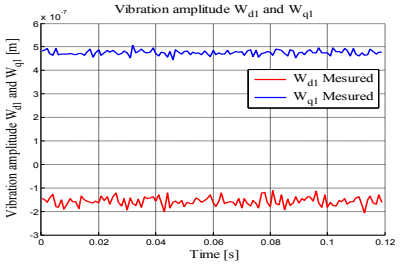
Abstract— This paper presents a new method to produce and control the vibration amplitude and direction of traveling wave in a finite beam, using multimodal approach. A closed loop control of the transducer vibration is applied using vector control method. This allows to regulate the vibration amplitude of the traveling wave directly. An analytical modeling is presented, with experimental validation, showing good performances even in the presence of perturbations.

Several studies are focused on the generation of traveling waves on a beam, to realize linear motor for instance. [1] Produced a traveling wave using two transducers in an early work by Sashida. One transducer was used to produce the traveling wave, while the other absorbed it to prevent the formation of standing wave. It should be noted that this method requires impedance matching, between the beam and that transducers.

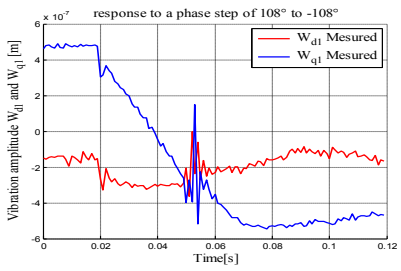
The second method [2] is based on the excitation of two successive flexion modes of the beam, which are excited by forces produced by two transducers. These forces are shifted by $\pi/2$ and generated at a frequency between the two mode frequencies. The advantage is that the impedance matching is no more required and so changing direction can be achieved by changing the phase difference from $\pi/2$ to $-\pi/2$.

However, these methods are in open loop control and cannot control the vibration amplitude in the presence of disturbance. In [3], the authors proposed a closed-loop control of transducers and the beam to produce a traveling wave using the second method. The main drawback is that it requires the identification of the whole system.

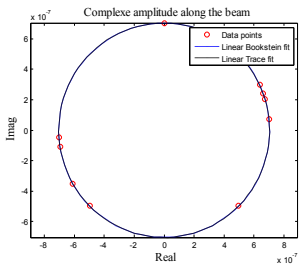
In this work, this latest approach is improved by controlling the vibration of each transducer in a rotating frame. It is then possible to control the amplitude of each actuator and their relative phase shift. This standing wave amplitude is directly controlled and the effect of the beam is rejected as a perturbation. Hence, it is necessary to model only the transducers. As depicted in the figure below, experiments have shown that it was possible to control phase and amplitude (left) even in transient (middle) and obtained a large traveling wave with standing wave ratio nearly equal to one.



Vibration amplitude of the left actuator in rotating frame with 0.5 µm and phase of 108°



Vibration amplitude response to a phase step to invert the travelling wave



Traveling wave with SWR ≃ 1

[1] T. Sashida and T. Kenjo, An Introduction to Ultrasonic Motors. Clarendon Press, 1993.

[2] B.-G. Loh and P. Ro, "An object transport system using flexural ultrasonic progressive waves generated by two-mode excitation," IEEE Transactions on Ultrasonics, Ferroelectrics, and Frequency Control, vol. 47, no. 4, pp. 994–999, Jul. 2000.

[3] F. Giraud, C. Giraud-Audine, M. Amberg, and B. Lemaire-Semail, "Vector control method applied to a traveling wave in a finite beam," IEEE Transactions on Ultrasonics, Ferroelectrics, and Frequency Control, vol. 61, no. 1, pp. 147–158, 2014.

Measurement and Analysis of a Circular Wedge Acoustic Waveguide using PZT Sensor

Yu, Tai-Ho
Department of Electronic Engineering, National United University
2 Lienda Road, Nan-Shi Li, Miaoli 36003, Taiwan
E-mail: yth@nuu.edu.tw

This study investigated the propagation of flexural waves along the outer edge of a circular cylindrical wedge, as well as phase velocities and the corresponding mode displacement. Thus far, only approximate solutions to these problems have been derived because of the complexity of boundary-value problems. In this study, the dispersion curves were determined using the bi-dimensional finite element method (Bi-d FEM), as derived through the separation of variables and the Hamilton principle. According to a calculation of modal displacement, the maximum deformation appeared at the outer edge of the wedge tip. Numerical examples also indicated how distinct thin-film materials deposited on the outer surface of the circular cylindrical wedge influenced the dispersion curves.

Additionally, the dispersion curves were measured using a laser-induced guided wave experiment, in which a PZT sensor measurement scheme and a two-dimensional fast Fourier transform (2D-FFT) method were used. According to the 2D-FFT calculation results of B-scan data from the laser-generated flexural waves at the circular cylindrical wedge tip, most of the measured signals belonged to the first and second modes.

The reliability of numerical solutions was confirmed, and the necessity of numerical solutions in the design and application of wedge-like acoustic waveguides was subsequently validated. Regarding the design of circular cylindrical wedge wave ultrasonic motors, a flexural wave with a low mode number *N* and high wavenumber *k* was selected as the driving mode.

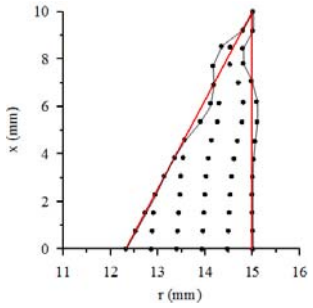


Fig. 1: Bi-d FEM simulation result.

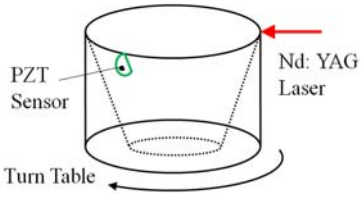


Fig. 2: Schematic of measurement process.

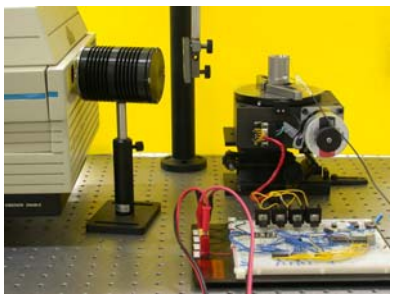


Fig. 3: Photograph of the experimental setup.

[1] P. E. Lagasse, Higher-order finite element analysis of topographic guides supporting elastic waves. *Journal of Acoustical Society of America*, **53** (1973), 1116-1122.

[2] A. C. Hladky-Hennion, Finite analysis of the propagation of acoustic waves in waveguides, *Journal of Sound and Vibration*, **194**(2), (1996), 119-136.

[3] V.V. Krylov and G.V. Pritchard, Experimental investigation of the aquatic propulsion caused by localized flexural wave propagation in immersed wedges and plates, *Appl. Acoustics*, **68** (2007)**,** 97-113.

The Characterization and Temperature Sensor Application of $Ca_3TaGa_3Si_2O_{14}$ Crystal Resonators

Hongfei Zu, Huiyan Wu, Quanming Lin*, Yanqing Zheng*, Qing-Ming Wang
Department of Mechanical Engineering & Materials Science, University of Pittsburgh, Pittsburgh, Pennsylvania, USA
*Shanghai Institute of Ceramics, Chinese Academy of Sciences, 588 Heshuo Road, Jiading, Shanghai, 201800 China
Email: qiw4@pitt.edu

Due to the increasing needs for advanced sensor technology which can be applied in extreme environments, the high-temperature sensors have won great attention in aerospace, automotive and energy industries in the past few years. Recently, langasite family crystals, especially the ordered ones have been widely studied for high temperature sensor applications due to their excellent electromechanical coupling properties and high temperature stability [1]. Among the ordered ones, the $Ca_3TaGa_3Si_2O_{14}$ (CTGS) crystal resonators have demonstrated the great promising as one of the best high temperature acoustic wave sensors [2].

In this paper, the temperature behavior (from ambient temperature to 800°C) of all CTGS's dielectric, piezoelectric and elastic coefficients were investigated according to IEEE standard method. Based on the sensitivity and linearity of crystal resonators with different cuts in high temperature test, the optimal orientation for the temperature sensors is determined. The high temperature stability of the selected crystal sensor is studied by repeatedly measuring the same type of signal with a certain time interval for months. The preliminary measurements demonstrate that the elastic stiffness coefficient c_{11}^{E} exhibits the best linearity and high sensitivity verse temperature, as shown in Fig. 1. The change of c_{11}^{E} value from room temperature to 800°C is about 6.1%. And the same sample (X-cut plate) was measured four times with one-month interval for a duration of four months. As can be seen in Fig. 2, the impedance essentially stays unchanged during the entire course of tests, indicating that the excellent temperature stability of X-Cut CTGS crystal resonator for temperature sensor.

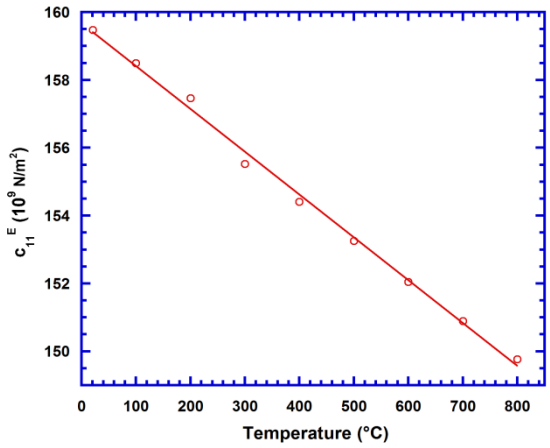


Fig. 1: The elastic stiffness coefficient (c_{11}^{E}) verse temperature.

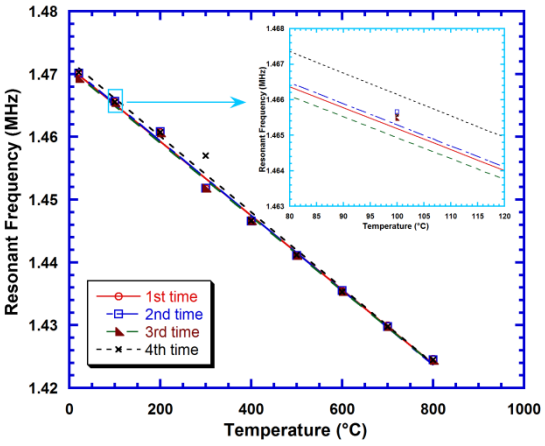


Fig. 2: The repeated impedance measurement of X-cut crystal resonator sample for duration of four months. The inset enlarges the result at 100°C.

[1] B. H. T Chai, A. N. P. Bustamante, and M. C. Chou, "A new class of ordered langasite structure compounds," *Proceedings*, 2000 IEEE/ELA Int. Frequency Control Symp., Kansas City, MO, Jun 1-5, 2000, pp. 163-168.

[2] X. Z. Shi, D. R. Yuan, X. Yin, A. J. Wei, S.Y. Guo, and F. P. Yu, "Crystal growth and dielectric, piezoelectric and elastic properties of $Ca_3TaGa_3Si_2O_{14}$," Solid State Commun., vol. 142, pp. 173-176.

Novel gyroscopic mounting for crystal oscillator applied in high dynamic GNSS receiver to improve tracking loops

Maryam Abedi, Tian Jin
Beihang University, School of Electronic and Information, Beijing 100191, China
E-mail: abedi_maryam@buaa.edu.cn

In high dynamic GNSS receivers, crystal oscillator output signal is polluted by dynamic loads modulated on it. Vibration loads such as sinusoidal and random vibrations cause clock drift on oscillator output. In GNSS receivers, the tracking loops will lost when clock drift exceeds the certain boundary. Thereby reduce the vibration loads induced disturbances, such as phase and frequency jitter, give arise the improvement in tracking thresholds for GNSS receivers.

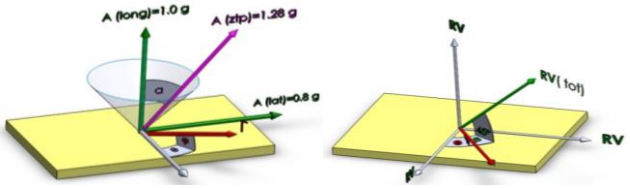


Figure1: (left) sinusoidal vibration,(right) random vibration applied on crystal oscillator by high dynamic receiver

A gyroscopic mounting introduces to install the oscillator on electronic board. It will give the freedom to rotate freely around roll, pitch and yaw. In the case of low frequency loads, gyro oscillates as dynamic load is perpendicular to crystal surface in any given moment. And in the case of high frequency loads, gyro has not enough time to oscillate, so crystal remains perpendicular to zero to peak vibration load. By this method, gyro-mounting can minimize the effect of vibration loads on crystal oscillator output and improves the tracking loops on PLL and FLL for GNSS receivers.

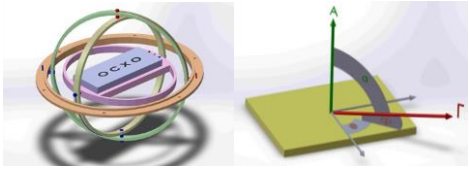
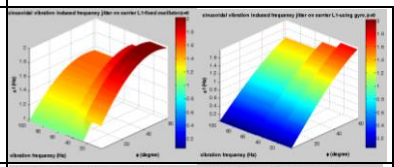
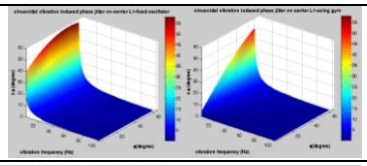
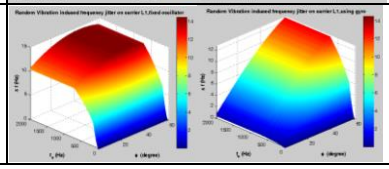
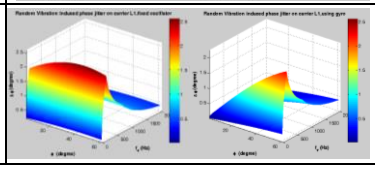


Figure2: (left) gyro-mounting (right) dynamic load orientation for oscillator installed on gyro

PLL tracking threshold: for BPSK $3\sigma \leq$ phase pull-in range of the PLL discriminator/4=180°/4→ $3\sigma \leq 45°$ & $\sigma \leq 15°$;
FLL tracking threshold: $3\sigma \leq$ frequency pull-in range of the FLL discriminator/4=1/4T→$3\sigma \leq 12.5$ & $\sigma \leq 4.6$ (Hz)(T=20 ms);

Numerical analysis is provided to illustrate the positive effect of this mounting on GNSS receiver tracking thresholds and compared performance before and after using it. High dynamic receiver assumed as a GPS receiver installed on launch vehicle ARIAN 5 and equipped with OCXO with Γ=10^(-9),Q-factor=10^(11) and uses L1 carrier=154×f0, f0=10.23 MHz.

A (Dynamic load)	Frequency jitter (Δf) (τ=1s)	Phase jitter (Δφ) (τ=1s)	Max gyro effect on		Explanation
	(left) before (right) after using gyro		FLL (Hz)	PLL (°)	
Sinusoidal Vibration (2-100 Hz)			-1.2446	-35.658	This load impacts PLL seriously. For φ<15°, gyro reduces phase jitter below 1σ threshold.
Random vibration (2-2000 Hz)			-10.056	-1.7782	This load impacts FLL seriously. For φ <18°, gyro reduces frequency jitter below 1σ threshold.

[1] "Arian 5 User's Manual Issue 5", Revision 1, July 2011.
[2] Jaap Wijker, "Random Vibrations in Spacecraft Structures Design", © Springer Science +Business Media B.V.2009.
[3] Jacob Job Wijker,"Spacecraft Structures", © 2008 Springer Science-Verlag Berlin Heidelberg.
[4] Elliott D.Kaplan, Christopher J.Hegarty, "understanding GPS Principles and Applications", second edition,ISBN-10: 1-58053-894-0,© 2006 ARTECH HOUSE, INC. 685 Canton Street Norwood, MA 02062.

The 3D Split-Ring Cavity Lattice: A New Metastructure for Sensing and Spectroscopy Applications

Maxim Goryachev and Michael E Tobar
ARC Centre of Excellence for Engineered Quantum Systems, School of Physics, University of Western Australia,
35 Stirling Highway, Crawley WA 6009, Australia
E-mail: michael.tobar@uwa.edu.au

A new patented electromagnetic cavity structure, a lattice of 3D cavities consisting of an array of posts and gaps is presented [1,2]. The individual cavity elements are based on the re-entrant cavity. We show that these cavities can also can be thought of as 3D split-ring resonators, which is confirmed by applying symmetry transformations, each of which is an electromagnetic resonator with spatially separated magnetic and electric field. The characteristics of the cavity are used to mimic phonon behavior of a 1D chain of atoms. It is demonstrated how magnetic field coupling can lead to phonon-like dispersion curves with acoustical and optical branches. The system is able to reproduce a number of effects typical to one-dimensional lattices exhibiting acoustic vibration, such as band gaps, phonon trapping, and effects of impurities. In addition, quasicrystal emulations predict the results expected from this class of ordered structures. The system is easily scalable to simulate 2 and 3D lattices and shows a new way to engineer arrays of coupled microwave resonators with a variety of possible applications to hybrid quantum systems proposed.

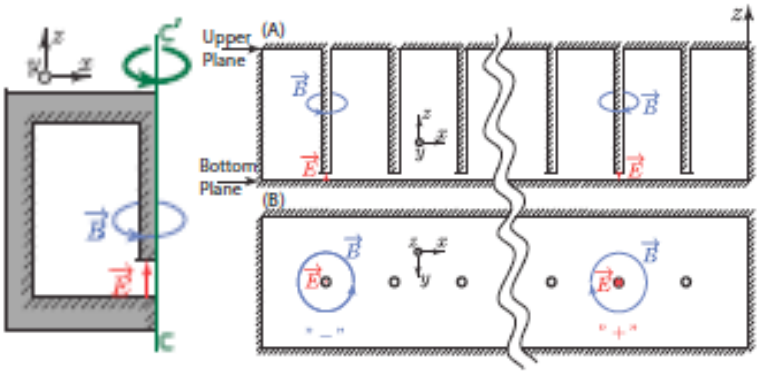


Fig. 1: Left, Rotation of the split-ring resonator surface required to construct a 3D microwave cavity. Right, (A) Side and (B) Top view, of a 1D lattice of 3D split ring resonators with for two possible field orientations shown.

Potential usages include: 1) Highly tunable multimode systems based on the closed cavity metamaterial [2]: 2) Applications in multi-frequency sensing: gas/fluids: 3) Probes of magnetic and dielectric properties of solids: 4) Space-resolved pressure sensors: 5) Spectroscopy of complex-shape small (sub-millimeter) crystals in the whole microwave region due to unique filling factors [3]: 6) Spatial separation of magnetic and electric fields required for some spectroscopy applications: 7) The system allows the engineering field structure in the cavity, with concentrated spots of magnetic field and dark field regions ideal for spectroscopy applications: 8) The possibility of future applications in quantum computing, a platform for hybrid quantum systems incorporating together superconducting circuits, conventional and superfluid optomechanics, spins in solids, etc.

[1] M. Goryachev and M. Tobar, "Microwave frequency magnetic field manipulation systems and methods and associated application instruments, apparatus and system," Patent: AU2014903143 (12 August 2014).
[2] M Goryachev, ME Tobar, "The 3D Split-Ring Cavity Lattice: A New Metastructure for Engineering Arrays of Coupled Microwave Harmonic Oscillators, arXiv:1408.3228[physics.ins-det], accepted New Journal of Physics 2015.
[3] NC Carvalho, Y Fan, J-M Le Floch, and ME Tobar, "Piezoelectric Voltage Coupled Reentrant Cavity Resonator," Rev Sci. Instrum., vol. 85, 104705, 2014.
[4] M Goryachev, WG Farr, DL Creedon, Y Fan, M Kostylev, ME Tobar, "High cooperativity cavity QED with Magnons at Microwave Frequencies," Phys. Rev. Applied, vol. 2, 054002, 2014.

Searching for High Frequency Gravitational Waves with High-Q Cryogenic BAW Resonators

Maxim Goryachev[1], Eugene Ivanov[1], Serge Galliou[2] and Michael E Tobar[1]
[1]ARC Centre of Excellence for Engineered Quantum Systems, School of Physics, University of Western Australia, 35 Stirling Highway, Crawley WA 6009, Australia
E-mail: michael.tobar@uwa.edu.au
[2]Time and Frequency Dept., FEMTO-ST Institute, UFC, CNRS, ENSMM, UTBM, Besançon, France

There are a number of theoretical predictions for astrophysical and cosmological objects, which emit high frequency ($10^6 - 10^9$ Hz) Gravitation Waves (GW) or contribute somehow to the stochastic high frequency GW background. In this work we show the possibility of a new sensitive detector in this frequency band, which is based on existing cryogenic ultra-high quality factor quartz Bulk Acoustic Wave cavity technology, coupled to near-quantum-limited SQUID amplifiers at 20 mK [1]. We show that spectral strain sensitivities reaching 10^{-22} per $\sqrt{\text{Hz}}$ per mode is possible, which in principle can cover the frequency range with multiple (> 100) modes with quality factors varying between $10^6 - 10^{10}$ allowing wide bandwidth detection. Due to its compactness and well established manufacturing process, the system is easily scalable into arrays and distributed networks that can also impact the overall sensitivity and introduce coincidence analysis to ensure no false detections.

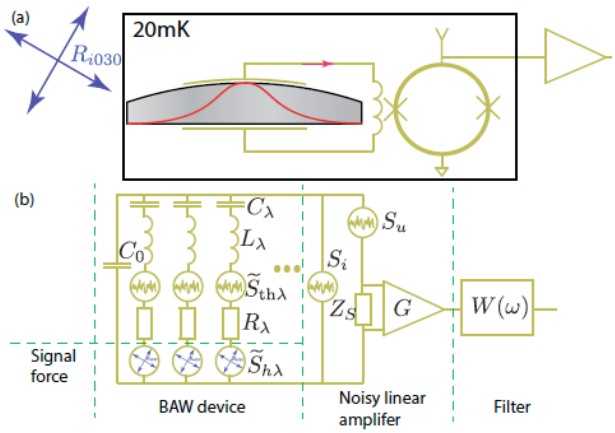


Fig. 1: (a) Experimental setup. (b) Equivalent electrical model.

A proto-type detector has been constructed to operate at 4K. The detector consists of a high-Q quartz BAW resonator coupled to a SQUID amplifier. Such systems are sensitive enough to be thermal noised limited at 4K [2]. Thus, besides introducing the theory of how GWs couple to BAW resonators. First results of implementation of such a detector at 4 K will be revealed.

[1] M Goryachev and ME Tobar, "Gravitational wave detection with high frequency phonon trapping acoustic cavities," Phys. Rev. D, vol. 90, 102005, 2014.

[2] M Goryachev, EN Ivanov, F van Kann, S Galliou, ME Tobar, "Observation of the fundamental Nyquist noise limit in an ultra-high Q-factor cryogenic bulk acoustic wave cavity," Appl. Phys. Lett., vol. 105, 153505, 2014,

Feasibility Study of Proximity Sensing by using a Conventional Airborne Transducer

Yamada, Ken, and Agatsuma, Shu

Department of Electronic Eng., Tohoku Gakuin Univ., Tagajo, Japan
E-mail: k-yamada@mail.tohoku-gakuin.ac.jp

Ultrasonic proximity sensors utilizing non-radiant (evanescent) acoustic fields created in the vicinity of piezoelectric vibrators were proposed [1]-[4]. When an object is brought into the evanescent field, electric admittance of the vibrator varies depending on the vibrator-to-object distance. In former reports [3], [4], the air-film damping effect occurred between the sensing plate attached to the length-extensional mode vibrator and the test-object plate was studied. In this configuration, lateral flow of the viscous fluid sandwiched in between the parallel plates undergoes resistive force that will act as a damper for the motion of vibration. Because the degree of damping varies depending on the gap width, it is applicable for detection of the gap width by observing the change in electrical properties of the piezoelectric vibrator. In this system, a 140° rotated *Y*-cut $LiNbO_3$ bar operating in the length-extensional mode at 80.9 kHz was employed for driving the sensor plate. Although it showed good sensing properties, it would be convenient if the system could be constructed by a conventional airborne transducer.

In this study, the sensing system is constructed by using a commercially-available airborne transducer (R40-16, NIPPON CERAMIC, Japan). The transducer is composed of a mono-morph-type bending plate with a radiation cone and housed in a metal case as shown in Fig. 1(a). The diameter and the height of the housing are 16.2 mm and 12.2 mm, respectively. The resonance (operation) frequency is 48.8 kHz. An acrylic plate of 5 mm thickness is approached to the face of the transducer using a pulse-motor stage, such as illustrated in Fig. 1(b). The variation in the peak value of the electric admittance at the resonance on the distance *d* between the transducer front surface and the target plate is observed by an impedance analyzer (IM3570, HIOKI E.E. Corp., Japan). The result is shown in Fig. 2. Distance dependent variation in the electric admittance level such as that observed in the former study has been confirmed. Feasibility of using the conventional airborne transducer for proximity sensing is discussed in detail in this paper.

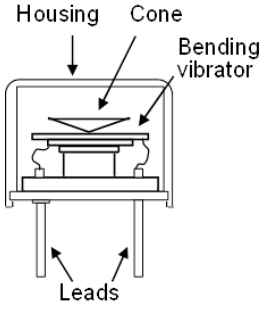


Fig. 1(a) Airborne transducer

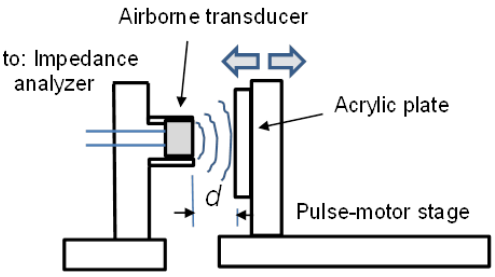


Fig. 1(b) Measurement setup

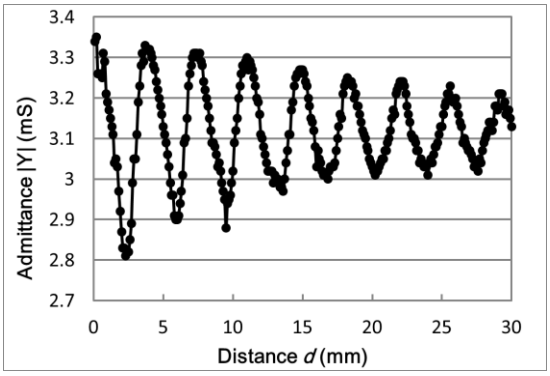


Fig. 2 Variation of electric admittance at resonance

[1] K. Yamada, D. Yamazaki, and K. Nakamura, "A Localized Acoustic Field Formed in the Vicinity of a Bending-Vibrator End and its Application to Piezoelectric Sensors," Proc. 2004 IEEE Ultrason. Symp., pp.1598-1602, 2004.

[2] K. Yamada, D. Yamazaki, and K. Nakamura, "Variation of Bending-Vibrator Characteristics when an Object is Brought into Close Proximity with the Vibrator End," Jpn. J. Appl. Phys., vol. 43, pp.2996-2999, 2004.

[3] K. Yamada, S. Kaneko, and T. Nagasawa, "Proximity Sensing through Air-Film Damping Effect Caused by Length-Extensional-Mode Piezoelectric Vibrator," Proc. 2008 IEEE Freq. Control Symp., pp.523-525, 2008.

[4] K. Yamada, S. Kaneko, and T. Nagasawa, "Basic Study on Proximity Sensors Utilizing Air-Film Damping Effect Caused by Longitudinal-Mode Piezoelectric Vibrator," Jpn. J. Appl. Phys., vol. 47, pp.3929-3930, 2008.

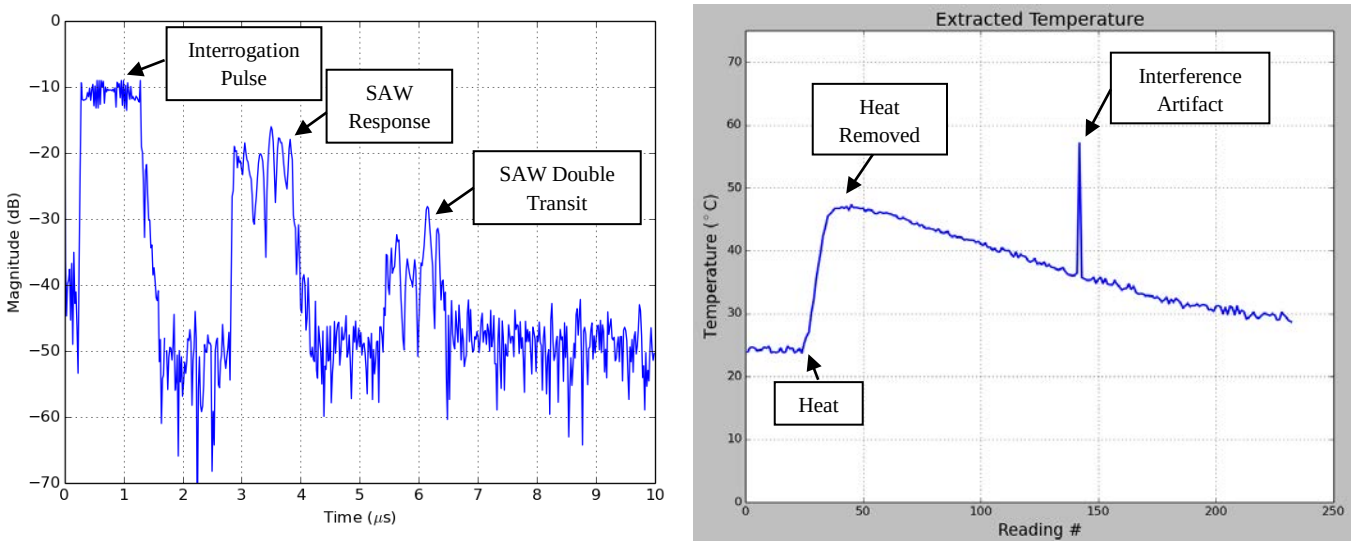
Interrogation of Orthogonal Frequency Coded SAW Sensors Using the USRP

Humphries, J.R., Gallagher, M.W., Gallagher, D.G., Weeks, A.R., and Malocha, D.C.
Department of Electrical Engineering and Computer Science, University of Central Florida, Orlando, FL
E-mail: James.Humphries@knights.ucf.edu

The universal software radio peripheral (USRP) is a versatile software defined radio (SDR) platform, developed by Ettus Research, which is intended for a wide variety of applications ranging from communication links to RADAR. We have investigated another application of the USRP by implementing a transceiver capable of interrogating passive, wireless surface acoustic wave (SAW) sensors at 915MHz. In particular, the USRP B200 is utilized for the transceiver design; it is a fully integrated transceiver based on the Analog Devices AD9361 RFIC and Xilinx Spartan 6 FPGA. It is an attractive platform for a passive sensor interrogator due to is small size (10x15x2 cm), relatively high output power (+10dBm), and large bandwidth (56MHz).

Interrogation of wideband orthogonal frequency coded (OFC) SAW sensors imposes strict requirements on the timing and synchronization of the transceiver. In the standard mode of operation, samples are generated and streamed between the USRP and host computer, introducing latency and bandwidth limitations due to the sampling bus. To achieve the performance required for this application, the USRP FPGA has been modified to introduce new functionality. Extraction of the sensor temperature is accomplished with a custom matched filter correlator. The system is capable of interrogating multiple sensors and can quickly reconfigure the USRP.

Demonstration of the USRP sensor interrogator is achieved by interrogating wireless SAW OFC sensors at 915MHz. Figure 1 shows (a) the received response from a SAW sensor and (b) the extracted temperature of the sensor over time.



(a) (b)

Figure 1: Example of received and processed data from the USRP B200. (a) Received data sweep from the USRP. The interrogation pulse and SAW responses are seen. (b) Extracted temperature of a single SAW sensor after being interrogated by the USRP. The sensor was heated and then let to cool over time.

SH-SAW Sensor Based Heavy Metal Detection

Ramshani, Zeinab, Narakathu, Binu B., Avuthu, Sai G. R., Obare, Sherine*, Atashbar, Massood Z.
Department of Electrical and Computer Engineering, Western Michigan University, Kalamazoo, Michigan
*Department of Chemistry, Western Michigan University, Kalamazoo, Michigan
E-mail: zeinab.ramshani@wmich.edu

Mercury (Hg), the second most toxic compound in the planet, is a neurotoxicant which targets the central nervous system as well as liver and heart muscles in human body [1]. Mercury ions, often released from a variety of natural and manmade sources easily accumulate in the vital organs and causes fatal effects [2]. Surface acoustic wave (SAW) sensors, which have been employed in various sensing applications, are an optimum choice for the detection of Hg due to its relatively small size, high resonant frequency, low power consumption and compatibility with CMOS technology. Moreover, SAW sensors operating in the shear horizontal mode cause parallel particle displacement which has a minimal energy loss in aqueous media. Therefore the development of detection systems, which incorporate shear horizontal surface acoustic wave (SH-SAW) sensors, for the highly sensitive detection of toxic heavy metals, such as Hg, in aqueous media is of utmost importance.

In this work, a SH-SAW sensor was photolithographically fabricated by patterning gold (Au) interdigitated electrodes (IDE) and reflectors on the surface of a 11 × 12 mm^2 64° YX-$LiNbO_3$ based piezoelectric substrate. The IDEs and reflectors for the two port resonator SH-SAW configuration were formed by sputtering 0.1 µm Au with electrode width and gap of 10 µm. The resonance frequency of the SH-SAW sensor was measured to be 112 MHz. A sensitive layer of phenol was deposited on top of the SH-SAW sensor surface, by drop-casting method, and placed in a custom built acrylic flow cell which consists of inlet and outlet ports for a polydimethylsiloxane (PDMS) based microfluidic channel (Fig. 1(a)). Varying concentrations of mercury nitrate ($HgNO_3$) were injected on the surface of the SH-SAW sensor using a programmable syringe pump. A PC based LabView™ application was used to control a network analyzer and measure the phase response (S_{21}) of the sensor. An average frequency shift of 184.83 kHz, 378.33 kHz, 458.33 kHz, 600.00 kHz and 748.33 kHz were observed for the 1 pM, 100 pM, 1 nM, 100 nM and 1 µM concentrations of $HgNO_3$ solution, when compared with the resonant frequency of DI water (Fig. 1(b)). The results obtained demonstrated detection levels as low as picomolar concentrations while the maximum permissible level for Hg in drinking water, by the United States Environmental Protection Agency, is 10 nM [2].The details of the SH-SAW sensor and the experiment setup as well as the response towards different heavy metal compounds such as nickel nitrate ($NiNO_3$) and iron nitrate ($FeNO_3$) will be presented.

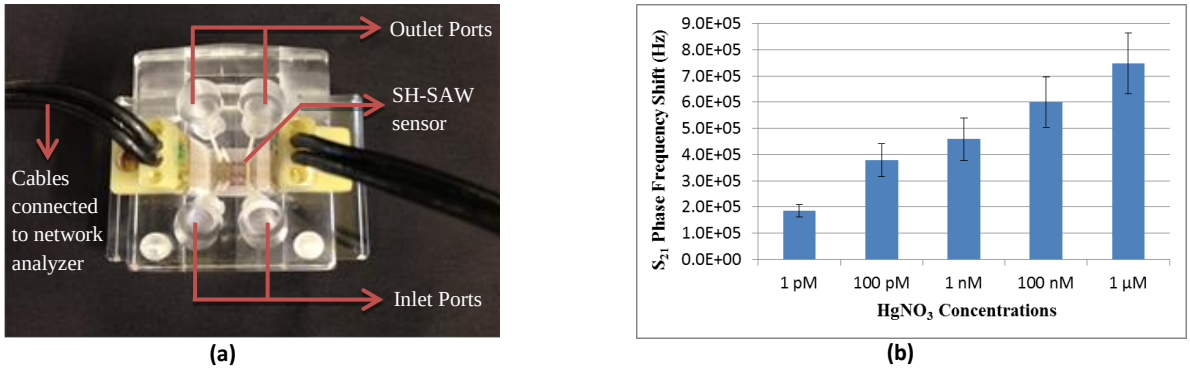


Fig. 1: (a) Flow cell with SH-SAW sensor and (b) SH-SAW sensor phase response towards varying concentrations of $HgNO_3$.

[1] G. K. Darbha, A. K. Singh, U. S. Rai, E. Yu, H. Yu, P. Chandra Ray, "Selective detection of mercury (II) ion using nonlinear optical properties of gold nanoparticles," J. Am. Chem. Soc., vol. 130, no. 25, pp. 8038-8043, Jun. 2008.

[2] S. C. S. Lin, X. Mao, T. J. Huang, "Surface acoustic wave (SAW) acoustophoresis: now and beyond," Lab Chip, vol. 12, no. 16, pp. 2766-2770, Jul. 2012.

The Study of BeiDou Timing Receiver Delay Calibration

Hongbo Wang, Hang Yi, Shengkang Zhang, Haifeng Wang, Huaiying Shang, Fan Shi, Zhenggang Ding

Science and Technology on Metrology and Calibration Laboratory, Beijing Institute of Radio Metrology and Measurement, Beijing, China

Email: wanghomeboy@139.com

The BeiDou System already provides continuous and reliable full operational services to most parts of Asia-Pacific region. Chinese government has made great efforts to extend the applications of BDS. Many Chinese companies put out their terminal products in a short time. To keep the time consistency and ensure the timing accuracy of BD receivers, it is very profitable to test the timing accuracy and make calibration of the BD receiver delay.

This paper gives the test method of receiver delay. A BeiDou System simulator and a time interval counter were used in the experiments. The receivers under test were given a fixed position and configured in timing mode. The BDS simulator was set in a static scene excluding all the error sources. The 10MHz signals from a cesium atomic clock were put into the simulator and the counter as reference. The BDS simulator output the simulated BDS signal into the receiver. The time interval between the two 1PPS signals output from the simulator and the receiver could be got from the counter. By substracting the delay of the BDS simulator and the difference of the two 1PPS cable delays, the receiver delay could be calculated. The most important step is to measure the delay of the simulator. This method can avoid the effect of errors from satellite orbit and satellite clock, ionospheric delay, tropospheric delay and multipaths, and get the accurate internal delay of receivers. The uncertainty of this method is analyzed to be less than 1.5ns.

With this method, four timing receiver models from three famous Chinese companies were chosen to test the internal delay. The test results are shown. These receivers showed different timing specification and delay. Furthermore, with these four receivers, the experiments of receiver delay variation with temperature have been done.

Developing of one time link calibrator with GNSS at NIM

LIANG Kun, YANG Hang*, ZHANG Aimin, YANG Zhiqiang, WANG Weibo
Division of Time and Frequency Metrology, National Institute of Metrology, NIM, Beijing, China
*School of Electronics and Information Engineering, Beijing JiaoTong University, Beijing, China
E-mail: liangk@nim.ac.cn

Time link calibration is the premise of time transfer. At present, we can have two kinds of time links in TAI(Temps Atomique International) corporation in summary, such as, GNSS(Global Navigation Satellite System) based links and TWSTFT(Two Way Satellite Time and Frequency Transfer) based links. GNSS based links can be calibrated using the methods of differential calibration (golden receiver method)[1] with the uncertainty of about 5 ns and using the whole link calibration with uncertainty of less than 2 ns, even 1 ns. Since 2001, BIPM has always implemented many GNSS time link calibration campaigns all over the world using the first method mostly because the method is easier to use. TWSTFT based links can be calibrated using two way mobile station with the uncertainty of about 1 ns, however the mobile station is hard to get for use of the calibration and the calibrated GNSS based links can be used for the alignment and calibration of TWSTFT based links and calibration for GNSS based links could be transferred to TWSTFT based links.

Base on the whole link calibration for GNSS based links, some successful experiments for calibration have been implemented by BIPM(Bureau International des Poids et Measures), ROA(Royal Institute and Observatory of the Armada) PTB(Physikalisch-Technische Bundesanstalt), NIM(National Institute of Metrology) and LNE-SYRTE(OP, Observatory of Paris) and so on. PTB and BIPM has developed the homemade precise mobile calibration setups for the time link calibration as described in [2] and [3]. Moreover, BIPM has started to draw up the new guideline for GNSS link calibration and assigned several NMIs including NIM as the group 1 laboratories to implement the possibility of calibration of group 2 laboratories in the local RMO(Regional Metrology Organization) that might give some assist to BIPM. Since 2014 NIM has also started to design and develop one kind of homemade calibration system for the time link calibration on the basis of NIMTFGNSS-2 receiver. The system has been constructed preliminarily and calibrated, and in the near future, with this calibrator we might implement the calibration campaigns of some TAI links in the APMP(Asia Pacific Metrology Programme) scheme.

[1] BIPM, BIPM guidelines for GNSS equipment calibration V2.0, 2014
[2] Thorsten Feldmann, Andreas Bauch, Dirk Piester, Michael Rost, Elizabeth Goldberg, Stephen Mitchell, and Blair Fonville, Advanced GPS-based time link calibration with PTB's new gps calibration setup, Proc. PTTI 2010, 2010
[3] Jiang Z., Arias F., Lewandowski W., Petit G., BIPM Calibration Scheme for UTC Time Links, Proc. EFTF 2011, 2011, 1064-1069

Calibration of the NICT's 2nd UTC generation station KOBE by using GPS, TWSTFT and Clock Transportation

Takiguchi H, Gotoh T, Fujieda M, Nakagawa F, Narita H, Matsubara K, Imamura K, Ito H, and Hanado Y
National Institute of Information and Communications Technology, Koganei, Tokyo, Japan
E-mail: htaki@nict.go.jp

The National Institute of Information and Communications Technology (NICT) has a role in the generation, comparison, and dissemination of Japan Standard Time and has contributed to the generation of the Coordinated Universal Time (UTC). Currently, NICT has operated these tasks only at NICT headquarters where is located at Koganei, Tokyo (KOGANEI). Therefore, NICT is advancing the decentralization of these tasks to NICT's branch facilities in order to prepare for future disasters and to improve the reliability and accuracy of these tasks [1]. The decentralization means the placement of atomic clocks at different site, the construction of time transfer links, the construction of database, and the installation of standard time generation system. At first, we selected the Advanced ICT Research Institute (KOBE) which is one of the NICT's branch institute where located at Kobe as the first place, and established a time transfer link using a real-time GPS common-view (GPSCV). If the emergency will occur at KOGANEI, KOBE has to take over all the functions and tasks from KOGANEI, that is, KOBE performs the UTC(NICT) generation instead of KOGANEI. At that moment, UTC(KOBE) which is generated at KOBE should be synchronized with UTC(NICT). Furthermore it is demanded that the time difference between them is enough small. Therefore, we must calibrate the time difference between the reference points of each UTC(NICT) and UTC(KOBE) and then steer the difference to zero. From above reason, before to start the operation officially, we carried out the calibration campaign at KOGANEI and KOBE.

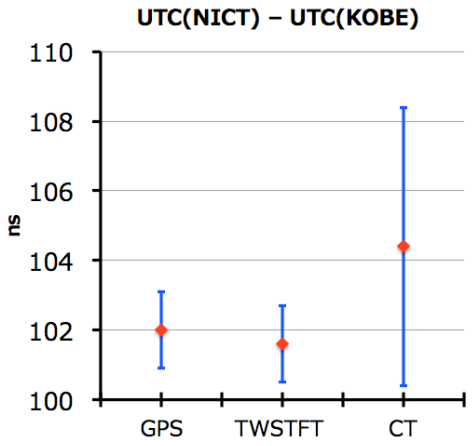


Fig. 1: UTC(NICT)-UTC(KOBE) which were determined by this calibration campaign. The error bars are the overall uncertainty of each technique.

In this campaign, we employed three time and frequency transfer techniques by GPSPPP, Two-way Satellite Time and Frequency Transfer (TWSTFT), and Clock Transportation (CT). The calibration measurements by GPSPPP and TWSTFT were performed using a GPS travelling receiver and a portable TWSTFT station, respectively. The clock used in CT was consisted of a cesium atomic clock (Cs) with AC/DC batteries and it was transported by a van between KOGANEI and KOBE. CT is simple way, such as measure the time difference between each UTC reference point and Cs by using a time interval counter directly.

The determined time difference of UTC(NICT)−UTC(KOBE) by GPS, TWSTFT and CT were 102.0, 101.6 and 104.4 ns respectively. The calibration uncertainty of GPS, TWSTFT and CT were 1.1, 1.1 and 4.0 ns respectively. Fig. 1 shows the time difference of UTC(NICT)−UTC(KOBE) determined by each technique with the error bars which are the overall calibration uncertainty. Each calibration result agreed within the uncertainty. We will explain about the details of the procedure of the calibration and the uncertainty estimation, in the presentation.

[1] F. Nakagawa, Y. Hanado, K. Imamura, H. Itoh, T. Gotoh, H. Narita, H. Takiguchi, and R. Tabuchi, “The Decentralization of Japan Standard Time (2)” *Proceedings*, 2014 IEICE Soc. Conf., Tokushima, Japan, September 23-26, 2014, B-2-3.

Discovery of Persistent Ionospheric Frequency Shifts of a few Herz and Impact on Time and Frequency Transfer.

Underhill, Michael J
Underhill Research Limited
Lingfield, UK
E-mail: mike@underhill.co.uk

Unexpected frequency shifts of Standard Frequency Signals have been 'discovered'. Fig. 1 shows a three day right to left frequency spectrum waterfall of 10MHz Standard Frequency signals as received at Lingfield, Surrey, UK. The first discovery was of the observation of the persistent formation of a dependent 'spurious' signal at an offset of ~10Hz below the 10MHz carrier frequency. The corresponding Doppler velocity is 300m/s or about 1000kph. For a one day duration the distance covered would be 24000 km if this was a Doppler frequency shift.

Such spurious signals have been observed on AM carrier frequencies and DRM signals between ~1MHz and 25MHz [2]. They correlate with the existence of an Ionospheric propagation path. At some times the dependent signal can be stronger than the original carrier signal. Then the Standard Frequency Signal cannot in any way be used as an accurate reference frequency. The error can be 1ppm.

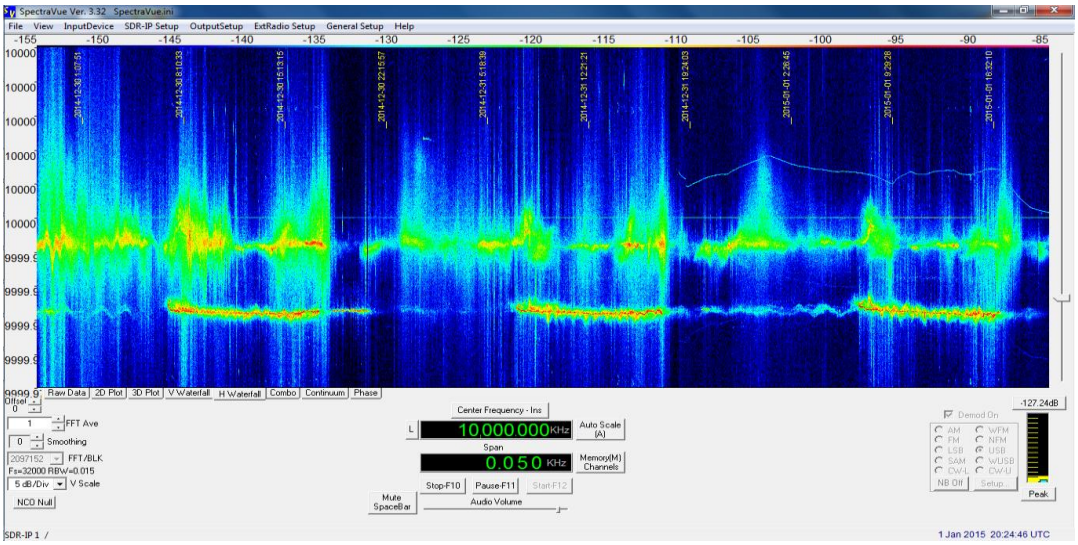


Fig. 1: Three day (to 01Jan15) right to left waterfall record of 50 Hz bandwidth at 10MHz of mixture of carriers from WWV Fort Collins USA (4700 mile NW path), BPM China (5200 miles NE path), PPE Rio de Janeiro, Brazil (5700 miles SW), WWVH Kekaha, Hawaii (7200 miles NNW). From RFSpace SDR-IP receiver using SpectraVue software with 15mHz resolution.

Frequency deviations of a few parts in 10^7 can persist for minutes to hours on both dominant components depending on the time of day. Are these detecting the earth's rotation and motion around the sun as effects on the ionosphere? Or even Gravity Waves?

The paper will present further evidence collected over at more than two years on various SDR receivers, and consider the impact on Time and Frequency Transfer and the operation of Radar, Navigation, GPS, and Loran Positioning Systems. The SDR techniques used are further described in [3] and [4].

[1] M. J. Underhill., "Coupling Theory for Fluctuating Spurs in Oscillators", *Proceedings,* 2014 IEEE Int. Frequency Control Symp., Taipei, Taiwan, 19-22 May 2014, pp. 1-5.

[2] M. J. Underhill, "Estimation of Ionospheric layer heights and velocities using available DRM signals", *IET IRST 2012 Conf. Proc.*, 15-17 May, 2012, pp. 1 - 5.

[3] M. J. Underhill, "Investigations into spectrum shape fluctuations of oscillators and signal sources," *Proceedings,* 2013 Joint UFFC, EFTF, and PFM Symposium, 21-25 July 2013, Prague, pp 729-732.

[4] M. J. Underhill., "SDR and Self-Focusing Radar Techniques for milliHerz Measurement of Multi-Component Phase Noise Spectra?", submitted to Group 2 of this conference.

Prediction of Navigation Satellite Clock Bias by Gaussian Processes

Yu Lei, Bian Li,Danning Zhao
National Time Service Center, Chinese Academy of Sciences, Xi'an, China
E-mail: leiyu@ntsc.ac.cn

Prediction of navigation satellite clock bias is a very important task in global navigation satellite system (GNSS) positioning and navigation. It is required for various applications, such as real precise point positioning (PPP) and autonomous satellite navigation. Traditional methods for predicting satellite clock bias are mainly based on some linear model, such as the quadratic polynomial model, grey model and Autoregressive moving average (ARMA) model. However, these models can not meet the requirements of high-accuracy prediction of satellite clock bias. One reason for this fact is that satellite clocks in space can be easily affected by various factors such as temperature and environment and this leads to complicated aspects like periodic and stochastic variations, which are not sufficiently described by conventional models.

In this paper, a kind of machine learning algorithm- Gaussian processes (GP) are employed for forecast of satellite clock bias. In order to enhance the learning speed and generalization performance of the GP-based predictor, the strategy of epoch differenced (ED) is proposed. The basis procedure is as follows. Two clock bias values between adjacent epochs firstly differenced so as to obtain the corresponding differenced time-series. Then the differenced series are used to train and validate the GP model. Finally, the predicted differenced series are recovered to the corresponding forecasted clock bias. The data of precise GPS clock bias collected from the International GNSS Service (IGS) are used to test the developed method. The results show that the prediction accuracy of the proposed method is substantially better than the quadratic polynomial and grey model, especially for long-term prediction.

Filtering Measurement Noise in GNSS Time-transfer Data Using a EMD Filter and Cross-Validation

Yu Lei, Bian Li,Danning Zhao
National Time Service Center, Chinese Academy of Sciences, Xi'an, China
E-mail: leiyu@ntsc.ac.cn

Measurement noise is one of the important error sources in high-accuracy global navigation satellite system (GNSS) positioning, navigation and timing (PNT). A new time-series filtering method, based on the empirical mode decomposition (EMD) filter and the technique of cross-validation, is developed for separating signals from noise in time-series, and applied to extract the noise in GNSS time-transfer data. Both simulated time-series and real GNSS time-transfer data are employed to test the proposed method. It is demonstrated that the method can be used to successfully separate signals from noise at different noise levels, and for varying signal frequencies as long as the noise level is lower than the magnitude of the signals. The time deviation is decreased and frequency stability is enhanced after the measurement noise in GNSS time-transfer data is removed by the presented algorithm.

Research on Time and frequency transfer based on BeiDou Common-View

Hang Yi, Hongbo Wang, Shengkang Zhang, Haifeng Wang, Huaiying Shang, Fan Shi, Zhenggang Ding

Science and Technology on Metrology and Calibration Laboratory, Beijing Institute of Radio Metrology and Measurement, Beijing, China

Email: 398009@163.com

Since there are already 5 GEO, 5 IGSO and 4 MEO BeiDou navigation satellites in orbit which can provide stable and continuous navigation services for the Asia-Pacific region, BeiDou Navigation Satellite System can be another choice for remote precise time and frequency transfer. A strict common-view test using BeiDou Navigation Satellite System is introduced in this paper.

In this paper, the zero-baseline common-view test is done and we are going to test the case of long-baseline in 2015. In the test, we use two BeiDou receivers which work in the position hold mode, use the same frequency standards and track the same BeiDou navigation satellite and the time difference of the two receivers is compared second by second. At first, only pseudo-range observation data is used in our test, however, the result is not so good. The peak-to-peak jitter of the clock comparison error is about 12ns.Then, a sample novel smooth method using the carrier phase data is introduced to our test. We use both the pseudo-range data and carrier phase data of the former 20 epochs to get an averaged pseudo-range of the current epoch. Finally, the zero-baseline common-view measurement shows that for the GEO with a high elevation the peak-to-peak jitter can keep in 8ns, for the GEO with a low elevation can keep in 15ns, for the IGSO and MEO the peak-to-peak jitter changes from 5ns to nearly 60ns according to the elevation. Then we give a different weight to each satellite according to its elevation, and the weighted-average result is better than 5 ns.

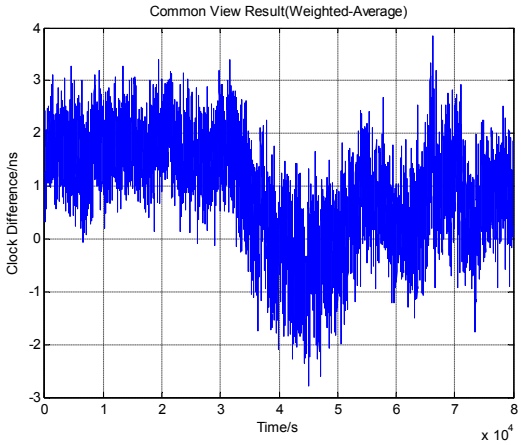


Figure 1 Common-View Results Using BeiDou Navigation Satellite System

Preparing ACES-PHARAO data analysis

[Meynadier, Frédéric] [2,1], [Delva, Pacôme] [2,1], [le Poncin-Laffite, Christophe] [1], [Guerlin, Christine] [2,3], [Laurent, Philippe] [1], [Wolf, Peter] [1]

[1] LNE SYRTE – Observatoire de Paris, PSL Research University, Paris, France
[2] Sorbonne Universités, UPMC Univ Paris 06, Paris, France
[3] Laboratoire Kastler-Brossel, Ecole Normale Supérieure, PSL Research University, Paris, France
E-mail: Frederic.Meynadier@obspm.fr

The Atomic Clocks Ensemble in Space (ACES-PHARAO mission [1]) will realize, on board of the International Space Station, a time scale of very high stability and accuracy, connected to a dedicated microwave link (MWL) for comparison to ground clocks. This will allow to perform high performance time transfers between distant ground stations, as well as fundamental physics tests, such as measuring the gravitational redshift with unprecedented accuracy, and search for a violation of the Lorentz local invariance.

Our team at SYRTE is currently developing a dedicated software for analyzing the data retrieved by the MWL. It will be a crucial component of the processing chain, allowing to reach the nominal scientific performances, thus complementing the quick-look data provided by the ground segment. During ACES flight, our software will run in a data processing center that will be set up in SYRTE, as requested by ESA.

We will present the current status of the data analysis software and its expected capabilities, mostly based on data generated by our own data simulator, but also some preliminary results of comparisons with actual test data from the instruments. Our simulator itself will also be presented, as it plays a key role in the validation of the data analysis software, and also allows to assert the sensitivity of ACES data to various theoretical signatures.

[1] C. Salomon, L. Caciapuoti and N. Dimarcq, 2007, International Journal of Modern Physics D., 16, 2511

Preparations for the ACES Mission at the National Physical Laboratory

Shemar S, Gill P, Kronjaeger J, Marra G, Whibberley P
Time, Quantum and Electromagnetics Division, National Physical Laboratory,
Teddington, Middlesex, TW11 0LW, UK
E-mail: setnam.shemar@npl.co.uk

ESA's forthcoming Atomic Clock Ensemble in Space (ACES) mission due to be launched in mid-2016 is an international collaboration involving several countries on a global scale. This will enable participating timing laboratories to conduct high accuracy ground-to-space and ground-to-ground comparisons of advanced atomic frequency standards at the 10^{-16} and 10^{-17} level respectively and to test General Relativity [1]. A summary will be presented here of the preparatory activities for the mission at the National Physical Laboratory (NPL) in the UK. We will focus on preparations for the installation of an ACES ground terminal at the NPL site.

Firstly, we will briefly outline the ACES mission and NPL's planned inputs. The latter includes a ground-to-space time and frequency link to the ACES payload to be located at NPL using a MicroWave Link (MWL) ground terminal, the available ground clocks (including H-masers, caesium fountains and optical clocks), frequency combs, operational satellite time and frequency transfer links and a potential contribution to one or more aspects of the MWL data analysis.

We then focus on the potential infrastructure for the ACES MWL ground terminal installation, including its location at the NPL site based on the ground terminal's requirements and the potential optical fibre link transfer methods for connecting the reference H-maser to the ground terminal. In the latter case, the aim is to achieve a frequency transfer accuracy of $3\text{x}10^{-18}$ at 1 day averaging times and a time transfer accuracy of 30 ps. The suitability of potential methods for both time and frequency transfer are discussed, including the use of a comb-based phase compensation technique under development at NPL, a method involving commercially available Satre modems often used for TWSTFT measurements [2] and some commercial off-the-shelf approaches. We mention the possibility of tests of the ACES MWL link using optical fibre links, such as the London-Paris link currently being implemented.

[1] L. Cacciapuoti & C. Salomon, 'Atomic Clock Ensemble in Space', Journal of Physics: Conference Series, vol. 327, 2011.

[2] D. Piester, M. Fujieda, M. Rost & A. Bauch, 'Time transfer through optical fibres (TTTOF): First results of calibrated clock comparisons', Proc. 41st Annual Precise Time and Time Interval (PTTI) Systems and Applications Meeting, 16-19 Nov. 2009, Santa Ana Pueblo, New Mexico, USA.

Impact of dead time of measurement on frequency estimate and uncertainty

Signorile Giovanna, Tavella Patrizia
Optics Division, INRIM, Turin, Italy

E-mail: g.signorile@inrim.it

During last years, some National Metrological Institutes (NMI) and laboratories developed and operates fountain frequency standards based on caesium atoms, achieving high level of accuracy. Such realizations of the SI second are used by BIPM for the steering of the International Atomic Time (TAI), as well as by single laboratories to realize a national time scale.

Primary Frequency Standards as well as the more recent Optical Clocks do not usually run in a continuous way, therefore using such measurements means dealing with period of missing data. The presence of dead time impacts any kind of analysis performed on such data set.

In the frame of a Seventh Framework Project named International Time Scale with Optical clocks (ITOC), we carried out an analysis based on least squares aimed to understand the impact of dead time on the frequency estimate and uncertainty. In particular the role of different parameters (e.g. the number of available measures, measures distribution in the considered time period, ...) is considered. This will help anyone wants to use dataset including dead times to use the available measures in an optimal way, being aware of the uncertainty level that could be expected in that particular case.

This work was supported by the European Metrology Research Programme EMRP. The EMRP is jointly funded by the EMRP participating countries within EURAMET and the European Union.

Investigating the Correlation between Hydrogen-Maser clocks in the Same Place

C. Gao[1,2], B. Wang[1,2], X. Zhu[1,3], T. C. Li[1,4], and L. J. Wang[1,2,3,4]

[1]Joint Institute for Measurement Science, Tsinghua University, Beijing 100084, P. R. China
[2]The state key lab of precision Measurement Technology and Instrument, Department of Precision Instruments, Tsinghua University, Beijing 100084, P. R. China
[3]Department of Physics, Tsinghua University, Beijing 100084, P. R.China
[4]National Institute of Metrology, Beijing 100013, P. R. China

Email: bo.wang@tsinghua.edu.cn

Atomic clocks in the same place always affected by common environments, such as temperature, pressure, gravity and so on. Consequently, for a group of clocks placed in the same environment, certain correlation always exists between them, but it cannot be easily measured. Thanks to the fiber based frequency dissemination techniques developed recently, we can give an estimation of this correlation through comparing them with the clocks at remote locations.

From 2013, we start the program of Beijing regional time and frequency network (Fig. 1) [1,2]. Based on this network and using three-corner-hat method, we can simultaneously compare four Hydrogen-masers (H-Masers) placed in the Changping site of National Institute of Metrology (NIM-CP), Tsinghua University (THU) and Beijing Institute of Radio Metrology (BIRM), respectively. There are two H-Masers (Maser A, Maser B) placed at NIM-CP. Through three-corner-hat comparisons between clocks A, C, D and clocks B, C. D, we can get the independent frequency stability of maser A ($\sigma(A)$) and B ($\sigma(B)$). The relative stability of these two clocks can be calculated as $\sigma(AB)_{cal}=(\sigma(A)^2+\sigma(B)^2)^{1/2}$. Compared $\sigma(AB)_{cal}$, with the measured relative stability of these two clocks $\sigma(AB)_{meas}$, we find that there is strong correlation between these two clocks at certain averaging time. The detailed results will be shown during the EFTF & IFCS conference.

This work was supported by the National Key Scientific Instrument and Equipment Development Project (No.2013YQ09094303) and the Beijing Higher Education Young Elite Teacher Project (No. YETP0088).

[1] B. Wang, C. Gao, W.L. Chen, J. Miao, X. Zhu, Y. Bai, J.W. Zhang, Y.Y.Feng, T.C. Li and L.J. Wang, "Precise and Continuous Time and Frequency Synchronisation at the 5×10-19Accuracy Level", Scientific Reports, Vol. 2, p556, 2012.

[2] C. Gao, B.Wang, X. Zhu, Miao, Y. Bai, T. C. Li and L. J. Wang. The Three Corner Hat Measurement of Three Hydrogen Masers in Remote Locations via Fiber Based Frequency Synchronization Network. 28th European Frequency and Time Forum, Neuchâtel, Switzerland , June 23-26, **pp259**,2014



Figue1. Beijing regional time and frequency network. The solid line is the synchronization link under used. The dash line is the synchronization link under construction. Symbol A, B, C, D are Hydrogen masers, while symbol E is a Sr optical clock.

LMJ Timing and fiducial System: overview of the global architecture and performances

Drouet Vincent, Prat Michel
CEA-DAM, DIF, F-91297 Arpajon, France
E-mail: Vincent.drouet@cea.fr

The Laser MegaJoule (LMJ) timing system has to synchronize 176 laser beams within 40 ps to compress symmetrically the millimeter-size target in order to ignite the deuterium and tritium filled capsule despite the fact that the quadruplet laser sources are separated within the building by several hundreds of meters. This kind of performance is also required for fiducial pulses used to temporally mark laser and plasma diagnostics.

After the LMJ was officially commissioned on 23rd October 2014 with a first physics successful campaign, this article offers an overview of the final overall timing system architecture and its performances.

The latest results from our presentation during the previous EFTF conference edition [1] as part of ongoing studies on time drifts are also presented.

[1] E. Meyer, V. Drouet, N. Gautherot, F. Vernotte, F. Meyer, M. Prat and P. Raybaut, "Picosecond time drift characterization of the Laser MegaJoule Timing System," *Proceedings*, 2014 IEEE European Frequency Time Forum, Neuchâtel, Suisse, June 23-27 , 2014, pp. 558-563.

Practical Limitations of NTP Time Transfer

Novick, Andrew N., Lombardi, Michael A.
National Institute of Standards and Technology, Boulder, Colorado, USA
E-mail: novick@nist.gov

The Network Time Protocol (NTP) is commonly utilized to synchronize computer clocks in packet-switched, wide area networks (WANs) such as the public Internet. The delay asymmetry in WANs, often due to inconsistent routing and/or bandwidth saturation, is usually the dominant source of error. It typically limits NTP time transfer uncertainty to about one millisecond. This paper is a study of the uncertainty of NTP time transfer when network asymmetry is largely eliminated. We perform NTP measurements over a local area network (LAN) when both the server and client are referenced to a common clock. Variations of a LAN are tested, including a direct connection between the server and client with an Ethernet crossover cable. The elimination of network asymmetry reveals other uncertainty sources that serve as practical limitations for NTP time transfer, including server instability, client software instability, and asymmetry in network interface cards.

Industrial White-Rabbit solutions

Díaz Javier, Gutierrez José-Luis, Rodriguez Rafael*, Rat Benoit*
Computer Architecture and Technology Department, University of Granada, Spain
*Seven Solutions S.L, Granada, Spain
E-mail: jda@ugr.es, jlgutierrez@ugr.es, rrodriguez@sevensols.com, benoit@sevensols.com

White Rabbit (WR) is an Open Source Ethernet-based technology developed to synchronize distributed networks with sub-nanosecond accuracy. It was born at CERN [1] and it is currently being developed in a collaborative framework formed by scientific and industrial partners. Its high performance is possible thanks to the extension of well-known network standards, such as Synchronous Ethernet (SyncE) and Precise Time Protocol (PTP, IEEE1588). Nowadays, WR is the most accurate, flexible and the easiest solution for network synchronization over Ethernet. The main features of the WR technology are:

- Sub-nanosecond accuracy synchronization
- It is possible to interconnect thousands of nodes
- Typical distances of 10km between nodes (can be extended to more than 100km)
- Ethernet-based Gigabit rate reliable data transfer
- Fully open hardware, firmware and software
- Multi-vendor commercially produced hardware

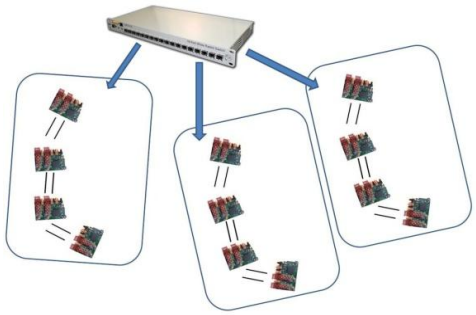


Fig. 1: White-Rabbit network topology composed by a WR switch (root node) and several low-cost WR standalone cards forming a daisy chain reliable topology.

Current efforts from industrial partners as Seven Solutions [2] are focused on moving this technology from scientific or academic applications (like [3]) to highly dependable industrial solutions. Different applications are presented and the requirements are clearly explained with strong focus on the incoming time and frequency dissemination specifications of next information technology products.

The current contribution describes the work done by the authors in this framework, including the development of new boards (Fig. 1) and functionalities to support the enhancement of the dependability of the solution as well as improved schemes for time and frequency distribution. The final goal is to provide White-Rabbit products with better long and short term clock stability compared to current White-Rabbit products and, at the same time, to provide dependable solutions for the industrial markets.

This paper evaluates the effects of new functionalities, such as external holdover oscillators, predictive mechanisms for clock correction under free running operation mode or enhanced clocking schemes in term of clock skew and jitter. Moreover, this work evaluates how the different mechanisms allow to enhance the dependability of the final product, quantifying each of them and explaining its applicability in different market domains such as telecomunations, Power Grid or industrial automatation.

[1] White-Rabbit Project: http://www.ohwr.org/projects/white-rabbit/wiki
[2] Seven Solutions S.L website http://www.sevensols.com/index.php
[3] Jimenez Lopez, Miguel; Gutierrez Rivas, Jose Luis; Diaz Alonso, Javier, "A White-Rabbit Network Interface Card for synchronized sensor networks," SENSORS, 2014 IEEE , vol., no., pp.2000,2003, 2-5 Nov. 2014.

Precise Three-Channel Integrated Time Counter

Szplet Ryszard, Kwiatkowski Paweł, Jachna Zbigniew, Różyc Krzysztof
Department of Electronics, Military University of Technology, Warsaw, Poland
E-mail: rszplet@wat.edu.pl

Various users in many countries are still more often obliged by local legislation for applying of a legal time in their activities. Typical way to achieve the legal time is based on synchronization of locally created time scale to national time scale generated by National Institute of Metrology (NIM). Quality of a local time scale and its ability for autonomous operation (unlocked to NIM) depends on the stability of clock sources involved. This stability can be verified through the measurements performed with the use of precise time counter. We propose the three-channel, high-precision, integrated time counter designed for a system of local time scale based on three clocks, which is developed as a part of LTDS EUREKA project.

Figure 1 shows the simplified block diagram of the time counter. The measurement method employed in the counter combines period counting and two-stage interpolation [1] to create a very precise time base that is common for all channels of the counter. The rough marks of the time base, distributed every single period of the reference clock, are created by the period counter operating continuously. When the rising edge of measured signal from the monitored clock source appears at the counter input (Clock1 to 3), the current content of period counter is saved in the channel register. To improve the resolution of the rough time base, the two-stage in-period interpolation is introduced in each channel. The first interpolation stage (FIS), based on a multiphase clock created with the use of reference clock, identifies the phase segment in which the measured signal appeared. Then the second interpolation stage (SIS) precisely quantizes relatively short time interval within the identified phase segment. Based on data from channel register, FIS and SIS, precise information about time of occurrence of measured signal is calculated in the code processor and saved as a time stamp [2].

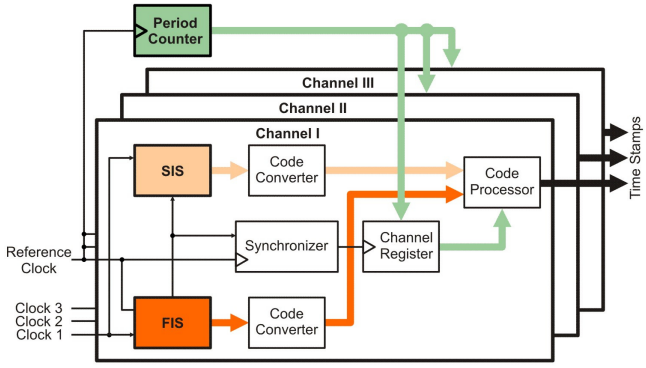


Fig. 1: Simplified block diagram of the time counter.

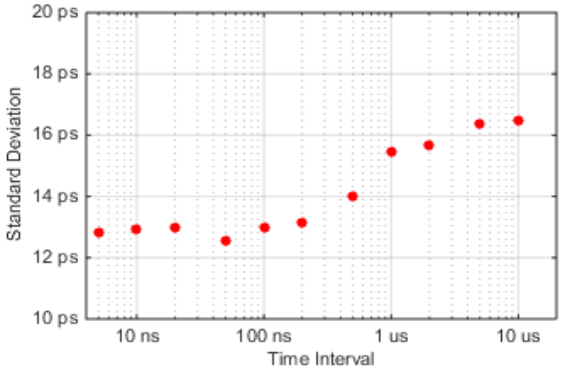


Fig. 2: Precision of the time counter.

The time counter was implemented in a low cost, off-the-shelf FPGA device Spartan-6 (*Xilinx*). Preliminary tests performed within the range of measured time intervals from 5 ns to 10 µs revealed that the precision of the counter is below 20 ps (fig. 2), while its resolution is about 18 ps.

This work was supported by the Polish National Centre for Research and Development under contract no. E 8727LTDS/1/2014

[1] R. Szplet, J. Kalisz, Z. Jachna, "A 45 ps time digitizer with two-phase clock and dual-edge two-stage interpolation in FPGA device", Measurement Science and Technology, vol. 20 (2009), 025108, 11 pp.

[2] R. Szplet, P. Kwiatkowski, K. Rozyc, Z. Jachna, T. Sondej, M. Sawicki, "Timestamps-Based Multichannel Time Interval Counter", *Proceedings*, 45th Annual PTTI Meeting, Bellevue, Washington, USA, December 25, 2013, pp. 158-162.

An optical fiber link for the remote comparison of optical clocks and geodesy experiments

Clivati Cecilia, Frittelli Matteo, Mura Alberto, Levi Filippo, Calonico Davide
Optics Division, Istituto Nazionale di Ricerca Metrologica, Turin, Italy

E-mail: c.clivati@inrim.it

In recent years, it has become evident that optical clocks, with systematic uncertainties at the 10^{-18} level are not only the strongest candidate for the redefinition of the second in the International System of Units, but represent a powerful tool to investigate Physics at deeper levels of precisions [1,2].

Among other applications, the project "International Timescales on Optical Clocks" [3] aims at demonstrating that optical clocks can be used a probe for the Earth's gravitational potential with a resolution at the 10 cm level. This achievement will be pursued by comparing two optical clocks placed at heights on the Earth differing by about 1000 m, and determining the related gravitational red-shift. The clocks will be located at INRIM, Turin, Italy and at the Laboratoire Souterrain de Modane (LSM) in the Frejus tunnel, on the Italy/France border.

To achieve this goal, the two remote clocks will be bridged by a 150-km long, Doppler-stabilized optical link. In addition, a stable radio-frequency reference must be disseminated at LSM, where GPS-disciplined oscillators cannot be reliably exploited.

The optical link is based on a multiplexed-fiber architecture where the metrological signal shares the fiber with Internet users and exploits a hybrid amplification technique based on bidirectional Erbium-Doped Fiber Amplifiers and a Brillouin amplifier at the remote end. The ultimate stability for this link achieves the $3 \cdot 10^{-19}$ level of stability in few hours of operation, which fulfils the requirements for the present applications. This span extends the present Italian fiber backbone for frequency metrology to a total length of 792 km [4].

The radio-frequency dissemination is obtained by 100 MHz amplitude modulation of a narrow-linewidth laser which is then launched in an un-stabilized fiber. The inherent stability of the fiber is in this case enough to deliver a RF signal with a long-term stability better than 10^{-13}.

We describe the implementation of the two links and their characterization, both from the metrological and from the reliability point of view. We then highlight some possible applications for this link, also in view of the realization of a continental network for frequency metrology in Europe.

This work was supported by the European Metrology Research Programme EMRP-SIB55. The EMRP is jointly funded by the EMRP participating countries within EURAMET and the European Union.

[1] B. J. Bloom, T. L. Nicholson, J. R. Williams, S. L. Campbell, M. Bishof, X. Zhang, W. Zhang, S. L. Bromley, J. Ye, "An optical lattice clock with accuracy and stability at the 10^{-18} level" Nature 506, pp. 71–75, Febr. 2014.

[2] N. Hinkley, J. A. Sherman, N. B. Phillips, M. Schioppo, N. D. Lemke, K. Beloy, M. Pizzocaro, C. W. Oates, and A. D. Ludlow, "An atomic clock with 10^{-18} instability," Science, Vol. 341 no. 6151 pp. 1215-1218, Aug. 2013.

[3] H. S. Margolis et al., "International Timescales with Optical Clocks (ITOC)," *Proceedings*, 2013 IEEE Joint UFFC, EFTF and PFM Symposium, Prague, Czech Republic, July 21-25, 2013, pp. 908-911.

[4] D. Calonico, E. Bertacco, C. Calosso, C. Clivati, G. A. Costanzo, M. Frittelli, F. Levi, A. Mura, N. Poli, D. V. Sutyrin, G. M. Tino, A. Godone, "High-accuracy coherent optical frequency transfer over a doubled 642-km fiber link," Appl. Phys. B, Vol. 117, no. 3, pp. 979-986, Nov. 2014.

OPTIME - the system grows - a new 330 km line

Bogacki Wojbor[5], Adamowicz Waldemar[4], Binczewski Artur[5], Buczek Łukasz[1], Czubla Albin[3], Dunst Piotr[2], Igalson Jacek[4], Kołodziej Jacek[1], Krehlik Przemysław[1], Lemański Dariusz[2], Lipiński Marcin[1], Nawrocki Jerzy[2], Nogaś Paweł[2], Ostapowicz Piotr[5], Pawszak Tadeusz[4], Pieczerak Janusz[4], Stroiński Maciej[5], Śliwczyński Łukasz[1], Turza Krzysztof[5], Zawada Michał[6]

[1] AGH University of Science and Technology (AGH), Krakow, Poland
[2] Astrogeodynamic Observatory (AOS), Borowiec, Poland
[3] Central Office of Measures (GUM), Warsaw, Poland
[4] Orange Polska S.A. (OPL), Warsaw, Poland
[5] Poznan Supercomputing and Networking Center (PSNC), Poznan, Poland
[6] Institute of Physics, Faculty of Physics, Astronomy and Informatics, Nicolaus Copernicus University, Torun, Poland
E-mail: wojbor@man.poznan.pl

The document describes the OPTIME project – which implements a self-calibrating, high precision dissemination system for time and frequency reference signals. The system consists of three main elements: reference time and frequency laboratories, local time and frequency repositories and distribution network, which is based on fiber optical network in Poland.

The distribution network consists of two fully operational links and one planned:

- the first one, which works more than 3 years, connects two UTC laboratories: UTC(PL) located in Central Office of Measures (GUM) – Warsaw and UTC(AOS) located in Astrogeodynamic Observatory, Space Research Centre - Borowiec. Link length is about 420 km.
- the second one, which became operational on December 2014, connects Astrogeodynamic Observatory (AOS) in Borowiec with National Laboratory of Atomic, Molecular and Optical Physics (KL FAMO) in Toruń. Link length is more than 330 km.
- planned third link between UTC(PL) laboratory and Orange Polska network synchronization center in Anin (Warsaw). Link length is about 40 km.

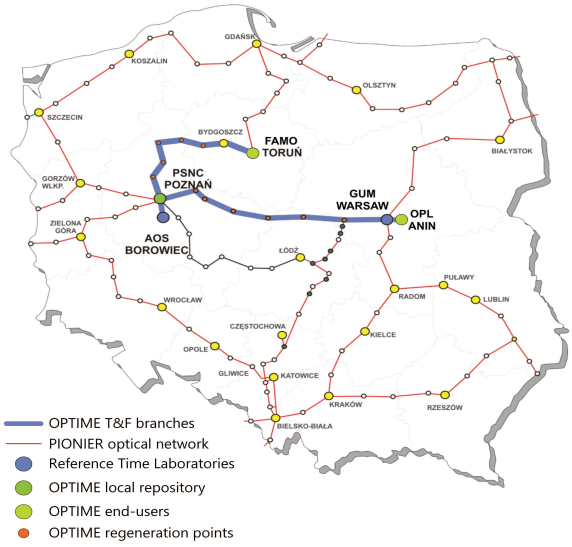


Fig. 1: National Distribution System for Atomic Clocks Time and Frequency (T&F) Signals

Right now the time and frequency dissemination system in Poland reaches more than 750 km. Fig. 1 shows topology of the OPTIME system.

Document provides also information about results of comparisons of UTC(PL) and UTC(AOS), and shows the first results of the new link between AOS in Borowiec and KL FAMO in Toruń, where two strontium optical lattice standards were build. Moreover, document describes a new local repository, where a passive H-maser will be installed. This local repository is being built in Poznan, and will be connected via optical fiber link, to both UTC laboratories, AOS and GUM.

Acknowledgement: Project OPTIME (no. PBS1/A3/13/2012) is co-founded by The National Centre for Research and Development – Poland. Strontium optical lattice standards were built by National Laboratory of Atomic, Molecular and Optical Physics (KL FAMO).

Towards international optical frequency transfer by fiber link between two metrology institutes, PTB and LNE-SYRTE

Lopez Olivier[1], Chiodo Nicola[1], Quintin Nicolas[1], Stefani Fabio[2,1], Wiotte Fabrice[1], Chardonnet Christian[1], Santarelli Giorgio[3], Amy-Klein Anne[1], Pottie Paul-Eric[2],
Raupach Sebastian M. F. [4], Koczwara Andreas[4], Schnatz Harald[4], Grosche Gesine[4]

[1]Laboratoire de Physique des Lasers (LPL), Université Paris 13, Sorbonne Paris Cité, CNRS, Villetaneuse, France
[2]Laboratoire National de Métrologie et d'Essais–Système de Références Temps-Espace (LNE-SYRTE), Observatoire de Paris, CNRS, UPMC, Paris, France
[3]Laboratoire Photonique, Numérique et Nanosciences (LP2N), Université de Bordeaux 1, Institut d'Optique and CNRS, Talence, France
[4]Physikalisch-Technische Bundesanstalt (PTB), Braunschweig, Germany
E-mail: Paul-Eric.Pottie@obspm.fr

The last decade has seen a dramatic improvement in the performance of optical clocks, which now reach a performance better than 10^{-17} [1]. Presently, *optical* frequency transfer via fiber links is the only means for clock comparisons at these levels of accuracy and instability. In recent years the transfer of optical and radio frequencies has seen considerable progress. Optical links with different technologies and over lengths up to 1800 km have been investigated ([2-5] and references therein), reaching instabilities in the low 10^{-19} range and better. While international r.f. links via fiber are being operated already [6], the transfer of ultra-stable *optical* frequencies up to now has been demonstrated on the national scale only. Now, within a French-German project two national metrological institutes will be connected by an optical frequency fiber link enabling optical clock comparisons at the highest stabilities and accuracies.

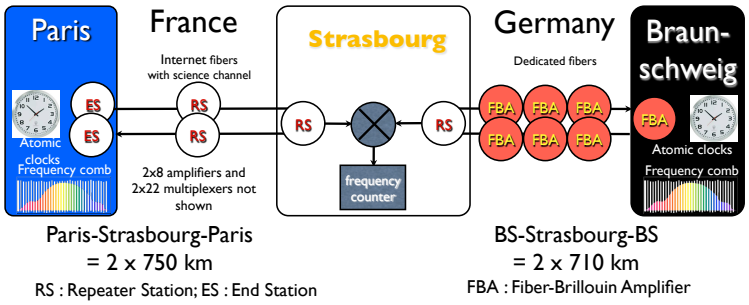


Fig. 1: Optical links connecting NMIs in France and Germany.

Within the European Metrology Research Program, project "NEAT-FT", the French project REFIMEVE+ and the German DFG-project SFB 1128 geo-Q, we are now implementing two anti-parallel optical frequency links of about 1500 km between the French and German national metrological institutes, in Paris and Braunschweig, as sketched in Fig. 1. The link combines the best techniques for long-haul frequency dissemination [2-3] and is expected to enable the comparison of the best German and French optical clocks without any limitation due to the frequency transfer. We will describe the link architecture and report recent progress on the interconnection of the national links in Strasbourg.

[1] B. J. Bloom et al., "An Optical Lattice Clock with Accuracy and Stability at the 10^{-18} Level," Nature 506, 71–75, 2014.
[2] S. M. F. Raupach, A. Koczwara and G. Grosche, "Optical frequency transfer via a 660 km underground fiber link using a remote Brillouin amplifier," Opt. Expr., vol. 22, pp. 26537-26547, 2014.
[3] O. Lopez et al., "Ultra-stable long distance optical frequency distribution using the Internet fiber network," Opt. Express, vol. **20**, pp. 23518-23526, 2012.
[4] S. Droste et al., "Optical-Frequency Transfer over a Single-Span 1840 km Fiber Link," Phys. Rev. Lett., vol. **111**, 110801, 2013.
[5] D. Calonico et al., "High-accuracy coherent optical frequency transfer over a doubled 642-km fiber link" Appl. Phys. **B** 117, 2014.
[6] S. C Ebenhag et al., "Time Transfer between UTC(SP) and UTC(MIKE) Using Frame Detection in Fiber-Optical Communication networks" in 43rd Precise Time and Time Interval (PTTI) Systems and Applications Meeting, 2011.

Design of the Optical Fiber Transmission Link in a Femtosecond-precision, Fiber-optic Timing Synchronization System

Huaiying Shang, Shengkang Zhang, Fan Shi, Hongbo Wang, Haifeng Wang, Hang Yi, Zhenggang Ding, Feng Nian, Keming Feng

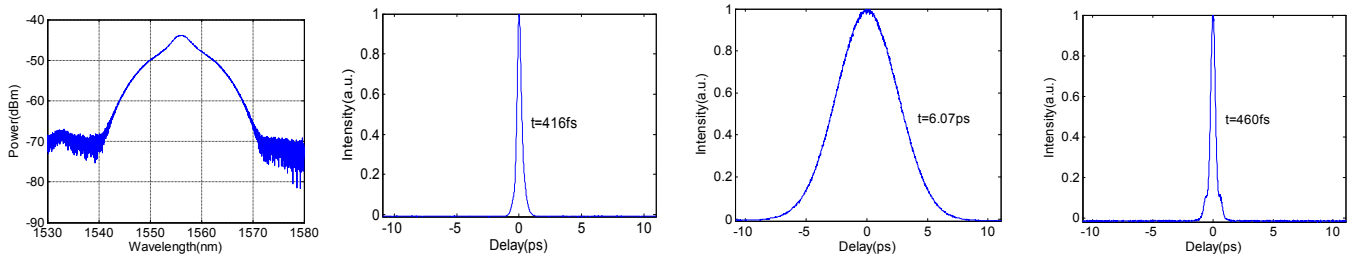
Science and Technology on Metrology and Calibration Laboratory, Beijing Institute of Radio Metrology & Measurement, Beijing 100854, China

E-mail: shanghuaiying2010@163.com

Due to the limited precision of the existing satellite-based time synchronization techniques such as GPS common-view or Two-Way Satellite Time and Frequency Transfer, and the emergence of optical clock, time transfer via optical fiber which has advantages of high precision and anti-jamming becomes the trend of high precision time synchronization. Time transfer via optical fiber has so far been investigated over regional distances with the use of two different methods for transmission: time signal transfer by means of an amplitude-modulated laser, or transmission of femtosecond laser pulses. With the development of ultrashort-pulse mode-locked laser, time synchronization technology based on femtosecond laser pulses is becoming more and more valued. We study on the femtosecond precision time synchronization technology based on femtosecond laser pulses, which measures timing jitter for transmitted pulse using balanced optical cross correlation scheme. [1]

The width of femtosecond laser pulses transmitted in optical fiber with dispersion will be broadened. The dispersion compensation of optical fiber transmission link in the femtosecond-precision fiber-optic timing synchronization system needs to be investigated. We should make the broadening amount as small as possible to reduce the influence on the balanced cross correlation detection progress of the timing synchronization system.

In this paper, The principle of dispersion compensation by dispersion compensation fiber is described, the details of the chirped femtosecond laser pulse used for timing synchronization when transferring in single mode fiber(SMF) and dispersion compensation fiber(DCF) are analyzed based on a numerical simulation. The broadening of the 416fs laser pulse used for timing synchronization by 9.7m DCF and then the compression by 33m SMF can be observed in the experiment(see Fig.1). Based on the simulation and experiment, a design of the optical fiber transmission link which is made up of SMF and DCF in the femtosecond-precision fiber-optic timing synchronization system is introduced: Firstly, the absolute value of the femtosecond laser pulse's initial chirp can be confirmed when the spectral width and pulse width of the laser source are known. Secondly, the sign of initial chirp can be confirmed with the broadening amount of the laser pulse transferred in a piece of DCF. At last, the length of DCF for dispersion compensation is calculated by the numerical simulation, after the final width of the pulse, the initial chirp of the laser source and the length of the SMF are figured out.



(a) (b) (c) (d)

Fig. 1 (a) spectrum of the femtosecond laser source; (b) auto-correlation trace of the initial laser pulse; (c) auto-correlation trace of the laser pulse transmitted by 9.7m DCF; (d) auto-correlation trace of the laser pulse transmitted by 9.7m DCF and 33m SMF;

[1] Jungwon Kim, Jonathan A. Cox and Jian Chen, et al., "Drift-free femtosecond Timing Synchronization of remote optical and microwave sources" Nature Photonics, www.nature.com/naturephotonics, vol. 2, pp. 733-736, Dec. 2008.

The method of determination of GEO satellite precise clock bias during maneuvering

Wu Mei-fang *, Yang Xu-hai, Wei Pei, Liu Tao
National Time Service Center /Key Lab of Precision Navigation and Timing Technology, Chinese Academy of Sciences, Xi'an, Shannxi China
*University of the Chinese Academy of Sciences, Beijing, China
Email: wumeifang@ntsc.ac.cn

The most important applications of GNSS include navigation, surveying and mapping, land resources monitoring, meteorology, seismology, security assistance and etc. So precision is not the only parameter to consider, availability and continuity are also worth taking on. BDS of China includes GEO satellite as one kind of its constellation. But during the lifetime of GEO satellite, it is necessary to orbital maneuver within some time intervals to avoid radio frequency interference. The orbital maneuvers bring errors into precise orbit determination and satellite clock bias determination. So the GEO satellite precise clock product during maneuvering was not included in precise clock product at present, which influences availability and continuity of BDS and brings trouble in researching with GEO satellite clock product.

In essence, determination of GEO satellite precise clock bias during maneuvering is a problem about interpolation. By analyzing of GEO satellite clock bias data, quadratic polynomials, cubic spline and Lagrange are chose as interpolation methods. Firstly, we construct GEO satellites maneuvering experimental data with GEO satellite precise clock bias when it doesn't maneuver. Secondly, we calculate satellite precise clock bias during maneuvering with experimental data by using three kinds of interpolation methods. At last, we compare the accuracy of the three kinds of interpolation methods and then draw a conclusion.

The experiment results show as follows. Because the error of quadratic polynomials interpolation is as high as 1ns, it cannot be used to determine GEO satellite precise clock bias during maneuvering. Both cubic spline and Lagrange interpolation can be chosen to determine GEO satellite precise clock bias during maneuvering, and the errors of them are at the level of 0.1ns. Besides, the difference of the errors of cubic spline and Lagrange interpolation is tiny, about at the level of 0.01ns.

The main conclusions in this dissertation are as follows. In most cases, cubic spline interpolation is the best one of the three interpolation methods which can determine the GEO satellite precise clock bias during maneuvering. The accuracy of cubic spline interpolation is at the level of 0.08ns～0.38ns (aiming at the data of sample) which can meet the actual demand; And the stability is obviously better than that of quadratic polynomials and Lagrange interpolations; besides these, cubic spline interpolation has the advantage of simple calculation and high calculation efficiency. Taken together, we should choose cubic spline interpolation to determine the GEO satellite precise clock bias during maneuvering.

Therefore, GEO satellite precise clock bias during maneuvering can be determined by interpolating, which is not only helpful to the research with GEO satellite clock product, but also improve the availability and continuity of BDS.

[1] Shin-Chan Han. Static and Kinematic Absolute GPS positioning and Satellite Clock Error Estimation. 2000.
[2] Wang-Jun and Fang Shun-shan, The three methods and the analysis of GPS precision satellite clock offset interpolation. GNSS World of China, 2012.
[3] Ye, C., et al., Research on interpolation of satellite clock bias. Journal of Geometrics. Feb. 2008; 33(1).
[4] Wu, J., et al., Research on interpolation method for IGS precise ephemeris and clock bias. Geotechnical Investigation & Surveying. 2008.

Stable Similariton Generation in All-fiber Hybrid Mode-locked Ring Laser for Frequency Metrology

Lazarev Vladimir[1], Krylov Alexander[2], Dvoretskiy Dmitriy[1], Sazonkin Stanislav[1], Leonov Stanislav[1], Shelestov Dmitriy[1], Karasik Valeriy[1], Kireev Alexey[3], and Gubin Mikhail[3,4]

[1]Science and Research Center Photonics and IR-Technics, Bauman Moscow State Technical University, Moscow, Russia
[2]Fiber Optics Research Center of the Russian Academy of Sciences, Moscow, Russia
[3]P.N. Lebedev Physical Institute of the Russian Academy of Sciences, Moscow, Russia
[4]National Research Nuclear University MEPhI, Moscow, Russia
E-mail: vladimir.al.lazarev@gmail.com

In the last decade ultra-short pulse (USP) fiber lasers became one of the most important instruments in frequency metrology [1-2]. It was shown earlier that a similariton generation may be realized with a hybrid mode-locking (ML) technique [3] that implies co-action of two ML mechanisms – a slow saturable absorber such as single-walled carbon nanotubes [4], and a fast one such as nonlinear polarization evolution based on the nonlinear Kerr-effect in fibers. Hybrid ML should undoubtedly enhance pulse quality and provide a reliable ML start-up by taking advantages of both fast and slow ML mechanisms, so that hybrid ML can significantly extend the laser service life. Fig. 1 shows 92.6-fs USP spectra at 11.2 mW output power. Obtained similariton generation regime was very reliable during several months.

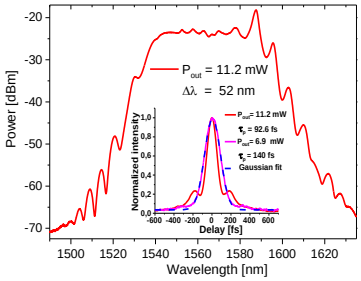


Fig. 1: USP spectrum and its fitting. Inset: USP auto-correlation traces.

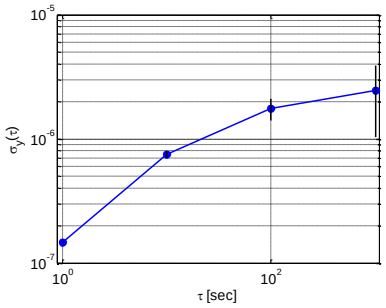


Fig. 2: Allan deviation of the repetition rate of the free-running similariton laser

Allan deviation of the repetition rate for the free-running similariton laser is shown in Fig. 2. Being compared with a 100-fs stretch-pulse fiber laser [5], similariton laser has low repetition rate deviation in the same averaging time interval 1-10^3 s and high reliability, which makes it highly promising for further development of the stabilized comb. Our current efforts are aimed now to demonstrate active stabilization for further generation of low-noise microwaves.

[1] T. Udem, "Optical frequency metrology", Nature 416, 233 (2002).

[2] S. Diddams [et al.], "Optical frequency synthesis and comparison with uncertainty at the 10^{-19} level," Science, 303, 1843 (2004).

[3] Krylov, A.A. [et al.], "Sub-100 fs similariton generation in the hybrid mode-locked erbium-doped fiber ring laser," Laser Optics, 2014 International Conference , vol., no., pp.1,1, June 30 2014-July 4 2014

[4] V. V. Grebenyukov [et al.], "Optical Studies of Single-Walled Nanotubes Synthesized from C:BN:B4C Catalytic Mixtures," J. Nanoelectronics and Optoelectronics, vol. 4, no 2, pp. 281-285, 2009.

[5] M. A. Gubin [et al.], "Femtosecond Er^{3+} Fiber Laser for Application in an Optical Clock", Las. Phys., 2007, V.. 17, N.. 11, pp. 1286–1291.

Generation and stabilization of optical frequency comb from on-chip microresonators

Huang, S.-W.[1], Yang, J.[1], Zhou, H[2]., Matsko, A.[3], Yu, M.[4], Kwong, D.-L.[4], Maleki, L.[3], and Wong, C. W.[1]
[1]University of California Los Angeles, Los Angeles, CA, United States
[2]University of Electronic Science and Technology of China, Chengdu, China
[3]OEwaves Inc, Pasadena, CA, United States
[4]Institute of Microelectronics, Singapore, Singapore
E-mail: swhuang@seas.ucla.edu

The current benchmark laser systems for optical frequency combs are self-referenced femtosecond mode-locked lasers. However, continuous-wave (cw) pumped microresonators recently emerge as promising alternative platforms for optical frequency comb generation [1]. Microresonator-based optical frequency combs, or Kerr frequency combs, are unique in their compact footprints and offer the potential for monolithic electronic and feedback integration, thereby expanding the already remarkable applications of frequency combs.

Here we report two recent progresses on optical frequency combs from on-chip Si_3N_4 microresonators: 1) generation of mode-locked ultrashort pulses from a ring resonator [2]; and 2) stabilization of 18 GHz Kerr frequency comb from a spiral resonator.

In the first half, we describe the generation of stable mode-locked pulse trains from normal dispersion microresonators. We show the importance of pump detuning and wavelength-dependent quality factors in stabilizing and shaping the pulse structure, to achieve a single pulse inside the cavity. We examine the mode-locking dynamics by numerically solving the master equation and provide analytic solutions.

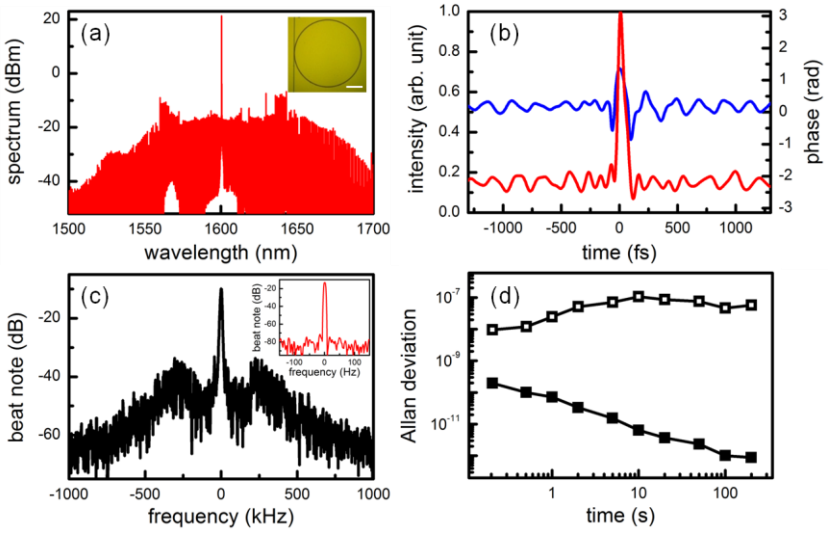


Fig. 1: (a) Example Kerr comb spectrum, with a spectral width spanning more than 200 nm. Inset: an optical micrograph of the ring resonator. Scale bar: 100μm. (b) Retrieved pulse shape (red curve) and temporal phase profile (blue curve), measuring a 74 fs FWHM pulse duration. (c) Out-of-loop beat note between the stabilized pump laser and the fiber laser reference comb. Inset: zoom-in view of the beat note (resolution bandwidth 6 Hz). (d) Allan deviation of the free-running (open squares) and the stabilized (closed squares) Kerr frequency comb spacing.

Then we report a low-phase-noise Kerr frequency comb with 18 GHz mode spacing, compatible with high-speed silicon optoelectronics. We show the frequency of the pump laser can be phase locked to an optical reference, *e.g.* a mode of a fiber laser frequency comb. On the other hand, the mode spacing of the Kerr frequency comb can also be stabilized to achieve frequency Allan deviations of 7×10^{-11} in 1 s.

[1] T. J. Kippenberg, R. Holzwarth, and S. A. Diddams, "Microresonator-Based Optical Frequency Combs" *Science* **332**, 555 (2011).

[2] S.-W. Huang, H. Zhou, J. Yang, J. F. McMillan, A. Matsko, M. Yu, D.-L. Kwong, L. Maleki, and C. W. Wong, "Mode-locked ultrashort pulse generation from on-chip normal dispersion microresonators" *Phys. Rev. Lett.* (accepted; arXiv: 1404.3256).

Noise Analysis of a Diode-Pumped Femtosecond Ti:Sapphire Laser

Gürel Kutan, Wittwer Valentin J, Hoffmann Martin, Saraceno Clara J*, Hakobyan Sargis, Resan Bojan+, Rohrbacher Andreas+, Weingarten Kurt+, Schilt Stéphane, Südmeyer Thomas

Laboratoire Temps-Fréquence, Université de Neuchâtel, Avenue de Bellevaux 51, CH-2000 Neuchâtel, Switzerland

* Institute for Quantum Electronics, ETH Zurich, 8093 Zurich, Switzerland

+ JDSU Ultrafast Lasers AG, Ruetistrasse 12, CH-8952 Schlieren/Zurich, Switzerland

E-mail: kutan.guerel@unine.ch

Ti:Sapphire lasers are widely used due to their large tunability, short pulse duration, and high stability, despite the need for complex and expensive pump lasers operating in the blue-green spectral region. In contrast, fiber lasers and diode-pumped solid-state lasers (DPSSLs) can be efficiently pumped by cost-effective and reliable laser diodes. With the advent of gallium nitride (GaN) laser diodes, Roth et al. demonstrated the first blue-pumped Ti:Sa DPSSL [1]. However, the pump wavelength of 452 nm led to slow deterioration of the output power [1]. The highest output power from a Ti:Sa DPSSL so far was 105 mW in 50-fs pulses, with a total pump power of 4 W [2]. The recent availability of green pump diodes enabled the first demonstration of a green-pumped Ti:Sa DPSSL achieving 23.5 mW average power and 62 fs pulses using a 1-W laser diode [3]. This power is too low for many applications, and it was not clear if higher efficiencies than 2.5% can be achieved at watt-level blue-green diode pumping. Moreover, the effect of the multi transverse mode pump on the noise was not evaluated, raising the question of their potential use for frequency comb applications.

Here, we report on a green-pumped ultrafast Ti:Sa DPSSL generating 200 mW average power, which is twice as high than the previous power record and which has a 4-times higher efficiency. The two laser diodes used for pumping (Nichia) deliver a total power of 2 W at 520 nm (Fig. 1 (a)). In order to achieve soliton pulse formation, we introduced two 150±40 fs^2 GTI-type mirrors. The output coupler has a transmission of 2%. In the other arm, the beam is focused onto a SESAM that is optimized for 810 nm with a modulation depth of around 1%. In modelocked operation, we achieved an average output power of 200 mW with 68-fs pulses and an optical bandwidth of 15.6 nm (FWHM) at a repetition rate of 378 MHz (Fig. 1 (b, c)). As a preliminary investigation towards the stabilization of this laser and its use as frequency comb, we analyzed its relative intensity noise (RIN) and the phase noise of the repetition rate beat, shown in Fig. 1 (d, e). The RMS integrated RIN is calculated to be 1.3% from 1 Hz to 50 MHz. Our result is a first step towards the realization of cheap, compact, air-cooled Ti:Sa lasers that will soon be available for numerous applications. In particular, we expect that CEO stabilization can be achieved in a simple way, either by direct diode modulation or SESAM opto-optical modulation [4], resulting in compact, air-cooled, and cost-efficient fully-stabilized diode-pumped Ti:Sa frequency combs.

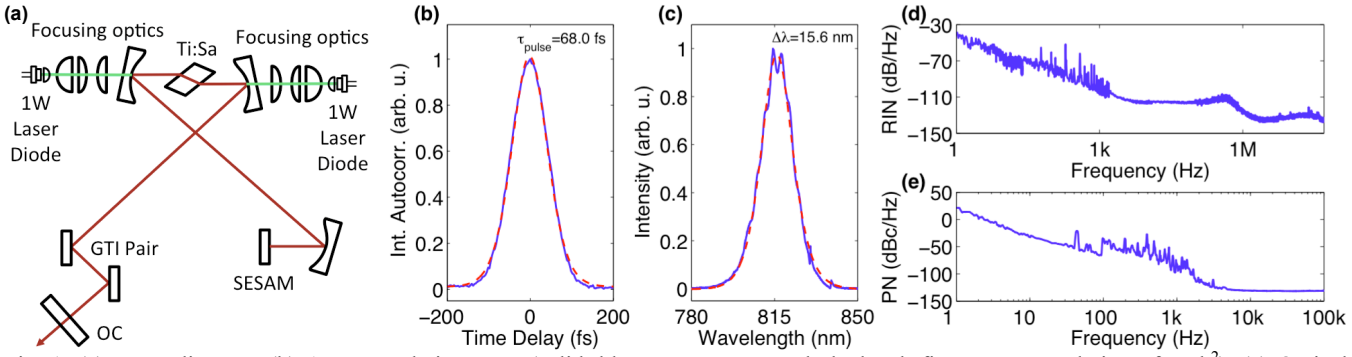


Fig. 1: (a) Laser diagram. (b) Auto-correlation trace (solid, blue: measurement; dashed red: fit to auto-correlation of $sech^2$). (c) Optical spectrum (solid, blue: measurement; dashed red: fit to $sech^2$). (d) Relative Intensity Noise (RIN). (e) Phase Noise (PN) spectrum.

[1] P. W. Roth, A. J. Maclean, D. Burns, and A. J. Kemp, Opt. Lett. **34**, 3334-3336 (2009).

[2] M. D. Young, S. Backus, C. Durfee, and J. Squier, Journal of Microscopy **249**, 83-86 (2012).

[3] S. Sawai, A. Hosaka, H. Kawauchi, K. Hirosawa, and F. Kannari, Appl. Phys. Exp. **7**, 022702-1-3 (2014).

[4] M. Hoffmann, S. Schilt, and T. Südmeyer, Opt. Exp. **21**, 30054-30064 (2013).

Versatile characterization of a passively carrier envelope phase stable frequency comb

Russell Kliese, Alexander Sell, Felix Rohde, Thomas Puppe, Armin Zach, Wilhelm G. Kaenders
TOPTICA Photonics AG, Lochhamer Schlag 19, 82166 Gräfelfing, Germany
E-mail: Thomas.Puppe@toptica.com

We demonstrate and characterize an Er:fiber frequency comb at a repetition rate of 80 MHz which is passively phase-stabilized via difference frequency generation to the initial wavelength of 1550 nm. A universal method to measure the phase noise spectra of comb lines at different wavelengths is demonstrated. With repetition-rate stabilization to an RF oscillator a linewidth of below 100 kHz at 1550 nm is achieved. It can be further reduced by locking the DFG comb to an optical reference. The measured phase noise spectra, after different nonlinear wavelength conversion stages, allows the analysis of noise properties in the laser system.

Optical frequency combs provide a greatly simplified clockwork to link the optical (~100 THz) and microwave (~100 MHz) frequency domain [1]. A comb spectrum generated from a short pulse mode-locked laser is defined by the repetition rate f_{rep} and the carrier envelope offset frequency f_{ceo}. The repetition rate is typically monitored by a photodiode and phase-locked to an RF or optical oscillator.

Several methods for stabilizing the f_{ceo} have been demonstrated. A well-established scheme detects f_{ceo} by f-2f interferometry and acts via a feed-back loop on the group-velocity dispersion (GVD), or alternatively by a feed-forward scheme on an external AOM [2]. Instead of stabilizing the f_{ceo}, it can be fundamentally removed from the comb output using difference frequency generation (DFG) [3], as has been previously realized in pulsed Ti:Sa lasers [4]. Broadening an Erbium doped fiber comb such that the DFG results at 1550 nm allows for a technologically elegant solution [5].

We characterize a passively carrier envelope phase stabilized Er:fiber frequency comb based on DFG at several wavelengths (Fig. 1). By transferring the properties of a comb line to a cw external cavity diode laser, the phase noise can be subsequently measured by tracking the self-heterodyne beat note [6]. The results are in agreement with the expectation from the elastic tape model. Furthermore, it has been shown that substantial phase noise improvement can be realized by locking a single comb line of the frequency comb to an optical reference. Since the fix point of the frequency and phase fluctuations of the DFG-comb is located strictly at the frequency origin, the phase noise at f_{rep} scales in an ideal way for RF clock signal generation. The DFG-comb is therefore an attractive solution for practical optical clocks.

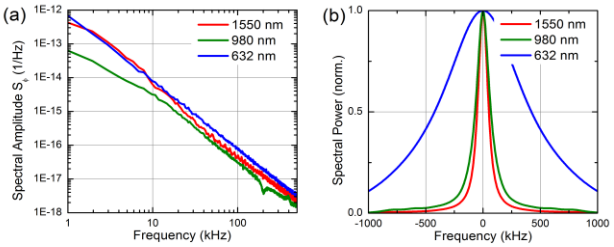


Fig. 1: Phase noise of the comb at different wavelengths normalized to an 800 MHz carrier frequency (a) and reconstructed line-shapes (b).

[1] S.A. Diddams, "The evolving optical frequency comb", J. Opt. Soc. Am. B. 11, B51 (2010).

[2] S. Koke, C. Grebing, H. Frei, A. Anderson, A. Assion, G. Steinmeyer, "Direct frequency comb synthesis with arbitrary offset and shot-noise-limited phase noise", Nature Photonics 4, 462 (2010)

[3] N. Haverkamp, H. Hundertmark, C. Fallnich, H.R. Telle, "Frequency stabilization of mode-locked Erbium fiber lasers using pump power control", Appl. Phys. B 78, 321 (2004)

[4] M. Zimmermann, C. Gohle, R. Holzwarth, T. Udem, and T.W. Hänsch, "Optical clockwork with an offset-free difference-frequency comb: accuracy of sum- and difference-frequency generation", Opt. Lett. 29, 310 (2004).

[5] G. Krauss et al., "All-passive phase locking of a compact Er:fiber laser system", Opt. Lett., 4, 540 (2011).

[6] T. Okoshi et al., "Novel method for high resolution measurement of laser output spectrum", Electron. Lett. 16, 630 (1980).

Comparison of different carrier-envelope frequency stabilization methods for a high performance DPSSL frequency comb

Kundermann Stefan, Lecomte Steve
Centre Suisse d'Electronique et de Microtechnique (CSEM), Jaquet-Droz 1, 2000 Neuchâtel, Switzerland
E-mail: stefan.kundermann@csem.ch

Carrier envelope frequency (f_{CEO}) stabilization of frequency combs is traditionally achieved via power modulation of the pump power of the comb oscillator [1]. A further possibility is to shift the laser f_{CEO} using an external acousto-optic frequency shifter (AOFS). In this case the optical frequency comb spectrum is shifted exactly by the RF modulation frequency of the AOFS [2,3].

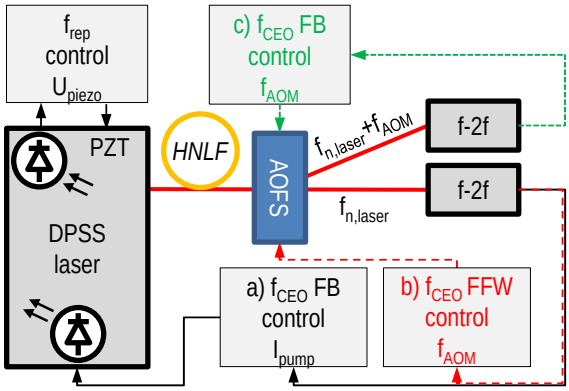


Figure 1: Block schematic of stabilization schemes.

In this work different stabilization schemes in self-referenced frequency comb system architecture are compared and the relevant block schematic is presented in figure 1. The used 100 MHz diode pumped solid state laser (DPSSL) emits 190 fs transform limited pulses at 1560 nm telecom wavelength at an average output power of 115 mW. Control of f_{rep} is achieved in a PLL using a high performance synthesizer locked to a hydrogen maser as local oscillator. The laser output spectrum is broadened to a bit more than an octave to enable f_{CEO} detection in f-2f interferometers. The spectrally broadened laser beam passes an AOM, where one part of the beam is frequency shifted and deflected. At both outputs of the AOFS f-2f interferometers detect f_{CEO}. The standard f_{CEO} lock via current modulation is implemented using the non-deflected beam (a). The output signal of the same interferometer is used for a feed forward (FFW) control of f_{CEO} (b). The measured f_{CEO} signal is directly sent to the AOFS after amplifying and shifting it to the frequency appropriate for the AOM. Furthermore a feedback (FB) lock via the AOFS is realized using the diffracted beam (c).

In case of the stabilization using the feedback lock via pump laser current (a), a stability at 1 s of $4 \cdot 10^{-11}$ of the stabilized harmonic of f_{CEO} at 390 MHz was achieved. This stability influences the stability of the193 THz optical modes by $8 \cdot 10^{-17}$. When the AOFS is driven with the measured f_{CEO} signal (b), the f_{CEO} frequency stability amounts to $1 \cdot 10^{-10}$ which is more than an order of magnitude worse than with the lock via the pump laser power. Using the AOFS with the FB control (c) a stability of f_{CEO} of $3 \cdot 10^{-12}$ could be attained with an integrated phase noise of 118 mrad. In conclusion feedback control of f_{CEO} via AOFS frequency shifting represents a high performance alternative to the standard feedback control via pump power modulation.

[1] S. Kundermann, E. Portuondo-Campa and S. Lecomte, "Ultra-low-noise 1 µm optical frequency comb", Electron. Lett. 50, 1231 (2014)

[2] S. Koke, C. Grebing, H. Frei, A. Anderson, A. Assion, G. Steinmeyer, "Direct frequency comb synthesis with arbitrary offset and shot-noise-limited phase noise", Nat. Photonics 4, 462 (2010)

[3] C. Benko, A. Ruehl, M. J. Martin, K. S. E. Eikema, M. E. Fermann, I. Hartl, and J. Ye, "Full phase stabilization of a Yb:fiber femtosecond frequency comb via high-bandwidth transducers", Opt. Lett. 37, 2196 (2012)

Radiation hard optical frequency comb from a diode-pumped solid-state femtosecond laser

Buchs Gilles, Kundermann Stefan, Portuondo-Campa Erwin, Lecomte Steve
Centre Suisse d'Electronique et de Microtechnique (CSEM), Jaquet-Droz 1, 2000 Neuchâtel, Switzerland
E-mail: gilles.buchs@csem.ch

Highly stable frequency combs generated by advanced mode-locked femtosecond lasers have led to several breakthroughs in the field of precision optical metrology, precision measurements and applications such as laser-based gas sensing and molecular fingerprinting [1]. Today such femtosecond lasers also show a high potential for space-related applications, *e.g.* Refs [2,3]. For this, optical frequency combs from mode-locked femtosecond lasers must be capable of surviving a whole set of challenging environmental conditions along the whole lifetime of a typical space mission, especially high energy radiations.

Here, we present results from standard ground-level radiation tests performed on a femtosecond diode-pumped solid-state laser (DPSSL) based on Yb:KYW gain medium and passively mode-locked with a semiconductor saturable absorber mirror (SESAM), similar to the laser reported in Ref [4]. Such lasers can be built in a compact way and they have shown properties like low cavity losses, high power and short pulse width, which surpass those of fiber lasers which are usually seen as a preferential choice for space applications. These properties, which are similar to those of Ti:sapphire lasers, would offer superior performance for specific space applications like ultra-precise distance measurement, time and frequency transfer, optical spectroscopy, etc. Furthermore, such laser architecture is not prone to radiation induced attenuation (RIA), as seen in fiber lasers [5].

The radiation tests have been conducted in the framework of the ESA M3 mission candidate STE-QUEST which aimed at precise measurements of general relativity effects [3]. We show that the DPSSL technology is capable to sustain a total gamma dose of 170 krad (H_2O) applied in 5 days and corresponding to 5 years dose in the highly elliptical STE-QUEST orbit behind a 3.5 mm spherical Al-shield. The laser was continuously running during the gamma irradiation and its key parameters were monitored. A 5% power loss and a 20% pulse length increase, while maintaining solitonic regime, have been observed at the end of the irradiation session. The laser power fully recovered within about 24h with the initial pump current applied continuously. About forty days later, the laser had roughly recovered its pre-irradiation pulse width as well. According to the rate of performance-loss during the high-flux gamma radiation and the recovery rate during normal operation, we could expect that the effects of the low-flux cosmic radiation during the mission are continuously counterbalanced by the observed self-healing effect with no or very low effective loss of performance over time. A proton irradiation test has been performed with a total fluence of $9.8 \cdot 10^{10}$ protons/cm^2 with energies between 20 and 100 MeV, equivalent to 7.5 years in the STE-QUEST orbit. During and after the test, no laser parameters degradation was observed. Additionally, the stability of the frequency comb generated by stabilizing the two degrees of freedom f_{rep} (comb spacing) and f_{CEO} (offset frequency) of the DPSSL laser are presented and discussed.

From these results, we claim that DPSSL technology is readily compatible with long duration space missions.

[1] N. R. Newbury, "Searching for applications with a fine-tooth comb", Nat. Photonics 5, 186 (2011)
[2] I. Coddington et al., "Rapid and precise absolute distance measurements at long range" Nat. Photonics 3, 351 (2009)
[3] http://sci.esa.int/ste-quest/
[4] S. A. Meyer, T. M. Fortier, S. Lecomte and S. A. Diddams, "A frequency-stabilized Yb:KYW femtosecond laser frequency comb and its application to low-phase-noise microwave generation", Appl. Phys. B 112, 565 (2013)
[5] J. Lee et al. "Testing of a femtosecond pulse laser in outer space", Scientific Reports 4, Article number: 5134

Development of an erbium-fiber-laser-based optical frequency comb at NTSC

Zhang Yanyan[1], Yan Lulu[1], Fan Songtao[1,2], Zhang Long[1], Zhao Wenyu[1,2], Guo Wenge[3], Zhang Shougang[1] and Jiang Haifeng[1*]
1 Key Lab. of Time and Freq. Primary Standards, National Time Service Center, Xi'an China
2 Graduate University of Chinese Academy of Sciences Beijing, China
3 School of Science, Xi'an Shiyou University, Xi'an, 710065, China
Email: zhangyanyan@ntsc.ac.cn; * haifeng.jiang@ntsc.ac.cn

Optical frequency combs based on mode mocked lasers are very powerful tools for many applications including spectroscopy[1], ultra-low noise microwave generation[2], time & frequency transfer[3]. Especially, erbium-fiber-laser-based optical frequency combs[4-6] play an outstanding role, owing to their robustness, compactness, reliability, user friendliness and directly covering telecommunication wavelength. In order to perform Sr optical clock frequency measurements and ultra-stable microwave generation at NTSC, we developed a home-made erbium-fiber-laser-based optical frequency comb system.

The laser source of optical frequency comb is a mode-locked erbium-doped fiber ring laser with an output of 50 mW and a 3dB optical bandwidth of 50 nm centered at ~1570nm. The repetition rate of the laser (209MHz), controlled by both an intra-cavity electro-optic modulator[7] and a piezo-transducer, enables a long term frequency stabilization. The carrier envelope offset frequency (f_{ceo}) of the frequency comb is controlled via the pumping power.

The in-loop frequency stability of the repetetion rate's 4th harmonic is about 0.1 mHz, limited by the resolution of the frequency counter. The signal-to-noise ratio of f_{ceo} is about 40 dB with 3 MHz resolution bandwidth. The in-loop frequency stability of f_{ceo} is about 0.6 mHz, corresponding to a relative stability of 4×10^{-18}@1s. Now, we are working on extending the comb's optical spectrum to the Sr clock transition (698nm).

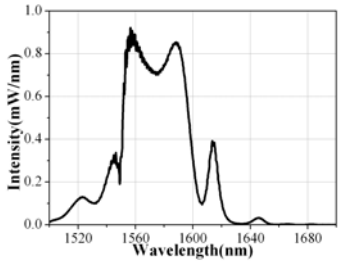


Fig. 1. Optical spectrum of the mode-locked laser.

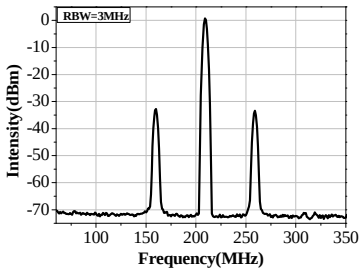


Fig. 2. Spectrum of the *f*-2*f* interference in 3 MHz resolution bandwidth (RBW)

REFERENCES

[1] Diddams S A, Hollberg L, and Mbele V, "Molecular fingerprinting with the resolved modes of a femtosecond laser frequency comb," *Nature*, **445**, 2007, 627-630.

[2] Fortier T M, Kirchner M S, Quinlan F, Taylor J, Bergquist J C, Rosenband T, and Diddams S A, "Generation of ultrastable microwaves via optical frequency division," *Nat. Photonics*, **5,** 2011, 425-429.

[3] Giorgetta F R, Swann W C, Sinclair L C, Baumann E, Coddington I, and Newbury N R, "Optical two-way time and frequency transfer over free space," Nat. Photonics, 7, 2013, 434-438.

[4] Nicolodi D, Argence B, Zhang W, Le Targat R, Santarelli G, and Le Coq Y, "Spectral purity transfer between optical wavelengths at the 10-18 level," Nat. Photonics, 2014, 8, 219-223.

[5] Tauser F, Leitenstorfer A, and Zinth W, "Amplified femtosecond pulses from an Er: fiber system: Nonlinear pulse shortening and self-referencing detection of the carrier-envelope phase evolution," Opt. Express, 2003, 11, 594–600.

[6] H. Udem, R. Holzwarth, and T. Hänsch, "Femtosecond optical frequency combs," Eur. Phys. J. Special Topics, 172, 2009, 69-79.

[7] Hudson D D, Holman K W, Jones R J, Cundiff S T, Ye J, and Jones D J, "Mode-locked fiber laser frequency-controlled with an intracavity electro-optic modulator," Opt. Lett., 30, 2005, 2948-2950.

Reference-source-free timing jitter measurement of a mode-locked laser using a fiber delay line

Jung, Kwangyun and Kim, Jungwon*
Korea Advanced Institute of Science and Technology (KAIST), Daejeon 305-701, South Korea
*E-mail: jungwon.kim@kaist.ac.kr

Mode-locked lasers can emit extremely short optical pulse trains with ultralow timing jitter. Their timing jitter properties are important for low phase noise microwave generation, photonic analog-to-digital converter, clock distribution, and large-scale particle accelerators. In order to utilize or optimize ultralow timing jitter properties of mode-locked lasers properly, timing jitter should be characterized prior to their specific applications. So far, most of high-resolution timing jitter measurements of mode-locked lasers have used a low-bandwidth phase-locked loop (PLL) with a reference oscillator (either a low-noise tracking electronic oscillator or a similar mode-locked laser with the same repetition rate). For the most accurate measurement, a balanced optical cross-correlator (BOC) method [1,2] can be used, but it requires a reference laser that has a similar or lower timing jitter compared to the laser under test (LUT). Furthermore, the repetition rate should be exactly matched to the integer multiple of the LUT. For these reasons, high-resolution and accurate timing jitter measurement of a femtosecond mode-locked laser has been challenging and resource consuming.

In this paper, for more convenient and versatile timing jitter measurement with ultrahigh resolution, we demonstrate a long optical fiber delay line-based timing jitter measurement technique that does not require an additional reference source. This method is based on Michelson interferometer including a km scale optical fiber delay line [3]. To verify the suggested delay line method, we built two similar 77-MHz Er-fiber lasers and compared the delay line method to the BOC method (Fig. 1). They show a fairly good agreement. Note that high frequency noise spikes are from integer multiples of the inverse delay time (not real laser noise). As the demonstrated method takes advantage of sensitive optical frequency comparison instead of RF/microwave frequency comparison that other delay line techniques [1,4] have used, the equivalent background phase noise floor is much lower at ~ -170 dBc/Hz (at 10-GHz carrier). The demonstrated result is in the very early stage, so we anticipate that the background floor can be improved after enhancing detection SNR using proper optical filters in the near future. As this method does not require additional low-noise reference oscillators, has an all-fiber configuration, and is almost repetition rate independent, we expect that it can be a convenient tool for accurate timing jitter measurement and optimization of mode-locked lasers.

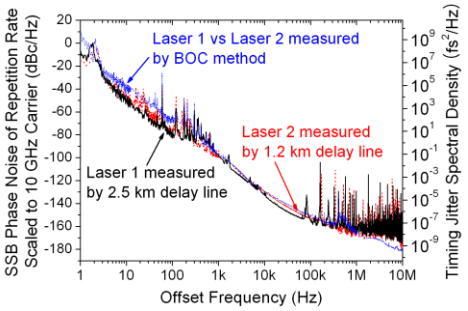


Fig. 1: Mode-locked lasers timing jitter spectral density measurement result.

[1] J. Kim, J. Chen, J. Cox, and F. X. Kärtner, "Attosecond-resolution timing jitter characterization of free-running mode-locked lasers," Opt. Lett., vol. 32, no. 24, pp. 3519-3521, Dec. 2007.

[2] T. K. Kim, Y. Song, K. Jung, C. Kim, H. Kim, C. H. Nam, and J. Kim, "Sub-100-as timing jitter optical pulse trains from mode-locked Er-fiber lasers," Opt. Lett., vol. 36, no. 22, pp. 4443-4445, Nov. 2011.

[3] F. Kéfélian, H. Jiang, P. Lemonde, and G. Santarelli, "Ultralow-frequency-noise stabilization of a laser by locking to an optical fiber-delay line," Opt. Lett., vol. 34, no. 7, pp. 914-916, Apr. 2009.

[4] E. Rubiola, E. Salik, S. Huang, N. Yu, and L. Maleki, "Photonic-delay technique for phase-noise measurement of microwave oscillators," J. Opt. Soc. Am. B, vol. 22, no. 5, pp. 987-997, May 2005.

Frequency Measurements with Yb-Laser Comb

Çağrı Şenel, Ramiz Hamid, Cihangir Erdogan, Mehmet Çelik,and F. Ömer Ilday*
TÜBİTAK National Metrology Institute (UME), PO 54, TR-41470, Gebze, Kocaeli, Turkey
*Department of Physics, Bilkent University, TR-06800, Ankara, Turkey
E-mail: cagri.senel@tubitak.gov.tr

Despite the prevalence of fiber frequency combs around 1.5 μm, few fully stabilized frequency combs have been demonstrated around 1.0 μm, despite the generally superior performance of Yb-fiber lasers compared to Er-fiber lasers [1] and even fewer absolute frequency measurements with these lasers are reported. Here, we report an Yb-doped fiber laser that operates at net-zero group-velocity dispersion and produces pulses that is compressed externally to 33-fs. The frequency comb generated by this system is locked to Cs atomic clocks.

Experimental setup is shown in Fig. 1(a). Oscillator design relies on self-similar amplification, followed by spectral filtering, then, purely linear dispersive propagation and finally spectral compression in fiber, returning to the original state at the end of the loop. The repetition rate is 49.6 MHz. Intracavity pulse energy before (after) the gain fiber is 60 pJ (4 nJ), limited by pump power. The oscillator was first designed using numerical simulations and then constructed. Extracted pulses are amplified externally in a fiber amplifier that is arranged to exactly mimic pulse propagation inside the oscillator, thereby eliminating gain narrowing. Consequently, the compressed pulse duration after amplification is the same from the oscillator, namely, 33 fs.

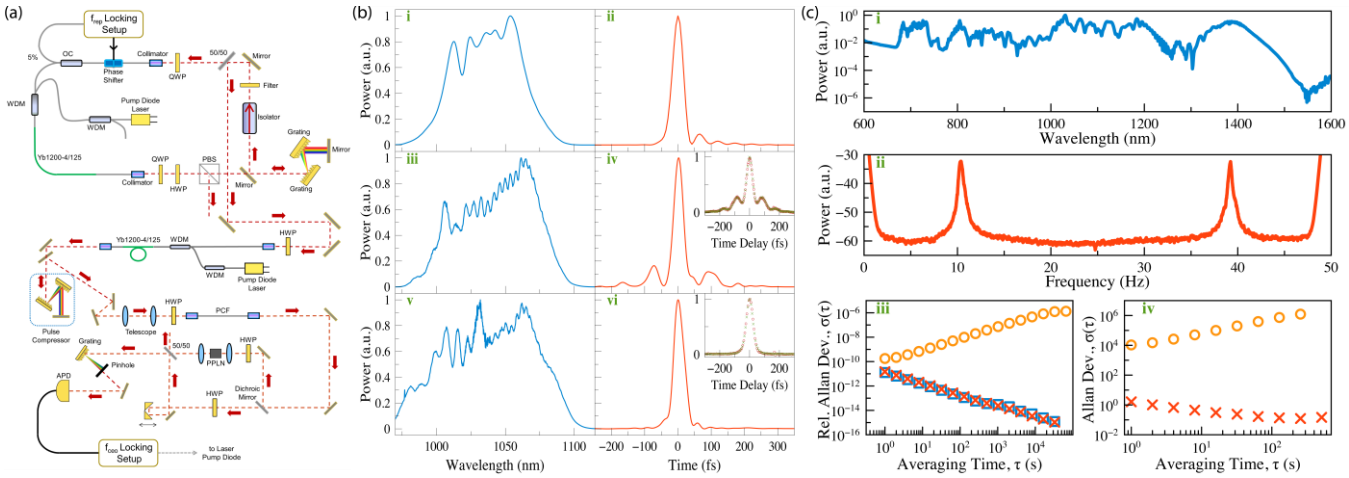


Fig. 1: (a) Schematic diagram of the setup. (b) Optical spectra obtained for (i) simulations of the oscillator, (iii) measured from the oscillator, (v) measured after amplification and retrieved pulse shapes obtained for (ii) the oscillator (simulated), (iv) the oscillator (experimental), (vi) the amplifier (experimental). Insets shows the measured autocorrelations. (c) (i) Spectrum of the generated supercontinuum, (ii) free-running f_{ceo} beat signals, Allan deviation of (iii) the repetition frequency and (iv) f_{ceo} of the free-running fiber comb (circles), Cs-locked fiber comb (crosses), and Cs atomic clock (squares)

Stability of the laser is characterized using relative intensity noise (RIN) and phase noise measurements in the short term and using Allan deviation measurements for frequency stability in the long term (Fig. 1(c)). Integrated RIN from 3Hz to 250 kHz is measured as 0.017%. Measured phase noise from 1 kHz to 25 MHz is 76 fs (limited by the measurement setup). After amplification 60 mW of compressed pulses is coupled to a 30 cm-long segment of photonic crystal fiber (PCF) with zero-dispersion-wavelength of 975 nm to generate supercontinuum (SC). An f-2f interferometer is built and carrier-envelope-offset beat signals are observed. Repetition and carrier-envelope-offset frequencies (f_{ceo}) are locked to Cs atomic clocks. The system has been used for absolute frequency measurement of an Nd:YAG/I_2 laser. The efforts to measure the absolute frequency of a 543 nm laser utilizing SHG is ongoing. In the future, spatial light modulator will be used for pulse compression at the amplifier output to obtain near-transform-limited pulses (~20 fs).

[1] S. A. Diddams, "The evolving optical frequency comb [Invited]," J. Opt. Soc. Am. B 27, B51 (2010).

High spectral purity laser characterization with a self-heterodyne frequency discriminator

O. Llopis[1], Z. Abdallah[1,3], V. Auroux[1,4], A. Fernandez[1,2]
[1]CNRS, LAAS, Univ. de Toulouse, Toulouse, France
[2] Univ. de Toulouse, UPS, Toulouse, France
[3]CNES, Toulouse, France ; [4]OSAT, Toulouse, France
E-mail: llopis@laas.fr

The today availability of small size narrow linewidth lasers, such as semiconductor lasers optically coupled to high quality factor optical resonators (WGM resonators, fiber resonators…), is an opportunity to develop new embedded applications for which the laser phase noise level is mandatory. This is the case, as an example, of high precision interferometers and of microwave to terahertz signal generation using optics. Before being used in these systems, this type of laser has to be characterized in terms of phase or frequency noise. However, phase noise measurement in the optical domain is not as developed as it is for radio frequency sources, although some commercial systems are already available (ex : OEwaves). The reason is that it is much more difficult to design a high quality optical frequency synthesizer than a low phase noise RF synthesizer. Therefore, the easier way to measure this type of sources is still to set up the frequency discriminator technique.

In this approach, the laser signal is split in two paths, one path is delayed with a delay smaller than the coherence length of the laser (contrarily to linewidth measurement case) and the signals are combined on a photodiode. In the self-heterodyne case, an acousto-optic modulator is added in one of the paths in order to shift the signal in frequency around a few tens of MHz. In this case, the noise is analyzed using an RF phase noise test bench at this frequency [1].

The main difficulty in this approach is to evaluate the measurement noise floor. In microwave frequency discriminators, it is measured using a bypass of the delay line. However, in the optical case, part of the noise may come from nonlinear effects in the fiber [2], and the noise floor has to be measured with the fiber maintained in the system.

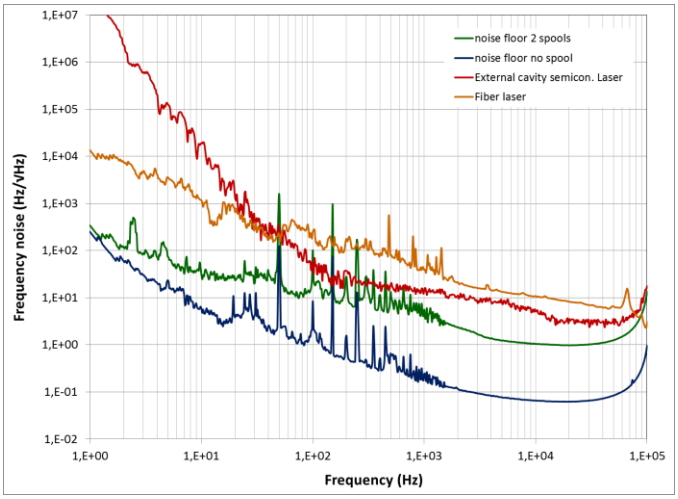


Fig 1 : Frequency noise of an external cavity semiconductor laser (red), of a fiber laser (orange) and noise floor of the bench measured by removing the fiber spool (blue) or by using two fiber spools to cancel the optical delay (green)

To this purpose, two fiber spools are used to cancel the delay, and the remaining noise is the uncorrelated noise of the two fibers. This raises largely the noise floor, and shows the limitation of the technique. However, a careful choice of the fiber spool and of the measurement conditions (such as the optical power in the fiber) can improve this noise floor. This behavior will be described at the conference.

[1] S. Camatel, V. Ferrero, Journal of Lightwave Technology, Vol. 26, Issue 17, pp. 3048-3055 (2008).

[2] O. Okusaga, J. Cahill, W. Zhou, A. Docherty, G.M. Carter, C.R. Menyuk, IEEE EFTF-IFCS 2011, May 2011.

A transportable optical cavity for laser frequency stabilization in space

Williams R. A.[1], Barwood G. P.[1], Gill P.[1], Koegel H.[2], Nicklaus K.[3], Herding M.[3], Wang X.[3], Herper M.[4], Fitzau O.[4], and Giesberts M.[4]

[1]National Physical Laboratory, Teddington, United Kingdom
[2]Airbus Defence and Space, Immenstaad, Germany
[3]SpaceTech GmbH, Immenstaad, Germany
[4]Fraunhofer Institute for Laser Technology, Aachen, Germany
E-mail: ross.williams@npl.co.uk

Laser frequency stabilization to high finesse optical cavities is a key enabling technology for a wide variety of fields, including optical frequency standards, ultra-low-noise microwave synthesis, and precision interferometry. While laboratory-based devices have continued to improve the state-of-the-art limits on oscillator stability [1], there is a complementary need for robust and portable lasers with excellent frequency stability. For example there is a growing requirement for transportable frequency-stable lasers for geodesy, space science, navigation, and earth observation.

In this presentation we describe an optical cavity system that has been built in the scope of an ESA-funded 'High Stability Laser' activity, which is concerned with developing a laser source for a satellite-to-satellite heterodyne interferometer. Such a satellite-satellite tracking scheme could be used for a Next Generation Gravity Mission, for which high resolution knowledge of changes in the intersatellite distance is needed to allow an accurate measurement of the earth's varying gravitational potential. A laser-ranging interferometer would enable significantly higher ranging accuracy compared to previous missions analyzing the earth's gravity field, such as GRACE, which used microwave ranging.

An optical cavity intended for operation in space must meet several criteria. It must be compact, low weight, modular, rigidly mounted, and be able to withstand the large inertial forces associated with launch and deployment. We present the design and performance testing of a Laser Stabilisation Unit (LSU) which meets these criteria, shown in Figure 1. It comprises a rigidly mounted Fabry-Pérot cavity based on a cubic spacer [2], a titanium vacuum chamber, and an integrated optics arm for launching light into the cavity.

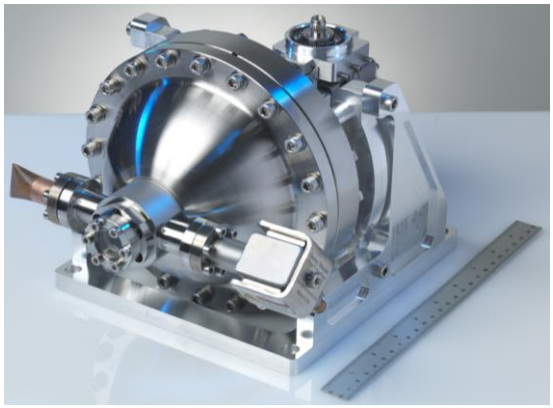


Fig. 1: The Laser Stabilisation Unit. The system has dimensions 19 cm ×18 cm ×28 cm and weighs less than 8 kg.

[1] T. Kessler, C. Hagemann, C. Greing, T. Legero, U. Sterr, F. Riehle, M. J. Martin, L. Chen and J. Ye, "A sub-40-mHz-linewidth laser based on a silicon single-crystal optical cavity," Nat. Photonics, vol 7, pp. 644-650, 2013.

[2] S. Webster and P. Gill, "Force-insensitive optical cavity," Optics Letters, vol. 36, no. 12, pp. 3572-3574, 2011.

Noise analysis in an ultra-stable laser system

X. H. Shi, X. Y. Zeng, W. Wu, Y. Liu, S. Y. Zhou, K. Deng, J. Zhang, and Z. H. Lu
MOE Key Laboratory of Fundamental Quantities Measurement, School of Physics,
Huazhong University of Science and Technology, Wuhan, P.R. China
E-mail: jie.zhang@mail.hust.edu.cn

Sub-Hertz linewidth lasers are essential as clock lasers in optical frequency standards. We are carrying on an Al^+ optical frequency standard experiment at Huazhong University of Science and Technology. The $^1S_0$ - $^3P_0$ clock laser transition is at 267.4 nm. This wavelength is reached by frequency quadrupling an external cavity diode laser at 1070 nm. We frequency stabilize the 1070 nm diode laser with the Pound-Drever-Hall (PDH) technique using a 10 cm long ultra-low expansion glass (ULE) cavity. To evaluate the achieved laser linewidth, we build two similar frequency stabilization systems, and measure the obtained beat note between the two stabilized lasers. A thermal noise limited performance is achieved with an Allan Deviation of 1.0×10^{-15} at 1 s for a single laser. Other noises have contributions at 5.0×10^{-16} level. The noise contribution is measured by locking two lasers to same cavity, and recording the beat frequency. In the present work, we evaluate the noise contributions due to cavity temperature fluctuation, vibrations, residual amplitude modulation (RAM), and electronic noise etc, and propose means to further lower these contributions to less than 1.0×10^{-16} level. By calculating the total noise contribution with the servo loop transfer function and measured different noise contribution terms, we have found that our calculation results agree with our measured noise contribution very well.

Temperature fluctuation will greatly vary the cavity length when the cavity temperature is far from its zero crossing temperature of the coefficient of thermal expansion even though the cavity spacer is made of ULE. The zero crossing temperatures of the two ULE cavities are measured by setting the cavities to different temperatures and measuring the locked laser frequencies. At the same time, the vacuum chambers' time constant are obtained which is useful to estimate the temperature fluctuation of the cavity itself. We use finite element analysis (FEA) to simulate the thermal property of our vacuum chambers, which shows a good agreement with the measured time constant. With FEA, we have a better understanding about the effects of materials used inside inner shielding layer of the vacuum chambers, which is of great use for us to design a new vacuum chamber with a much longer thermal time constant. Vibration is a limiting factor for us to reach the thermal noise limit at different frequency range. To minimize the vibration environment of the cavity, the whole laser stabilization system is installed on an optical breadboard which is supported by an active vibration isolation system. An acoustic shielding box is built which also minimize air turbulence. Vibration sensitivity of the ULE cavity is measured, and noise due to vibration is analyzed.

RAM due to the electro-optic modulator (EOM) is found to be a limitation at a stability level of 10^{-15} when the temperature of the EOM is not controlled. There is an offset voltage in the error signal when the RAM is not zero. This is caused by EOM's temperature fluctuation and the polarization of the injected light, etc. The effect of RAM due to temperature is measured, and the RAM-induced fractional frequency instability is estimated with Eq. (1) to be[1]

$$\sigma_y(\tau) = \sigma_{RAM}(\tau)\frac{\Gamma}{\nu}, \tag{1}$$

where Γ is the cavity linewdith and ν is the laser frequency. With the temperature of the EOM stabilized, the contribution of RAM is lowered to 5.0×10^{-16} level.

[1] W. Zhang, *et al.*, "Reduction of residual amplitude modulation to 1×10^{-6} for frequency modulation and laser stabilization," Optics Letters, vol. 39, no. 7, pp. 1980–1983, 2014.

Stable diode laser with integrated microresonator

Xie, Zhenda [1,2,*], Liang, Wei [3], Savchenkov, Anatoliy [3], McDonald, Michael [4], Zelevinsky, Tanya [4], Ilchenko, Vladimir [3], Matsko, Andrey [3], Maleki, Lute [3,*], and Wong, Chee-Wei [1,2,*]

1 Optical Nanostructures Laboratory, Columbia University, New York, NY 10027
2 Mesoscopic Optics and Quantum Electronics Laboratory, University of California, Los Angeles, CA 90095
3 OEwaves Inc., 465N. Halstead Str., Pasadena, CA 91107
4 Department of Physics, Columbia University, New York, NY 10027
E-mail: zhenda@seas.ucla.edu; cheewei.wong@ucla.edu; lute.maleki@oewaves.com

Stable lasers at specific atomic transitions are of special interest for optical atomic clocks. High-Q whispering-gallery-mode resonators (WGMR) may be used as portable frequency references for such laser sources. By actively [1] or passively [2] locking its frequency to WGMR, the laser can be stabilized with narrow linewidth.

Here we report the first external cavity diode laser (ECDL) comprising an integrated semiconductor reflective amplifier and a WGMR. Lasing originates from resonant feedback from the WGMR to the amplifier. The ECDL linewidth is measured by beating with a stable reference laser, showing an instantaneous sub-kHz linewidth. An 8.8 nm tuning range is realized by adjusting the angle of the grating. Single-longitudinal-mode (SLM) lasing around the Strontium (Sr) ^1S_o-^3P_o transition at 698nm is achieved by mode selection using a diffraction grating.

The WGMR we use is made from MgF_2 crystal with fine polishing, down to 7 mm diameter and 0.1 mm thickness. It is prism-coupled and sealed in a temperature-controlled package. The quality factor is tested by scanning a 698 nm tunable laser across the resonances, and Fig. 1(a) shows a spectrum corresponding to Q of ~10 billion. Our setup is depicted in Fig. 1(b). An anti-reflection coated semiconductor amplifier is used as a gain medium. Its emission is collimated and directed onto a ruled diffraction grating, and then focused at the coupling point into the WGMR. When properly coupled, a significant amount of light within the WGMR is backscattered creating feedback necessary for lasing. The diffraction grating ensures SLM lasing despite of the high mode-density of the WGMR. The output wavelength can be tuned by changing the angle of the diffraction grating.

SLM lasing specta is studied with an optical spectrum analyzer in a broad tuning range of 8.8 nm from 690.5 nm to 699.3 nm (see Fig. 2(a)-(d)). Fig. 2(e) shows radio frequency signal obtained by beating our laser output with a cavity-stabilized reference laser on a fast photodiode. The beat signal exhibits a short-term laser linewidth of ~1 kHz. Increasing the lasing power results in parametric lasing within the WGMR (Fig. 2f, [3])

In summary, we have created a stable laser source around Sr ^1S_o-^3P_o transition based on a monolithic WGMR comprising a narrow band mirror of the laser cavity. Unlike other laser stabilization schemes using WGMR, the reflective amplifier does not generate coherent light if spontaneous emission from the amplifier is not coupled to WGMR. This completely new configuration results in significant broadening of the range of applicability of WGMR for creation of spectrally pure stable lasers.

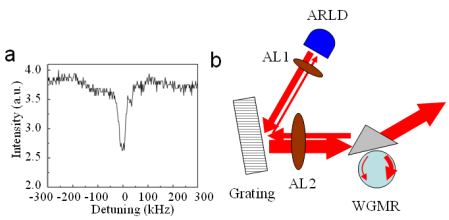


Fig. 1 (a) The WGMR has a measured linewidth of 30 kHz, corresponding to *Q* of 1.43 billion. (b) Schematic of our setup. ARLD: anti-reflection coated laser diode. AL: aspherical lens.

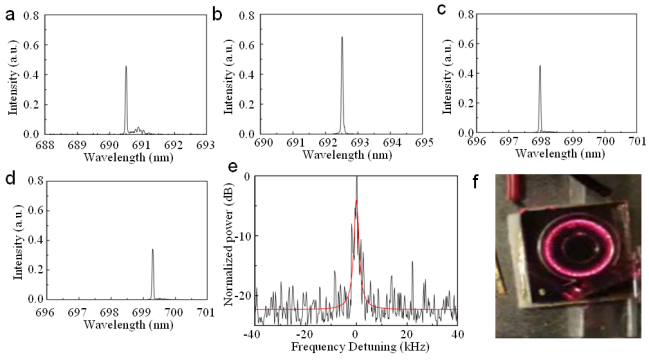


Fig. 2 (a)-(d) Laser spectra. (e) Beat signal. (f) WGMR photo.

[1] W. Liang, et al., Opt. Lett. 35, 2822 (2010).
[2] J. Alnis, et al., Phys. Rev. A 84, 011804 (2011).
[3] W. Liang, et al. Optica 2(1), (2015), TBP.

External cavity diode laser with long-term frequency stabilization based on mode boundary detection

Zhouxiang Xu, Kaikai Huang, Xuanhui Lu

Physics Department, Zhejiang University, Hangzhou, 310027, P. R. China

E-mail: xhlu@zju.edu.cn

Frequency stabilization for external cavity diode laser (ECDL) has played an important role in quantum optics, cold atom physics, and optical clocks [1]. Theoretically, mode hopping is caused by the drift of temperature and other influences such as aging of diode[2]. In the past several methods have been used to suppress mode hopping. They are divided into passive [3,4]and active methods[5].

We have implemented a long-term frequency stabilization system for external cavity diode laser (ECDL) based on mode boundary detection method. In this system, the saturated absorption spectroscopy was used. The current and the grating of the ECDL were controlled by a computer-based feedback control system. By checking any mode boundaries in the spectrum, the control system determined how to adjust current to avoid mode hopping. This procedure was executed periodically to ensure the long-term stabilization of ECDL in the absence of mode hops. This laser diode system without antireflection-coating had operated in the condition of long-term mode hopping free stabilization for almost 1200 hours (Seen in Fig.1), which is a significant improvement of ECDL frequency stabilization system. This technique is very useful in some applications such as laser atomic cooling and atom fountain etc.

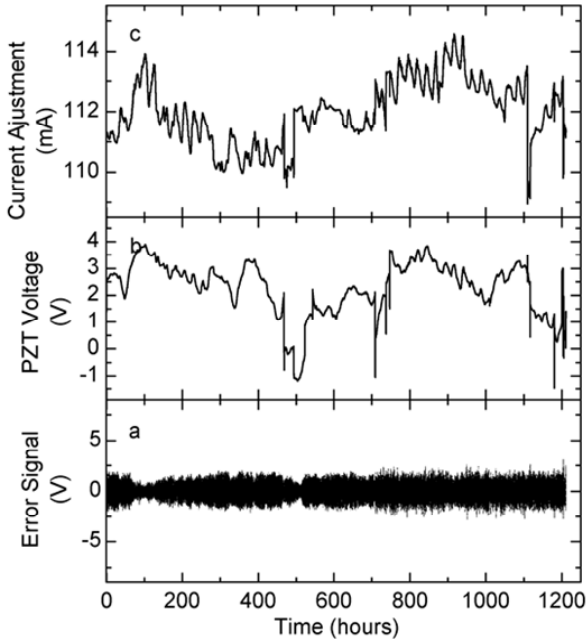


Fig.1 a. Locking error signal which is almost a straight line in 1200 hours shows that the frequency of ECDL didn't lose lock for any time. b. Grating's PZT voltage trace indicates the actions of normal PID. c. Current adjustment eliminated mode boundaries successfully for hundreds of times.

References:

[1] C. E. Wieman and L. Hallberg, Rev. Sci. Instrum. **62**, 1-20 (1991).
[2] A. S. Arnold, J. S. Wilson, and M. G. Boshier, Rev. Sci. Instrum. **69**, 1236-1239 (1998).
[3] J. Hult, I. S. Burns, and C. F. Kaminski, Appl. Opt. **44**, 3675-3685 (2005).
[4] C. Petridis,et al , Rev. Sci. Instrum. **72**, 3811-3815 (2001).
[5] Sheng-wey Chiow, Quan Long, Christoph Vo, Holger Müller, and Steven Chu, Appl. Opt. **46**, 7997-8001 (2007).

Birefringence effects in a fiber-coupled AOM-RN

Baryshev Viacheslav, Aleinikova Ekaterina, Aleinikov Mikhail

FGUP "VNIIFTRI", Mendeleevo, Moscow Region, Russian Federation

Email: baryshev@vniiftri.ru

We have presented in [1] the results of the comparative analysis of the residual amplitude modulation (RAM) and birefringence effects in EOM and AOM-RN. The birefringence deteriorating the noise performances of the signals obtained by FM spectroscopy (FMS) was experimentally investigated in particular case of commercial 20 MHz resonant EOM and broadband AOM-RN fabricated at "VNIIFTRI". No driving signals were applied to them. It has been shown that AOM-RN is much less sensitive to the birefringence effect than commercial EOM.

In this work we present the investigation of the birefringent and possible anisotropic performances of AOM-RN induced by strong driving signals applied to it. The power P_S of the driving signals exceeded considerably the level sufficient to conduct FMS with AOM-RN as a phase modulator. The simple experimental set-up (fig. 1) has been used to measure the detrimental polarization rotation of the AOM-RN output radiation consisted of the carrier and a couple of the first diffraction order optical beams. The input laser radiation at wavelength λ=795 nm was delivered to the AOM-RN by the single-mode, polarization-maintaining optical fiber. Thus the birefringent performances of AOM-RN and fiber itself contributed to the output beams polarization rotation. Fig. 2 shows a fractional power of the first diffraction order output beam component produced by the birefringence effect in AOM-RN in dependence of the angle θ between crystal optical axis *z* and vertical direction of the input laser beam polarization. We can conclude that the strength of the birefringence effect is still of the same order (tenths per cent) as that we observed and presented in [1] when no driving signals were applied to AOM-RN. This fact encouraged us to build a fiber-coupled AOM-RN whose FM output radiation performances will be presented at the conference.

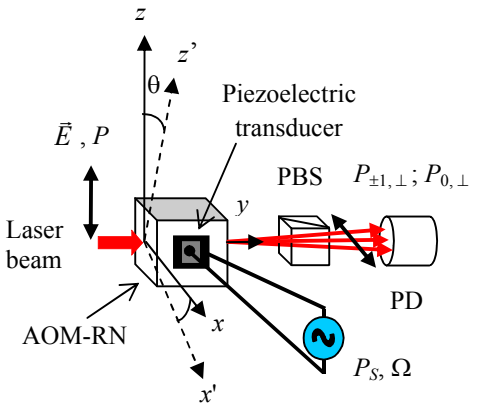


Fig. 1. Experimental set-up for measuring the birefringence performances of AOM-RN crystal. PBS –polarizing beam splitter, PD – photo-detector.

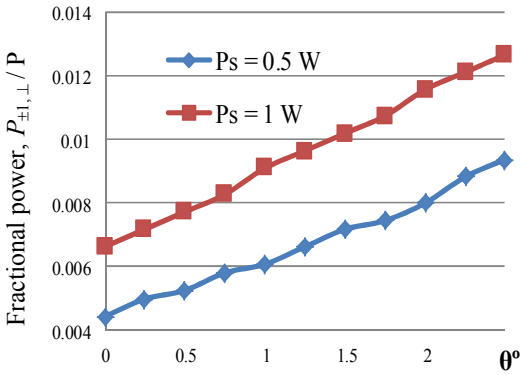


Fig. 2. Fractional power of the first diffraction order output beam component produced by the birefringence effect.

[1] V. Baryshev, E Aleinikova, "Residual Amplitude Modulation and Birefringence Effects in EOM and AOM-RN", *Proceedings*, 28th European Frequency and Time Forum, Neuchatel, Switzerland, 23-26 June, 2014, pp. 525-527.

created using
BCL easyPDF
Printer Driver
Click here to purchase a license to remove this image

Micro-integrated semiconductor laser modules for precision quantum optical experiments in space

Krueger, Mandy*, Bawamia, Ahmad*, Kuerbis, Christian*, Lewoczko-Adamczyk, Wojciech*+, Pyrlik, Christoph*, Wicht, Andreas*, Erbert, Goetz*, Peters, Achim*+, Traenkle, Guenther*

*Ferdinand-Braun-Institut, Leibniz-Institut fuer Hoechstfrequenztechnik, Berlin, Germany

+Humboldt-Universitaet zu Berlin, Germany

E-mail: mandy.krueger@fbh-berlin.de

We present a new technology platform for compact, robust and energy-efficient semiconductor laser modules that are suitable for field operation and for a deployment in space. Applications include coherent optical communication and coherent manipulation of atoms and molecules, as in optical atomic clocks and matter-wave interferometers.

We report on the integration of two arbitrary laser chips, micro-optics, DC and RF electronics including fiber-coupling into a single-mode, polarization maintaining fiber on a structured AlN substrate within a footprint of 80 x 30 mm². The AlN substrate is encapsulated into a hermetically sealed housing with custom-made feed-throughs for all DC, RF and optical signals.

We present a MOPA module that is based on this technology. It consists of a distributed feedback laser (DFB) emitting at 780 nm as master oscillator. The fiber coupled output power exceeds 500 mW and the intrinsic linewidth is less than 50 kHz. These features make the laser suitable for laser cooling and atom interferometry with Rb atoms.

In addition, we report on the application of the integration technology to an ultra-narrow-linewidth semiconductor laser module consisting of a DFB diode at 780 nm optically self-locked to a mode of an external Fabry-Pérot resonator. The unique combination of a DFB diode and external Fabry-Pérot resonator enables a reduction of frequency noise of at least a factor 1000 for all Fourier frequencies above 1 kHz as compared to a standard grating-based extended-cavity laser. The corresponding intrinsic linewidth is of the order of a few Hz.

We further outline the implementation of a laser system emitting in the UV range. A micro-integrated MOPA module emitting in the NIR forms a local oscillator of a UV laser system. The UV wavelength is then achieved through two consecutive frequency-doubling stages, at least one of which consisting of a micro-integrated monolithic enhancement cavity.

High-precision ring laser gyro for planar angle metrology

Astrua M[1], Belfi J[2], Beverini N [2,3], Di Virgilio A[2], Carelli G[2,3], Maccioni E[2,3], Ortolan A[4], Pisani M[1]

[1]INRIM Torino, Italy
[2]INFN, section of Pisa, Pisa, Italy
[3]Dept. of Physics, University of Pisa, Pisa, Italy
[4]Laboratori Nazionali di Legnaro, INFN, Legnaro (PD), Italy

E-mail: belfi@pi.infn.it

Ring laser gyroscopes (RLGs), based on the Sagnac effect, transduce the rotation rate of their reference frame in a frequency signal produced by the optical beat between the two counter-propagating beams circulating in their optical cavity. RLGs with side-length of tens of centimeters are nowadays commonly used for inertial navigation applications while larger systems (side-length larger than one meter), rigidly fixed to the ground, provide precise measurements of the Earth rotation rate and of the small superimposed local rotations coming from geophysical and geodetic phenomena.

Applications of RLGs in Angular Metrology have been foreseen since the end '60s [1], just after the invention of the LASER. The basic idea is to use the interference fringes by the two counterpropagating modes as an ultra-fine angular scale (see Fig. 1) dividing the full angle into a number $N=L/\lambda$ intervals, where L is the cavity perimeter and λ is the laser wavelength. The most effective realization of such kind of goniometer is the ring laser developed by Yu. V. Filatov and collaborators since the end of 70s [2]. This consists in a monolithic cavity 11 cm in side-length equipped with total reflection prisms in optical contact with the zerodur cavity frame. The typical resolution of these systems is at the level of 100 nrad, typically limited by the errors due to the influence of environmental parameters on the ring laser dynamics (magnetic field effects on the corner prisms, mechanical instabilities of the rotator, non-optimization of the geometrical parameters of the laser cavity).

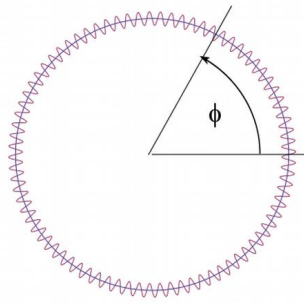


Fig.1 Ring laser goniometer concept.

We present the main characteristics of a new kind of laser goniometer being developed by a collaboration between INRIM and INFN. The target accuracy is 10 nrad, being the accuracy of the most precise angular encoders at the level of some 100 nrad. Our key idea is to setup a square non-monolithic cavity [3] of about 0.5 m in side making use of the last generation dielectric super-mirrors employed in the much larger gyroscopes for geodetic and geophysical applications.
We will discuss the main issues and proposed strategies concerning the implementation of an extremely accurate transportable rotational standard, the realization of a very sensitive gyroscope for the measurement of seismic effects, the demonstration of a self-calibration concept leading to the design of a larger rotating RLG for geodetic and relativistic experiments.

[1] Catherin J. M., Dessus B., French Patent No. 1511089; granted 26.01.68.
[2] Yu. V. Filatov, D. P. Loukianov, R. Probst, ”Dynamic angle measurement by means of a ring laser”, Metrologia, 34, 343-351, (1997).
[3] J. Belfi et al., “A 1.82 m^2 ring laser gyroscope for nanorotational motion sensing”, Appl. Phys. B ,106, 271-281, (2012).

Improving the Frequency Stability of a Laser Using a "Paper" Laser

C. A. Ortiz Cardona*,+, E. de Carlos López*, J. M. López Romero* and S. López López*

* Dirección de Metrología de Tiempo y Frecuencia, Centro Nacional de Metrología, CENAM, km 4.5 carretera a los Cues, El Marqués, 76241, Querétaro, México.
+ Centro de Investigación y de Estudios Avanzados del Instituto Politécnico Nacional (IPN), CINVESTAV, Unidad Querétaro, Libramiento Norponiente No 2000, Fracc. Real de Juriquilla, Querétaro, Querétaro 76230, México.
E-mail: cortiz@cenam.mx

The Dirección de Metrología de Tiempo y Frecuencia of the Centro Nacional de Metrología (*CENAM*) has developed and implemented a novelty strategy to improve the frequency stability of a laser. That strategy consists in generate a "paper" laser using some ideas of the algorithm employed on time scales [1] but in the frequency domain. Particularly, we used a *GaAs* laser (852 nm) coupled to an Ultra Low Expansion (*ULE*) optical cavity. The laser's light is splitted to be controlled in frequency by three different Acousto-optic modulators (*AOM´s*), which are arranged using cat's eye configuration [2]. Each *AOM* is frequency stabilized through three independent and analogous polarization spectroscopy experiments, using the most probable Cesium´s-133 D_2 line transition [$|6^2s_{1/2}, F = 4\rangle \rightarrow |6^2p_{3/2}, F' = 5\rangle$]. Therefore, three independent lasers (oscillators) with similar metrological characteristics are obtained.

In order to measure simultaneously the frequency of each member of the ensemble every second, a portion of the signal that is feed to the *AOM´s*, is sent to a frequency counter to establish the frequency variations as a time function. From data of frequency measurements, the equation (1) is used to calculate a frequency value $\nu_k(t+\tau)$ and generate a "paper" laser.

$$\nu_k(t+\tau) = \sum_{j=1}^{N} \omega_j \left[\nu_j(t) - \nu_{jk}(t+\tau)\right] \quad (1)$$

In the equation (1), ω_j represents the weight of each member of the ensemble. Of course, the condition of normalized weights is given by $\sum_{i=1}^{N} \omega_i = 1$. For simplicity and due to the experiments are similar, those weights are equal ($\omega_1 = \omega_2 = \omega_3 = 1/3$) and the initial frequency values are fixed to zero ($\nu_1 = \nu_2 = \nu_3 = 0\ Hz$). In the equation the term $\nu_{jk}(t+\tau)$, corresponds with frequency differences between members of the ensemble.

As mentioned above, the main objective of this idea consists in obtain a "paper" laser with better metrological characteristics (compared with lasers of the ensemble) using a simple technique. Preliminary results are promising because, by observing the stability data presented in figure 1, the relative stabilities, which correspond with the frequency differences between the lasers (Cs_1, Cs_2 and Cs_3), are lower than the relative stabilities of the frequency differences between those lasers and the "paper" laser (*PL*).

[1] J. M. López Romero, and N. Diaz-Muñoz, " Progress in the Generation of the UTC(CNM) in terms of a virtual clock", *Metrologia,* vol. 45, pp. S59-S65, Dec. 2008.

[2] E. A. Donley, T. P. Heavner, F. Levi, M. O. Tataw, and S. R. Jefferts, "Double-pass acousto-optic modulator system", *Review of Scientific Instruments*, vol. 76, 063112, Jun. 2005.

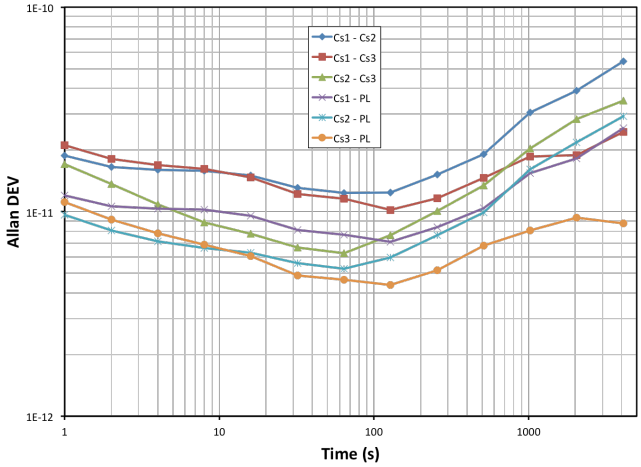


Fig. 1: Allan Deviation of the virtual lasers in comparison with real lasers (Cs_1, Cs_2 and Cs_3).

Faraday Anomalous Dispersion Optical Filter at 461nm Utilizing a Strontium Hollow-cathode Lamp

Duo Pan, Xiaobo Xue, Bin Luo*, Xiang Peng, Jingbiao Chen, and Hong Guo
State Key Laboratory of Advanced Optical Communication, Systems and Networks, School of Electronics Engineering and Computer Science, and Center for Quantum Information Technology, Peking University, Beijing 100871, China.
*State Key Laboratory of Information Photonics and Optical Communications, Beijing University of Posts and Telecommunications, Beijing 100876, China
E-mail: panduo@pku.edu.cn

Faraday anomalous dispersion optical filter (FADOF) has an advantage of ultra-narrow bandwidth, which makes it an excellent frequency selection component in laser system. Thus it can be used for laser frequency stabilization [1, 2] and directly made into an optical clock [3].

In this paper, a Faraday anomalous dispersion optical filter at 461 nm (^{88}Sr, $^1S_0$-$^1P_1$) is demonstrated utilizing a strontium hollow-cathode lamp, the experimental setup is displayed schematically in Fig. 1. The configuration in the dashed box is a FADOF using ^{88}Sr hollow-cathode lamp, with H1 and H2 being a pair of permanent magnets, and P1 and P2 being a pair of crossed polarizer. A 461 nm diode laser provides the probing beam, and the transmission spectrum is detected by a photodiode (PD). A twin-peak transmission spectrum at the ^{88}Sr $^1S_0$-$^1P_1$ transition is obtained, with a maximum transmittance of 0.5%, as shown in Fig. 2.

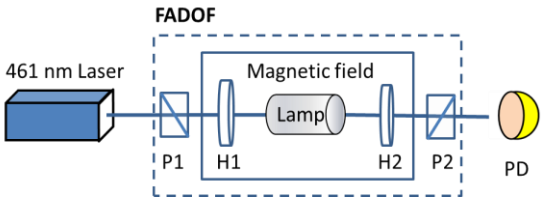


Fig. 1: Experimental setup of a FADOF utilizing Sr hollow-cathode lamp. 461 nm laser: the probe laser, P1 and P2: crossed polarizer, H1 and H2: permanent magnets, PD: photodiode.

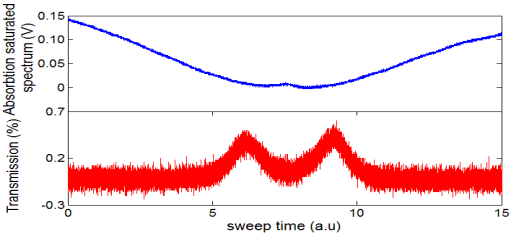


Fig. 2: Measured transmission spectrum at 461nm (red), in comparison with the saturated absorption spectrum (blue).

When combined with the all-optical locking technique, the FADOF can be used to realize a compact frequency-stabilized laser system [2], in which the laser would work immediately at the ^{88}Sr $^1S_0$-$^1P_1$ resonance line when turned on. This demonstration is simpler and more effective for 461 nm laser frequency stabilization, compared with those using Sr atomic beam for stabilization.

In the next step, the transmittance of the FADOF will be optimized by adjusting the magnetic field strength and density of atoms. Then an all-optical locking technique will be applied to stabilize the laser frequency to ^{88}Sr $^1S_0$-$^1P_1$ transition. For future work, we will build a Faraday laser system [1, 3] working at 461 nm resonance line used for ^{88}Sr optical clock. The frequency of this laser will be immune to the fluctuations of injection current and laser diode temperature.

[1] X. Miao, L. Yin, W. Zhuang, B. Luo, A. Dang, J. Chen, and H. Guo, "Note: Demonstration of an external-cavity diode laser system immune to current and temperature fluctuations", Rev. Sci. Instrum. 82, 086106 , 2011.

[2] X. Zhang, Z. Tao, C. Zhu, Y. Hong, W. Zhuang, and J. Chen, "An all-optical locking of a semiconductor laser to the atomic resonance line with 1 MHz accuracy", Opt. Express. Vol. 21, Issue 23, pp. 28010-28018, 2013.

[3] W. Zhuang, and J. Chen, "Active Faraday optical frequency standard", Opt. Lett., Vol. 39, Issue 21, pp. 6339-6342, 2014.

Cavityless Laser as An Optical Frequency Standard Using Cesium Cell with 459 nm Laser Pumping

Xiaobo Xue, Duo Pan, Jingbiao Chen
State Key Laboratory of Advanced Optical Communication, Systems and Networks, School of Electronics Engineering and Computer Science, and Center for Quantum Information Technology, Peking University, Beijing 100871, China
E-mail: xbxue@pku.edu.cn

In this paper, we present a laser scheme without cavity in a cesium cell. In this scheme, a 1469.9 nm laser light is emitted with 459 nm laser pumping. Since no cavity is applied, the stimulated light is emitted from the atoms directly and the center frequency of output laser light is solely determined by atoms without cavity pulling. Thus a better long term stability can be expected and the experimental demonstration is more compact. We name this a "cavityless laser" temporarily. This experimental method can be further extended to generate other frequency standard signals.

The experimental demonstration is shown in Fig. 1. The upper part is the cavityless laser scheme and the lower part is the active optical frequency standard scheme which we have reported earlier [1, 2]. Both of the two parts will generate a 1469.9 nm stimulated light. The photodetector (PD) is used to detect the emitted 1469.9 nm laser light when the beamspliter (BS) is not placed and the beat signal when the BS is placed to investigate the linewidth of the cavityless laser.

The threshold at different temperature is measured. Fig. 2 shows the detected amplitude, which is proportional to the power of the emitted 1469.9 nm laser light, with different pumping laser power. The threshold decreases with temperature increasing. The temperature is tuned from 157 °C to 184 °C at present. More data about the linewidth and power of the cavityless laser, and threshold characteristics under different temperature will be given in the fully written letter later.

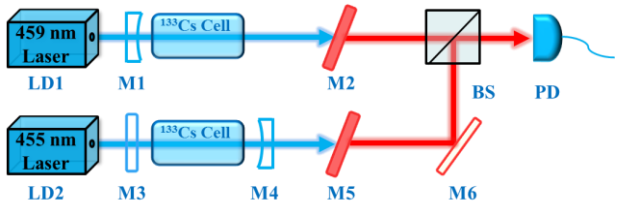


Fig.1: The experimental setup of cavityless laser scheme. M1 is a coated concave mirror with 459 nm laser light anti-reflection and 1469.9 nm laser light high reflection. The radius of curvature is 8000 mm. M3 and M4 constitute a low-finesse cavity for 1469.9 nm laser oscillation. M2 and M5 are 1469.9 nm optical filters. PD is a photodetector.

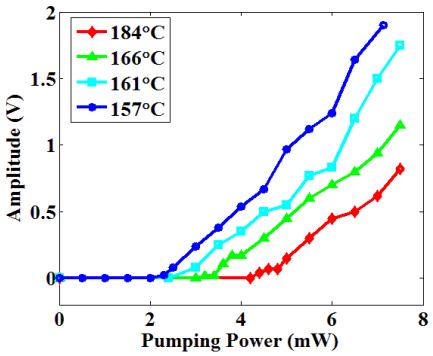


Fig. 2: The detected amplitude of 1469.9 nm laser light changing with pumping laser power and temperature.

[1] D. Pan, Z. Xu, X. Xue, W. Zhuang and J. Chen, "Lasing of Cesium Active Optical Clock with 459 nm Laser Pumping", *Proceedings*, 2014 IEEE Int. Frequency Control Symp, May 19-22, Taipei, pp. 242-245.

[2] Z. Xu, W. Zhuang, and J. Chen, "Lasing and suppressed cavity-pulling effect of Cesium active optical clock", arXiv: 1404.6021.

Active Optical Frequency Standard Based on Narrow Bandwidth Faraday Atomic Filter

Xiaogang Zhang, Wei Zhuang*, Jingbiao Chen
State Key Laboratory of Advanced Optical Communication, System and Network,
School of Electronics Engineering and Computer Science, Peking University, Beijing 100871, China
*National Institute of Metrology, Beijing 100013, China
E-mail: ganggunther@gmail.com

Proposed in 2005[1], active optical clock based on the stimulated emission in a bad cavity has become a very promising optical clock. With a bad cavity, the frequency of active optical clock is insensitive to the Brownian thermo-mechanical noise of optical cavity. In addition, the principle of the stimulated emission will make the linewidth of the laser frequency surpass the limitation of quantum-limited linewidth. Millihertz level of the linewidth is expected.

With these prior advantages, active optical clock also suffers the low laser output power. For now, several experimental schemes have been realized[2,3]. In this paper, we demonstrate an active optical frequency standard based on narrow bandwidth Faraday atomic filter, which it is called active Faraday optical frequency standard.

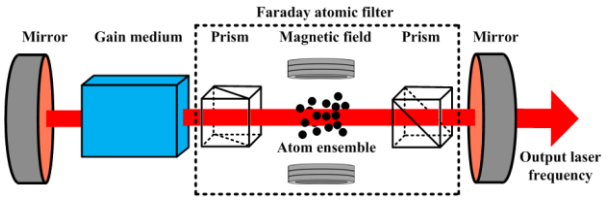


Fig. 1: Active optical frequency standard based on narrow bandwidth Faraday atomic filter

Due to its narrow bandwidth, Faraday atomic filter is further utilized as a frequency reference in active optical frequency standard in a new-mechanism configuration. As shown in Figure 1, the atom ensemble which dips in a homogeneous magnetic field can be vapor cell atoms, atomic beam, neutral cold atoms or trapped ions with narrow transition lines. On both sides of the atom ensemble, there are two crossing Glan-Taylor prisms to realize Faraday atomic filter. The gain medium could be Ti:Sapphire, dye or semiconductor. The two mirrors constitute a bad cavity with one mirror having a low reflectivity. In this unique active Faraday optical frequency standard, the spatial departure of frequency reference and gain medium overcomes the limitation of low laser output power in the active Faraday optical frequency standard, and open the door for any two-level atom optical transitions with reasonable linewidth for active optical clocks.

In this system, active Faraday optical frequency standard is based on Cs 852 nm narrow bandwidth Faraday atomic filter in an extended bad cavity of a semiconductor diode. The narrow bandwidth Faraday atomic filter is realized by using a velocity selection spectroscopy with a pumping laser and a probing laser in opposite propagation direction. The stimulated emission is realized by using Faraday atomic filter and semiconductor gain medium in a bad cavity. The output laser frequency is determined by the Cs $6^2S_{1/2}$ F=4 to $6^2P_{3/2}$ F'=4, 5 crossover transition line. The preliminary experimental results have been published[3]. We redesign the system in an integrated construction to reduce the influence of the mechanical and thermal vibrations. The whole experimental system with two separated active Faraday optical frequency standard has been built. The transmission of Faraday atomic filter has achieved to 20% and the bandwidth is 26 MHz. The bad cavity with 300 MHz linewidth of cavity mode has been built. The improved experimental results with compact setup will be reported.

[1] J. Chen, "Active optical clock," ArXiv Physics e-prints(2005), physics/0512096.
[2] D. Pan, Z. Xu, X. Xue, W. Zhuang, and J. Chen, "Lasing of Cesium active optical clock with 459 nm laser pumping," 2014 IEEE Int. Frequency Control Symp., Taipei, Taiwan, May 18-23, 2014, pp. 19-22.
[3] W. Zhuang and J. Chen, "Active Faraday optical frequency standard," Optics Letters **39**, pp. 6339-6342(2014) .

All-fiber Implementation of Modulation Transfer Spectroscopy for ^{4}He Atoms

Wei Gong, Xiang Peng, Wenhao Li, Teng Wu, Haidong Wang, Jingbiao Chen and Hong Guo
State Key Laboratory of Advanced Optical Communication, Systems and Networks, School of Electronics Engineering and Computer Science, and Center for Quantum Information Technology, Peking University, Beijing 100871, China.
E-mail: gongwei@pku.edu.cn

The metastable ^{4}He atoms with no nuclear spin are commonly used in fields like laser cooling, optical pumping and optical magnetometry [1], where frequency stabilization of the laser source around 1083 nm is necessary. In our previous work [2], modulation transfer spectroscopy (MTS) of ^{4}He atoms is observed with a free-space experimental scheme and applied for locking a fiber laser to the transition lines of metastable ^{4}He atoms around 1083 nm. In this paper we present the demonstration of MTS for ^{4}He atoms with an all-fiber experimental scheme, which exhibits more flexibility and superior performance than the free-space one.

The experimental setup is shown in Fig. 1, where all optical elements are fiber-connected. The laser beam from the 1083 nm fiber laser enters a 50:50 coupler and splits into two beams——the probe and the pump beams. A $LiNbO_3$ electro-optic modulator (EOM) is used to modulate the phase of the pump beam. The probe and pump beams are aligned collinearly within a ^{4}He atomic vapor cell which is fixed on a U-bench fiber-to-fiber collimator. With the four-wave-mixing effect, the modulation of the pump beam can be transferred to the originally unmodulated probe beam. Finally the probe beam with sidebands is heterodyne detected with an InGaAs photodetector (PD). By utilizing standard phase-sensitive detection with a lock-in amplifier, the dispersive-like MTS signal can be generated. MTS signal could be further optimized with beam power adjustment as well as polarization manipulation.

In our experiment, MTS signals at D_0, D_1, D_2 lines and the cross line between D_1 and D_2 are obtained respectively, which is displayed in Fig. 2. It is obvious that the MTS signals exhibit sharp slopes around resonance and sit on zero baseline, which is particularly suitable for laser frequency locking. More details about the application of the laser frequency-locking performance will be given in the fully written paper.

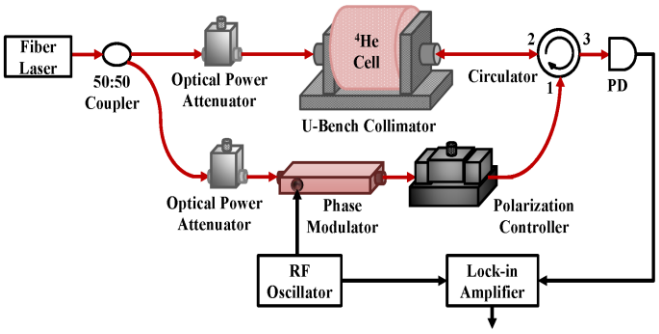


Fig. 1: The experimental setup of the all-fiber MTS scheme for metastable Helium.

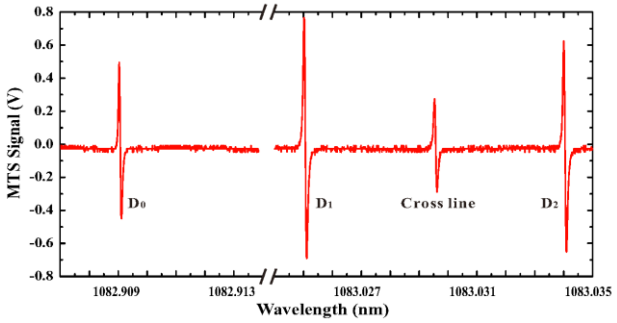


Fig. 2: The MTS signals of ^{4}He atoms at D_0, D_1, D_2 lines and the cross line between D_1 and D_2.

[1] D. D. McGregor, "High-sensitivity helium resonance magnetometers," Rev. Sci. Instrum., Vol. 58, Issue 6, pp. 1067–1076, Jun. 1987.

[2] W. Gong, X. Peng, W. Li, and H. Guo, "Frequency stabilization of a 1083 nm fiber laser to 4He transition lines with optical heterodyne saturation spectroscopies," Rev. Sci. Instrum., Vol. 85, Issue 7, 073103, Jul. 2014.

A two-photon transition in calcium for portable optical frequency standards

Vutha, Amar C.
Department of Physics and Astronomy
York University
Toronto ON M3J 1P3, Canada
Email: avutha@yorku.ca

Advances in the performance of optical lattice clocks and trapped-ion optical clocks have opened up the need for portable optical frequency standards. These are expected to find a use in clock ensembles for time-keeping [1], and could be used for applications such as geodesy [2] and low-phase-noise microwave frequency synthesis [3]. High-performance frequency standards aboard satellites could also be used to detect gravitational waves [4]. We have proposed the use of the $^1S_0 \rightarrow {}^1D_2$ two-photon clock transition in laser-cooled and magneto-optically trapped calcium atoms, as the atomic reference in a portable optical frequency standard [5].

In our poster, we describe the practical advantages of using this two-photon transition, and point out the features that lend this scheme to a simple, portable implementation. The measurement scheme (outlined in Figure 1) takes advantage of the level structure of calcium atoms, which enables efficient detection of the probability that atoms that have undergone the clock transition. We will describe our progress towards the implementation of this scheme.

The precision of an optical frequency standard based on this transition could reach $< 10^{-16}$ within a short averaging time. We will present calculations of the size of systematic frequency shifts that can be expected in such a standard, and show that these shifts can be controlled to below the 10^{-16} level, commensurate with the expected statistical performance.

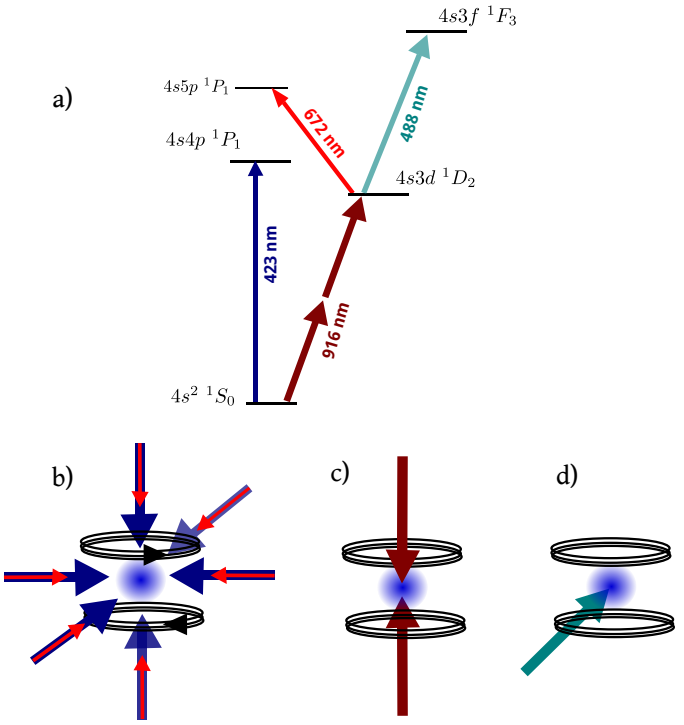


Fig. 1. The two-photon $^1S_0 \rightarrow {}^1D_2$ clock transition in neutral calcium (916 nm, 327 THz) is an attractive candidate for constructing a portable optical frequency standard. The relevant transitions are shown in (a). All the laser wavelengths can be obtained from commercial laser diodes. The measurement sequence involves the following steps: (b) atoms are cooled and trapped in a magneto-optical trap (MOT) operating on the 423 nm $^1S_0 - {}^1P_1$ transition, (c) they are excited from $^1S_0 \rightarrow {}^1D_2$ by two counter-propagating photons from the 916 nm laser oscillator, and (d) the excited state fraction can be detected using laser-induced fluorescence on the $^1D_2 - {}^1F_3$ cycling transition at 488 nm.

References

[1] T. E. Parker, *Rev. Sci. Instrum.*, vol. 83, no. 2, p. 021102, 2012.

[2] C. W. Chou, D. B. Hume, T. Rosenband, and D. J. Wineland, *Science*, vol. 329, no. 5999, pp. 1630, 2010.

[3] J. McFerran, E. Ivanov, and A. Bartels, *Electron. Lett.*, vol. 41, no. 11, pp. 40, 2005.

[4] J. Armstrong, *Living Rev. Relativity*, 2006.

[5] A. C. Vutha, *arXiv:1501.01733*, submitted to Phys. Rev. A, 2015.

Large Waist Cavity for Ultra Narrow Transition Spectroscopy

Schäffer, Stefan A., Adsersen, Sigrid S., Christensen, Bjarke T. R., Henriksen, Martin R., Thomsen, Jan W.
Niels Bohr Institute, University of Copenhagen, Blegdamsvej 17, 2100 Copenhagen, Denmark
E-mail: schaffer@nbi.dk

State-of-the-art optical atomic and molecular clocks employ spectroscopy on ultra narrow atomic transitions which exert high demands on the spectral quality and stability of the laser. Using a cavity to enhance the light matter interaction one can greatly improve the locking signal of the system [1-4], thus allowing for a large signal to noise ratio without the high demands on cooling and shielding of a bare reference cavity [5]. This is especially useful as a frequency discriminator used to reduce the instability of a local oscillator. Such a system, however, will typically have a small intracavity beam waist resulting in a restriction on the velocity classes of the sample or a spectral broadening of the resonance feature due to transit time broadening.

Here we present a resonator designed with an intracavity telescope in order to increase the waist radius of the beam while maintaining a robust construction. We have investigated the optical limitations of a variety of different focal configurations, and present a general characterization (see figure 1). The system finesse of the cavity ensemble alone is in the few hundreds and limited by the quality of the optical coating as well as spherical aberrations.

In a typical large-waist cavity, end mirrors with a radius of curvature of 9 m provides a waist radius of the order of 0.5 mm. By using an intracavity telescope a beam diameter of the order of centimetres can be achieved. We are currently developing a system for use in a molecular clock setup for iodine (I_2) or ethyne as well as an atomic strontium beamline. For these experiments we plan a waist radius of 5 mm. This is an increase in cavity waist size by an order of magnitude while still maintaining a resonator that is well stabilized within a convenient range of parameters.

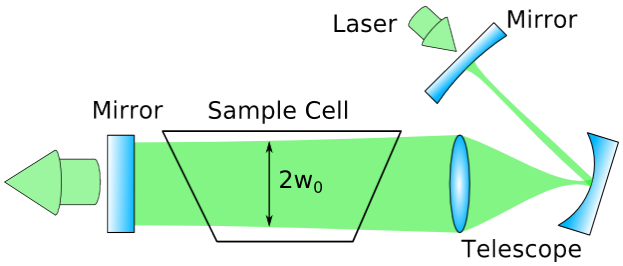


Fig. 1: *Sketch of the resonator with intracavity telescope and Brewster-angled windows in the sample cell. The dimension of w_0 is 5 mm. Rather than using a linear cavity the angled telescope mirror yields a reduction in cavity size and reduces the number of surfaces. The length of the cavity is limited by the sample cell and is of the order of 40 cm.*

In molecular spectroscopy a large waist diameter greatly reduces the transit time broadening of the hot molecules. We interrogate the 514.6 nm line in iodine and the 1542 nm line in ethyne which has transition widths of 284 kHz and a few kHz respectively. These simple systems are very promising for compact clock systems [6-8] relevant e.g. for space applications. The use of a cavity will effectively increase the interrogation length by a factor of the order of the finesse, and when combined with the great reduction in transit time broadening due to the large waist size, this system could exceed current state-of-the-art iodine clock systems in terms of frequency stability [8].

In a strontium beamline the cooperativity enhancement achieved by the cavity can be taken advantage of in order to exceed current limitations on laser frequency stability due to brownian motion in the mirrors [1]. This allows for continuous direct interrogation of the clock transition, contrary to usual clock setups. Here the large waist allows probing of a broader range of velocity classes, effectively increasing the number of atoms interrogated in the system. Cavity finesse and atom number both boosts our cooperativity and thus facilitates a better error signal, reducing the local oscillator instability.

[1] P. G. Westergaard et al., "Observation of Motion Dependent Nonlinear Dispersion with Narrow Linewidth Atoms in an Optical Cavity", *arXiv*:1408.3983 (2014).
[2] M. J. Martin et al., "Extreme nonlinear response of ultranarrow optical transitions in cavity QED for laser stabilization", *Phys. Rev. A*, vol. 84, issue 6, 063813 (2011).
[3] D. Meiser et al., "Prospects for a Millihertz-Linewidth Laser", *Phys. Rev. Lett.*, vol. 102, issue 16, 163601 (2009).

[4] D. Meiser and M. Holland, "Steady-state superradiance with alkaline-earth-metal atoms", *Phys. Rev. A*, vol. 81, issue 3, 033847 (2010).
[5] T. Kessler et al., "A sub-40-mHz-linewidth laser based on a silicon single-crystal optical cavity", *Nature Photonics,* vol. 6, pp. 687–692 (2012).
[6] J. Hald, et al., "Fiber laser optical frequency standard at 1.54 um", *Optics Express*, vol. 19, pp. 2052-2063 (2011).
[7] W.-Y. Cheng et al., "Sub-Doppler molecular-iodine transitions near the dissociation limit (523-498 nm)", *Opt. Lett.*, vol. 27, pp. 571-573 (2002).
[8] E. Zang et al., "Realization of Four-Pass I2 Absorption Cell in 532-nm Optical Frequency Standard", *IEEE Tran. Ins. Meas.*, vol. 56, no. 2, (2007).

Progress on a Calcium Ramsey-Bordé Thermal-Beam Optical Frequency Reference

Fox, R. W., Olson, J. B.*, de Carlos-Lopez, E.[+], Oates, C. W., and Ludlow, A. D.
National Institute of Standards and Technology, Boulder, CO, USA
*Department of Physics, University of Colorado, Boulder, CO, USA
[+] Time and Frequency Division Centro Nacional de Metrología, Querétaro, México
E-mail: richard.fox@nist.gov

We report progress in the development of an optical frequency standard at 456 THz (657 nm) based on the $^1S_0 - {}^3P_1$ intercombination line in neutral calcium. Excitation of this narrow (~400 Hz) linewidth transition via Ramsey- Bordé (RB) spectroscopy was first demonstrated [1] more than three decades ago, however with the advent of frequency combs in recent years interest has been renewed because of the potential low instability and simplicity that the calcium line offers. Previously, we reported [2] an instability of $5.5 \times 10^{-15}\,\tau^{-1/2}$ at one second, obtained with a system that collected only a fraction of the weak 657 nm fluorescence from the thermal beam emerging from the RB interferometer. Significant improvements in the detection efficiency are difficult as the mean atomic velocity (~700 m/s) and long upper state lifetime result in fluorescence spread over approximately 30 cm.

Here we discuss a new detection strategy to measure the $^3P_1$ upper state population with enhanced S/N by utilizing a closed cycling transition as shown in Fig.1. We have built a 431 nm laser system and observed high S/N Ramsey fringes with a photo-multiplier detecting blue light. The 431 nm transition has a lifetime on the order of a few nanoseconds, which allows for multiple excitation and emission cycles during the transit of a blue probe beam downstream from the red Ramsey zones. Simply put, the opportunity exists for greatly enhanced S/N relative to detection of 657 nm light since not only is the detector efficiency higher and the fluorescence tightly confined, but most importantly large blue photon numbers are possible from the closed cycling transition until the $^3P_1$ decays with the emission of a single red photon. In this way, an optical frequency instability of $< 10^{-16}\,\tau^{-1/2}$ is possible at short times.

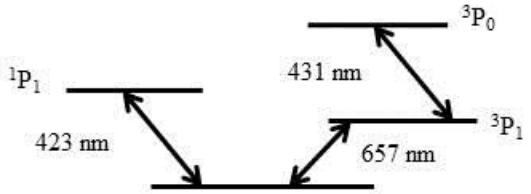


Fig. 1: Calcium energy level diagram. The 657 nm laser crosses the atomic beam to create four Ramsey-Bordé zones and the 431 nm beam crosses downstream in front of a photo-multiplier. The 423 nm cooling transition is not used in this work.

The fast atomic velocities present in thermal-beam systems means that Doppler effects can easily become an important mechanism limiting the stability. In particular, we have often observed an upturn of the Allan deviation beyond about 1 minute, likely caused by the environmentally-induced drift of optical mounts and laser beam directions over time in the presence of the nearby ~600 C calcium oven. In this paper we also report on partially correcting these Doppler effects by alternating the direction of the 657 nm laser beam through the Ramsey zones, thus reversing the Ramsey fringe sensitivities to many of the laser beam angular deviations.

[1] R. L. Barger, J. C. Bergquist, T. C. English, and D. J. Glaze, "Resolution of photon-recoil structure of the 6573-A calcium line in an atomic beam with optical Ramsey fringes," Appl. Phys. Lett., vol. 34, pp. 850-852, 1979.

[2] R. W. Fox, J. A. Sherman, W. Douglas, J. B. Olson, A. D. Ludlow, and C. W. Oates, "A high stability optical frequency reference based on thermal calcium atoms," *Proceedings* 2012 IEEE Int. Frequency Control Symp., Baltimore, MD, May 21-24, 2012, pp. 1-3.

Hybrid mode-locked fiber laser comb of milihertz relative linewidth with a polarization-maintaining fiber-pigtailed waveguide electro-optic modulator

Jin-Long Peng, Tze-An Liu, Ren-Huei Shu, and Yuh-Chuan Cheng
National Measurement Laboratory, Center for Measurement Standards/Industrial Technology Research Institute, Hsinchu, Taiwan
E-mail: jlpeng@itri.org.tw

Narrow linewidth optical frequency comb is important for the applications in optical clock, high resolution multi-heterodyne laser spectroscopy and coherent lidar. In recent years, narrow linewidth of fiber laser comb has been demonstrated with mode-locking based on nonlinear polarization rotation (NPR) [1, 2] or semiconductor saturable absorber mirror (SESAM) [3]. In this paper, we report a fiber laser comb hybrid mode-locked by NPR and SESAM with a polarization-maintaining (PM) fiber-pigtailed intra-cavity waveguide electro-optic modulator (EOM). The linewidth of the carrier-envelope-offset (CEO) beat signal of the fiber laser comb is controlled to mHz-level by a feedback control loop with phase-lead compensation.

The laser oscillator has a sigma cavity, similar to the one published in [4], except that an SESAM in the linear arm and a free-space isolator, a half-wave plate and a PM fiber pigtailed EOM with collimators on both ends located after the polarization beam splitter (PBS) are used. Highly Er-doped fiber of 92 cm-long is used as the gain medium and pumped by a 660 mW diode laser through a wavelength division multiplexer. The laser delivers pulse trains of 100 MHz from the PBS rejection port. The output beam is coupled into a single mode fiber and one third of the output power is amplified by an Er-fiber amplifier and then compressed by standard single mode-fiber. A highly nonlinear fiber is used to generate octave-spanning supercontinuum. The CEO beat signal detected with a collinear f-2f interferometer has a signal-to-noise ratio of 40 dB at 100 kHz resolution bandwidth.

The CEO beat signal is phase-locked to an RF synthesizer through feedback to the pump power with phase-lead compensation. Figure 1 shows the in-loop CEO beat signal with resolution bandwidth (RBW) of 100 Hz. The central peak contains 99% of total power. Inset shows the spectrum near the central peak measured by an FFT analyzer. Narrow linewidth of 3.3 mHz limited by the measurement time is obtained. Phase-lock of the fiber laser comb to a CW laser using the EOM for high bandwidth control is presented in the conference.

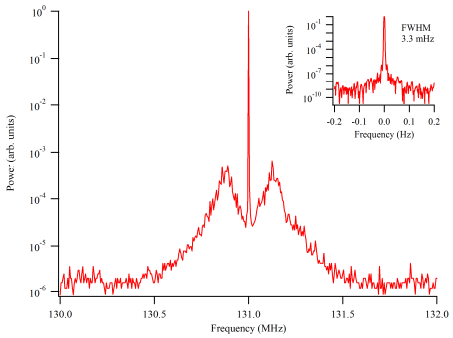


Fig. 1: RF spectrum of the in-loop CEO beat signal with RBW of 100 Hz. Inset, FFT spectrum with 0.4 Hz span.

[1] W. C. Swann, J. J. McFerran, I. Coddington, N. R. Newbury, I. Hartl, M. E. Fermann, P. S. Westbrook, J. W. Nicholson, K. S. Feder, C. Langrock and M. M. Fejer, "Fiber-laser frequency combs with subhertz relative linewidths," Opt. Lett., vol. 31, no. 20, pp. 3046-3048 (2006).

[2] K. Iwakuni, H. Inaba, Y. Nakajima, T. Kobayashi, K. Hosaka, A. Onae, and Feng-Lei Hong, "Narrow linewidth comb realized with a mode-locked fiber laser using an intra-cavity waveguide electro-optic modulator for high speed control," Opt. Express, vol. 20, no. 13, pp. 13769-13776 (2012).

[3] T. R. Schibli, I. Hartl, D. C. Yost, M. J. Martin, A. Marcinkevicius, M. E. Fermann and J. Ye, "Optical frequency comb with submillihertz linewidth and more than 10W average power," Nature Photon., vol. 2, no. 6, pp. 355-359 (2008).

[4] S. Kim, Y. Kim, J. Park, S. Han, S. Park, Y.-J. Kim, and S.-W. Kim, "Hybrid mode-locked Er-doped fiber femtosecond oscillator with 156 mW output power," Opt. Express, vol. 20, no. 14, pp. 15054-15060 (2012).

Resonant Infrared Detector Based on a Piezoelectric Fishnet Metasurface

Hui Yu, Qian Zhenyun and Rinaldi Matteo
Department of Electrical and Computer Engineering, Northeastern University, Boston, MA/USA
E-mail: yhui@ece.neu.edu

This paper presents, for the first time, a high resolution (noise equivalent power NEP of *2.3 nW/Hz*$^{1/2}$ at 200 Hz bandwidth) and fast (thermal time constant of *5.3 ms*) infrared (IR) detector based on a nanoelectromechanical system (NEMS) resonant piezoelectric fishnet-like metasurface (Fig. 1-a,b). For the first time, an ultra-thin (650 nm) piezoelectric fishnet-like metasurface is employed to form the vibrating body of a nanomechanical resonator with a unique combination of optical, thermal and electromechanical properties: (1) Efficient sensing and actuation (electromechanical coupling coefficient, k_t^2*~1.4%*) of a high frequency (*172 MHz*) and high quality factor (*Q~2254*) bulk acoustic mode of vibration in the free-standing ultra-thin structure is achieved thanks to the intrinsic piezoelectric transduction properties of the proposed metasurface (based on a thin-film Aluminum Nitride, AlN). (2) Strong absorption (60%) of short wavelength infrared (SWIR) radiation in the ultra-low volume resonant device (without the need of any additional IR absorbing material) is obtained thanks to the properly engineered optical properties of the fishnet-like metasurface which provide a Fabry-Perot like resonance at ~4 μm to the structure (Fig. 1-d inset). (3) Maximum thermal isolation of the resonant metasurface from the heat sink (thermal resistance *~2.3×10*^{5} *K/W*, one order of magnitude higher than previous demonstrations), hence maximum device responsivity (*~442 Hz/μW*), are attained by using nanoscale metallic anchors (with minimum cross-section) to support the freestanding vibrating body of the structure [1]. Thanks to such unique features, the fabricated piezoelectric metasurface resonant IR detector shows a *7X* enhanced responsivity and unchanged noise performance compared to a conventional AlN nano-plate resonant thermal detector (Fig. 1-d). The demonstrated properties of the proposed piezoelectric fishnet-like metasurface address the most important and fundamental challenges associated with the development of performing resonant IR detectors, marking a milestone towards the implementation of a new class of high performance, miniaturized and low power IR spectroscopy and multi-spectral imaging systems.

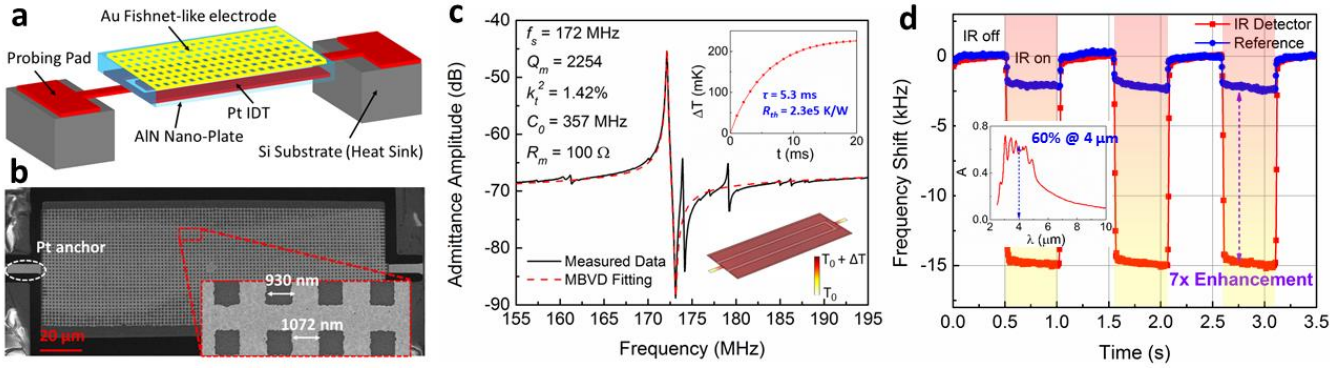


Figure 1: (a) 3D mock view of the NEMS resonant piezoelectric fishnet-like metasurface. (b) SEM image of the fabricated device: the inset shows the dimensions of the fishnet-like metasurface. (c) Measured admittance versus frequency of the NEMS resonator showing high mechanical quality factor (*Q~2254*) and electromechanical coupling coefficient (k_t^2*~ 1.42%*). The inset shows 3D FEM simulated thermal resistance, time constant and temperature profile. (d) Measured responses of the fabricated IR detector and a reference device (conventional AlN MEMS resonator) to a 5 μm quantum cascaded laser (QCL) IR source, showing a 7X enhancement in the device responsivity. The inset shows the measured absorption of the fishnet-like metasurface.

[1] Y. Hui, Z. Qian, G. Hummel, M. Rinaldi, "Pico-Watts Range Uncooled Infrared Detector Based on a Freestanding Piezoelectric Resonant Microplate with Nanoscale Metal Anchors," *Proc.* Hilton Head 2014, 8-12 June, pp. 387-390.

NSPUDT using c-axis Tilted ScAlN Thin Film

Abhay Kochhar[1], Yasuo Yamamoto[2], Akihiko Teshigahara[2],
Ken-ya Hashimoto[3], Shuji Tanaka[1] and Masayoshi Esashi[1]
[1]Tohoku University, Sendai (JAPAN), [2]Research Laboratories, DENSO CORPORATION, Nisshin (JAPAN),
[3]Chiba University, Chiba (JAPAN)
E-mail: abhay.kochhar@ieee.org

Introduction/Motivation: This paper reports finding of directionality in the 48% Sc-doped Aluminum Nitride thin film sezawa mode based surface acoustic wave (SAW) devices. SAW devices are low cost, simple fabrication and has outstanding reproducibility for various applications from sensors to high-end RF filters. Unidirectional SAW IDTs are widely used for low-loss transducers and specifically suppress the Triple Transit Echo (TTE). Some bulk substrates produces higher power of acoustic signals in either forward or backward direction depending on their crystal orientations and are called natural single-phase unidirectional transducers (NSPUDT) [1]. NSPUDTs were reported previously for oriented quartz and $LiNbO_3$ substrates [1], ST-25 X quartz, Y-51.25Z $LiTaO_3$, 50Y-25X $La_3Ga_5SiO_{14}$ substrates [2]. These substrates observed 15-20 dB of directivity, comparing forward & backward direction insertion loss. The reason behind the directionality is shift in the transduction and reflection coefficient [3], [4]. As reported NSPUDTs were in bulk substrates, in this paper, we report NSPUDT using c-axis tilted Sc-doped AlN (ScAlN) thin film SAW devices on sapphire. In addition, we also examined the c-axis tilt dependency to improve transducers return loss. It is worth to put in notice here that our observance of directionality is specifically in sezawa mode.

Method: To confirm the directionality in ScAlN/Sapphire devices, previously reported IDT structure [1] is utilized as shown in Figure 1(a). Two device structures are compared, NS: "normal IDT (port 1) – split IDT (port 2)" and SN: "split IDT (port 1) – normal IDT (port 2)". All configurations have spacing of 50 λ between port 1 and port 2. In normal IDT, fingers are spaced at λ/4 having finger width of 0.5 μm. Number of finger pairs are 40 and the aperture is 40 λ. In split IDT, finger width is 0.5 μm and each pair of fingers is spaced at 0.5 μm. Split IDT is utilized to eliminate internal reflections and thus ensure that it is bidirectional on any crystal orientation [1]. The number of finger pairs is limited to 10 and the aperture is 40 λ. For observing transducer's return loss, the NN type configuration: "normal IDT (port 1) – normal IDT (port 2)", is utilized. In both configurations, the SAW propagation direction is 90° with respect to sapphire orientation. SAW IDT is patterned by EB lithography on 2 μm ScAlN/Sapphire and metallized with Au electrode using EB evaporation, following lift-off process.

Experimental results: The tilt in ScAlN's (002) orientation is confirmed by XRD pole figure measurement. By comparing NS & SN type for 3° c-axis tilted ScAlN film; the directivity is 7 dB as shown in Fig. 1(a). For NN type, the return loss is improved and is dependent on the c-axis tilt of ScAlN film. S22 is improved to as high as 20 dB for 4.5° c-axis tilt (when compared with no tilt) as shown in Fig. 1(b). The difference in S11 & S22 is somewhat saturated, however, the improvement of around 4 dB in S22 is still observed in the saturated region (3° & 4.5°). Such improvement is valuable for the sensor applications.

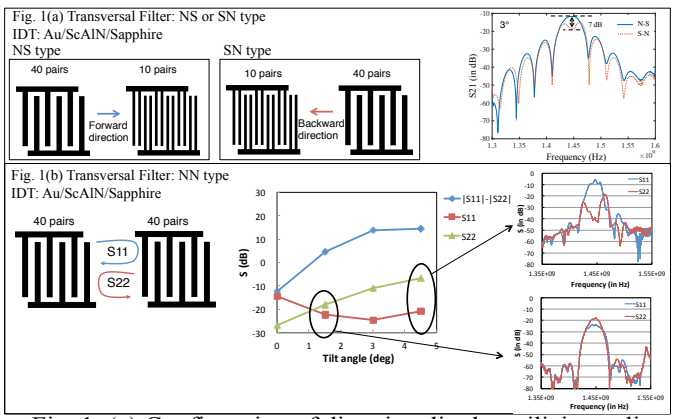


Fig. 1: (a) Confirmation of directionality by utilizing split IDT, (b) Improvement in return loss by varying c-axis tilt.

[1] P. V. Wright, "The Natural Single-Phase Unidirectional Transducer: A New Low-Loss SAW Transducer," *IEEE Ultrasonics Symposium,* pp. 58-63, 1985.

[2] K. Hasegawa, et. al, "Extraction of all Coefficients of Coupled-Mode Equations for Natural, Single-Phase, Unidirectional SAW Transducers from Dispersion Characteristics Computed by Hybrid Finite Element Method," *IEEE UFFC Transactions,* vol. 48, no. 5, pp. 1341-1350, 2001.

[3] C. S. Hartmann, et. al, "An Analysis of SAW Interdigital Transducers with Internal Reflections and the Application to the Design of Single-Phase Unidirectional Transducers," *IEEE Ultrasonics Symposium* , pp. 40-45, 1982.

[4] M. Takeuchi, et. al, "SAW Transducer Configurations for Reversing the Directivity of NSPUDT substrates," *IEEE Ultrasonics Symposium*, pp. 17-22, 1995.

ZIF-coupled Resonant Sensors

Candler RN*+, Hwang Y*
*Department of Electrical Engineering, University of California, Los Angeles, CA, USA
+California NanoSystems Institute, Los Angeles, CA, USA
E-mail: rcandler@seas.ucla.edu

We present a novel method for fabrication of resonant sensors using dielectrophoretic assembly of zeolitic imidazolate frameworks (ZIFs) onto microscale resonant sensors for highly sensitive and selective gas detection. ZIFs are part of a recently invented class of materials and are constructed from transition metals bridged by imidazolate. ZIFs have attracted wide attention for their tailorable nanoporosity and functionalized cavities for various sensing methodologies, such as detecting changes of impedance, refractive index and strain [1-2]. Other research has independently investigated the potential for sensitivity enhancement with porous material coatings on resonant sensors [3]. This work marks the *first demonstration of resonant sensors using ZIFs*, which is noteworthy because ZIFs have *2.8 times* more surface area than any material previously used for resonant sensing. Also, ZIFs hold the potential for *selective* absorption of gases based on their tailorable nanoporosity.

ZIFs were assembled onto the surface of resonators through dielectrophoresis (DEP). To achieve assembly, first ever measurements were performed of the Clausius-Mosotti factor for the nanoparticles of interest, ZIF-69 [4]. After DEP assembly of ZIFs, the resonant sensors were tested in the presence of Isopropyl alcohol (IPA) and CO_2. The ZIF-coupled resonators demonstrated sensitivity improvement up to 150 times over a bare silicon resonator with identical dimensions. Perhaps more importantly, real-time absorption measurements of ZIFs revealed different absorption time constants for IPA and CO_2 (figure 2). The distinguishable absorption time constants provide the possibility of inherent selectivity for these resonant-based sensors. This presentation will include latest measurements results along with discussions of the prospects and open challenges for resonant sensing.

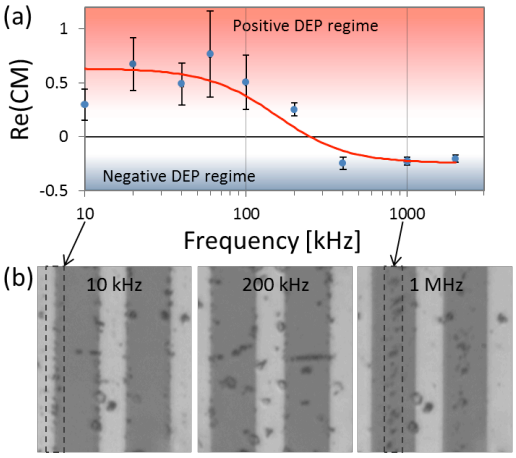


Figure 1. (a) Real part of the Clausius-Mosotti factor for ZIF-69. (b) Particle assembly with positive (10 kHz) and negative (1 MHz) DEP (c) Picture of resonator with assembled ZIFs

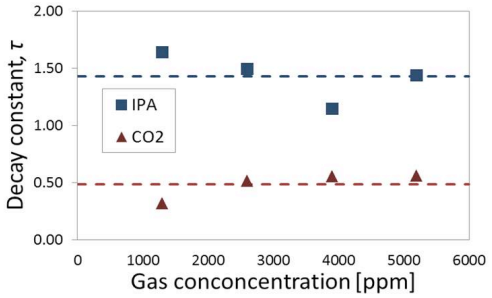


Figure 2. Absorption time constants for Isopropoyl alcohol (IPA) and CO_2 are 1.43±0.28 s and 0.49±0.17 s, respectively, demonstrating the potential to discern different gases based on absorption time

[1] G. Lu and J. T. Hupp,"Metal−Organic Frameworks as Sensors: A ZIF-8 Based Fabry−Pérot Device as a Selective Sensor for Chemical Vapors and Gases," *J. Am. Chem. Soc.,* vol. 132, pp. 7832-7833, 2010.

[2] S. Achmann*, et al.*,"Metal-Organic Frameworks for Sensing Applications in the Gas Phase," *Sensors,* vol. 9, pp. 1574-1589, 2009.

[3] P. C. Xu*, et al.*,"Functionalized Mesoporous Silica for Microgravimetric Sensing of Trace Chemical Vapors," *Anal Chem,* vol. 83, pp. 3448-3454, 2011.

[4] Y. Hwang, H. Sohn, A. Phan, O. M. Yaghi, R. N. Candler, "Dielectrophoresis-Assembled Zeolitic Imidazolate Framework Nanoparticle-Coupled Resonators for Highly Sensitive and Selective Gas Detection," Nanoletters, 13 (11), pp. 5271-5276, 2013

Ultimate and Practical Limits to Micro- and Nanomechanical Frequency-Shift-Based Sensing

Roukes, Michael L.
Robert M. Abbey Professor of Physics, Applied Physics and Bioengineering
California Institute of Technology, Pasadena, CA
E-mail: roukes@caltech.edu

Frequency-shift sensing has emerged as the basis for important new applications in metrology employing micro- and nano- electromechanical systems (MEMS/NEMS). Prominent among these are new approaches to magnetic resonance [1], radiation detection [2], and chemical and biological analyte detection by inertial mass sensing in gas [3], liquid [4], and vacuum [5,6]. I will briefly review recent achievements in these areas, and then describe the physics underlying the ultimate and practical limits of frequency-shift sensing with MEMS/NEMS. Unlike their macroscale counterparts, these devices permit detection down to the thermodynamic, even quantum, noise floor in the mechanical domain. At the other end of their dynamic range, NEMS can easily be driven well beyond the onset of mechanical nonlinearity. The smallest of NEMS devices, which provide unprecedented mechanical responsivities useful for sensing, have a vanishingly small linear dynamic range [7]. Hence, it becomes important to consider the operation of NEMS sensors well into the regime of nonlinear response. Such operation is conventionally avoided, given the increased phase noise that usually arises in this regime. I will describe three new, robust, and very general paradigms to harnessing *nonlinear* nanomechanical dynamics to achieve substantial performance gains with ultra miniature frequency-shift-based sensors [8,9,10].

[1] D. Rugar, R. Budakian, H.J. Mamin, and B.W. Chui, "Single spin detection by magnetic resonance force microscopy," *Nature* **430,** 753-758 (2004).

[2] X.C. Zhang, E.B. Myers, J.E. Sader, and M.L. Roukes, "Nanomechanical torsional resonators for frequency-shift infrared thermal sensing," *Nano Letters* **13** (4), 1528-34 (2013).

[3] I. Bargatin, E.B. Myers, J.S. Aldridge, C. Marcoux, P. Brianceau, L. Duraffourg, E. Colinet, S. Hentz, P. Andreucci, and M.L. Roukes, "Large-Scale Integration of Nanoelectromechanical Systems for Gas Sensing Applications," *Nano Letters* **12** (3), 1269-74 (2012)

[4] J.L. Arlett, E.B. Myers, and M.L. Roukes, "Comparative advantages of mechanical biosensors," *Nature Nanotechnology* **6** (4), 203-15 (2011)

[5] M.S. Hanay, S. Kelber, A.K. Naik, D. Chi, S. Hentz, E.C. Bullard, E. Colinet, L. Duraffourg, and M.L. Roukes, "Single-protein nanomechanical mass spectrometry in real time," *Nature Nanotechnology* **7** (9), 602-8 (2012).

[6] M.S. Hanay, S. Kelber, C. O'Connell, P. Mulvaney, J.E.Sader, and M.L. Roukes, "Inertial Imaging with Nanomechanical Systems," *Nature Nanotechnology*, in press (2015).

[7] H.W.C. Postma, I. Kozinsky, A. Husain, and M.L. Roukes, "Dynamic range of nanotube- and nanowire-based electromechanical systems," *Applied Physics Letters* **86**, 223105 (2005).

[8] L.G. Villanueva E. Kenig, R.B. Karabalin, M.H. Matheny, R. Lifshitz, M.C. Cross, and M.L. Roukes, "Surpassing Fundamental Limits of Oscillators Using Nonlinear Resonators," *Physical Review Letters* **110**, 177208 (2013).

[9] L.G. Villanueva, R.B. Karabalin, M.H. Matheny, E. Kenig, M.C. Cross, and M.L. Roukes, "A Nanoscale Parametric Feedback Oscillator," *Nano Letters* **11** (11), 5054-9 (2011).

[10] M.H. Matheny, M. Grau, L.G. Villanueva, R.B. Karabalin M.C. Cross, and M.L. Roukes, "Phase Synchronization of Two Anharmonic Nanomechanical Oscillators. *Physical Review Letters* **112**, 014101 (2014).

Rubiclock, cold-atom based clock in microgravity: signal optimization and clock operation on a moving platform

[De Sarlo, Luigi], [Langlois, Mehdi], [Schaff, Jean-François]*, [Lours, Michel], [Holleville, David], and [Dimarcq, Noël]

SYRTE – Observatoire de Paris, CNRS, LNE, UPMC, Paris France
*Muquans, Talence, France

Email: Luigi.de-sarlo@obspm.fr

In autumn 2014, the compact cold-atom based clock Rubiclock participated to a second parabolic flight campaign on the Airbus A300-0g. During these flights, several studies were conducted:

- Building upon the results of the first flight campaign [1], we characterized and optimized in microgravity the signal to noise ratio (SNR) of the atomic interrogation for Ramsey times between 10 ms and 300 ms. By comparing the measurement in microgravity to those obtained on the ground and in flight at 1g and 2g of acceleration, we could elucidate the influence of the fluctuations of vertical acceleration of the plane on the atomic noise. The ensemble of the results of the two flight campaign allows us to estimate the expected short term stability of Rubiclock both on the airplane and on a less noisy microgravity platform.

- We operated the clock in-flight by locking the local oscillator frequency onto the atomic transition. Taking advantage of the flexibility of the Rubiclock concept, we adapted the Ramsey interrogation time to the local acceleration decreasing it during 1g and 2g phases, and increasing it during 0g phases in order to suppress the variations in the number of detected atoms. This original technique allowed us to maintain the local oscillator locked throughout the flight, including during the 30 0g phases.

We begin this presentation by briefly describing the experimental setup and the particular characteristics of the 0g environment in Airbus A300. We will then present the results of the SNR measurements and discuss the predominant effects that limit the SNR in the plane, and thus the short-term performances of the clock. A curve demonstrating the lock of the quartz during the entire flight will be presented. We end this presentation by introducing a few improvements that we plan to implement on our device for the next flight campaign scheduled for October 2015.

[1] L. De Sarlo *et al.*, "Preliminary Test of a Cold-Atom Based Clock Prototype on a Microgravity Platform: Rubiclock on the a-300 0g", oral presentation at EFTF 2014, Neuchâtel, Swizerland, 24-26th June 2014.

Approaching Readiness for Flight with the ACES Mission Elements

L. Cacciapuoti[1], R. Much[1], S. Carli[1], L. de Parolis[1], J. Kehrer[2], M.P. Hess[2], A. Helm[2], T. Niedermaier[2], D. Massonnet[3], W. Schaefer[4], X. Stehlin[5], P. Mosset[5], D. Goujon[5], P. Rochat[5], I. Moric[6], P. Laurent[6], P. Wolf[6], F. Meynadier[6], P. Delva[6], C. Le Poncin Lafitte[6], C. Guerlin[6], D. Piester[7], M. Prevedelli[8], I. Prochazka[9], A. Schlicht[10], U. Schreiber[10], C. Salomon[11]

[1] European Space Agency, ESTEC, Noordwijk, The Netherlands
[2] Airbus Defence and Space, Friedrichshafen, Germany
[3] CNES, Toulouse, France
[4] TIMETECH, Stuttgart, Germany
[5] Spectratime, Neuchâtel, Switzerland
[6] SYRTE, Observatoire de Paris, CNRS, UPMC, LNE, Paris, France
[7] Physikalisch-Technische Bundesanstalt (PTB), Braunschweig, Germany
[8] Bologna University, Bologna, Italy
[9] Czech Technical University in Prague, Prague, Czech Republic
[10] Technical University of Munich, Munich, Germany
[11] Laboratoire Kastler Brossel, ENS, Paris, France
Email: Luigi.Cacciapuoti@esa.int

From the International Space Station (ISS), the Atomic Clock Ensemble in Space (ACES) payload will distribute a clock signal with fractional frequency instability and inaccuracy of $1 \cdot 10^{-16}$. Space-to-ground and ground-to-ground comparisons of atomic frequency standards via ACES will be used to test Einstein's theory of general relativity.

The ACES mission elements are now close to flight maturity. The flight model of the cold cesium clock PHARAO has been tested and delivered for integration into the ACES payload. Tests on the engineering models of the active H-maser SHM and of the time transfer microwave link MWL have been completed and manufacturing of the flight models is ongoing. The SHM insensitivity to the thermal and magnetic environment is being optimized. End-to-end tests of MWL have been performed and procedures for its calibration are being finalized. The time transfer optical link ELT is also well advanced. The ACES ground segment is close to completion, with the first two terminals of the ACES microwave link expected to be delivered to LNE-SYRTE and PTB in the first half of 2015.

This paper will present the progress of the ACES mission. Recent test results on instruments and subsystems and the status of the ACES science ground segment will be discussed.

Space Rubidium Atomic Frequency Standard for BeiDou Navigation Satellite System

Ganghua Mei, Da Zhong, Shaofeng An, Feng Zhao, Feng Qi, Fang Wang, Gang Ming
Key Laboratory of Atomic Frequency Standards,
State Key Laboratory of Magnetic Resonances and Atomic and Molecular Physics,
Wuhan Institute of Physics and Mathematics, Chinese Academy of Sciences, Wuhan 430071, Hubei, China
E-mail: mei@wipm.ac.cn

In this talk, we outline development of the BeiDou system and its space primary frequency standard, the rubidium atomic frequency standard.

China's navigation satellite system BeiDou is developed according to a three step strategy [1]. The first step construction begun in 1994 and ended in 2000, as the BeiDou Navigation Demonstration System, as known as BeiDou I, provided radio determination satellite service (RDSS). The second step covers from 2004 to 2012, and is to construct the BeiDou navigation satellite System (BDS, also called BeiDou II sometimes), providing radio navigation satellite service (RNSS) for users in China and nearby regions. The third step involves functional enhancement of the system, making the BDS system able to provide high precision RNSS service for the worldwide users in 2020. As result of the second step construction, the current BDS system consists 16 satellites, including 5 MEO, 6 GEO and 5 IGSO satellites, and could provide the service with positioning precision of 10m in both horizontal and height, velocity measurement precision of 0.2m/s, and timing precision of 50ns. The service has covered the whole Asia Pacific region.

The rubidium atomic frequency standard (RAFS) is the only one type of space clock employed so far in BDS satellites. As one of the three domestic space RAFS suppliers, Wuhan Institute of Physics and Mathematics (WIPM), Chinese Academy of Sciences has been engaging in research of space RAFS since the late 1990's. Earlier work focused on realization of performance and adaptability for space environment. In the work, main attention was paid to developing a new structure slotted tube microwave cavity [2] with mode similar to TE_{011}, designing a high SNR physics package [3], verifying that the rubidium spectral lamp is of long operation time and ability to work in vacuum environment, optimizing operational parameters of the RAFS unit, and so on. To avoid element failure in space, no digital frequency synthesizing technique was used in the electronics. A test model was built in 2005, and the product was space qualified in 2006. Since then, the performance of the RAFS has been improved further [4]. 10 space RAFS products were used in the BDS satellites. Statistics obtained on ground showed that the key performance of the RAFS, the frequency stability per day, is within $2.0\sim5.0\times10^{-14}$ in Hadamard deviation, comparable with those used in GPS Block IIR[5] and Galileo satellites.

To meet the needs of the third step construction of the BDS system, further improvement of the RAFS is being performed at WIPM.

[1] "Report on the Development of BeiDou (COMPASS) Navigation Satellite System", http://www.beidou.gov.cn/

[2] G.H. Mei and J. T. Liu, "A Miniaturized Microwave Resonator for Rubidium Frequency Standards", *Proceedings*, 1999 Joint Meeting EFTF- IEEE IFCS, Besancon, April 13-16, 1999, pp. 601.

[3] Baihua Xia, Da Zhong, Shaofeng An, Ganghua Mei, "Characteristics of A Novel Kind of Miniaturized Cavity-cell Assembly for Rubidium Frequency Standards", IEEE Trans. Instrum. and Meas., vol. 55, no. 3, pp. 1000-1005, June 2006.

[4] Da Zhong, Ganghua Mei, "Study of a High Performance Rubidium Atomic Frequency Standard", *Proceedings*, 2011 IEEE Int. Frequency Control Symp., San Francisco, California, May 1-5, 2011, pp. 215-217.

[5] R. T. Dupuis, T. J. Lynch, J. R. Vaccaro, "Rubidium Frequency Standard for the GPS IIF Program and Modifications for the RAFSMOD Program," *Proceedings*, Joint IEEE IFCS-EFTF, Toulouse, April 22-25, 2008, pp.655-660.

GNSS RAFS latest improvements

Droz Fabien, Rochat Pascal, Boillat Sébastien, Scheidegger Batiste
Orolia Switzerland SA (SpectraTime), Vauseyon 29, Neuchâtel 2000, Switzerland
E-mail: droz@spectratime.com

Accurate and ultra-stable atomic clocks have been recognized as the critical equipment for the precision Global Navigation Satellite Systems (GNSS). In parallel to Rb clocks produced for industrial applications, SpectraTime (SpT) is space clocks manufacturer of Rubidium Atomic Frequency Standard (RAFS) for various navigation systems (European, Chinese and Indian) and other programs. In the last ten years, the 56 SpT RAFS units in-orbit have cumulated 170 years of flight heritage. In addition, almost 130 SpT RAFS flight units have been manufactured and characterized. Those compact clocks (3 kg only) provide good performances and reach the expected reliability figure. The foreseen stability up to two hours was well in specification and analysis of the telemetries demonstrates a nominal behavior over the time. Nevertheless, from the long term records of the frequency stability of those units, it appears that a weakness exists when considering the predictability of their behavior over time period interval longer then few hours. As long as the GNSS infrastructure was designed to compensate the frequency variations within an interval of one or two hours, this issue was not too critical.

According to new latest GNSS requirements, such RAFS behavior becomes critical. Predictability of the frequency is expected over much longer period of operation. In order to reach such new requirements, an update of the RAFS physics package was initiated through ESA EGEP funding in 2012. This paper describes the achieved results of this new space RAFS through the description of the internal coefficients influence reduction and the positive consequences in term of clock frequency stability and predictability improvements. Performances achievements during uninterrupted operation of several months demonstrate a monotonic behavior, a stability of $1x10^{-14}$ $@10^{5}$ sec. and a drift per day of few 10^{-14} already after only few days of operation.

An industrial prototype of Chinese optically pumped Cesium clock

Yuanhong Cao, Xingwen Zhao, Runchang Du, Lin Yang, Leiji Liu, Xingshi Zheng, Haijun Chen*, Shougang Zhang +

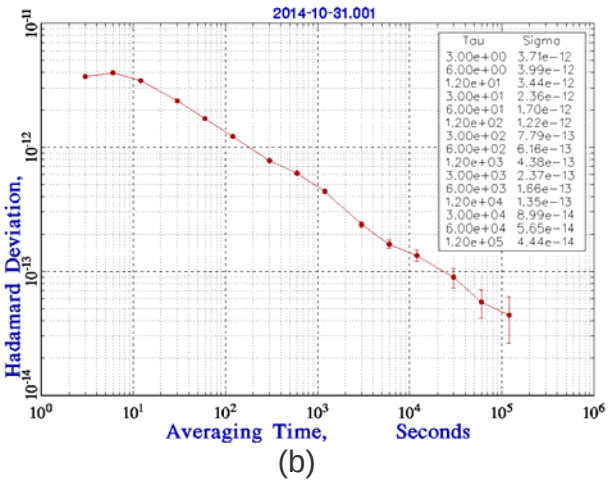
Chendu Spaceon Electronics CO., LTD., Chengdu, China
*CETC-12 institute, Beijng, China
+National Time Service Center, Chinese Academy of Sciences, Xi'an, China
E-mail: sccyh@163.com

As a new primary frequency standard, optically pumped cesium atomic clock has excellent accuracy and low cost in comparison with traditional Cesium beam with magnetic state selection, and will be used in telecom, power synchronization network. Aiming to market demanding, Chinese government has been supporting Cesium atomic clock development by National Key Scientific Instrument and Equipment Development Project. In order to satisfy the engineer requirements, the first industrial prototype has been realized in the end of 2014.

This clock has better performance in long-term frequency stability and in robustness than the original principal clock realized in 2013. In this turn, there are three modified points in the industrial prototype. At first, the Cesium oven was redesigned to prevent Cesium leakage in movement or high temperature work condition. The Cesium mass was added properly, and the lifetime will be enhanced to 12 years. In Laser module, two layers shielded the saturation absorption cell and some optical devices were integrated, which will keep the wavelength and Laser intensity stable. Laser electronics samples the discrimination signal from the saturation absorption cell and synchronously checks the frequency with Cesium atoms. The output is an error which will be to lock the Laser frequency. In addition, this Laser electronics can automatically find the saturation absorption line and be into holding on the locked point. Especially, the Laser will be relocked while unlocked incident occurs. All of the electronics including OCXO servo, RF circuits and temperature controller have been renewed, and the clock's work parameters can be adjusted and recorded by PC locally or remotely. The clock frame and other mechanics have been reinforced and the panel has been relocated simultaneously so as to work normally in engineering condition. The size is 446×177×550(mm^3), and the height is 4 U. Until now, we have completed three industrial prototypes, and have tested them more than a month. The Allan deviation of frequency stability is prior to 1.2E-11/s, 4.4E-14/100000s. According to the test data and estimation, the clock can be provided to customers in 2015.



(a)



(b)

Fig. 1: (a) The industrial prototype of the Cesium. (b) The Allan deviation of the clock.

The new GNSS calibration scheme of the BIPM

Arias Felicitas, Petit Gérard, Jiang Zhiheng, Tisserand Laurent
BIPM 92312 Sèvres France

E-mail: farias@bipm.org

All laboratories contributing to UTC are equipped with GNSS receivers, almost all of them providing the official time link, either by one-technique links (GPS) of by combined-techniques links (GPS/GLONASS and TW/GPSPPP). Most laboratories contributing to UTC operate redundant time transfer equipment, providing backups to the official UTC links. The characterization of the delays in the time transfer equipment (known as "calibration") is essential to the accuracy of time transfer and time dissemination. The set of GNSS equipment in laboratories used for time transfer in UTC needs to be calibrated, and the system is to be maintained through a programme of repeated calibrations over time.

Over the past years, the system of calibration procedures for GNSS equipment that has been in operation at the BIPM was twofold: one system for GPS C/A based on calibration trips with closure using a reference receiver based at OP; one system for GPS P3 based on a set of BIPM reference receivers visiting laboratories ("golden receiver" calibration). Because geodetic receivers are now used in the majority of UTC laboratories, the past procedure cannot be sustained on the BIPM resources. Furthermore, it is expected that the global calibration uncertainty could be significantly improved by using a procedure of calibration trips with closure.

The BIPM now proposes a new procedure in which the BIPM, the Regional Metrology Organizations (RMOs) and the laboratories can cooperate. In the new calibration scheme, the BIPM will maintain, at regular intervals, the calibrations of a set of equipment distributed in so-called "Group 1" laboratories in the regions. RMOs and some national laboratories will organize calibration campaigns to the other "Group 2" laboratories where at least one "Group 1" system will serve as a reference. The "Group 2" trips will follow guidelines provided by the BIPM and the results will be reported to the BIPM for UTC use. In addition, the BIPM could conduct "Group 2" trips as necessary to accommodate special cases, using either one BIPM system or a "Group 1" system as a reference.

Some 10 UTC laboratories have been selected as "Group 1" and an initial reference calibration for those systems has been started using the visits of BIPM equipment over 2013-2014. Visits to Group 1 laboratories will continue through 2015. The paper will present the main features of the new scheme along with practical information on the initial Group 1 results and the progressive implementation of the new scheme.

Use of two traveling GPS receivers for a relative calibration campaign among European laboratories

Uhrich P., Rovera G.D., Chupin, B., Galindo J.*, Esteban H*, Jaldehag K.°, Rieck C.°, Bauch A.#, Polewka T.#, Cerretto G.+, Fantino G.+, and Piriz R.$.
LNE-SYRTE, Observatoire de Paris, LNE, CNRS, UPMC, Paris, France
* ROA, San Fernando, Spain
° SP Technical Research Institute of Sweden, Borås, Sweden
Physikalisch-Technische Bundesanstalt, 38116 Braunschweig, Germany
+ INRIM, Torino, Italy
$ GMV, Tres Cantos, Spain
E-mail: Pierre.Uhrich@obspm.fr

One well-known limiting factor of GPS receiver relative calibration of hardware delays is the stability during the measurement campaign of the traveling equipment against which all local receivers are measured. One way to estimate that stability is to measure the deviation from closure of the traveling equipment with respect to the reference receiver of the campaign, that is the difference in the hardware delays between the start and the end of the campaign. But unexpected events on the traveling receiver delays at a given location might remain unnoticed, introducing that way a bias in the calibration results for this site. The use of two receivers as traveling equipment might help to detect abnormal behavior during the campaign or to study effects not clearly understood yet.

We report about a GPS receiver relative calibration campaign, which took place during Autumn 2014 between five European National Measurement Institutes or Designated Institutes: LNE-SYRTE in Observatoire de Paris (OP, Paris, France), where the reference receiver of the campaign was located, ROA (San Fernando, Spain), SP (Borås, Sweden), PTB (Braunschweig, Germany) and INRIM (Torino, Italy). We used as traveling equipment two main units, which have been independently calibrated against the reference receiver of the campaign in OP, both connected to a single antenna plus antenna cable. We kept track of the offset between both traveling units in all the visited sites, and, by using the ionosphere free P3 linear combination of P-Code data based on the BIPM standard (TAIP3), we computed the Common-Views (CV) between both traveling units as shown in Fig. 1.

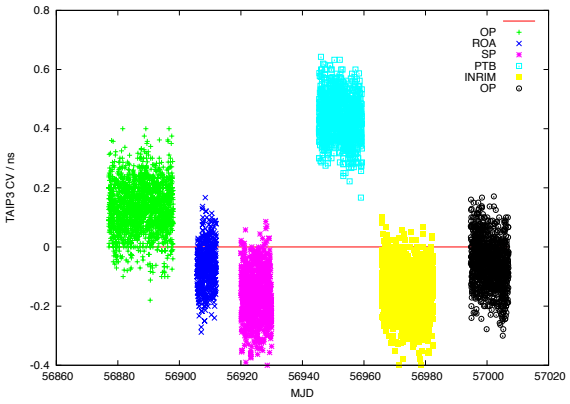


Fig. 1: *Averaged TAIP3 CV between the OP traveling receivers in the visited sites during the relative calibration campaign: OP at the start (green), ROA (blue), SP (lilac), PTB (light blue), INRIM (yellow), and back to OP at the end (black).*

Thanks to a very good stability of the traveling equipment, the instability taken into account in the uncertainty budget computations was finally issued from such an analysis. We obtained expanded uncertainty estimates of about 2 ns (k = 2) for the hardware delays in all visited sites, which is an excellent result. An external validation of the resulting hardware delays is to compare the TAIP3 CV computed with calibrated delays to the time scale differences derived from the UTC – UTC(k) data published by BIPM in its monthly Circular T. Taking into account the fact that the Circular T is mostly based on Two-Way Satellite Time and Frequency Transfer data for the laboratories considered here, we obtained results very close to what was expected.

The calibration campaign was made in the frame of the Galileo Time and Geodetic Validation Facility contract between European Space Agency and GMV as industrial Prime.

GPS Time Link Calibrations in the Frame of EURAMET Project 1156

Esteban, Héctor, Galindo, F. Javier, Bauch, Andreas*, Polewka, Thomas*, Cerretto, Giancarlo^, Costa, Roberto^, Whibberley, Peter.§, Uhrich, Pierre.+, Chupin, Baptiste+

Real Instituto y Observatorio de la Armada, San Fernando, Spain
* Physikalisch-Technische Bundesanstalt, 38116 Braunschweig, Germany
^INRIM, Torino, Italy
§National Physical Laboratory, Teddington, UK
+LNE-SYRTE, Observatoire de Paris (OP), LNE, CNRS, UPMC, Paris, France
E-mail: hesteban@roa.es

Since 2010 ROA has supported the coordination of the EURAMET Technical Committee for Time and Frequency (TC-TF) Project 1156, a reaction from EURAMET TC-TF to Recommendation 2 of CCTF 2009: to study the characterization of GNSS equipment in use for establishing the time links between institutes contributing with their clocks to TAI. Starting that year, it organized a GPS calibration campaign between three contributing laboratories: ROA (Spain), PTB (Germany) and INRIM (Italy). The time transfer results were achieved by using the P3 method, and also carrier phase PPP comparison techniques. These results were also used to re-calibrate the TWSTFT (Two-Way Satellite Time and Frequency Transfer, TW for short) links between Labs, with an uncertainty slightly higher than that of the GPS links.

During 2011 and 2012, the experience was repeated, and in 2012 two other laboratories were included in the calibration trip: NPL (United Kingdom) and OP (France). This project has been stopped since then, but currently we are taking the appropriate steps to reactivate it, once we have solved some equipment limitations. The intention is to extend during this year the calibration to any other institute participating in the Project: ÚFE/IPE (Czech Republic), BEV (Austria), DMDM (Serbia), EXHM/GSCL-EIM (Greece), IPQ (Portugal), JV (Norway), METAS (Switzerland), MIKES (Finland), MIRS (Slovenia), SMD (Belgium), SP (Sweden).

In this paper we report the calibration results, with a focus on the long term stabilities of GPS and TW links between the visited Labs, some technical issues related with the calibration procedure, the current status since the recent approval of BIPM guidelines for GNSS equipment calibration, and finally some lessons learned.

$1x10^{-16}$ frequency transfer by GPS PPP with integer ambiguity resolution

Petit Gérard[1], Kanj Amale[1,3], Loyer Sylvain[2], Delporte Jérôme[3], Mercier Flavien[3], Perosanz Félix[3]
[1] BIPM 92312 Sèvres France
[2] CLS 31520 Ramonville Saint-Agne France
[3] CNES 31401 Toulouse France

E-mail: gpetit@bipm.org

Since many years, the BIPM has been using the Precise Point Positioning (PPP) technique using GPS phase and code observations to compute time and frequency links. We estimate the present typical uncertainty of PPP frequency comparisons to be about $1x10^{-15}$ at 1-day averaging and about $1x10^{-16}$ at 30 day averaging. This is a significant limiting factor in comparing frequency standards in view of the accuracy of the standards which is in the low 10^{-16} for those presently reported with 10^{-17} and below coming soon. Besides improving the performance of frequency transfer at many-day averaging, it is also important to gain at shorter averaging time in order to access more rapidly to the true performance of the compared clocks.

One main limiting factor of PPP with real-valued ambiguities comes from the effect on the clock solution of the simultaneous resolution of floating phase ambiguities together with other parameters such as the tropospheric delay and station position. An approach to overcome these limitations of "classical PPP" is to consider the integer nature of phase ambiguities. We have implemented procedures that allow applying the Integer-PPP (IPPP) technique developed by the CNES to perform frequency transfer over long durations. We quantify the improvement brought by IPPP by several examples of links between stable clocks and characterize the achieved accuracy by comparisons with other techniques.

We present results showing that a frequency transfer accuracy of $2x10^{-15}$ is achieved at ~5-hour averaging for all links and that an accuracy of $1x10^{-16}$ is reached at ~5-day averaging for regional links while a similar performance is likely achievable for long distance links. Such a frequency transfer accuracy of $1x10^{-16}$ at 5-day averaging represents a significant improvement over the present situation to compare remote frequency standards and it will allow a better characterization of new frequency standards. The complete set of results is documented in an upcoming publication [1].

[1] Petit G., Kanj A., Loyer S., Delporte J., Mercier F., Perosanz F., "$1x10^{-16}$ frequency transfer by GPS PPP with integer ambiguity resolution", Metrologia, submitted.

Comparison of Two Continuous GPS Carrier-Phase Time Transfer Techniques

Jian Yao, Skakun Ivan*, and Judah Levine
Time and Frequency Division and JILA, National Institute of Standards and Technology and University of Colorado, Boulder, CO, USA
*PNT Information and Analysis Center, Central Research Institute of Machine Building, Korolyov City, Russia
E-mail: jian.yao@nist.gov

Global Positioning System (GPS) carrier-phase (CP) time transfer is a widely accepted high-precision time transfer method. This method provides much lower short-term noise than other time transfer methods, such as Two Way Satellite Time and Frequency Transfer (TWSTFT) and Common View (CV) Time Transfer. However, CP time transfer solutions frequently show day boundary discontinuity of up to 1 ns due to the inconsistency of the phase ambiguity between two independent days.

To eliminate the day boundary discontinuity, several methods have been proposed in recent years. The question is how large the solutions of these methods differ from each other and how well the solutions are faithful to the clocks. To answer these questions, we here choose two methods to study: Revised RINEX-Shift (RRS) method [1], and Phase Common-View method (Phase-CV) [2]. The RRS is actually an updated version of PPP (precise point positioning). It runs PPP for a data batch of 10 days and extracts the middle epoch. Then it shifts the data batch by a small step of 10 min, runs PPP, and extracts the new middle epoch. It does the data-batch shift by 10 min again and again. The solutions at all middle epochs form the RRS result. The advantages of the RRS method are as follows: it requires only a single station; its solution is unique, no matter what the start date is; it uses both phase and code measurements, which can be helpful when there is some phase drift. However, it increases the computation burden. The Phase-CV is similar to the GPS Common-View time transfer, but using phase rather than code. The advantages of this method are as follows: it cancels out the common errors from satellites and path; the integer ambiguity resolution makes it more likely to be insensitive to small noise. However, it does not work well for a long baseline because of few common-view GPS satellites and no common path. Besides, it sometimes cannot keep the integer ambiguity property, which leads to a re-start of the processing.

Here, we show the time comparison between OPMT and PTBB (baseline is approximately 700 km) by RRS, Phase-CV, and TWSTFT (Fig. 1). Note, slope has been removed and some constant offsets are added to the three curves to overlap each other. We can see that both RRS and Phase-CV provide continuous solutions. And they match each other very well. Further study shows that the time deviation of the difference between RRS and Phase-CV is below 100 ps for an averaging time of less than 10 days. Especially, for an averaging time of less than 1 day, the time deviation is less than 40 ps. We can also find that both RRS and Phase-CV match TWSTFT quite well, although there is approximately 0.5 ns discrepancy during MJD 56887-56895. This discrepancy could come from either GPS time transfer or TWSTFT or both.

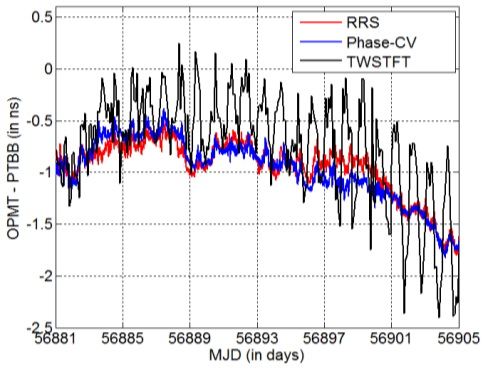


Fig. 1: Time comparison between OPMT and PTBB, using RRS, Phase-CV, and TWSTFT.

We want to do further comparisons between RRS and Phase-CV for more baselines (short and long). We may also do a comparison between RRS and optical fiber time transfer. Latest results will be presented.

[1] J. Yao, and J. Levine, "An improvement of RINEX-Shift algorithm for continuous GPS carrier-phase time transfer," Proc. 27th ION GNSS+ 2014 Conference, pp. 1253-1260, 2014.

[2] J. Delporte, *et al*, "GPS carrier-phase time transfer using single-difference integer ambiguity resolution," International Journal of Navigation and Observation, 2008.

Correction for code-phase clock bias in PPP

P. Defraigne[1], J.-M. Sleewaegen[2], W. Aerts[1]
[1]Royal Observatory of Belgium, Brussels, Belgium
[2]Septentrio Satellite Navigation NV, Leuven, Belgium
Email: p.defraigne@oma.be

Precise Point Positioning (PPP) is a zero-difference single-station technique that has proved to be very effective for time and frequency transfer, enabling the comparison of atomic clocks with a precision of a hundred picoseconds and a one day stability below the 1e-15 level. PPP is based on the joint analysis of dual-frequency ionosphere-free combinations of codes and carrier phases measured in one station, to determine its position and its clock synchronization error at each observation epoch. It was however noted that for some receivers, a frequency difference is observed between the clock solution based on the code measurements and the clock solution based on the carrier phase measurements. This is reflected by a non-zero average of the discontinuities between successive batch solutions [1], and by systematic effects between the code and carrier phase residuals of the PPP solutions [2]. These observations reveal some inconsistency between the code and carrier phases measured by the receiver.

This paper proposes to explain this discrepancy by the time offset that can exist for some receivers between the code and carrier phase latching. In a first step, we explain the origin of this code-phase bias in the receiver hardware and firmware. Its effect on PPP is quantified and it is shown by simulation that it can result in an apparent frequency difference between the code and the carrier phase clock solutions. In a second step, an improved PPP modelling is proposed, in which the code-phase bias is estimated and corrected for. The improvement in the final PPP solution is then estimated for a set of stations participating to the TAI and IGS networks.

[1] G. Petit and F. Mercier, “The time stability of PPP links for TAI,” Proc. IFCS-EFTF 2011, pp.1041-1045.

[2] D. Matsakis, Precise Point Positioning when GNSS Carrier Phase and Pseudorange Disagree, presentation at the PTTI 2014, Boston, MS.

All Digital Frequency Synthesis Based on New Sigma-Delta Modulation Architectures

Sotiriadis, Paul
Department of ECE, National Technical University of Athens, Greece
E-mail: pps@ieee.org

This paper presents an overview of high dynamic range (DR) all-digital frequency synthesis techniques based on a new class of Σ-Δ modulation architectures.

Over the past thirty years all-digital frequency synthesis has attracted the interest of the scientific community because of the advantages of the digital circuits like design-automation, testability, robustness to noise, temperature, supply and process variations, etc. Downscaling of integration technologies makes all-digital frequency synthesis even more desirable as digital circuitry becomes faster and smaller in area while analog RF becomes more challenging to design and with limited area-scaling capability. All-digital frequency synthesizers [1] are finite state machines driven by a clock whose rising and falling edges specify those of the output. This implies that only integral division frequencies of the clock result in clean spectra, instead, all other generated frequencies result in spectra polluted with many and strong spurs. Techniques have been proposed to alleviate the spurs / timing jitter, most are summarized in [1], with random dithering being the only purely digital one.

Published work has demonstrated that dithering can eliminate all or selected spurs, however, it introduces a high noise-floor typically in the order of $10\log_{10}\left(f_{sampling}\right)$ dBc/Hz [2]. In contrast to previous work, this paper introduces all-digital frequency synthesis architectures with embedded new structures of band-pass sigma-delta modulators with frequency translation, generating the single-bit output via a digital non-linear feedback loop. This allows powerful noise shaping and spurs elimination in the pass-band of interest, yet, it raises many new challenges related to the selection of the noise transfer function, stability of the loop and realistic hardware implementation, all of which will be discussed in the presentation. A typical example of the output spectrum is shown in Fig. 1 where the pass-band is 2% of $f_{Nyquist} = f_{sampling}/2$ and the indicated DR is 140dB with RBW=333Hz. There is an inherent trade-off between the pass-band and DR which will also be discussed.

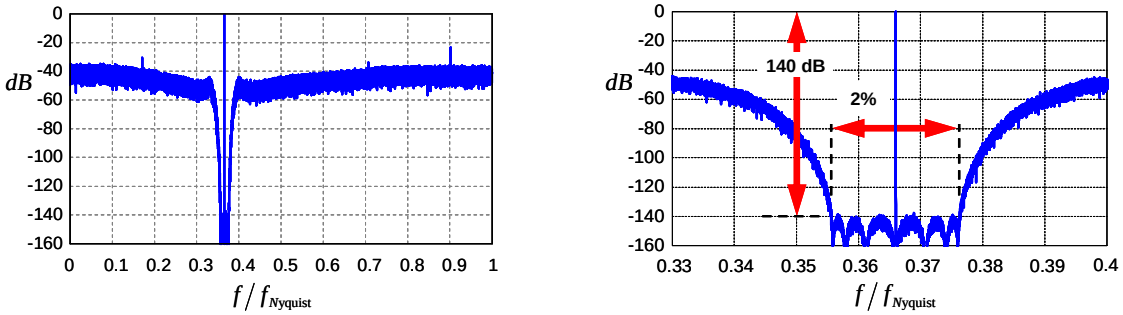


Fig. 1: Typical spectrum of the new all-digital frequency synthesizers based on Σ-Δ modulation. Spectrum (left) and zoom-in (right). Spectrum parameters: Resolution BW = 333Hz, $f_{Nyquist} = f_{sampling}/2 = 500\text{MHz}$, Clean 2% BW is 10MHz.

[1] P. Sotiriadis, K. Galanopoulos, "Direct All-Digital Frequency Synthesis Techniques, Spurs Suppression, and Deterministic Jitter Correction", IEEE Trans. on Circuits and Systems-I, Vol. 59, No. 5, May 2012, pp. 958-968.

[2] P. Sotiriadis, "All Digital Frequency Synthesis Based on Pulse Direct Digital Synthesizer with Spurs Free Output and Improved Noise Floor", IEEE Int. Frequency Control Symposium. 2014.

Noise in High-Speed Digital-to-Analog Converters

Bourgeois P.-Y, Imaike T *, Goavec-Merou G. and Rubiola E
Time & Frequency dpt, FEMTO-ST Institute, Besancon, France
*Dept of Electronics Engineering, Nihon University, Japan

E-mail: pyb2@femto-st.fr

As a part of the Oscillator Instability Measurement Platform project, we target fully digital phase noise measurements with the lowest background noise.

We started with the selection of high-speed cards exhibiting state of the art sampling frequency (250 MS/s), high resolution (16 bits), low analog noise, integrated FPGA computing power, and fully Unix/Linux/Windows compatibility.

First we measured the background noise in the presence of a large HF sinusoidal signal (+12 dBm), the same at the two inputs of a card. The difference of the two data streams cancels the input signal and the external clock, which are in the common mode. There remain the noise of the two ADCs, including the distortion noise, and the noise of the differential clock path.

Then, we measured the background noise in the cross-spectrum mode, using four channels (two cards) to compare two differential signals in the same conditions as before. This configuration rejects the common mode, and also averages out the noise of the two ADC pairs. Theory states that the rejection is of 5 dB per factor-of-ten in the measurement time. After that, the background is set by the crosstalk and by some effects in the clock distribution path.

The noise of one ADC is of 14 nV/√Hz (white) and approximately 1 μV/√Hz (1-Hz flicker). White noise is consistent with the number of bits, with no negligible contribution of the analog frontend. After averaging on up to 4×10^6 spectra, we got 0.56 nV/√Hz (white), and aproximately 100 nV/√Hz (1-Hz flicker, to be confirmed). Referred to the +12 dBm carrier, this is equivalent to a SNR of –156 dB (white) and –119 dB (1-Hz flicker), in 1 Hz bandwidth; and to a SNR of –184 dB (white) and –139 dB (1-Hz flicker) with correlation, in 1 Hz bandwidth. However, actual phase noise may be somewhat higher, due to the asymmetry between AM and PM introduced by the clock distribution. This problem is still under study.

As an example of application, we measured the phase noise of two cryogenic sapphire oscillators, after beating the 10 GHz out down to the HF region, with no need of correlation. These oscillators exhibit a stability of 10^{-15} at 1 s, and 3×10^{-16} (floor).

Our setup compares favorably to other experiments and to all commercial instruments in background noise, processing speed, and absence of spurs and artifacts.

Needless to say, the whole data processing algorithm is under full control.

Simple Method for ADC Characterization under the Frame of Digital PM and AM Noise Measurement

Cárdenas-Olaya Andrea C.*ⁱ, Rubiola Enrico+, Friedt Jean-M.ˣ , Ortolano Massimoⁱ, Calosso Claudio E.*
* Department of Time and Frequency, INRiM, Turín, Italy
ⁱDepartment of Electronics and Telecommunication, Politecnico di Torino, Turín, Italy
+ CNRS/UFC FEMTO-ST Institute, Besançon, France
ˣDepartment of Time and Frequency, FEMTO-ST Institute, Besançon, France
E-mail: a.cardenas@inrim.it

Since the phase noise is a critical parameter in the selection of the appropriated system source(s) for systems and processes highly sensitive to oscillator frequency fluctuations, such as radars, data communication links, multichannel receivers and ultra-stable oscillator applications (timekeeping)., different techniques have been developed in order to measure it, most of them based on the use of spectrum analyzers and analog systems [1]. Due to the fact that analog systems, in general, are not easily reconfigurable and are affected by mechanical noise, temperature dependence, drift, aging and tuning, digital architectures have started to be used for the implementation of phase-meters taking advantage of the flexibility that this kind of approach offers for the system reconfiguration [2].

Considering that the ADC is the front end and the core of a digital phase-meter, see Fig.1, its residual noise has an important impact on the instrument performance. In consequence, the characterization of the ADC becomes an imperative issue in order to guarantee the minimum contributions of noise on the phase noise measurement. Currently, the information available in literature does not provide data about ADC characterization close to the carrier, an important range for time and frequency applications.

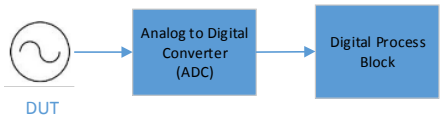


Fig. 1: General description of the architecture used for digital implementation of phase-meters.

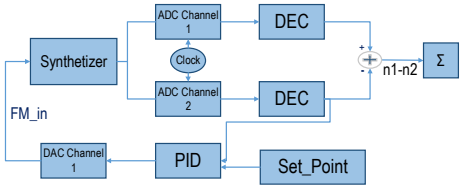


Fig. 2: Method for ADC characterization, based on the PLL definition for phase and amplitude noise detection.

In this work, a method for ADC characterization is proposed, Fig.2, based on a digital test bench with the objective of provide a simple and flexible tool for performing tests on diverse ADCs, in order to find the proper component for phase noise measurement, avoiding time consuming in the reconfiguration and setup of the hardware for each ADC. As test bench was used Red Pitaya platform, a system based on the System on Chip (SoC) Zynq (Xilinx) which integrates two ADCs and two DACs, providing capability and flexibility for developing the tests of characterization in the frequency range of interest.

The method proposed, uses the PLL definition for tacking the zeros crossing samples acquired by the ADCs and based on the slope of the sine input signal is possible convert these zero crossing samples to phase noise information. In the same way, the samples of maximum values could be tack detecting the amplitude noise contributions as well. With this information an ADC model is build and validated.

[1] D. Owen, “Good Practice Guide to Phase Noise Measurement”, Measurement Good Practice Guide No. 68. National Physical Laboratory. United Kingdom. May 2004. ISSN 1368-6550.

[2] J. Grove, J. Hein, J. Retta, P. Schweiger, W. Solbrig and S.R. Stein, “Direct-Digital Phase-Noise Measurement”, *Proceedings*, 2004 IEEE Int. Frequency Control Symp.and Exposition, Aug. 23-27, 2004, pp. 287-291.

6/12-channel Synchronous Digital Phasemeter for Ultrastable Signal Characterization and Use

Caligaris Massimo, Costanzo Giovanni A.[§], Calosso Claudio E.[*]
Department of Electronics and Telecommunication, Politecnico di Torino, Torino, Italy
[*]Division of Optics, INRIM, Torino, Italy
[§]Inrim and Politecnico di Torino
E-mail: c.calosso@inrim.it

Nowadays, in primary time and frequency laboratories we can find high spectral purity signals in the 10 MHz – 10 GHz range generated from cryogenic oscillators or ultrastable lasers together with frequency combs. Their short-term stability surpasses by about two orders of magnitude the performances of active hydrogen masers (AHM), while in the long-term AHMs still have a better behaviour. The new technology can be considered mature for what concern spectral purity, but we cannot say the same about complexity, power consumption and reliability. In this sense it is important to measure ultra-stable sources with respect to AHMs. First, to test their spectral purity or, at least, to give it an upper bound; second to have a continuous monitoring; finally, to combine them in order to get the best of all in term of phase noise and frequency stability.

All of these requirements can be satisfied by the system we are developing. It is a multi-channel synchronous and real-time phasemeter based on tracking Direct Digital Synthesizer (DDS) technique [1]. Here, it has been thought to operate at 100 MHz, nevertheless it can accept arbitrary frequencies in the 5–400 MHz range, with small degradation at low frequency. The expected stability at 1 s is of the order of $2–3\times10^{-14}$, and can be further reduced by about one order of magnitude with the help of cross-correlation technique and three-cornered hat method (the latter for the medium-term). The possibility to measure a wide range of frequencies also allows to use an external pivot oscillator to furtherly reduce the contribution of tracking DDSs. Finally the internal local oscillator has the possibility to be phase-locked and is externally available. It runs at 1 GHz and, if necessary, it can be directly multiplied to 10 GHz, allowing a direct comparison with the ultra-stable source(s) without any significant degradation. These features are particularly interesting to generate a real-time composite clock.

In the medium-long term we expect to have a resolution better than 10^{-16}, thanks to the low temperature sensitivity of the choosen DDS (of the order of 2 ps/K). In any case, it is possible to stabilize the temperature of the board at the milliKelvin level by means of a thermal shield and of several digital temperature sensors, placed close to the temperature-sentitive components.

Fig. 1 shows the design of the main board of the system. In the center of the hexagon, we can see the local oscillator with its distribution that feeds the six tracking DDSs. In the lower part there is the field programmable gate array (FPGA) that drives the six channels and interfaces the single board computer (SBC, not shown in figure). The complete system with 12 channels (two boards), power supply and regulation, and SBC can be hosted in a 1-unit sub-rack.

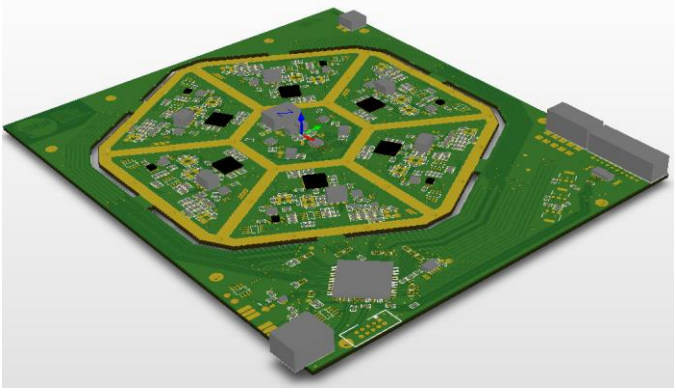


Fig. 1: Design of the multi-channel synchronous phasemeter.

At the conference, we plan to show the first prototype, its characterization and use for averaging time longer than 0.1 s.

[1] C. E. Calosso, "Tracking DDSs in time and frequency metrology," *Proc.* Joint IFCS / EFTF Symposium (Prague, 2013).

Mode-Resolved Direct Frequency-Comb Spectroscopy

James D. Anstie[1], Sarah K. Scholten[1], Nicolas Bourbeau Hébert[2], Richard T. White[1], Jérôme Genest[2] and Andre N. Luiten[1],
[1]Institute for Photonics and Advanced Sensing (IPAS) and School of Physical Sciences, University of Adelaide, Adelaide, SA 5005, Australia
[2]Centre d'Optique, Photonique et Laser, Université Laval, Québec, G1K7P4, Canada
E-mail: james.anstie@adelaide.edu.au

Stabilized frequency combs have been shown to be nearly ideal sources for broadband absorption spectroscopy because they combine broad spectral coverage with high frequency resolution and accuracy [1-4]. High sensitivity can be gained by exploiting the coherence of the comb, which allows both resonant enhancement and heterodyne detection. Nonetheless, to gain all the potential benefits flowing from a stabilized comb's frequency stability, accuracy and uniformity it is necessary for the detection technology to be able to resolve the individual comb teeth. For a 250MHz repetition rate comb with a spectral width of 100nm this means detecting around 50,000 teeth.

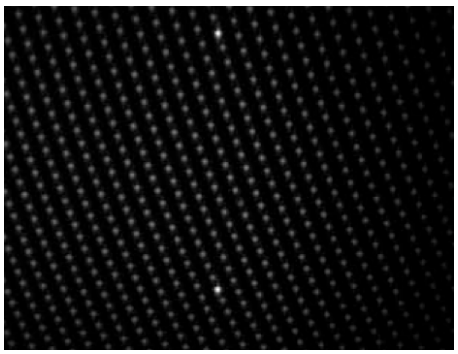


Fig. 1: Frequency comb showing individual modes on the VIPA detector after pre-filtering through a 9.5GHz mode filter cavity. The bright spots relate to a calibration cw laser.

One of the most popular comb detection approaches is based on a combination of a virtually imaged phase array (VIPA), a diffraction grating and an IR camera [1-3]: its popularity derives from its broad spectral resolution, and simplicity. Unfortunately, its frequency resolution is insufficient to resolve individual comb modes from conventional fiber comb sources.

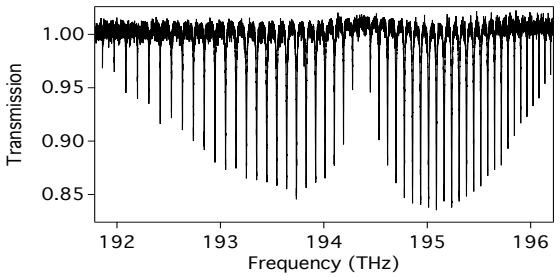


Fig. 2: A spectra of HCN formed by interleaving the 38 unique spectra derived by stepping the cavity length through each set of modes

To overcome this limitation we have augmented the VIPA with a pre-filtering optical resonator that has a free spectral range (FSR) of 9.5GHz – exactly 38 times the comb repetition rate. We rapidly step-tune the cavity so that it becomes resonant with each unique subset of comb modes to generate 38 unique mode-resolved spectra (see Figure 1 to see one of these). These filtered combs are then sent through an optical apparatus that alternately passes the light through a molecular sample and then bypasses the sample to provide a reference comb. Eventually the light falls onto a conventional VIPA detector. By ratioing the two filtered combs (sample and reference) we obtain a measurement of the transmission through the sample at a 9.5GHz frequency spacing. We combine all 38 measurements to generate a complete broadband transmission spectrum that is sampled with a 250 MHz resolution but with an accuracy equal to that of the comb – which is around 100Hz in our case. The entire process takes just a few seconds. We will report on the performance of this high-resolution, high-speed molecular spectrometer and discuss the requirements for high quality spectra.

[1] F. Adler, M. J. Thorpe, K. C. Cossel, and J. Ye, Annual Review of Analytical Chemistry 3, 175–205 (2010).
[2] S. A. Diddams, L. Hollberg, and V. Mbele, Nature 445, 627–630 (2007).
[3] M. J. Thorpe, K. D. Moll, R. J. Jones, B. Safdi, and J. Ye, ,Science 311, 1595–1599 (2006).
[4] I. Coddington, W. C. Swann, and N. R. Newbury, ,Phys. Rev. Lett. 100, 013902 (2008).

Coherent octave-span microcavity frequency combs

Scott Papp, Katja Beha, Pascal Del'Haye, Daniel Cole, Aurélien Coillet, Fred Baynes, Frank Quinlan, Tara Fortier, Scott Diddams
Time and Frequency Division, National Institute of Standards and Technology, Boulder, CO USA
E-mail: scott.papp@nist.gov

Modelocked-laser frequency combs have revolutionized optical frequency metrology and precision time keeping by providing an equidistant set of absolute reference lines that span in excess of an octave. Their typically sub-GHz repetition frequency and <100 fs optical pulses enable nonlinear broadening for self-referencing, and feature among the highest spectral purity of any oscillator.

Frequency combs generated from a CW laser via parametric nonlinear optics in microcavities (microcombs) and electro-optic modulation (EOM) [1] are interesting new platforms for experimenters. The 10's of GHz or higher repetition frequency and the offset frequency of such combs are tunable to match a fuller range of comb applications in communications, metrology, arbitrary waveform generation, and quantum information. Moreover, the physics of comb generation in microcombs [2] and EOM combs [3] offers access to novel regimes of spectral phase apart from requirements of modelocking.

An important goal for microcombs and EOM combs is self-referencing to connect microwave and optical frequencies. In this talk, we report on the first coherent octave-span combs with both technologies, and on experiments that use these spectra. The figure below shows a simplified apparatus diagram for our EOM comb and microcomb systems. We have refined a two-stage nonlinear fiber (HNLF) broadening approach and applied it to both combs. The plot at right shows data traces of the resulting octave-span spectra.

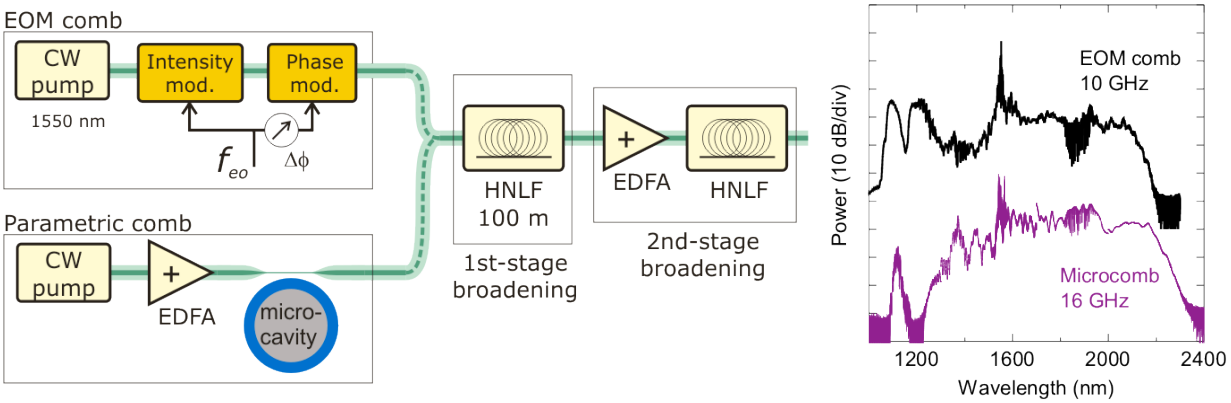


Figure 1: (Left) Optical comb generators feed into a two-stage nonlinear fiber broadening system. (Right) Optical spectra from the two seed comb generators. In both cases the spectrum cover an optical octave.

[1] H. Murata, A. Morimoto, T. Kobayashi, and S. Yamamoto, IEEE J. Sel. Top. Quant. Electron. 6, 1325–1331 (2000).
[2] P. Del'Haye, K. Beha, S. B. Papp, and S. A. Diddams, Phys. Rev. Lett. 112, 043905 (2014).
[3] R. Wu, V. R. Supradeepa, C. M. Long, D. E. Leaird, and A. M. Weiner, Opt. Lett. 35, 3234 (2010).

Towards efficient octave-spanning comb with micro-structured crystalline resonator

Ivan S Grudinin and Nan Yu

Jet Propulsion Laboratory, California Institute of Technology, Pasadena, California 91109, USA

[*] *nan.yu@jpl.nasa.gov*

250-word-Abstract:

Optical frequency combs, typically produced by mode locked lasers, have revolutionized many applications in science and technology. Frequency combs were recently generated by micro resonators through nonlinear Kerr processes. However, the comb span from micro resonators was found to be limited by resonator dispersion and mode spectrum. While dispersion engineering has been reported in on-chip devices, monolithic crystalline resonators offer an advantage of high optical quality factor. Moreover, most resonators used for comb generation support many mode families, leading to unavoidable crossings in resonator spectrum. Such crossings strongly influence comb dynamics and may prevent stable coherent mode-locking and soliton states. We report a new crystalline resonator appraoch supporting dispersion control and single mode spectrum while maintaining high quality factor. Dispersion engineering by waveguide micro-structuring is used to flatten the dispersion in our MgF2 resonator. Both absolute magnitude of dispersion and its slopes can be altered over a wavelength span exceeding an octave. Dispersion flattening leads to generation of an octave-spanning frequency comb with repetition rate of 46 GHz and coupled pump power below 100 mW. We also demonstrate that the micro-structuring dispersion engineering approach can be used to achieve flattened and anomalous dispersion in a CaF2 resonator near 1550 nm wavelength. In addition, we describe observation of discrete steps between the modulation instability states of the primary comb and on the three-stage comb unfolding dynamics. The micro-structured resonators may enable efficient low repetition rate coherent octave spanning frequency combs without external broadening, ideal for applications in optical frequency synthesis, metrology, spectroscopy, and communications.

100-word-Abstract:

Optical frequency combs were recently generated by micro--resonators through nonlinear Kerr processes. However, the comb span from micro resonators was found to be limited by resonator dispersion and mode spectrum. Here we report generation of a low repetition rate comb in a new crystalline resonator supporting dispersion control, single mode spectrum, and ultra--high quality factor. We show that flattening of dispersion allows the frequency comb to reach an octave span with record efficiency. The micro-structured resonators may enable efficient low repetition rate coherent octave spanning frequency combs without external broadening, ideal for applications in optical frequency synthesis, metrology, spectroscopy, and communications.

Research was carried out at the Jet Propulsion Laboratory, California Institute of Technology under a contract with the National Aeronautics and Space Administration.

Precision spectroscopy of N_2O by a phase-locked quantum cascade laser to a mid-IR comb

Gambetta A, Cassinerio M, Coluccelli N, Fasci E*, Castrillo A*, Gianfrani L*, Gatti D, Marangoni M, Laporta P, and Galzerano G

Istituto di Fotonica e Nanotecnologie - CNR and Dipartimento di Fisica - Politecnico di Milano, Milano, Italy
* Dipartimento di Matematica e Fisica - Seconda Università di Napoli, Caserta, Italy
E-mail: gianluca.galzerano@polimi.it

We report on metrological-grade mid-IR spectroscopic system based on frequency-comb-assisted distributed-feedback (DFB) QCL, tunable in the wavelength range from 8.56 to 8.63 μm. The QCL laser is phase-locked to a tooth of a difference frequency generation mid-IR comb [1] using a beat note generated directly in the mid-IR region without any conversion scheme: the result is a compact spectroscopy system combining the broadband parallel detection capabilities of a mW-level mid-IR comb to the high-precision performances of a mid-IR narrow linewidth source. The achieved ~30 dB signal-to-noise ratio of the detected beat-note together with the achieved closed-loop locking bandwidth of ~500 kHz allows for a residual integrated phase noise of 0.78 rad (1 Hz - 5 MHz), for an ultimate resolution of ~21 kHz, limited by the measured linewidth of the mid-IR comb. By tuning the comb repetition rate, f_{rep}, the QCL frequency is scanned across nitrous oxide (N_2O) transition lines with an ultimate accuracy of a GPS-disciplined Rb frequency standard.

Figure 1 shows the transmission spectrum of the ν_2 vibrational band of N_2O at a pressure of 800 Pa, resulting from a 180-kHz wide Rb-referenced scan of f_{rep}, corresponding to an optical frequency tuning of 0.9 cm^{-1} (0.05 cm^{-1}/minute frequency scan speed), sufficiently wide to precisely identify different rovibrational lines. Without any control of the QCL power, an absorption sensitivity of the order of 10^{-4} cm^{-1}, mainly limited by unwanted etalon effects, is achieved, as demonstrated by the inset of Fig. 1 showing a well resolved doublet with a fractional absorption of 2%. We also performed several acquisitions of the N_2O P(8)-e rovibrational transition at different pressure in the range from 55 to 1000 Pa (at a temperature of 296 K). A linear fit of the retrieved line-centre frequencies as a function of the gas pressure allowed us to determine a pressure shifting parameter of -99(14) Hz/Pa, as well as to extrapolate the zero-pressure value of the center frequency, which resulted to be 1161.4792366(3) cm^{-1} (corresponding to a relative precision of 3×10^{-10}). This value deviates from the one of the HITRAN database by 2.6×10−5 cm^{-1}, well within the HITRAN accuracy, and results to be 2 orders of magnitude more precise. The statistical uncertainty on the extrapolated zero-pressure value of the line-center frequency is mostly limited by the SNR of the recorded spectra and by the pressure-dependent repeatability of the line-center frequency retrievals. On the other hand, the main source of systematical deviation is the pressure reading (whose contribute amounts to 6×10^{-10}); other sources, including the electronic detection chain bandwidth and the RF-standard accuracy are negligible, being at the 2×10^{-12} level.

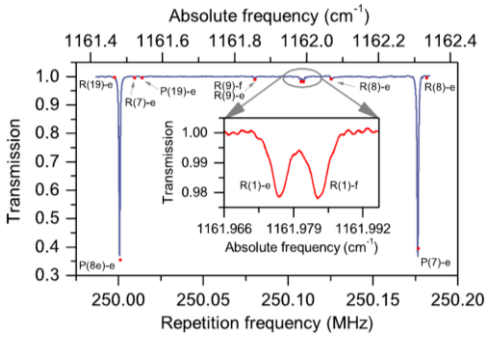


Fig. 1: N_2O transmission spectrum at 800 Pa pressure. Inset: detail of the R(1)-e - R(1)-f doublet.

[1] A. Gambetta, N. Coluccelli, M. Cassinerio, D. Gatti, P. Laporta, G. Galzerano, and M. Marangoni, "Milliwattlevel frequency combs in the 8-14 μm range via difference frequency generation from an Er:fiber oscillator," Opt. Lett. 38, 1155-1157 (2013).

Optical Bloch band spectroscopy with laser cooled magnesium atoms

Kulosa André, Rühmann Steffen, Fim Dominika, Zipfel Klaus, Jha Nandan, Sauer Steffen, Ertmer Wolfgang, and Rasel Ernst M.

Institut für Quantenoptik, Leibniz Universität Hannover, Hannover, Germany

E-mail: kulosa@iqo.uni-hannover.de

Optical lattices are an important tool for many applications in physics ranging from frequency metrology, with recently demonstrated record uncertainties and instabilities in the low 10^{-18} regime, to simulation of solid state physics with quantum degenerate gases. Optical lattice clocks are typically operated at deep traps, such that the periodic band structure and tunneling between the lattice sites normally have a minor impact on the spectroscopy signal. However, in magnesium, featuring a small atomic mass and a magic wavelength in the blue regime of the optical spectrum, these effects are more prominent and demand higher optical powers for the lattice beams.

Here we report on Bloch band spectroscopy of laser cooled magnesium atoms trapped in a magic wavelength lattice at 468 nm. Atoms are interrogated on the magnetic field-induced $^1S_0 \rightarrow {}^3P_0$ clock transition at 458 nm. Operating the optical lattice at a trap depth of a few recoil energies, we expect the bandwidth of the lattice ground state to be larger than the spectroscopic linewidth of the atomic resonance. We observe a symmetric frequency shift of the carrier transition into a doublet-like structure whereas the order of the shift is in the order of the ground state bandwidth. For an increasing trap depth and as a consequence a decreasing ground state bandwidth, we see the corresponding decreasing in the carrier frequency shift as it has been postulated by Wolf and Lemonde [1].

However, this spectroscopic feature arising in the regime of shallow lattices, can be used to extract information about atomic properties being relevant for precision spectroscopy. A difference in the atomic polarizabilities of the ground and excited state, respectively, appears in an asymmetry of the observed feature. Thus, the magic wavelength can also be determined by measuring this asymmetry at different lattice wavelengths.

[1] P. Lemonde and P. Wolf, *Phys. Rev. A* **72**, 033409 (2005)

Time Signals Converging within Cyber-Physical Systems

Weiss, Marc, Chandhoke, Sundeep*,Melvin, Hugh+
Time and Frequency Division, NIST, Boulder, CO, USA
*Research & Development, National Instruments, Austin, TX, USA
+National University of Ireland, Galway, Ireland
E-mail: mweiss@nist.gov

Time is central to predicting, measuring and controlling properties of the physical world, and is one of the most important constraints distinguishing Cyber-Physical Systems (CPS) from distributed computing in general. However mixing the cyber and the physical has a fundamental challenge, since computers and communications systems have abstracted away the physical layer and timing is fundamentally a physical signal. While such abstractions have yielded significant benefits, time has been a casualty. CPS used in industry today achieve time-awareness by making use of time-aware fieldbuses and devices with specialized proprietary software. However, this approach has proved restrictive in both the topologies achievable and the scalability of networks beyond a certain size. The new era of the Internet-of-Things and the Industrial Internet is paving the way for convergence, where time needs to be an integral part of the cyber, making integration of cyber and physical seamless. However, this requires successful research in a number of different areas.

Time in CPS can be referenced to a local time scale or a national one, such as UTC. UTC is generally provided via a Global Navigation Satellite System (GNSS) such as GPS. There are various standards for transferring time through networks, such as the Precise Time Protocol (PTP). For PTP to transfer time accurately, significant hardware is necessary in the network path, called on-path support. Once precise time arrives at a CPS node, its use often must incorporate some degree of computation. Modern processors cannot provide predictable execution needed to support required precise time in many CPS. Research is needed at all of these stages of time transfer to support time in CPS with scalability and in systems-of-systems [1].

NIST has formed a CPS Public Working Group (PWG), with members from global industry, academia and government [2]. This CPS PWG is tasked with creating a set of frameworks and reference architectures for CPS, to promote proper function and interoperability. Public documents from this effort are now available [3]. We discuss the current status of the CPS PWG and of the research that aims to better integrate time with cyber-systems, and the potential future of how CPSs may be built on these new converged networks (with integrated time).

[1] M. Weiss, J. Eidson, C. Barry, L. Goldin, B. Iannucci, E. Lee, and K. Stanton, “The Case for Cross Disciplinary Research on Time Aware Applications, Computers and Communication Systems (TAACCS),” Sep 18, 2013, available from http://taaccs.org/

[2] webpage: http://www.nist.gov/cps/

[3] webpage: http://www.cpspwg.org/

Ns-level time transfer over a microwave link using the PTP-WR protocol

M. Rico, C. Botteron, J.-P. Aubry, P.-A. Farine

EPFL-STI-IMT-ESPLAB, Electronic & Signal Processing Laboratory, Neuchâtel, Switzerland
mathieu.rico@epfl.ch; cyril.botteron@epfl.ch; jean-pierre.aubry@epfl.ch; pierre-andre.farine@epfl.ch

Many infrastructures require very accurate and secure time synchronization, such as for example electronic intelligence systems and smart grid PMUs (Phasor Measurement Units). For these types of applications, a GNSS-free time reference is often mandatory or desired because of the acknowledged vulnerabilities of GNSS-based time transfer. Optic fiber based time dissemination is one alternative and thanks to the various PTP profiles (Energy, Telecom), micro-second time transfers may be obtained. Recently, an improved variant of PTP has been introduced by CERN's team called the PTP-White Rabbit (PTP-WR). This improved protocol has been demonstrated to provide time transfer in the sub-ns range over a 5 km optical fiber link [1].

While today µs-level synchronization over wireless can be achieved, what is still missing is a protocol adapted to a microwave link that can provide ns-level of time transfer accuracy.

After reviewing the different technologies available (SDH/SONET or E1/T1 time stamp, amplitude modulation), we have selected PTP and PTP-WR as the preferred protocols, mainly because of momentum and equipment availability.

Then our goal was to identify existing radio links that could support ns range time dissemination over medium distances. As a microwave link can support various radio link technologies (QAM/PSK, FDD/TDD, PTP Transparent Clock), our experimental plan was to apply successively PTP protocol, PTP with SyncE, then PTP-WR, over candidates wireless links. PTP and PTP-WR master/slave were used to qualify respectively PTP & PTP-SyncE and PTP-WR performances. The experimental setup was a PPS master/slave delay comparison and a typical record is shown on figure 1. In this example, performances are qualified in terms of time delay mean (50.5 ns) and standard deviation (6.6 ns).

PTP only presents a gaussian distribution, and performances over wireless are expected in the sub-100 ns level. Offset distribution is highly sensitive to radio configuration. Also we noticed that an initial transient behavior is generally observed.

PTP-WR provides better accuracy, but PTP-WR deployment requires dedicated fiber infrastructure and interfaces, while PTP or PTP-SyncE may be used with common equipment.

In conclusion, radio link supporting PTP & PTP-SyncE are able to provide some sub-100 ns range time transfer link, and we will show that we can deploy radio configuration supporting PTP-WR and providing sub-ns time transfer accuracy over a microwave link.

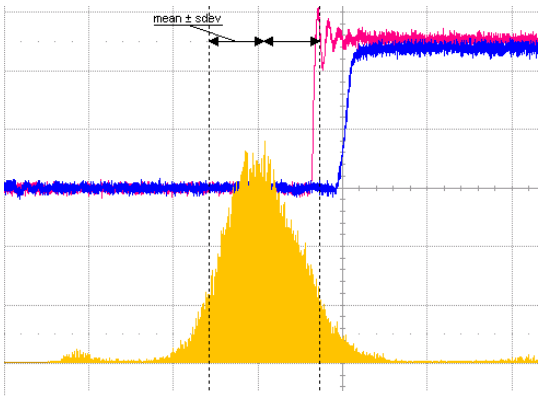


Figure 1: PTP time transfer over wireless link, using PTP transparent clock radio

[1] M. Lipinski, T. Wlostowski, J. Serrano, P. Alvarez, "White rabbit: a PTP application for robust sub-nanosecond synchronization", ISPCS 2011.

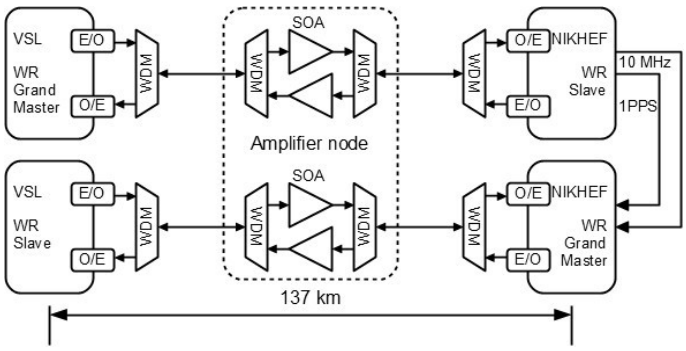
Using White Rabbit PTP for accurate time and frequency transfer in long haul optical fiber links

DIERIKX, Erik[1]; PINKERT, Tjeerd[2]; KOELEMEIJ, Jeroen[2]; PEEK, Henk[3]; SMETS, Rob[4]
[1]VSL, Delft, The Netherlands
[2]LaserLaB and Department of Physics & Astronomy, VU University, Amsterdam, The Netherlands
[3]Nikhef, Amsterdam, The Netherlands
[4]SURFnet, Utrecht, The Netherlands
E-mail: edierikx@vsl.nl

Within the framework of a European collaboration, NEAT-FT, an investigation has been made on the application of White Rabbit PTP for accurate time and frequency (TF) transfer through long haul optical fibers. The White Rabbit (WR) [1] protocol was originally developed to synchronize instruments and equipment within a perimeter of 10 km with an accuracy of 1 ns. In this work, it is demonstrated that WR can be used over much longer distances. If implemented appropriately, the accuracy can be maintained over long distance.

In contrast to other optical fiber TF transfer techniques (e.g. [3], [4]) the transmitted signals in WR are based on existing Ethernet protocols. This allows integration of WR with data traffic in telecom fiber networks. WR implements the precise time protocol (PTP)[2], in a synchronous 1 Gbps Ethernet environment. In a WR network, all switches and nodes are frequency locked in a hierarchical structure to a single reference clock. This clock determines the transmission rate of all data in the network. PTP provides coarse synchronization between the different nodes and the phase of the transferred data bits is used for fine synchronization.

As an experimental test bed, SURFnet (the Dutch national research and education network) and Delft University of Technology have provided a pair of dark fibers of 137 km between VSL in Delft and Nikhef in Amsterdam. In each fiber, a bidirectional path is created for 1470 nm one way and 1490 nm the other way. These wavelengths could coexist with C-band data transmission. The total attenuation (fibers, patches and multiplexers) is ca 50 dB each. A delay-calibrated quasi-bidirectional optical amplifier is used to compensate the losses.



With two cascaded WR links, a loop has been created from VSL to Nikhef and back to VSL. From this loop, the performance of this combined link has been evaluated by monitoring the 1PPS output from the grand master and the 1PPS output from the slave at VSL. The stability of the frequency transfer is well below 1 x 10^{-15} Hz/Hz averaged over 24 hours. The stability of the time delay is below 50 ps averaged over 24 hours. The absolute time transfer accuracy of the link is currently within 8 ns. The most important uncertainty contribution is related to the estimated effect of chromatic dispersion on the time delay.

[1] J. Serrano, P. Alvarez, M. Cattin, E. G. Cota, P. M. J. H. Lewis, T. Włostowski *et al.*, "The White Rabbit Project," in Proceedings of ICALEPCS TUC004, Kobe, Japan, 2009.

[2] IEEE, "IEEE 1588: Standard for a Precision Clock Synchronization Protocol for Networked Measurement and Control Systems", http://standards.ieee.org/, 2008.

[3] V. Smotlacha, A. Kuna, W. Mache, "Time transfer using fiber links", EFTF-2010 24th European Frequency and Time Forum, Noordwijk, The Netherlands, 13-16 April 2010.

[4] P. Krehlik, Ł. Sliwczynski, Ł. Buczek, M. Lipinski, "Fiber-Optic Joint Time and Frequency Transfer With Active Stabilization of the Propagation Delay", IEEE Trans. Instrum. Meas., vol. 61, no. 10, pp. 2844–2851, Oct. 2012.

Precise UTC Dissemination through future Telecom Synchronization Networks

Wen-Hung Tseng, Sammy Siu, Shinn-Yan Lin, and Chia-Shu Liao
Telecommunication Laboratories, Chunghwa Telecom Co., Ltd., Taoyuan, Taiwan
E-mail: whtseng@cht.com.tw

Traditional telecommunication networks require precise frequency synchronization to ensure the quality of data streams. Owing to the need of broadband Internet access for smart phones, the mobile system operators have to manage wireless spectrum more efficiently. For the coming in 4G or future 5G mobile networks, the accurate time synchronization is vital for a larger number of base stations. The study and investment of synchronization network are inevitable for today's telecommunications industries. Meanwhile, for emerging critical information infrastructures, the demands for precise standard time have also increased recently, e.g., financial market for recording low-latency trading data and cloud computing for time-stamping of events. In order to satisfy different applications, it is necessary to provide the standard Coordinated Universal Time (UTC) through protocol level support at the various network nodes. Towards the best investment-effectiveness, the plans [1][2] for disseminating precise UTC time through commercial telecommunications network will become attractive to both telecommunications industries and official regulations.

The Precision Time Protocol (PTP, IEEE 1588), is a protocol for clock synchronization in networks. With the support of hardware and Synchronous Ethernet (Sync-E), its dynamic (short-term) time stability can be as low as a few ns. Several experimental measurements in mobile backhaul networks have been performed in Chunghwa Telecom. This paper will introduce the result of network performance measurements, which is a time transfer from a telecom grandmaster clock (T-GM) to a telecom time slave clock (T-TSC) over a chain of 9 cascaded telecom boundary clocks (T-BCs) with Sync-E frequency support. For the network cover a range of about 30 km in a metro area, the maximum time interval error (MTIE) is only 4 ns for a period of 19 h. Although the dynamic time variation can be kept low, the asymmetry of the backhaul network still cause a constant time bias of up to 37 ns.

Fig. 1 shows a prospective architecture for time synchronization distribution in a mobile network. Currently, most critical timing infrastructure systems rely on GNSS signals, which can support sub-microsecond accuracy for general receivers, and reach accuracies of no more than 5 ns with respect to UTC with dual-frequency receivers for time-keeping purposes. With the help of alternative timing systems based on Sync-E and the IEEE-1588 protocol, the GNSS receivers can move from base stations to the backhaul network, and then ideally to the core network. For being traceable to UTC, the primary reference time clock (PRTC) of a core network needs to be calibrated and monitored in real-time by a national timekeeping institute. Now, the GNSS common-view time transfer can provide near real-time monitoring. A dedicated fiber link would be a future solution to calibrate the reference clock. The network asymmetry calibration and related issues will be discussed in the full paper.

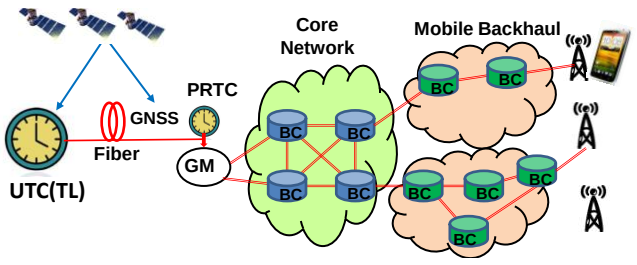


Fig. 1: A prospective architecture for time synchronization distribution through mobile networks.

[1] M. Weiss, L. Cosart, J. Hanssen, S. Hicks, and et al., "Ethernet time transfer through a U.S. commercial optical telecommunications network," *Proceedings*, 2014 Precise Time and Time Interval Meeting, ION PTTI 2014, Boston, Massachusetts, Dec. 2014, pp. 214-220.

[2] H. Imlau, "Synchronization network migration with focus on coherent network primary reference time clocks," Time and Sync in Telecoms, ITSF 2014, Nov. 2014.

Multi-functional and Reconfigurable Piezoelectric MEMS/NEMS Resonators for Advanced Sensing and Wireless Communications

Matteo Rinaldi, Yu Hui, Zhenyun Qian, Gwendolyn Hummel
Department of Electrical and Computer Engineering, Northeastern University, Boston, MA, USA
E-mail: rinaldi@ece.neu.edu

Sensors are nowadays found in a wide variety of applications, such as smart mobile devices, automotive, healthcare and environmental monitoring. The recent advancements in terms of sensor miniaturization, low power consumption and low cost allow envisioning a new era for sensing in which the data collected from multiple individual smart sensor systems are combined to get information about the environment that is more accurate and reliable than the individual sensor data. By leveraging such sensor fusion it will be possible to acquire complete and accurate information about the context in which human beings live, which has huge potential for the development of the Internet of Things (IoT) in which physical and virtual objects are linked through the exploitation of sensing and communication capabilities with the intent of making life simpler and more efficient for human beings.

This trend towards sensor fusion has dramatically increased the demand of new technology platforms, capable of delivering multiple sensing and wireless communication functionalities in a small foot print. In this context, Micro- and Nanoelectromechanical systems (MEMS/NEMS) technologies can have a tremendous impact since they can be used for the implementation of high performance sensors and wireless communication devices with reduced form factor and Integrated Circuit (IC) integration capability.

This work presents a new class of Aluminum Nitride (AlN) piezoelectric nano-plate NEMS resonant devices that can address some of the most important challenges in the areas of physical, chemical and biological detection and can be simultaneously used to synthesize high-Q reconfigurable and adaptive radio frequency (RF) resonant devices. By taking advantage of the extraordinary transduction properties of AlN combined with the unique physical, optical and electrical properties of advanced materials such as graphene, photonic metamaterials, phase change materials and magnetic materials, multiple and advanced sensing and RF communication functionalities are implemented in a small footprint. Particular attention is dedicated to the key attributes of such piezoelectric MEMS/NEMS devices in realizing intrinsically switchable and reconfigurable RF MEMS components, high performance gravimetric chemical sensors, ultra-fast and high resolution un-cooled IR/THz detectors and ultra-miniaturized and low power magnetoelectric sensors.

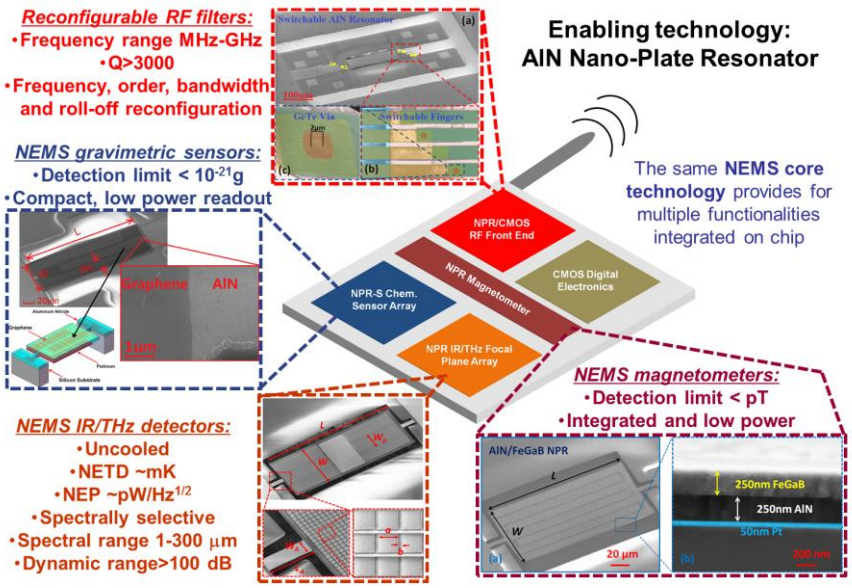


Fig. 1: Schematic representation of multiple sensing and wireless communication functionalities implemented by the core AlN Nano-Plate Resonator technology.

Gap Reduction Based Frequency Tuning for AlN Capacitive-Piezoelectric Resonators

Robert A. Schneider, Thura Lin Naing, Tristan O. Rocheleau, and Clark T.-C. Nguyen
EECS Department, University of California, Berkeley, CA/USA
E-mail: schneid@berkeley.edu

A voltage-controlled resonance frequency tuning mechanism, capable of effecting 1,547 ppm frequency shifts or more, is demonstrated for the first time on an AlN capacitive-piezoelectric two-disk array-composite resonator, shown in Fig. 1. The key enabler here is a compliant top electrode suspension that moves with applied voltage to effectively vary capacitance in series with the device, hence changing its frequency. Capacitive-piezoelectric AlN micromechanical resonators, i.e., those with electrodes not directly attached to the piezoelectric material, already exhibit high *Q*-factors compared to attached-electrode counterparts, e.g., 8,800 versus 2,100 at 300 MHz; are "on/off" switchable [1]; and (as shown in this work) can exhibit respectable electromechanical coupling C_x/C_0 of 1.0%. This new ability to tune frequency without the need for external components now invites the use of on-chip corrective schemes to improve accuracy or reduce temperature-induced frequency drift, making an even more compelling case to employ this technology for frequency control applications.

Fig. 1 presents an annotated SEM of the device. Here, two central-stem supported 1.6-μm-thick AlN disks mechanically coupled via an extensional-mode beam of acoustic length λ/2 are sandwiched by top and bottom electrodes spaced 135- and 100-nm, respectively, by air gaps. The use of two resonators allows one to accept input/output electrodes, while the other sports a dedicated electrode to tune frequency. This separation decouples the I/O and tuning, thereby allowing tuning without changes in motional impedance. Fig. 2 presents cross sections of the variable-top-gap tuning mechanism. Here, an applied bias voltage attracts the spring-supported top electrode to a fixed bottom electrode, changing the top-gap series capacitance, C_{gt}, which then changes the mode frequency for both resonators, effectively changing the frequency f_s for the array-composite. Again, there is no need for the external digitally addressable capacitor banks [2] or external varactors [3] normally required by conventional AlN resonator technology. Fig. 3 presents measurements confirming voltage-controlled frequency tuning for 1) the device of Fig. 1, where a V_{tune} of 24V yields 630 ppm of frequency tuning with constant motional impedance; and in the inset 2) 1547 ppm frequency tuning on a single resonator, but with variable motional impedance. In both cases, f_s decreases as V_{tune} increases, as expected.

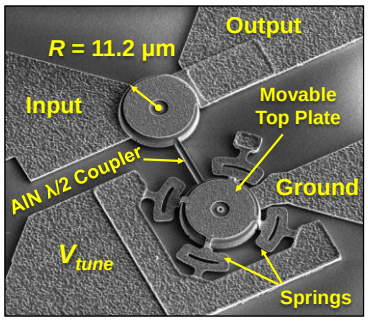


Fig. 1: Annotated SEM of a tunable AlN capacitive-piezo 2-disk array-composite resonator using a dedicated tuning transducer.

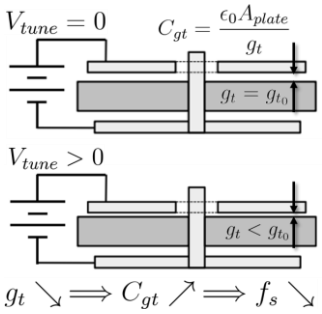


Fig. 2: Illustrative cross sections of an untuned (top) and a tuned (bottom) capacitive-piezoelectric AlN radial-contour-mode disk resonator.

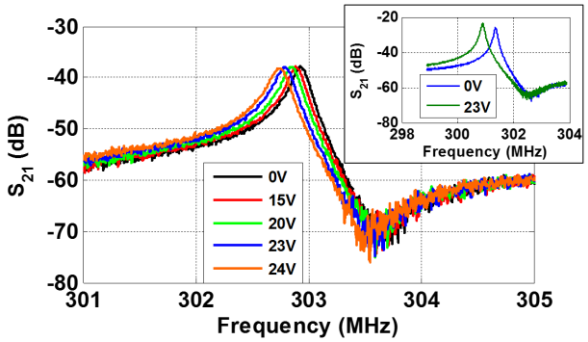


Fig. 3: Measurements confirming voltage-controlled frequency tuning for 1) the device of Fig. 1, where motional resistance remains constant; and 2) (in the inset) a single resonator device using a single port for both input/output and tuning, for which motional resistance varies with voltage.

[1] R. Schneider and C. Nguyen, "On/off switchable high-Q capacitive-piezoelectric AlN resonators," *Proc. MEMS*, 2014, pp. 1265–1268.
[2] J. Hu, et al., "A wide-tuning digitally controlled FBAR-based oscillator for frequency synthesis," *Proc. IFCS*, 2010, pp. 608–612.
[3] B. Kim, et al., "Capacitive frequency tuning of AlN micromechanical resonators," *Proc. Transducers*, 2011, pp. 502–505.

GHz Range Graphene-Aluminum Nitride Nano Plate Resonators

Zhenyun Qian, Yu Hui, Fangze Liu*, Swastik Kar* and Matteo Rinaldi
Dept. of Electrical and Computer Engineering, Northeastern University, Boston, MA, USA
*Dept. of Physics, Northeastern University, Boston, MA, USA
E-mail: qian@ece.neu.edu, rinaldi@ece.neu.edu

This paper reports on the design and experimental verification of Graphene-Aluminum Nitride (G-AlN) Nano Plate Resonators (NPRs) operating at *GHz* frequencies. For the first time we demonstrate that by using a virtually massless and high electrical conductivity graphene electrode, floating at the van der Waals separation of a few angstroms from a piezoelectric nano-plate, it is possible to implement nanomechanical resonators operating in the GHz range with improved electromechanical performance (up to *4X* improved $f \cdot Q$) compared to conventional devices employing a metal electrode (Fig. 1).

An individual prototype of G-AlN NPR operating at *245 MHz* was previously reported [1]. In this work we demonstrate for the first time (with statistical data over *120* devices) that, when the operating frequency of the resonator is scaled in the *GHz* range (Fig. 1), the use of a virtually massless graphene electrode not only boosts the operating frequency of the resonator but it also enables the achievement of higher electromechanical performance without introducing any electrical loading compared to conventional devices employing a metal electrode. Unlike metal electrodes that form chemical bonds with underlying substrates, graphene virtually "floats" at the van der Waals separation of a few angstroms over the AlN nano-plate with minimal mechanical interactions; which minimizes energy dissipation due to electrode damping and interfacial strain (high Q). Simultaneously, high confinement of electric field within the active volume of the piezoelectric nano-plate is maintained (unchanged electromechanical coupling) thanks to the high electrical conductivity of the graphene sheet and its minimal van der Waals separation of only a few angstroms from the AlN nano-plate. Furthermore, despite the sheet resistance of a single atomic layer graphene sheet is approximately 3 orders of magnitude higher than that of a *100 nm* thick Au layer (used as a reference) the contribution of the graphene top-electrode (ΔR_s in Fig. 2(c)) to the overall electrical loss of the device (R_s in Fig. 2(b)) becomes negligible as the operating frequency of the device is increased due to the effective shortening of the electrical path of the current flowing in the top electrode (smaller pitch and larger number of fingers forming the bottom interdigital electrode for a similar device area, Fig. 1(b)).

70 G-AlN NPRs and *70* reference devices (employing a *100 nm* thick top Au electrode) with *7* different pitch sizes from *20 μm* to *4 μm* (*0.2~1.3GHz*) were simultaneously fabricated on a single wafer and tested. The device performance metrics were extracted and compared (Fig. 1 (c)), showing that the use of the massless graphene van der Waals electrode enables the achievement of higher electromechanical performance in nanomechanical structures with reduced volume and higher vibration frequency which really represents a trend inversion in the scaling of piezoelectric electromechanical resonators.

[1] Z. Qian, et al., *Proceedings*, 2013 IEEE Int. Frequency Control Symp., Prague, Czech Republic, July 21-25, 2013, pg. 559-561.

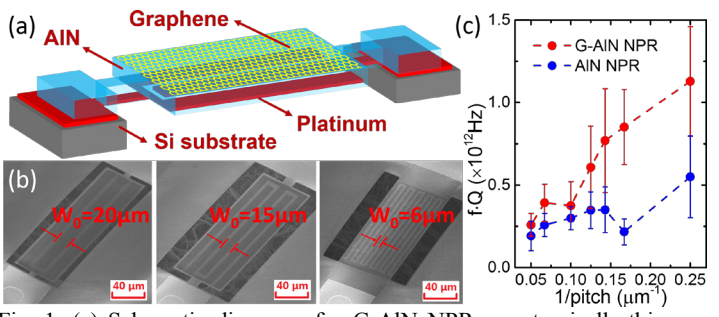


Fig. 1: (a) Schematic diagram of a G-AlN NPR: an atomically-thin graphene sheet is employed, in lieu of a conventional metal film, as top electrically floating electrode in the lateral field scheme used to excite a higher order lateral-extensional mode vibration in the AlN piezoelectric nano-plate. (b) A set of SEM images of G-AlN NPRs with 3 different pitch sizes. (c) Comparison of $f \cdot Q$ values for the G-AlN NPRs and reference devices.

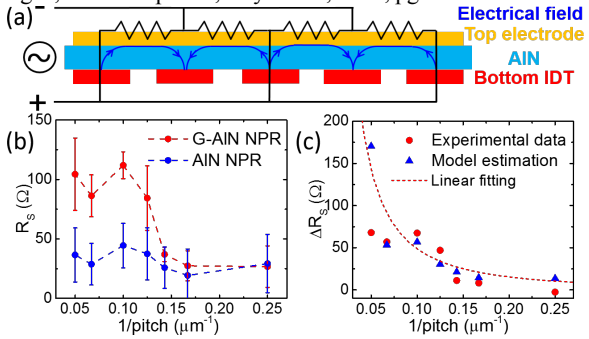


Fig. 2: (a) Schematic illustration of the geometrical model used to estimate ΔR_s. (b) Extracted values of total electrical resistance, R_s, for different pitch sizes. (c) Extracted graphene electrode resistance, ΔR_s, for different pitch sizes, compared to the geometrical model estimations. The linear fitting confirms $\Delta R_s \propto pitch$.

Switchable 2-Port Aluminum Nitride MEMS Resonator Using Monolithically Integrated 3.6 THz Cut-Off Frequency Phase-Change Switches

Hummel, Gwendolyn and Rinaldi, Matteo
Electrical and Computer Engineering, Northeastern University, Boston, MA, USA
E-mail: hummel.gw@husky.neu.edu, rinaldi@ece.neu.edu

This work presents the first experimental demonstration of an intrinsically switchable Aluminum Nitride (AlN) 2-port MEMS resonator using monolithically integrated chalcogenide phase change material (PCM) switches. Effective ON/OFF switching of the device transmission (*~42dB* variation for fixed *50 Ω* termination) is demonstrated for the first time, without increasing the complexity of the device fabrication process (only 2 additional masks) or requiring substantial modification of the device layout (only an additional probing pad per via), thanks to the monolithic integration of 3 ultra-miniaturized (*2 μm×2 μm*) PCM switches with radio frequency (RF) performance superior to the one of more conventional RF switch technologies: an ON-state resistance of *2 Ω* with an OFF-state capacitance and resistance of *22 fF* and *~20 MΩ*, respectively, were measured for the PCM switches of this work resulting in an RF switch cutoff frequency of *3.6 THz* and an improved figure of merit ($FOM=R_{ON}\cdot C_{OFF}$*~44 fs*) compared to the *~100s fs* of typical solid-state RF switches [1]. This monolithic solution enables dense integration of resonators and switches with reduced resistive losses and capacitive loading effects (this work demonstrates a Port 1 capacitance as low as *70 fF* in the OFF state, determined by 2 OFF switches and *~25 fF* parasitics), setting a milestone towards the development of AlN/PCM single-chip multi-band RF systems with the highest level of reconfigurability and minimum possible effect on the RF performance.

Differently from previous demonstrations, a 2-port configuration is chosen since it enables the synthesis of reconfigurable narrow-band filters by simply electrically cascading multiple switchable resonator stages. The lateral-extensional mode resonator is composed of an AlN thin-film (*500 nm*) sandwiched between a bottom (Pt) plate electrode connected to electrical ground and top interdigital electrode (Al) patterned in 3 parallel fingers: 2 of which are connected to form the input port and 1 is connected to form the output port. 3 programmable PCM vias are employed to connect each of the metal fingers to the corresponding device terminal through a *250 nm* SiO_2 layer (Fig. 1). Each programmable PCM via is composed of a *100 nm* thick $Ge_{50}Te_{50}$ film deposited in a *2 μm×2 μm* via (etched in the SiO_2 isolation layer). The transition temperature needed for the switching of the PCM vias was achieved by passing current directly through the PCM. Voltage pulses of *1.5 V, 200 μs* were used to turn the PCM switches ON and pulses of *4.7 V, 2 μs* were used to trigger the ON-to-OFF transition.

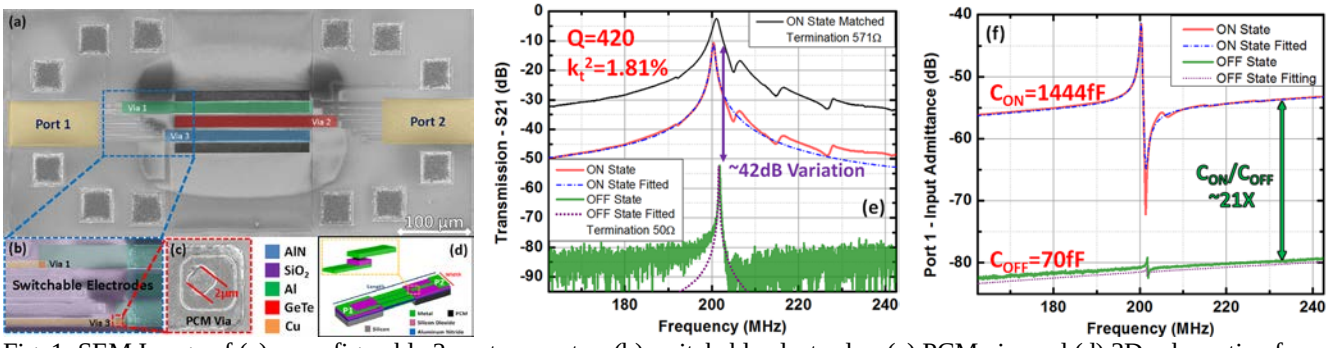


Fig. 1: SEM Image of (a) reconfigurable 2-port resonator, (b) switchable electrodes, (c) PCM via, and (d) 3D schematic of resonator design. (e) Transmission for ON and OFF states and equivalent circuit fittings. (f) Admittance of input port for ON and OFF states and equivalent circuit fittings.

[1] J. Moon, H. Seo, and D. Lee, SPIE Proceedings, vol. 9096, 90960A, June 2014.

Analysis of the Impact of Release Area on the Quality Factor of Contour-Mode Resonators by Laser Doppler Vibrometry

Gibson, B.*, Cassella, C.+, Qalandar, K.*, Piazza, G.+, Turner, K.L.*
*University of California at Santa Barbara, Santa Barbara, CA 93106, USA
+Carnegie Mellon University, Pittsburgh, PA 15213, USA

Energy dissipation through the anchors of an aluminum nitride (AlN) MEMS contour-mode resonator (CMR) accounts for a significant portion of the total energy loss and degradation of the quality factor at frequencies around 220MHz [1]. This energy takes the form of strain energy, not only in the anchor but also in the portion of the surrounding device layer that has been released from the substrate during fabrication (Figure 1). Typical device simulations do not take into account the motion of this additional area. We show a direct effect on the device Q as a result of this released region.

Device Q was extracted from electrical measurements taken from a 220MHz AlN CMR (Figure 1). Then, using a laser Doppler vibrometer (LDV), displacement data was collected along a path from the edge of the device's active region to the edge of the released region. The device was then etched using XeF_2 to release additional device layer area from the substrate. These measurements were taken again and this process was repeated eight times on the same device.

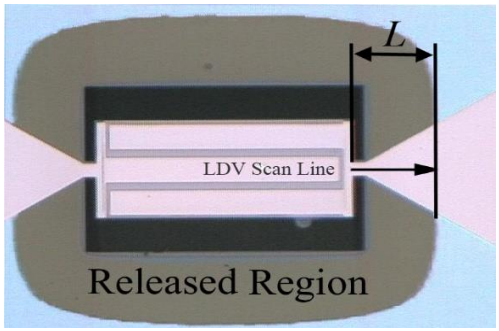


Figure 1: A 220MHz AlN contour-mode resonator. The device layer imediately around the CMR has been released from the substrate and exhibits strain as the result of energy dissipated out of the anchors.

The LDV displacement data for each etch step was squared and summed in order to obtain a value that is proportional to the strain energy outside the body of the resonator (for publication, this will be validated by COMSOL simulations). This was compared to the device Q. Figure 2 shows these values plotted with respect to distance, *L*, taken from the edge of the resonator to the end of the released area. There is a direct relationship between displacement and Q. A 28% increase in Q can be seen as *L* is varied. In addition, these values vary sinusoidally with respect to *L*. The wavelength of this sine wave is 19.1μm, which is exactly half of the acoustic wavelength of the 220MHz AlN device. It is believed that this is the result of energy escaping the anchor, reflecting off of the edge of the released region and returning into the resonator. Constructive interference will occur if $L=n\lambda/2$, where $n=1,2,3\ldots$ and λ is the acoustic wavelength at the resonance frequency. Maximum device Q occurs when $L\approx 3\lambda/2$ which further validates our hypothesis.

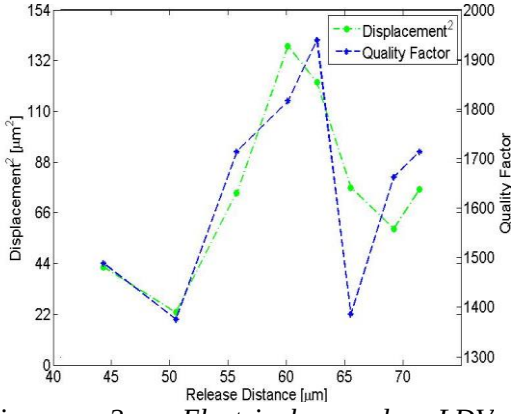


Figure 2: Electrical and LDV measurements demonstrate the effect of the released region on Q, which is optimized at the released length, $L=n\lambda/2$.

The released length, *L* is set arbitrarily during fabrication as a result of the etch radius needed to release the resonator body and anchor from the substrate. Instead, we show that this parameter should be carefully designed so as to maximize resonator Q.

[1] J. Segovia-Fernandez, M. Cremonesi, C. Cassella, A. Frangi, and G. Piazza, "Experimental study on the impact of anchor losses on the quality factor of contour mode AlN resonators," *Proceedings, 2013 Transducers & Eurosensors XXVII: The 17th International Conference on*, 2013, pp. 2473-2476.

Control of residual amplitude modulation below 1×10^{-6} for laser frequency stabilization

Hall, John L.; Zhang, Wei; Ye, Jun
JILA, University of Colorado and NIST, Boulder CO, USA
E-mail: jhall@jila.colorado.edu

Modulation schemes can encode interesting resonance information to higher Fourier frequencies, thus avoiding excess noise at low frequencies. However, Residual Amplitude Modulation (RAM) usually accompanies optical phase modulation processes, and presents a major limitation to the accurate determination of the resonance center. Early progress came with cascaded modulation techniques, or finding parameter-insensitive operating points, etc. One approach involves testing the modulated probe beam *before*, as well as *after* it interacts with the chosen frequency reference system, in principle allowing suppression of RAM-induced offsets, whatever their origin. The first effort [1] illustrated the idea, but added an excessive level of measurement noise. A narrow-band intensity noise servo using 2 phases was demonstrated [2]. Recently, Zhang et al [3] have shown a very simple means to implement two Degrees of Freedom (DoF) servos, achieving stability in the part-per-million (ppm) domain.

Here we report a fully explicit two DoF measurement of the probe light, combined with the in-phase (I) and quadrature (Q) servos that actuate I and Q compensating amplitude modulators operating on the light beam, prior to sampling. The first task is to minimize direct rf pickup in the photodetector systems, presently about 1ppm RAM equivalent. The control rf signal is bandpass-filtered, amplified and demodulated by the two doubly-balanced mixers (DBM), using I and Q reference waves. Similarly the spectroscopy rf signal is prepared for single-channel detection. With light blocked, the static offsets of the mixers (<1 mV) are suppressed by dc offsets of the low-drift 10x gain buffers, which precede the double-integrator servo controllers. (The RAM processes rise very strongly toward dc, and a single integrator is insufficient.) The next task is to introduce compensating I and Q amplitude modulation onto the laser beam, according to these servo requests. We have used a tip-tilt PZT mirror between a free-space EOM and a PM fiber that feeds to the optical sampler and then the reference cavity (or spectroscopy) setup. The I-phase of the detected RAM signal controls this vertical PZT and provides 0 ppm I-component AM on the beam, due to the designed-in vertical position modulation synchronous with the EO crystal voltage. Via weak deliberate interference fringes, the Q-phase is controllable by tilting the horizontal PZT of the relay mirror, and this servo achieves 0 ppm Q-phase RAM. In an improved version we inject these error signals as rf amplitude requests onto the AOM.

An out-of-loop proof of this ZERO RAM claim uses the 500x-amplified output of the cavity frequency lock PDH error signal. Its deliberate 10 dB excess ac gain before its DBM scales 1 ppm of RAM into ~1.1 mV dc. Of course the unlocked laser can drift a little and encounter a higher spatial mode, which leads to the big "noise" bursts in the trace. We find a light ON/OFF dc shift of 0.6 mV, where the shotnoise at 6s averaging is 0.5 mV. The equivalent Allan Deviation of locating the resonance center is below 1 ppm for times >10s (Fig.1). The frequency-shifted residual RAM carrier is just seen after 25 scans with 0.25 Hz BW for the FFT.

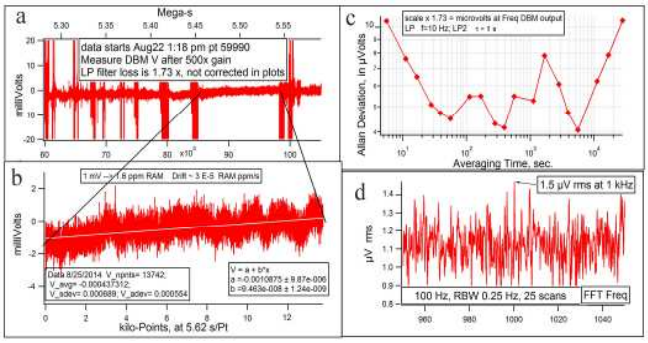


Fig 1. **a**, Out-of-loop RAM; **b**, Data without bursts; **c**, Corresponding Allan deviation; **d**, FFT of down-shifted rf error sig.

[1] N. C. Wong, and J. L. Hall, Servo control of amplitude modulation in frequency-modulation spectroscopy: demonstration of shot-noise-limited detection ," J. Opt. Soc. Am. B, Vol. 2, No. 9, pp. 1527-1533, Sept. 1985.

[2] F du Burck, G Tetchewo, A N Goncharov and O Lopez, "Narrow band noise rejection technique for laser frequency and length standards: application to frequency stabilization," Metrologia, Vol 46, No. 4, pp. 599-606, Sept. 2009..

[3] W. Zhang , M. J. Martin, C. Benko, J. L. Hall, J. Ye, C. Hagemann, T. Legero, U. Sterr, F. Riehle, G. D. Cole, and M. Aspelmeyer, "Reduction of residual amplitude modulation to 1×10^{-6} for frequency modulation and laser stabilization," OPT. LETT, Vol. 39, No. 7, pp.1980-1982, Apr. 2014.

Recent Advancements in Substrate-Transferred Crystalline Coatings

Garrett D. Cole,[1,2] David Follman,[1] Markus Aspelmeyer[3]
[1]Crystalline Mirror Solutions LLC, 114 E. Haley, Suite N, Santa Barbara, California 93101, USA
[2]Crystalline Mirror Solutions GmbH, Seestadtstraße 27, Top 1.05, A-1220 Vienna, Austria
[3]Vienna Center for Quantum Science and Technology (VCQ), Faculty of Physics, University of Vienna, A-1090 Vienna, Austria
E-mail: g.cole@crystallinemirrors.com

Substrate-transferred crystalline coatings represent an entirely new concept in high-performance optical coatings. This technology was originally developed as a solution to the long-standing thermal noise limitation found in ultrastable optical interferometers, impacting cavity-stabilized laser systems for precision spectroscopy and optical atomic clocks, as well as interferometric gravitational wave (GW) detectors [1]. In such interferometers, minimization of the limiting thermal-noise requires mirrors that simultaneously exhibit excellent optical and mechanical quality. The ultimate stability of these systems is currently dictated by coating Brownian noise, driven by the elevated mechanical losses of the materials that comprise the highly reflective elements of the cavity end mirrors. Preliminary research in the field of cavity optomechanics revealed that monocrystalline semiconductors, specifically AlGaAs-based heterostructures, are capable of significantly reduced mechanical damping, while achieving competitive reflectivity when compared with state-of-the art ion-beam sputtered dielectric coatings [2]. However, the implementation of such single-crystal multilayers in a high-finesse cavity presents a number of challenges. Direct deposition onto typical optical substrates is precluded by lattice matching constraints, or in the case of amorphous substrates, by the lack of a crystalline template for seeded growth. Additionally, high-quality epitaxy is incompatible with the curved surfaces required for a stable resonator design. Overcoming these obstacles, we have developed a microfabrication technique that enables the transfer of low-loss monocrystalline multilayers onto essentially arbitrary optical surfaces.

Employed as end mirrors in a Fabry-Pérot cavity, our crystalline coatings exhibit high reflectivity (with a demonstrated finesse of 150,000 at 1064 nm), as well as a thermally-limited noise floor consistent with a tenfold reduction in mechanical damping at room temperature [3]. Building upon this initial demonstration, investigations have now shown the potential for realizing parts-per-million levels of optical losses, including both absorption and scatter, in GaAs-based Bragg mirrors at wavelengths spanning 1000 to nearly 4000 nm. In collaboration with colleagues from the LIGO-scientific collaboration, we have experimentally verified absorption coefficients below 0.1 cm^{-1} in the near infrared [5], enabling an absorption of 3 ppm or below in this spectral region. These recent advancements have opened up additional application areas including but not limited to crystalline coatings for next-generation ring-laser gyroscopes [4], as well as chemical and trace gas sensing in the mid-infrared spectral range. Further efforts include a focus on increasing the current maximum bond diameter of 16 mm, aiming for tens-of-cm-diameter GW-relevant optics, while we have also begun fabricating active devices including semiconductor saturable absorber mirrors and laser gain media transferred to high thermal conductivity substrates [6].

[1] G. M. Harry, T. P. Bodiya, and R. DeSalvo (Eds.). *Optical coatings and thermal noise in precision measurement.* New York, NY: Cambridge University Press, 2012.

[2] G. D. Cole, "Cavity optomechanics with low-noise crystalline mirrors," *SPIE Optics & Photonics, Optical Trapping and Optical Micromanipulation IX*, San Diego, CA, USA, 12–16 August 2012 [8458–07].

[3] G. D. Cole, W. Zhang, M. J. Martin, J. Ye, and M. Aspelmeyer, "Tenfold reduction of Brownian noise in high-reflectivity optical coatings," *Nature Photonics*, vol. 7, no. 8, pp. 644-650, August 2013.

[4] J. Steinlechner, I. W. Martin, A. Bell, G. D. Cole, J. Hough, S. Penn, S. Rowan, S. Steinlechner, "Mapping the optical absorption of a substrate-transferred crystalline AlGaAs coating at 1.5 µm," preprint arXiv:1412.3627, December 2014.

[5] A.A. Velikoseltsev, D.P. Luk'yanov, V.I. Vinogradov, K.-U. Schreiber, "Super-large optical gyroscopes for applications in geodesy and seismology: state-of-the-art and development prospects," *Quantum Electronics*, vol. 44, no. 12, pp. 1151-1156, December 2014.

[6] A. Diebold, T. Zengerle, M. Mangold, C. Schriber, F. Emaury, M. Hoffmann, C.J. Saraceno, M. Golling, D. Follman, G. D. Cole, M. Aspelmeyer, T. Südmeyer, and U. Keller, "Optimized SESAMs for kilowatt ultrafast lasers," *Conference on Lasers and Elecro-Optics (CLEO)*, San Jose, CA, USA, 10–15 May 2015.

A Second-Generation Cryogenic Silicon Resonator

Matei, D.G., Zhang, W. *, Legero, T., Grebing, C., Häfner, S., Lisdat, C., Riehle, F., Ye, J. *, Sterr, U.
Physikalisch-Technische Bundesanstalt (PTB), Bundesallee 100, 38116 Braunschweig, Germany
*JILA, National Institute of Standards and Technology and University of Colorado,
440 UCB, Boulder, CO 80309-0440, USA
E-mail: dan.matei@ptb.de

The tremendous progress with optical atomic clocks asks for super-stable lasers to interrogate the best clock transitions with only a few mHz line width. Previously, we have developed a cryogenic silicon Fabry-Pérot resonator that provides short-term instability of *mod* $\sigma_y(\tau) \leq 1 \times 10^{-16}$ for averaging times of $\tau = 1 - 10$ s [1] and a long-term fractional frequency drift of less than 5×10^{-19} /s [2]. We are currently setting up two independent systems where we reduce the different perturbations to the overall frequency stability of each system, with the goal of reaching a thermal-noise limited fractional frequency instability of about 7×10^{-17}.

The new systems are operated again at 124 K, where the coefficient of thermal expansion of silicon has a zero crossing as a function of temperature. The control of the resonator temperature is greatly enhanced using a combination of several temperature sensors, heat shields and low-thermal conductivity materials. Owing to the anisotropic elasticity of the single-crystal silicon, we find from both finite element (FEM) simulations and experiment that the vertical acceleration sensitivity can have a zero crossing when the support points of the resonator are suitably chosen and the azimuthal angle between the internal crystal axis and the chosen three-point support structure is properly adjusted (Fig. 1). Both the vibration and thermal systems are operated as closely as possible to these zero crossings.

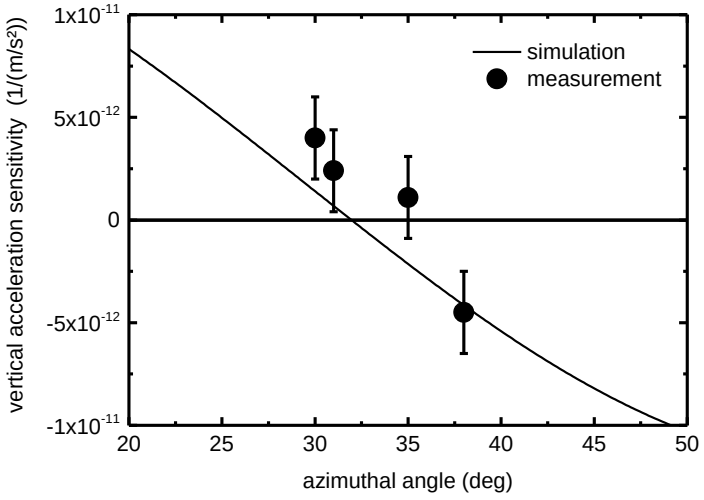


Fig. 1: Vertical acceleration sensitivity of the silicon resonator on a three-point support structure, as a function of the azimuthal angle: FEM simulation (line) and measurement (points).

Additional improvements with respect to [1] comprised the reduction of pressure fluctuations in the vacuum and of residual amplitude modulation [3], and the improved cavity finesse ($F > 400\,000$). We report on the current progress and on the possible use of the resonator in PTB's optical Sr lattice clock [4].

We gratefully acknowledge support from the Centre for Quantum Engineering and Space-Time Research (QUEST), NIST, and DARPA.

[1] T. Kessler et al., "A sub-40-mHz-linewidth laser based on a silicon single-crystal optical cavity", Nature Photonics, vol. 6, pp. 687–692, 2012

[2] Ch. Hagemann et al., "Ultrastable laser with average fractional frequency drift rate below 5×10^{-19} /s", Optics Letters, vol. 39, no. 17, pp. 5102–5105, 2014.

[3] W. Zhang et al., "Reduction of residual amplitude modulation to 1×10^{-6} for frequency-modulation and laser stabilization" Optics Letters, vol. 39, no. 7, pp. 1980-1983, 2014.

[4] S. Falke et al., "A strontium lattice clock with 3×10^{-17} inaccuracy and its frequency", New J. Phys.,vol.16, 073023, 2014.

Cryogenic silicon optical cavities for high spectral purity lasers

Fang S., Light P. S., Marmet L., Döringshoff K.*, Peters, A.*, Sterr, U.[+], Webster S.[#], Ma L. S.[△], Hartnett J., Luiten A. N.

Institute for Photonics and Advanced Sensing (IPAS) and School of Physical Sciences,
University of Adelaide, Adelaide, SA 5005, Australia
*Department of Physics, Humboldt University, Berlin, Germany
[+]Physikalisch-Technische Bundesanstalt (PTB), 38116 Braunschweig, Germany
[#]M Squared Lasers, 1 Kelvin Campus, West of Scotland Science Park, Maryhill Road, Glasgow, G20 0SP, United Kingdom
[△]State Key laboratory of Precision Spectroscopy (LPS), East China Normal University, Shanghai, China
E-mail: su.fang@adelaide.edu.au

Stable, narrow-linewidth lasers have long been used to provide high-precision measurement for a wide range of physical parameters. Their performance is such that they find wide use in the most extreme examples of measurement i.e tests of fundamental physics, driving optical atomic clocks, and enabling gravitational wave detection.

We are developing sources to meet the demands of these high-precision experiments: our target is a laser with fractional frequency fluctuations in the 10^{-17} range, corresponding to frequency fluctuations of 2 mHz at the optical frequency of 200 THz (~1560 nm).

We are focused on solving two outstanding technical barriers for optical cavity stabilization: the deleterious effects of external accelerations and of thermal noise on the cavity length. To address the problem of external accelerations, we have designed a monocrystalline silicon cavity, that when mounted from four points in a tetrahedral configuration, will have a cavity length that is nearly immune to external vibrations [1]. The silicon cavity spacer and the spring-loaded mounting pins are shown in Fig 1. For reducing thermal noise we operate the cavity inside a closed-cycle cryostat, either operating at the lowest possible temperature (~4 K) or at a turning point in the thermal expansion of silicon (~18 K). The laser is delivered to the cavity via optical fiber feedthroughs. We employ active stabilization of the optical alignment to the cavity mode as well as active stabilization of the fiber length. In a second generation version of the cavity we intend to use crystalline mirror coatings, which will have a thermal noise contribution an order-of-magnitude lower than that of conventional dielectric high-reflectivity coatings [2], although for the current version we are using conventional coating technologies.



Fig. 1: Silicon cavity spacer and aluminium support pin.

We will detail the cavity and mounting structures that deliver the ultra-low thermal noise and high immunity to vibration. We will also discuss how we guarantee good thermal conductivity and good coupling efficiency throughout the cooling process. Furthermore, we will present experimental progress using prototype Al optical cavities that show 10^{-14} range stability at room temperature. We expect that we should also be able to present the first results using monocrystalline silicon cavities.

[1] S. Webster and P. Gill, "Force-insensitive optical cavity," Opt. Lett. vol. **36**, No 18, pp. 3572-3574, Sep. 2011.

[2] G. D. Cole, W. Zhang, M. J. Martin, J. Ye and M. Aspelmeyer, "Tenfold reduction of Brownian noise in high-reflectivity optical coatings," Nature Photon. Vol. **7**, pp. 644-650, Aug. 2013.

Toward Chip Integrated Ultra-Low-Noise Lasing Using a Microrod Resonator

J. Becker[1], W. Loh[1], F. Baynes[1], D. Cole[1], F. Quinlan[1], H. Lee[2], K. Vahala[2], S. Papp[1], and S. Diddams[1]
[1]Time and Frequency Division, National Institute of Standards and Technology (NIST), Boulder, CO 80305, USA
[2]T.J. Watson Laboratory of Applied Physics, California Institute of Technology, Pasadena, CA 91125, USA
E-mail: Joe.Becker@nist.gov

Stimulated Brillouin scattering (SBS) as a gain medium for lasing has been demonstrated in bulk fiber rings, crystalline resonators, and silica microdisks [1-4]. Our previous microdisk SBS lasers showed linewidths below 100 Hz but required a second silica microrod cavity to lower the noise level near the carrier frequency [4]. By expanding the mode volume of the resonator relative to that of a microdisk, we demonstrated an overall decrease in the noise level both at the noise floor and near carrier frequency. This promising result opens a path towards low-noise operation in a single silica microrod resonator [5].

A schematic of the SBS microrod system is shown in Figure 1a. We lock the semiconductor pump laser to a whispering gallery mode having $Q=10^7$. This generates SBS lasing in the direction counter-propagating to the pump on an adjacent cavity mode offset by the cavity free spectral range of 11 GHz. The frequency noise of the SBS microrod laser is shown in comparison to the pump laser in Figure 1c. Near the carrier frequency we have an improvement of up to 2 orders of magnitude in the frequency noise, and the noise floor approaches 0.2 Hz^2/Hz. We are presently investigating noise contribution due to thermal refractive and photo-thermal effects, such that further expansion of the mode-volume, improved control of the pump power, and overall thermal stabilization of the microrod should lead to still lower noise levels.

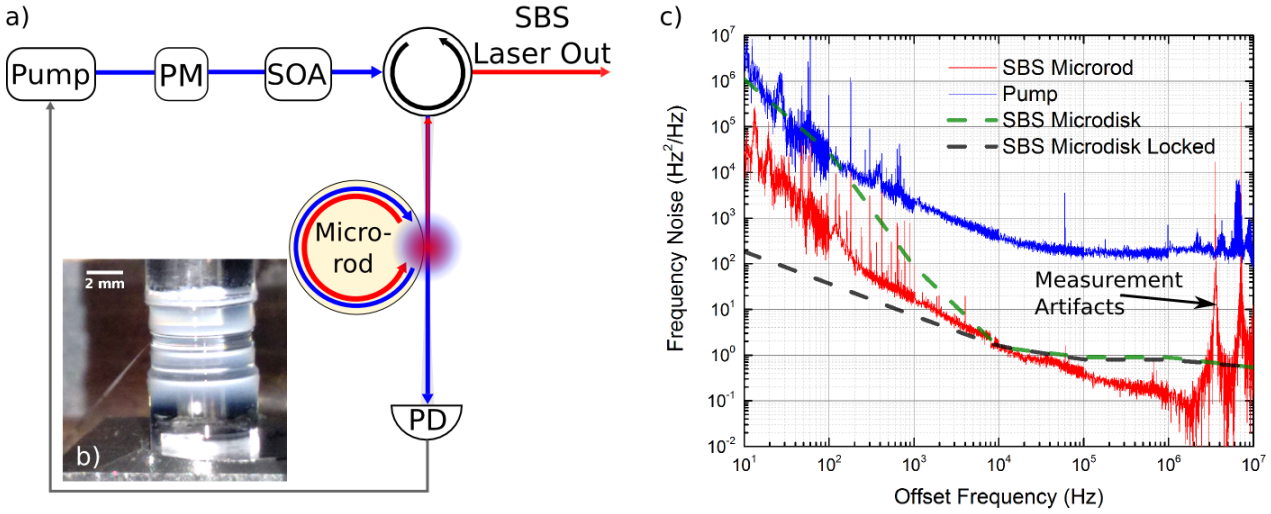


Figure 1: a) Schematic of the SBS microrod system using an external phase modulator (PM) and photodetector (PD) to implement a Pound-Drever-Hall locking. b) An image of the microrod resonator with tapered optical fiber for coupling. c) Measured SBS microrod laser frequency noise versus measured pump laser frequency noise. The dashed lines represent the previous SBS results in a smaller mode volume microdisk laser both by itself and locked to a second microrod.

[1] S. P. Smith et al., "Narrow-linewidth stimulated Brillouin fiber laser and applications," Opt. Lett. **16** (1991).
[2] I. S. Grudinin et al., "Brillouin lasing with a CaF2 whispering gallery mode resonator," Phys. Rev. Lett. **102** (2009)
[3] H. Lee et al., "Chemically etched ultrahigh-Q wedge-resonator on a silicon chip," Nature Photon. **6**, 369-373 (2012)
[4] W. Loh et al., "Dual-microcavity narrow-linewidth Brillouin Laser," arXiv:1410.2912
[5] P. Del'Haye et al, "Laser-machined ultra-high-Q microrod resonators for nonlinear optics," Appl. Phys. Lett. **102**, (2013).

Diode Laser For Atomic Clock Applications

Wei Liang, Danny Eliyahu, Elijah Dale, Anatoliy Savchenkov, Jerry Byrd, Vladimir Ilchenko, David Seidel, Andrey Matsko, Lute Maleki
OEwaves Inc., 465 North Halstead Street, Suite 140, Pasadena, California 91107, U.S.A.
E-mail: andrey.matsko@oewaves.com

We have developed a miniature frequency modulatable semiconductor laser based on self-injection locking a bare diode to a whispering gallery mode microresonator. The laser is characterized with frequency noise better than 300 Hz/Hz$^{1/2}$ at offset frequencies ranging from 10 Hz to 10 MHz. Lasers at 1,550 nm and 795 nm are demonstrated, though lasers at nearly any desired wavelength, for which a diode is available, may be realized with our scheme. We stabilized 795 nm laser by locking it to Rb saturation absorption transition and demonstrating frequency stability better than 10^{-12} for integration time spanning 1 s to 1 day. The residual amplitude modulation measured for the locked laser was below -80dB. Using similar technique we locked the 1,550nm phase modulatable laser to a thermally stabilized microresonator and achieved phase noise of 0 dBc at 10 Hz offset frequency. The demonstrated stability of the locked devices, combined with their compact packages makes them useful for application in atomic clocks, magnetometers, wavelength references and other high precision instruments.

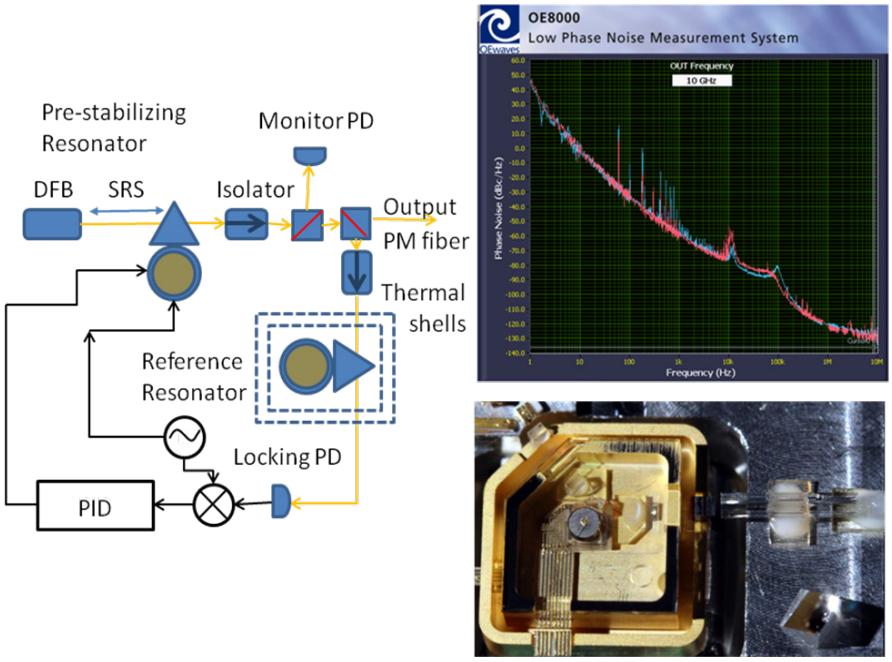


Fig. 1: Schematic of low noise microresonator-stabilized laser. The laser is frequency modulated using PZT-actuated pre-stabilizing resonator and then is locked to a thermally-stabilized reference resonator. Pre-stabilization reduces instantaneous linewidth of the laser to less than 300 Hz. Reference resonator improves long term stability of the laser. The reference resonator was replaced with a Rb atomic cell for 795 nm laser. Top inset: Phase noise of the laser locked to both resonators. Bottom inset: A picture of the reference MgF_2 resonator. The resonator has 2 mm in diameter and 0.1 mm in thickness.

We built the external cavity distributed feedback (DFB) semiconductor laser using a monolithic whispering gallery mode (WGM) resonator. The modulation of the laser frequency was produced via the external cavity (pre-stabilizing resonator in Figure 1). The frequency of the WGM resonator was modified by changing its temperature and by stress applied via a piezo-electric transducer (PZT) actuator. The measured modulation rate was 10 MHz/V, with respect to the voltage at the PZT element. In this scheme the resonant stimulated Rayleigh back-scattering (SRS) is used for self-injection locking. Because self-injection locking feedback is rather fast, it results in significant reduction of the laser phase and, to a lesser extent, amplitude noise, in a broad frequency range. This feedback also allows transferring frequency modulation from the resonator to the laser. Miniature, high performance lasers supporting atomic clocks based on various ions and atoms can be realized with this scheme.

Carrier Phase Frequency Biases in Receivers Used for UTC-Generation

Matsakis, Demetrios, Jiang, Zhiheng*
U.S. Naval Observatory, Washington DC, USA
*Time, Frequency, and Gravimetry Department, BIPM, Sevres, France
E-mail: dnm,@usno.navy.mil

Precise Point Positioning (PPP) uses both code and phase data to determine local parameters, including those of the local time reference. Extremely precise results are obtained when data are well-behaved and consistent within the errors. On the other hand, in cases where the receiver's phase data display a frequency offset compared to the pseudorange it is possible to obtain obviously discrepant solutions, and we will show an example persistently evident between individual days. We report the results of a search for such instrumental discrepancies in data submitted to the BIPM, using typically discarded parameter solutions from multiday solutions.

Long-Term Uncertainty in Time Transfer Using GPS and TWSTFT Techniques

Zhang, Victor, Parker, Thomas, Yao, Jian
Time and Frequency Division, National Institute of Standards and Technology, Boulder, Colorado, U.S.A.
E-mail: vzhang@boulder.gov

The techniques of GPS time and frequency transfer (code based and carrier phase) and two-way satellite time and frequency transfer (TWSTFT) are widely used in remote clock comparison and in the computation of International Atomic Time (TAI). Many timing laboratories in the world utilize both techniques (GPS and TWSTFT transfer links) to compare each other's' clocks. The time transfer accuracy of these links is an important parameter, but in many cases calibration campaigns have been very infrequent due to the expense and lack of suitable equipment. In lieu of repeated calibrations, some information regarding the long-term stability of these links can be obtained through comparisons between the two links (a so called double difference). Without frequent calibrations it is impossible to tell where the instabilities originate, but information regarding the magnitude of the instabilities can be obtained from double difference data. We have been investigating the combined delay variations of GPS and TWSTFT links for a number of laboratory pairs, including both long and short base lines. Our preliminary results show that the relative delay change between GPS and TWSTFT transfer links can be as large as 2 to 3 ns over a few years and that all of the laboratory pairs that have been investigated show similar magnitudes in the double difference data. Currently the longest set of good double difference data is about 8 years. The data point out the need for frequent calibration campaigns if accuracies at the nanosecond level are required.

In this paper, we will present the results of a study of the relative long-term delay changes between GPS and TWSTFT links for timing links between laboratories in Europe and the USA, as well as links within Europe, and in the USA.

Broadband Two-Way Satellite Link Performance for Optical Clock Comparison

F. Riedel[1], E. Benkler[1], J. Leute[1], D. Piester[1], J. Achkar[2], P. Delva[2], D. Rovera[2], I. Sesia[3], G. Cerretto[3], P. Defraigne[4], S. Shemar[5], P.B. Whibberley[5], and H.S. Margolis[5]

[1] Physikalisch-Technische Bundesanstalt, Braunschweig, Germany
[2] LNE-SYRTE / Observatoire de Paris, LNE, CNRS, UPMC, Paris, France
[3] Istituto Nazionale di Ricerca Metrologica, Torino, Italy
[4] Royal Observatory Belgium, Brussels, Belgium
[5] National Physical Laboratory, Teddington, UK

Email: franziska.riedel@ptb.de

Enhancements of the commonly used time and frequency transfer techniques are required to prepare for steering timescales with optical clocks having relative frequency instabilities of less than 10^{-17}. To explore the potential of two-way satellite time and frequency transfer (TWSTFT), we performed a 1-week test of simultaneous broadband (20 Mchip/s) TWSTFT satellite links between the four European national metrology institutes (NMIs) PTB, LNE-SYRTE, INRIM and NPL through ASTRA 3B in the Ku-band. This test prepared for a 3-week optical clock comparison campaign in June 2015.

The 1 Mchip/s TWSTFT employed for regular international clock comparisons is limited to an instability of roughly 10^{-15} at 1 day [1]. To deploy the potential of optical clocks, at least an order of magnitude lower instability at 1 day is required, which in principle is feasible by increasing the TWSTFT chip rate to the maximum of the employed SATRE modems of 20 Mchip/s. However, technical and environmental effects in a real satellite link may obstruct this theoretical limit. In addition to TWSTFT link data, GPS data were recorded. Cs fountains were run at all four NMIs and optical clocks at NPL, OP and PTB. In each institute, a hydrogen maser signal was used as a reliable common reference for the SATRE modems and GPS receivers, as well as for the Cs fountain and optical clock (via an optical frequency comb) frequency measurements.

Here, we present the performance of the broadband TWSTFT satellite links. We observe short-term instabilities of the level of 2×10^{-11} ($\tau = 1$ s). Even though several disturbances can be observed, which at lower chip rates are usually hidden below the link noise, we reach instabilities of 3×10^{-16} at one day (MDEV), limited by the hydrogen masers used. We discuss the origins of the technical disturbances, such as multipath effects and temperature influence. As an independent method, GPS frequency comparisons have been carried out using the precise point positioning (PPP) concept; the performance of these two techniques is compared and discussed.

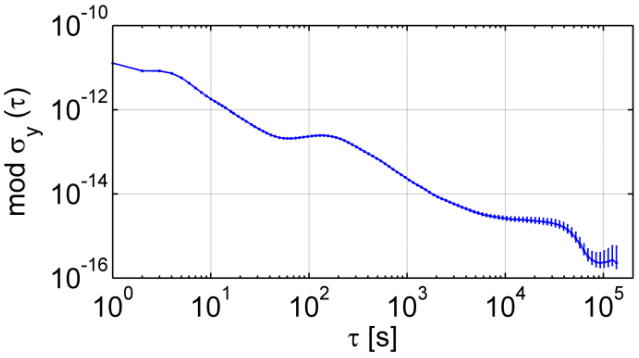


Fig. 1: Modified Allan deviation of a 20 Mchip/s TWSTFT link between OP and PTB.

This work was supported by the European Metrology Research Programme EMRP. The EMRP is jointly funded by the EMRP participating countries within EURAMET and the European Union.

[1] A. Bauch et al., "Comparison between frequency standards in Europe and the USA at the 10^{-15} uncertainty level," Metrologia, vol. 43, pp. 109-120, 2006.

Optical clock evaluation without a hydrogen maser by carrier-phase two-way satellite frequency transfer

Fujieda M, Ido T, Gotoh T, Takiguchi H, Hayasaka K, Toyoda K*, Yonegaki K*, Tanaka U*, Urabe S*
Space-Time Standards Laboratory, National Institute of Information and Communications Technology, Koganei, Japan
*Graduate School of Engineering Science, Osaka University, Toyonaka, Japan
E-mail: miho@nict.go.jp

Frequency evaluation of a remote optical clock is typically performed by an optical frequency comb and a satellite link connected to International Atomic Time (TAI). Conventional satellite links such as GPS and TWSTFT require an integration time longer than some hours to reach an uncertainty in the 10^{-15} level. From this reason, a hydrogen maser whose frequency drift is negligible for some hours is used as a mediate microwave reference in the frequency evaluation of an optical clock. There are not so many institutes that equip a hydrogen maser, however. We developed a frequency evaluation system of an optical clock without a hydrogen maser, where carrier-phase two-way satellite frequency transfer (TWCP) [1] enables to reduce the integration time and track a frequency variation in the 10^{-13} level at 1 second. A microwave signal was generated from a repetition frequency of an optical frequency comb which is stabilized to an optical clock. The 10-MHz reference signal down-converted from the microwave signal was supplied to the TWCP system.

Fig.1 shows the schematic of the frequency evaluation system. We utilized a linearly-trapped single $^{40}Ca^{+}$ ion which was developed at Osaka University for experiments related to quantum information processing [2]. The clock transition frequency ($^2S_{1/2}$-$^2D_{5/2}$, 729 nm) was evaluated. An Yb optical frequency comb was stabilized to the clock laser, where the reference frequency of the optical PLL was adjusted so that the repetition rate was 250 MHz. The 1-GHz signal as the fourth harmonic of the repetition frequency was detected by a photodetector. A 100-MHz VCXO was phase-locked to it and the one-tenth-frequency signal was used as a reference of the TWCP system. The frequency difference relative to UTC(NICT) was measured. The measurements were performed for five days in November of 2014. One measurement continued from several tens of minutes to ninety minutes and total number of measurements was seventeen. As a result, we achieved that the frequency stability of 3×10^{-13} and 4×10^{-15} at 1-sec and 1000-sec averaging times, which includes the instabilities of the TWCP system and optical-to-microwave conversion. Our frequency evaluation system realized the stability compatible to that of a hydrogen maser and could be applied to the remote optical-clock comparison.

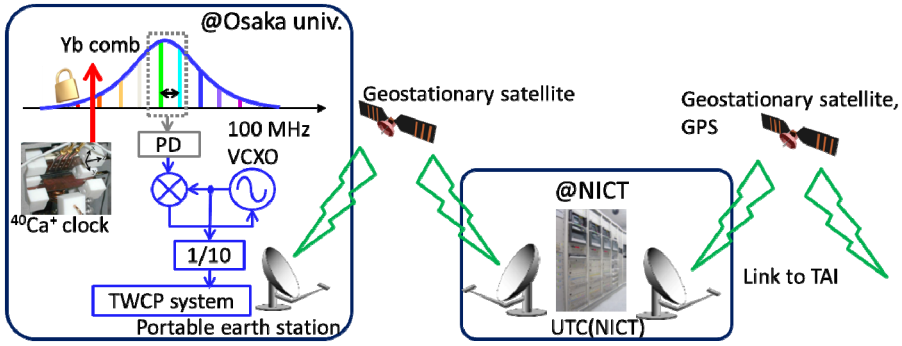


Fig. 1: Schematic of the frequency evaluation system. A portable TWSTFT station was installed at Osaka University. PD: photo detector.

[1] M. Fujieda, D. Piester, T. Gotoh, J. Becker, M. Aida, and A. Bauch, "Carrier-phase two-way satellite frequency transfer over a very long baseline," Metrologia, 51, pp. 253-262, 2014.

[2] A. Noguchi, Y. Shikano, K. Toyoda, and S. Urabe, "Aharonov-Bohm effect in the tunneling of a quantum rotor in a linear Paul trap," Nature Commun. 5, 3868, 2014

CGTTS results with Beidou using the R2CGTTS

W. Huang, P. Defraigne
Royal Observatory of Belgium, Brussels, Belgium
Email: w.huang@oma.be

Measurements from Global Navigation Satellite Systems (GNSS) are used since the eighties to perform precise and accurate Time and Frequency Transfer. Only GPS and GLONASS have been used to date for operational applications. With the development of new navigation satellite systems, the CCTF Working Group on GNSS Time Transfer upgraded the general standard for time transfer, in order to include Galileo, QZSS and Beidou as well. The Beidou constellation is growing with presently 5 MEO and 5 IGSO satellites. The goal of this paper is to present some first results of using Beidou signals for time transfer using this international standard CGTTS V3. We use the RCGGTTS software [1] developed at the Royal Observatory of Belgium (ROB) and upgraded to Beidou, in order to produce the time transfer solutions in the CGTTS format using data from geodetic type receivers providing raw data as well as broadcast ephemeris data in the RINEX 3.02 format [2]. A comparison between the Beidou, GPS, GLONASS and Galileo results will then be proposed.

[1] Defraigne, P. and Petit, G., 2003. Time transfer to TAI using geodetic receivers *Metrologia* **40** 184-188.

[2] RINEX: The Receiver Independent Exchange Format, Version 3.02 ftp://igs.org/pub/data/format/rinex302.pdf

RIOS: first iGMAS tracking station in Brazil

Junqueira, Selma, Rocha, Pedro Senna*, Andrei, Alexandre[+], Cacau, Diego Carriço*
DSHO, Observatorio Nacional/MCTI, Rio de Janeiro, RJ/Brazil
*DSHO, Observatorio Nacional/MCTI, Rio de Janeiro, RJ/Brazil
[+]GPA, Observatorio Nacional/MCTI, Rio de Janeiro, RJ/Brazil
E-mail: selma@on.br

We present the preliminary results obtained from the analysis of data generated by RIOS station (first GNSS iGMAS tracking station in Brazil), installed in August/2014 at Observatorio Nacional of Rio de Janeiro (ONRJ) in partnership with the Astronomical Observatory of Shanghai (SHAO). The goal of the station is to track the satellites of the BEIDOU Chinese constellation and analyze their performances. Figure 1 shows the configuration of RIOS station[1]. To achieve our purpose 2 GNSS receivers were used: a UR4B0 Chinese receiver (Unicore-NovAtel) and a PolaRx4TR (Septentrio). The GNSS receiver UR4B0 is a high precision receiver processing 11 frequency signals from BEIDOU, GPS, GALILEO and GLONASS satellite navigation systems. It is based on NebulasTM multi-system, multi-frequency high performance SoC chip. It tracks BEIDOU B1/B2/B3, GPS L1/L2/L5, GALILEO E1/E5a/E5b and GLONASS G1/G2, with high-precision external clock input and 1PPS output. It provides high-quality raw observation storage and output, remote network upgrade and control firmware, multi-path suppression algorithm in shelter environment and it is equipped with a high gain antenna NovAtel GNSS750. We performed a statistical analysis of carrier codes and phases from BEIDOU and GPS satellites generated continuously and simultaneously by the 2 receivers in a period of 46 days (MJD56918-56964). Initial results obtained with a software, modified from that one available on the BIPM ftp server (ftp: tai.bipm.org, remote directory: /soft/r2cggtts)[2], originally developed to treat GPS and GLONASS time transfer data using P3 method[3], are presented.

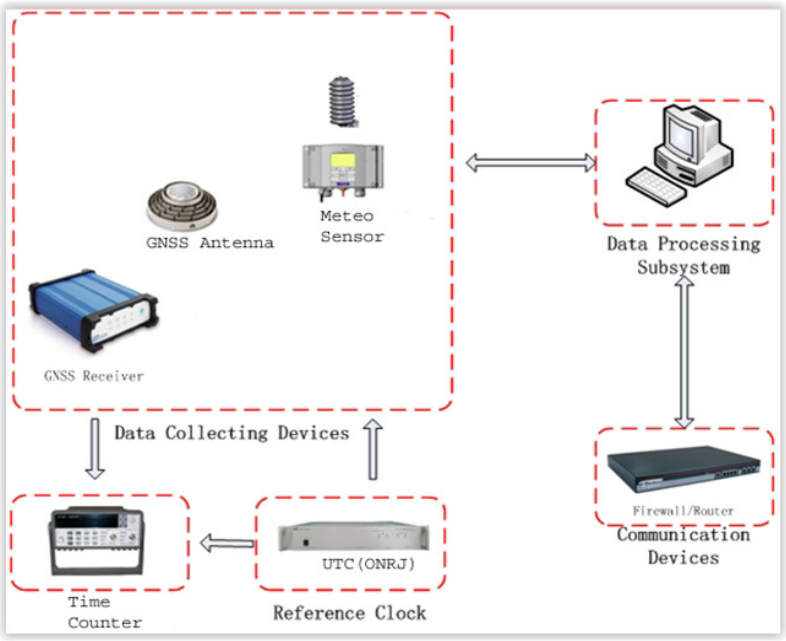


Fig. 1: RIOS iGMAS tracking station configuration

[1] S. Junqueira, E. V. Raymundo, P. Rocha, J. Grosman, and S. Song, “RIOS: first BeiDou monitoring station in Brazil”, 2014 Conference on Precision Electromagnetic Measurements, Rio de Janeiro, Brazil, August 24-29, 2014.

[2] http://www.bipm.org/ws/CCTF/TAI_TRAINING/Allowed/Fundamentals/Training-2012-GNSS-Defraigne.pdf

[3] P. Defraigne, G. Petit, 2004, *"Time Transfer to TAI using geodetic receivers,"* **Metrologia, Vol. 40,** 184-188.

Temperature Stable Silicon and Piezo-MEMS for Timing and Frequency Reference Applications

Pensala, Tuomas
Microelectronic Systems, VTT Technical Research Centre of Finland, Espoo, Finland
E-mail: Tuomas.Pensala@vtt.fi

Silicon MEMS resonators for timing and frequency reference applications have taken significant performance steps in recent years. Of fundamental importance is the temperature stability of Si versus quartz. We have developed passive compensation of Si based on modifying materials properties. In many-valley semiconductor like Si the electronic properties exhibit a coupling to the elastic constants that can be tailored by doping to yield temperature stable resonance modes in properly chosen resonator geometries. The temperature stability can be reached not only in the linear temperature coeffiecient of frequency but also in the second order resulting in Si MEMS resonators on par with quartz in temperature stability: we report frequency within ±15 ppm over -40 to +85 C range (Fig. 1.)

As Si is not intrinsically piezoelectric like quartz, the driving force for oscillation has to generated either electrostatically, thermally, or by an integrated piezoelectric thin film transducer. We have developed a versatile AlN-on-CSOI piezoMEMS platform with various advantages and some trade-offs as compared to electrostatic MEMS. We report work in improving the electromechanical coupling coefficient K^2 of the resonators up to 0.3 % via using piezo-drive and discuss the other benefits and drawbacks of the approach. Other applications of the piezo-MEMS platform, including the possiblities opened up by introducing ScAlN with much stronger piezoelectric effect than that of AlN in strength are discussed.

As an application demonstration, we report an agressively miniaturised integrated generic timing system performing real time clock and on-demand programmable frequency synthesizer developed in the Go4Time project. This system utilises piezo-actuated AlN-on-CSOI MEMS platform to co-integrate a 440 kHz tuning fork resonator for the RTC function with an 26 MHz bulk wave resonator for the frequency reference, metal-based wafer level sealing, and Cu through-Si vias. The oscillator IC is matched in size to the MEMS die.

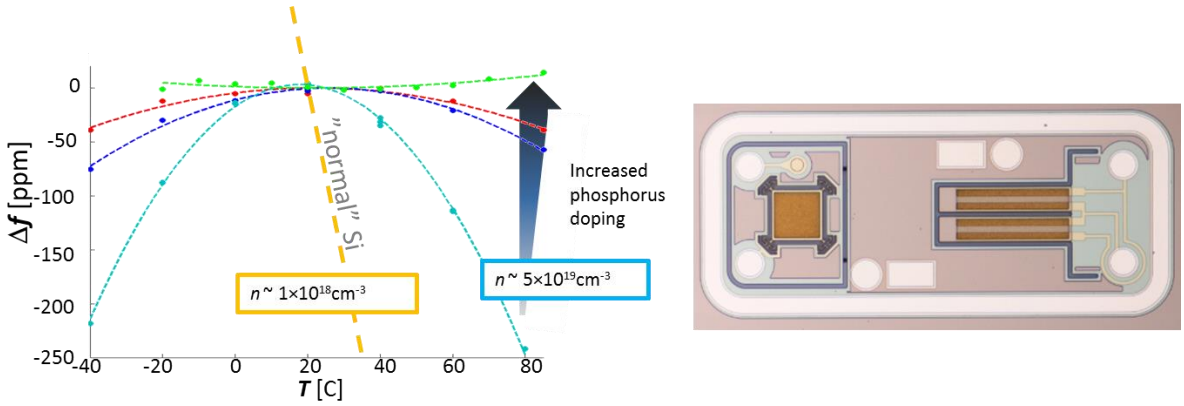


Figure 1 : Frequency vs. Temperature curves for resonators having different levels of compensation doping (left). Photograph of the Go4Time dual-resonator chip with a 26 MHz square resonator and 440 kHz tuning fork, both piezo-driven (right).

Quality Factors of Quartz Crystal Resonators Operating at 4 Kelvins

Galliou Serge, Abbé Philippe, Goryachev Maxim*, Tobar Michael* and Bourquin Roger

Time and Frequency Dept., FEMTO-ST Institute, UFC, CNRS, ENSMM, UTBM, Besançon, France
* ARC CE for Engineered Quantum Systems, School of Physics, University of Western Australia, Crawley, Australia
E-mail: serge.galliou@femto-st.fr

Recently, quality factors greater than 1 billion have been measured on bulk acoustic wave quartz crystal resonators working at liquid-helium temperature [1]. This feature offers the opportunity to use such low-loss resonators as acoustic cavities in quantum hybrid systems or similar physical experiments [2]. Beyond this specific use, such high-Q resonators are obviously also attractive for applications involving frequency sources.

Nevertheless, all the tested resonators do not exhibit Q-factors greater than 1 billion at 4 K. Indeed, Q-factors of some of them can even be limited to just a few tens of millions. This depends on various factors or conditions that are discussed in this paper. The tested resonators are state-of-the-art devices, typically SC-cuts initially optimized to work at 5 or 10 MHz at room temperature. Actually, it is shown that such Q-measurements can reveal defects invisible at room temperature but becoming predominant when resonators operate at low temperature.

Firstly, a short review reminds that the devices under test are operating in the Landau-Rumer regime for which the usual relationship $Qxf = const.$ does not hold anymore. Then the analysis is mainly based on a new set of experimental data extracted from resonators tested within [3.5 K – 12 K] over a wide range of overtones of A, B, and C modes, up to 300 MHz.

As a matter of fact, it is shown that Q-values differ from one design to another, according to engineering options, as expected or not. In addition, Q-values depend on the vibration mode, and of course on the material quality. Nonlinearities are also considered with regard to the issue of the energy stored inside the device.

[1] S. Galliou, M. Goryachev, R. Bourquin, P. Abbé, J. Aubry, and M. Tobar, "Extremely Low Loss Phonon-Trapping Cryogenic Acoustic Cavities for Future Physical Experiments," Scientific Reports 3: 2132, 2013.

[2] M. Aspelmeyer, T. J. Kippenberg, F. Marquardt, "Cavity Optomechanics " arXiv:1303.0733 [cond-mat.mes-hall], accepted for publication in Review of Modern Physics, 4 June 2014.

Frequency tuning with lithium niobate composite BAW resonators

N.Boudou, J.S.Moulet, L.Benaissa, G. Audoit, A.Reinhardt
Univ. Grenoble Alpes, F-38000 Grenoble, France
CEA, LETI, MINATEC Campus, F-38054 Grenoble France
E-mail: nicolas.boudou@cea.fr

The multiplication of telecommunications bands dramatically increases the complexity, size and cost of mobile terminals RF front-ends. Therefore, the introduction of tunability in these architectures becomes mandatory. This requires RF resonators and filters capable to be tuned over different communication standards [1]. In this context, tunable composite piezoelectric resonators, in which a piezoelectric layer serves as a tuning layer and another one as a transducer, have been identified as a promising way to add tunability in BAW resonators [2]. Modifying the electrical boundary conditions across the tuning layer, for instance by using a tuning capacitor, induces a frequency shift of the whole resonator response. Since the structure is a composite resonator and the tuning mechanism is directly induced from the electromechanical nature of the acoustic waves exploited only materials showing very high piezoelectric properties allow an acceptable trade-off between effective resonator electromechanical coupling factor and tuning range. Single-crystal X-cut lithium niobate ($LiNbO_3$) was therefore identified as the best candidate for such tunable RF filters [2]. However, so far, no experimental demonstration of composite $LiNbO_3$ resonators has been shown.

In this paper, we demonstrate the tunability of a $LiNbO_3$ composite resonator. We first present the fabrication of a composite resonator made of two layers of single-crystal X-cut $LiNbO_3$ film on top of a silicon wafer, each of them sandwiched between two electrodes, as presented in Fig.1. As $LiNbO_3$ cannot be grown with an a-axis orientation, we used successive steps of wafer bonding and thinning, ending up in $LiNbO_3$ film thicknesses lying around 7 µm.

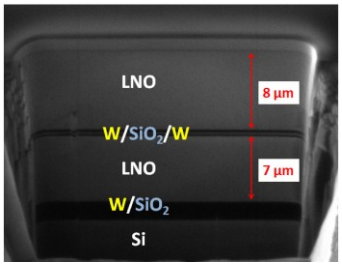


Fig. 1: Cross-section SEM imaging of the $LiNbO_3$/ $LiNbO_3$ composite resonator stack

Electrical characterization presented in Fig.2 of this composite resonator reveals the first three thickness shear overtones of the complete composite stack, providing a first confirmation of the operation as a composite resonator and of the quality of the bonding between transferred layers.

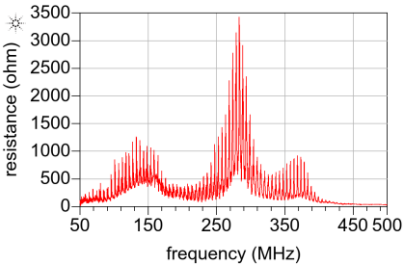


Fig. 2: Electrical response of the composite resonator

Finally, we accessed buried tuning electrodes via plasma FIB etching. By measuring the resonator with and without short-circuiting theses electrodes, we were able to measure the electric response with two extreme electrical boundary conditions applied across the tuning layer, and thus to quantify the frequency tunability: a shift of 10 MHz of the 265 MHz resonance peak is measured after short-circuiting the tuning electrodes. This is in line with theoretical evaluations for the precise configuration of the resonator, hence validating the concept of tunable composite resonator, and opening new perspectives towards further developments of this technology.

[1] R. Aigner, "Tunable Acoustic RF-Filters: Discussion of Requirements and Potential Physical Embodiments", in *Proc. 40th European Microwave Conference*, 2010, pp. 787-790

[2] A. Reinhardt, E. Defaÿ, F. Perruchot, C. Billard, "Tunable Composite piezoelectric resonators: a possible "Holy Grail" of RF filters?" *2012 IEEE MTT-S International Microwave Symposium Digest*

Analysis of Contributions of Nonlinear Material Constants to Temperature-induced Velocity Shifts of Quartz and Langasite Surface Acoustic Wave Resonators

Haifeng Zhang[1], John A. Kosinski[2] and Lei Zuo[3]

[1]Department of Engineering Technology, University of North Texas, Denton, TX, 76207
[2]MacAulay-Brown, Inc., Advanced Technology Group (ATG), Dayton, OH 45430
[3]Department of Mechanical Engineering, Virgina Tech., Blacksburg, VA 24061

Email: haifeng.zhang@unt.edu

Temperature-induced surface acoustic wave (SAW) velocity shifts are analyzed for quartz and langasite SAW resonators. The analytical methodology has been verified by comparing experimental results and analytical results for quartz resonators. Sensitivity of the analytical results to different groups of nonlinear material constants (third-order elastic constants (TOE), third-order piezoelectric constants (TOP), third-order dielectric constants (TOD) and electrostrictive constants (EL)) for SAW quartz resonators is discussed; it was found that in general, the third-order elastic constants contribute most significantly to the wave velocity shift. The contribution from the third-order dielectric constants and electrostrictive constants are negligible. For some specific cases, the elimination of the third-order piezoelectric constants may cause significant errors. The sensitivity of each third-order elastic constants to the temperature-velocity effect is analyzed by applying 10% error to the third-order elastic constants separately. The analysis for SAW quartz resonators has been extended to langasite SAW resonators as well. It is worthy to mention that commonly used thermoelastic expansions provide a good but not exact description of the temperature effects on frequency in piezoelectric resonators. These commonly used expansions do not include the effects of higher order material constants. In this paper we examine the significance of the various higher order effects as regards calculating temperature behavior from a set of material constants and their temperature coefficients. Fig. 1 shows an exemplar analysis for an X-cut SAW quartz resonator.

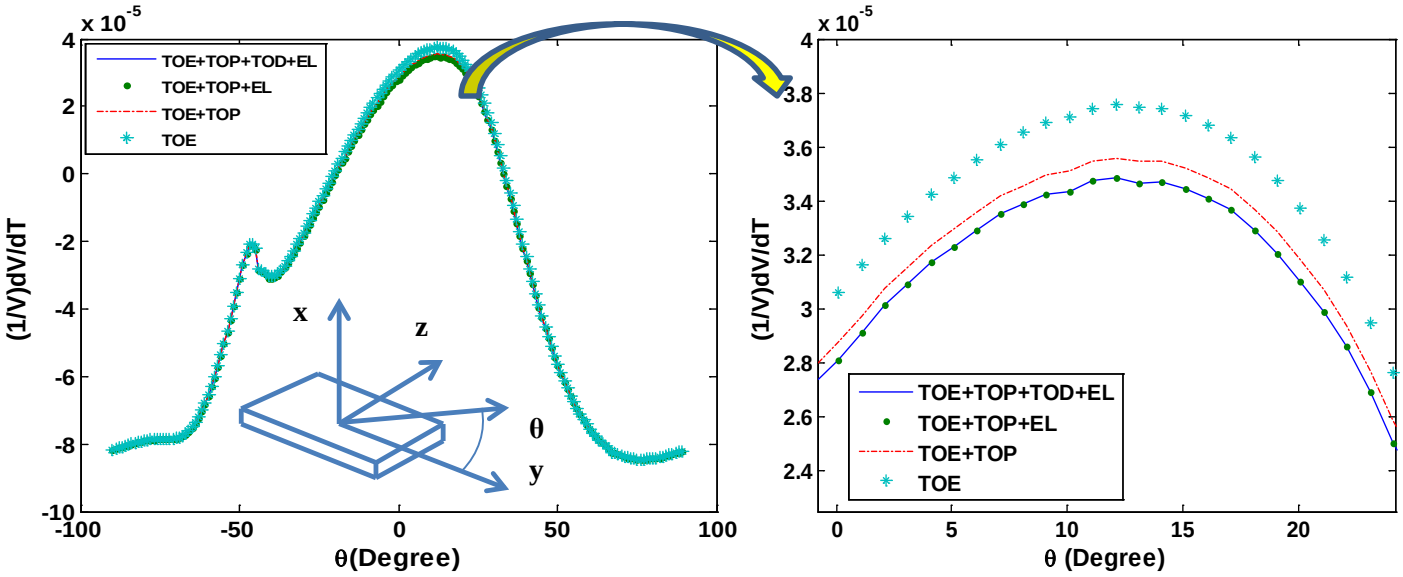


Fig. 1. The sensitivity analysis for temperature-induced velocity shifts as a function of wave propagation direction (θ) for an X-cut SAW quartz resonator. (a) The sensitivity analysis; (b) The enlarged view.

Tungsten oxide as high acoustic impedance material for fully insulating acoustic reflectors

DeMiguel-Ramos M., González S., Clement M., Mirea T., Olivares J., Iborra E.
GMME-CEMDATIC. ETSI de Telecomunicación Universidad Politécnica de Madrid, Spain
E-mail: mmramos@etsit.upm.es

Bulk acoustic wave (BAW) resonators are currently applied in various fields, such as telecommunications or sensors, showing excellent performance. The confinement of the acoustic energy in the piezoelectric area is a major concern for BAW designers and fabricators, because it affects the quality factor of the device. Two different structures are used to achieve this confinement, the free-standing bulk acoustic wave resonator and the solidly mounted resonator (SMR). This last technology displays some advantages in terms of robustness and ease of fabrication, and is based on the use of a stack composed of alternated high and low acoustic impedance layers that reflects almost completely the acoustic energy. The mismatch between the high and low acoustic impedance (Z_A) of the two materials used in the stack must be as high as possible, and depends directly on the density (ρ) and the acoustic velocity (V_A) of the material ($Z_A=\rho \cdot V_A$). To this end, metals such as Mo, Ir or W are used as high acoustic impedance layer and SiO_2 is used as low acoustic impedance layer. However, the use of metallic layers in the reflector is very damaging for certain applications, especially when the contacts must be extended, because the parasitic capacitance generated between the line and the first metallic layer of the reflector destroys the signal of the device and causes cross-talk between different ones. To overcome this problem alternative high acoustic impedance insulating materials, such as AlN or Ta_2O_5, are used. However these materials offer much lower acoustic impedances compared to metals, which forces fabricators to increase the number of layers of the reflector, making the fabrication process more difficult.

In this work we present high-electrical-resistivity sputtered tungsten oxides (WO_x) as high acoustic impedance layer for fully insulating acoustic reflectors. We have deposited different layers by varying the concentration of oxygen between 50% and 100%, while maintaining the pressure (1 mTorr) and the power applied to the target (1200 W). We have characterized the material using X-Ray diffraction (XRD) and infrared reflectance spectroscopy (R-IR). The density of the material was assessed by X-Ray reflection (XRR). We have measured both the shear and the longitudinal acoustic velocities by inducing a half wavelength standing wave in the WO_x layer under study placed into an AlN-based SMR, as explained in [1].

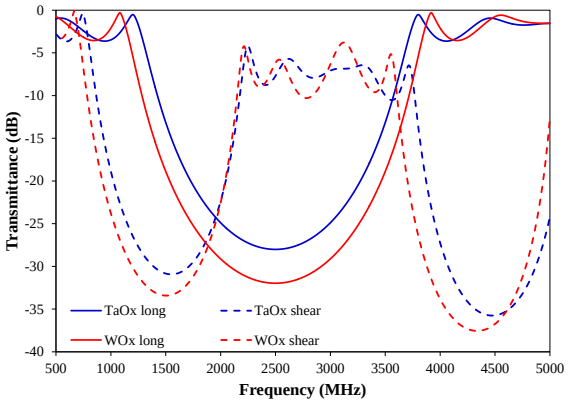


Fig. 1: Transmittance of the five-layer acoustic reflectors

We have obtained WO_x thin films that display a density of 7080 kg/m^3, and longitudinal and shear acoustic velocities of 6900 m/s and 3800 m/s, respectively. These values give a Z_A considerably higher than that obtained for the most used insulating high acoustic impedance materials (AlN and Ta_2O_5). Figure 1 compares the reflectivity of both the shear mode and the longitudinal mode for acoustic reflectors using WO_x and Ta_2O_5 as high acoustic impedance layer. It can be observed that the acoustic reflectivity increases considerably with the WO_x.

[1] J. Capilla, J. Olivares, M. Clement, J. Sangrador, E. Iborra, and A. Devos, "High-acoustic-impedance tantalum oxide layers for insulating acoustic reflectors.," *IEEE Trans. Ultrason. Ferroelectr. Freq. Control*, vol. 59, no. 3, pp. 366–72, Mar. 2012.

Primary frequency standard NPL-CsF3: first results

Lea S N[1], Głowacki P[2], Acharya A[3], Liu K[4], Marra G[1], Johnson L A M[1], Kyriacou S[1], King S A[1], Williams R A[1], Margolis H S[1], Gibble K[5], and Szymaniec K[1]

[1]National Physical Laboratory, Teddington, United Kingdom
[2]Poznan University of Technology, Poznan, Poland
[3]National Physical Laboratory India, New Delhi, India
[4]National Institute of Metrology, Beijing, China
[5]The Pennsylvania State University, University Park, PA, USA
E-mail: stephen.lea@npl.co.uk

NPL-CsF3 is a new caesium fountain made operational recently at the National Physical Laboratory. Its main features are in common with the fully evaluated standard NPL-CsF2, which has already been regularly contributing to the evaluations of TAI/UTC scale: a single-stage vapour-loaded magneto-optical trap as the source of cold atoms, easy to align (0,0,1) optical configuration, and accumulation of the $m_F = 0$ sublevel population by optical pumping. The latter requires only a minor modification to the optical set-up with no additional lasers and gives a 5-fold increase in the number of atoms reaching detection. This relatively simple physics package nevertheless yields a short-term stability and a type B uncertainty similar to that achieved by more complex devices. The potentially high cold collision frequency shift is approximately cancelled by manipulation of the atomic cloud size before launch and the clock state population probabilities [1]. The distributed cavity phase (DCP) frequency shift is minimised in a newly designed Ramsey cavity [2]. The cavity is the major novelty in this new fountain and we present experimental verification of reduction of the $m = 0$ and $m = 1$ components of the DCP shift.

The short-term stability, as in NPL-CsF2, is normally limited at 1.5×10^{-13} at 1 s by a room temperature quartz-based local oscillator. Using an interrogation signal synthesized from an ultra-stable laser by means of a femtosecond optical frequency comb, we demonstrate short-term stability of 3.7×10^{-14} at 1 s (fig. 1); from the highest atom number observed in detection we infer an even lower value of 2.5×10^{-14}. The master laser for this optical local oscillator (OLO) is stabilized to a 30 cm-long ultra-stable optical cavity [3]. The OLO stability is transferred to 9.21 GHz using a transfer oscillator scheme to eliminate comb instability [4].

Further improvements of the new set-up aim to ensure more robust operation and include: an integrated electronic control unit, repumper light obtained by a sideband of the master laser frequency generated by an electro-optic modulator, and a compact optical set-up for cooling and detection.

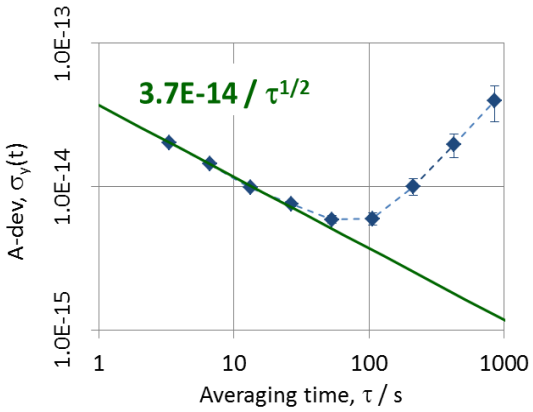


Fig. 1: Improved short-term stability obtained with the OLO. The OLO was drifting at a rate of approximately 1×10^{-16} s^{-1}.

[1] K. Szymaniec and S. E. Park, "Primary Frequency Standard NPL-CsF2: Optimized Operation near the Collisional Shift Cancellation Point," IEEE Trans. Instrum. Meas., vol. 60, pp. 2475–2481, 2011.

[2] K. Gibble, S. N. Lea, and K. Szymaniec, "A microwave cavity designed to minimize distributed cavity phase errors in a primary cesium frequency standard," 2012 Conference on Precision Electromagnetic Measurement, pp. 700–701, 2012.

[3] S. A. Webster and P. Gill, "Low-thermal-noise optical cavity," Proceedings of the 2010 IEEE International Frequency Control Symposium, pp. 470–473 2010.

[4] B. Lipphardt, G. Grosche, U. Sterr, Chr. Tamm, S. Weyers, and H. Schnatz, "The Stability of an Optical Clock Laser Transferred to the Interrogation Oscillator for a Cs Fountain," IEEE Trans. Instrum. Meas, vol. 58, pp. 1258–1262, 2009.

Operation of the KRISS-F1(Cs) Fountain Clock with a Cryocooled Sapphire Oscillator

Sang Eon Park, Myoung-Sun Heo, Taeg Yong Kwon, Kurt Gibble*, John G. Hartnett+, Andre N. Luiten+, Ashby Hilton+, Sang-Bum Lee, Hyun-Gue Hong, Chang Yong Park, Won-Kyu Lee, Dai-Hyuk Yu

Center for Time and Frequency, Korea Research Institute of Standards and Science, Daejeon 305-340, Korea
*Department of Physics, The Pennsylvania State University, University Park, Pennsylvania 16802, USA
+IPAS and the School of Physical Sciences, University of Adelaide, Adelaide 5005, Australia
E-mail: parkse@kriss.re.kr

The short-term stability of a microwave atomic fountain clock using a room-temperature quartz-crystal oscillator (XO) as a local oscillator (LO) is mostly limited by the short-term stability of the XO, near several 10^{-13} at 1-s integration time [1, 2]. Therefore it takes more than 10 days to reach the 10^{-16} frequency stability level. An ultra-low-phase-noise microwave source enables quantum-projection-noise limited performance of an atomic fountain clock. There are two common ways to realize such a low noise local oscillator. Recently, ultra-low noise microwave signals have been extracted from an optical frequency comb by locking it to an ultra-stable optical reference cavity [2, 3]. Here we use the established technique of a liquid helium Cryocooled Sapphire Oscillator (CSO) to generate an ultra-stable X-band signal [4].

Our CSO implementation is collaboration with the University of Adelaide under an ARC (Australian Research Council) Linkage project. A closed system ultra-low-vibration pulse-tube cryocooler reduces the operating cost. The CSO is the source for a new low-noise frequency synthesizer we developed for the KRISS-F1 Cs/Rb dual fountain. The short-term stability of KRISS-F1(Cs) is 5×10^{-14} at 1-s integration time with MOT (magneto-optical trap) operation.

The total uncertainty of the KRISS-F1(Cs) with optical molasses operation was evaluated to be 5.6×10^{-16} when the BVA XO was used as a LO. At the end 2014 the KRISS-F1 was moved to a new building with improved temperature and humidity control. We will now reevaluate the uncertainty using the CSO. We anticipate a lower uncertainty of KRISS-F1(Cs) along with a shorter duration of the uncertainty evaluation with the CSO.

[1] G. Santarelli et al., "Quantum Projection Noise in an Atomic Fountain: A High Stability Cesium Frequency Standard," Phy. Rev. Lett., vol. 82, pp. 4619-4622, 1999.

[2] S. Weyers et al., "Reaching the quantum limit in a fountain clock using a microwave oscillator phase locked to an ultrastable laser," Phy. Rev. A, vol. 79, pp. 031803(R), 2009.

[3] J. Millo et al., "Ultralow noise microwave generation with fiber-based optical frequency comb and application to atomic fountain clock," Appl. Phys. Lett., vol. 94, pp. 141105, 2009.

[4] J. G. Hartnett et al., "Ultra-low-phase-noise cryocooled microwave dielectric-sapphire-resonator oscillators," Appl. Phys. Lett., vol. 100, pp. 183501, 2012.

The Microwave Lensing Frequency Shift

Kurt Gibble
Department of Physics, The Pennsylvania State University, University Park, PA USA
E-mail: kgibble@psu.edu

The lensing of atomic wave functions by resonant microwave dipole forces leads to a frequency shift of fountain clocks. The calculated biases for several primary frequency standards are 0.6×10^{-16} to 0.9×10^{-16} [1-5], a fraction of their total inaccuracies, which are as low as 2×10^{-16}. More recently, two primary standard evaluations have treated this systematic differently [6-8]. Both use models that predict no shift for infinitesimally small microwave amplitudes, whereas the previous treatments yield a generally non-zero shift in this limit. One evaluation reports a total inaccuracy of 1.1×10^{-16} [6,9], whose largest contribution is the microwave lensing shift in combination with other microwave amplitude dependent shifts, such as microwave leakage.

We will describe the behavior of the lensing shift in the limit of zero microwave amplitude. In this limit, dipole forces go smoothly to zero and therefore give a perturbation to the transition probability that also goes to zero. To get the frequency shift, the perturbation of the transition probability is divided by the Ramsey fringe amplitude, which also goes to zero, resulting in a constant and generally non-zero frequency shift.

The small amplitude limit has an interesting connection to photon recoil frequency shifts [1,10], for example, of optical frequency transitions. Standing wave excitations are necessarily multi-photon absorptions of traveling wave photons. For small amplitudes, only a coherent excitation from two counter-propagating photons has to be considered. The destructive interference near the antinode of a standing wave yields the microwave lensing frequency shift for an atomic wave function that is much smaller than the microwave wavelength [1,10]. Allowing the size of the wave packet to grow, our treatment smoothly transitions to the well-known photon recoil frequency shift. As expected, the recoil shift we calculate is non-zero in the limit of small field amplitudes.

[1] K. Gibble, "Difference between a Photon's Momentum and an Atom's Recoil," Phys. Rev. Lett. **97**, 073002, 2006.

[2] K. Gibble, "Ramsey Spectroscopy, Matter-Wave Interferometry, and the Microwave Lensing Frequency Shift," Phys. Rev. A **90**, 015601, 2014.

[3] R. Li, K. Gibble, and K. Szymaniec, "Improved accuracy of the NPL-CsF2 primary frequency standard: evaluation of distributed cavity phase and microwave lensing frequency shifts," Metrologia **48**, 283-289, 2011.

[4] S. Weyers, V. Gerginov, N. Nemitz, R. Li and K. Gibble, "Distributed cavity phase frequency shifts of the caesium fountain PTB-CSF2," Metrologia **49**, 82–87, 2012.

[5] J. Guéna, M. Abgrall, D. Rovera, Ph. Laurent, B. Chupin, M. Lours, G. Santarelli, P. Rosenbusch, M. E. Tobar, R. Li, K. Gibble, A. Clairon, and S. Bize, IEEE Trans. Ultrason. Ferroelectr. Freq. Control **59** 391–410, 2012.

[6] T. P. Heavner, E. A. Donley, F. Levi, G. Costanzo, T. E. Parker, J. H. Shirley, N. Ashby, S. Barlow and S. R. Jefferts, "First accuracy evaluation of NIST-F2," 2014 Metrologia **51** 174–182.

[7] N. Ashby, S. Barlow, T. P. Heavner and S. R. Jefferts, "Frequency shifts in NIST Cs primary frequency standards due to transverse RF field gradients," arXiv:1404.4101v2, 2014.

[8] Levi F, Calonico D, Calosso C E, Godone A, Micalizio S, and Costanzo G A, 2014 "Accuracy evaluation of ITCsF2: a nitrogen cooled caesium fountain," Metrologia, **51**, 270–284.

[9] K. Gibble, 'Comment on "First accuracy evaluation of NIST-F2,"' 2015 Metrologia **52**, 163-166.

[10] P. Wolf and Ch. Borde, "Recoil Effects in Microwave Ramsey Spectroscopy," quant-ph/0403194, 2004.

High Stability Comparison of Atomic Fountains using two Different Cryogenic Oscillators

Abgrall M.[1], Guéna J.[1], Lours M.[1] , Santarelli G[1], Tobar M. E. [2], Bize S.[1], Grop S.[3], Dubois B.[3], Fluhr Ch.[3], Giordano V[3]

[1]SYRTE, Observatoire de Paris – LNE- CNRS –UPMC, Paris, France
[2]School of Physics, University of Western Australia, Crawley, Australia
[3]Time and Frequency Dpt., FEMTO-ST Institute, Besançon, France
E-mail: michel.abgrall@obspm.fr

It is well known that the use of an ultra-stable reference based on a cryogenic sapphire oscillator (CSO) benefits to the stability of atomic fountains that can then be operated at the quantum projection noise limit [1, 2, 3]. A stability of 1.6×10^{-14} at 1 s has been demonstrated at SYRTE in FO2Cs using a CSO developed by University of Western Australia (UWA), together with dedicated ultra-low noise synthesizers [4]. The CSO signal, once slowly phase locked to a hydrogen maser, is at the basis of the ultra-stable reference that is in continuous operation at SYRTE since more than 10 years. Thanks to this reference, the fountains operate routinely with a stability of $\sim 4 \times 10^{-14}$ at 1 s for many applications, such as improving the accuracy evaluations, real time steering of the local timescale UTC(OP) or contributing to international timescales.

This paper presents the results of an experiment performed in collaboration with FEMTO-ST that develops state of the art CSO systems. The transportable CSO ULISS [5] was set-up at SYRTE for a few months. This CSO operates with a pulse-tube cryocooler, whereas the UWA CSO has to be periodically helium refilled. Both CSO systems include an ultra-low noise synthesizer including a DDS for phase-locking the output signal on a common hydrogen maser with a time constant of about 1000 s, in order to compensate the frequency drift of the oscillators. The main output signals are at 10 GHz and 11.98 GHz respectively. Signals at 100 MHz and 1 GHz are also generated by the synthesizers. We will present the characterization of the two independent set-ups based on the two CSOs, leading to relative frequency instabilities below 10^{-15}.

Next, we compared the operation of two fountains referenced to the two different CSOs. For this test, the cesium part of FO2 dual fountain was operated using the down conversion to 9.192… GHz of the 11.98 GHz signal provided by the UWA CSO, as usual, while the 6.834… GHz synthesizer of FO2Rb was referenced to the 1 GHz output of ULISS. The differential stability between the two fountains was found the same as for measurements with a common CSO, except for a small bump at a few thousand seconds. Concerning accuracy, FO2Cs and FO2Rb remained in agreement within $\sim 1 \times 10^{-16}$ during the measurement campaign, compared to previous comparisons with a common CSO.

[1] C. Vian, et al., "BNM-SYRTE Fountains: Recent Results," IEEE Trans. Instrum. Meas., vol. 54, p. 833, 2005.

[2] J. Guéna, et al., "Progress in atomic fountains at LNE-SYRTE", IEEE Trans. Ultrason. Ferroelectr. Freq. Control,59 (.3), 391-410, 2012.

[3] A. Takamizawa, et al, "Atomic Fountain Clock With Very High Frequency Stability Employing a Pulse-Tube-Cryocooled Sapphire Oscillator", IEEE Trans. Ultr. Ferr. Freq. Contr., vol. 61, no. 9, p1463, 2014

[4] D. Chambon, et al, "Design and metrological features of microwave synthesizers for atomic fountain frequency standard," IEEE Trans. Ultr. Ferr. Freq. Contr., vol. 54, p. 729, 2007.

[5] S. Grop, Ch. Fluhr, B. Dubois, J-L. Masson,Y. Kersale, E. Rubiola, G. Haye and V. Giordano: "*Latest Improvements in the Performances of a Cryogenic Sapphire Oscillator",* Proceedings of the 2014 EFTF, 23-26 June 2014, Neuchâtel (CH)

Precision Measurements of Quantum Scattering Phase Shifts through Feshbach Resonances

Aaron Bennett and Kurt Gibble
Department of Physics, The Pennsylvania State University, University Park, PA USA
E-mail: awb5334@psu.edu

We precisely measure quantum scattering phase shifts of ultracold cesium atoms through a series of Feshbach resonances. Using an atomic fountain clock, we scatter atoms in a coherent superposition of the clock states off target atoms in another F, m_F state. Excluding the forward scattering direction and detecting only scattered atoms, the Ramsey fringes in Fig. 1 have a phase shift that is the difference of the clock states' quantum scattering phase shifts for scattering off of the target atoms [1].

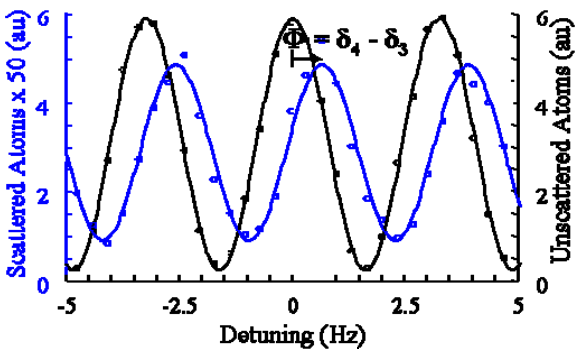


Fig. 1: The Ramsey fringes of scattered atoms have a phase shift Φ, which is the difference of quantum scattering phase shifts.

In a previous experiment [2], we juggled two clouds of atoms and used this technique to observe a series of Feshbach resonances for magnetic fields up to 1.8 G and collision energies between 12 and 50 μK. At these energies, even low 400 nK cloud temperatures give a spread of collision energies of order 10 μK, broadening the resonances.

Here, we instead collide atoms within a single cloud with collision energies less than 1 μK, giving a much smaller spread of collision energies. Fig. 2 shows variations of the scattering phase shifts of nearly π through Feshbach resonances. The error bars are statistical, and comparable to our systematic error bars. We have developed an extensive mathematical model of the experiment and account for the systematic errors from cold collision frequency shifts, inelastic spin-exchange collisions, and several measurement backgrounds. We use target atoms in all F, $m_F \neq 0$ target states to accurately probe the phase variations through a number of Feshbach resonances.

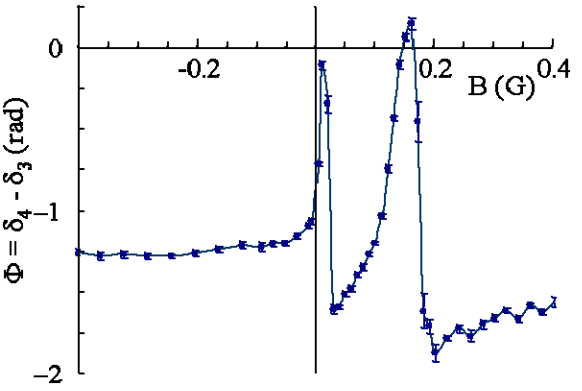


Fig. 2: Difference of scattering phase shifts vs. magnetic field for clock atoms scattering off of target atoms in F=3, m_F=3. Feshbach resonances at 0.02 and 0.18 G produce large variations of the scattering phase shifts.

These measurements promise a precise picture of cesium interactions that can resolve existing discrepancies. A precise picture is in turn expected to significantly reduce the uncertainty of the size and sign of the ultracold collision frequency shift for laser-cooled space clocks. An improved understanding of the cesium interactions may also enable this technique to set stringent limits on the time variation of fundamental constants, such as the electron-proton mass ratio, by observing the constancy of the scattering phase shifts near these narrow Feshbach resonances [3].

[1] R. Hart, X. Xu, R. Legere, and K. Gibble, "A quantum scattering interferometer," *Nature* **446**, 892-895, 2007.

[2] S. D. Gensemer, R. B. Martin-Wells, A. W. Bennett, and K. Gibble, "Direct Observation of Resonant Scattering Phase Shifts and Their Energy Dependence," *Phys. Rev. Lett.* **109**, 263201, 2012.

[3] C. Chin and V. V. Flambaum, "Enhanced Sensitivity to Fundamental Constants in Ultracold Atomic and Molecular Systems near Feshbach Resonances," *Phys. Rev. Lett.* **96**, 230801, 2006.

Bias Corrections in Primary Frequency Standards

Parker, Thomas E., Heavner, Thomas H., Jefferts, Steven R.
National Institute of Standards and Technology, 325 Broadway, Boulder, CO/USA
Email: tparker@boulder.nist.gov

Primary frequency standards (PFS) serve the function of calibrating the rate (frequency) of International Atomic Time, TAI, and therefore play a critical role in the accuracy of the world's time. The Working Group on Primary and Secondary Frequency Standards, WGPSFS, is an advisory body to the Time Department of the International Bureau des Poids et Mesures, BIPM, and to the Consultative Committee for Time and Frequency, CCTF, on matters related to primary and secondary frequency standards that are used to determine the rate of TAI. A current issue to be considered by the WGPSFS is establishing guidelines for deciding when and how to make corrections for newly discovered frequency biases in primary frequency standards. This paper is intended to generate discussions on this topic in an audience wider than just the WGPSFS.

First a historical retrospective will be presented using a few biases that have been included as corrections to PFS that report to BIPM. These include biases that were once corrected and no longer are, biases that were unrecognized until long after the definition of the second and have now been included in all PFS bias tables, as well as corrections that are outside of the definition of the SI second but are applied for the generation of TAI.

The Millman effect is an example of a frequency bias that was once applied to some PFS. The correction was a generalization of an effect that had long been recognized in atomic beam physics. The generalization was accepted and a "correction" applied in spite of the fact that no experimental evidence of the effect existed. Wineland & Hellwig later showed that, in fact, the physics of the effect was incorrectly described and that the frequency shift was not allowed on the clock transitions in Cs [1]. Consequently, the frequency bias was no longer considered in PFS. The Blackbody correction is a good example where a previously unknown frequency bias of significant magnitude was proposed theoretically, measurements were made to confirm it, and it was formally recommended by the CCTF in 1996. This bias is unusual in that it actually required a clarification to the formal definition of the second [2]. When the accuracy of clocks and frequency standards improved to the level where shifts due to relativity needed to be included, there was no consensus on how this was to be accomplished. For example, for some period TAI was incorrectly considered a form of *proper time* rather than *coordinate time*. While the gravitational redshift was experimentally verified in the late 1950s, it was not until 1991 that the IAU adopted the specific metric for use in comparing frequency standards which is in use today [3]. The gravitational red shift correction is, in fact, not part of the definition of the second, but is part of the implementation of TAI.

Currently the situation exists where a significant bias correction is being applied to some PFS based on a theoretical calculation with no experimental confirmation, and that is not universally accepted. It is this current issue that prompted the more general discussion here pertaining to when and how "new" biases should be applied to PFS.

In addition to the above specific issue, there is an even more general question of how to assign a total uncertainty in situations where there are very likely unknown biases. In most cases these are usually sufficiently small as to have a negligible impact on the total uncertainty, but there are exceptions. For example, with the blackbody correction, nearly all PFS were uncorrected for this bias prior to 1996, and therefore their total uncertainties did not account for this frequency error. Some thoughts on possible ways to approach this issue will be presented. It is hoped that this paper will generate a broad discussion among the frequency standard community that can be used by the WGPSFS to shape its recommendations to the CCTF.

[1] David J Wineland and Helmut Hellwig, Comment on "The Millman Effect in Cesium Beam Atomic Frequency Standards", *Metrologia,* **13**, 173-174 (1977).

[2] http://www.bipm.org/en/publications/si-brochure/second.html

[3] Bernard Guinot and Elisa Felicitas Arias, "Atomic time-keeping from 1955 to the present", *Metrologia,* **42**, S20-S30 (2005).

Two-way optical frequency comparisons over tele-communication network fibers

Bercy Anthony*,+, Stefani Fabio+,*, Lopez Olivier*, Lee Won-Kyu+, Chardonnet Christian*, Pottie Paul-Eric+, Amy-Klein Anne*

*Laboratoire de Physique des Lasers, Université Paris 13, Sorbonne Paris Cité, CNRS, Villetaneuse, France
+Laboratoire National de Métrologie et d'Essais–Système de Références Temps-Espace, Observatoire de Paris, CNRS, UPMC, Paris, France
E-mail: amy@univ-paris13.fr

High-resolution time and frequency transfer between remote locations are of major interest for many applications, such as tests of general relativity and temporal variation of fundamental constants, future redefinition of the second, relativistic geodesy, and navigation (see [1], and references herein). It is usually performed through satellites but with performance now insufficient for state-of-the-art optical clocks. As a very promising alternative, optical fiber links demonstrated impressive results far beyond the GPS capabilities on distances of more than 1000 km. If one focuses on optical frequency comparisons, and puts the frequency transfer aside, the optical link setup can be drastically simplified with a two-way method [2-3]. At each end of the fiber link, a laser is sent to the other end and one detects the frequency difference between the local laser and the remote laser. Assuming that the propagation frequency noise is equal for the two propagation directions, one can efficiently reject the propagation contributions by subtracting and dividing by 2 the two data sets recorded at each end, after their synchronization.

We consider here two alternative two-way schemes which can be practically implemented between distant laboratories [4]. We demonstrated them over a 100-km urban link, making a loop in Paris area, with simultaneous data transfer. One scheme uses a single fiber through which the light is propagated in both directions. It exhibits a very low instability of 7×10^{-18} at 1-s integration time and 5×10^{-21} at 10^4 s, thanks to the very good rejection of the fiber noise. The other one uses two parallel fibers, each one transmitting the light in a single direction. The relative frequency stability is 10^{-15} at 1-s integration time and reaches 2×10^{-17} at 4×10^4 s, three orders of magnitude below the one-way fiber instability. This unidirectional scheme outperforms satellite comparison techniques for short averaging time. The fractional uncertainty of the frequency comparisons was evaluated for the best case to 2×10^{-20}. These results open the way to frequency comparisons over a telecommunication network with minimal modification of the network backbone.

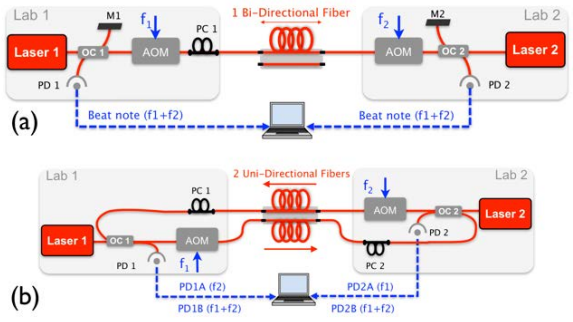


Fig. 1: experimental set-ups for two-way optical frequency comparisons using (a) one fiber and bidirectional propagation or (b) two fibers and unidirectional propagation.

[1] F. R. Giorgetta, W. C. Swann, L. C. Sinclair, E. Baumann, I. Coddington, and N. R. Newbury, "Optical two-way time and frequency transfer over free space," Nat. Photonics, vol. **7**, pp. 434-438, 2013.

[2] D. W. Hanson, "Fundamentals of two-way time transfers by satellite," *Proceedings of 43rd Annual Symposium on Frequency Control, Denver, CO* (IEEE, Piscataway, NJ, 1989),pp. 174–178.

[3] C. E. Calosso et al, "Frequency transfer via a two-way optical phase comparison on a multiplexed fiber network," Opt. Lett., vol. 39, pp. 1177-1180, 2014

[4] A. Bercy, F. Stefani, O. Lopez, C. Chardonnet, P.-E. Pottie, and A. Amy-Klein, "Two-Way Optical Frequency Comparisons Over 100 km Telecommunication Network Fibers," Phys. Rev. A Rapid Comm., vol. 90, pp. 001802(R), Dec 2014.

Transmission of a Frequency Channel Through a Long-Haul Optical Fiber Communications Link

Menyuk, Curtis R.
CSEE Dept., University of Maryland Baltimore County, Baltimore, MD 21250 USA
E-mail: menyuk@umbc.edu

It has been demonstrated that it is possible to transfer frequencies over 1840 km in a two-way optical fiber link with a modified Allan deviation of 10^{-18} after 100 s of averaging [1]. However, these results were obtained by using dark fibers and specialized Brillouin amplifiers. There has been a persistent interest in the possibility of transmitting a frequency channel in a long-haul optical fiber communications link [2]. Due to its interaction with neighboring WDM channels, a frequency channel in an optical fiber communications link will be subject to impairments that are not present in a dark fiber link. In this work, we systematically examine the impairments that are present in a long-haul optical fiber communications link to determine their impact on a frequency channel.

Figure 1 shows a diagram of the physical impairments that are present in an optical fiber communications link [3]. These include linear impairments—amplified spontaneous emission (ASE) noise from erbium-doped amplifiers, chromatic dispersion, and polarization mode dispersion (PMD). The nonlinear impairments include Rayleigh, Brillouin, and Raman scattering, as well as the Kerr effect, which can be divided into self-phase modulation (SPM), cross-phase-modulation (XPM), and four-wave mixing (FWM).

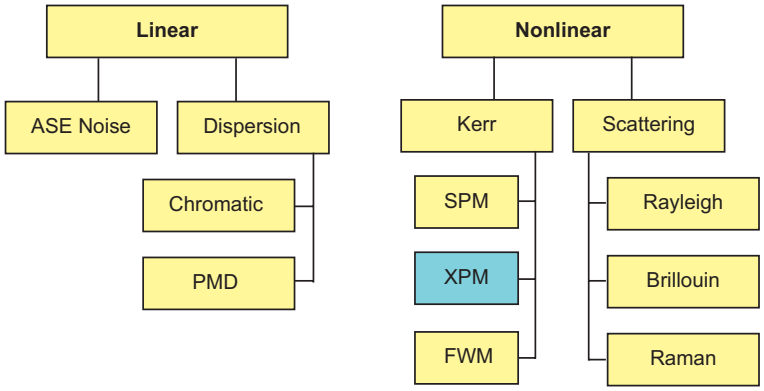


Fig. 1: Diagram of the impairments in an optical fiber communications system.

We have considered in detail an 800-km link that has 10 amplifiers, spaced 80 km apart, which is typical for a terrestrial long-haul link. We find that ASE noise sets a lower limit that is proportional to the bandwidth of the signal and equals 1 nW for a 10 MHz frequency channel. The dispersive impairments are negligible. Raman scattering is negligible. Brillouin scattering sets an upper limit on the power of the frequency channel of 1 mW. Rayleigh scattering is an important noise source, but its effect can be greatly reduced by modulating the frequency channel [4]. Self-phase modulation and four-wave mixing are negligible. However, cross-phase modulation, in which nearby WDM channels interact dispersively with the frequency channel, lead to phase fluctuations. We estimate that these fluctuations cause a fractional uncertainty of $< 10^{-15}$ in 1 s and $< 10^{-17}$ in 100 s in a typical on-off-keyed 10-gigabit/sec system in which each channel has 1 mW of power.

This work was supported by Raytheon Corporation.

[1] F. Droste et al., "Optical Frequency Transfer Over a Single-Span 1840 km Fiber Link," Phys. Rev. Lett., vol. 111, no. 11, 110801, 13 Sep. 2013.

[2] O. Lopez et al., "Ultra-Stable Long Distance Optical Frequency Distribution Using the Internet Fiber Network," Opt. Exp., vol. 20, no. 21, pp. 23518–23526, 8 Oct. 2012.

[3] G. P. Agrawal, *Fiber-Optic Communication Systems* (2nd edition), Wiley: 1997.

[4] J. P. Cahill et al., "Optimization of Modulation Techniques for Suppression of GEMRS in Frequency Transmission Systems," Proc. Int. Freq. Control Symp., 2014.

Joint Frequency and Time Transfer over A Cascaded Fiber Link of 250km

Qin Liu, Wei Chen*, Dan Xu*, Nan Cheng*, Fei Yang*, Youzhen Gui, Haiwen Cai*, Shenshen Han
Key Laboratory for Quantum Optics, Shanghai Institute of Optics and Fine Mechanics, Chinese Academy of Sciences, Shanghai, China
* Shanghai Key Laboratory of All Solid-State Laser and Applied Techniques, Shanghai Institute of Optics and Fine Mechanics, Chinese Academy of Sciences, Shanghai, China
E-mail: yzgui@siom.ac.cn and hwcai@siom.ac.cn

Abstract: We have demonstrated the transfer of joint 1GHz frequency and 1 pulse per second (1PPS) time signals based on WDM technology over a compensated cascaded fiber link of 250km in the laboratory, which consists of a repeater station and two fiber links of 100km and 150km. Meanwhile, in the center of each fiber link there inserts a bi-directional Erbium-doped fiber amplifier (Bi-EDFA) to compensate the big optical attenuation. After every stage achieving steady state by optical compensation method, the reached Allan deviation (ADEV) of frequency signal is 6.3×10^{-14} and 1.8×10^{-17} at averaging time of 1s and 10^4s respectively and the time deviation (TDEV) of time signal is 1.7ps at averaging time of 10^3s. Simultaneously after calibration, the time synchronization accuracy is within 120ps.

Reference:

[1] H. Jiang, F. Kefelian, S. Crane, O. Lopez, M. Lours, J. Millo, D. Holleville, P. Lemonde, Ch. Chardonnet, A. Amy-Klein, and G. Santarelli, "Long-distance frequency transfer over an urban fiber link using optical phase compensation," J. Opt. Soc. Am. B, vol. 25, no. 12, pp. 2029–2035, 2008.

[2] M. Fujieda, M. Kumagai, and S. Nagano, "Coherent Microwave Transfer Over a 204-km Telecom Fiber Link by a Cascaded System," IEEE Trans. Ultrason., Ferroelect., Freq. Contr., vol. 57, no. 1, pp. 168-174, Jan. 2010.

Optical Frequency Transfer over 1400 km using cascaded Remote Fibre Brillouin Amplifiers

Raupach, S. M. F.; Koczwara, A.; Grosche, G.
Physikalisch-Technische Bundesanstalt (PTB), Bundesallee 100, D-38116 Braunschweig, Germany
E-mail: sebastian.raupach@ptb.de

The transfer of ultrastable optical frequencies is required for the comparison of optical clocks and for applications in relativistic geodesy. It furthermore allows the dissemination of an optical reference frequency to remote users. Frequency transfer faces two major challenges: the attenuation of the signal and the noise added to the signal by the transmission. Low instabilities are achieved by using underground fiber links as a transmission path and by suppressing the phase noise of the optical frequency transfer actively by stabilizing the phase of the transferred signal [1-3]. Also the two-way technique can be used here [4,5], if applicable. Very recently, phase-stabilized frequency transfer was demonstrated with an instability (modADEV) of 3×10^{-20} over a 540 km loop of cascaded fiber links [5]. In optical frequency transfer via fiber, the typical attenuation of around 0.2 dB/km (at 1550 nm) usually is compensated for by broad-band, bidirectional Erbium doped fiber amplifiers (EDFA) [1-5]. To avoid spontaneous lasing, these amplifiers are typically operated at low gain around 17 dB.

Here we present results form the world's first continental-scale link relying on an entirely different technology: field-able fibre Brillouin amplifiers (FBA) developed at PTB within a European project [6]. Fiber Brillouin amplification achieves narrow-band amplification, with a gain bandwidth of order 10 MHz. This allows selectively amplifying the frequency-shifted return signal, without amplifying back reflections. Therefore signal gains in excess of 40 dB can be realized here. We have installed field-able FBA along a 1400 km underground fibre loop PTB-Strasbourg-PTB. During a single path the signal experiences seven Brillouin amplifications achieving an average distance between individual amplifications of around 200 km.

We will present first results from phase-stabilized optical frequency transfer over this 1400 km "Brillouin-link".

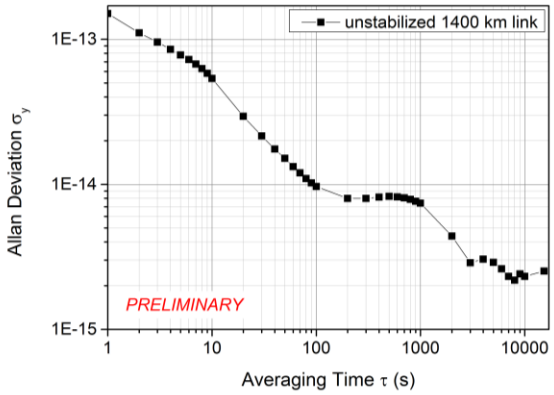


Fig. 1: Fractional optical frequency transfer instability (Allan deviation) of the unstabilized 1400 km link.

This project is supported by the DFG in SFB 1128 geo-Q, and by EMRP SIB-02 (``NEAT-FT''). The EMRP is jointly funded by the EMRP participating countries within EURAMET and the European Union.

[1] O. Lopez et al., "Ultra-stable long distance optical frequency distribution using the Internet fiber network," Opt. Express, vol. 20, pp. 23518-23526, 2012.

[2] K. Predehl et al., "A 920-Kilometer optical fiber link for frequency metrology at the 19th decimal place," Science, vol. 336, pp. 441-444, 2012.

[3] D. Calonico et al., "High-accuracy coherent optical frequency transfer over a double 642-km fiber link," Appl. Phys. B, vol. 117, pp. 979-986, 2014.

[4] C. E. Calosso et al., "Frequency transfer via a two-way optical phase comparison on a multiplexed fiber network," Opt. Lett., vol. 39, pp. 1177-1180, 2014.

[5] F. Stefani et al., "Tackling the limits of optical fiber links," arXiv:1412.2496v1, 2014.

[6] S. M. F. Raupach, A. Koczwara, and G. Grosche, "Optical frequency transfer via a 660 km underground fiber link using a remote Brillouin amplifier," Opt. Expr., vol. 22, pp. 26537-26547, 2014.

Preliminary time transfer through optical fiber at NIM

LIANG Kun, ZHANG Aimin, YANG Zhiqiang, WANG Weibo
Division of Time and Frequency Metrology,National Institute of Metrology, NIM
Beijing, China
E-mail: liangk@nim.ac.cn

Since 2012, we have finished building the new timekeeping system at the Changping campus of National Institute of Metrology(NIM) and changed the realization of UTC(NIM) to this campus from the Hepingli campus. There is still one H-maser and two cesium clocks located at the Hepingli campus, based on which one time scale UTC(NIM)Hepingli is generated, and we provide most of the calibration and traceability services directly reference to the time scale at this campus. So we need one precise time and frequency transfer method to link our two campuses which are about 40 km away.

TWSTFT(Two Way Satellite Time and Frequency Transfer) is a famous precise time transfer method to compare two time scales with a very long distance. BIPM(Bureau international des poids et mesures) evaluates the method with the uncertainty A of 0.5 ns. According to the similar principles, we use one local modem referenced to the local time scale to generate the microwave signal modulated by the local time information, after the conversion of E/O, the signal is transferred through the optical fiber instead of satellite and free space, and then at remote site after the conversion of O/E, the other modem is used to demodulated the local time information referenced to the remote time scale from the local microwave signal, at the same time we do vice verse, and at last combining the two time information demodulated by the two modems separately located at the two sites will give access to compare the two time scales and we call it two way optical fiber time and frequency transfer (TWOTFT) as BIPM did. PTB has finished the first successful implementation on the baseline between the Physikalisch-Technische Bundesanstalt (PTB) and the Institut für Quantenoptik(IQ) at Leibniz Universität Hannover with the length of 73 km, and the uncertainty was below 100 ps[1].

In terms of this kind of principles, some experiments have been implemented at NIM. First, we compare the same time scale, which is common clock difference(CCD), using 1 m, 50 km and 102 km optical fiber in the laboratory. Then we implemented the transfer with the real optical fiber link partly underground and partly over ground at the length of 109 km with the two fibers between our two campuses ring-connected. We can get the time stability of less than 6 ps/s and 0.9 ps/100s as follows in Fig. 1.

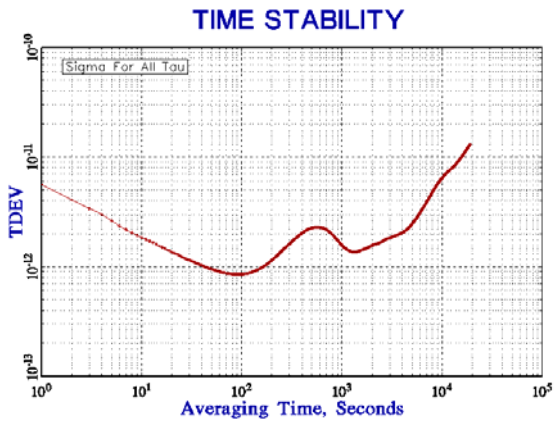


Fig. 1: TDEV of CCD on the real baseline of 109 km

Next step, we will implement the experiment in the 63 km optical fiber with the two fibers between our Changping campus and BSNC(Beijing Satellite Navigation Center) campuses ring-connected and then finish the time link calibration to give the time transfer results and evaluate the corresponding uncertainty.

[1] A. U. Name, A. U. Name2, and A. U. Name3, “Time transfer through optical fibers over a distance of 73 km with an uncertainty below 100 ps” Metrologia 49 (2012) 772–778

Active and Passive Compensated RF Frequency Disseminations on Branching Fiber Network

Bo Wang[1, 2], Xi Zhu[1, 3], Yu Bai[1, 3], Chao Gao[1, 2], and Lijun Wang[1, 2, 3, 4]

[1]Joint Institute for Measurement Science, Tsinghua University, Beijing 100084, China
[2]State Key Lab of Precision Measurement Technology and Instruments, Department of Precision Instruments, Tsinghua University, Beijing 100084, China
[3]Department of Physics, Tsinghua University, Beijing 100084, China
[4]National Institute of Metrology, Beijing 100013, China

Email: bo.wang@tsinghua.edu.cn

Over the past decade, ultra-stable optical and RF frequency disseminations via fiber link have been demonstrated by many groups. To improve its accessibility, multi-access frequency dissemination methods have been proposed and demonstrated by several groups. How to apply these techniques to satisfy the frequency synchronization requirements of different large-scale Scientific and Engineering facilities is the next challenge to many us. Currently, the European FT-Neat consortium is constructing the time and frequency synchronization network through the telecommunication fiber network; the Beijing regional time and frequency synchronization network is under construction, 5 remote institutes (5 H-Masers) have been linked by the network; the square kilometer array telescope (SKA) requires reference frequency synchronization for thousands of dish antenna. These practical applications required a frequency dissemination methods suitable for the branching network.

In this paper, we demonstrate two RF frequency dissemination methods (active and passive phase fluctuation compensation) for branching network. For the active one, the phase noise compensation function placed at the client site. One transmitting module hence can be linked with multiple client sites. As a performance test, using two separate 50 km fiber spools, we recover the 100 MHz disseminated reference frequencies at two remote sites, separately. Relative frequency stabilities between two recovered frequency signals of 2.8×10^{-14}/s and $2.5\times10^{-17}/10^{5}$s are obtained.[1] For the passive one, without any phase control on the disseminated rf signals or usages of active feedback loop, the highly stable reference radio frequency signal can be delivered to several remote sites simultaneously and independently. Relative frequency stability of 6×10^{-15}/s and $7\times10^{-17}/10^{4}$s is obtained for 10km dissemination. Detailed experimental results will be shown during the conference.

This work was supported by the National Key Scientific Instrument and Equipment Development Project (No.2013YQ09094303) and the Beijing Higher Education Young Elite Teacher Project (No. YETP0088).

[1] B. Wang, X. Zhu, C. Gao, Y. Bai, J. Miao and L.J. Wang, “Fiber-based ultra-stable frequency synchronization using client-side, 1f-2f active compensation method”, arXiv:1409.3342 [physics.optics]

Phase noise of Kerr frequency combs based microwave oscillators

A. Coillet[1], P. Del'Haye, A. Rolland, T. Fortier, H. Lee[2], K. Vahala[2], S. B. Papp and S. A. Diddams
[1]National Institute of Standards and Technology, 325 Broadway MS 847, Boulder CO 80305
[2]T.J. Watson Laboratory of Applied Physics, California Institute of Technology, Pasadena, CA 91125, USA
E-mail: aurelien.coillet@nist.gov

The purest microwave to date is generated through the photodetection of the output light from an optically-stabilized Ti-sapphire laser [1]. These lasers are however bulky, which limits their use outside of the laboratory. In this context, a Kerr frequency comb produced in a micrometer size resonator present undeniable advantages for the realization of photonic oscillators in compact systems, with low power requirements and widespread use. This work is dedicated to the analysis of the phase noise performance of a photonic oscillator based on a Kerr frequency comb generated in a silica wedge disk [2].

Our setup consists of a 4-mm-diameter silica disk with Q-factor above 10^8 pumped by an amplified continuous-wave laser. When power levels in the 100 mW range are reached, different regimes of frequency combs can be observed, depending on the detuning between the pump wavelength and the resonance. Some of the comb states are phase-locked [3], and the photodetection of the optical signal leads to the generation of a unique frequency at 16.4 GHz, corresponding to the free-spectral range of the resonator.

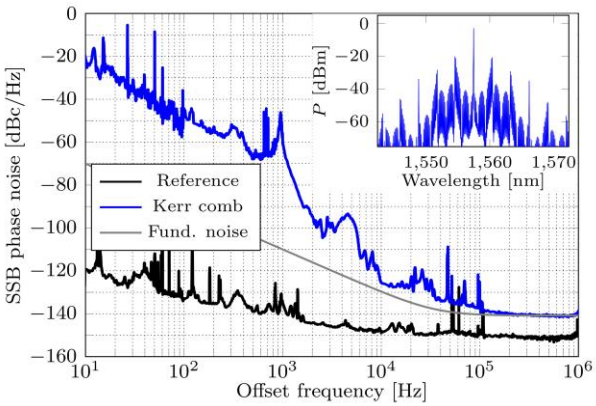


Fig. 1: Single sideband (SSB) phase noise of the 16.4 GHz RF signal generated by an optical Kerr frequency comb. This signal is measured by electronic mixing against the 16th harmonic of a 1.02 GHz Ti-sapphire laser. The black curve corresponds to the phase noise of the beat between the Ti-sapphire laser and another similar laser. The gray curve shows the fundamental noise level, as described in [4]. The optical spectrum of the comb is shown in the inset.

In order to characterize the noise properties of this 16.4 GHz microwave beatnote, we mix it with the 16th harmonic of the output of a 1.02 GHz repetition rate Ti-sapphire laser, whose phase noise is known to be at the state-of-the-art of microwave purity. The phase noise power spectral density of this signal at around 50 MHz is then measured with a phase-noise analyzer.

The measured phase noise of the Kerr comb generated microwave beat is shown in Fig. 1. The most notable feature of this 16.4 GHz oscillator is the noise floor at -140 dBc/Hz between 100 kHz and 1 MHz. For lower frequency offsets, the phase noise is limited by the pump laser, whose intensity and frequency noise are converted to RF phase noise through thermal and Kerr mechanisms within the resonator. It should be noted that the pump laser and cavity are both free-running, and therefore, this technical noise could be lowered by using well-known locking technics.

[1] T. M. Fortier et al, "Generation of ultrastable microwaves via optical frequency division," Nat. Phot., vol. 5, pp. 425-429, 2011.
[2] H. Lee et al, "Chemically etched ultrahigh-Q wedge-resonator on a silicon chip," Nat. Phot., vol. 6, pp. 369-373, 2012.
[3] P. Del'Haye et al, "Phase steps and resonator detuning measurements in microresonator frequency combs," Nat. Com., vol. 6, no. 5668, 2015.
[4] A. B. Matsko et al, "On timing jitter of mode locked Kerr frequency combs," Optics Express, vol. 21, no. 23, 28862, 2013

Low-Noise RF Oscillator with Frequency-Conversion Pair and Matched Photonic Delay

Yitang Dai, Ruixin Wang, Feifei Yin, Jian Dai, Yue Zhou, Jianqiang Li, and Kun Xu

State Key Laboratory of Information Photonics & Optical Communications (Beijing University of Posts and Telecommunications), P. O. Box 55 (BUPT), Beijing, 100876, China. E-mail: ytdai@bupt.edu.cn

High performance radio frequency (RF) oscillators are of prime importance in a wide range of scientific and technological fields, such as communications, navigation, radar and precise scientific measurements. Optoelectronic oscillator (OEO) is one of the most potential technologies to generate RF signals with ultra-high spectral purity, which is even expected to replace classical oscillators such as multiplied quartz crystals or phase-locked dielectric resonator oscillators [1]. The fiber transmission, with advantages of low loss and high bandwidth, enables the generation of high-frequency carrier with low and frequency-independent phase noise, as well as the broadband tunability. However, the fiber is filtering-less: the oscillation mode spacing is greatly decreased (usually less than 1 MHz), so that significant side modes are generated which are highly undesirable for most applications. Multiple fiber loops are then usually employed, which together function as a side-mode-suppression filter in the RF domain [2]. Recent reports demonstrate that such filtering can be achieved in the optical domain by ultra-high-*Q* optical cavity [3]. However, the compound cavity is vulnerable to environment, while the high-Q optical filtering requires state-of-the-art fabrication as well as precise and careful optical alignment or coupling.

Here we propose, for the first time to our knowledge, the side-mode filtering can be achieved equivalently in the intermediate frequency (IF) domain, which consists of a pair of frequency conversions, an IF filter, and a RF local oscillation (LO), as shown in Fig. 1(a). In the cavity, the oscillating RF carrier is firstly down-converted to an IF tone, which is then band-pass filtered and finally up-converted to recover the RF oscillating with the same LO. Thanks to the down-conversion, the challenging narrow RF filtering is achieved by the IF filter, which is much easier for even kHz-level filtering due to the greatly decreased carrier frequency. Meanwhile, large delay is provided by the IF filter because of its causality, so that long fiber is no longer required inside the cavity. Note that the key issue is to precisely preserve the phase noise of the input RF carrier after the proposed filtering (i.e. the phase noise should be independent from that of LO), which requires, predicted by our theory, that the delay of the second LO matches that of the IF filter. Such LO delay is usually long, and is achieved by fiber transmission outside of the cavity.

Our design is experimentally demonstrated. The 3-dB bandwidth of the IF filter, centered at 20 MHz, is 560 kHz. When the LO is 10.02 GHz, the oscillation occurs at 10 GHz, and the equivalent 560 kHz-@-10 GHz filtering eliminates any possible side modes around 10 GHz. Note the image tone at 10.04 GHz after up-conversion, far from the target 10 GHz carrier, can be easily removed by an ordinary RF filter or an I/Q up-convertor. The IF filter delay is ~1 μs, and the matched delay of the second LO is achieved by a 200-m-around fiber. As shown in Fig.1 (b), low phase noise of -120 dBc/Hz at 10-kHz offset is observed, which shows, to our knowledge, competitive performance compared with an ordinary 200-m-long-cavity fiber OEO. Note a much worse phase noise exists in the LO (-90 dBc/Hz at 10-kHz offset), which illustrates the effectivity of our proposed delay match.

References:

[1] L. Maleki, "The opto-electronic oscillator (OEO): review and recent progress," 2012 IEEE European Frequency and Time Forum, pp. 497-500.

[2] D. Eliyahu and L. Maleki, "Low phase noise and spurious level in multi-loop opto-electronic oscillators," 2003 IEEE Frequency Control Symposium and PDA Exhibition Jointly with the 17th European Frequency and Time Forum, pp. 405-410.

[3] A. Savchenkov, et al. "Whispering-gallery mode based opto-electronic oscillators," 2010 IEEE International Frequency Control Symposium, pp. 554-557.

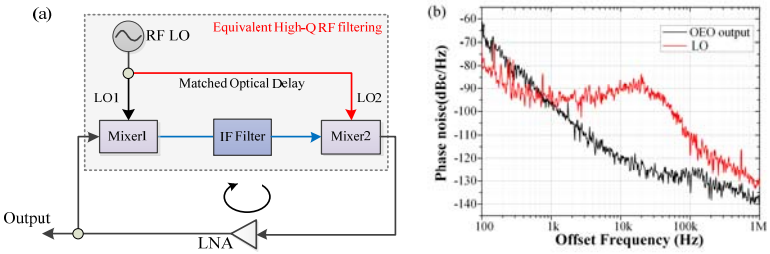


Fig. 1: (a) The oscillator design; LNA: low-noise amplifier. (b) The phase noise of the 10.02-GHz LO and 10-GHz oscillation output.

Ultra-low noise Er frequency combs

Kuse. N, Lee. C. -C*, Jiang. J, Mohr. C, Schibli. T. R*, and Fermann. M. E.
IMRA America Inc., 1044 Woodridge Avenue, Ann Arbor, MI, 48105, USA
*Department of Physics, University of Colorado at Boulder, 2000 Colorado Avenue, Boulder, Colorado 80309-0390, USA
E-mail: nkuse@imra.com

Ultra-low noise microwave signals have many applications in radar, navigation, remote sensing, and long baseline interferometry. Recently, optical frequency division has been considered to be one of the promising approaches to generate low noise microwaves, in which frequency combs are used as a precision gear for optical to microwave conversion. Although the phase noise of the generated microwaves has been mainly limited by the saturation current inside the photo diode, high power photo diodes were recently developed, which produced -135 /*f* dBc/Hz of phase noise and reached -170 dBc/Hz at 10 kHz for a 10 GHz carrier [1]. Here, *f* is the offset from the carrier. Thus, ultra-low noise frequency combs are highly sought. Furthermore, not only low noise is required, but frequency combs have also be compliant with harsh environments, since frequency combs will ultimately be used by non-experts. In this report, we demonstrate an all polarization maintaining (PM) Er frequency comb with ultra-low noise. The PM configuration can in principle satisfy stringent requirements for usability and stability.

The oscillator consists of a linear cavity, in which only PM components are used. The oscillator is self-starting and reproducible. To use frequency combs for microwave generation, two degrees of freedom, the offset (f_{ceo}) and repetition (f_{rep}) frequencies, are preferably stabilized. The repetition frequency is set by stabilizing the beat (f_{beat}) between the comb and an optical reference. The f_{ceo} and f_{beat} are stabilized by a graphene-based EOM and a bulk EOM inside the oscillator with large feedback bandwidth, respectively. Figure 1 (a) and (b) show the power spectral density (PSD) of locked f_{ceo} and f_{beat}, respectively. -92 dBc/Hz and -96 dBc/Hz of f_{ceo} and f_{beat} phase noise at 10 kHz, and -75 dBc/Hz and -80 dBc/Hz at 100 kHz are demonstrated. Since our laser has large intensity noise, intensity noise is also suppressed by feedback to a waveguide EOM outside the oscillator. The result is shown in Fig. 1 (c). -150 dBc/ Hz at 10 kHz and -136 dBc/Hz at 100 kHz of in-loop root mean square intensity noise (RIN) are obtained. The amplitude noise suppressed frequency range can be selected by changing the RF filter design in the locking electronics. In conclusion, we demonstrated record-low noise all PM Er frequency combs, whose phase noise is better than other Er frequency combs used for microwave generations [2, 3].

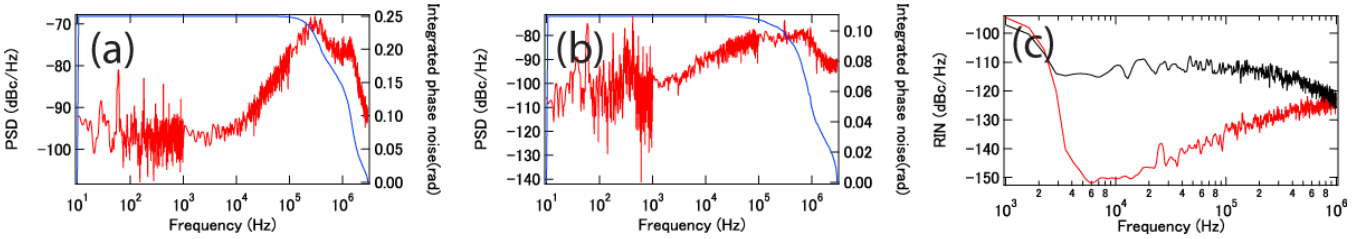


Figure 1. (a) PSD of locked f_{ceo} (red) and integrated phase noise of locked f_{ceo} (blue). (b) PSD of locked f_{beat} (red) and integrated phase noise of locked f_{beat} (blue). (c) Black is RIN without RIN feedback. Red is RIN with RIN feedback.

[1] F. N. Baynes, F. Quinlan, T. Fortier, Q. Zhou, A. Beling, J. Cambell, and S. A. Diddams, "Attosecond Timing in Optical-to-Electrical Conversion,"arXiv;1410.7461 (2014).

[2] F. Quinlan, T. M. Fortier, M. S. Kirchner, J. A. Taylor, M. J. Thorpe, N. Lemke, A. D. Ludlow, Y. Jiang, and S. A. Diddams, "Ultralow phase noise microwave generation with an Er:fiber-based optical frequency divider," Opt. Lett. 36(16), 3260–3262 (2011).

[3] W. Zhang, M. Lours, M. Fischer, R. Holzwarth, G. Santarelli, and Y. Coq, "Characterizing a fiber-based frequency comb with electro-optic modulator," IEEE Trans. Ultrason. Ferroelectr. Freq. Control 59(3), 432–438 (2012)

Wideband photonic synthesizer with 10^{-15} instability

T.M. Fortier, A. Rolland, F.J. Quinlan, F. Baynes A.Hati, A.Ludlow, N. Hinkley, N. Shimizu[+], T. Ishibashi[+], J. Campbell[*] and S.A. Diddams[1]

Time and Frequency Division, NIST Boulder 325 Broadway MS 847 Boulder CO 80305

* Department of Electrical and Computer Engineering, University of Virginia, 351 McCormick Road, Charlottesville, VA 22904, USA

+ NTT Electronics Techno Corporation Atugi-shi, Kanagawa, 243-0198, Japan

E-mail: fortier@boulder.nist.gov

Photonic approaches to signal processing and generation have been developed with the aim of addressing the ever-increasing demand for higher data rates, faster detection and better synchronization. Optical frequency division (OFD) of cavity-stabilized lasers has demonstrated microwave signals with exquisite spectral purity [1], providing a room temperature alternative to quartz crystal oscillators. One shortcoming of OFD is its limited tuning rage of 1-2 % about quantized microwave harmonics. Using a combination of optical frequency division, direct digital synthesis and opto-electronic multiplication we demonstrate synthesis of agile signals from radio frequencies up to the W-band (100GHz).

As seen in Figure 1, using these techniques we obtain tunable signals at radio frequencies with a spectral purity comparable to the best crystal quartz oscillators. In the X-band (10GHz) and the W-band (100 GHz) we can produce tunable signals with a fractional frequency instability of 2 $\times 10^{-15}$ at 1s, corresponding to a combined phase noise levels of -97 dBc/Hz and -80 dBc/Hz at 1 Hz offset respectively. These levels represent greater than a 30 dB reduction in the close in noise as compared to the best possible quartz based synthesizer.

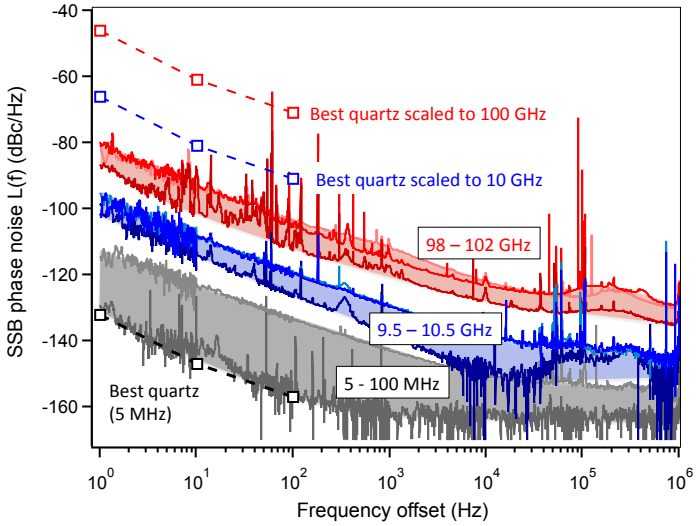


Fig. 1: Two oscillator comparison of agile signals synthesized via optical frequency division, DDS and electro-optic multiplication for 3 frequency bands: grey (rf frequencies from 10 – 100 MHz), blue (X-band frequencies centered at 10 GHz) and red (W-band signals centered at 100 GHz). For comparison we also show the phase noise of the best (BVA) crystal quartz oscillator at 5 MHz, and what its noise would be if scaled to 10 and 100 GHz.

[1] T.M. Fortier et al, "Generation of ultrastable microwaves via optical frequency division," Nature Photonics **5**, 425–429 (2011)

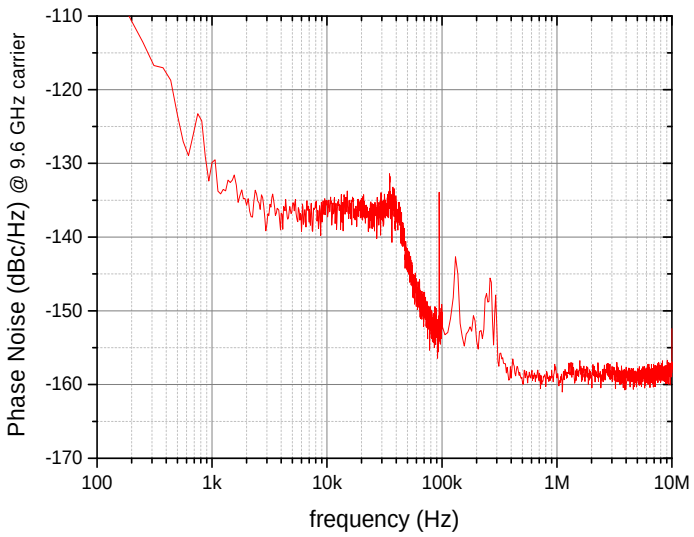
[2] J. Chauvin et al, "A New Generation of Very High Stability BVA Oscillators," *Proceedings*, 2011 IEEE Int. Frequency Control Symp. Geneva Switzerland, May 29, 2007, pp. 1261 – 1268.

Ultra-low phase noise microwave generation from a diode-pumped solid-state laser

Portuondo-Campa Erwin, Buchs Gilles, Kundermann Stefan, Lecomte Steve
Centre Suisse d'Electronique et de Microtechnique (CSEM), Jaquet-Droz 1, 2000 Neuchâtel, Switzerland
E-mail: erwin.portuondo@csem.ch

Photonics-based technologies offer new routes to generate ultra-low phase noise signals at microwave frequencies. Record low-level phase noise at 10 GHz carrier frequency has been demonstrated using an ultra-narrow cavity-stabilized continuous-wave laser, an optical frequency comb as a coherent frequency divider and a photodiode as an optical-to-electrical converter [1,2]. This approach has been implemented with different types of femtosecond lasers, including Ti:sapphire oscillators [2] and Er-doped fiber oscillators [3, 4]. In the case of fiber lasers with repetition rates in the 100-250 MHz range, the pulse repetition rate has been multiplied using fiber interleavers in order to enhance the microwave signal power at 10 GHz, thus improving the phase noise floor [3].

In this contribution we present a system based on femtosecond diode-pumped solid-state laser technology that implements a semiconductor saturable absorber mirror for passive modelocking. These lasers emit a 150 fs pulse train at 1560 nm with 100-MHz repetition rate. Previous measurements of optical pulse timing jitter using a balanced optical cross-correlator demonstrated sub-100 attoseconds integrated timing jitter [10 kHz - 50 MHz] [5]. Two such optical frequency combs have been stabilized using a single ultra-narrow cavity-stabilized continuous-wave laser. Self-referenced stabilization of f_0 is achieved with standard *f*-2*f* interferometers. Five-stage pulse interleavers with timing error < 1 ps per stage have been constructed using polarization maintaining fiber combiners to produce 3.2 GHz pulse trains. The pulses are detected with photodiodes of the type Discovery Semiconductors HLPD DSC50S generating a power of about 0 dBm at 9.6 GHz carrier with a photocurrent of 10 to 13 mA. First phase noise measurements presented in the shown figure demonstrate a very low phase noise floor in the -160 dBc/Hz range (presently limited by the instrument noise floor). Further work is ongoing in order to increase the phase noise sensitivity of the characterization setup and to reduce the AM to PM noise conversion at the photodetection stage.



[1] A. Bartels et al., "Femtosecond-laser-based synthesis of ultrastable microwave signals from optical frequency references", Opt. Lett. 30, 667 (2005)

[2] T. M. Fortier et al., "Generation of ultrastable microwaves via optical frequency division", Nat. Phot. 5, 425 (2011)

[3] F. Quinlan et al., "Optical amplification and pulse interleaving for low-noise photonic microwave generation", Opt. Lett. 39, 1581 (2014)

[4] J. Millo et al., "Ultra-low-noise microwave extraction from fiber-based optical frequency comb", Opt. Lett. 34, 3707 (2009)

[5] E. Portuondo et al., "Sub-100 attosecond timing jitter from low-noise passively mode-locked solid-state laser at telecom wavelength", Opt. Lett. 38, 2650 (2013)

Comparison of Self-ILPLL Forced Oscillators

Zhang, Li; Sun, Tianchi; Receveur, Kevin; Poddar, Ajay*; Rohde, Ulrich*; Daryoush, Afshin
Department of ECE, Drexel University, Philadelphia, Pennsylvania/USA
*Synergy Microwave Corp., Patterson, New Jersey/USA
E-mail: daryoush@coe.drexel.edu

Oscillator phase noise reduction of dielectric resonator oscillator (DRO) using self-injection locking (SIL) and phase locked loop (SPLL) techniques and their combination as SILPLL have been reported [1]. Fiber optic (FO) delay elements using both Mach-Zehnder modulator (MZM) and electro-absorption modulator (EAM) [2] are constructed for implementation of self-forced oscillation topologies, where the former is lower in noise figure, while the latter is cost effective and smaller in size. This paper compares close-in to carrier phase noise of a DRO with various forced oscillation techniques using both MZM and EAM links as depicted in Fig. 1. The FO link realization using MZM is a push-pull dual drive, while the EAM is a single ended drive. The optical signal in both cases is amplified using Erbium doped fiber amplifier (EDFA) in order to compensate for the FO link loss. The delays in Path 1 and Path 2 are 5 km and 3 km respectively. The measurement results are summarized in Table 1 for various circuit topologies using both MZM and EAM for the first time. We can see that MZM link provides better phase noise reduction compared to EAM link due to a lower noise figure.

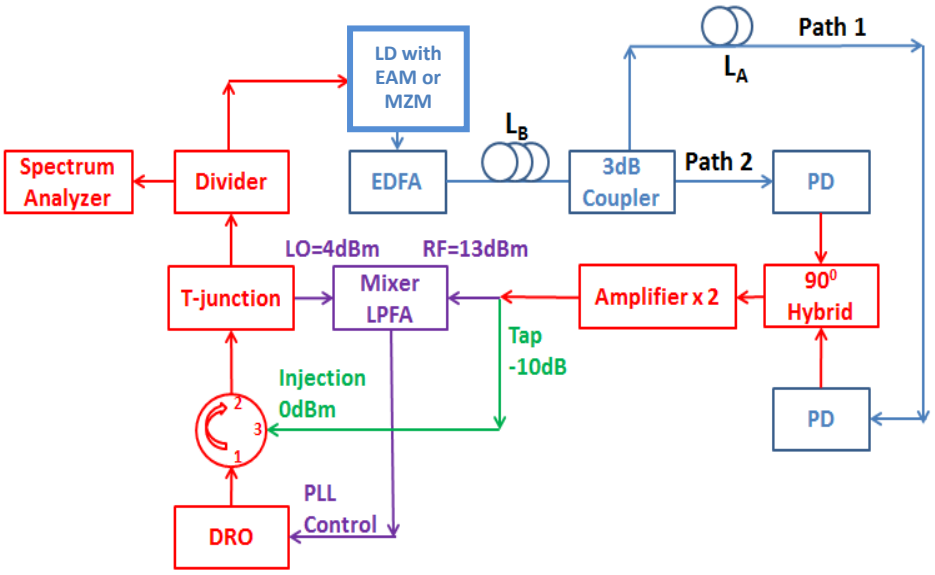


Fig. 1: Experimental set-up for SILPLL using either laser diode (LD) with EAM or MZM.

Table 1: Measured Phase Noise for MZM or EAM-based fiber optic links

	DRO / EAM	DRO / Dual Drive MZM
Free Running @ 1kHz	-83.16 dBc/Hz	-83.16 dBc/Hz
DSIL Phase Noise @ 1kHz	-88.33 dBc/Hz	-95.04 dBc/Hz
DSPLL Phase Noise @ 1kHz	-94.26 dBc/Hz	-96.45 dBc/Hz
DSILPLL Phase Noise @ 1kHz	-97.67 dBc/Hz	-100.75 dBc/Hz

[1] L. Zhang *et al.*, "Oscillator phase noise reduction using self-injection locked and phase locked loop (SILPLL)," in *Proc. IEEE Int. Freq.Control Symp.*, 2014, pp. 592–595

[2] L. Zhang *et al.*, "Self-ILPLL using Optical Feedback for Phase Noise Reduction in Microwave Oscillators" in *IEEE Photonics Technology Letters*, 30 Dec 2014

Miniature Trapped-Ion Frequency Standard with $^{171}Yb^{+}$

Schwindt, Peter D. D., Yuan-Yu Jau, Heather Partner, Darwin Serkland, Adrian Casias, Ronald Manginell, Matthew Moorman, John Prestage*, Nan Yu*, Igor Kosvin†, Dan Boschen†, David Scherer†, David Mailoux†

Sandia National Laboratories, Albuquerque, NM/USA

*Jet Propulsion Laboratory, Pasadena, CA/USA

†Microsemi, Inc., Beverly, MA/USA

Email: pschwin@sandia.gov

We are developing a highly miniaturized trapped-ion clock by probing the 12.6 GHz hyperfine transition in the $^{171}Yb^{+}$ ion. The goals of our project are to develop a clock that consumes 50 mW of power, has a size of 5 cm^3, and has a long-term fractional frequency instability of 10^{-14} at one month. Trapped ion systems are an excellent candidate for such extreme miniaturization because ions are well isolated from the environment independently of the size of the trap. Significant miniaturization has already been demonstrated with the $^{199}Hg^{+}$ trapped ion clock developed at the Jet Propulsion Laboratory [1].

We will discuss the development of the ion trap physics package [2] and its integration with other key elements of the frequency standard, including miniaturized laser sources at 369 and 935 nm, a local oscillator, control electronics, and a microfabricated Yb source for trap loading. We have recently demonstrated operation of the 1 cm^3 ion trap vacuum package. The package is made from titanium with sapphire windows. The ion trap is built up on a high temperature co-fired ceramic (HTCC) substrate to which Ti trap electrodes and microfabricated Yb sources are brazed. With the HTCC substrate forming one wall of the package, electrical vias in the HTCC substrate route electrical signal from the outside of the package to the inside components. The package is evacuated through a copper tube, and once the appropriate vacuum conditions are achieved in package, the copper tube is crimped to form a cold weld seal. Vacuum conditions are maintained by an internal non-evaporable getter. We implemented the vacuum package in an atomic clock and demonstrated $2 \times 10^{-11}/\tau^{1/2}$ performance. In addition, we will show results of using a methane buffer gas to quench the low-lying $^2F_{7/2}$ state in ^{171}Yb.

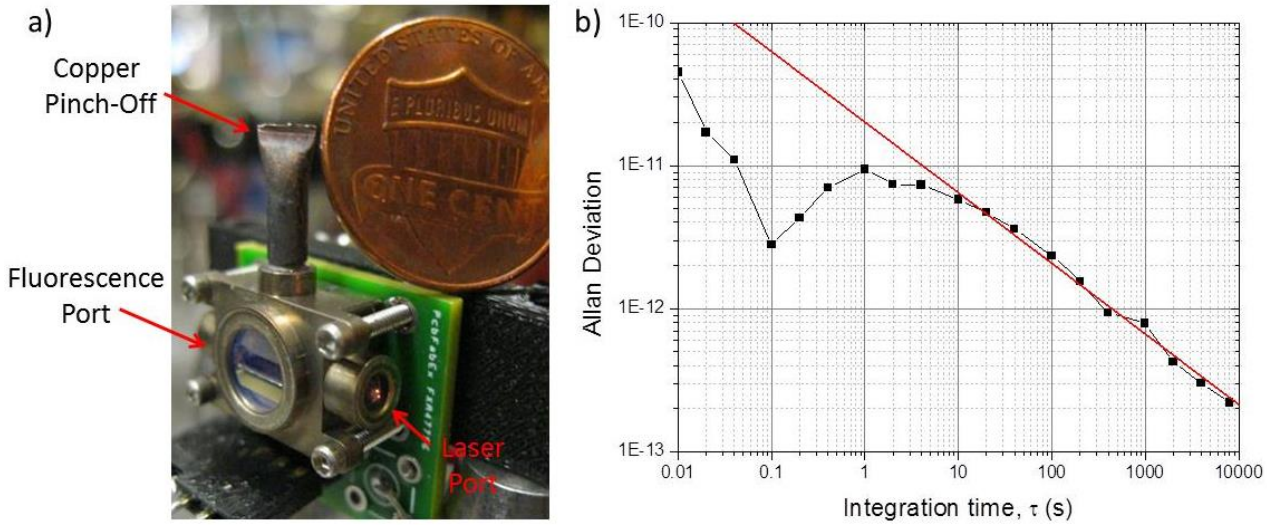


Fig. 1.(a) Picture of the 1 cm^3 vacuum package. (b) Performance of the vacuum package in an atomic clock.

[1] J.D. Prestage, G L. Weaver, 2007, "Atomic clocks and oscillators for deep-space navigation and radio science," Proceedings of the IEEE, Vol. 95 No. 11, pp. 2235-2247.

[2] Y.-Y. Jau, H. Partner, P. D. D. Schwindt, J. D. Prestage, J. R. Kellogg, N. Yu, 2012, "Low-power, miniature ^{171}Yb ion clock using an ultra-small vacuum package," Appl. Phys. Lett., Vol. 101, pp. 253518.

Towards a high-performance microwave frequency standard based on $^{113}Cd^{+}$ ions

Jiawei Zhang, Kai Miao, Xiaolin Sun*, Lijun Wang*
Department of Precision Instrument, Tsinghua University, Beijing, China
State Key Laboratory of Precision Measurement Technology and Instruments, Tsinghua University, Beijing, China
* Department of Physics, Tsinghua University, Beijing, China
Joint Institute for Measurement Science (JMI), Tsinghua University, Beijing, China
E-mail: zhangjw@tsinghua.edu.cn

The microwave frequency standard based on laser-cooled $^{113}Cd^{+}$ ions has a promising performance of frequency stability and uncertainty [1]. Since 2010, a project is carried out to build a Cd^{+} clock at the Joint Institute for Measurement Science (JMI), China. With the experimental setup of Cd^{+} clock, we measured the ground-state hyperfine splitting of $^{113}Cd^{+}$ and obtained the result 15 199 862 854.96(0.12) Hz [2]. Later, we improved it to 15 199 862 855. 0125(87) Hz [3] based on an upgraded setup. As a preliminary measurement result, the short-term frequency stability is less than $1.7\times10^{-12}\tau^{-1/2}$ [1]. Recently, we improved it to less than $6\times10^{-13}\tau^{-1/2}$ [4].

We investigated the reasons for the undesirable frequency stability, and the results indicate that the temperature rising of ions due to the radio frequency heating degrades the signal-to-noise-ratio (SNR) [4]. The other limit is the Dick effect caused by the phase noise of the local oscillator, a crystal oscillator, and the Dick-effect-limited Allan deviation is about $4\times10^{-13}\tau^{-1/2}$. Keeping these in mind, we designed a new experimental setup with two identical ion traps (Fig. 1) to realize the interleaving interrogation of the local oscillator. Thus, the Dick-effect-limited frequency stability is expected to be $1.2\times10^{-14}\tau^{-1/2}$. In each ion trap, $^{24}Mg^{+}$ ions and $^{113}Cd^{+}$ ions are trapped simultaneously. Mg^{+} ions are laser cooled, and used to sympathetically cool Cd^{+} ions. The SNR of the clock signal will be improved greatly due to the low temperature of Cd^{+} ions. With the new setup, the frequency stability of the Cd^{+} clock will decrease as $1/\tau$ over a long sampling time from the lock-loop time until that the stability reaches the quantum-noise limit [5]. Based on the new setup, a high-performance Cd^{+} clock with promising frequency stability and uncertainty is expected.

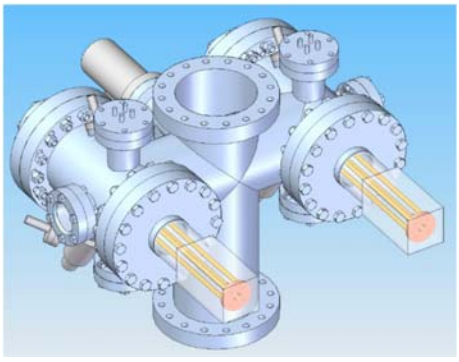


Fig. 1: Design diagram of the new experimental setup of the Cd^{+} clock with two identical ion traps.

This work was supported by 973 Program (Grant No. 2010CB922901) and by NSFC (Grant No. 11304177).

[1] J. W. Zhang, S. G. Wang, K. Miao, Z. B. Wang, and L. J. Wang, "Toward a transportable microwave frequency standard based on laser-cooled $^{113}Cd^{+}$ ions", Appl. Phys. B, vol. 114, pp. 183–187, Jan. 2014.

[2] J. W. Zhang, Z. B. Wang, S. G. Wang, K. Miao, B. Wang, and L. J. Wang, "High-resolution laser microwave double-resonance spectroscopy of hyperfine splitting of trapped $^{113}Cd^{+}$ and $^{111}Cd^{+}$ ions," Phys. Rev. A, vol. 86, no. 2, p. 022523, 2012.

[3] S. G. Wang, J. W. Zhang, K. Miao, Z. B. Wang, and L. J. Wang, "High-accuracy measurement of the $^{113}Cd^{+}$ ground-state hyperfine splitting at the milli-Hertz level," Optics express, vol. 21, no. 10, pp. 12434–12442, 2013.

[4] K. Miao, J. W. Zhang, S. G. Wang, Z. B. Wang, and L. J. Wang, "Improvement of the signal-to-noise ratio of the clock signal for the frequency standard based on $^{113}Cd^{+}$ ions," *Proceedings*, 2014 IEEE Int. Frequency Control Symp., Taipei, May 19-22, 2014, pp. 1–3.

[5] L.-J. Wang, "On a New Class of Self-Referencing, $1/\tau$ Atomic Clocks," Chin. Phys. Lett., vol. 31, no. 8, p. 080601, Aug. 2014.

Deep Space Atomic Clock (DSAC) for a Technology Demonstration Mission

R.L. Tjoelker, J.D. Prestage, E.A. Burt, A. Berg, P. Chen, Y. Chong, S. Chung, W. Diener, D. Enzer, H. Mojaradi, C. Okino, M. Pauken, D. Robison, M. Schoppers, B. Swenson, B. Tucker, R. Wang
Jet Propulsion Laboratory, Caltech, Pasadena, CA USA
E-mail: tjoelker@jpl.nasa.gov

There are many different atomic clock technologies but few meet the demanding performance, reliability, size, mass, and power constraints required for space based navigation applications. JPL is currently developing a mercury trapped ion clock [1,2] for a NASA Technology Demonstration Mission (TDM) referred to as DSAC (Deep Space Atomic Clock) [3]. A one year flight demonstration as a hosted payload is planned following a 2016 launch. Ion clock development, status, and a brief mission overview will be presented.

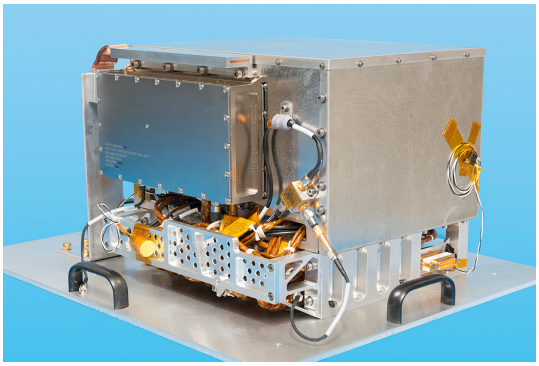


Fig. 1: Mercury ion clock Demonstration Unit (DU) for the DSAC Technology Demonstration Mission.

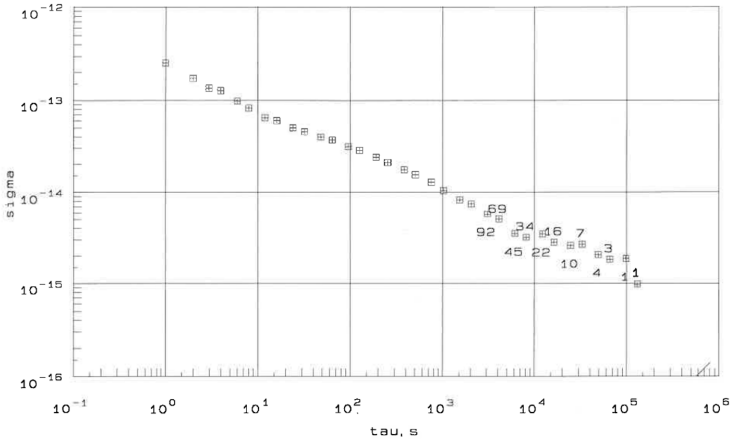


Fig. 2: Seven day Allan Deviation of the DSAC mercury ion clock compared to a hydrogen maser. The performance at one second is limited by the user synthesizer used to generate a 20.456 MHz reference signal.

[1] R.L. Tjoelker et al, "Mercury Atomic Frequency Standards for Space Based Navigation and Timekeeping," Proc. of the 43rd annual PTTI, 2011.

[2] J. D. Prestage et al, "Atomic Clocks and Oscillators for Deep-Space Navigation and Radio Science," Proc. of the IEEE, vol. 95, Nov. 2007, pp. 2235–2247.

[3] Todd A. Ely et al, "The Deep Space Atomic Clock Mission" ; Proc. of the 23rd International Symposium on Space Flight Dynamics, At Pasadena, CA, 2012.

Next Generation JPL Ultra-Stable Compensated Multipole Trapped Ion Atomic Clock for the Naval Research Laboratory

Eric Burt, Lin Yi, Blake Tucker, Robert Hamell, Scott Crane*, and Robert Tjoelker

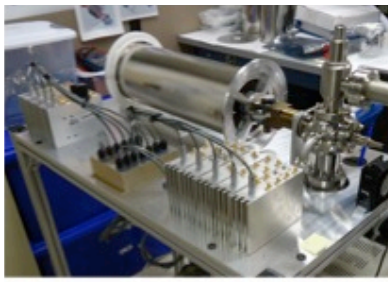
Jet Propulsion Laboratory, California Institute of Technology, Pasadena, CA
*Naval Research Laboratory, Washington, DC

Email: eric.a.burt@jpl.nasa.gov

Over the past decade, trapped ion atomic clock development at the Jet Propulsion Laboratory (JPL) has proceeded in two parallel directions: 1) new atomic clock technology for space flight applications that require strict adherence to size, weight, and power requirements, and 2) ultra-stable atomic clocks, usually for terrestrial applications focusing on ultimate performance. In this paper we will present first results from a new ultra-stable trapped ion clock in the second category recently delivered to the Naval Research Laboratory.

Two new identical clocks, based on a compensated multipole design, build on the successful demonstration of exceptionally low drift at the 3×10^{-17}/day level [1] by their predecessor, LITS-9, with changes in design intended to further improve ultimate long-term performance. The first has been delivered to the Naval Research Lab, while the second, and eventually a third and fourth, will be retained as in-house standards at JPL.

The excellent long-term stability of LITS-9, and the anticipated equivalent or better performance of the new clocks, has both engineering and scientific applications. It will be invaluable for characterizing the performance of flight clocks both at JPL and at NRL, as well as that of clocks being delivered to, and operated in NASA's Deep Space Network. In addition, the new standard at JPL will be used as a reference for an ACES ground station [2] at JPL when the ACES laser-cooled atomic clock becomes operational on the International Space Station in the 2016 time frame.



The new multipole trapped ion clock during assembly.

As with LITS-9, the new clocks use a quadrupole trap for loading ions and a separate 12-pole [3] trap for sensitive microwave clock interrogation that greatly reduces one of the largest systematic effects in this type of clock, the second order Doppler (SOD) shift. A key additional enhancement to LITS-9 was the use of magnetic compensation to reduce the SOD by a further order of magnitude [1]. The newer clocks use an improved version of magnetic compensation fully integrated into the design. Other enhancements include a sealed vacuum system bakeable to 450 C for improved stability of background gases, improved magnetic field uniformity, enhanced microwave coupling, improved optical efficiency, and a dedicated FPGA-based controller for better reliability.

In this paper we will presents first results from the new standard installed at NRL, which is now achieving $\sim 1 \times 10^{-15}$ maser-limited long-term stability at four days of averaging time.

[1] E.A. Burt, W.A. Diener, and R. L. Tjoelker, IEEE Trans. UFFC **55**, 2586 (2008)

[2] E. Daganzo, et al., Proceedings of the 2009 joint IFCS-EFTF, 1146 (2009)

[3] J.D. Prestage, R.L. Tjoelker, and L. Maleki, Proceedings of the 1999 joint IFCS-EFTF, 121 (1999)

Towards a miniature lamped-pumped Hg^+ standard

Bandi, Thejesh, Le, Thanh, Kellogg, James, Chung, Sang, Prestage, John, Yu, Nan
Jet Propulsion Laboratory, California Institute of Technology, Pasadena, California, USA.
E-mail: thejesh.n.bandi@jpl.nasa.gov

Discharge lamp pumped Hg^+ standards using linear traps has shown to provide excellent frequency stabilities leading towards the next generation space clock, Deep Space Atomic Clock (DSAC) [1]. We are aiming at further miniaturizing the $^{199}Hg^+$ standard. Our preliminary study suggests that a miniaturized standard would be able to support the fractional frequency stabilities at 1×10^{-14} in one day with 100 mW power consumption. To demonstrate the feasibility, we address the key challenges for developing an efficient miniature Hg+ UV lamp and a micro Hg+ trap package. We present our recent feasibility studies towards miniaturizing the lamps and demonstrating ion trapping and clock operation in a completely sealed micro trap vacuum package.

We have fabricated a number of miniature Hg discharge lamps and investigated scaling of the UV output with the reduction in size and power consumption. We investigated the performance of a miniature discharge lamp (2 mm ID) compared to that of typical sized one (10.6 mm ID) used so far. Fig 1(a) shows a miniature lamp in operation. Presently, the absorption power is dramatically reduced from 4 W to ~300 mW that is enough to optically pump the ^{199}Hg ions. We also use simulation tools to confirm simple predictions and explore new approaches for design optimizations.

We have also designed and fabricated an all-metal miniature vacuum trap package. The design leveraged our previously demonstrated approaches that allowed for successful fabrication of the recent micro Yb+ trap tubes in the DARPA IMPACT program [2]. The miniature Hg+ trap package is made of titanium with sapphire windows brazed in place and has an overall volume of 77 cm^3. A quadrupole trap assembly with a thermionic electron emitter (LaB6) as an initial demonstration was assembled in the package, shown in Fig 1(b). We will discuss approach differences between the Hg+ package used in this work and that used in Yb+ trap tubes.

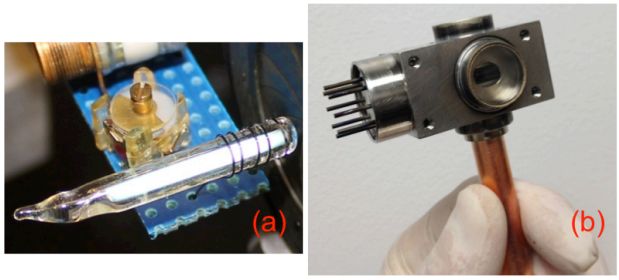


Fig 1: (a) Miniature $^{202}Hg^+$ lamp (V = 0.9 cm^3) and (b) miniature trap package with integrated electron emitter (V = 77 cm^3).

In the first small Hg+ package, we demonstrated the ion trapping with lifetimes up to 80 mins and observed clock signals. We have investigated the possibility of using silicon field emitters (FE) instead of thermionic electron emitters (LaB6). FEs do not require a heater current for their operation and will greatly reduce the electron source power consumption to less than a mW.

Acknowledgements: This work was carried out at the Jet Propulsion Laboratory under contract with the National Aeronautics and Space Administration. Support from the Defense Advanced Research Projects Agency is acknowledged. Thejesh Bandi thank Swiss National Science Foundation for the fellowship through Early Postdoc Mobility grant.

[1] NASA future mission -NASA: http://www.nasa.gov/mission_pages/tdm/clock/index.html#.VGvFLFbO70A
[2] Y.-Y.Jau, H.Partner, P.D.D. Schwindt, J.D. Prestage, J.R.Kellog, N.Yu, "Low-power, miniature ^{171}Yb ion clock using an ultra-small vacuum package", Appl. Phys. Lett., 101, 253518 (2012).

ELSTAB - electronically stabilized time and frequency distribution over optical fiber - an overview

Krehlik Przemysław, Śliwczyński Łukasz
Department of Electronics, AGH University of Science and Technology, Krakow, Poland
E-mail: krehlik@agh.edu.pl

This presentation is an overview of the technology developed at AGH University of Science and Technology for time and RF-frequency distribution over optical fibers. The main part of the presentation is a systematic and organized description of the ELSTAB solution, spread in pieces in our previous papers, [1 - 3]. Some new achievements however, not published till now, are also presented.

In the first section the characteristic effects limiting a quality of T&F transfer in optical fibers is described, and various ideas for overcoming this limitations are briefly shown.

Next, the core idea of our system is described, which is an active stabilization of the fiber propagation delay by means of a pair of precisely matched electronic variable delay lines, controlled in a close-loop arrangement - see Fig. 1. Then the time signal embedding is introduced, and time signal delay calibration with its uncertainty budget is presented. The experimental data of a T&F distribution stability are discussed - see Fig. 2.

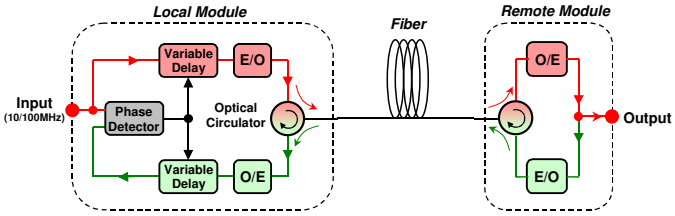


Fig. 1: Simplified block diagram of the delay stabilizing system.

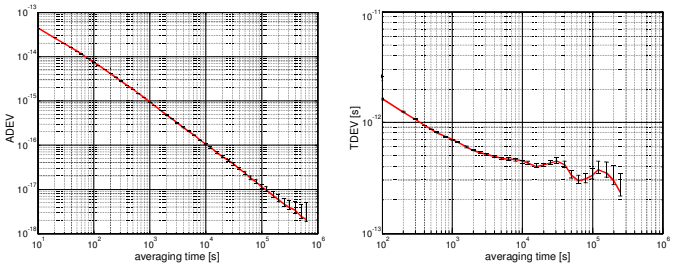


Fig. 2: Overlapping Allan deviation for 10 MHz frequency distribution (left), and Time Deviation for 1PPS distribution (right). Transmission in 60 km-long urban fiber.

Then, various extensions of the basic system are introduced. They are: single-path bidirectional optical amplifiers needed in case of large attenuation of an optical path, hybrid electronic-and-optical delay stabilization useful in long-distance links displaying the seasonal delay fluctuations higher than 100 ns, and finally stabilized tapping nodes and side-branches allowing to build a point-to-multipoint dissemination network.

Finally, two field-deployed installations of the ELSTAB system in Poland are described, and general characterization of our technology with reference to other solutions is presented.

Acknowledgement: This work was partially supported by EMRP (SIB-02 NEAT-FT project), NCN (DEC-2011/03/B/ST7/01833 project), and NCBiR (PBS1/A3/13/2012 project).

[1] Ł. Śliwczyński, P. Krehlik, Ł. Buczek and M. Lipiński, "Active propagation delay stabilization for fiber optic frequency distribution using controlled electronic delay lines," IEEE Trans. Instrum. Meas. vol. 60, pp. 1480–8, 2011.

[2] P. Krehlik, Ł. Śliwczyński, Ł. Buczek and M. Lipiński, "Fiber optic joint time and frequency transfer with active stabilization of the propagation delay," IEEE Trans. Instrum. Meas. vol. 61, pp. 2844–51, 2012.

[3] Ł. Śliwczyński, P. Krehlik, A. Czubla, Ł. Buczek and M. Lipiński , "Dissemination of time and RF frequency via a stabilized fibre optic link over a distance of 420km," Metrologia vol. 50, pp. 133–45, 2013.

Comparison of forward- and backward-propagating optical-fiber-induced noise for application to optical fiber frequency transfer

James P. Cahill[*,+], Olukayode Okusaga[+], Weimin Zhou[+], Curtis R. Menyuk[*], and Gary M. Carter[*]
[*]University of Maryland: Baltimore County, Baltimore, MD, USA
[+]U.S. Army Research Laboratory, Adelphi, MD, USA
E-mail: james.p.cahill.ctr@us.army.mil

Frequency transfer over optical fibers is a promising technique to enable transmission of highly stable frequency sources between metrology laboratories and to other users across the world. It is well-known that noise occurring in the optical fiber limits the frequency stability that can be transmitted via optical fibers. Previous schemes have mitigated this noise by using active feedback [1] that requires light to be sent bi-directionally through the same optical fiber [2]. This requirement is not readily compatible with the majority of installed fiber-optic networks. Hence, it is important to identify the physical mechanisms that lead to the optical-fiber-induced noise and to use this knowledge to explore alternate methods of mitigating this noise. In our past work, we have shown experimentally that optical intensity noise that is induced in the optical fiber can be converted into phase noise of the transmitted frequency reference [3]. While we initially concluded that the physical mechanism causing the optical intensity noise was a third-order nonlinear scattering mechanism—guided entropy mode Rayleigh scattering—in the linear regime [4], recent experimental results have shown that this physical picture is inadequate to describe the noise source [5]. As we search for a theory that completely explains our results, it is helpful to further characterize the optical-fiber-induced intensity noise.

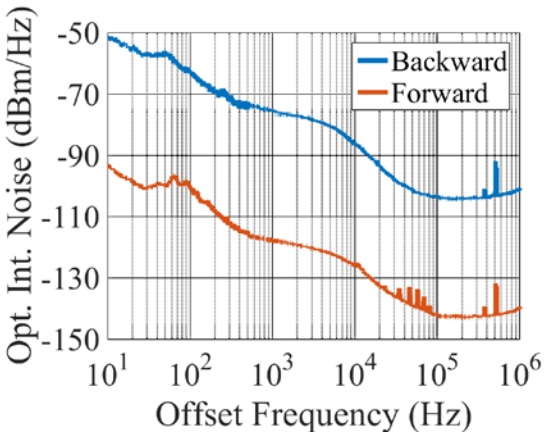


Fig. 1 Optical intensity noise spectra of the forward- (red) and backward- (blue) propagating light.

In this work, we will experimentally compare the intensity noise of the forward- and backward-propagating light. Figure 1 shows preliminary results, measured for an optical fiber length of 10 km and an input optical power of 6 dBm. The shape of the intensity noise spectra of the forward- and backward-propagating light is similar, but the power is approximately 40 dB higher in the backward direction. This result suggests that similar mechanisms cause intensity noise in both directions and that an asymmetry exists that causes the 40 dB power difference.

[1] S. Droste, et al, "Optical-frequency transfer over a single-span 1840 km fiber link," *Phys. Rev. Lett.*, vol. 111, 110801, Sept. 2013.

[2] P. A. Williams, et al, "High-stability transfer of an optical frequency over long fiber-optic links," *J. Opt. Soc. Am. B*, vol. 25, no. 8, pp. 1284-1293, Aug. 2008.

[3] J. P. Cahill, et al, "Effect of optical scattering on one-way RF frequency transfer over optical fibers," *Proceedings*, 2013 ION Precise Time and Time Interval Systems and Applications Meeting, Bellevue, Washington, Dec. 2013.

[4] O. Okusaga, et al, "Spontaneous inelastic Rayleigh scattering in optical fibers," *Opt. Lett.*, vol. 38, no. 4, pp. 549-551, Feb. 2013.

[5] J. P. Cahill, et al, "Superlinear growth of Rayleigh scattering-induced intensity noise in single-mode fibers," under review. Preliminary text available at: http://arxiv.org/abs/1501.01015.

The optical fiber link LIFT for radioastronomy

Calonico Davide[1], Clivati Cecilia[1], Frittelli Matteo[1], Mura Alberto[1], Zucco Massimo[1], Levi Filippo[1]
Perini Federico[2], Bortolotti Claudio[2], Roma Mauro[2] Ambrosini Roberto[2]
[1]INRIM, Istituto Nazionale di Ricerca Metrologica, Turin, Italy
[2]INAF, Istituto di Radioastronomia, Radiotelescopi di Medicina (Bo), Italy
E-mail: d.calonico@inrim.it

We present a coherent optical fiber link for radioastronomy realized in Italy between the Istituto Nazionale di Ricerca Metrologica (INRIM) in Torino and the Institute for Radioastronomy of the National Insitute of Astrophysics (INAF-IRA) in Medicina (Bologna).

Optical fiber links are the most performant technique for time and frequency transfer and remote clocks comparisons. In Europe, there is an effort to establish a network of accurate clocks by optical fiber links, a unique facility for metrology, fundamental physics, relativistic geodesy. Further, optical links will benefit the improvement of global navigation satellite systems and the synchronization of very long baseline interferometry (VLBI) antennas.

In Italy, INRIM developed LIFT [1], a coherent optical fiber link that connects INRIM to the scientific pole in Sesto Fiorentino, Florence, for atomic physics application (642 km), and INRIM to the Italian-French border in Modane (150 km). After the 642 km fiber haul, LIFT provides a frequency reference with an instability of 3×10^{-19} at 1000 s (Allan deviation), and an accuracy of 5×10^{-19}.

INAF-IRA joined LIFT to study the possible benefits of fiber links to radioastronomy, such as the dissemination of better frequency references and the fiber synchronization of remote radiotelescopes, e.g. for VLBI and for ambitious projects as the Square Kilometer Array (SKA). IRA operates 3 radiotelescope facilities: the "Northern Cross Radiotelescope", in Medicina, two 32-m single dish antennas, in Medicina and Noto (Sicily) and the Sardinia Radio Telescope, a 64-m antenna in Cagliari. The dish antennas are part of the VLBI global network (150 days a year). As well, IRA is member of the Joint Institute for VLBI in Europe (JIVE), of the European VLBI Network (EVN) and of the International VLBI Service for Geodesy and Astronomy (IVS). It is involved in the astronomical projects ALMA, e-VLBI, SKA, LOFAR.

The coherent optical link from INRIM to IRA radiotelescopes in Medicina is an extension of the link connecting INRIM to Florence, obtained splitting the optical signal in Bologna into two equal arms to Medicina and Florence. The operation of the two arms at the same time is expected by the end of this year, implementing the proper noise compensations. The link INRIM-IRA is 544 km long, with a total losses of 144 dB and it is based on a hybrid fiber architecture: a dedicated fiber is used from INRIM to Bologna (514 km) and then from Bologna to IRA (30 km), the dedicated ITU-44 channel in Dense Wavelenght Division Multiplexing is used. The metrological channel is operated at the same time with data channels. The losses are compensated by seven Bidirectional Erbium-Doped Fiber Amplifiers (EDFA) along the fiber and a remote amplification stage is implemented at Medicina, realized testing both EDFA and Brillouin amplification.

At INAF-IRA, a diode laser at 1542 nm is phase locked to the incoming optical carrier from the link, and the locked diode laser is the reference for an optical frequency comb that generates the RF at 100 MHz to be used at the radio-telescope facility. The 100 MHz signal is compared to the radiotelescope present reference, an active Hydrogen Maser, monitored by a GPS receiver on the long term.

At the conference we will present the details of the implementation and the first results in terms of the comparison between the RF synthesized from the optical link and the local H-Maser. The further steps of the experiment and the perspectives of the use of optical links in radioastronomy will be described and discussed.

This work is supported by the project SIB02-NEAT-FT of the European Metrology Research Programme EMRP. The EMRP is jointly funded by the EMRP participating countries within EURAMET and the European Union.

[1] D. Calonico, et al., “High-accuracy coherent optical frequency transfer over a doubled 642-km fiber link,” Appl. Phys. B, Vol. 117, no. 3, pp. 979-986, Nov. 2014.

4-span cascaded optical link of 1500 km using the Internet fiber network

Chiodo Nicola*, Quintin Nicolas*, Fabio Stefani[+,]*, Wiotte Fabrice*, Chardonnet Christian*, Santarelli Giorgio[#], Amy-Klein Anne*, Pottie Paul-Eric[+], Lopez Olivier*

*Laboratoire de Physique des Lasers, Université Paris 13, Sorbonne Paris Cité, CNRS, Villetaneuse, France
[+]Laboratoire National de Métrologie et d'Essais–Système de Références Temps-Espace, Observatoire de Paris, CNRS, UPMC, Paris, France
#Laboratoire Photonique, Numérique et Nanosciences, Université de Bordeaux 1, Institut d'Optique and CNRS, Talence, France
E-mail: paul-eric.pottie@obspm.fr

High-resolution frequency comparisons between remote locations are of major interest for time and frequency metrology and for many applications, such as tests of general relativity and of temporal variation of fundamental constants and relativistic geodesy. Optical fiber links are intensively studied for a decade by several groups for and demonstrate impressive results of ultra-stable and accurate frequency transfer far beyond the GPS capabilities on distances of several hundreds of km [1] with a record of 1850 km [2].

In order to face the issue of the fiber availability, we have extended the technique of optical fiber link to installed telecommunication network, simultaneous used for digital data transfer. In order to improve the fiber noise rejection that is limited by the optical propagation delay on long haul link, we also implement cascaded optical link, where the propagation noise is compensated by successive fiber spans. Thus the optical signal has to be repeated from one span to the other using a so-called repeater station, as sketched on Fig. 1. Such a station contains a laser source to boost the optical signal injected in the successive span. Part of the light of the remote laser is sent backward to enable the stabilization of the upstream link. The other part of the light is sent forward and allows the stabilization of the following span. With such a technique, we demonstrated a 1100-km cascaded link composed of four sub-links using two parallel fibres between the LPL laboratory at Villetaneuse and Nancy. The complete link uses 3 repeater stations and 2 stations at both ends. The end-to-end stability is 3×10^{-16} at 1-s integration time and reaches 2×10^{-19} at 10^4 s.

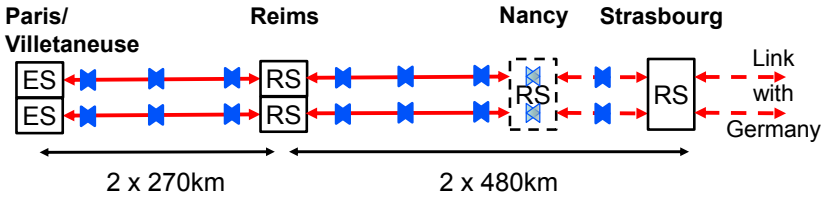


Fig. 1: Schematic of the 4-span cascaded link between Paris/Villetaneuse and Strasbourg. Optical add-drop multiplexers are not shown. ES : end station, RS : repeater station. ⋈ Bidirectional Erbium-doped fiber amplifiers. At Nancy is installed either a repeater station or 2 amplifiers.

Further results on a 1500-km cascaded link between LPL and Strasbourg, at the German border, will be given at the conference. This will represent a first step towards a transnational link between the French and German national metrological institutes.

[1] O. Lopez, A. Haboucha, B. Chanteau, C. Chardonnet, A. Amy-Klein, and G. Santarelli, "Ultra-stable long distance optical frequency distribution using the Internet fiber network," Optics Express, vol. 20, pp. 23518-23526, 2012.

[2] S. Droste, F. Ozimek, T. Udem, K. Predehl, T. W. Hänsch, H. Schnatz, G. Grosche, and R. Holzwarth, "Optical-Frequency Transfer over a Single-Span 1840 km Fiber Link," Physical Review Letters vol. 111, pp. 110801, 2013.

A Round-Trip Fiber-Optic Time Transfer System Using Bidirectional TDM Transmission

Guiling Wu, Liang Hu*, Hao Zhang, Jianping Chen
State Key Laboratory of Advanced Optical Communication Systems and Networks, Department of Electronic Engineering, Shanghai Jiao Tong University, Shanghai 200240, China
*Dipartimento di Fisica e Astronomia and LENS, Università di Firenze - INFN Sezione di Firenze, Via Sansone 1, 50019 Sesto Fiorentino, Italy
E-mail: wuguiling@sjtu.edu.cn

Due to the advantages of low loss, high reliability, wide bandwidth, and high stability, optical fiber link is considered to be a promising option for high-precision time transfer and has attracted an intensive research interest in recent years [1-2]. In this paper, we propose a round-trip time transfer system over single optical fiber employing the same wavelengths in both directions. It can suppress the impact of the Rayleigh backscattering (RB) and the dispersion-induced symmetric deviation over fiber links at the same time by using bidirectional time division multiplexing (TDM)mechanism. Figure 1 illustrates the proposed round-trip fiber-optic time transfer system based on bidirectional TDM transmission schematically. The time signals (1PPS, 1 Pulse Per Second) from clocks at the local site are entered to the local end connected by an optical fiber links. At the local end, the input 1PPS from local end clock are encoded into time code by encoder, and carried to lights through optical transmitters (E/O converter). The lights from the local optical transmitter are launched to the fiber link by switching on optical switchers (OS), which are switched off after the sending of the time codes. At the remote end, the optical signals carrying time codes are converted to electrical signals by O/E converter, which are sent to decoders to extract the 1PPSs in it. Then the 1PPS go through the Time Delay Adjustment Unit (TDAU). In this way, it can realize bidirectional TDM transmission and suppress the noise of the RB. Then the delayed 1PPS are transferred to the local end, which has the same processes with sending 1PPS from the local end to the remote end. At the local end, it has a time interval counter A (TIC A, measured value: ΔT_{LL}) to measure time difference between entered 1PPS at the local end and returned 1PPS from the remote end. In order to verify the effectiveness of the system, we also utilize a TIC B (measured value: ΔT_{LR}) to measure the one-way propagation delay directly between the 1PPS at the local end and extracted 1PPS at the remote end. We use $\Delta T=\Delta T_{LL}/2-\Delta T_{LR}$ to verify the stability and the bidirectional propagation delay asymmetry of round-trip time transfer. Figure 2 shows the time deviations (TDEVs) of 100 km and 200 km (with one SFBA) round-trip time transfer at different averaging time, and TDEVs less than 40ps/s and 11ps/d are obtained. Figure 3 shows that the bidirectional propagation delay asymmetry is less than 27 ps with fiber length up to 200 km without any calibration, which is closed to the floor of the used TICs.

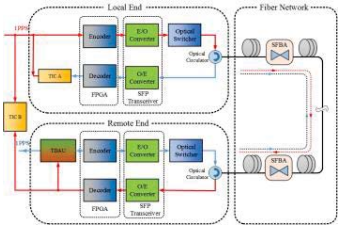


Fig. 1: The scheme of the round-trip time transfer using bidirectional TDM transmission. SFP: Small Form-factor Pluggable; SFBA: Single-Fiber Bidirectional amplifier.

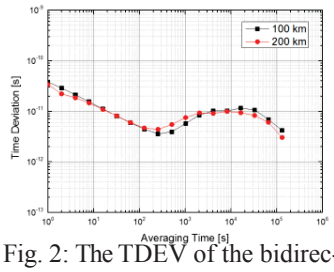


Fig. 2: The TDEV of the bidirectional TDM round-trip time transfer over different fiber lengths.

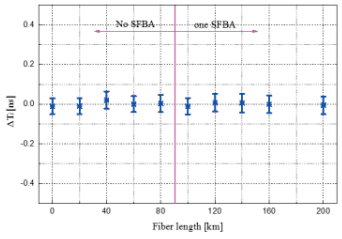


Fig. 3: The ΔT based on bidirectional TDM round-trip time transfer scheme over different lengths of fiber

[1] L. Hu, G. Wu, H. Zhang, and J. Chen. A 300-Kilometer Optical Fiber Time Transfer Using Bidirectional TDM Dissemination . Proc. 46th PTTI Meeting, 2014.

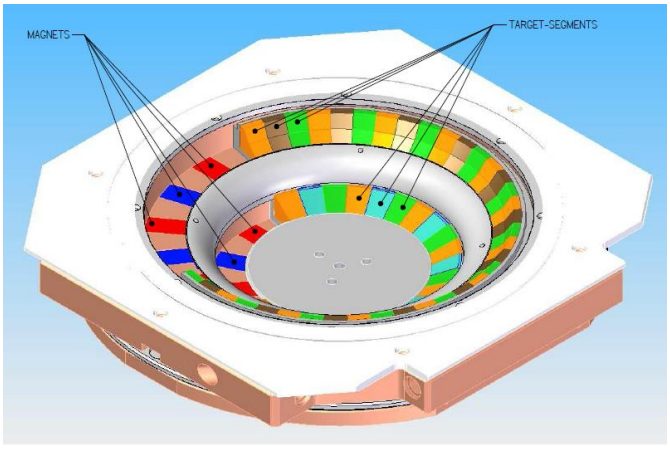
[2] O. Lopez, A. Kanj, P. E. Pottie, D. Rovera, J. Achkar, C. Chardonnet, A. Amy-Klein, and G. Santarelli, "Simultaneous remote transfer of accurate timing and optical frequency over a public fiber network." Applied Physics B, 2013, 110(1): 3-6.

Manufacturability of highly doped Aluminum nitride films

Sergey Mishin
Yury Oshmyansky
Advanced Modular Systems, Inc
Goleta, CA/USA
smishin@amssb.com
yoshmyansky@amssb.com

Abstract—There have been several investigations [1], [2], [3] that demonstrated benefits of adding dopants such as (Sc) or combination of other materials to the aluminum nitride (AlN) films in order to increase coupling coefficient (kt^2) of the Bulk Acoustic Wave (BAW) devices. For Sc, for example, with concentrations below atomic 10%, it is possible to use a composite target with a standard magnetron design. Most R&D systems that performed initial investigations on AlScN films, for example, with high concentration of Sc, used two separate targets: one with pure Al and one with pure Sc to compensate for the large difference in sputtering rates of the two materials. Unfortunately, depositing from two different targets is only viable for low volume R&D experiments, due to non-uniform film properties. The system described in this article uses standard dual conical magnetron with AC deposition source. Targets are cut into multiple segments as shown in Figure 1. Unfortunately, Al is eroded at much higher rate than Sc at the same potential and same magnetic field. Over the target life, concentration of Sc increases in the deposited films. In order to maintain same Sc composition over the entire target life, it is necessary to vary magnetic field locally over the surface of the Al and Sc pieces to provide same erosion rate of Al vs. Sc at the same target potential. Adjusting magnetic field for each segment of both Al and Sc allows for constant concentration over the entire target life solves this problem.

Figure 1. Multiple material targets



REFERENCES

[1]Morito Akiyama, "Influence of temperature and scandium concentration on piezoelectic response of scandium aluminum nitride alloy thin films", Applied Physics Letters, Oct. 2009, Vol.95, Iss. 16, pp. 2107-2107-3

[2]Pau Muralt, et.al.. "Electromechanical properties of AlScN thin films evaluated at 2.5 GJz film bulk acoustic resonators", Applied Physics Letters 99, 2011

[3]Keiichi Umeda1, et.al.. "PIEZOELECTRIC PROPERTIES OF ScAlN THIN FILMS FOR PIEZO-MEMS DEVICES", MEMS 2013, Taipei, Taiwan, January 20 – 24, 2013

PZT nanofilm-based, wafer-scale nano-resonators

Dezest Denis, Mathieu Fabrice, Mazenq Laurent, Soyer Caroline*, Costecalde Jean*, Remiens Denis*, Nicu Liviu
LAAS CNRS, Toulouse, France
*IEMN-CNRS, Villeneuve D'Ascq, France
E-mail: nicu@laas.fr

In this work, we present an unprecedented level of integration of piezoelectric actuation means on arrays of functional nanoresonators at the wafer scale. We use lead titanate zirconate (PZT) as piezoelectric material mainly because of its excellent actuation properties even when geometrically constrained at extreme scale.

For nanoelectromechanical systems (NEMS) to start being a viable alternative to their microscale counterparts (i.e. microelectromechanical systems or MEMS), the fully integrated transduction at the wafer scale represents the ultimate goal to be achieved. So far, relevant results in that sense have been obtained mostly at the chip level either by transposing traditional transduction schemes at the nanoscale [1] or delivering brand new schemes exclusively adapted to the NEMS realm [2].

Here, the fabrication method was performed on SOI 4" P-type (100) wafer (340nm/1µm/525µm). Arrays of four cantilevers of different lengths (from 2µm to 10.5µm) and similar width have been placed on the wafer. The width was varied from 1µm to 2.8µm. A piezoelectric stack including top Ti-Pt (12-120nm thick) and bottom LNO (100nm thick) electrodes as well as the PZT material (150nm thick) has been patterned on each nanocantilever in two covering configurations: full-length or half-length of the nanocantilever. The elastic support beneath the piezoelectric stack was made of the SOI device silicon layer covered by a 30nm thick thermal silicon dioxide (see Figure 1(a)). The whole fabrication process was performed at the wafer scale, the lithography steps being realized using a UV stepper photo repeater (CANON FPA 3000i4/i5). The piezoelectric actuation at the nanodevice level was tested by biasing the top and bottom electrodes as shown in Figure 1(a). Measurements were performed in a home-made fully-automated Fabry-Perot interferometer configuration, under secondary vacuum at ambient temperature. In a first attempt to confirm the piezoelectric actuation efficiency, no electrical poling of the PZT layer was performed. The nanocantilevers' mechanical responses notably showed linear dependence with respect to the AC applied voltage (Figure 1(b)) with a quality factor of 878 at 5.472 MHz for an AC voltage level of 200 mV under secondary vacuum at room temperature.

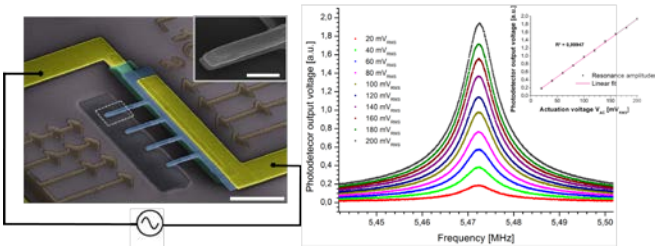


Fig. 1: (a) SEM image (false colors) of an array of four nanocantilevers showing the biasing scheme for the internal piezoelectric actuation. The cantilevers dimensions are 2µm wide and respectively 10.2, 8.2, 6.2 and 4.2µm long (scale bar corresponds to 20µm). The inset is a close view of the 10.2 µm long cantilever showing the different layers (scale bar corresponds to 3µm). (b) Effect of the AC actuation voltage on a cantilever resonance amplitude under secondary vacuum at room temperature. The inset shows a linear dependence between the cantilever response and the actuation voltage ($R^2 = 0.99964$). The cantilever is 4.5 µm wide, 11.5 µm long in the full-length configuration. The structure exhibits a quality factor of 878 at 5.472MHz.

In conclusion, we demonstrated functional of PZT nanofilm-based piezoelectric actuation on NEMS. This work paves promising ways for NEMS to be used in configurations where transduction capabilities are integrated at the nanodevice level providing effective fabrication process flow at the wafer-scale.

[1] L. G. Villanueva, R. B. Karabalin, M. H. Matheny, E. Kenig, M. C. Cross, M. L. Roukes, *Nano Lett.* 11 (2011), pp. 5054-5059

[2] Q. P. Unterreithmeier, E. M. Weig, J. P. Kotthaus, *Nature* 458 (2009), pp. 1001-1004

Observation of Strong Temperature Hysteresis in Molybdenum Disulfide (MoS_2) Nanomechanical Resonators

Zenghui Wang*, Rui Yang, Philip X.-L. Feng*
Electrical Engineering, Case Western Reserve University, Cleveland, OH 44106, USA
*E-mail: zenghui.wang@case.edu, philip.feng@case.edu

Temperature-related hysteresis is an important phenomenon that affects the performance of MEMS resonators and oscillators. For timing applications the hysteresis is highly undesirable, and can be largely mitigated through techniques such as encapsulation [1]. Resonant nanoelectromechanical systems (NEMS) based on atomic-layer two-dimensional (2D) crystals have demonstrated interesting properties such as high tunability of frequency [2] and very broad dynamic range [3]. However, their temperature-dependent resonant responses, such as temperature coefficient of frequency (TC*f*) and possible temperature hysteresis, remain to be characterized. In this work, we report observations of a strong temperature hysteresis in molybdenum disulfide (MoS_2) diaphragm nanomechanical resonators, with new features that differ from those known in MEMS devices.

Figure 1 shows the temperature hysteresis measured in a 5μm-diameter, 56nm-thick MoS_2 diaphragm resonator (Fig. 2 inset). As temperature T increases, resonance frequency f_{res} decreases (Fig. 1a red curves), exhibiting very large TC*f* (>4000ppm/°C). As T further increases, f_{res} shift significantly slows down. During cooling, f_{res} follows a different pattern (Fig. 1a green curves). Such behavior is reproducible and does not depend on the step size in temperature sweep (Fig. 1b), and can be observed at different pressures. The observed hysteresis exhibits several attributes that are in contrast to typical temperature hysteresis observed in MEMS resonators [4]: (i) it is much stronger (~15% near 50°C *vs.* ~1–100 ppm levels in typical MEMS devices); (ii) it is strongly T-dependent; (iii) the f_{res} shift precedes T-change (*vs.* that f_{res} always lags behind T change in hysteresis due to thermal lag). These phenomena suggest that the observed hysteresis may be dominated by a different mechanism than those commonly found in MEMS and quartz oscillators [4,5], such as thermal lag, changes in strain or the crystal, and circuit hysteresis.

Compared with conventional devices, 2D resonators have very high surface-to-volume ratios (~$10^9 m^{-1}$), which can make their f_{res} more sensitive to surface adsorption. Thus adsorption may play an important role in the observed strong hysteresis with varying temperature. If completely verified (currently ongoing in control experiments), such hysteresis may be exploited for engineering temperature-programmed surface processes such as surface diffusion [6] and phase transitions [7] in adsorbed particles or atoms.

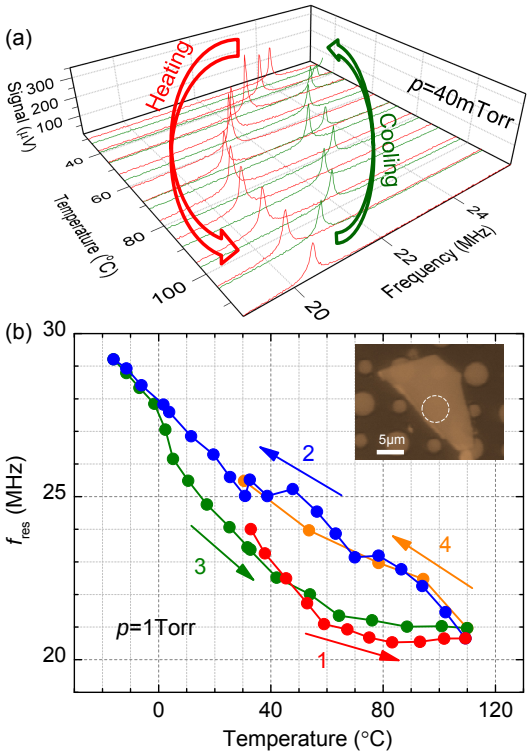


Fig. 1: Temperature hysteresis of a MoS_2 nanomechanical resonator. (a) A set of measured resonances as the device temperature is swept up and down. (b) f_{res} as a function of T for several cycles of temperature sweep. *Inset*: Device image.

[1] B. Kim *et al.*, "Frequency stability of wafer-scale encapsulated MEMS resonators", in *Transducers'05*, **2**, 1965 (2005).
[2] P. X.-L. Feng *et al.*, "Two-dimensional nanoelectromechanical systems (2D NEMS) via atomically-thin semiconducting crystals vibrating at radio frequencies", in *IEDM'14*, paper no. 8.1, 196 (2014).
[3] Z. Wang, P. X.-L. Feng, "Dynamic range of atomically thin vibrating nanomechanical resonators", *Appl. Phys. Lett.* **104**, 103109 (2014).
[4] C. Jha *et al.*, "CMOS-compatible dual-resonator MEMS temperature sensor with milli-degree accuracy", in *Transducers'07*, 229 (2007).
[5] J. Kusters, J. Vig, "Hysteresis in quartz resonators-a review", *IEEE Trans. Ultrason. Ferr. Freq. Contr.* **38**, 281 (1991).
[6] Y.T. Yang, *et al.*, "Surface adsorbate fluctuations and noise in nanoelectromechanical systems", *Nano Lett.* **11**, 1753 (2011).
[7] Z. Wang, *et al.*, "Phase transitions of adsorbed atoms on the surface of a carbon nanotube", *Science* **327**, 552 (2010).

New Capacitive Micro-Acoustic Resonators machined in single-crystal silicon stacked structures

Belkadi Nesrine, Baron Thomas, Robert Laurent, Bernard Florent, Herth Etienne, Dulmet Bernard
Time and Frequency Dpt., FEMTO-ST Institute, Besançon/France
E-mail: nesrine.belkadi@femto-st.fr

We present new MEMS resonators structures based on silicon [1] to take advantage of the availability of this material together with low unit cost, large-scale production, and robustness. The present work aims to undoing the technological locks encountered during the realization of capacitive silicon MEMS resonators exploiting true Bulk Acoustic Wave resonances instead of structural ones [2,3]. We propose here a new type of acoustic resonator carried out in the technology shown in Fig. 1. These resonators are driven through a 700 nm-thick electrostatic gap parallel to the substrate surface. The combined static bias and dynamic voltages are applied through existing interconnections between the existing conductive layers.

To realize these interconnections, two technologies have been tested: direct wire contacting through etched holes and so-called TSS "Through Silicon Stacking" technology [4], in order to ease the electric access to both sides of the gap from a single face of the plate, at the difference of the topology previously experimented in Refs. [2,3]. The thin electrostatic gap cavity is realized by a local over-thickening of the gold layers used in the gold-gold bonding process of the resonant silicon plate with the external electrode support structure, also made from silicon. This allows for very thin gaps on surfaces in the range of a few square millimeters while avoiding the shallow machining in the silicon that would require an additional technological step.

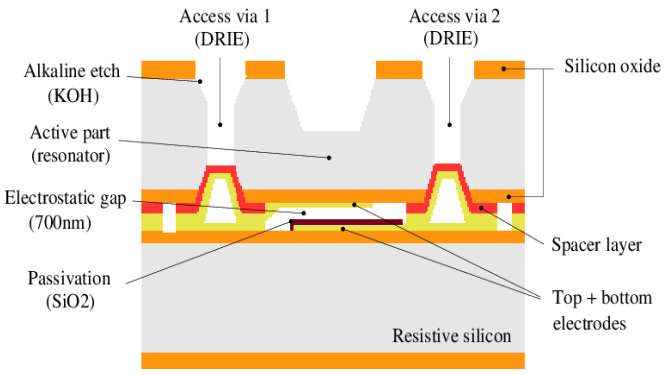


Fig. 1: Schematic view of capacitive BAW resonator with TSS integrated technology.

The design of our resonators rely on thickness-extensional modes, exploiting energy-trapping of elastic waves resonant modes in order to minimize anchor losses, thereby achieving a new type of so-called C-MAR (Capacitive Micro-Acoustical Resonators) structure. The Thickness-Extensional (TE) modes yield a fundamental frequency close to 16 MHz with a 250 µm-thick Si wafer. The second originality of the work lies in the realization of the electrostatic gap for (100) silicon resonant structures, preferably full plate, *ie* without machining of silicon other than the final dicing of components. Our design is aimed to comply with MOS (Metal-Oxide Semi-conductor) co-integration to optimize the specific electrical response of C-MAR structures. The technology of here-developed resonators is detailed through the process steps and designs implemented during the so-called ORSEPEE R&T project from CNES. And finally, experimental results are provided.

[1] W-T. Hsu, “Vibrating RF MEMS for Timing and Frequency Control, Microwave Symposium Digest,” pp 672-675, IEEE-MTT-S, DOI 10.1109/MWSYM.2006.249704, (2006).

[2] M. Ivan, *et al.*, “New electrostatically-excited single crystal silicon resonator vibrating in a Thickness-Extensional mode, ”Proceedings, European Frequency and Time Forum (EFTF), Gothenburg, Sweden, April 23-27, 2012, pp. 221-226.

[3] M. Ivan, *et al.*, “A new electrostatically-excited silicon structure for CMUT and TE-modes resonators and sensing applications,” Proceedings, IEEE Int. Frequency Control Symp., San Francisco, California, May 1-5, 2011, pp. 753-758.

[4] T. Defforge, *et al.*, “Copper-selective electrochemical filling of macropore arrays for through-silicon via applications”, July 2012. Nanoscale research letters, 7(1), 1-7.

Anisotropy in Stiffnesses of Amorphous Silicon Dioxide Films Estimated by Ultrasonic Microscopy

Kensuke Sakamoto[1], Tatsuya Omori[1], Jun-ichi Kushibiki[1,2], and Ken-ya Hashimoto[1]
[1]Graduate School of Engineering, Chiba University, Chiba, Japan
[2]Professor Emeritus, Tohoku University, Sendai, Japan
E-mail: x0t0931@students.chiba-u.jp

Amorphous silicon dioxide (SiO_2) thin films are often used in radio frequency (RF) surface and bulk acoustic waves (SAW/BAW) devices for their temperature compensation. It is known that elastic properties of SiO_2 thin films change dramatically with used deposition apparatus and conditions, and give serious impacts to device performances. The authors measured the propagation direction θ dependence of the water-loaded SAW velocity on SiO_2 thin films deposited on a Si (001) substrate by the Line-Focus-Beam (LFB) ultrasonic microscopy, and tried to estimate stiffnesses of SiO_2 films from the measured θ dependence[1]. However, agreement was poor between the measurement with the fitted result when isotropy was assumed to SiO_2 films.

This paper describes evaluation of stiffnesses of SiO_2 thin films when the anisotropy in elasticity is taken into account. The result indicates that SiO_2 films possess the strong 6mm anisotropy. Namely, stiffnesses normal to the surface are significantly larger than those along the surface. This anisotropy may be induced during the deposition.

Fig. 1 shows the measured water-loaded SAW velocity as a function of θ with the fitted result when the 6mm anisotropy is taken into account. The SiO_2 thickness is 1 μm and the measurement frequency is 225 MHz. It is seen that the fitted result agreed well with the experiment under the comparison with the result given in [1]. Discrepancies can be seen at $\theta \sim \pm 15^o$ and $\theta \sim \pm 75^o$. They are due to change of the propagation mode detected by the LFB, and the SAW propagation loss becomes extremely large at these θ regions.

We have applied the same procedure to four SiO_2 samples prepared by sputtering or chemical vapor deposition (CVD) with two different deposition conditions each, and the agreement was excellent for all these samples.

Table I shows stiffnesses of four SiO_2 samples estimated by the fitting described above. In addition to the large variation, strong anisotropy in elasticity can be clearly seen among four samples. It is seen that variation of C_{11} and C_{12} is much larger than that of C_{33} and C_{13}, respectively. This means SiO_2 sometimes become very stiff along the surface, and the variation is very dependent on the film preparation condition.

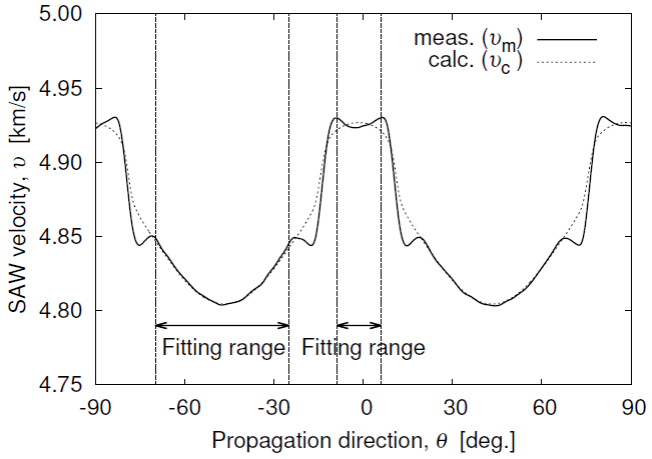


Fig. 1: Measured SAW velocity and fitted result as a function θ. (Sample (a): SiO_2/Si deposited by CVD)

[1] K.Sakamoto, S.Suzuki, T.Omori, K.Hashimoto, J.Kushibiki, and S.Matsuda, "Characterization of Elastic Properties of SiO_2 Thin Films by Ultrasonic Microscopy," Proc. IEEE Ultrason. Symp. (2014) pp. 893-896
[2] B. A. Auld, "Appendix 2 Properties of Materials," in *Acoustic Field and Waves in Solids*, Volume 1, Second edition, Kringer, FL, USA (1989) pp. 365–390

Table I Estimated stiffnesses of four SiO_2 samples

	Stiffness [GPa]					
Sample	C_{11}	C_{12}	C_{13}	C_{33}	C_{44}	C_{66}
(a)	125.7	84.7	21.1	63.6	29.1	20.5
(b)	129.7	95.3	39.1	60.7	20.7	17.2
(c)	104.8	79.8	35.9	64.4	20.2	12.5
(d)	95.8	61.8	33.6	63.7	18.9	17.0
Ref.[2]	78.5	16.1	16.1	78.5	31.2	31.2

Coherent interaction of intracavity pulses and Rb-87 vapor

K. Masuda[1], C. Affolderbach[2], G. Mileti[2], J.-C. Diels[1] and Ladan Arissian[1]

[1] *Center for High Technology Materials, University of New Mexico, Albuquerque, New Mexico 87106, USA*
[2] *Laboratoire Temps-Fréquence, University of Neuchâtel, Neuchâtel, Switzerland*

Email: jcdiels@unm.edu

Motivation Combining the spectral resolution of optical frequency comb with a narrow transition in alkali atoms can create the most sensitive laser sensor for measurement of a magnetic field through Intracavity Phase Interferometry [1]. Towards the realization of such a device, we performed experiments of intracavity interaction between alkali atoms and a mode-locked laser.

Setup A rubidium-87 vapor cell is inserted in a Ti-sapphire laser cavity passively mode-locked by a saturable absorber. The optical frequency and the repetition rate are adjusted by an intracavity birefringent filter and by translating one end mirror, respectively. This setup enable the study of the intracavity near-resonant interaction of rubidium atoms and the comb of pulses.

Results Figure 1 (a) shows the autocorrelations of a pulse in the absence of resonant interaction. A reshaping is observed [Fig. 1 (b)] by tuning the laser to the D1 transition of Rb. The oscillations observed in the interferometric autocorrelation (b) indicate π phase shifts characteristic of zero-area pulse propagation. However the broad intensity autocorrelation and the large intensity are characteristics of 2π pulses of self-induced transparency [2]. The pulse shaping and intracavity pulse area indicate that a combination of 0π and 2π-pulses is generated in the laser. A numerical calculation of Maxwell-Bloch equations supports this claim.

By tuning the repetition rate to the frequency of the ground state hyperfine splitting, while remaining resonant with the D1 transition, coherent population trapping [3] is observed as a dip in fluorescence [Fig. 1 (c)] centered at the 54th sub-harmonic of the 6.8 GHz of the ground state hyperfine splitting. This is the first observation of CPT with a pulse area on the order of π as well as being inside a mode-locked laser cavity.

Our study reveals the nature of coherent interaction of frequency comb with alkali atoms in a previously unexplored regime, and opens the possibility to control and utilize nonlinearity of intracavity interaction for novel applications such as magnetometer.

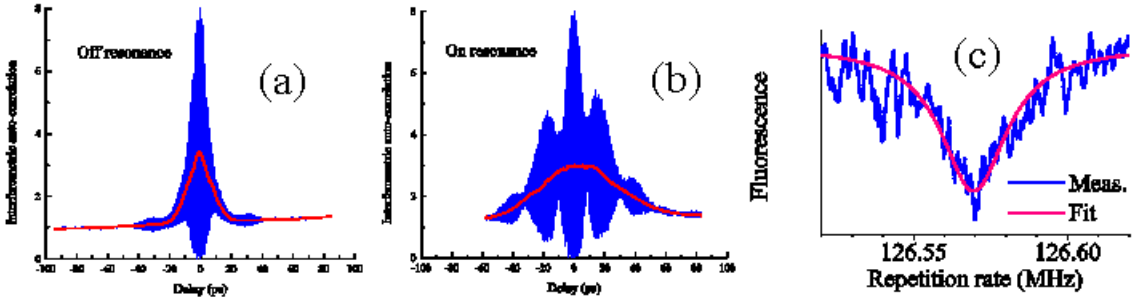


Figure 1: Interferometric (blue) and intensity (red) autocorrelations of the laser pulses (a) off-resonance and (b) at resonance with the D1 line of Rb. (c) Fluorescence versus repetition rate.

[1] L. Arissian and J.-C. Diels, "Intracavity phase interferometry", *Laser Photonics Review* **8**:799-826 (2014)

[2] S. McCall and E. L. Hahn, "Self-induced transparency" *Phys. Rev.*, **183**:457 (1969).

[3] L. Arissian and J.-C. Diels. "Repetition rate spectroscopy of dark line in Rb." *Optics Comm.*, **264**:169–173 (2006).

Study on double-modulation coherent population trapping clock

Yun Peter, Mejri Sinda, Tricot Francois, De Clercq Emeric, Guérandel Stéphane
LNE-SYRTE, Observatoire de Paris, PARIS, FRANCE
Email: enxue.yun@obspm.fr

A high performance passive coherent population trapping (CPT) clock can be based on lin⊥lin configuration [1], or on a compact push-pull optical pumping scheme [2,3] using a Michelson interferometer-like phase delay set-up. This can also be implemented by a more compact and robust setup based on the constructive polarization modulation [4], in which a phase modulation is applied between the two optical components of the bichromatic laser synchronously with the polarization modulation, we simply called it double-modulation scheme. In this scheme, the two CPT dark states produced successively by the alternate polarizations ($\sigma^+\sigma^+ - \sigma^-\sigma^-$) add constructively, thus the atomic population no longer leaks to the end Zeeman states but to the wanted ($m_F = 0$) clock states [4]. As a result, an increased contrast of clock transition is observed.

Here we give a detailed study of the impact of several experimental parameters, modulation frequency, detection time, laser power, etc., on such a clock. For example, as shown in Fig.1, there exists a range of the modulation frequency that maximizes the CPT clock transition contrast. The detailed theoretical and experimental studies will be presented at the conference.

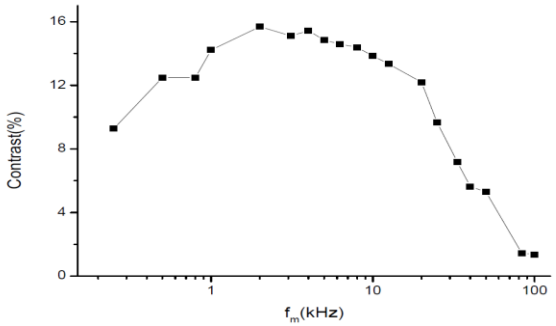


Fig. 1: Contrast of clock transition as function of modulation frequency. In this experiment, light power is 2.63 mW with beam diameter of 15mm. The cylinder vapor cell with length 50 mm and diameter 20 mm, is filled with 21 torr mixed buffer gas with argon and nitrogen. The cell temperature is controlled at 33 ℃. The static magnetic field is 6.87 μT.

This work is supported by the European Metrology Research Programme (EMRP project IND55-MClocks). The EMRP is jointly funded by the EMRP participating countries within EURAMET and the European Union.

[1] J.-M. Danet, M. Lours, P. Yun, S. Guérandel, E. de Clercq, "Frequency Instability Investigations on a Cs Cell Clock Based on Pulsed Coherent Population Trapping," 2013 Joint UFFC, EFTF and PFM Symposium, p. 586-589, 2013.

[2] Y. Y. Jau, E. Miron, A. B. Post, N. N. Kuzma, and W. Happer, "Push-Pull optical pumping of pure superposition states," Phys. Rev. Lett., 93, 160802, 2004.

[3] X. Liu, J.-M. Mérolla, S. Guérandel, C. Gorecki, E. de Clercq, and R. Boudot, "Coherent-population-trapping resonances in buffer-gas-filled Cs-vapor cells with push-pull optical pumping," Phys. Rev. A 87, 013416, 2013.

[4] P. Yun, J.-M. Danet, D. Holleville, E. de Clercq, and S. Guérandel, "Constructive polarization modulation for coherent population trapping clock," Appl. Phys. Lett. 105, 231106, 2014.

Compact and high-performance Rb clock based on pulsed optically pumping for industrial application

Songbai Kang, Mohammadreza Gharavipour, Florian Gruet, Christoph Affolderbach, Gateano Mileti
Laboratoire Temps-Fréquence, Institute of Physics, University of Neuchâtel, Neuchâtel, Switzerland.
E-mail: Gaetano.mileti@unine.ch

We report on the development of a compact laser-pumped Rb clock based on pulsed optically pumping (POP) technique, in view of future industrial applications. The clock Physics Package (PP) is based on a compact magnetron-type microwave cavity of 45 cm^3 volume [1], and our current clock PP has a volume of only 0.8 liters, including temperature control and magnetic shields. This clock PP is completed by a newly-developed frequency-stabilized laser head [2] of 2.5 liters overall volume, with an acoustic optical modulator (AOM) integrated within the laser head for switching the laser output. The laser head's optical setup occupies less than half of the laser head volume, leaving room for further reduction in size in view of the realization of a highly compact vapor-cell atomic clock with state-of-the-art frequency stability.

Due to the highly uniform magnetic field inside the microwave cavity, Ramsey signals with high contrast of up to 35% and with a linewidth of 160 Hz have been demonstrated. A typical short-term clock stability of $3.0\times10^{-13}\ \tau^{-1/2}$ is measured. Thanks to the pulsed operation, the light-shift effect has been considerably suppressed as compared to previously demonstrated continuous-wave clock operation using the same clock PP [3], which is expected to enable improved long-term clock stabilities down to the 10^{-14} level or better (at τ = 1 day). The clock development status will be presented at the conference. Such a compact and high-performance POP Rb clock could find great applications in telecommunication and space navigation and also can be used as high-performance local oscillator (LO) reference.

This work was supported by the Swiss National Science Foundation (SNSF) and the European Metrology Research Programme (EMRP project IND55-Mclocks). The EMRP is jointly funded by the EMRP participating countries within EURAMET and the European Union. We thank C. Calosso (INRIM, Italy) for providing the microwave local oscillator.

[1] C. Stefanucci, T. Bandi, F. Merli, M. Pellaton, C. Affolderbach, G. Mileti and A. K. Skrivervik, "Compact Microwave Cavity for High Performance Rubidium Frequency Standards", *Review of Scientific Instruments*, vol. 83, 104706 (2012).

[2] F. Gruet, M. Pellaton, C. Affolderbach, T. Bandi, R. Matthey, G. Mileti, "Compact and Frequency Stabilized Laser Heads for Rubidium Atomic Clocks", *Proceedings of the International Conference on Space Optics (ICSO)*, Ajaccio, Corsica, October 9 – 12 (2012).

[3] T. Bandi, C. Affolderbach, C. Stefanucci, F. Merli, A. K. Skrivervik, G. Mileti, "Compact high-performance continuous-wave double-resonance rubidium standard with $1.4 \times 10^{-13}\ \tau^{-1/2}$ stability", *IEEE Transactions on Ultrasonics, Ferroelectrics, and Frequency Control*, vol. 61, 1769 – 1778 (2014).

Compact atomic clock prototype based on CPT: Towards the $10^{-13}\,\tau^{-1/2}$ level frequency stability

Sinda Mejri, Francois Tricot, Jean-Marie Danet, Peter Yun, Emeric De Clercq and Stephane Guerandel
LNE-SYRTE Observatoire de Paris, 61 avenue de l'Observatoire, Paris, France

E-mail: Sinda.mejri@obspm.fr

Towards the next generations of compact atomic clocks [1, 2], clocks based on coherent population trapping (CPT) [3] offer a very interesting alternative. In fact thanks to their simple scheme and high performance stability they represent a promising candidates for on-board space and industrial applications [4].

We report in this paper on the performance obtained with a laboratory compact CPT cesium clock. The CPT signal is observed on the Cs D1 line transmission, using a double Λ scheme and a Ramsey interrogation technique. A great deal of work has been done to investigate the two mains frequency noise source: the local oscillator noise and the laser intensity noise. It led to a state-of-the art stability measurement at the level of $3.2\text{x}10^{-13}$ at 1s [5].

In order to reach the ultimate performance of our system, further investigations are carried on in order to improve the short-term and the mid-term stability. For the short-term stability a new frequency chain build with collaboration of INRIM FEMTO-ST [6] will be used in order to minimize further the contribution of the Dick effect, which originates from the down-conversion of the local oscillator intrinsic frequency noise. An optimization of the time sequence and the operating parameters of our clock is under investigations. We are also aiming to improve the signal-to-noise ratio by stabilizing the intensity of the lasers and normalizing the absorption signal by the laser power measured on the cell input, in order to compensate the noise added by the acousto-optic modulator chopping the beam.

For the mid-term stability, a careful study will be conducted on the influence of the laser power and the magnetic field on the clock frequency.

The results of these studies will be presented at the conference.

[1] S. Micalizio, C.E. Calosso, A. Godone and F. Levi, Metrologia 49 425-436 (2012).
[2] Thejesh Bandi et al, IEEE Transactions on ultrasonic, ferroelectrics, and Frequency control, Vol. 61, NO.11 (2014).
[3] Knappe et al, Vol. 18, No. 11/ November/ J. Opt. Soc. Am. B, 1545 (2001).
[4] P. Waller et al, Trans. Ultrason., Ferroelect., Freq. Contr., 57, 738 (2010).
[5] J. M. Danet, O. Kozlova, P. Yun, S. Guerandel and E. De Clerq, EPJ Web of Conference 77, 00017 (2014).
[6] B. François, C. E. Calosso, J. M. Danet, and R. Boudot, Review of Scientific Instruments 85, 094709 (2014).

Light Shifts in a cold-atom CPT Clock

E. A. Donley, E. Blanshan, X. Liu, and J. Kitching

NIST, Boulder, CO, USA
E-mail: elizabeth.donley@nist.gov

A detailed study of the light shift in our cold-atom coherent population trapping (CPT) clock [1] will be presented. In our clock, laser-cooled atoms are interrogated with lin || lin CPT [2] by use of Raman-Ramsey spectroscopy [3]. The clock interrogates a sample of 2×10^5 atoms under free-fall with typical cycle and Ramsey periods of 50 ms and 16 ms, respectively. The clock typically demonstrates a short-term fractional frequency stability of $4\times10^{-11}/\sqrt{\tau}$, limited by frequency noise on the phase-locked interrogation lasers.

The light shift for Raman-Ramsey CPT interrogation was first studied in a sodium beam clock [4], where it was shown that the dominant light shift behaves fundamentally differently than the well-known AC Stark shift that arises when the energy levels are shifted by harmonic electric fields. In contrast, the light-shift in Raman-Ramsey interactions is present only while the dark state coherence is approaching steady state during the first Ramsey pulse, and it is independent of the intensity ratio of the two frequency components provided the total intensity is constant. Counterintuitively, the light shift vanishes in the limit of sufficiently large intensity and duration for the first pulse. Low intensity and/or detuned CPT frequencies, however, generate low excitation rates that prevent the dark state from fully forming during the finite length of the first pulse. The resulting shift scales inversely with the Ramsey period and changes sign depending on the initial hyperfine ground state.

Measured light shifts in our Raman-Ramsey CPT clock do not vanish at high intensity as predicted by this established model [4]. A set of typical light-shift measurements is presented in Fig. 1, which shows an intensity independent shift that persists at high intensity. The residual shift scales inversely with the Ramsey period but is independent of laser intensity, pump pulse duration, and initial hyperfine level.

We can explain the observed shifts in terms of phase shifts that arise during the formation of dark-state coherences combined with optical-pumping effects caused by incoherent light in the CPT laser spectrum. Measurements compared with an expanded version of the existing model that includes optical pumping from incoherent light in the CPT spectrum show good agreement.

A laser configuration is identified and demonstrated that should reduce clock drift from light shifts to $< 1\times10^{-14}$ for the current system. Improving the fraction of beat-note power in the coherent carrier from its current value of 72 % would also reduce the light shift. Current efforts are directed toward improving the fraction of coherent light in the CPT spectrum and testing other CPT interrogation schemes for sensitivity and long-term stability.

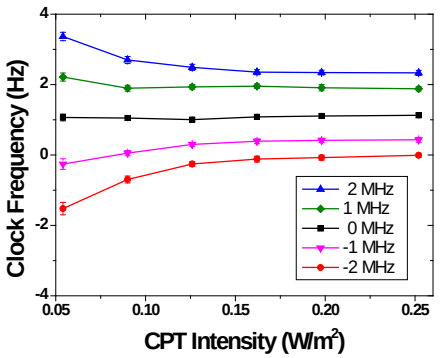


Fig. 1: Typical light shift measurements. Absolute frequency measurements are performed, and the clock frequency is referenced to the hyperfine ground state splitting for ^{87}Rb. Here the Ramsey period was 16 ms, the first pulse length was 400 μs, and the initial hyperfine ground state was F=2. There is a 1 Hz frequency offset from the Zeeman shift.

[1] F. X. Esnault, E. Blanshan, E. N. Ivanov, R. E. Scholten, J. Kitching, and E. A. Donley, "Cold-atom double-Λ coherent population trapping clock," *Physical Review A*, vol. 88, 2013.

[2] A. V. Taichenachev, V. I. Yudin, V. L. Velichansky, and S. A. Zibrov, "On the unique possibility of significantly increasing the contrast of dark resonances on the D1 line of 87Rb," *JETP Lett.*, vol. 82, pp. 398-403, 2005.

[3] J. E. Thomas, P. R. Hemmer, S. Ezekiel, J. C. C. Leiby, R. H. Picard, and C. R. Willis, "Observation of Ramsey fringes using a stimulated, resonance Raman transition in a sodium atomic beam," *Phys. Rev. Lett.*, vol. 48, pp. 867-870, 1982.

[4] P. R. Hemmer, M. S. Shahriar, V. D. Natoli, and S. Ezekiel, "Ac Stark shifts in a two-zone Raman interaction," *J. Opt. Soc. Am. B*, vol. 6, pp. 1519-, 1989.

Free-Space Optical Time-Frequency Transfer Over 4 km

Sinclair, Laura C., Deschênes, Jean-Daniel, Swann, William C., Giorgetta, Fabrizio R., Baumann, Esther, Coddington, Ian, and Newbury, Nathan R.
National Institute of Standards and Technology, 325 Broadway, Boulder, Colorado 80305
E-mail: laura.sinclair@nist.gov
Work of the U.S. government, not subject to copyright.

Optical two way time frequency transfer (TWTFT) in conjunction with linear optical sampling supports time-frequency comparison at the 10^{-18} level [1,2]. Here we demonstrate optical TWTFT over a 4 km bi-directional free-space link with a common clock. Unlike earlier efforts [1], we take advantage of the development of robust fiber frequency combs [3] to implement the system with self-referenced frequency combs co-located at the terminals. Self-referenced combs result in a lower pulse-to-pulse timing jitter and contribute to the lower residual stability compared to earlier measurements (Fig 1a). Furthermore, these improved combs also remain phase locked with glitch free operation for days [3] as opposed to the limitation of a few hours for earlier efforts due to phase slips. In addition, redesigned free-space optical terminals resulted in higher link availability. The low residual stability relies on the reciprocity of the single-mode link to cancel any pathlength variations [1].

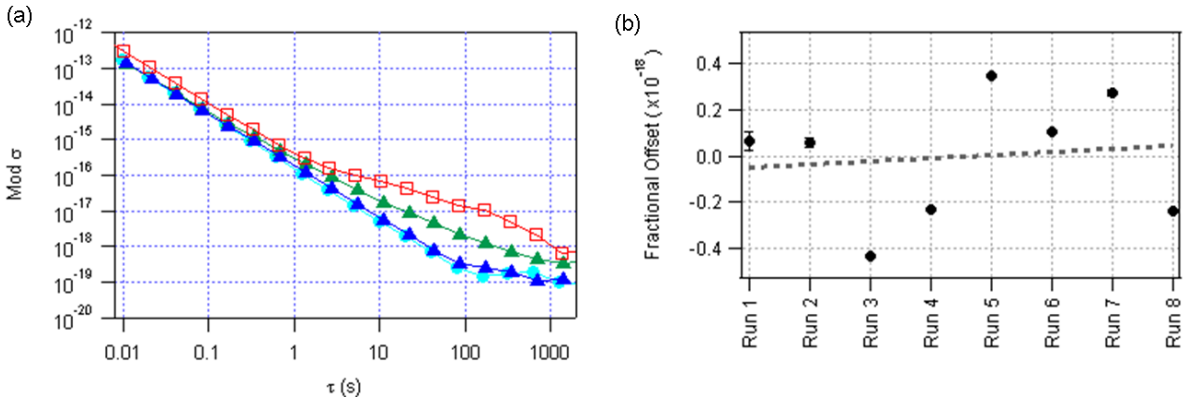


Fig. 1. (a) Two-way Modified Allan deviation for 4 km link for 90% link availability (dark blue triangles) and 72% link availability (green triangles) and for a "shorted path" (light blue circles). In addition, the red open squares show the residual stability for the 2 km link measurement described in Ref. [1]. (b) Fractional offset for 8 datasets (circles) and a linear fit (dashed line). The fit gives an offset of -5.4×10^{-20} +/- 1.9×10^{-19}, which is consistent with zero as expected, demonstrating a lack of a bias.

When the link is available 90% of the time, the residual stability is below 10^{-18} at 44 seconds and reaches a floor of 1.2×10^{-19} at 1400 seconds. This is below the performance of the best optical clocks [4-7]. In this case, the residual stability is dominated by the small amount of out-of-loop fiber as shown by the agreement between the shorted path and 4 km data. Even when the link is only available for two-thirds of the time, the time-frequency comparison is still possible. Fig. 1b shows a fractional offset consistent with zero for 8 datasets with acquisition times ranging from 30 minutes to 16 hours.

[1] F. R. Giorgetta et al., Nat. Photonics, 7, 434–438 (2013).
[2] I. Coddington et al, Nat. Photon, 3, 351–356 (2009).
[3] L. C. Sinclair et al., Opt. Express, 22, 6996–7006 (2014).
[4] C. W. Chou et al, Science, 329, 1630–1633 (2010).
[5] N. Hinkley et al., Science, 341, 1215–1218 (2013).
[6] I. Ushijima et al., ArXiv14054071 Phys. (2014).
[7] B. J. Bloom, et al., Nature, 506, 71–75 (2014).

Identification and Calibration of Ground System Biases in Ground to Space Laser Time Transfer

Prochazka, Ivan*; Blazej, Josef*; Kodet, Jan*+
*Dept. of Physical Electronics, Czech Technical University in Prague, Prague, Czech Republic
+Forschungseinrichtung Satellitengeodäsie, Technische Universität München, Germany
E-mail: blazej@fjfi.cvut.cz

Laser time transfer is an attractive technique to transfer time ground to space with picosecond precision and systematic errors on the level of tens in picoseconds. Recently the European Laser Timing (ELT) experiment is under construction [1]. It is an optical link prepared in the frame of the European Space Agency mission Atomic Clock Ensemble in Space. The objective of this laser time transfer is the synchronization of the ground based clock and the clock on board the International Space Station with picosecond precision and the accuracy better than 50 picoseconds. Several other laser time transfer missions are under consideration by various space agencies [2]. In addition one way laser ranging ground to space over interplanetary distances is and attractive technique foreseen for future deep space missions.

In all the foreseen applications the systematic errors – biases – associated with the ground segment of the process represent a significant limitation of the overall performance. We are reporting on a progress in identification and calibration of these biases. To reach the ultimate accuracy in European Laser Timing experiment the Calibration Device has been developed and tested. It enables to calibrate the ground based laser systems for their systematic timing biases. As a result the ground to ground and ground to space time transfer in and ELT experiment should be accomplished with systematic errors not higher than 20 picoseconds. The design and construction of the ELT Calibration Device will be presented along with the results of its application in field tests.

The typical structure of the ground segment of the laser time transfer system is illustrated in Fig. 1. The laser is is generating a short pulse (usually at 532 nm), the pulse is split, a part is triggering a photodiode and its signal is time tagged in reference with ground 1 pps signal. The majority of optical energy is transmitted by a telescope with single optical reference point. The goal of our work is to find time interval between electrical signal at event timer input connector and optical signal in telescope reference point.

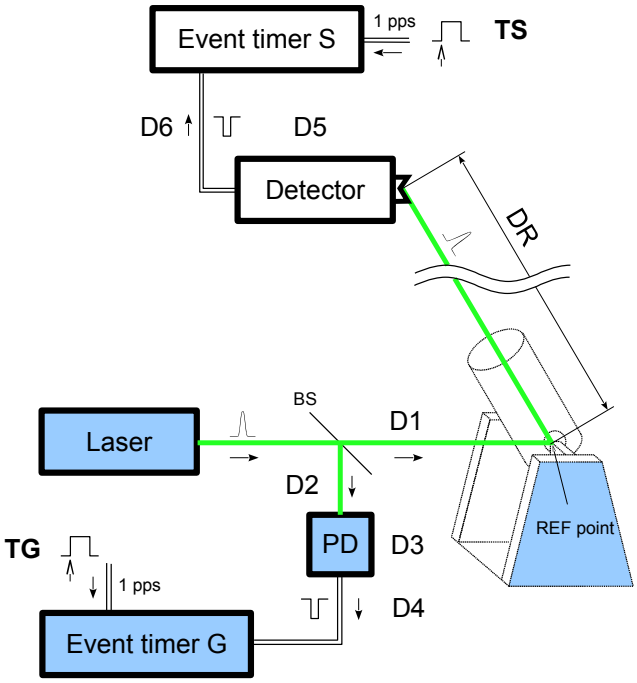


Fig. 1: Block scheme of signals and delays between instruments involved in laser time transfer. Single green line – optical signals, double line – electrical signals, ground segment instruments are in blue color.

[1] K. U. Schreiber, I. Prochazka, P. Lauber, U. Hugentobler, W. Schäfer, L. Cacciapuoti, and R. Nasca, "Ground-based demonstration of the European Laser Timing (ELT) experiment," IEEE Trans. Ultrason., Ferroelect., Freq. Contr., vol. 57, no. 3, pp. 728-737, Mar. 2010.

[2] I. Ciufolini, et al. "Testing General Relativity and gravitational physics using the LARES satellite," The European Physical J. Plus, vol. 127, no. 11, p. 133, 2012.

Concept for Space-Time Reference via Laser-Comm Link

Berceau, Paul and Hollberg, Leo
Department of Physics and Hansen Experimental Physics Laboratory
Stanford University, Stanford, CA 94305-4085
E-mail: leoh@stanford.edu

A high performance Space-Time Reference (STR) could be realized using a stable atomic clock in a precisely defined orbit and synchronizing the orbiting clock to high-accuracy atomic clocks on the ground. The synchronization would be done using a two-way laser-comm link between ground and space. The basic idea is to take advantage of the highest performance cold-atom atomic clocks at national standards laboratories and to transfer that performance to the orbiting clock that has good stability over times-scales of a few orbits. The two-way laser-comm link could also provide range information and thus precise orbit determination. With a well-defined orbit and a synchronized clock, the satellite could serve as a high accuracy Space-Time Reference, and provide precise time world-wide and a valuable reference frame for geodesy.

A diagram of the major system components is shown in Fig. 1. High accuracy atomic frequency references on the ground stabilize femtosecond-Optical Frequency Comb (OFC) with the usual "self-referencing" techniques. The train of phase-coherent and ultra-short pulses emitted from the stabilized fs-optical comb serves as the heart of the optical timing reference for the laser-comm link. The precise timing information available from the comb and optical pulses are then transferred to the data stream of the two-way laser-comm link between the ground and the satellite. At Stanford, we are beginning to explore these concepts and testing subsystems using an optical fiber network plus a short free-space distance that mimics the ground to space link. Using microwave frequency references and a 1550 nm OFC we have measured timing noise levels of a few fs/√Hz, which are more than adequate to support precise time transfer at the ps level. We have also demonstrated the pointing and tracking of a moving target using a low power laser and MEMS mirrors as actuators. The achieved performance and robustness of these sub-systems are compatible with the requirements for space.

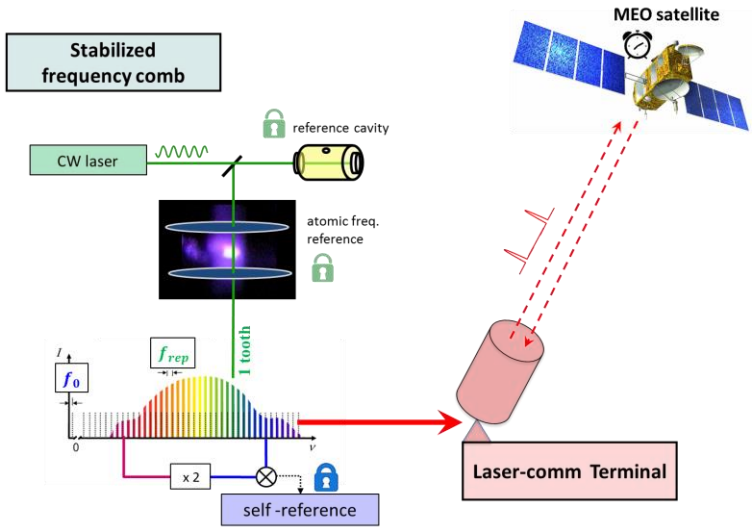


Fig. 1: Diagram of a high performance optical time transfer link between the ground and a middle earth orbit satellite. A stable CW laser is locked to both an ultra-stable Fabry-Pérot cavity and a narrow atomic transition. That laser stabilizes an OFC that serves as the timing reference for the two-way laser-comm link, which synchronizes the clock to the ground clocks.

Integrating these systems and technologies with actual laser-comm links to space would allow us to create a very high performance nearly-inertial orbiting STR. This could provide very compelling performance in a practical system with time transfer (~ 1ps) world-wide, and a highly accurate reference frame for coordinate position (~ 1mm). This would provide unique capabilities in navigation, earth sciences, geodesy and testing fundamental physics in space. System performance could provide even higher performance as better space-qualified clocks become available.

Characterization of an ultra stable quartz oscillator thanks to Time Transfer by Laser Link (T2L2, Jason-2)

A. Belli[1,2], P. Exertier[1], E. Samain[1], C. Courde[1], F. Vernotte[2], A. Auriol[3], C. Jayles[3]
[1] Géoazur Valbonne, France
[2] Observatoire de Besançon UTINAM, Besançon, France
[3] CNES *French Space Agency*, Toulouse, France
Email: belli@geoazur.unice.fr

Abstract

The experiment T2L2 (*Time Transfer by Laser Link*), on-board Jason-2, with an orbit at 1335 km, since June 2008 allows the clock synchronization between ground clock (generally H-maser) and space clock (quartz Ultra Stable Oscillator (USO) DORIS) with a stability of a few picoseconds over 100 seconds. In common view, when two laser stations see T2L2, the time transfer stability is less than 10 picosecondes over few seconds. In order to perform non-common view time transfer for synchronizing distant ground clocks, it is important to precisely characterize the on-board oscillator at least on 10 000 seconds (maximal flight time between two distant stations). The key is to study the space environment on the Jason-2 orbit, to separate deterministic and stochastic behaviors of the USO (shift and drift). We show that T2L2 is able to provide accurate frequencies, which are deduced from the ground to space time transfer over each laser station (few 10^{-13}). Since 2008, these time transfers helped us to create an on-board frequency data base.

The major contributors to these frequency variations on 10 000 seconds are temperature and space radiation especially due to the South Atlantic Anomaly (SAA) (due to Jason-2 orbit). Aging can be considered as a linear drift during 10 000 seconds and the effect of radiation like a very small shift over each SAA overflight. The effect of the temperature is drived by the on-board temperature measurement. A model is realized to represent these effects on USO with a RMS of few 10^{-13} over 10 000 seconds.

Space phenomena are also playing an important role in long term. Actually, if we consider both accumulation dose received by radiation and aging, we can explain 99.9 % of the global frequency variation of the USO since the beginning of the T2L2 mission.